

QA: QA

**Civilian Radioactive Waste Management System
Management & Operating Contractor**

Unsaturated Zone Flow and Transport Model Process Model Report

TDR-NBS-HS-000002 REV00 ICN02

August 2000

Prepared for:

U.S. Department of Energy
Yucca Mountain Site Characterization Office
P.O. Box 30307
North Las Vegas, Nevada 89036-0307

Prepared by:

TRW Environmental Safety Systems, Inc.
1180 Town Center Drive
Las Vegas, Nevada 89144-6352

Under Contract Number
DE-AC08-91RW00134

NM5507
WM-11

QA: QA

**Civilian Radioactive Waste Management System
Management & Operating Contractor**

Unsaturated Zone Flow and Transport Model Process Model Report

TDR-NBS-HS-000002 REV00 ICN02

August 2000

Prepared for:

U.S. Department of Energy
Yucca Mountain Site Characterization Office
P.O. Box 30307
North Las Vegas, Nevada 89036-0307

Prepared by:

TRW Environmental Safety Systems, Inc.
1180 Town Center Drive
Las Vegas, Nevada 89144-6352

Under Contract Number
DE-AC08-91RW00134

INFORMATION COPY
LAS VEGAS DOCUMENT CONTROL

DISCLAIMER

This report was prepared as an account of work sponsored by an agency of the United States Government. Neither the United States Government nor any agency thereof, nor any of their employees, nor any of their contractors, subcontractors or their employees, makes any warranty, express or implied, or assumes any legal liability or responsibility for the accuracy, completeness, or any third party's use or the results of such use of any information, apparatus, product, or process disclosed, or represents that its use would not infringe privately owned rights. Reference herein to any specific commercial product, process, or service by trade name, trademark, manufacturer, or otherwise, does not necessarily constitute or imply its endorsement, recommendation, or favoring by the United States Government or any agency thereof or its contractors or subcontractors. The views and opinions of authors expressed herein do not necessarily state or reflect those of the United States Government or any agency thereof.

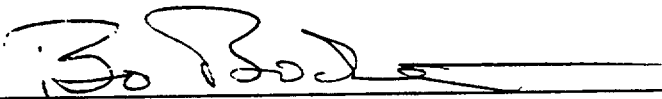
**Civilian Radioactive Waste Management System
Management & Operating Contractor**

Unsaturated Zone Flow and Transport Model Process Model Report

TDR-NBS-HS-000002 REV00 ICN02

August 2000

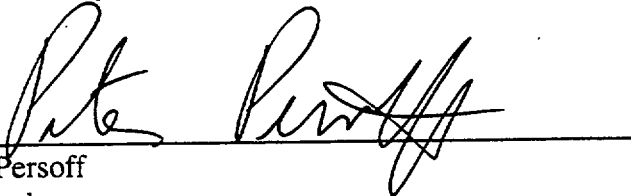
Prepared by:



G.S. Bodvarsson
UZ PMR Lead Author

8/9/00
Date

Checked by:



P. Persoff
Checker

8/9/00
Date

Approved by:



G.S. Bodvarsson
Responsible Manager, UZ PMR Department Manager

8/9/00
Date

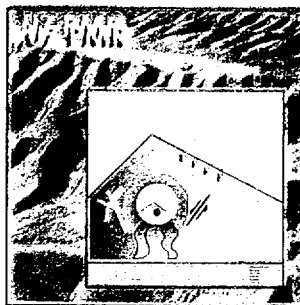
INTENTIONALLY LEFT BLANK

**Civilian Radioactive Waste Management System
Management & Operating Contractor**

Unsaturated Zone Flow and Transport Model Process Model Report

TDR-NBS-HS-000002 REV00 ICN02

August 2000



Authors:

G.S. Bodvarsson, Lead

C.F. Ahlers
M. Cushey
F.H. Dove
S.A. Finsterle

C.B. Haukwa
J. Hinds
C.K. Ho
J. Houseworth

Q. Hu
H.H. Liu
M. Pendleton
E.L. Sonnenthal

A.J. Unger
J.S.Y. Wang
M. Wilson
Y.-S. Wu

Editors:

G.S. Bodvarsson, Lead

F.H. Dove
C.K. Ho
M. Pendleton

Production:

M. Villavert, Lead
K. Eaton
L. Montgomery

Illustrations:

D. Swantek, Lead
M. Fink
R. Reen
F. Robles

Technical Editing:

J. Geller, Lead
D. Hawkes
Y. Tsang

INTENTIONALLY LEFT BLANK

CHANGE HISTORY

<u>Revision Number</u>	<u>Interim Change No.</u>	<u>Effective Date</u>	<u>Description of Change</u>
00		03/14/2000	Initial Issue
00	1	06/21/2000	Interim change to address comments per AP-7.5Q <i>Submittal, Review, and Acceptance of Deliverables</i> . Changes indicated by sidebar in margin.
00	02	08/09/2000	Interim change to modify text language in Executive Summary, Section 1, and Section 6.2 to meet Regulatory requirements. Changes indicated by sidebar in margin.

INTENTIONALLY LEFT BLANK

EXECUTIVE SUMMARY

The Unsaturated Zone (UZ) Process Model Report (PMR) describes the modeling, analysis and current understanding of fluid flow and chemical (solute and colloidal) transport through the UZ at Yucca Mountain. The UZ PMR is supported by 24 Analysis/Model Reports (AMRs) which provide detailed descriptions of the various UZ models and analyses. The primary purpose of the UZ PMR is to document models and analyses for Total System Performance Assessment (TSPA) that evaluate the post-closure performance of the UZ. The models in the UZ PMR consider two principal factors (factors identified by the Yucca Mountain Project that greatly affect the performance of the potential repository), which are seepage into drifts and radionuclide retardation in the UZ. Seven other factors (factors of secondary importance) that relate to climate/infiltration, percolation flux, and coupled processes are also considered. The other factors are climate, net infiltration into the mountain, UZ flow above the repository, coupled processes-effects on UZ flow, advective pathways in the UZ, colloid-facilitated transport in the UZ and coupled processes-effects on UZ transport.

The UZ PMR models are built upon the Integrated Site Model (ISM) and conceptual models for flow and transport through the UZ that have been developed from site-specific data, together with scientific and technical knowledge associated with flow and transport at analog sites and other UZ studies. The construction of mountain- and drift-scale numerical grids for the models is based upon the geological characterization of the site at scales relevant to the intended purpose of, or process(es) described by, the specific model. Most of the models in the UZ PMR are based on continuum approximations and employ the dual-permeability approach with van Genuchten equations to describe characteristic curves of both the fracture and matrix continua. The models are supported by site data collected since the early 1980's and the results of field testing in boreholes and underground drifts, which allow for model calibration against field observations, and validation using independent data sets and/or field tests. Uncertainties associated with the models range from uncertainties in individual parameters and processes, to uncertainties in the conceptual and numerical models employed. Some of these uncertainties are due to the fact that the UZ at Yucca Mountain is very heterogeneous. Uncertainty is included in the models for use in TSPA.

The major hydrogeologic units identified at Yucca Mountain are, in order from the land surface to the water table, the Tiva Canyon welded unit (TCw), the Paintbrush nonwelded unit (PTn), the Topopah Spring welded unit (TSw), the Calico Hills nonwelded unit (CHn), and the Crater Flat undifferentiated unit (CFu). These units are partially saturated with water. Generally, water occupies about half of the pore space in the TCw and the PTn, except for values near 90% at the transition between the TCw and PTn. Within the TSw, water saturations range from 60% to almost fully saturated, and saturations in the CHn are mostly greater than 90%. The water table elevation is approximately 400 to 800 meters (m) below ground surface.

Current climate is expected to persist for approximately the next 600 years, followed by a warmer and wetter monsoon climate for another 1,400 years, and then a cooler, still wetter glacial-transition climate for the remainder of the 10,000-year compliance period. The current best estimate of average net-infiltration of 4.6 mm/yr is expected to increase to an average of 12.2 and 17.8 mm/yr for the monsoon climate and glacial-transition climate, respectively. Percolating water derived from precipitation flows primarily in fractures in the welded units

(e.g., TCw and TSw), and in the rock matrix in the nonwelded units (e.g., PTn and CHn (vitric)). Although infiltration is highly episodic, with significant amounts expected to infiltrate for only a few days every 3 to 5 years, the PTn is expected to dampen these pulses, so that water flow below the PTn is assumed to be steady.

The potential repository will reside at a depth ranging from 200 to 425 m below ground surface, and from 175 to 365 m above the water table, in three geological units within the TSw. About ten percent of the potential repository volume is located in the middle nonlithophysal unit, 78% in the lower lithophysal unit, and 12% in the lower nonlithophysal unit. More than 80% of water flow at the potential repository horizon is through fractures, while the remainder flows through the low permeability (10^{-16} to 10^{-18} m²) rock matrix. In general, as the infiltration/percolation flux increases, the fraction of the total water flow in the fractures also increases. Bomb-pulse ³⁶Cl data have verified the existence of fast flow from the land surface to the potential repository horizon; most of the fast flow is associated with known faults. The fracture network permeability in the upper nonlithophysal unit is high but scale-dependent, with large-scale (100 m scale) permeability on the order of 5×10^{-11} m², and smaller-scale (1 m scale) permeability ranging from 10^{-14} to 10^{-11} m². Preliminary field tests show that the average permeability of the lower lithophysal unit may be an order of magnitude higher than that of the upper nonlithophysal unit. Geochemical data such as total chloride (Cl), nonbomb-pulse ³⁶Cl and calcite fillings in fractures are used to build confidence in the conceptual and numerical models of flow and transport processes occurring in the mountain, and to constrain the predictions of local and global percolation flux.

As a result of the varied geology, critical flow and transport processes differ between the northern and southern parts of the potential repository. Below the horizon of the potential repository, perched water bodies have been found primarily in the northern part of the potential repository area, where low permeability zeolitic rock units are abundant. The presence of the perched water bodies creates the potential for the lateral flow of water to nearby high-permeability vertical features, such as faults. The three-dimensional (3-D) simulations of flow and radionuclide transport in the northern part indicate that flow down the faults increases with depth below the repository, resulting in over 40% of the groundwater recharge occurring through faults. The potential lateral flow and flow through faults have important implications for radionuclide transport, by allowing rapid advective transport from the potential repository to the water table and bypassing of the rock matrix where matrix diffusion and sorption could promote retardation. Larger-size colloids (e.g., plutonium (Pu) colloids) that cannot diffuse into the matrix are particularly susceptible to rapid transport. Beneath the southern part of the potential repository, vitric rock units are present; the vitric rocks potentially provide efficient sorption of some radionuclides such as neptunium (²³⁷Np). Technetium (⁹⁹Tc) and iodine (¹²⁹I) are non-sorbing and potentially may provide the highest dose rates for the first 10,000 years of the potential repository's life. Daughter products of plutonium (²³⁹Pu) such as uranium (²³⁵U) become important after 10,000 years, and therefore must be considered in the abstractions and models for Total System Performance Assessment (TSPA).

The rate of water seepage into drifts is expected to be considerably less than the prevailing percolation flux and may be zero for areas where the percolation flux is lower than the seepage threshold for that location. This is because the drifts act as capillary barriers which divert most of the flowing water around the drifts. The seepage threshold, defined as the percolation flux below

which no seepage occurs (for a given location within a hydrogeological unit), depends upon various hydrological parameters, especially fracture permeability and the fracture van Genuchten "alpha" value. The average seepage threshold of the upper nonlithophysal unit is estimated to be 200 mm/yr. Based on limited hydrological data and understanding of seepage processes, it is expected that the seepage behavior of the lower lithophysal and lower nonlithophysal units is similar to that of the upper nonlithophysal unit. Changes in the drift shape due to rock fall may increase seepage; however, estimates based on the current rock fall model show negligible effects on seepage.

As the radioactive waste emits heat, coupled thermal-hydrological-chemical (THC) processes in the UZ rock mass may be important for time periods of up to about 10,000 years. The energy emitted will heat up the entire UZ extending 600 m from the potential repository footprint, with estimated temperature increases of 30 to 35°C at the water table, and up to 5°C at the ground surface. With the assumed design options (Enhanced Design Alternatives II and 50-year ventilation, currently under revision), boiling will occur around the drifts; the region experiencing the boiling temperature (~97°C) will extend out to a maximum of 50 meters into the rock. Temperatures in the mid-pillar regions will increase to 80 to 85°C, but sufficient drainage of condensate is predicted because of the relatively high fracture permeabilities of the potential repository hydrogeological units. As a result, the percolation flux during the thermal period will not greatly exceed the ambient percolation flux for most locations within the potential repository.

The drift-scale models of THC coupled processes predict the chemistry of water and gases entering and occurring around the drifts, and the changes in hydrological properties expected from precipitation/dissolution processes. The results from the models indicate that the water entering the drifts will have relatively neutral pH values, ranging from 7 to 9, and total chloride concentrations that increase to a maximum of about four times the concentrations in the ambient pore water. The precipitation/dissolution of various chemical species and/or minerals was found to have negligible effects on fracture and matrix hydrological properties.

The UZ PMR process models, specifically the Flow Model, the Seepage Model, the Drift-Scale THC Model and the Transport Model, are abstracted for use in TSPA. The degree of abstraction of these models varies from direct use of the process model in TSPA to using the model to justify neglecting certain processes. In the development of the process models, the uncertainties in parameters, processes, and conceptual models are identified and qualified where possible; TSPA then evaluates the importance of these uncertainties on the performance of the potential repository.

In addition to the treatment of the various technical issues on UZ flow and transport, the UZ PMR summarizes concerns and comments by various overseeing bodies such as the Nuclear Regulatory Commission (NRC), the Nuclear Waste Technical Review Board (NWTRB), various peer review groups convened by the Yucca Mountain Site Characterization Project (YMP), and from various internal YMP workshops discussed in Section 2.5. The issues raised by the NRC are of particular interest. In support of the Site Recommendation (SR), the NRC will review current information about the Yucca Mountain site in the UZ PMR, as part of their statutory role in the high-level waste management program. The NRC issues are discussed in detail in Chapter 4 of the UZ PMR.

ACKNOWLEDGMENTS

The authors and contributors of the UZ PMR appreciate very valuable comments from the following M&O and DOE reviewers; Bob Andrews, Norma Biggar, Jim Blink, R. Bradbury, John Case, Steve Dana, Tom Doe, Harvey Dove, Dwight Hoxie, Rick Kossik, Levy Kroitoru, Mike Lugo, Bimal Muhkopadhyay, Kathryn Mrotek, W. Mark Nutt, Pasu Pasupathi, Lew Robertson, Ralph Rogers, Rick Salness, Mike Scott, David C. Sassani, David Stahl, Mark Tynan, and Mark Wisenburg. Other thanks go out to the LBNL staff who worked diligently on components of the document, for without their help, this would have not been possible; N. Aden-Gleason, M. Cuzner, V. Fissekidou, J.D. Jackson, P. Lau, S. Link, D. Mangold, I. McClung, and C. Valladao. Thank you to Roy Kaltschmidt, photographer for LBNL, for providing some of the photos for the graphics.

ACRONYMS AND ABBREVIATIONS

1-D	One-dimensional, one dimension
2-D	Two-dimensional, two dimensions
3-D	Three-dimensional, three dimensions
ACC	Accession Number
ACNW	Advisory Committee on Nuclear Waste
AGM	Ambient Geochemistry Model
AMR	Analysis/Model Report
AP	Administrative Procedure
CFR	Code of Federal Regulations
CM	Climate Model
CPM	Calibrated Properties Model
CPU	Central Processing Unit
CRWMS	Civilian Radioactive Waste Management System
CSNF	Commercial Spent Nuclear Fuel
DCPT	Dual Continuum Particle Tracker
DDSM	Disturbed Drift Seepage Model
DECOVALEX	DEvelopment of COupled models and their VALidation against EXperiments
DFNM	Discrete Fracture-Network Model
DHLW	Defense High Level Waste
DIRS	Document Input Reference System
DOE	Department of Energy
DP	Development Plan
DSNF	DOE Spent Nuclear Fuel
DSPR	Drift Scale Peer Review
DST	Drift Scale Test
DTN	Data Tracking Number
EBS	Engineered Barrier System
ECM	Effective Continuum Model
ECRB	Enhanced Characterization of Repository Block
EDA	Enhanced Design Alternative
EDZ	Excavation-Disturbed Zone
EIS	Environmental Impact Statement
EPA	Environmental Protection Agency
ESE	East South East
ESF	Exploratory Studies Facility
FEHM	Finite Element Heat and Mass Transfer
FEP	Features, Events, and Processes
FM	Flow Model
FTM	Flow and Transport Model

ACRONYMS AND ABBREVIATIONS (Continued)

FY	Fiscal Year
GDF	Ghost Dance Fault
GFM	Geologic Framework Model
HGU	Hydrogeologic Unit
HLW	High Level Waste
IFDM	Integral Finite Difference Method
IM	Infiltration Model
INEEL	Idaho National Engineering and Environmental Laboratory
ISM	Integrated Site Model
IRSR	Issue Resolution Status Report
ITN	Input Tracking Number
KTI	Key Technical Issue
LA	License Application
LANL	Los Alamos National Laboratory
LBNL	Lawrence Berkeley National Laboratory
LBT	Large Block Test
LHS	Latin Hypercube Sampling
LLNL	Lawrence Livermore National Laboratory
MAI	Mean Annual Infiltration
M&O	Management and Operating Contractor
MINC	Multiple Interacting Continua
MM	Mineralogic Model
N/A	Not Applicable
NC	Nye County
NEA	Nuclear Energy Agency
NFE	Near Field Environment
NOAA	National Oceanic and Atmospheric Administration
NR	North Ridge
NRC	Nuclear Regulatory Commission
NS	North South
NTS	Nevada Test Site
NWTRB	Nuclear Waste Technical Review Board
OCRWM	Office of Civilian Radioactive Waste Management
OECD	Organization for Economic Cooperation and Development
PA	Performance Assessment
PARP	Total System Performance Assessment Peer Review Panel

ACRONYMS AND ABBREVIATIONS (Continued)

PMR	Process Model Report
Q	Qualified
QA	Quality Assurance
QAP	Quality Administrative Procedure
QARD	Quality Assurance Requirements and Description
QIP	Quality Implementing Procedure
RPM	Rock Properties Model
RSS	Repository Safety Strategy
RT	Radionuclide Transport
RTM	Radionuclide Transport Model
RTTF	Residence-Time Transfer Function
SCM	Seepage Calibration Model
SCP	Site Characterization Plan
SHT	Single Heater Test
SMPA	Seepage Model for Performance Assessment
SN	Scientific Notebook
SNL	Sandia National Laboratories
SR	Site Recommendation
SRR	Site Recommendation Report
STN	Software Tracking Number
SZ	Saturated Zone
TBD	To Be Determined
TBV	To Be Verified
TDMS	Technical Data Management System
TEF	Thermal Effects on Flow
TH	Thermal-Hydrologic
THC	Thermal-Hydrological-Chemical
THCM	Thermal-Hydrological-Chemical Model
THCMe	Thermal-Hydrological-Chemical-Mechanical
THM	Thermal-Hydrologic Model
THMe	Thermal-Hydrological-Mechanical
TM	Transport Model
TMe	Thermal-Mechanical
TOUGH	Transport Of Unsaturated Groundwater and Heat
TSPA	Total System Performance Assessment
TU	Tritium Units
US	United States
USGS	United States Geological Survey
UZ	Unsaturated Zone
UZEE	Unsaturated Zone Flow Expert Elicitation

ACRONYMS AND ABBREVIATIONS (Continued)

UZFTEP	Unsaturated Zone Flow and Transport Evaluation Panel
VA	Viability Assessment
WFD	Waste Form Degradation
WNW	West North West
WP	Waste Package
WPO	Waste Package Operations
WPPS	Work Package Planning Summary
XRD	X-Ray Diffraction
YM	Yucca Mountain
YMP	Yucca Mountain Site Characterization Project
YMSD	Yucca Mountain Site Description

ACRONYMS AND ABBREVIATIONS (Continued)

UNITS

ky	thousand years
m	meters
Ma	million years
masl	meters above sea level
mg/L	milligrams/liter
mm	millimeters
MPa	megapascals
Pa	Pascals
yr	year

MAJOR HYDROGEOLOGICAL UNITS

(Also see Table 3.2-2 for the following and other geological units and model layers.)

CFu	Crater Flat undifferentiated hydrogeological unit
CHn	Calico Hills nonwelded hydrogeological unit
PTn	Paintbrush Tuff nonwelded hydrogeological unit
TCw	Tiva Canyon welded hydrogeological unit
TSw	Topopah Spring welded hydrogeological unit

INTENTIONALLY LEFT BLANK

GLOSSARY

DEFINITIONS:

Abstraction: The process of reducing a system or model to its salient features, i.e., the features that significantly affect the behavior of interest.

Advection: Transport of solute in a fluid due to the flow of the fluid.

Ambient: Prevailing thermodynamic conditions prior to waste emplacement.

Aperture: Width of open space between fracture walls.

Argillic: Containing clay or clay minerals.

Capillarity: The tendency of a liquid to be held in the pore space by virtue of its surface tension and adhesion to the solid surface.

Capillary barrier: Contact between a medium of stronger capillarity and a medium of weaker capillarity (or an underground opening), at which flow is obstructed due to the tendency of liquid to be retained in the medium of stronger capillarity.

Capillary pressure: The pressure difference across the interface between two immiscible fluids (e.g., gas and liquid).

Colloid: Particle, micelle and/or macromolecule of sizes ranging from 10^{-6} to 10^{-9} m.

darcy: A unit for permeability approximately equal to 10^{-12} m².

Darcy's Law: The linear relationship between the specific discharge through porous media and the pressure, or hydraulic, gradient; permeability or hydraulic conductivity is the constant of proportionality.

Diffusion: The movement of a solute in a fluid due to random molecular motion (see also matrix diffusion).

Drift: A tunnel.

Flux: Flow rate per unit area.

Flow rate: Volumetric or mass flow per unit time.

Fracture flow: Water flowing through fractures.

Fracture-matrix interaction: The flow and transport of mass and energy between fractures and the rock matrix.

Hydraulic conductivity: A measure of the ability of a porous medium to transmit fluid, expressed as a proportionality constant (units of length/time) relating specific discharge through the medium to hydraulic gradient.

Hydraulic gradient: The ratio of the change in water potential, or hydraulic head, to flow path length.

Hydrodynamic dispersion: The spreading of a solute as a result of variations in fluid flow velocity.

Lithophysae: (= Lithophysal Cavities) Cavities resulting from trapped vapor phase inclusions during cooling of magma.

Matrix diffusion: Solute transport into and through the matrix by diffusion.

Matrix flow: Water flowing through rock matrix.

Infiltration: The penetration of liquid water through the ground surface. Also used to refer to net infiltration, i.e., the amount of water that has penetrated to a depth where it can no longer be removed by evapotranspiration.

Matrix: Bulk rock mass between explicitly considered fractures.

Nonwelded tuffs: Tuffs that were not subjected to the welding process (see Welded Tuff).

Perched water: Locally water-saturated zones with positive pressure head above the water table.

Percolation: The flow of liquid water through the unsaturated zone.

Permeability: A measure of the ability of a porous medium to transmit fluid, expressed as a proportionality constant (units of length²) relating specific discharge through the medium to pressure gradient.

Porosity: The fraction of the total rock volume occupied by voids.

Pyroclastic: Pertaining to fragmented rock material formed by volcanic explosion.

Retardation: Slowing-down of solute migration relative to the travel of the fluid phase. This may arise from the solute sorption onto the solid phase, matrix diffusion, or fracture-matrix interaction.

Saturation: The fraction of the pore space occupied by a fluid (gas, liquid). Throughout this PMR, saturation that is not modified by the specific fluid phase refers to liquid saturation.

Seepage: The flow of liquid water into an underground opening such as a niche, alcove, or waste emplacement drift.

Seepage Fraction: The fraction of waste packages affected by seepage.

Seepage Threshold: The critical percolation flux below which no seepage occurs.

Sorption: Attachment of chemical components to the solid phase as a result of chemical and/or physical interactions.

Specific discharge: Flow rate per unit cross-sectional area through which flow occurs.

Tuff: Rock formed from the consolidation of pyroclastic material.

Unsaturated zone: The region above the water table and below the ground surface where the pore space is only partially filled with liquid water.

van Genuchten parameters (α and m): Parameters used in the van Genuchten equations that relate relative permeability and capillary pressure to saturation.

Vitric: Fused by heat to a glassy (non-crystalline) substance.

Water table: The surface of the water-saturated zone, where the fluid pore pressure is equal to atmospheric pressure. In this report, the water table specifically refers to the surface of the saturated zone and not of perched water bodies.

Weep: Localized feature where episodic or persistent water flow may occur.

Welded tuff: A glass-rich pyroclastic rock solidified under the combined action of heat retained by the glass particles, pressure resulting from the weight of overlying material, and hot gases. Welded tuffs have comparatively lower porosity and higher bulk density than nonwelded tuffs.

Zeolite: Secondary minerals of hydrous silicates.

INTENTIONALLY LEFT BLANK

CONTENTS

	Page
EXECUTIVE SUMMARY	ix
ACRONYMS AND ABBREVIATIONS	xiii
GLOSSARY	xix
1. INTRODUCTION.....	1
1.1 OBJECTIVES	5
1.2 PMR SCOPE AND BACKGROUND INFORMATION	6
1.2.1 Scope of UZ Flow and Transport PMR	6
1.2.2 Principal Factors and Other Factors Considered	7
1.2.3 Features, Events, and Processes (FEPs)	9
1.2.4 Summary of Current Understanding of Flow and Transport at Yucca Mountain	14
1.3 QA STATUS OF DATA AND SOFTWARE.....	20
1.3.1 Acquired and Developed Data	21
1.3.2 Software	21
1.3.2.1 TOUGH2.....	21
1.3.2.2 iTOUGH2.....	22
1.3.2.3 TOUGHREACT	22
1.3.2.4 Transport Codes	22
1.4 RELATIONSHIP TO OTHER PROCESS MODEL REPORTS AND KEY PROJECT DOCUMENTS	25
2. EVOLUTION OF THE UZ SITE CHARACTERIZATION PROGRAM – DATA COLLECTION AND MODEL DEVELOPMENT SUPPORTING THE UZ PMR	27
2.1 UZ CHARACTERIZATION PROGRAM AT YUCCA MOUNTAIN	27
2.1.1 Development and Documentation of the Site Characterization Program	28
2.1.2 Chronology of Drilling/Excavation, Testing, and Modeling	28
2.1.3 Stimulating Issues for the UZ.....	29
2.1.4 Yucca Mountain Boreholes and ESF Drifts	31
2.2 DATA COLLECTION AND <i>IN SITU</i> FIELD TESTING.....	33
2.2.1 Geological Reconnaissance and Data Collection.....	33
2.2.2 Hydrological Testing and Data Collection.....	34
2.2.2.1 Surface-Based Investigations and Hydrological Property Measurements.....	35
2.2.2.2 Underground Testing and Monitoring.....	37
2.2.3 Geochemical Data Collection.....	41
2.2.3.1 Mineral and Solubility Measurements	41
2.2.3.2 Geochemical Measurements	41
2.2.3.3 Isotopic Measurements.....	42
2.2.3.4 UZ Transport Tests.....	42
2.2.4 Thermal Testing	43

CONTENTS (Continued)

	Page
2.2.4.1 Thermal-Hydrological Modeling	43
2.2.4.2 Thermal Characterization and Pre-ESF Testing	44
2.2.4.3 Underground Thermal Tests	44
2.3 NATURAL ANALOGS AS CORROBORATIVE INFORMATION	45
2.4 EVOLUTION OF UZ AND TSPA MODELS	49
2.5 KEY ISSUES FOR UNSATURATED ZONE FLOW AND TRANSPORT	52
2.5.1 Summary of Key Issues from External Reviewers	52
2.5.1.1 Summary of the TSPA Peer Review Panel	52
2.5.1.2 Summary of the UZ Flow and Transport Model Independent Evaluation Panel	57
2.5.1.3 Summary of the Drift-Scale Seepage Peer Review	57
2.5.1.4 Summary of the Unsaturated Zone Flow Expert Elicitation	58
2.5.1.5 Summary of Nuclear Waste Technical Review Board Issues	58
2.5.1.6 Summary of Nye County Issues	59
2.5.2 Summary of Key Project Issues	59
2.5.2.1 TSPA-VA	59
2.5.2.2 Summary of PA Workshop on UZ Flow and Transport	61
2.5.2.3 Summary of the UZ Flow and Transport Model Workshop	62
3. UZ FLOW AND TRANSPORT MODEL AND ABSTRACTIONS	65
3.1 INTRODUCTION	65
3.2 GEOLOGICAL CONSIDERATIONS FOR FLOW AND TRANSPORT	67
3.2.1 Overview	67
3.2.2 Major Hydrogeological Units	69
3.2.2.1 Tiva Canyon Welded (TCw) Hydrogeological Unit	71
3.2.2.2 Paintbrush Nonwelded (PTn) Hydrogeological Unit	72
3.2.2.3 Topopah Spring Welded (TSw) Hydrogeological Unit	72
3.2.2.4 Calico Hills Nonwelded (CHn) Hydrogeological Unit	73
3.2.2.5 Crater Flat Undifferentiated (CFu) Hydrogeological Unit	74
3.2.2.6 Water Table Configuration	74
3.2.3 Structural Setting	74
3.2.4 Mineral Alteration and the Vitric-Zeolitic Boundary	75
3.2.5 Summary	77
3.3 PHYSICAL PROCESSES	79
3.3.1 Climate	79
3.3.2 Infiltration	79
3.3.3 Fracture and Matrix Flow Component	80
3.3.3.1 Flow Through the TCw Unit	80
3.3.3.2 Flow Through the PTn Unit	80
3.3.3.3 Flow Through the TSw Unit	81
3.3.3.4 Flow Below the Potential Repository	82
3.3.4 Fracture-Matrix Interaction	82
3.3.5 Effects of Major Faults	84

CONTENTS (Continued)

	Page
3.3.6 Transient Flow	85
3.3.7 Flow Focusing.....	85
3.3.8 Perched Water.....	86
3.3.9 Seepage into Drifts.....	86
3.3.10 Gas Flow Processes.....	86
3.3.11 Radionuclide Transport Processes	87
3.3.12 Effects of Coupled Processes.....	88
3.3.12.1 TH Processes.....	88
3.3.12.2 TMe Processes	89
3.3.12.3 TC Processes.....	89
3.3.13 Current and Alternative Conceptual Models	90
3.3.14 Summary and Conclusions	91
3.4 NUMERICAL MODELS AND GRIDS.....	93
3.4.1 Numerical Models for UZ Flow and Transport	93
3.4.1.1 Continuum Models	93
3.4.1.2 Discrete Fracture-Network Models.....	94
3.4.1.3 Numerical Models for UZ Flow and Transport at Yucca Mountain.....	95
3.4.1.4 Some Important Issues for Flow and Transport Modeling.....	95
3.4.2 Development of Numerical Grids.....	97
3.4.2.1 Input.....	97
3.4.2.2 Data Integration and Grid Generation.....	99
3.4.2.3 Output	101
3.4.2.4 Grid Refinement Studies.....	102
3.4.3 Summary.....	102
3.5 CLIMATE AND INFILTRATION	105
3.5.1 Future Climate Analysis	106
3.5.1.1 Introduction.....	106
3.5.1.2 Analyses and Assumptions	107
3.5.1.3 Timing of Climate Change.....	108
3.5.1.4 Nature of Future Climates.....	109
3.5.1.5 Uncertainties	112
3.5.1.6 Alternative Conceptual Models	112
3.5.1.7 Corroborative Evidence	112
3.5.1.8 Summary and Conclusions	113
3.5.2 Infiltration Model.....	114
3.5.2.1 Introduction.....	114
3.5.2.2 Analyses and Assumptions	114
3.5.2.3 Hydrological Data Collected at Yucca Mountain.....	115
3.5.2.4 Conceptual Model for Net Infiltration	116
3.5.2.5 Net Infiltration for the Three Climate Scenarios	116
3.5.2.6 Uncertainties	119
3.5.2.7 Alternative Conceptual Models	119

CONTENTS (Continued)

	Page
3.5.2.8 Corroborative Evidence	120
3.5.2.9 Model Validation	120
3.5.2.10 Summary and Conclusions	121
3.5.3 Abstraction of Climate and Infiltration	121
3.5.3.1 Climate	121
3.5.3.2 Infiltration	122
3.6 UZ PROPERTIES DEVELOPMENT	123
3.6.1 Introduction	123
3.6.2 Issues	125
3.6.3 Analysis of Hydrologic Properties Data	126
3.6.3.1 Matrix Property Data	126
3.6.3.2 Fracture Property Data	128
3.6.3.3 Fault Property Data	129
3.6.3.4 Thermal Property Data	130
3.6.4 Calibrated Properties Model	130
3.6.4.1 1-D Inversions	132
3.6.4.2 2-D Inversions	133
3.6.5 Results and Discussion	134
3.6.5.1 Results	134
3.6.5.2 Uncertainty	135
3.6.5.3 Validation	135
3.6.5.4 Alternative Conceptual Models	136
3.6.6 Summary and Conclusions	137
3.7 FLOW MODEL	139
3.7.1 Introduction	139
3.7.1.1 Objectives	139
3.7.1.2 UZ Flow Issues	140
3.7.2 Description of the Flow Model	141
3.7.3 UZ Flow Submodels	144
3.7.3.1 PTn Flow Studies	144
3.7.3.2 Effects of Major Faults	146
3.7.3.3 Investigations of Calico Hills and Perched Water Occurrence	149
3.7.4 Site-Scale Flow Analysis	153
3.7.4.1 Percolation Flux at the Potential Repository Horizon	153
3.7.4.2 Repository Percolation Flux Frequency Distribution	154
3.7.4.3 Fracture and Matrix Flow Components	155
3.7.4.4 Model Validation and Confidence Building	156
3.7.4.5 Bounds on Percolation and Uncertainties/Limitations	158
3.7.4.6 Corroborative Evidence and Natural Analog	159
3.7.4.7 Alternative Conceptual Models	160
3.7.5 UZ Flow Abstractions for TSPA-SR	160
3.7.5.1 Abstraction of Flow Fields	160

CONTENTS (Continued)

	Page
3.7.5.2 Abstraction of Water-Table Rise	161
3.7.5.3 Abstraction of Perched Water Models	161
3.7.5.4 Abstraction of Groundwater Flow Patterns	162
3.7.6 Summary and Conclusions	162
3.8 AMBIENT GEOCHEMISTRY ANALYSIS AND MODELS	165
3.8.1 Introduction	165
3.8.2 Chloride and $^{36}\text{Cl}/\text{Cl}$ Data and Analysis	166
3.8.3 Evidence for Fast Flow Paths and Transport from $^{36}\text{Cl}/\text{Cl}$ and Tritium	169
3.8.4 Calcite Simulation Results and Data	170
3.8.5 Uncertainties and Limitations	174
3.8.6 Alternative Conceptual Models	175
3.8.7 Corroborating Evidence	175
3.8.8 Analogs	176
3.8.9 Model Validation	176
3.8.10 Summary and Conclusions	177
3.9 DRIFT SEEPAGE MODELS	179
3.9.1 Introduction	179
3.9.2 Objectives and General Modeling Approach	182
3.9.3 Key Issues and Corresponding Modeling Assumptions	184
3.9.3.1 Percolation Flux and Channeling Effects	184
3.9.3.2 Episodic Flow	185
3.9.3.3 Ventilation, Evaporation, and Condensation Effects	186
3.9.3.4 Excavation Effects, Surface Roughness, and Drift Degradation	187
3.9.3.5 Capillary Barrier and Seepage Threshold	189
3.9.4 Seepage Calibration Model	190
3.9.4.1 Objectives and General Approach	190
3.9.4.2 Air-Permeability and Liquid-Release-Test Data	190
3.9.4.3 Model Assumptions	191
3.9.4.4 Model Development	192
3.9.4.5 Model Calibration	192
3.9.4.6 Model Validation	193
3.9.4.7 Seepage Threshold Prediction	194
3.9.4.8 Summary	194
3.9.5 Seepage Model for PA	195
3.9.5.1 Objectives and General Approach	195
3.9.5.2 Model Development	195
3.9.5.3 Selection of Parameter Ranges and Case Studies	195
3.9.5.4 Results	197
3.9.6 Abstraction of Seepage into Drifts	197
3.9.6.1 Introduction and Objectives	197
3.9.6.2 Initial Abstraction of Seepage Results	200
3.9.6.3 Adjustments	200

CONTENTS (Continued)

	Page
3.9.6.4 Abstraction Results	202
3.9.7 Corroborative Evidence and Analog Studies	203
3.9.7.1 Calcite Depositions in Lithophysal Cavities	203
3.9.7.2 Rainier Mesa	203
3.9.7.3 Altamira	204
3.9.7.4 Absence of Seepage into Sealed Drift Segments	204
3.9.8 Alternative Conceptual Models	204
3.9.8.1 Discrete Fracture Network Model	204
3.9.8.2 Seepage Governed by Ponding Probability	205
3.9.9 Summary and Conclusions	205
3.10 DRIFT-SCALE THERMAL-HYDROLOGICAL-CHEMICAL PROCESSES AND MODELS	207
3.10.1 Introduction	207
3.10.2 Thermal-Hydrological-Chemical Conceptual Model	207
3.10.2.1 TH Processes	207
3.10.2.2 Effects of TH Processes (Boiling, Condensation, and Drainage) on Water and Gas Chemistry and Mineral Evolution	208
3.10.2.3 Effects of Infiltration and Climate Changes on THC Processes	209
3.10.2.4 Hydrologic Property Changes in Fractures and Matrix	209
3.10.3 Modeling Approach, Assumptions, Inputs and Outputs	210
3.10.3.1 Dual-Permeability Model For Reaction-Transport Processes	210
3.10.3.2 Active Fracture Model For Reaction-Transport Processes	211
3.10.3.3 Equilibrium and Kinetic Models for Mineral–Water–Gas Reactions	211
3.10.3.4 Initial and Infiltrating Water and Gas Chemistry and Mineralogy	211
3.10.3.5 Relations for Mineral Reactive Surface Areas	213
3.10.3.6 Relations for Hydrological Property Changes	214
3.10.3.7 Basis for Numerical Code TOUGHREACT V2.2	214
3.10.4 DST THC Model Results and Validation	215
3.10.4.1 Gas-Phase CO ₂ Evolution	215
3.10.4.2 Water Chemistry Evolution	216
3.10.4.3 Mineralogical Changes	216
3.10.5 THC Seepage Model	217
3.10.5.1 THC Seepage Model Description	217
3.10.5.2 TH Effects	217
3.10.5.3 Gas-Phase CO ₂ Evolution	217
3.10.5.4 Water Chemistry Evolution	218
3.10.5.5 Porosity and Permeability Changes and Assessment of Precipitation Cap Formation	219
3.10.6 Uncertainties and Limitations	219

CONTENTS (Continued)

	Page
3.10.7 Alternative Conceptual Models	220
3.10.8 Corroborative Evidence	220
3.10.9 Analogs	221
3.10.10 Model Validation	223
3.10.11 Abstraction of Drift-Scale THC Modeling for TSPA-SR.....	223
3.10.12 Summary and Conclusions	227
3.11 UZ TRANSPORT MODEL.....	229
3.11.1 Introduction.....	229
3.11.1.1 Issues.....	229
3.11.1.2 Approach.....	230
3.11.1.3 Assumptions.....	230
3.11.2 Physical Processes	231
3.11.2.1 Flow Processes.....	231
3.11.2.2 Advection.....	231
3.11.2.3 Hydrodynamic Dispersion	231
3.11.2.4 Sorption.....	232
3.11.2.5 Matrix Diffusion	232
3.11.2.6 Radioactive Decay and Daughter Products.....	233
3.11.2.7 Colloidal Transport	233
3.11.3 Transport Properties.....	234
3.11.3.1 Dispersion	234
3.11.3.2 Sorption Coefficients	235
3.11.3.3 Matrix Diffusion Coefficients.....	237
3.11.3.4 Fracture Aperture and Spacing	237
3.11.3.5 Parameters for Colloid-Facilitated Radionuclide Transport.....	238
3.11.4 Geological Layers below the Potential Repository.....	238
3.11.5 2-D Radionuclide Transport Simulations	239
3.11.5.1 2-D Semi-Analytical Code FRACL.....	240
3.11.5.2 Simulation Approach	240
3.11.5.3 Transport in the Individual Hydrogeologic Unit	240
3.11.5.4 Transport Simulations below the Potential Repository	241
3.11.6 3-D Site-Scale Radionuclide Transport	241
3.11.6.1 EOS9nT Code	242
3.11.6.2 Transport Simulation of ⁹⁹ Tc	242
3.11.6.3 Transport Simulations of ²³⁷ Np and its Daughters.....	242
3.11.6.4 Transport Simulations of ²³⁹ Pu and its Daughters	243
3.11.6.5 Transport-Controlling Features.....	244
3.11.7 3-D Site-Scale Transport of Pu True Colloids.....	244
3.11.7.1 Colloidal Forms, Properties, and Filtration Model	245
3.11.7.2 Colloid Transport Simulations.....	245
3.11.8 Estimates of Mass Breakthrough	245
3.11.9 Alternative Models.....	247
3.11.9.1 Effects of Matrix Diffusion on Radionuclide Transport.....	247

CONTENTS (Continued)

	Page
3.11.9.2 Colloidal Transport Simulation	247
3.11.10 Uncertainty and Limitations	248
3.11.10.1 Assumptions.....	248
3.11.10.2 Sorption.....	248
3.11.10.3 Matrix Diffusion	249
3.11.10.4 Radioactive Decay and Daughter Products.....	249
3.11.10.5 Radionuclide Transport Simulations.....	250
3.11.10.6 Colloidal Transport	250
3.11.11 Model Validation	250
3.11.11.1 Alcove Tracer Test.....	250
3.11.11.2 Busted Butte Tracer Test	251
3.11.12 Analogs to Radionuclide Transport in the UZ	252
3.11.12.1 Natural Analog Studies at Peña Blanca, Mexico	253
3.11.12.2 Uranium Deposits in Northwestern Nevada/Southeastern Oregon.....	253
3.11.12.3 Akrotiri Archeological Site, Santorini, Greece.....	253
3.11.13 Abstraction of Transport Model.....	254
3.11.13.1 Introduction.....	254
3.11.13.2 Assumptions.....	254
3.11.13.3 Approach.....	255
3.11.13.4 Results.....	256
3.11.14 Summary and Conclusions	258
3.12 MOUNTAIN-SCALE TH MODEL	261
3.12.1 Introduction.....	261
3.12.2 Modeling Approach	262
3.12.2.1 Conceptual Model.....	263
3.12.2.2 Numerical Grids.....	263
3.12.2.3 Potential Repository Thermal Load	264
3.12.2.4 Boundary and Initial Conditions	265
3.12.2.5 Input Data and Parameters	265
3.12.3 Results of TH Simulations.....	266
3.12.3.1 Temperature	267
3.12.3.2 Saturation	269
3.12.3.3 Water Flux	270
3.12.4 Model Validation	272
3.12.5 Summary and Conclusions	273
3.13 OVERVIEW OF UNCERTAINTIES IN UZ FLOW AND TRANSPORT MODELS	277
4. RELATIONSHIP TO NRC ISSUE RESOLUTION STATUS REPORTS	281
4.1 SUMMARY OF THE KEY TECHNICAL ISSUES.....	281
4.2 RELATIONSHIP OF THE UZ FLOW AND TRANSPORT PMR TO THE KTIS.....	282

CONTENTS (Continued)

	Page
4.2.1 Evolution of the Near-Field Environment	282
4.2.1.1 Effects of Coupled THC Processes on Seepage and Flow	282
4.2.1.2 Effects of Coupled THC Processes on Radionuclide Transport	284
4.2.2 Radionuclide Transport	284
4.2.2.1 Radionuclide Transport through Porous Rock	284
4.2.2.2 Radionuclide Transport through Fractured Rock	285
4.2.3 Structural Deformation and Seismicity	286
4.2.3.1 Fracturing and Structural Framework of the Geologic Setting	286
4.2.4 Thermal Effects on Flow (TEF)	286
4.2.4.1 Is DOE's Thermal Modeling Approach Sufficient to Predict the Nature and Bounds of TEF in the Near Field?	287
4.2.4.2 Does DOE's TSPA Adequately Account for TEF?	287
4.2.5 TSPA and Integration	288
4.2.5.1 System Description and Demonstration of Multiple Barriers	288
4.2.5.2 Scenario Analysis	288
4.2.5.3 Model Abstraction	289
4.2.6 UZ and SZ Flow under Isothermal Conditions	289
4.2.6.1 Future Climates and Hydrological Effects on Climate Change: What Is the Likely Range of Future Climates at Yucca Mountain and What Are the Likely Hydrological Effects of Climate Change?	290
4.2.6.2 Present-Day Shallow Infiltration: What Is the Estimated Amount and Spatial Distribution of Present-Day Shallow Infiltration?	290
4.2.6.3 Deep Percolation: What Is the Estimated Amount and Spatial Distribution of Percolation through the Proposed Repository Horizon (Present Day and through the Period of Repository Performance)?	290
4.2.6.4 Matrix Diffusion: To what Degree Does Matrix Diffusion Occur in the UZ and SZ?	291
4.3 NRC ACCEPTANCE CRITERIA	291
5. SUMMARY AND CONCLUSIONS	317
5.1 SUMMARY OF THE UZ FLOW AND TRANSPORT PMR	317
5.2 SUMMARY OF MODELS AND ABSTRACTIONS FOR TSPA-SR	320
5.2.1 UZ Flow	321
5.2.2 Drift Seepage	322
5.2.3 Drift-Scale THC	323
5.2.4 UZ Transport	324
5.2.5 Treatment of Uncertainties	325

CONTENTS (Continued)

	Page
6. REFERENCES AND INPUTS.....	327
6.1 CITED DOCUMENTS.....	327
6.2 CODES, STANDARDS, REGULATIONS, AND PROCEDURES.....	354
6.3 SOURCE DATA, LISTED BY DATA TRACKING NUMBER.....	355
6.3.1 Data Tracking Numbers Listed for Tables and Figures in Attachment II.....	355
7. ATTACHMENTS.....	361
ATTACHMENT I – UZ DATA AND ASSOCIATED DATA TRACKING NUMBERS (DTNS)	
ATTACHMENT II – LIST OF DTNS FOR FIGURES AND TABLES	
ATTACHMENT III – FIGURES	

FIGURES

(All figures are included in Attachment III)

	Page
1-1. Schematic Diagram Showing the Relationships among Major YMP Documents, Including Analysis/Model Reports (AMRs), PMRs, SDs, SRR, and TSPA Documents	III-2
1-2. Main Models Included in the UZ PMR, Their Interrelations, and Their Connections to TSPA.....	III-3
2.1-1. Chronology of Drilling/Excavation, Testing, and Modeling Activities of the UZ Site Characterization Program at Yucca Mountain.....	III-4
2.1-2. Schematic Illustration of the Main Surface-Based Deep Boreholes and Underground Drifts of the ESF, and the Major Faults in the Vicinity of Yucca Mountain.....	III-5
2.1-3. Schematic Illustration of Alcove and Niche Locations in the Exploratory Studies Facility at Yucca Mountain.....	III-6
2.1-4. Schematic Illustration of the ECRB Cross Drift, Geological Units and Test Sites. (a) Generalized geological map at the Cross Drift level. (b) Generalized geological cross-section along the ECRB Cross Drift, showing the potential repository horizon.	III-7
2.2-1. Geological and Geophysical Studies on the Surface and along the ESF	III-8
2.2-2. Infiltration Study on the Bedrock and in Washes (USGS 2000, U0010, Sections 6.3 and 7.1)	III-9
2.2-3. Drift Seepage Test at Niche 3650 (CRWMS M&O 2000, U0015, Section 6.2.) ..	III-10
2.2-4. Damp Feature Observed during Dry Excavation of Niche 3566 and Bomb-Pulse ³⁶ Cl/Cl Signals along the ESF (Wang et al. 1999, pp. 331–332; CRWMS M&O 2000, U0085, Section 6.6)	III-11
2.2-5. Lower Lithophysal Seepage Test at ECRB Cross Drift Niche 1620	III-12
2.2-6. Fracture-Matrix Interaction Test at Alcove 6 (CRWMS M&O 2000, U0015, Section 6.6)	III-13
2.2-7. Paintbrush Fault and Porous Matrix Test at Alcove 4 (CRWMS M&O 2000, U0015, Section 6.7)	III-14
2.2-8. El Niño Infiltration and Seepage Test at Alcove 1	III-15
2.2-9. Cross-Drift Test between ECRB Cross Drift Alcove 8 and ESF Main Drift Niche 3107 (CRWMS M&O 2000, U0015, Section 6.9).....	III-16

FIGURES (Continued)

	Page
2.2-10. Geochemical Studies of Tuff Samples (CRWMS M&O 2000, U0050, Section 6.5; Sonnenthal and Bodvarsson 1999, p. 146).....	III-17
2.2-11. Isotopic Studies of Tuff Samples (CRWMS M&O 2000, U0085, Section 6.6)....	III-18
2.2-12. UZ Transport Test at Busted Butte (CRWMS M&O 2000, U0100, Section 6.8) .	III-19
2.2-13. Single Heater Test at Alcove 5 (Tsang and Birkholzer 1999, pp. 411–415).....	III-20
2.2-14. Drift Scale Test at Alcove 5 (CWRMS M&O 2000, U0110/N0120, Section 6.2)	III-21
2.4-1. One-Dimensional Column Simulations with the UZ-1986, the TSPA-1991, and the TSPA-1993 Models (Rulon et al. 1986, Barnard et al. 1992, and Wilson et al. 1994)	III-22
2.4-2. The Mesh and Approximations Used in the UZ-1995 Model (Wittwer et al. 1995, pp. 46–47)	III-23
2.4-3. Simulations of ²³⁷ Np Transport by the UZ Transport-1995 Model (Robinson et al. 1995, p. 61, p. 125)	III-24
2.4-4. The Mesh and the Approximations Used in the UZ-1997 Model for TSPA-VA (adapted from Wu et al. 1999b, pp. 190–193)	III-25
3.2-1. Yucca Mountain Site-Scale Geology: (a) in 3-D Perspective and (b) along an East-West Cross Section (adapted from GFM3.1 data, CRWMS M&O 2000, I0035) .	III-26
3.2-2. Lithostratigraphic Transitions at the Upper and Lower Margins of the PTn Hydrogeological Unit. (a) Photos and schematic at the TCw-PTn interface, where tuffs grade downward from densely welded to nonwelded, accompanied by an increase in matrix porosity and a decrease in fracture frequency. (b) Photo and schematic at the PTn-TSw interface, where tuffs grade downward from nonwelded to densely welded, accompanied by a decrease in matrix porosity and an increase in fracture frequency.	III-27
3.2-3. Thickness Contour Plots of the (a) PTn, (b) TSw, (c) CHn, and (d) CFu Hydrogeological Units (Adapted from DTN: MO9901MWDGFM31.000). Contours are in meters.	III-28

FIGURES (Continued)

	Page
3.2-4. Lithophysal Transitions within the TSw Unit. (a) Photo and schematic of the contact between the upper nonlithophysal (Ttpul) and the middle nonlithophysal (Ttpmn) zones showing a downward decrease in lithophysal volume. (b) Photo and schematic of the contact between the middle nonlithophysal (Ttpmn) and lower lithophysal (Ttpll) zones showing a downward increase in lithophysal volume. Fractures in the nonlithophysal unit are generally smoother, more planar, and more continuous than fractures in the lithophysal units.	III-29
3.2-5. Lithostratigraphic Transitions at the TSw-CHn Interface. (a) Schematic with prevalent alteration at the TSw-CHn contact. (b) Schematic with variable alteration at the TSw-CHn contact. (c) Schematic with minimal alteration at the TSw-CHn contact. (d) Schematic representation of a fault zone as a well-connected fracture network that may represent a fast flow pathway. (e) Schematic representation of a fault zone showing alteration within the fracture network that creates a flow barrier.	III-30
3.2-6. Occurrence of Lithostratigraphic Units at the Water Table (730 meters above sea level) (Adapted from DTN: MO9901MWDGFM31.000).....	III-31
3.2-7. Distribution of Zeolites in Certain Layers below the Potential Repository Horizon. (CRWMS M&O 2000, I0045, Section 6.3.2; DTN: MO9910MWDISMMM.003). Areas with less than or equal to 3% zeolite are considered vitric, or unaltered.	III-32
3.3-1. Schematic Showing Temporal and Spatial Variabilities of Net Infiltration Rates Resulting From the Nature of the Storm Events and Variation in Soil Cover and Topography. The size of the arrow indicates the relative magnitude of infiltration rates.	III-33
3.3-2. Schematic Showing Overall Water Flow Behavior in the UZ Including the Relative Importance of Fracture and Matrix Flow Components in the Different Hydrogeologic Units. The blue and red colors on the land surface correspond to high and low infiltration rates, respectively, while the other colors correspond to intermediate infiltration rates (CRWMS M&O 2000, U0030, Figure 1).	III-34
3.3-3. Schematic Showing Water Flow Behavior within the PTn Characterized by Dominant Matrix Flow and a Few Fast Flow Paths	III-35
3.3-4. Water Flow in Fractures Characterized by Fingering Flow at Different Scales....	III-36
3.3-5. Major Faults Can Act as Fast-Flow Conduits or Capillary Barriers. The size of the arrows in (a) and (b) indicates the relative magnitude of flow.	III-37

FIGURES (Continued)

	Page
3.3-6. Schematic Showing Flow Patterns within and near a Perched Water Body Characterized by Strong Lateral Flow within the Perched Water Body and the Associated Fault-Dominated Flow	III-38
3.3-7. Important Radionuclide Transport Processes. (Note that the radionuclides also undergo radioactive decay, but this is not shown in the schematic.)	III-39
3.3-8. TH Processes at Mountain and Drift Scales	III-40
3.4-1. Schematic Demonstrating (a) ECM, (b) Dual-Porosity with One Matrix Gridblock, (c) Dual-Permeability with One Matrix Gridblock per Fracture Gridblock, and (d) MINC with Three Matrix Gridblocks per Fracture Gridblock	III-41
3.4-2. Flow Diagram Showing Key Input Data Used in Numerical Grid Development, the Types of Grids Generated, and their End Users	III-42
3.4-3. Distribution of Percent Zeolite Mineral Abundance in the Calico Hills Formation (lithostratigraphic unit Tac): (a) MM2.0, (b) MM3.0. (DTNs: MO9901MWDISMMM.000, MO9910MWDISMMM.003, respectively). Areas with less than or equal to 3% zeolite by weight are considered vitric, or unaltered.	III-43
3.4-4. Distribution of Matrix Permeability (m^2) in Select Layers of the CHn Hydrogeologic Unit: (a) RPM3.0, (b) RPM3.1. (DTNs: MO9901MWDISMRP.000, MO9910MWDISMRP.002, respectively). In order to maintain consistent parameters within the UZ Flow and Transport Model PMR, saturated hydraulic conductivity (K_{sat} , m/s) from the RPM was converted to permeability (m^2) by multiplying K_{sat} values by 10^{-7}	III-44
3.4-5. Extent of Vitric Region (Indicated by Pattern of Diagonal Lines) in Model Layers (a) ch1, (b) ch2, (c) ch3, (d) ch4, and (e) ch5. White areas indicate prevalent zeolitization (from CRWMS M&O 2000, U0000, Figure 5).	III-45
3.4-6. Plan-View (a) Schematic Showing the UZ Model Boundary, the Repository Outline, Major Fault Locations Adapted from GFM3.1, Select Boreholes, the ESF, and the ECRB, (b) Numerical Grid Design for the Mountain-Scale Model Used for UZ Calibration (adapted from Figure V-1 of CRWMS M&O 2000, U0000), and (c) Numerical Grid Design for the Mountain-Scale Model Used for PA Calculations (Adapted from CRWMS M&O 2000, U0000, Figure VI-1).	III-46
3.4-7. East-West Cross-Section through Borehole UZ-14: (a) Adapted from Data Contained in CRWMS M&O (2000, I0035) (b) from the 3-D UZ Model Numerical Grid for PA (Adapted from CRWMS M&O 1999a, Figure VI-2). The 3-D UZ Model Grid in plan view (c) shows the location of the cross section. Bottom elevation along cross sections is 730 m above mean sea level.	III-47

FIGURES (Continued)

	Page
3.4-8. East-West Cross-Section through Boreholes SD-6, SD-12, UZ#16: (a) Adapted from Data Contained in CRWMS M&O (2000, I0035) (b) from the 3-D UZ Model Numerical Grid for PA (Adapted from CRWMS M&O 1999a, Figure VI-3). The 3-D UZ Model Grid in plan view (c) shows the location of the cross section. Bottom elevation along cross sections is 730 m above mean sea level.	III-48
3.4-9. North-South Cross-Section through Boreholes UZ-14, H-5, and SD-6: (a) Adapted from Data Contained in CRWMS M&O (2000, I0035) (b) from the 3-D UZ Model Calibration Grid (Adapted from CRWMS M&O 1999a, Figure V-4). The 3-D UZ Model Calibration Grid in plan view (c) shows the location of the cross sections. Bottom elevation along cross sections is 730 m above mean sea level.	III-49
3.5-1. Summary of Issues, Modeling Methodology, Data, and Results for both the Climate and Infiltration Models	III-50
3.5-2. (a) Generalized View of Present-Day Atmospheric Circulation (USGS 2000, U0005, Figure 2) and (b) Daily Precipitation Record Between 1980 and 1995 at Yucca Mountain (USGS 2000, U0010, Figure 6-18) with (c) an Areal View of the Arid Conditions at the Yucca Mountain Site	III-51
3.5-3. (a) Field-Scale Water Balance and Processes Controlling Net Infiltration (USGS 2000, U0010, Figure 5-1) and (b) Major Components of the Net Infiltration Modeling Process (USGS 2000, U0010, Figure 6-1).....	III-52
3.5-4. (a) Precipitation (USGS 2000, U0010, Figure 7-1), (b) Surface Run-On (USGS 2000, U0010, Figure 7-3) and (c) Net-Infiltration Rates (USGS 2000, U0010, Figure 7-4) for the Mean Modern Climate Scenario.....	III-53
3.5-5. Net-Infiltration Rates for (a) Mean Monsoon (USGS 2000, U0010, Figure 7-7) and (b) Mean Glacial-Transition (USGS 2000, U0010, Figure 7-14) Climates.....	III-54
3.5-6. Histogram of Log of Potential Repository-Average Infiltration for Glacial-Transition Climate (adapted from CRWMS M&O 2000, U0095, Figure 6-2).....	III-55
3.6-1. Relationship of the Analysis of Hydrologic Properties Data and the Calibrated Properties Model to Input Data and Models and to Analyses and Models that use the Developed UZ Properties.....	III-56
3.6-2. Issues for Development of UZ Properties.....	III-57
3.6-3. Calibrated Property Development.....	III-58

FIGURES (Continued)

	Page
3.6-4. Calibrated 1-D Simulation Match to Saturation, Water Potential, and Pneumatic Data. Data from Borehole USW SD-12 for the Base Case Infiltration Scenario (adapted from CRWMS M&O 2000, U0035, Figures 2, 3, and 4)	III-59
3.6-5. Calibrated 2-D Simulation Match to Saturation, Water Potential, and Pneumatic Data from Borehole USW UZ-7a Base Case Infiltration Scenario (adapted from CRWMS M&O 2000, U0035, Figures 9, 10, and 11)	III-60
3.6-6. Initial Estimate of and Calibrated Fracture and Matrix Permeability for the Base Case, Present-Day Infiltration Scenario (adapted from data in CRWMS M&O 2000, U0035, Table 13). The calibrated values for the vitric ch1 through ch5 layers are shown in a lighter color than the zeolitic. The prior information (initial estimate) is shown as a red line (green for the vitric ch1 through ch5).	III-61
3.6-7. Initial Estimate of and Calibrated Fracture and Matrix van Genuchten α Parameter for the Base Case, Present-Day Infiltration Scenario (adapted from data in CRWMS M&O 2000, U0035, Table 13). The calibrated values for the vitric ch1 through ch5 layers are shown in a lighter color than the zeolitic. The prior information (initial estimate) is shown as a red line (green for the vitric ch1 through ch5).	III-62
3.6-8. Comparison of Predictions from the 3-D Model with <i>In Situ</i> Water Potential Data from the ECRB Cross Drift and Pneumatic Pressure Data from Borehole USW SD-12 (adapted from CRWMS M&O 2000, U0050, Figures 6-69 and 6-70)	III-63
3.6-9. Important Results of Analysis of Hydrologic Properties Data and Calibrated Properties Model	III-64
3.7-1. Diagram Showing the Important UZ Flow and Transport Issues, Addressed by the Flow Model and Its Submodels	III-65
3.7-2. Perspective View of the UZ Model Domain of Yucca Mountain, Showing the Hydrogeological Units and Layers and Major Faults: (a) Geological Model and (b) Numerical Grid	III-66
3.7-3. Plan View of the 3-D UZ TSPA Model Grid, Showing the Model Domain at Yucca Mountain, Faults Incorporated and Borehole Locations (Adapted from CRWMS M&O, 2000, U0000, Figure VI-1)	III-67
3.7-4. Three Base-Case Maps of Mean Surface Infiltration over the Flow Model Domain for (a) Present-Day Climate, (b) Monsoon Climate, (c) Glacial-Transition Climate (Adapted from CRWMS M&O, 2000, U0050, Figures 6-3, 6-4 and 6-5)	III-68
3.7-5. Schematic of the Major Input Data to, and Output Models from, the UZ Flow Model	III-69

FIGURES (Continued)

	Page
3.7-6. Geological Profiles in Cross Sections Crossing the Model Domain, (a) North-South Transect at Yucca Mountain, Showing Thickness of the Hydrogeologic Units (b) East-West Transect at Yucca Mountain, Showing Incorporated Faults and Displacements as well as Hydrogeologic Units.....	III-70
3.7-7. Simulated Vertical Percolation Fluxes at the PTn-TSw Interface with the Present-Day, Mean Infiltration Map (Data from CRWMS M&O, 2000, U0050, Section 6.6.3)	III-71
3.7-8. Effects of Faults on UZ Flow for the Present-Day, Mean Infiltration Rate; (a) Simulated Vertical Percolation Fluxes at the Water Table, (b) Simulated Groundwater Flow paths along the West-East Cross Section within Fracture-Fracture Flow Fields (Data from CRWMS M&O, 2000, U0050, Section 6.6.3)	III-72
3.7-9. Simulated 3-D View of Perched Water Bodies along the Base of the TSw, Using the Simulation Results of Conceptual Model #1 with Present-Day, Mean Infiltration Rate (the blue contours denote the domain with 100% water saturation and the green for the areas with less than 100% water saturation) (CRWMS M&O, 2000, U0050, Figure 6.9).....	III-73
3.7-10. Comparison between Percolation Flux (mm/yr) Contours Simulated: (a) at the Potential Repository Horizon; (b) at the Water Table with Conceptual Model #1; and (c) at the Water Table with Conceptual Model #2, under the Present-Day, Mean Infiltration Rate (Data from CRWMS M&O, 2000, U0050, Section 6.6.3).....	III-74
3.7-11. Simulated Percolation Fluxes at the Potential repository Under Three Mean Infiltration Rates: (a) Present-Day; (b) Monsoon; and (c) Glacial-Transition (Data from CRWMS M&O, 2000, U0050, Section 6.6.3)	III-75
3.7-12. Areal Frequency and Distribution of Simulated Percolation Fluxes within the Potential Repository Horizon Under Three Mean Infiltration Rates: (a) Present Day; (b) Monsoon; and (c) Glacial Transition (Data from CRWMS M&O, 2000, U0050, Section 6.6.3)	III-76
3.7-13. (a) Matrix Flow (mm/yr) and (b) Fracture Flow at Potential Repository Horizon, Simulated Using the Present-Day, Mean Infiltration Rate. Data from CRWMS M&O, 2000, U0050, Section 6.6.3.....	III-77
3.7-14. Comparison to the Simulated and Observed Matrix Liquid Saturations and Perched Water Elevations for Borehole UZ-14, Using the Simulation Results for the Mean Infiltration Rates of the Three Climates Scenarios (Data from CRWMS M&O, 2000, U0050, Section 6.6.3, Figure 6-41).....	III-78

FIGURES (Continued)

	Page
3.7-15. Comparison of 3-D Pneumatic Prediction to Data from Borehole UZ-7a (CRWMS M&O 2000, U0050, Figure 6-70).....	III-79
3.7-16. Locations of Particle Breakthrough at the Water Table for the Mean Infiltration, Glacial-Transition Climate Using Two Perched Water Models (CRWMS M&O 2000, U0160, Figure 3).....	III-80
3.7-17. Comparison of Cumulative Normalized Breakthrough Curves at the Water Table Using Perched Water Model #1 and #2 with a Non-Sorbing Tracer (Tc) for Mean-Infiltration, Glacial-Transition Climate (CRWMS M&O 2000, U0160, Figure 8).....	III-81
3.7-18. Effect of Infiltration (lower, mean, and upper) on Cumulative Normalized Breakthrough Curves at the Water Table for a NonSorbing Tracer (Tc) Using FEHM V2.0 (STN: 10031-2.00-00) with Present-Day Climate (CRWMS M&O 2000, U0160, Figure 12).....	III-82
3.7-19. Summary of the UZ Flow Model Results and Issues to be Resolved.....	III-83
3.8-1. Conceptual Model of Yucca Mountain Showing Major Processes Affecting Cl and ³⁶ Cl/Cl Distributions and Important Issues for Performance.....	III-84
3.8-2. Model Diagram Showing Inputs and Outputs for Ambient Geochemistry Model. Icons are described in the text.....	III-85
3.8-3. Infiltration Rates (USGS 2000, U0010) Plotted on UZ 3-D Calibration Grid. Simulated (using base-case infiltration rates), calibrated, and measured Cl concentrations in the ESF and the ECRB (Adapted from CRWMS M&O 2000, U0050, Figure 6-18).....	III-86
3.8-4. Percolation Flux Map for 3-D Calibration Grid (Adapted from CRWMS M&O 2000, U0050, Figure 6-24).....	III-87
3.8-5. Analytical Results of ³⁶ Cl/Cl Along ESF (Using Calibrated Infiltration) for Transient Changes in Initial Ratios, Compared to Measured Ratios (CRWMS M&O 2000, U0050, Figure 6-31).....	III-88
3.8-6. Simulated Calcite Abundance (Lines) with Infiltration Rate After 10 Million Years in the WT-24 Column Together with Measured Calcite Mass Abundances (Diamond Symbols) (Data from CRWMS M&O 2000, U0085, Section 6.10, Figure 53; CRWMS M&O 2000, U0050, Figure 6-36).....	III-89

FIGURES (Continued)

	Page
3.8-7. Prediction of Cl Concentrations in Pore Waters Made Prior to Excavation of the ECRB Compared to Data Collected Subsequently (Adapted from Sonnenthal and Bodvarsson (1999, Figure 14) and CRWMS M&O 2000, U0050, Figure 6-23)	III-90
3.8-8. Conceptual Model of UZ Flow and Transport at Yucca Mountain, Showing Results Gained from Analysis of Geochemical Data and Modeling	III-91
3.9-1. Schematic of Phenomena and Processes Affecting Drift Seepage. Numerals refer to list items in text	III-92
3.9-2. Schematic Showing Data Flow and Series of Models Supporting Evaluation of Drift Seepage	III-93
3.9-3. Seepage Issues	III-94
3.9-4. Schematic Showing General Approach for the Development of the Seepage Calibration Model (Adapted from CRWMS M&O 2000, U0080, Section 6).....	III-95
3.9-5. Schematic Showing Location and Layout of Niche 3650 as well as Log-Permeability Field of the Three-Dimensional Seepage Calibration Model (Adapted from CRWMS M&O 2000, U0080, Figures 12, 13, and 18)	III-96
3.9-6. Comparison between the Measured Seepage Mass (Circles) and That Calculated with Two- and Three-Dimensional, Homogeneous and Heterogeneous Models (Squares). The four models are visualized on the left. The uncertainty of the model predictions is shown as error bars on the 95% confidence level. The three-dimensional heterogeneous Seepage Calibration Model matches the data best (Adapted from CRWMS M&O 2000, U0080, Figure 19).	III-97
3.9-7. Schematic Showing Relationships between Seepage-Relevant Factors. The red solid lines schematically indicate the expected behavior; uncertainty is schematically shown as blue dashed lines; the green dotted line shows the conservative assumption that no capillary-barrier effect exists.	III-98
3.9-8. Schematic Showing Percolation-Flux and Seepage-Threshold Distributions, Which Determine the Seepage-Fraction Probability	III-99
3.9-9. Schematic Illustrating Monte Carlo Sampling Approach for Seepage TSPA Calculations.....	III-100
3.9-10. Effect of Flow Focusing on Seepage Fraction (CRWMS M&O 2000, U0120, Figure 5).....	III-101

FIGURES (Continued)

	Page
3.9-11. Effect of Flow Focusing on Mean Seep Flow Rate (CRWMS M&O 2000, U0120, Figure 6).....	III-102
3.9-12. Summary of Results.....	III-103
3.10-1. Schematic Diagram of THC Processes Around a Heated Drift.....	III-104
3.10-2. Schematic Diagram Showing Relation Between TH Processes and Geochemical Processes.....	III-105
3.10-3. Model Diagram Relating Inputs and Outputs for the THC Seepage Model and Drift Scale Test THC Model.....	III-106
3.10-4. Simulated CO ₂ Volume Fractions in Fractures and Matrix After 6 (a&b) and 20 (c&d) Months of Heating During the Drift Scale Test (adapted from CRWMS M&O 2000, N0120/U0110, Figures 5 and 6). Temperature contours are superimposed. "OD" refers to the Observation Drift.	III-107
3.10-5. Simulated CO ₂ Volume Fractions at Grid Nodes near Borehole (BH) Intervals Where Gas-Phase CO ₂ Measurements were Made (CRWMS M&O 2000, N0120/U0110, Figure 10). Filled circles are measured CO ₂ concentrations in the gas phase. Modeled data come from locations in 2-D grid close to center of borehole interval.....	III-108
3.10-6. THC Seepage Model Mesh Showing Hydrogeologic Units in Proximity of the Drift: Topopah Spring Tuff Upper Lithophysal (tsw33), Middle Nonlithophysal (tsw34), and Lower Lithophysal (tsw35) Units, and Blowup Showing Discretization of In-Drift Design Components (adapted from CRWMS M&O 2000, N0120/U0110, Figures 18 and 19)	III-109
3.10-7. Contour Plot of Modeled Liquid Saturations and Temperatures (Labeled Contour Lines) in the Matrix at 600 Years (Near Maximum Dryout) for Three Climate Change Scenarios: (a) Lower Bound, (b) Mean, and (c) Upper Bound (Calcite-Silica-Gypsum System) (CRWMS M&O 2000, N0120/U0110, Figure 26).....	III-110
3.10-8. Time Profiles of Modeled CO ₂ Concentrations in the Gas Phase in Fractures at Three Drift Wall Locations for Different Climate Change Scenarios (Calcite-Silica-Gypsum System) (CRWMS M&O 2000, N0120/U0110, Figure 29).....	III-111
3.10-9. Time Profiles of Modeled Total Aqueous Chloride Concentrations in Fracture Water at Three Drift Wall Locations for Different Climate Change Scenarios (Case 2). The dryout period is left blank. Numbers by each curve indicate the last output liquid saturation before dryout and the first output liquid saturation during rewetting (CRWMS M&O 2000, N0120/U0110, Figure 38).	III-112

FIGURES (Continued)

	Page
3.10-10. Time Profiles of the Modeled pH of Fracture Water at Drift Wall Locations for Different Climate Change Scenarios (Case 2 Calcite-Silica-Gypsum System). The dryout period is left blank. The last output liquid saturation before dryout and the first output liquid saturation during rewetting are noted on each curve (CRWMS M&O 2000, N0120/U0110, Figure 31).	III-113
3.10-11. Time Profiles of Modeled Total Aqueous Carbonate Concentrations (as HCO_3^-) in Fracture Water at Drift Wall Locations for Different Climate Scenarios (Calcite-Silica-Gypsum System) (CRWMS M&O 2000, N0120/U0110, Figure 33).....	III-114
3.10-12. Contour Plot of Calculated Total Fracture Porosity Change at 10,000 Years for Three Climate Change Scenarios (Calcite-Silica-Gypsum System): (a) Lower Bound, (b) Mean, and (c) Upper Bound. Red areas indicate the maximum decrease in porosity as a result of mineral precipitation (CRWMS M&O 2000, N0120/U0110, Figure 42).	III-115
3.10-13. Conceptual Model of TH Processes Around a Heated Drift and Summaries of Important Results of Drift-Scale THC Simulations and Analyses	III-116
3.11-1. Key Issues Related to Potential Radionuclide Transport in the UZ	III-117
3.11-2. Relationships of Other Models and Data Feeds to the Transport Model.....	III-118
3.11-3. Schematic Illustration of Flow and Transport in the UZ Model Layers below the Potential Repository (Boreholes SD-6 and UZ-14).....	III-119
3.11-4. Concentration Profiles of ^{237}Np in 2-D Cross Sections of SD-6 and UZ-14 (Adapted from CRWMS M&O 2000, U0060, Figures V.2 and V.8).....	III-120
3.11-5. Concentration Profiles of ^{99}Tc , ^{237}Np , ^{239}Pu and its Daughters at the Water Table for Varying Present-day Climatic Scenarios (Adapted from CRWMS M&O 2000, U0060, Figures 6.12.1, 6.13.1, 6.14.1, and 6.14.2).....	III-121
3.11-6. Normalized Mass Fraction Distribution of ^{99}Tc in the Fractures at the Bottom of the TSw and the Water Table (Adapted from CRWMS M&O 2000, U0060, Figures 6.12.2, 6.12.4, 6.12.12, and 6.12.14)	III-122
3.11-7. Influence of Colloid Size and Kinetic Model Parameters on Colloidal Transport (Adapted from CRWMS M&O 2000, U0060, Figures 6.16.1 and 6.16.2)	III-123
3.11-8. Correlations of Average Infiltration Rates and Tracer Transport Times at 50% Mass Breakthrough for 36 Simulation Scenarios (Data from CRWMS M&O, 2000, U0050, Section 6.7.3)	III-124

FIGURES (Continued)

	Page
3.11-9. Simulated Breakthrough Curves of Cumulative Tracer (^{36}Cl) Mass Arriving at the Repository Level, Since Release from the Ground Surface, Using the Present-Day, Mean Infiltration and Four Simulation Scenarios (Data from CRWMS M&O, 2000, U0050, Section 6.7.3)	III-125
3.11-10. Effects of Matrix Diffusion: Concentration of Radionuclides and Colloids at the Water Table for the No-diffusion Alternative Model (Adapted from CRWMS M&O 2000, U0060, Figures 6.17.1 and 6.17.2).....	III-126
3.11-11. Schematic of the RTTF Technique for Determining Particle Residence Time in a Cell (CRWMS M&O 2000, U0065, Figure 2)	III-127
3.11-12. Comparison of the Particle-Tracking Solution and a Direct Finite-element Solution to the Transport (FEHM V2.10) for a 1-D, Dual-permeability Model (CRWMS M&O 2000, U0065, Figure 9).....	III-128
3.11-13. Comparison of the Particle-Tracking Solution and a Direct Finite-element Solution to the Transport for a 1-D, Dual-permeability Model. Red curves: finite element solution, black curves: particle tracking (solid – no diffusion, dashed – diffusion) (CRWMS M&O 2000, U0065, Figure 10)	III-129
3.11-14. Comparison of Cumulative Normalized Breakthrough Curves at the Water Table Using FEHM V2.10 and DCPT V1.0 software with the Nonsorbing Tc for Mean-Infiltration, Glacial-Transition Climate (CRWMS M&O 2000, U0160, Figure 11).....	III-130
3.11-15. Comparison of Cumulative Normalized Breakthrough Curves at the Water Table Using FEHM V2.10 and DCPT V1.0 software with the Sorbing Np for Mean-Infiltration, Glacial-Transition Climate (CRWMS M&O 2000, U0160, Figure 11).....	III-131
3.11-16. Results Related to Radionuclide Transport in the UZ	III-132
3.12-1. Schematic of the TH Modeling Issues	III-133
3.12-2. Schematic Showing Input Data and the UZ Models that Support the Development of the TH Model	III-134
3.12-3. Plan View of the UZ TSPA Grid, Showing the Location of the Potential Repository Submodel Domain (in Red) and the Cross Sections, NS#1 and NS#2. Locations #1 and #2 are Used for Detail Plots. Large solid circles refer to boreholes; small circles refer to centers of grid columns (adapted from CRWMS M&O 2000, U0105, Figure 1).....	III-135

FIGURES (Continued)

	Page
3.12-4. Lateral and Vertical Discretization at the NS#2 Cross-Section Based on the Refined Numerical Grid. Plot shows location of the potential repository and the hydrogeologic units layering (adapted from CRWMS M&O 2000, U0105, Figure 3).	III-136
3.12-5. Temperature Distribution along NS#2 Cross-Section Grid at 1,000 Years (a) No Ventilation, (b) with Ventilation (Adapted from CRWMS M&O 2000, U0105, Figures 45 and 59).	III-137
3.12-6. Temperature at Location #1, NS#2 Cross-Section Grid (a) No Ventilation (b) with Ventilation (Adapted from CRWMS M&O 2000, U0105, Figures 46 and 60).	III-138
3.12-7. Temperature along a Section of the Potential Repository Horizon of the NS#2 Cross-Section Grid (a) No Ventilation, (b) with Ventilation (Adapted from CRWMS M&O 2000, U0105, Figures 48 and 62).	III-139
3.12-8. Matrix Liquid Saturation (SI) along NS#2 Cross-Section Grid at 1,000 Years (a) No Ventilation, (b) with Ventilation (Adapted from CRWMS M&O 2000, U0105, Figures 50 and 64).	III-140
3.12-9. Matrix Liquid Saturation at Location#1, NS#2 Cross-Section Grid (a) No Ventilation, (b) with Ventilation (Adapted from CRWMS M&O 2000, U0105, Figures 51 and 65).	III-141
3.12-10. Matrix Liquid Saturation along a Section of the Potential Repository Horizon, NS#2 Cross-Section Grid (a) No Ventilation, (b) with Ventilation (Adapted from CRWMS M&O 2000, U0105, Figures 52 and 66).	III-142
3.12-11. Fracture Liquid Flux at Location #1, NS#2 Cross-Section Grid (a) No Ventilation, (b) With Ventilation (Adapted from CRWMS M&O 2000, U0105, Figures 53 and 67).	III-143
3.12-12. Fracture Liquid Flux along a Section of the Potential Repository Horizon, NS#2 Cross-Section Grid (a) No Ventilation, (b) with Ventilation (Adapted from CRWMS M&O 2000, U0105, Figures 55 and 69).	III-144
3.12-13. Matrix Liquid Flux along a Section of the Potential Repository Horizon, NS#2 Cross-Section Grid (a) No Ventilation, (b) with Ventilation (Adapted from CRWMS M&O 2000, U0105, Figures 56 and 70).	III-145
3.12-14. Summary of TH Model Results.	III-146
5.1-1. Conceptual Sketch of the UZ with Icons Representing Major Model Components	III-147

FIGURES (Continued)

	Page
5.1-2. Schematic of Major Inputs and Outputs for UZ Flow Model and its Submodels.....	III-148
5.1-3. Schematic of Major Inputs and Outputs of the Drift Seepage Models.....	III-149
5.1-4. Schematic of Major Inputs and Outputs of the Drift-Scale THC Models	III-150
5.1-5. Schematic of Major Inputs and Outputs of the UZ Transport Models	III-151

TABLES

	Page
1-1. The Main Models of the UZ PMR.....	2
1-2. Roadmap for the UZ PMR.....	3
1.2-1. Principal Factors, Other Factors, and the PMRs where Addressed	8
1.2-2. FEPs for the UZ PMR.....	11
1.2-3. Summary of Current Understanding Used to Develop Conceptual and Numerical Models for UZ Flow and Transport at Yucca Mountain	14
1.3-1. Software for UZ Flow and Transport Model and Abstractions for TSPA-SR	24
2.3-1. Natural Analogs for Process Evaluation.....	45
2.5-1. Key External Issues for the Unsaturated Zone Flow and Transport Process Model Report.....	53
3.2-1. Geological Issues Related to Performance	67
3.2-2. Major Hydrogeological Unit, Lithostratigraphic Unit, Detailed Hydrogeological Unit, and UZ Model Layer Nomenclatures (adapted from CRWMS M&O 2000, U0000, Table 10).....	70
3.4-1. Summary of Grids Developed for UZ Flow and Transport Model PMR Activities (Adapted from CRWMS M&O 2000, U0000, Table 6)	101
3.5-1. Meteorological Stations Selected as Analogs for Future Climate States.....	109
3.5-2. Mean Annual Precipitation for Analogs for the Lower and Upper Bound of the Three Climate Scenarios	113
3.5-3. Mean Annual Temperature for Analogs for the Lower and Upper Bound of the Three Climate Scenarios	114
3.5-4. Average Net-Infiltration Rates over the UZ Flow and Transport Model Domain.....	121
3.7-1. The Average Value (mm/yr) of Infiltration Rates over the UZ Model Domain (Adapted from CRWMS M&O 2000, U0050, Table 6-3).....	143
3.7-2. Comparison of the Water Flux through Matrix and Fractures as a Percentage of the Total Flux at the Middle PTn and at the Potential Repository (CRWMS M&O 2000, U0050, Section 6.6.3)	146

TABLES (Continued)

	Page
3.7-3. Comparison of the Water Flux through Faults as a Percentage of the Total Flux at Four Different Horizons (1) on Ground Surface; (2) Interface between PTn and TSw; (3) at the Potential Repository; and (4) at the Water Table (Data from CRWMS M&O 2000, U0050, Section 6.6.3)	149
3.7-4. Average Percolation Fluxes Simulated within the Potential Repository Footprint for the Three Mean Infiltration Scenarios (Data from CRWMS M&O 2000, U0050, Section 6.6.3)	154
3.7-5. Comparison of the Water Flux through Fractures as a Percentage of the Total Flux at Two Different Horizons (1) at the Potential Repository and (2) at the Water Table, Using the Nine Infiltration Scenarios and Two Perched Water Conceptual Models (Data from CRWMS M&O 2000, U0050, Section 6.6.3)	156
3.8-1. Aqueous and Gaseous Chemical Concentrations (mg/L) Used for Initial and Boundary Conditions of Hydrochemical Transport Simulations (CRWMS M&O 2000, U0050, Table 6-14)	172
3.9-1. Parameter Ranges for Which Seepage Is Evaluated Using the SMPA (Adapted from CRWMS M&O 2000, U0075, Section 6.3)	196
3.9-2. Uncertainty in Seepage Parameters as Function of Percolation (Table from CRWMS M&O 2000, U0120, Table 11)	202
3.10-1. TSw Porewater Composition and CO ₂ Partial Pressure (CRWMS M&O 2000, N0120/U0110, Table 3)	212
3.10-2. Model Mineral Assemblage, Aqueous and Gas Species (Full Geochemical System; CRWMS M&O 2000, N0120/U0110, Table 7)	213
3.10-3. THC Abstraction for the Mean Infiltration Rate Case with Climate Change (CRWMS M&O 2000, N0125, Table 3)	227
3.11-1. Sorption Coefficient Distributions for UZ Units (adapted from CRWMS M&O 2000, U0100, Table 2a)	236
3.11-2. Summary of Diffusion Coefficient Data (CRWMS M&O 2000, U0100, Section 6.6.3)	237
3.11-3. Breakthrough Time of Radionuclides at the Water Table (Years) (CRWMS M&O 2000, U0060, Table 6.15)	243

TABLES (Continued)

		Page
3.11-4.	Summary of Radionuclide Sorption Results from Busted Butte Tests (adapted from CRWMS M&O 2000, U0100, Tables 27-28).....	251
3.12-1.	Summary of Numerical Model Cases for Mountain-Scale TH.	267
3.13-1.	Uncertainty in Major Model Components of the UZ Flow and Transport Model.....	277
3.13-2.	Uncertainties in UZ Flow and Transport Products for TSPA-SR.....	280
4.2-1.	Issue Resolution Status Report/Key Technical Issues (IRSR/KTI) Related to the UZ PMR.....	283
4.3-1.	Issue Resolution Status Reports, Subissues, Technical Acceptance Criteria, and PMR Approach (NRC 1997, 1999a-e, 2000)	293

INTENTIONALLY LEFT BLANK

1. INTRODUCTION

The United States (US) Department of Energy (DOE) is evaluating Yucca Mountain, Nevada, for the development of a potential geological repository for the permanent disposal of the nation's commercial and defense spent nuclear fuel and high-level radioactive waste. This evaluation includes analyses of the ability of the natural geologic and engineered barrier systems of this potential repository to prevent the migration of radionuclides to the accessible environment. The primary pathway to the accessible environment has been determined to be via the groundwater aquifer below the potential repository (CRWMS M&O 2000b).

As the site-characterization effort at Yucca Mountain (YMP) is near completion, and the preliminary design of an Engineered Barrier System (EBS) and the potential repository layout are completed, the DOE is deciding whether to recommend the site. This activity is termed Site Recommendation (SR), and if the site is recommended, a License Application (LA) may be submitted to the Nuclear Regulatory Commission (NRC). A series of project documents that include the Yucca Mountain Site Description (YMSD), the Total System Performance Assessment (TSPA), and Process Model Reports (PMRs) will support any SR. The PMRs provide the technical basis for the higher-level YMSD and TSPA documents. Figure 1-1 is a schematic diagram that shows the relationships amongst all of these project documents. Regulatory requirements and the SR/LA design feed the allocation analysis and the Repository Safety Strategy (RSS) (CRWMS M&O 2000b). The RSS identifies the most important factors (principal factors) that are expected to affect the performance of the potential repository.

TSPA is conducted to evaluate the postclosure performance of a potential repository at Yucca Mountain. Nine Process Models Reports (PMRs), of which this document is one, are being developed to summarize the technical basis for each of the process models supporting the TSPA. These reports cover the following areas:

- Integrated Site Model
- Unsaturated Zone Flow and Transport
- Near Field Environment
- Engineered Barrier System Degradation, Flow, and Transport
- Waste Package Degradation
- Waste Form Degradation
- Saturated Zone Flow and Transport
- Biosphere
- Disruptive Events

These PMRs are supported by Analysis/Model Reports (AMRs) that contain the more detailed technical information to be input into each PMR and the TSPA. This technical information consists of data, analyses, models, software, and supporting documentation that will be used to show the applicability of each process model for its intended purpose of evaluating the postclosure performance of the potential Yucca Mountain repository system. The PMR process will ensure the traceability of this information from its source through the AMRs, PMRs, and eventually to how that information is used in the TSPA. The PMRs also support the Site Description, a document that contains detailed information about the various aspects of the Yucca Mountain Site (see Figure 1-1).

This document is the PMR for unsaturated zone (UZ) flow and transport, hereafter referred to as the UZ PMR. The UZ PMR considers those features, events, and processes (FEPs) concerning flow and transport through the UZ that are expected to be important for evaluating the performance of the potential repository system; the FEPs are discussed in detail in Section 1.2.3. The UZ PMR is supported by 24 AMRs that cover all aspects of UZ flow and transport (see Figure 1-1).

Some of these AMRs are, in essence, data reports with limited in-depth analysis; others primarily discuss development and documentation of computer codes and models, and the remainder document Performance Assessment (PA) abstractions of the models for subsequent use in TSPA. The main models included in the UZ PMR and the citations for their respective AMRs are listed in Table 1-1. The models form the basis of the UZ PMR both as integration and performance evaluation tools. Figure 1-2 is a graphic illustration of the interrelations of the models and their connections to TSPA.

Table 1-1. The Main Models of the UZ PMR

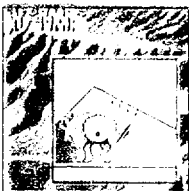
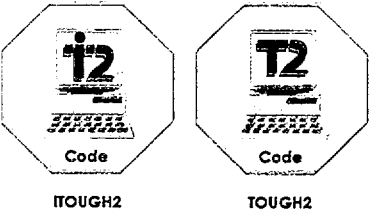
Model Title	Acronym	AMR Reference	Dimensionality	Abstracted for PA	UZ PMR Section
Climate Model	CM	USGS 2000, U0005	N/A	Yes	3.5
Infiltration Model	IM	USGS 2000, U0010	3-D	Yes	3.5
Calibrated Properties Model	CPM	CRWMS M&O 2000, U0035	1-D and 2-D	No	3.6
Flow Model	FM	CRWMS M&O 2000, U0050	3-D	Yes	3.7
Ambient Geochemistry Model	AGM	CRWMS M&O 2000, U0050	Analytical and 3-D	No	3.8
Seepage Calibration Model	SCM	CRWMS M&O 2000, U0080	2-D and 3-D	No	3.9.4
Seepage Model for Performance Assessment	SMPA	CRWMS M&O 2000, U0075	3-D	Yes	3.9.5
Drift Scale Test Thermal-Hydrological-Chemical Model	DST THCM	CRWMS M&O 2000, N0120/U0110	2-D	No	3.10
THC Seepage Model	THCM	CRWMS M&O 2000, N0120/U0110	2-D	Yes	3.10.5
Transport Model	TM	CRWMS M&O 2000, U0060	2-D, 3-D	No	3.11
Mountain-Scale Thermal-Hydrological Model	THM	CRWMS M&O 2000, U0105	2-D, 3-D	No	3.12




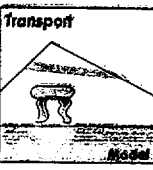


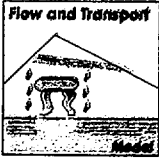


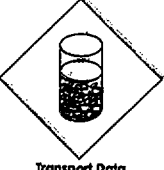

NOTE: N/A—Not applicable

The basic approach of the UZ PMR is to provide a comprehensive summary of UZ flow and transport issues discussed in the UZ AMRs as well as to provide the following additional information:

1. New data and analyses that are important to one or more of the main models, and have been collected or compiled since the AMRs were prepared.
2. Information from journal references to other sites worldwide that address issues considered in the AMRs and the UZ PMR.

Table 1-2. Roadmap for the UZ PMR

Information	Icon (Examples)	Report Chapter/Section	Cross-Referencing
Objectives and scope of the PMR		Sections 1.1 and 1.2	N/A
Features, Events, and Processes and their screening	N/A	Section 1.2.3	N/A
Key hypotheses and alternative hypotheses for the UZ PMR	N/A	Section 1.2.4	Pointers to sections of PMR for detailed discussions
Key issues from NRC, NWTRB, Peer Review Groups, and others	N/A	Section 2.5	Pointers to sections of the PMR where each issue is discussed
Software used in AMRs that support the PMR		Section 1.3.2	Pointers to sections of the PMR supported by AMRs using the software
Evolution of field testing and model development	N/A	Chapter 2	N/A

Information	Icon (Examples)	Report Chapter/Section	Cross-Referencing
Geological data, conceptual models and numerical grids	   Numerical Grids	Sections 3.2 to 3.4	N/A
Key UZ PMR models and analyses	   	Sections 3.5 to 3.12	For each model, the data inputs, relationships to other models, the data outputs, and intended use in TSPA are described.
Key NRC issues and subissues	N/A	Chapter 4	Pointers to sections in PMR where each issue is discussed
Summary and conclusions	N/A	Chapter 5	N/A
Summary of field and laboratory data used in AMRs and PMR	  Seepage Data Geochemistry Data	Attachment I	A brief description of the different data sets with appropriate DTN numbers is given.
	  Transport Data Perched Water Data		

NOTE: N/A—Not applicable

Table 1-2 provides a roadmap for the UZ PMR, indicating the chapters/sections in which key points of information are located. Most of this chapter (Chapter 1) describes the objectives and scope of the PMR, the principal factors, and other factors addressed by this PMR. Features, Events, and Processes (FEPs) and the key hypotheses for the PMR are also described.

Section 1.3 summarizes the Quality Assurance (QA) status and issues regarding the data and software used in this PMR. Chapter 1 concludes with a brief section describing the relationships between the UZ PMR and other key Project documents.

Chapter 2 summarizes the evolution of field and laboratory testing, data-collection activities and process/TSPA modeling of flow and transport in the UZ, and UZ flow and transport issues raised by various overseeing bodies, peer review groups, PA and UZ Workshops, NRC, and others. The Chapter describes the rationale for the evolution of the testing program and the major advances that have been made in modeling of the UZ. Chapter 2 refers to Attachment I, which summarizes the various data sets used in the UZ AMRs with appropriate pointers to Data Tracking Numbers (DTNs).

Chapter 3 contains the main technical sections of the UZ PMR. This chapter describes and summarizes all of the models that are considered in the UZ PMR. These include models on calibrated properties, 3-D flow fields, seepage, ambient chemistry, radionuclide transport, mountain-scale thermal-hydrological (TH) processes, and drift-scale thermal-hydrological-chemical (THC) processes (see Figure 1-2). In addition, Chapter 3 provides the necessary framework for the models in terms of the geological information, conceptual models, and numerical grids.

Chapter 4 deals with the Key Technical Issues (KTIs) on UZ flow and transport identified by the NRC. Each of the subissues is identified and pointers are provided to the relevant chapters/sections in the UZ PMR that address it. Finally, Chapter 5 gives the summary and conclusions of the UZ PMR, primarily focusing on the models that feed TSPA.

Table 1-2 shows examples of the various icons used in this PMR. The icons were developed to provide the reader with easily identifiable representations of the various components of the UZ PMR. Data icons are represented by diamond shapes, and model icons as squares. The icons are used in the various subsections of Chapter 3 to show the flow of data and information, as well as the interrelations among the various models.

1.1 OBJECTIVES

The following are the main objectives of the UZ PMR:

1. To synthesize all important data, analyses, models, and model abstractions of flow and transport within the UZ in a single document
2. To document the development of key models used to analyze the various data sets from the UZ
3. To document the development of key models for UZ flow and transport used in TSPA
4. To document the abstraction process and results for key UZ flow and transport models used by TSPA

5. To summarize the key products that are provided to TSPA for performance analysis.

The various AMRs that support the UZ PMR and the PMR itself are key documents that the Yucca Mountain Site Characterization Project (YMP) will rely upon and reference in the SR and LA documents.

1.2 PMR SCOPE AND BACKGROUND INFORMATION

1.2.1 Scope of UZ Flow and Transport PMR

The UZ Flow and Transport Model generates numerical simulations of spatial and temporal distributions of water flow and potential radionuclide transport through the UZ, and of water seepage into the potential repository waste emplacement drifts. The UZ models account for infiltration processes near the ground surface of the mountain, and the effect of climate changes. The spatial and temporal variability of net infiltration is specified as the main boundary condition for the UZ Flow and Transport Model. Numerical grids for the UZ models are developed based on the Geologic Framework Model (GFM, CRWMS M&O 2000, I0035), the Rock Properties Model (CRWMS M&O 2000, I0040), the Mineralogic Model (CRWMS M&O 2000, I0045) and Hydrological Property Data (CRWMS M&O 2000, U0090).

The Calibrated Properties Model (CPM) uses the estimated infiltration rates at various boreholes and adjusts various hydrological properties (CRWMS M&O 2000, U0090), such as permeability, to match observed matrix saturations, water potentials and pneumatic signals, using inverse modeling techniques. The calibrated property sets produced by this analysis are used for a wide variety of downstream models, including the 3-D Flow Model (FM), the Transport Model (TM), the Seepage Calibration Model (SCM), the Seepage Model for Performance Assessment (SMPA), the Thermal-Hydrological Model (THM), and the Thermal-Hydrological-Chemical Model (THCM).

The 3-D Flow Model and its submodels use the calibrated property sets (CRWMS M&O 2000, U0035) as initial values for further 3-D calibrations against various geochemical, temperature, and perched water data. These models generate numerous 3-D flow fields for TSPA that are based upon different assumptions regarding important hydrological properties, conceptual models, and infiltration cases. These 3-D flow fields are used as input to the Seepage Model for PA and for transport calculations.

The Seepage Calibration Model (SCM) (CRWMS M&O 2000, U0080) uses the calibrated property sets (CRWMS M&O 2000, U0035) as initial values to match the observed seepage data from the niche studies (CRWMS M&O 2000, U0015). The SCM supports the Seepage Model for PA, which evaluates the relationships between seepage and important hydrological parameters as a function of percolation flux. The results of the Seepage Model for PA are further abstracted to predict the fraction of waste packages that will encounter water seeping into open drifts and the flow rate of seepage into a drift (CRWMS M&O 2000, U0120).

Transport calculations (Transport Model) are performed using particle trackers (CRWMS M&O 2000, U0155; CRWMS M&O 2000, U0065; CRWMS M&O 2000, U0160), as well as numerical solutions of the conventional advection/dispersion equations. Comparison among these different

numerical approaches yield estimates for their accuracy and the extent to which they are conservative. Transport properties are mostly derived from laboratory data and from the Busted Butte transport test (CRWMS M&O 2000, U0100). Potential radionuclide transport in the colloidal phase is evaluated using various models and formulations for colloid transport mechanisms (CRWMS M&O 2000, U0070; CRWMS M&O 2000, U0060).

This PMR is intended for providing models and analyses to TSPA for their evaluation of the overall system behavior. In general, the PMR uses a more realistic approach in its treatment of processes identified as principal factors (see Section 1.2.2) and bounding or conservative values for processes controlling other factors, such as climate and coupled processes (see Table 1.2-1) related to unsaturated zone flow and transport. This is in accordance with the *Repository Safety Strategy* (CRMWS M&O 2000b). For these reasons, the results presented in this PMR should not be used to directly evaluate regulatory or other requirements.

Heat released by the emplaced waste potentially affects both the 3-D flow fields and the seepage rates into underground openings. Mountain-scale models (CRWMS M&O 2000, U0105) of the TH conditions near the emplacement drifts are included in the UZ PMR to evaluate the impact of these coupled processes on two-phase (water and gas) flow. These models investigate the extent of two-phase and dry-out zones, water drainage between pillars, and critical temperature conditions, occurring at various locations, such as at the drift walls, within mid-pillar regions, and within perched water bodies and zeolitic rocks. THC models (CRWMS M&O 2000, N0120/U0110) investigate the chemistry of water and gases entering drifts, and associated changes in important hydrological properties near the emplacement drifts.

1.2.2 Principal Factors and Other Factors Considered

The YMP has identified those factors most important to performance, hereafter named the principal factors, based on the Repository Safety Strategy (RSS) (CRWMS M&O 2000b). A series of workshops were conducted to develop the RSS (including the list of principal factors), review of each modeling area and discuss sensitivities from the perspective of the process models and TSPA. Project personnel from each of the scientific areas and from performance assessment took part in these workshops. The RSS lists seven principal factors and twenty other factors of second-order importance. The selection of the principal factors was based on preliminary TSPA analyses and expert judgment, which showed that these factors significantly affected the performance of the potential repository. The other factors were deemed to have second-order effects on the repository performance in terms of dose to the accessible environment (CRWMS M&O 2000b, Section 3.1). Table 1.2-1 lists the seven principal factors, the twenty other factors, and the PMRs that address each factor.

Table 1.2-1. Principal Factors, Other Factors, and the PMRs where Addressed

	Factor	Process Model Report
Principal Factors (Nominal Scenario)	Seepage into drifts	Unsaturated Zone Flow and Transport
	Performance of the drip shield	Waste Package Degradation
	Performance of the waste package barriers	Waste Package Degradation
	Solubility limits of dissolved radionuclides	Waste Form Degradation
	Retardation of radionuclide migration in the unsaturated zone	Unsaturated Zone Flow and Transport
	Retardation of radionuclide migration in the saturated zone	Saturated Zone Flow and Transport
	Dilution of radionuclide concentrations during migration	Saturated Zone Flow and Transport
Other Factors (Nominal Scenario)	Climate	Unsaturated Zone Flow and Transport
	Net infiltration into the mountain	Unsaturated Zone Flow and Transport
	Unsaturated zone flow above the repository	Unsaturated Zone Flow and Transport
	Coupled processes - effects on unsaturated zone flow	Unsaturated Zone Flow and Transport
	Coupled processes - effects on seepage	Near-Field Environment
	Environments on the drip shield	Engineered Barrier System Degradation, Flow, and Transport
	Environments on the waste package	Engineered Barrier System Degradation, Flow, and Transport
	Environments within the waste package	Waste Form Degradation
	CSNF waste form performance	Waste Form Degradation
	DHLW glass waste form performance	Waste Form Degradation
	DSNF, Navy fuel, Pu disposition waste form performance	Waste Form Degradation
	Colloid-associated radionuclide concentrations	Waste Form Degradation
	In-package radionuclide transport	Waste Form Degradation
	Transport through the drift invert	Engineered Barrier System Degradation, Flow, and Transport
	Advective pathways in the unsaturated zone	Unsaturated Zone Flow and Transport
	Colloid-facilitated transport in the unsaturated zone	Unsaturated Zone Flow and Transport
	Coupled processes – effects on unsaturated zone transport	Unsaturated Zone Flow and Transport
	Advective pathways in the saturated zone	Saturated Zone Flow and Transport
	Colloid-facilitated transport in the saturated zone	Saturated Zone Flow and Transport
	Biosphere transport and uptake	Biosphere
Factors for Disruptive Event Scenarios	To be determined. See Disruptive Event PMR for preliminary considerations	Disruptive Events

SOURCE: CRWMS M&O 2000b

The UZ PMR addresses the following principal factors:

1. Seepage into drifts (see Section 3.9)
2. Retardation of radionuclide migration in the UZ (see Sections 3.3 and 3.11).

Seepage into drifts is a principal factor as the amount of water entering the drift affects waste mobilization rates and transport of radionuclides out of the drifts into the UZ. Retardation of radionuclide migration in the UZ is a principal factor as this process is effective in delaying the migration of many radionuclides due to matrix diffusion and sorption (see Sections 3.3 and 3.11 for descriptions of these processes.)

In addition, the following seven other factors are within the scope of the UZ PMR:

1. Climate (Section 3.5)
2. Net infiltration into the mountain (Section 3.5)
3. UZ flow above the repository (Section 3.7)
4. Coupled processes-effects on UZ flow (Section 3.12)
5. Advective pathways in the UZ (Sections 3.3 and 3.11)
6. Colloid-facilitated transport in the UZ (Sections 3.3 and 3.11)
7. Coupled processes-effects on UZ transport (Section 3.12).

The general guidelines for addressing the seven other factors are to use conservative bounding analysis for the safety case. The two principal factors will be studied and evaluated using rigorous realistic numerical evaluations as well as bounding analyses.

1.2.3 Features, Events, and Processes (FEPs)

The Yucca Mountain Project has established a database of all features, events, and processes (FEPs) that could affect the potential repository performance. Rev. 00C of the database (CRWMS M&O 1999d) contains 1786 entries, derived from the following sources:

- General FEPs from other international radioactive waste disposal programs
- YMP-specific FEPs identified in YMP literature
- YMP-specific FEPs identified in technical workshops

The YMP FEPs list was initially populated with FEPs compiled by other international radioactive waste programs. The Nuclear Energy Agency (NEA) of the Organization for Economic Co-operation and Development (OECD) maintains an electronic FEP database that currently contains 1261 FEPs from seven programs, representing the most complete attempt internationally at compiling a comprehensive list of FEPs potentially relevant to radioactive waste disposal.

The YMP FEP list was supplemented with YMP-specific FEPs identified in past YMP work during site characterization and preliminary performance assessments. Because the YMP is the only repository proposed for an unsaturated fractured tuff, many of these FEPs represent events and processes not otherwise included in the international compilation. A search of YMP literature identified these 443 additional FEP entries.

Relevant FEPs from the 1704 entries identified from the NEA database and YMP literature were taken from a series of technical workshops convened between December, 1998 and April, 1999. At these workshops, the relevant FEPs were reviewed and discussed by subject matter experts within the project. As a result of these discussions, workshop participants proposed 82 additional YMP-specific FEPs.

From this project-wide list, there are 515 FEPs identified for UZ flow and transport. FEPs were selected for the UZ based on the processes identified in each FEP and the processes that are known to affect the UZ. UZ flow and radionuclide transport are components of the natural geologic barriers that affect the overall performance (including engineered barriers) of the potential repository. The UZ flow and transport FEPs were evaluated systematically to determine their relevance to UZ subsystem performance. Models were developed to address the FEPs identified as potentially important to performance. These models are the subject of the AMRs supporting the UZ PMR. This report summarizes the scientific bases for these models. The TSPA model and underlying process models of the natural barrier capture some, but not all, of the 515 FEPs that are associated with this natural barrier. The reasons for exclusion of a FEP are low probability and/or low consequence, discussed further below. The identification and treatment of all 515 FEPs are given in CRWMS M&O (2000, U0170).

A large degree of overlap exists among these 515 FEPs, and this overlap has been used to group FEPs into two broad categories, "primary" and "secondary" FEPs. Eighty-one primary FEPs that incorporate the topics represented by the entire list of 515 FEPs have been identified. Thus, the 434 secondary FEPs are subsets of the primary FEPs.

The primary FEPs have been further subdivided into the categories identified and described in Table 1.2-2. Both primary and secondary FEPs are discussed in CRWMS M&O 2000 (U0170).

Table 1.2-2. FEPs for the UZ PMR

FEP Category	Description	YMP Primary FEP Numbers
Included FEPs	Those FEPs that are completely included in the TSPA.	1.3.01.00.00, 1.3.07.02.00, 2.1.08.01.00, 2.1.08.02.00, 2.2.03.01.00, 2.2.03.02.00, 2.2.07.01.00, 2.2.07.02.00, 2.2.07.03.00, 2.2.07.04.00, 2.2.07.08.00, 2.2.07.09.00, 2.2.08.04.00, 2.2.08.08.00, 2.2.08.09.00, 2.2.08.10.00, 2.2.10.03.00, 2.2.10.10.00, 2.3.01.00.00, 2.3.11.01.00, 2.3.11.02.00, 3.1.01.01.00
Boreholes and Repository Seals	FEPs concerning site characterization boreholes and repository drift openings generally excluded from TSPA.	1.1.01.01.00, 1.1.01.02.00, 1.1.02.01.00, 1.1.04.01.00, 1.1.11.00.00, 1.4.04.02.00, 2.1.05.01.00, 2.1.05.02.00, 2.1.05.03.00
Extreme Climate/Episodic Transient Flow	FEPs concerning major changes in climate and/or episodic transient flow driven by episodic infiltration or thermal-hydrologic effects. Generally excluded from TSPA.	1.3.04.00.00, 1.3.05.00.00, 1.3.07.01.00, 1.4.01.01.00, 2.2.07.05.00, 2.2.07.06.00, 2.2.07.07.00, 2.3.11.03.00
Erosion/ Dissolution/ Subsidence	FEPs concerning surface erosion and deposition, large-scale rock dissolution, and subsidence. Generally excluded from TSPA.	1.2.07.01.00, 1.2.07.02.00, 1.2.09.02.00, 2.2.06.04.00
Human Influences on Climate/Soil	FEPs concerning effects of greenhouse gas emissions, destruction of ozone layer, and changes in soil chemistry due to human activities. Excluded from TSPA.	1.4.01.00.00, 1.4.01.02.00, 1.4.01.03.00, 1.4.01.04.00, 1.4.06.01.00
Natural Gas/Gas Generation Effects	FEPs concerning formation of gases in the emplacement drifts due to interactions with repository materials, intrusion of natural gas. Excluded from TSPA.	2.1.12.01.00, 2.2.10.11.00, 2.2.11.01.00, 2.2.11.02.00, 2.2.11.03.00
Seismic/Igneous/Rock Characteristics	FEPs concerning existing geologic characteristics and the effects of seismic or igneous activity on these characteristics. Mixture of items included in and excluded from TSPA.	1.2.02.01.00, 1.2.02.02.00, 1.2.03.01.00, 1.2.04.02.00, 1.2.06.00.00, 1.2.10.01.00, 1.2.10.02.00, 2.2.06.02.00, 2.2.06.03.00, 2.2.12.00.00
Repository Perturbed Thermal-Hydrologic-Mechanical-Chemical (THMC)	FEPs concerning coupled effects of thermal-hydrologic-mechanical-chemical processes in the repository environment. Effects of repository heat and materials on hydrology and geochemistry. Mixture of items included in and excluded from TSPA.	1.1.02.00.00, 2.2.01.01.00, 2.2.01.05.00, 2.2.07.10.00, 2.2.07.11.00, 2.2.08.01.00, 2.2.08.02.00, 2.2.08.03.00, 2.2.08.05.00, 2.2.08.06.00, 2.2.08.07.00, 2.2.09.01.00, 2.2.10.01.00, 2.2.10.04.00, 2.2.10.05.00, 2.2.10.06.00, 2.2.10.07.00, 2.2.10.09.00

SOURCE: CRWMS M&O 2000, U0170

FEPs designated as “included” are those directly represented in TSPA models and process-level models that support TSPA. Therefore, the treatment of these FEPs is described in other chapters/sections of this document and the corresponding supporting AMRs. Some FEPs (representing broad categories) are not fully in the “included” FEP category, but are also not fully excluded; these broad-category FEPs address some aspects that are included and some aspects that are excluded from TSPA. In other words, different aspects of the same FEP have different treatments. A summary of the included FEPs that affect UZ flow and transport is given in Section 1.2.4. FEPs in the other categories are mostly (but not entirely) excluded from the TSPA. The exclusion of FEPs from the TSPA is based on arguments demonstrating low probability or low consequence of occurrence. Most of the exclusion arguments are based on low consequence. For example, the FEP “Flow and Transport in the UZ from Episodic Infiltration” is argued to have low consequence. This is based on the findings by existing studies of episodic infiltration and percolation showing that flow through one of the hydrogeologic units above the potential repository (the Paintbrush nonwelded unit (PTn)) damps out the transient nature of the percolation. Consequently, UZ flow near the potential repository and below is essentially steady. In some cases, the low-consequence argument takes the form of a conservative assumption that bounds the potential effects of the FEP. For example, the FEP “Human Influences on Climate” is treated by assuming the onset of a wetter climate (the glacial-transition climate) early (after 2000 years) in the 10,000-year regulatory period. This bounds the impact of human activity on the climate by using a much earlier transition to the wetter climate than would be expected from the climate cycles indicated by the paleoclimate record. A few of the excluded FEPs, such as the FEP on glaciers, are excluded on the basis of low probability as shown by the paleoclimate record. An event may be excluded on the basis of low probability if the probability of occurrence is less than 0.0001 in 10,000 years.

Six assumptions used in the FEPs exclusion arguments are based on scientific rationale, but never-the-less may continue to be verified. These six assumptions are identified as “to be verified” (TBV). The six TBV assumptions and a brief description of their bases (CRWMS M&O 2000, U0170) follow. All FEPs excluded on the basis of TBV assumptions are identified in CRWMS M&O (2000, U0170, Chapter 7).

Assumption 1 (assumption 10 in CRWMS M&O 2000, U0170, Sections 6.3.8 and 6.8.6): Changes in aqueous geochemistry in the repository environment are dominated by thermal-chemical interactions associated with the potential repository.

Basis: With the exception of climate change, the potential repository is the only perturbation that will potentially affect the aqueous geochemistry of the UZ over the 10,000 year regulatory period. The assumption that the effects of climate change on the geochemistry will be smaller than the effects of the potential repository is based on the fact that temperature changes driven by the potential repository will be much larger than temperature changes that occur as a result of climate change. Also, the potential repository introduces a large number of new materials (some of them are in substantial quantities) that will influence the geochemistry. Climate change may influence the concentrations of dissolved salts in water that percolates, but will not introduce new materials. This is a reasoned argument based on the knowledge that temperature and chemical components affect the system chemistry. Temperature changes and introduction of new materials will be more drastic as a result of the repository than due to climate change.

Because the effects of climatic factors that affect the chemistry will be smaller, the resulting changes in chemistry are assumed to also be less.

Assumption 2 (assumption 11 in CRWMS M&O 2000, U0170, Sections 6.8.7, 6.8.8, 6.8.10, 6.8.17, and 6.8.18): Results from the near-field THC coupled processes model can be used to bound the effects of similar coupled processes on far-field flow and radionuclide transport.

Basis: Model results show that THC coupled processes in the near-field have a negligible effect on flow and transport. The effects of coupled processes in the far-field unsaturated zone are expected to be less severe than in the near-field. This is caused by the higher temperatures that will occur near the waste emplacement drifts, including boiling of the rock-water, and the associated precipitation of minerals and condensation of water. The near-field temperatures clearly bound the temperatures in the far field. Further THC process modeling at the mountain scale may be conducted, and data showing thermal-chemical effects on minerals in the Calico Hills will be considered, as appropriate, for further verification.

Assumption 3 (assumption 12 in CRWMS M&O 2000, U0170, section 6.8.12): The quantities of organic matter and microbes either emplaced or generated (through microbial growth processes) in the waste emplacement drifts are sufficiently small that they are unlikely to be of significance for far-field flow and transport processes.

Basis: This assumption is based on the limited use of organic matter in the emplacement drifts and the limited quantities of natural organic matter and nutrients, such as phosphorus, in the unsaturated zone. Analyses conducted for the viability assessment (CRWMS M&O 1998i; pp. 4-108 and 4-109) and the analysis of in-drift microbial communities (CRWMS M&O 2000, E0040, Section 7.3) provide additional support for this assumption. This assumption relies on the premise that organic and microbial material will interact with dissolved metals in a relatively uniform way. Although this assumption is qualitatively reasonable, it is important to show that microbial and organic matter that may be present in the potential repository environment does not have specific affinity for interaction with particular radionuclides, such as plutonium, which requires an investigation of existing data.

Assumption 4 (assumption 13 in CRWMS M&O 2000, U0170, Sections 6.3.5, 6.8.4, and 6.8.5): TH flow processes will have a minimal effect on radionuclide transport.

Basis: The major effects of TH flow processes will be near the emplacement drifts in the early part (first 10,000 years) of the postclosure time period. Radionuclide releases will likely be after the main portion of the thermal pulse (after waste heat begins to dissipate), and a large part of the radionuclide transport process in the UZ will take place at locations outside the envelope of the main TH effects. Therefore, the effect of TH flow processes on radionuclide transport is expected to be negligible, i.e. TH effects on flow will be small by the time radionuclide transport occurs. These qualitative arguments require quantitative verification with transport calculations using mountain-scale TH flow fields.

Assumption 5 (assumption 14 in CRWMS M&O 2000, U0170, Section 6.8.14): Thermal-mechanical effects on hydrogeologic properties near waste emplacement drifts will be limited to a time period (first 1000 years) occurring before any significant seepage occurs into the drifts.

Basis: The main compressive stresses caused by thermal-mechanical effects will occur during the period when temperatures are increasing. Drift seepage is not expected during this time period when temperatures are increasing because water boils and is removed as vapor from the vicinity of the waste emplacement drifts. The effects of thermal-mechanical stress around the waste emplacement drifts are expected to be small by the time water is present to seep into the drifts. Additional thermal-hydrologic-mechanical process modeling will be performed to verify this assumption.

Assumption 6 (assumption 15 in CRWMS M&O 2000, U0170, Section 6.7.1): Mechanical stresses around waste emplacement drifts after the thermal period are dominated by the existing in-situ stresses created by the presence of the opening. Therefore, changes to mechanical stresses due to fault movement around waste emplacement drifts are negligible.

Basis: Drift stability analyses have found that seismic activity has only a minor influence on rockfall in drifts (CRWMS M&O 2000b, Section 7). Therefore, the effects of fault movements on stresses around the emplacement drifts are expected to be minor. Additional hydrologic-mechanical process modeling will be performed to verify this assumption.

1.2.4 Summary of Current Understanding of Flow and Transport at Yucca Mountain

The UZ PMR considers many parameters, processes, and models that describe UZ flow and transport at Yucca Mountain. Current understanding of flow and transport issues have been gained through collections of site data and modeling of the relevant processes. Table 1.2-3 is intended to summarize the current understanding of flow and transport parameters and processes, and to provide pointers for each statement to the relevant section(s) of the PMR, where a more detailed discussion is given. This summary given here describes the aspects of the included FEPs (Section 1.2.3) that are believed to be important for UZ flow and transport processes. The specific titles used here are different than those in the formal FEPs database to allow for a more uniform and detailed discussion of the relevant FEPs. However, the content of all FEPs discussed below fall within the framework of the formal list of included FEPs. The statements listed under the column "Current Understanding" are a mixture of observations, hypotheses, and modeling insights and should only be considered as brief summary information. This column also includes alternative views to the current understanding that were either investigated in analyses or models, or previously proposed. A more detailed summary of the current understanding is given in Section 3.3 and in other sections identified in the table below.

Table 1.2-3. Summary of Current Understanding Used to Develop Conceptual and Numerical Models for UZ Flow and Transport at Yucca Mountain

Feature, Event or Process	Current Understanding	Section(s) Addressed
Climate/infiltration	Rainfall for the modern mean climate is about 190 mm/yr resulting in average steady-state net infiltration of 4.6 mm/yr.	3.5.1.8, 3.5.2.10
Climate/infiltration	After 600 years, the average rainfall is forecast to increase to about 300 mm/yr for monsoon climate; in response the average net infiltration is predicted to increase to 12.2 mm/yr.	3.5.1.8, 3.5.2.10

Table 1.2-3. Summary of Current Understanding Used to Develop Conceptual and Numerical Models for UZ Flow and Transport at Yucca Mountain

Feature, Event or Process	Current Understanding	Section(s) Addressed
Climate/infiltration	After 2,000 years, the average rainfall is predicted to increase to about 320 mm/yr for a glacial-transition climate; in response the average net infiltration is predicted to increase to 17.8 mm/yr.	3.5.1.8, 3.5.2.10
Infiltration	The net infiltration is episodic with a significant amount infiltrating only every few years.	3.3.2
Infiltration	There is large spatial variability of infiltration, with most water infiltrating on ridgetops and in the upper reaches of washes where there is little alluvial cover. Alternative View: Use of different models of groundwater/surface interaction results in different spatial distribution.	3.3.2, 3.5.2.5, Figures 3.5-4c, 3.5-5a and b 3.5.2.7
Flow through TCw	Flow through Tiva Canyon welded hydrogeologic unit (TCw) is episodic as controlled by infiltration.	3.3.3.1, 3.7.3.1
Flow through TCw	Fracture flow dominates in TCw.	3.3.3.1, 3.7.3.1
Flow through TCw	Fracture permeability of TCw is high ($\sim 10^{-11}$ to 10^{-10} m ²).	3.6.5.1, Figure 3.6-6
Flow through TCw	Water flow is transmitted rapidly through TCw.	3.3.3.1, 3.7.3.1
Flow through PTn	Flow through Paintbrush tuff nonwelded hydrogeologic unit (PTn) is primarily porous medium flow. Alternative View: Flow through the PTn is primarily fracture flow.	3.3.3.2, 3.7.3.1 3.3.3.2
Flow through PTn	The PTn consists of 5 to 10 bedded units with different degrees of welding and alterations and different hydrological properties.	3.2.2.2
Flow through PTn	The average matrix permeability of the PTn is about 10^{-13} m ² , with estimated variability of the major layers from 7×10^{-14} to 3×10^{-12} m ² .	3.6.5.1, Figure 3.6-6
Flow through PTn	Limited lateral flow occurs in the PTn. Alternative View: Significant lateral flow occurs in the PTn.	3.3.3.2, 3.7.3.1, 3.7.3.2 2.4, 3.3.3.2
Flow through PTn	Most of the fast flow through the PTn occurs via faults, and this represents only a very small fraction of the total flow. Alternative View: Fast flow through the PTn occurs via fractures and faults, and this represents a large fraction of the total flow.	3.3.7, 3.11.8 3.7.3.1
Flow through TSw	Episodic flow through Topopah Spring welded hydrogeologic unit (TSw) is damped by the PTn to the extent that flow can be considered steady-state when it enters the TSw. The exception is at or near major faults where episodic flow may still persist through the PTn. Alternative View: Episodic flow through the TSw is pervasive.	3.3.3.2, 3.3.3.3, 3.3.5, 3.3.6, 3.7.3.1, 3.7.3.2 3.7.3.1

Table 1.2-3. Summary of Current Understanding Used to Develop Conceptual and Numerical Models for UZ Flow and Transport at Yucca Mountain

Feature, Event or Process	Current Understanding	Section(s) Addressed
Flow through TSw	Fracture flow dominates in the TSw because this unit is densely welded and highly fractured; additionally, the low-permeability matrix is incapable of transmitting the percolation flux estimated to be moving through the unit.	3.3.3.3, 3.7.4.3
Flow through TSw	Fracture flow in the potential repository horizon, which intersects the Topopah Spring middle nonlithophysal, lower lithophysal and lower nonlithophysal stratigraphic units, is estimated to range from 84-94% of the total water flow for the three present-day climate scenarios. For the three scenarios of the two future climates, the percentage of fracture flow increases to 87%-96% of the total water flow.	3.7.4.2, 3.7.4.3
Flow through TSw	Water drainage in the potential repository units, Topopah Spring middle nonlithophysal, lower lithophysal and lower nonlithophysal stratigraphic units, is expected to be good due to the generally high fracture permeability ($\sim 10^{-11}$ to 10^{-10} m ²).	3.6.5.1, Figure 3.6-6
Flow through TSw	Current average percolation flux in the potential repository horizon is estimated to be about 5 mm/yr, with spatial variability between 0 and 60 mm/yr. Alternative View: Chloride data suggest that the percolation flux at the potential repository horizon is more uniform with values ranging from 1 to 10 mm/yr.	3.7.4.1, 3.7.4.2, 3.7.4.5 3.8.2, Figure 3.8-4
Flow through TSw	Long-term average percolation flux at the potential repository horizon, averaged over the last 1000 to 10,000 years, is estimated to be about 6 mm/yr based on calcite abundances, with a range of 2 to 20 mm/yr.	3.8.4.2
Flow through TSw	Evidence for fast/preferential flow is seen at the potential repository horizon, primarily near major faults. It is estimated that the fast component of flow is a less than a few percent of the total flow. Alternative View: Fast flow is the major component of the total flow.	2.2.3.3, 3.3.7, 3.8.3, 3.11.8
Perched water	Several perched water bodies have been found below the potential repository horizon, with the perching layer generally being the basal vitrophyre of the TSw or the zeolitic part of the Calico Hills nonwelded hydrogeologic unit (CHn).	3.3.3.4, 3.3.8, 3.7.3.3
Perched water	Perched water bodies formed due to permeability barriers (basal vitrophyre of the TSw or zeolitic portion of the CHn) and an absence of water-draining fractures. Alternative View: The perched water bodies in the northern region resulted from a historically elevated water table.	3.7.3.3 3.7.3.3
Perched water	The largest perched water body is found in the vicinity of borehole UZ-14, north of the potential repository region; this perched water body may be connected to those found in boreholes WT-24, SD-9 and SD-12. Alternative View: The perched water bodies found in the northern part of the potential repository region at boreholes UZ-14, WT-24, SD-9 and SD-12 are all disconnected.	3.7.3.3 3.7.3.3

Table 1.2-3. Summary of Current Understanding Used to Develop Conceptual and Numerical Models for UZ Flow and Transport at Yucca Mountain

Feature, Event or Process	Current Understanding	Section(s) Addressed
Perched water	A very small perched water body is found in the southern part of the potential repository region at borehole SD-7. This perched water body is expected to have little impact on the performance of the potential repository.	3.7.3.3
Perched water	The perched water bodies contain a mixture of Pleistocene and Holocene water, with average ages ranging from 3,500 to 11,000 years old.	2.2.3.3, 3.3.3.3, 3.8.3, 3.10.3.4
Perched water	Infiltration rates needed to form perched water bodies are higher than present-day values	3.8.2, 3.8.3
Perched water	The minute fractions of bomb-pulse ^{36}Cl and tritium in perched water suggest that the fast flow fraction over the last 50 years is very small.	3.8.3
Flow through CHn	The CHn consists of unaltered vitric zones, primarily in the south, and altered zeolitic zones, primarily in the north. Water flow through the zeolitic units is primarily fracture flow, but mostly or all matrix flow through the vitric units.	3.7.3.3, 3.3.3.4
Flow through CHn	Lateral flow in perched water bodies toward faults and other major permeable features causes partial bypassing of the low permeability zeolitic units of the CHn. Alternative View: Flow from the perched water bodies is primarily vertical through the zeolitic CHn, partly through fractures and partly through the low permeability matrix.	3.7.3.2, 3.7.3.3 3.7.3.3
Flow through CHn	Water entering the CHn vitric unit from the TSw transitions from discrete fracture flow to heterogeneous matrix flow	3.11.4
Perched water	Perched water is formed when percolation flux exceeds the capacity of the geologic media to transmit vertical flux through underlying low-permeability units. Water may either flow through the units, or laterally to major faults or other vertical conduits for flow. Alternative View: Perched water bodies are primarily formed by water infiltrating in the Solitario Canyon area flowing vertically downward until the water encounters low permeability units, such as the basal vitrophyre of the TSw, and then flows laterally to form the observed perched water bodies.	3.7.3.2, 3.7.3.3 3.7.3.3, 3.7.4.7
Flow through faults	Fault properties are variable, and generally controlled by rock type and stratigraphic displacement.	3.2.3, 3.3.5
Flow through faults	Faulting enhances fracturing in the fault zones contributing to increased permeability. Permeability in the TCw and TSw fault zone is $6 \text{ to } 9 \times 10^{-11} \text{ m}^2$. In the PTn fault zone it is $\sim 2 \times 10^{-11} \text{ m}^2$.	3.7.3.2, 3.6.5.1
Flow through faults	Faults are high permeability features through the CHn and Crater Flat undifferentiated hydrogeologic unit (CFu), provide a fast flow path from the TSw to the water table, and allow discharge from perched water bodies. Alternative View: Alteration of faulted rocks in the CHn and CFu causes them to be of low permeability, slowing travel time from the TSw to the water table.	3.3.5 3.3.5
Seepage	Open emplacement drifts act as capillary barriers, impeding water from seeping into the drifts and diverting some fraction of the prevailing	3.3.9, 3.9.1, 3.9.9, 3.9.3.5

Table 1.2-3. Summary of Current Understanding Used to Develop Conceptual and Numerical Models for UZ Flow and Transport at Yucca Mountain

Feature, Event or Process	Current Understanding	Section(s) Addressed
	percolation flux around the drifts. Alternative View: 1) Seepage is governed by local heterogeneity and ponding probability. 2) Weep-type flow will be unaffected by the presence of the drift.	3.9.8.2
Seepage	A critical percolation flux (seepage threshold) exists below which no seepage occurs. The distribution of seepage thresholds depends on the hydrological characteristics and variability of the unit, especially the fracture permeability and the van Genuchten alpha values.	3.9.3.5
Seepage	Seepage flux is always smaller than the percolation flux as a result of partial flow diversion around the drift. Alternative View: Seepage flux is equal to percolation flux.	3.9.1, 3.9.6.1 3.9.6.1
Seepage	Ventilation reduces seepage of liquid water. Neglecting ventilation effects in seepage models is conservative. Alternative View: Neglecting ventilation may not be conservative, because ventilation increases vapor flow, which may condense in the drift.	3.9.3.3 3.9.3.3
Seepage	Seepage percentages are expected to be similar for all potential repository units because permeability and capillary strength are inversely related, canceling their respective effects on seepage.	3.9.6.2
UZ transport	The main geological units below the potential repository expected to retard selected radionuclides are the Calico Hills vitric units, and the Prow Pass unit (in certain areas).	3.11.4
UZ transport	A small fraction of the expected nuclear waste inventory consists of radionuclides that are soluble in water and non-sorbing. These include iodine, technetium and others; they are not retarded as they migrate through the UZ.	Table 3.11-1, 3.11.5, 3.11.6
UZ transport	The bulk of the expected nuclear waste inventory consists of radionuclides that have very low solubility in water, and commonly have large sorption capacity in the UZ rocks. These radionuclides, including plutonium and others, will migrate very slowly through the UZ and do not contribute significantly to dose for tens of thousands of years. Alternative View: Discrete flow along fast paths from the repository to the water table will bypass the majority of the sorbing capacity and contribute to dose soon after release.	3.11.5, 3.11.6 3.11.9.1
UZ transport	The UZ contributes to the retardation of several important radionuclides that are rather soluble in water, including neptunium, strontium and others. For most radionuclides the sorptivity of the CHn zeolitic rocks is the highest, followed by CHn vitric and TSw.	Table 3.11-1, 3.11.4

Table 1.2-3. Summary of Current Understanding Used to Develop Conceptual and Numerical Models for UZ Flow and Transport at Yucca Mountain

Feature, Event or Process	Current Understanding	Section(s) Addressed
UZ transport	<p>The retardation processes are matrix diffusion and sorption in the rock matrix. Sorption in the fractures is not considered because of limited data and conservative nature of the assumption.</p> <p>Alternative View:</p> <p>Matrix diffusion is not effective in retarding radionuclides.</p>	<p>3.11.2.4, 3.11.2.5</p> <p>3.11.9.1</p>
UZ transport	<p>The most efficient retardation of radionuclides is found in the CHn vitric unit, which behaves as a porous medium. In spite of its large sorption potential, the low matrix permeability of the CHn zeolitic rock, causes water flow through fractures, thus limiting the amount of radionuclide sorption.</p> <p>Thermal alteration of zeolites was excluded as an alternative view because mountain-scale TH modeling indicates that temperatures in the zeolites will not exceed 70°C (CRWMS M&O 2000, U0105, Section 6.8.2.1).</p>	3.11.4, 3.11.5, 3.11.6
UZ transport	Significant colloidal transport may occur for radionuclides such as plutonium, americium, and others. Colloidal transport is believed to be most critical and important in the fracture-dominated flow. Furthermore, the larger size colloids pose the greatest threat for rapid transport as they cannot diffuse into the adjacent matrix.	3.3.11, 3.11.2.7, 3.11.3.5, 3.11.7, 3.11.9.2
Coupled processes	The heat released by the emplaced waste will have an important impact on water flow around the drifts in the potential repository, seepage into drifts, and the chemistry of water and gases entering the drifts.	3.3.12, 3.10.2, 3.12.1
Coupled processes	The heat released by the emplaced waste will increase wall temperatures of the drift to boiling conditions of approximately 97°C; some localized drifts in low percolation flux areas may completely boil off all fracture water and consequently reach higher peak temperatures (generally below 120°C).	3.12.3.1
Coupled processes	Peak temperature conditions in the drift walls will be reached after about 500 years, but closer to 1,000 years in the mid-pillars.	3.12.3.1, Figure 3.12.7
Coupled processes	Peak temperatures in the mid-pillars will reach 85 to 90°C depending upon the location and the prevailing percolation flux. Water saturation in the entire pillar will decline significantly primarily due to boiling near the drifts, and capillary suction further away.	3.12.3.1, 3.12.3.2, 3.12.3.3, Figure 3.12.7
Coupled processes	The extent of the maximum boiling zone around the drifts is estimated to be on the order of 10 m in all directions from the drifts. No significant water accumulation is found above or below the drifts.	3.12.3
Coupled processes	The water that may seep into the drifts will be near neutral in pH and mostly reflect the chemical composition of condensate waters mixed with infiltration waters at elevated temperatures. The predicted pH is about 7.2 to 9.0.	3.10.5.4
Coupled processes	Gas is mostly expected to flow away from drifts due to gas pressure gradients induced by increased temperatures. In specific locations, and at certain times during the thermal load period, the CO ₂ concentration in the gas phase may increase to about 10 % (~ 100 times ambient concentrations).	3.10.5.3, Figure 3, 10-8

Table 1.2-3. Summary of Current Understanding Used to Develop Conceptual and Numerical Models for UZ Flow and Transport at Yucca Mountain

Feature, Event or Process	Current Understanding	Section(s) Addressed
Coupled processes	Thermal-hydrological-chemical processes resulting in precipitation and dissolution of minerals will not significantly alter important fracture and matrix hydrological properties.	3.10.5.5
	Alternative View: Thermal-hydrological-chemical processes resulting in precipitation and dissolution of minerals significantly alter important fracture and matrix hydrological properties.	3.10.7, 3.10.9
Coupled processes	The thermal-hydrological processes will affect percolation fluxes and seepage in a beneficial way. No seepage will occur into any of the emplacement drifts for the bulk of the first 1,000 years after emplacement. A small spike in the percolation flux will occur, which will then quickly drop to the ambient system flux. After that, the percolation fluxes will slowly reach those of the ambient system.	3.12.3.3
Coupled processes	Excavation of the emplacement drifts will increase fracture permeability around the drifts up to two orders of magnitude due to mechanical stress release.	2.2.2, 2.2.2.2
Coupled processes	The coupled processes due to heat released from the emplaced waste will have insignificant effects on radionuclide transport through the UZ.	3.3.12.1
	Alternative View: The changing flow patterns around drifts will have significant effects on radionuclide transport in the UZ.	3.11

1.3 QA STATUS OF DATA AND SOFTWARE

Pursuant to evaluations (CRWMS M&O 1999a, 1999b, Wemheuer 1999) performed in accordance with QAP-2-0, *Conduct of Activities* (now superseded by AP-2.16Q, *Activity Evaluation*), it was determined that activities supporting development of the UZ PMR, its component models, and their documentation are quality-affecting activities subject to the quality assurance (QA) requirements of the *Quality Assurance Requirements and Description* (DOE 2000). The UZ PMR was produced by the Civilian Radioactive Waste Management System (CRWMS) Management and Operating (M&O) Contractor in accordance with the CRWMS M&O quality assurance program, using Office of Civilian Radioactive Waste Management (OCRWM) Administrative Procedures (APs) identified in the Development Plan for the UZ Flow and Transport PMR (CRWMS M&O 2000a).

The UZ PMR was prepared in accordance with AP-3.11Q, *Technical Reports*, the Development Plan for the UZ PMR (CRWMS M&O 2000a), and the *Work Package Planning Summary for UZ Flow and Transport Process Model Report FY00* (CRWMS M&O 1999c). It was reviewed at LBNL in accordance with YMP-LBNL-QIP-6.1, *Document Review*, prior to checking and review per AP-3.11Q and AP-2.14Q, *Review of Technical Products*, respectively. The electronic management of data complied with procedural requirements identified in the Development Plan (CRWMS M&O 2000a). The QA procedures under which the supporting Analysis/Model

Reports (AMR) were developed are identified in the respective AMRs and associated planning documents. The AMRs were prepared in accordance with AP-3.10Q, *Analyses and Models*.

This document may be affected by technical product input information that requires confirmation. Any changes to the document that may occur as a result of completing the confirmation activities will be reflected in subsequent revisions. The status of the input information quality may be confirmed by review of the Document Input Reference System (DIRS) database. The QA status of technical inputs to this PMR and the supporting AMRs are provided in the DIRS. The DIRS database is updated to indicate changes to the QA status of these data.

1.3.1 Acquired and Developed Data

The acquired data used in the development of the UZ AMRs are discussed in Attachment I.

The QA status of the acquired and developed data supporting the UZ PMR is provided in the DIRS Database for each of the AMRs supporting the UZ PMR. These data reside in the Technical Data Management System (TDMS) and are tracked by Data Tracking Numbers (DTNs). Their status is further classified depending on whether or not the data are relied upon to support a principal factor for the postclosure safety case. For the UZ PMR, there are two principal factors—"Seepage into drifts" and "Retardation of radionuclide migration in the unsaturated zone" (Section 1.2.2). These are discussed in Section 1.2.2 and listed in Table 1.2-1. These principal factors will be the focus of postclosure safety considerations for the SR and LA decision-making process, and therefore data supporting these principal factors require confirmation of their QA status. Approximately fifty data sets have been identified as relied upon to support the two principal factors for the UZ. These data sets are being confirmed in accordance with AP-3.15Q, *Managing Technical Inputs*.

The DTNs for the figures and tables in this document are listed separately in Attachment II. The QA status of these data can also be found in the DIRS Database.

1.3.2 Software

The software codes used in the AMRs that support the UZ PMR and their version number, and software tracking number, are listed in Table 1.3-1. These codes were managed in accordance with AP-SI.1Q, *Software Management*, or used under Section 5.11 of AP-SI.1Q. All software codes and routines are listed in the supporting AMRs. In the following subsections, the primary software codes used in the development of the models supporting the UZ PMR are discussed.

1.3.2.1 TOUGH2

TOUGH2 (Transport Of Unsaturated Groundwater and Heat) is an integral finite difference numerical simulator for nonisothermal flow of multi-component, multiphase fluids in porous and fractured media. It is used for numerical simulation of unsaturated and saturated flow, under both isothermal (constant temperature) and nonisothermal (variable temperature) conditions.

When considering flow in fractured porous media, a key issue is how to evaluate the interface area for fluid exchange between the matrix and fracture continua. The preferred method now

employed in TOUGH2 is the active fracture model (see Section 3.3.4). It was developed to describe gravity-dominated, nonequilibrium, preferential liquid flow in fractures, which is expected to be similar to flow fingering in unsaturated porous media. In this model, the fractures contributing to liquid flow are referred to as “active fractures.”

1.3.2.2 iTOUGH2

iTOUGH2 provides forward and inverse modeling capabilities for the numerical simulator TOUGH2. All TOUGH2 input parameters can be considered unknown or uncertain. The parameters are estimated based on any type of observation for which a corresponding TOUGH2 output is available, including prior information about the parameters to be estimated. One of the key features of iTOUGH2 is its extensive error analysis, which provides statistical information about residuals, estimation uncertainties, and the ability to discriminate among model alternatives.

The key elements of iTOUGH2 are (1) a simulation program to model flow and transport in the hydrogeologic system (“forward modeling”), (2) the objective function, which measures the misfit between the model output and the data, (3) the minimization algorithm, which reduces the objective function by automatically updating parameter values, and (4) the error analysis, which allows one to judge the accuracy of the estimates.

1.3.2.3 TOUGHREACT

TOUGHREACT is a numerical code designed to simulate coupled thermal-hydrological-chemical processes. It was developed for the Drift Scale Test and Single Heater Test, to simulate boiling conditions and fracture-matrix interactions (diffusion and advection of aqueous and gaseous species across fracture-matrix interfaces). The core of TOUGHREACT is the EOS3 module of the TOUGH2 code which solves the equations for the flow of water, air, and heat under nonisothermal and variably saturated conditions.

In TOUGHREACT, a transport module and a geochemical speciation module are sequentially coupled to the TOUGH2 module. The transport module solves for transport of dissolved species in water and transport of gases such as CO₂ and O₂ in a “carrier” gas phase consisting of H₂O and air. Transport of the latter two gas phases is computed by the TOUGH2 module. The geochemical module incorporated in TOUGHREACT simultaneously solves a set of chemical mass-action and mass-balance equations under equilibrium and/or kinetic conditions to compute the extent of reaction and mass transfer between a set of given aqueous species, minerals, and gases at each gridblock of the flow model.

1.3.2.4 Transport Codes

EOS9nT

EOS9nT is a TOUGH2 module for simulating flow and transport of an arbitrary number (n) of tracers (solutes and/or colloids) in the subsurface. The module first solves Richards’ equation, which describes saturated or unsaturated water flow in subsurface formations, and obtains the flow regime. A second set of transport equations, corresponding to the n tracers/colloids, is then solved sequentially. The very low concentrations of the tracers are considered to have no effect

on the density of the liquid phase, thus allowing the decoupling of transport from the flow equations.

The tracer transport equations account for sorption, radioactive decay, advection, hydrodynamic dispersion, molecular diffusion, filtration (for colloids only), first-order chemical reactions, and colloid-facilitated tracer transport. A total of $n-1$ daughter products of radioactive decay or of a chemical reaction chain can be tracked. EOS9nT can handle gridblocks of irregular geometry in 3-D domains and offers the option of a Laplace space formulation of the transport equations (in addition to conventional time-stepping) after the flow field becomes time-invariant. The Laplace transform formulation eliminates the need for time discretization and the problems stemming from the treatment of the time derivatives in the transport equations, and it yields solutions semi-analytical in time. This allows an unlimited time step size without loss of accuracy.

T2R3D

T2R3D has been developed to handle transport of sorbing and nonsorbing tracers in fractured media. A special module of T2R3D has been created for efficient simulation of radionuclide transport in porous media, in which the transport process is decoupled from fluid and heat flow. This module can be used when flow fields are established or reached steady state. The mass balance equation for the tracer/radionuclide component solved in this case is exactly the same as that of the coupled case. However, flow fields needed for calculating tracer or radionuclide transport are treated as input parameters, determined by a previous EOS9 or EOS3 flow simulation under the same boundary condition(s). This option provides substantial savings in both execution times and storage requirement for large problems of flow and transport in fractured rock. The coupled version of T2R3D as well as the decoupled version are both modified for implementation of a new computational scheme for handling the dispersion tensor.

FEHM

FEHM (Finite Element Heat and Mass Transfer) calculates hydrological flow and the transport of radionuclides, the latter by a particle-tracking algorithm. The particle-tracking method in FEHM views the computational domain as an interconnected network of fluid storage volumes. The two steps in the particle-tracking approach for steady-state flow fields are: (1) determine the time a particle spends in a cell, and (2) determine which cell the particle travels to next. The domain can consist of a single-continuum or dual-continua (e.g., fracture plus matrix) representation of the flow field. FEHM can be used to model transport breakthrough times in porous and fractured media.

DCPT

DCPT (Dual Continuum Particle Tracker) is a particle-tracking code used for modeling transport in dual-continuum media, such as fractured porous media. It receives as input the flow field calculated by another code, such as TOUGH2, and a grid developed by a mesh generator, such as WinGridder. It simulates transport by particle-tracking incorporating advection, dispersion, and linear sorption. Dispersion can be expressed as a tensor. The grid may be an irregular 3-D grid.

WinGridder

WinGridder is a Windows-based grid-generating software program that generates 1-D, 2-D, or 3-D grids for numerical modeling of flow and transport problems based on the integral finite difference method. For a given geological model and engineering-structure information, this software can be used to design, generate, and visualize discrete 1-D, 2-D, or 3-D grids for numerical modeling of flow and transport problems. The generated grid can be designed to describe special geological and engineering features (e.g., inclined faults, potential repository horizons). The major output file contains all the data required for the TOUGH2 input file MESH. WinGridder also allows users to produce other ASCII and EPS output files as well as hard copies of grid figures, for inspection or other purposes.

Table 1.3-1. Software for UZ Flow and Transport Model and Abstractions for TSPA-SR

Software Name/Version	Software Tracking Number	Short Description	Used in AMR(s) Supporting PMR Section
AMESH V1.0	10045-1.0-00	Generates numerical grids used for modeling drift-scale processes	3.9
DCPT V1.0	10078-1.0-00	Transport modeling with particle tracking	3.11
EARTHVISION V4.0	30035-2 V4.0	Graphical display in 3-D	3.4, 3.7
EOS9nT (TOUGH2 V1.11 Module EOS9nT V1.0)	10065-1.11MEOS9NTV1.0-00	EOS for TOUGH2 with tracers and colloids for transport modeling	3.11
EXT V1.0	10047-1.0-00	Extracts data from TOUGH2 for visual display	3.7, 3.9
FEHM V2.00	10031-2.00-00	Flow and transport modeling with particle tracking	3.11
FEHM V2.10	10086-2.10-00	Flow and transport modeling with particle tracking (new)	3.11
FRACL V1.0	10191-1.0-00	Semi-analytical solution for transport in heterogeneous fractured media	3.11
GSLIB V1.0 Module GAMV2 V1.201	10087-1.0MGAMV2V1.201-00	Analyzes spatial correlation of 2-D data	3.9
GSLIB V1.0 Module SISIM V1.203	10001-1.0MSISIMV1.203-00	Generates 3-D spatially correlated fields	3.9
GSLIB V2.0 Module SISIM V2.0	10098-2.0MSISIMV2.0-00	Generates 3-D spatially correlated fields	3.9
INFIL V2.0	10127-2.0-00	Calculates field water balance and net infiltration	3.5
INFIL2GRID V1.6	10077-1.6-00	Maps infiltration onto grids for simulating flow and transport	3.6, 3.7, 3.8
ITOUGH2 V3.2	10054-3.2-00	Inverse calculations for TOUGH2	3.6

Software Name/Version	Software Tracking Number	Short Description	Used in AMR(s) Supporting PMR Section
iTOUGH2 V3.2_DRIFT	10055-3.2_DRIFT-00	Inverse calculations for TOUGH2 (for drift calculations)	3.9
iTOUGH2 V4.0	10003-4.0-00	Inverse calculations for TOUGH2 with additional features	3.9
LAGRIT V1.0	10212-1.0-00	Developing grid for Busted Butte	3.11
LHS V2.50	10205-2.50-00	Monte Carlo simulation using Latin Hypercube Sampling	3.5
SOLVEQ/CHILLER V1.0	10057-1.0-00	SOLVEQ calculates species, CHILLER simulates equilibria	3.10
STO-UNSAT V1.0	10292-1.0-00	Stochastic method simulations for Busted Butte	3.11
SUPCRT92 V1.0	10058-1.0-00	Calculation of thermodynamic properties to 500 MPa, 1,000°C	3.10
T2R3D V1.4	10006-1.4-00	Transport modeling with active fracture concept	3.7, 3.11
TOUGH2 V1.3	10061-1.3-00	TOUGH2 with fracture-matrix interaction and enhancements	2.3
TOUGH2 V1.4	10007-1.4-01	TOUGH2 with active fracture concept and further upgrades	3.7, 3.8, 3.11
TOUGHREACT V2.2	10154-2.2-00	TOUGH2 with reactive transport chemistry	3.8, 3.10
TOUGHREACTE9 V1.0	10153-1.0-00	EOS9 for TOUGHREACT	3.8
WinGridder V1.0	10024-1.0-00	Interactive mesh generator for TOUGH2 family	3.4

1.4 RELATIONSHIP TO OTHER PROCESS MODEL REPORTS AND KEY PROJECT DOCUMENTS

Figure 1-1 shows the relationship between the UZ PMR and other key project documents; this relationship is also briefly described in the beginning of this chapter. The UZ PMR uses directly the geological framework, mineralogical and rock properties information from the ISM PMR. The UZ PMR is also closely connected to three other PMRs, the Near-Field Environment (NFE), Engineered Barrier System (EBS) and Saturated Zone (SZ) Flow and Transport PMRs through analysis performed in TSPA. The NFE models describe the evolving thermodynamic conditions near the emplacement drift using fine-grid, drift-scale, coupled process models. The EBS models in TSPA utilize information on water seepage and chemistry as well as gas chemistry from models provided to TSPA from the UZ PMR and the NFE PMR. Finally, the models developed within the UZ PMR provide temporal and spatial distributions of water recharge and radionuclide concentrations at the water table to the flow and transport models developed within the SZ PMR. All of these interfaces and data flows occur in the TSPA and not within the individual PMRs.

The specifications for the reference repository design used in the development of the UZ PMR and its supporting AMRs were from design input transmittals (CRWMS M&O 1999e; CRWMS M&O 1999f). These designs were based on the technical requirements baseline of Enhanced Design Alternative II (Wilkins and Heath 1999; CRWMS M&O 2000, EBS PMR, Section 2.5). Since that time, a number of modifications to the repository design have been under consideration. For example, backfill is no longer part of the design (Stroupe 2000) and the final design may extend the northern boundary of the repository approximately 600 meters. These design changes were not issued when the analysis and modeling work for the UZ was being performed and therefore could not be incorporated into the UZ AMRs. Evaluation of the impact of all of these design changes may require modification of models and additional simulations. The impact of these, or any, design changes will have to be evaluated once all of the design changes are finalized. The impact of excluding backfill is briefly discussed qualitatively at the end of Section 3.10.2.1.

2. EVOLUTION OF THE UZ SITE CHARACTERIZATION PROGRAM – DATA COLLECTION AND MODEL DEVELOPMENT SUPPORTING THE UZ PMR

This chapter summarizes the evolution of data-collection activities and the development of models for the unsaturated zone (UZ) of Yucca Mountain. The testing and modeling activities are used to characterize the site, evaluate the processes, and assess the viability of Yucca Mountain as a site for a potential nuclear waste repository. This chapter also summarizes issues identified by overseeing bodies, peer review groups, and other parties. The Department of Energy (DOE) Yucca Mountain Site Characterization Project (YMP) has evaluated the Yucca Mountain site for over two decades. The data-collection activities have evolved from intensive surface-based investigations in the early 1980s to the current focus on testing in underground drifts. The models have evolved from early conceptual descriptions of the site to current numerical model representations at relevant site- and drift-scales. The Yucca Mountain site investigations have contributed to the improved scientific understanding of UZ processes, and have benefited from studies at other analog sites and from the technical developments in the earth science disciplines.

Section 2.1 presents the chronology of the site characterization activities and a summary of the main characteristics of the Yucca Mountain site. Section 2.2 describes the specific activities associated with geological mapping, hydrological studies, geochemical samplings, and thermal testing activities. Information used as corroborative evidence obtained from analog studies is summarized in Section 2.3. The site-specific data, together with scientific and technical knowledge associated with flow and transport at analog sites and UZ studies, form the basis for the Yucca Mountain UZ model formulation, calibration, and validation. The evolution of the UZ models is summarized in Section 2.4. UZ flow and transport issues raised by peer review groups and panels, Nuclear Regulatory Commission (NRC), and Nuclear Waste Technical Review Board (NWTRB), and in the TSPA-VA, PA Workshop and UZ Model Workshop are presented in Section 2.5. The overview presented in this section provides some background and context for the detailed discussion of the current UZ models and analyses in Section 3. Any inferred conclusions in this section will be substantiated in detailed analyses in Section 3 or in cited Analysis/Model Reports (AMRs).

2.1 UZ CHARACTERIZATION PROGRAM AT YUCCA MOUNTAIN

This section summarizes the development of the site characterization program in Section 2.1.1, presents the chronology of the site characterization activities in Section 2.1.2, discusses some specific process issues for the UZ in Section 2.1.3, and summarizes characteristics, boreholes and underground facilities at the Yucca Mountain site in Section 2.1.4.

As a site for a potential nuclear waste repository, Yucca Mountain is considered to have the favorable hydrogeological characteristics: (1) a desert setting with arid climate and (2) a deep water table with a thick UZ. In a desert environment, the total amount of available water is small. The potential UZ repository will be designed to complement the hydrological environment of limited water flux by further diverting the small flow of water that does occur away from the wastes emplaced between the ground surface and the deep water table. Multiple natural barriers and engineered barriers are expected to contribute to limiting the contact between water and waste packages, and retarding radionuclide migration.

2.1.1 Development and Documentation of the Site Characterization Program

The concept of emplacing nuclear waste in the UZ in the arid region in and around the Nevada Test Site (NTS) was first proposed by the U.S. Geological Survey (USGS) (McKelvey 1976; Winograd 1981, pp. 1457–1464). DOE selected Yucca Mountain, near the southwest corner of NTS, for detailed study and extensive surface-based drilling and investigations in the 1980s. The Nuclear Waste Policy Act of 1982 was amended in 1987 to focus the U.S. effort on the Yucca Mountain site. A *Site Characterization Plan* (SCP) was completed in 1988 for systematic surface-based investigations, underground testing, laboratory studies, and modeling activities (DOE 1988). The *in situ* field testing was planned to be conducted in boreholes and in an underground tunnel, the Exploratory Studies Facility (ESF).

The *Yucca Mountain Site Description* (YMSD, CRWMS M&O 1998a through 1998f) summarizes the results of the site characterization program up to 1998. The *Viability Assessment of a Repository at Yucca Mountain* (VA, DOE 1998, Section 3.1) applies the available data to (and discusses the uncertainties in) a total system performance assessment (TSPA). This UZ Process Model Report (PMR), together with eight other PMRs and associated AMRs, is being developed to support the TSPA for Site Recommendation (SR) and Licensing Application (LA) with traceable and verifiable data. The VA (DOE 1998, p. 2–5) and the repository safety strategy (CRWMS M&O 2000b, p. 3–2) identify four attributes for safe disposal: limited water contact with waste packages, long waste-package lifetime, low rate of radionuclide release from breached waste packages, and reduction of radionuclide concentration during transport. Seepage into drifts and the reduction in radionuclide concentration by matrix diffusion and sorption in the UZ are two principal factors evaluated by this UZ PMR for assessment of the potential repository performance and safety.

2.1.2 Chronology of Drilling/Excavation, Testing, and Modeling

The evolution of the UZ site characterization activities in (1) drilling/excavation, (2) testing, and (3) modeling are summarized in Figure 2.1-1. The activities in Figure 2.1-1 are discussed throughout Section 2 of this PMR. Figure 2.1-2 illustrates the locations of the main deep surface-based boreholes and the underground ESF drifts in the vicinity of the potential repository block at Yucca Mountain.

The evolution of the drilling/excavation, testing, and modeling activities are closely coupled in the site characterization program. In the following discussion, the focus of each category of activities is described in terms of four distinct periods: (1) the early 1980s, (2) the period from 1986 to 1991, (3) the early 1990s, and (4) the current period (mid-1990s to the present). Specific references to technical advances and highlights of testing and modeling activities are not cited here; further details follow this discussion of the chronology of the site characterization program.

(1) *Drilling/Excavation.* To characterize the site and to conduct *in situ* testing, extensive borehole drilling and excavation have been conducted at Yucca Mountain to characterize the tuff layers and structures and to access the potential repository underground environment. During the first period, the drilling of boreholes from the land surface was the main focus of activity. The second period was devoted to the development of characterization plans, including the formulation of the quality assurance (QA) programs. The design of the original shaft access for

the ESF in the SCP (DOE 1988) was revised to adopt ramp access by the end of this period. The third period launched the specific design, preparation, and excavation of the ESF for underground access to the rock units surrounding the potential repository emplacement drifts. Borehole drilling was resumed over the site for UZ hydro-chemical investigations and along the North Ramp of the ESF for design and geotechnical evaluations. During the current period, the excavation of the main loop of the ESF and the Cross Drift was completed, alcoves and niches were excavated, and boreholes were drilled for enhanced characterization of the repository block (ECRB).

(2) *Testing.* Surface-based investigations and underground tests have been conducted to characterize and to evaluate the suitability of the site for a potential repository. The surface-based reconnaissance era of the first period collected most of the data used to establish the geological framework of Yucca Mountain. During the near-surface monitoring era of the second period, intensive laboratory measurements of flow and transport parameters were conducted. In the deep-borehole testing era in the third period, collections of samples for hydrological and geochemical characterization (especially for ^{36}Cl and calcite studies) were intensified and networks of boreholes were instrumented for pneumatic and moisture monitoring. As the project has matured, it has identified key scientific studies that are required to increase the understanding of hydrologic and transport processes. In the current underground testing era, the main focus of testing activities is on the UZ processes that control seepage into the drifts, heat transfer around the drifts, and transport through the UZ. Section 2.2 describes the data collection activities.

(3) *Modeling.* The scientific studies have included testing and modeling for a range of processes and for a range of scales. The conceptual models for Yucca Mountain site were formulated in the early 1980s. The heat transfer and thermal-hydrological (TH) modeling methodologies were established in the late 1980s. During the third period, the integration of site data into models was initiated and the basic probabilistic approach for TSPA was improved. In the current period, the calibration, validation, and integration of UZ process models and the direct inputs to TSPA models were conducted. The process models include UZ site scale flow and transport models, drift-scale seepage models, and coupled models for various combination of thermal, hydrological, mechanical, and chemical processes in site and in drift scales. The integration of UZ modeling with testing and the interaction of UZ process models with TSPA models illustrate how scientific methods have worked for the evaluation of UZ flow and transport at Yucca Mountain. Section 2.4 describes the evolution of the modeling activities.

2.1.3 Stimulating Issues for the UZ

The basic issues of limited water flow to the potential repository horizon and retarded radionuclide transport through the UZ were formulated in the early 1980s and were assessed consistently for over two decades. In the course of site characterization of this unique system, new concepts and hypotheses were developed and controversial issues were evaluated and resolved (or uncertainties addressed). The topics of focus within the site characterization program evolved dynamically, especially in the early period before the SCP. The stimulating topics in the 1980s include the origins of near-surface caliches, the possibility of water table rise under conditions of wet climates and seismic events, and the potential benefit of a hot potential repository with high temperatures induced by concentrated waste-loading. The topics of focus in the 1990s include the detection of bomb-pulse signals from chloride-36 (^{36}Cl) measurements in

borehole and ESF samples, the estimation of higher percolation fluxes than previously modeled, and the field observation of seepage thresholds that may limit the water flux into drifts. Currently, the YMP also places more emphasis on the potential benefit of the engineered barrier system (EBS) with drip shield and/or backfill protecting the waste packages, and with ventilation and wide-drift spacing maintaining the temperature of most of the water in the potential repository rock below its boiling point.

These topics are related to issues associated with keeping the water away from the waste packages and reducing the radionuclide concentration that could reach the accessible environment. The UZ processes and mechanisms addressing these and related topics are discussed in sections of this chapter on the evolution of the UZ site characterization program and in sections of Chapter 3 on UZ flow and transport models. A brief summary of relevant sections for the topics evolved in the site characterization program is given below.

The origin of near-surface caliches and the potential for water-table rise are discussed in Section 2.2.1. The possibility of upward movement of water from the deep water table was evaluated extensively in the 1980s.

The possibility of keeping water out of the vicinity of waste packages by boiling it away motivated the hot repository concept, as discussed in Section 2.2.4.1 on TH modeling. The drift-scale thermal-hydrological-chemical (THC) processes induced by the heat released by emplaced wastes are discussed in Section 3.10.

The detection of ^{36}Cl bomb-pulse signals stimulated the evaluation of fast flow paths, as discussed in Section 2.2.3. Since the water flows through the UZ in the matrix and in the fractures, most of the hydrological tests and geochemical studies discussed in Sections 2.2.2 and 2.2.3 are related to the quantification of the partitioning of total flux between fracture flow component and matrix flow component.

Over the site scale, percolation-flux magnitude and distribution are evaluated and updated as more site characterization data are collected. The evolution of percolation-flux estimate from low to high values is discussed in Section 2.4. The diversion of infiltrating water to steeply dipping and near-vertical faults above the potential repository horizon can reduce the percolation flux reaching the potential emplacement drifts. The perching of water and the diversion of percolation flux to faults at tuff unit interfaces below the repository horizon can affect the effectiveness of zeolites and clays for radionuclide retardation.

In the drift scale, the seepage into drifts can be a fraction of percolation, as discussed in Section 2.2.2.2 on tests conducted at the potential repository horizon. The capillary forces arising from unsaturated conditions can prevent water from entering waste emplacement drifts. If the percolation flux is less than a seepage threshold, no seepage into drifts occurs. The seepage models and analyses are discussed in Section 3.9.

To protect waste packages further from seepage into drifts, engineered barriers with drip shields and/or backfill are being evaluated. The performance of engineered barriers is closely related to the amount of water available to contact the waste packages.

In addition to seepage from the ceiling, lateral influx through the walls may also contribute to the water available in the drifts. Some of the tests discussed in Section 2.2.2.2 evaluate the lateral flows at tuff unit interfaces. Perching at the tuff interface can enhance the potential of lateral flow and lateral seepage for drifts intercepted by tuff unit interfaces. The drainage below the drifts is another important process for fluid to move away from the waste packages and transport through the UZ. The monitoring of water migration is discussed in Section 2.2.2.2.

One of the more recent topics addressed by the site characterization program is on the benefits of keeping the water in tuff rocks surrounding the waste emplacement drifts from boiling, with wide drift spacing to allow bulk of flow moves through the pillars and with long-term ventilation to remove heat from the emplaced wastes. The TH analyses of multiple drifts are presented in Section 3.12.

The topics listed in this section are subsets of issues for the UZ addressed in the site characterization program. Most of these topics are also identified by overseeing bodies, peer review groups, and other interested parties, as discussed in Section 2.5.

2.1.4 Yucca Mountain Boreholes and ESF Drifts

This section describes the surface-based boreholes and the ESF drifts. A summary of the Yucca Mountain site characteristics is also presented.

Over two hundred vertical boreholes have been drilled from the surface for the YMP. These boreholes are referred to as surface-based boreholes. The first YMP borehole was drilled in 1978. Over one-fourth of the surface-based boreholes are over 300 m deep, with 80% of deep boreholes drilled in the early 1980s and 20% drilled in the 1990s. Most of the early boreholes penetrating the entire UZ were drilled away from the potential repository block along nearby washes. The geological (G) series, hydrological (H) series, water table (WT) series, and unsaturated zone (UZ) series of boreholes were all initiated in the late 1970s or early 1980s. (Additional official prefixes UE25 for boreholes located within the NTS and USW for boreholes outside the NTS boundary are omitted in this section.)

The early deep boreholes are used to define the stratigraphy, to locate the water table, to collect cores, and to test *in situ* borehole monitoring techniques. The main tuff units in the UZ at Yucca Mountain are the Tiva Canyon welded hydrogeologic unit (TCw), the Paintbrush nonwelded hydrogeologic unit (PTn), the Topopah Spring welded hydrogeologic unit (TSw), and the Calico Hills nonwelded hydrogeologic unit (CHn). The nomenclature of hydrogeologic units is adapted from Montazer and Wilson (1984, pp. 9–19) and explained in Section 3.2 of this PMR.

Nearly one hundred shallow boreholes were drilled with depths less than 100 m for near-surface infiltration studies, with three-quarters of the infiltration boreholes drilled in the early 1980s and the remainder in the early 1990s. The infiltration study collected water-content profile data for over ten years and provided input data to the UZ flow and transport models at the upper UZ boundary.

The construction of the starter tunnel for the ESF was initiated in 1992. Construction of the ESF was supported by additional surface-based boreholes drilled along the North Ramp (NRG series of boreholes) and along the Main Drift for systematic drilling (SD series of boreholes) in the

potential repository block. Pneumatic and moisture monitoring sensors were installed in most of the boreholes in the NRG and SD series, together with selected boreholes in the UZ series. Figure 2.1-2 includes the main deep boreholes in the vicinity of the Yucca Mountain potential repository block. A borehole drilled by the Nye County (borehole ONC-1) was also instrumented with sensors for monitoring.

The 8 km long, 8 m diameter ESF main loop was excavated with a Tunnel Boring Machine (TBM) from 1994 to 1997. The 2.7 km long, 5 m diameter ECRB Cross Drift was excavated with a smaller TBM in 1997 and 1998. Underground testing, calcite and ^{36}Cl sampling, and moisture monitoring studies were initiated during the ESF North Ramp excavation in 1995, intensified in 1998, and continued to the present time.

The ESF is the largest effort of the site characterization program and provides direct underground access to the upper tuff units. Yucca Mountain is a flat-topped ridge running 10 km from north to south and rising approximately 300 m above the adjacent valleys. With the ridge-top and underlying tuff layers gently tilted to the east, the middle of the UZ can be accessed by nearly horizontal ramps of the ESF from the base of the eastern slopes. The ESF ramps penetrate TCw, PTn, and the upper lithophysal zone of TSw.

The primary potential repository block is located between the north-south trending ESF Main Drift and Solitario Canyon to the west. The Main Drift is at the depth of the potential repository. Most of the Main Drift is located in the middle nonlithophysal zone of TSw (Tptpmn, the stratigraphic nomenclature of Buesch et al. 1996, pp. 5–8, labeled as tpmn in figures of this section). During and after the construction of the ESF, seven alcoves and four niches were excavated along the ESF for *in situ* testing and monitoring of UZ processes, as illustrated in Figure 2.1-3.

Photographs and schematic illustrations of the test sites are presented in Section 2.2. The ESF tests include air-injection tests in all alcoves (including Alcove 2 for the Bow Ridge fault and Alcove 6 for the Ghost Dance fault) and niches, the infiltration test at Alcove 1, the fault-damping test at Alcove 4, the Single Heater Test (SHT) and Drift-Scale Test (DST) at Alcove 5, seepage tests at Niches 3650, 3107, and 4788, the fracture-matrix interaction test at Alcove 6, and moisture monitoring in sealed Niche 3566, in sealed Alcove 7, and along open (ventilated) tunnel segments.

Figure 2.1-4 illustrates the stratigraphic units penetrated by the ECRB Cross Drift and the locations of two test sites (Alcove 8 and Niche 1620) under excavation for testing of seepage. The ECRB Cross Drift provides underground access to the lower lithophysal and lower nonlithophysal tuff zones of TSw (tpll and tpIn in Figure 2.1-4) respectively, and to the Solitario Canyon fault. Approximately 10% of the potential repository area is located in the middle nonlithophysal zone of TSw, 78% in the lower lithophysal zone, and 12% in the lower nonlithophysal zone.

Figure 2.1-4b also illustrates that PTn and the upper lithophysal zone (tpul in Figure 2.1-4) of TSw are exposed on the steep outcrop below the crest of Yucca Mountain on the Solitario Canyon wall. Some of the lower tuff units can be seen at outcrops of other more remote ridges to the east and to the southeast of Yucca Mountain. At one of these locations, Fran Ridge, the

fractures of middle nonlithophysal zone of TSw were mapped, and an above ground thermal test was conducted in a block carved from the outcrop of middle nonlithophysal zone of TSw (the large block test or LBT). At Busted Butte, the vitric CHn is exposed. A test facility was excavated for UZ transport testing at Busted Butte. (A photograph presented in Figure 2.2-12 in Section 2.2 illustrates the locations of Fran Ridge and Busted Butte relative to the Yucca Mountain ridge.) The deeper units, including the zeolitic CHn, can only be accessed by the available deep boreholes.

2.2 DATA COLLECTION AND *IN SITU* FIELD TESTING

This section describes the evolution of activities for geological data collection in Section 2.2.1, the hydrological testing and data collection in Section 2.2.2, the geochemical data collection in Section 2.2.3, and the thermal testing in Section 2.2.4. The surface-based data collection activities have evolved from surface surveys, trench studies, and infiltration studies with shallow boreholes, to testing and monitoring of deeper boreholes. The underground data collection activities have evolved from sampling and testing in short horizontal and slanted boreholes to seepage, thermal, and transport testing in niches, alcoves, and test beds.

2.2.1 Geological Reconnaissance and Data Collection

The stability of the geological structures and spatial distribution of the tuff units and faults were the focus of early geological studies. This section focuses on the UZ, delineated by the upper ground surface and the deep water table.

The stability of the geological environment is one of the early issues addressed in the study of Yucca Mountain. The tuff units from TCw to TSw were formed 12.7 to 12.8 million years (Ma) ago by eruptions from volcanic vents associated with calderas to the north. The Yucca Mountain landform has changed little since its formation. The erosion in the Yucca Mountain region generally has proceeded slowly. The modern landforms of ridges and valleys had been established 11.6 Ma ago when the Rainier Mesa tuff was deposited (Sawyer et al. 1994, pp. 1304–1318). Most of the surface deposits are alluvium in the washes and valleys. Only rock rubbles and a very thin to nonexistent veneer of colluvium cover the bedrock ridges and slopes. Near-surface carbonate deposits (caliche) extend to shallow depths as fracture fillings. Evidence from trench studies indicates that the caliche deposits are pedogenic in origin, related to the formation of soil under arid and semi-arid climates. In the pedogenic process, downward infiltrating rainwater dissolves carbonate minerals at the surface and reprecipitates them at shallow depth as a result of evapotranspiration. The speculation that caliche forms from seismic pumping from the water table has not been substantiated (Stuckless et al. 1991, pp. 551–554; CRWMS M&O 1998d, Section 3.4.3.4.2).

The bedrock of Yucca Mountain is mainly in the fractured TCw hydrogeological unit. The bedrock is incised by a series of east-to-southeast-trending stream channels. In the north, the ridge is cut by northwest-to-southeast trending washes associated with faults. The early geological mapping of Yucca Mountain by Scott and Bonk (1984) was updated and refined by Day et al. (1998) to include additional small faults on the surface (e.g., the Sundance fault in the potential repository block, Spengler et al. 1994, pp. 9–11; Potter et al. 1999, pp. 1–15). The fracture patterns in the bedrock were also mapped in pavement studies (with thin soil covers

removed) and in shallow-pit studies of fractures exposed on the walls. Mapping and sampling data along transects, especially along washes and valleys, together with regional geophysical surveys were used to construct early stratigraphic and structural models for Yucca Mountain.

The stratigraphic description of the tuff units were refined with coring, mapping, and geophysical logging data from surface-based boreholes, and confirmed by data collected in the underground drifts. The division of tuff units into members, zones, and subzones is based on variations in degree of welding (compaction and fusion at high temperatures), abundance of lithophysae (cavities formed by bubbles of volcanic gases trapped in the tuff matrix during cooling), depositional features, crystal content, mineral composition, pumice and rock fragment abundance, and fracture characteristics (Moyer et al. 1996, pp. 7–79; Buesch et al. 1996, pp. 4–16) (see Section 3.2 of this PMR). Detailed line surveys and full peripheral mapping of fracture networks were conducted along the ESF drifts (Barr et al. 1996, pp. 133–135; Albin et al. 1997, pp. 161–163; see data sources listed in Appendix I of this PMR). New features were mapped, including the observations of an intensely fractured zone in the southern part of the ESF Main Drift (Buesch and Spengler 1998, p. 19) and several new faults in the western part of the ECRB Cross Drift (see data sources listed in Appendix I of this PMR). The geologic mapping and geophysical studies conducted on the surface and in the ESF are summarized in Figure 2.2-1.

The water table defines the lower boundary of the UZ. The water table at Yucca Mountain is approximately 500 to 750 m below the ground surface. A large hydraulic gradient just north of the potential repository area was inferred from the relatively high water tables observed in three boreholes north of the Pagany Wash (Luckey et al. 1996, pp. 21–37; CRWMS M&O 2000, U0000, Section 4.1). Alternative hypotheses have been proposed to interpret the large gradient, involving either the de-coupling of the northern aquifer system from the southern aquifer system or the existence of perched water bodies (Ervin et al. 1994, pp. 5–12; Czarniecki et al. 1994, pp. 249–250; 1995, pp. 191–192). The other issue associated with the water table is its potential rise in response to wetter climates or to seismic events. Analyses of the mineral alternations indicate that the highest water rise of the ancient water table was less than 120 m above the current water table.

The results of the geological data collection for Yucca Mountain are summarized in the YMSD (CRWMS M&O 1998d, Section 3), incorporated in the Geologic Framework Model (GFM)/Integrated Site Model (ISM) (CRWMS M&O 1997a and CRWMS M&O 2000, ISM PMR), and used in developing the numerical grid for the UZ Model (CRWMS M&O 2000, U0000, Sections 6.5, 6.6, 6.7; see Section 3.2 of this PMR).

2.2.2 Hydrological Testing and Data Collection

YMP hydrological testing and data collection evaluate climate/infiltration, percolation, seepage, and migration. The net infiltration into the tuff layers is a small fraction of the precipitation at the ground surface and represents the inflow to the UZ model at the upper boundary. The percolation process redistributes the infiltration, determines the fluxes throughout the UZ and at the potential repository horizon, and provides the source of recharge to the saturated zone below the potential repository. Diversions to the boundary faults (steeply dipping to near vertical faults at the boundaries of the potential repository block) reduce the percolation flux through the potential repository block from the net infiltration value. The seepage process determines the fraction of

percolation dripping or seeping into the drifts. Seepage into drifts occurs at the interface between the natural geological barriers of the UZ and engineered barriers within the drift. As such, seepage depends not only on rock characteristics, but also on the drift opening size and shape, as well as excavation-induced perturbations in the vicinity of the drift. Water drainage through the drift floor and radionuclide transport through the UZ constitutes the migration process.

The climate/infiltration studies were initiated in the mid-1980s. The percolation studies were intensified in the 1990s with more data collected and finer models developed, as discussed in Section 2.4 of this PMR. The seepage tests and moisture monitoring in the ESF were conducted in the late 1990s. The transport test at Busted Butte is summarized in Section 2.2.3 and the thermal tests in the ESF are summarized in Section 2.2.4. Before discussing the thermal and transport tests and modeling, the following sections focus on hydrological testing and monitoring activities. Section 2.2.2.1 is on the surface-based investigations and hydrological property measurements. Section 2.2.2.2 is on the underground testing and monitoring of drift seepage, fracture-matrix interaction, fault flow, large-scale infiltration and seepage tests, air-permeability tests and potential monitoring.

2.2.2.1 Surface-Based Investigations and Hydrological Property Measurements

Modern climate data have been collected in and around the Yucca Mountain site since 1988. The climate at Yucca Mountain is arid. On average, Yucca Mountain receives about 190 mm of rain and snow per year; nearly all the precipitation (about 95 percent) is either run-off or lost to evaporation (Hevesi et al. 1994, pp. 2520–2529). The climate study also evaluates the long-term records of analog sites, e.g., calcite dating data from Devils Hole (Winograd et al. 1992, pp. 255–260), and microfossil records from Owens Lake (Forester et al. 1999). Geological information indicates that the regional climate has changed over the past million years and that long-term average precipitation is somewhat greater than modern conditions. Future climate scenarios use available climate data from wetter analog sites in western states (CRWMS M&O 1998a, Section 4.3; USGS 2000, U0005, Section 6.6; see Section 3.5 of this PMR).

The infiltration study at Yucca Mountain was initiated in 1984. To date, the infiltration study has used nearly 100 shallow boreholes across washes and on the crest to measure the changes in water-content profiles in response to precipitation and snow-melt events (Flint and Flint 1995; USGS 2000, U0010, Sections 6.3 and 7.1; see Section 3.5 of this PMR). Weekly or monthly measurements were collected from 1984 through 1995. The Pagany Wash and three other washes were instrumented for run-on and run-off measurements. Water-balance calculations from precipitation, evapotranspiration, run-on, and run-off along washes are used to derive the net infiltration flux values over the ridge top, side slopes, and stream channels. Areas with exposed bedrock and no soil cover have a different infiltration flux compared to areas with soil covers that have substantial storage capacity for excess water. Figure 2.2-2 provides a summary of the surface infiltration studies performed. The net infiltration distributions for different climate states over the bedrock are used as upper boundary conditions for the UZ Flow and Transport Model and TSPA models.

The collection and processing of drill cores began with the surface-based borehole program. The characteristic curves of water content (saturation times porosity) as a function of water potential, together with permeability, porosity, and rock densities, were measured in the laboratory on

samples and cores collected from bedrock transects, surface-based boreholes, and alcove, drift, and niche boreholes in the ESF. The laboratory measurements indicate that the matrix of the PTn and CHnv units have high-enough permeabilities to conduct net infiltration, while the TCw, TSw, and CHn (zeolitic) units have low matrix permeabilities that could promote a larger fracture flow component. The laboratory techniques for tuff samples have evolved from the adoption of established soil-testing methods (e.g., submerged pressure cell, chilled-mirror psychrometer, transient diffusivity measurements) to the use of an ultracentrifuge for relative permeability measurements. The matrix properties of thousands of samples are used to define hydrogeological units (Flint 1998, pp. 3–4; CRWMS M&O 2000, U0090, Section 6.2; see Sections 3.2 and 3.6 of this PMR). Soil properties were also measured to support geotechnical evaluation of the near surface, especially during the ESF preparation period.

The surface-based borehole testing program in the early 1980s included the instrumentation of the first UZ borehole, UZ-1, in the Drill Hole Wash (Montazer 1987, pp. 31–42) and the measurement of pneumatic signals in a pair of boreholes, UZ-6 and UZ-6a, on the crest near the Solitario Canyon cliff (Weeks 1987, pp. 165–170). Eight deep boreholes were instrumented in the 1990s for extensive testing and monitoring. This program included the measurement of barometric pressures in sealed borehole intervals or in the borehole annulus with an inflatable borehole sealing system (Rousseau et al. 1999, pp. 55–122). The pneumatic data (damping and lag of barometric signals) were used to derive the effective parameters for the PTn unit and the properties of the Ghost Dance fault (CRWMS M&O 2000, U0035, Sections 6.1, 6.2, 6.3). Air permeability was measured along four surface-based boreholes with straddle packers (LeCain 1997, pp. 9–23). *In situ* moisture potentials and temperatures were also measured in sealed borehole intervals. The data sets obtained through the surface-based borehole testing program, specifically pneumatic signals between boreholes, core saturation data from laboratory measurements, and *in situ* moisture potential profiles, were used to calibrate the Flow Model for the UZ and determine the effective fracture-flow component of the total flow through the hydrogeological units (CRWMS M&O 2000, U0050, Section 6.6; see Sections 3.6 and 3.7 of this PMR).

The partitioning of total flux between fracture flow component and matrix flow component is one of the most important processes to determine in the UZ flow field. Percolation or UZ flow distribution determines the amount of water that could potentially contact the waste packages and other components of the Engineered Barrier System (EBS). The magnitude of percolation flux and its distribution between the fractures and matrix are predicted by the UZ Flow and Transport Model based on calibration against all available data. Early estimates of percolation flux were based on the assumption of matrix-dominated flow that was calibrated by saturation profile data alone (see Section 2.4 of this PMR on early percolation flux estimates of < 1 mm/yr). Subsequent investigations have shown that the welded tuff matrix has low permeability and that therefore matrix flow is a small fraction of the percolation flux in the TCw and TSw units. Currently, the estimates of percolation flux range from 1 to 10 mm/yr. These higher values result from the inclusion of temperature, age-dating, and geochemical data together with pneumatic and hydrological data. The additional field data that indicate higher values of percolation flux include the prevailing low geothermal gradient associated with convective heat transfer, the relatively young water found at depth, and the low concentration of dissolved salts in pore water and in perched water bodies. The evolution of the percolation flux estimate dramatically illustrates its

close coupling with the evolution of data-collection activities in the UZ site characterization program (see Sections 3.6 and 3.7 of this PMR).

Perched water information is one of the most important pieces of hydrological data for UZ site-scale model calibration. While most of the tuff units are unsaturated, perched water bodies exist in the north below the potential repository horizon and in the south in the vicinity of the Ghost Dance fault. Perched water bodies (i.e., localized zones that are fully water-saturated) can occur either above a low-permeability barrier or above a capillary barrier. Perched water bodies have been encountered in boreholes at both the vitrophyre between the TSw and CHn units and at the vitric-zeolitic interface (CHnv-CHnz) within the CHn unit. Pumping tests were conducted to evaluate the spatial extent of the perched water bodies, and water samples were collected for age dating. When water perches at tilted interfaces, lateral redistribution of percolation flux can occur. The absence of perched water bodies at the boundaries of the PTn unit and the presence of perched water bodies at interfaces within the CHn unit suggest that lateral redistribution is relatively ineffective above the potential repository horizon, but significant below. The process of lateral diversion by the CHn interfaces and the mechanism of mixing within the perched water bodies greatly affect radionuclide transport in terms of both the retardation potential of the CHn and the capacity for dilution within the UZ (see Sections 3.3.8, 3.7 and 3.11 of this PMR).

2.2.2.2 Underground Testing and Monitoring

The ESF provides direct access to the UZ environment. The locations of the alcoves and niches for underground studies were shown previously in Figure 2.1-3. The underground studies have evolved rapidly through three stages as they develop new emphases and different approaches. For the first stage during the North Ramp excavation period, methodologies developed and deployed in surface-based borehole testing were applied to the underground ESF. Four alcoves were excavated in the first part of the ESF North Ramp to provide access to specific features and hydrogeological units. Alcove 1 provides access to the upper TCw unit, Alcove 2 to the Bow Ridge fault, Alcove 3 to the upper PTn contact, and Alcove 4 to the lower PTn contact. These alcoves were largely used in the mid-1990s as drill bays for horizontal and slanted boreholes to collect cores, measure air permeability, and sample gases (LeCain 1998, pp. 12–28; Rousseau et al. 1999, pp. 55–122). In the second stage, three alcoves were excavated along the Main Drift. Alcove 5 was dedicated to thermal testing. Alcoves 6 and 7 were designed to measure the properties of the Ghost Dance fault located to the east of the Main Drift. The thermal tests are discussed in Section 2.2.4 and Section 3.10 of this PMR.

In the third stage, four niches (Niches 3566, 3650, 3107, and 4788—niches are short drifts, typically 10 m long) were excavated along the ESF Main Drift in the northwest direction into the potential repository block to test the drift seepage processes. Two test beds with slot undercuts were constructed in Alcoves 4 and 6 to conduct fracture-matrix and fault-matrix interaction tests. Alcove 1 was instrumented with seepage collectors and wall sensors for a large-scale infiltration and seepage test. The tests in these sites have one feature in common: the use of water and aqueous phase tracers to directly evaluate hydrological processes. This is a drastic departure from the previous approach in UZ testing, where the concerns about contamination and perturbation of the ambient unsaturated states discouraged the use of water in surface-based drilling and testing. The change in approach arises from the fact that it is much easier to control water releases and quantify water movement in the underground (ESF) environment compared to

injection into deep boreholes. In addition, while boreholes could be drilled dry, the use of construction water to control dust during TBM excavation already perturbed the ambient saturation state. Evaluating the migration of the construction water itself provided useful site data. This was done by coring below the ESF and by monitoring below the ECRB Cross Drift, at the starter tunnel of the Cross Drift and at the crossover point (where the Cross Drift passes ~20 m over the ESF Main Drift) (CRWMS M&O 2000, U0015, Section 6.9).

The underground testing and monitoring activities are discussed in the following four sections, with Section 2.2.2.2.1 on drift seepage tests and moisture monitoring, Section 2.2.2.2.2 on fracture-matrix interaction and fault flow tests, Section 2.2.2.2.3 on large-scale infiltration and seepage tests, and Section 2.2.2.2.4 on air-permeability tests and potential monitoring.

2.2.2.2.1 Drift Seepage Tests and Moisture Monitoring

A number of drift seepage studies are the current focus of underground ESF testing. The seepage tests were motivated by the observed absence of continuous seepage in the ESF drifts following their excavation. The capillary barrier mechanism may explain the lack of seepage in underground drifts in the UZ. Under unsaturated conditions, capillary forces can hold the water within the rock mass. For seepage or dripping into a drift opening to occur, the percolation flux must be greater than the seepage threshold. Above the seepage threshold, the local accumulation of water is large enough to overcome capillarity. The absence of seeping water in the ESF may indicate that the prevailing percolation flux, on the order of 10 mm/yr (CRWMS M&O 2000, U0050, Section 6.6), may not be large enough to break the capillary barrier (see Section 3.9 of this PMR).

Seepage tests involve the release of liquid water above the niche ceiling and collection of seeps if they occur. Niche seepage tests are designed to evaluate the capillary barrier mechanism and to quantify seepage and the seepage threshold. Aqueous dye tracer are released as pulses above the niche ceiling to represent episodic percolation events, as illustrated in Figure 2.2-3 for the seepage tests at Niche 3650. Tracers used in the seepage tests are sampled to evaluate the spatial distribution of flow paths. The seepage flow paths indicated by the presence of dyes on the niche ceilings are associated with transient wetting-front movement through the fractures. The seepage threshold data and the wetting-front movement data are used to derive characteristic curves for the fractures for *in situ* conditions. The seepage threshold for releases at a given borehole interval is determined by a series of tests with decreasing flow rates until no seep occurs. The wetting-front arrival at the niche ceiling is determined by visual or video observations. Available seepage test data and seepage calibration model results indicate that the seepage threshold could be larger than the percolation flux for releases above the niche ceiling (CRWMS M&O 2000, U0015; Section 6.2; CRWMS M&O 2000, U0080, Section 6.6; see Section 3.9 of this PMR).

Ventilation, needed for underground operations and construction activities, may also explain the lack of observed seepage. Ventilation can remove a large amount of moisture, dry the rock behind the drift walls, and suppress seepage. Ventilation is also being considered as an important component in potential repository design to remove heat during the thermal periods. The concept of constructing niches along the ESF Main Drift was originally motivated by the need to isolate a drift-size opening with a bulkhead from the ventilation in the Main Drift. The niches were excavated by an Alpine Miner, a mechanical device (shown in Figure 2.2-5) with no water

spreading upward at the cutter head into the ceiling. Drift seepage tests at Niche 3107 near the crossover point and at Niche 4788 in the intensely fractured zone are conducted behind bulkheads and under high humidity conditions.

With dry excavation, it is possible to observe flow paths visually. In the dry excavation of Niche 3566 in the vicinity of the Sundance fault, a damp feature was observed in 1997, as illustrated in Figure 2.2-4. The 0.3 m wide by over 3 m long, nearly vertical feature dried up before the bulkhead could be installed. The full rewetting of this feature was not observed after over two years of bulkhead closure at this niche site. Figure 2.2-4 also illustrates that the Sundance fault is one of several faults and features with bomb-pulse signals detected by $^{36}\text{Cl}/\text{Cl}$ measurements along the ESF. The $^{36}\text{Cl}/\text{Cl}$ measurements are further discussed in Section 2.2.3.3.

In addition to the niches, two additional drift-sealing studies are ongoing. The first study is at Alcove 7 in an over 100 m long segment intersecting the Ghost Dance fault. The second study is in the second half of the ECRB Cross Drift for a 1,000 m scale segment that intersects the Solitario Canyon fault. Both sealing studies deploy double bulkheads for better isolation from ventilation. No continuous seeps have been observed so far in either of these two long drift segments.

Most of the potential repository area is located in the lower lithophysal zone of TSw (tp11 in Figure 2.1-4). The lower lithophysal tuff is more permeable than the middle nonlithophysal tuff, the fractures are shorter, and large lithophysal cavities are pervasive. Figures 2.2-5c and d show an example of a large lithophysal cavity in the lower lithophysal tuff and a borehole image of lithophysal cavities intersected by a borehole for the test site of Niche 1620 in the ECRB Cross Drift. Figure 2.2-5 also summarizes the objective and results of the seepage testing in this niche. The presence of lithophysal cavities makes packer installation and test setup in the lower lithophysal zone more challenging than in the middle nonlithophysal zone.

The larger permeability of the lower lithophysal tuff may enhance the capillary barrier effect, i.e. reduce seepage, either by the presence of permeable fractures that can divert flow around the drift opening, or by higher porosity in the matrix rock that can absorb more water. Geological mapping along the Cross Drift indicates that the lower lithophysal zone is very heterogeneous. The effects of spatial heterogeneity on pneumatic and seepage characteristics are evaluated by systematic hydrological testing along the Cross Drift, using slanted boreholes drilled into the crown of the drift ceiling.

2.2.2.2.2 Fracture-Matrix Interaction and Fault Flow Tests

Two tests were conducted to evaluate the contribution of the rock matrix to overall flow and tracer transport. If the contact time between the water flowing along fractures or faults and the unsaturated matrix is long, water can imbibe into the matrix. Fracture-matrix interaction refers to the flow of water from the fracture to the matrix. While the results of the niche seepage tests for episodic flow conditions are adequately analyzed with fracture parameters alone, analysis of the long-term tests requires the quantification of fracture-matrix interaction.

The dominance of fracture flow and the dependence of the fraction of flow occurring through the fractures on the total flux magnitude were evaluated in a test bed in Alcove 6, as illustrated in

Figure 2.2-6. The slot below the test bed was used to collect the fast fracture flow component. The amount of water imbibed into the welded tuff matrix was estimated from mass balance of the water injected and collected. A series of tests were conducted over time periods longer than the episodic releases in the niche tests, and with larger volumes of traced water. The approach to steady-state outflow occurred in irregular steps, which reflect the intrinsic instability of the flow field. The fracture flow fractions have an oscillatory dependence on injection rates, ranging from 60% to 80% for this test bed in the TSw middle nonlithophysal unit for large flow rates (Figure 2.2-6).

The first fault test with liquid water in the ESF was conducted at Alcove 4. (The Bow Ridge fault and Ghost Dance fault were characterized by air injection tests before the Alcove 4 liquid test.) The same mass-balance approach used in Alcove 6, with a slot for recovery of the outflow, was adopted. The Alcove 4 test bed includes a small fault and the PTn layers, as illustrated schematically in Figure 2.2-7c and in the photograph in Figure 2.2-7b. Figure 2.2-7 also summarizes the testing performed in Alcove 4. In contrast to the TSw unit occurring in Alcove 6 and in the niches, the matrix of the PTn unit has a large capacity to absorb water and to dampen the flow pulses along the fault. The data in Figure 2.2-7 show a slow decline in water intake rates with time. One hypothesis to explain the slow decline is the possible swelling of the PTn argillic layers and subsequent reduction of fault permeability. With sequential wetting, the wetting front moves faster, with more water introduced into the flow system. These preliminary findings help determine the behavior of flow through the PTn layers.

2.2.2.2.3 Large-Scale Infiltration and Seepage Tests

The first of two large-scale infiltration and seepage tests is located in Alcove 1 near the North Portal and is illustrated in Figure 2.2-8. In this test, a drip irrigation system on the outcrop directly above Alcove 1 is used to simulate large infiltration events associated with the El Niño conditions of high precipitation. The test results have shown that matrix diffusion is important in diluting the tracer concentration and reducing the tracer breakthrough times in the TCw unit.

At the location where the ECRB Cross Drift crosses over the ESF Main Drift, the migration of construction water from the excavation of the Cross Drift was monitored below at the Main Drift near Niche 3107, as illustrated in Figure 2.2-9. No seepage was observed when the Tunnel Boring Machine passed over the Main Drift. A new Alcove 8 has been excavated in the Cross Drift for controlled liquid-release tests directly above the Niche 3107 which is instrumented for seepage detection. The test bed includes the interface between the upper lithophysal zone and the middle nonlithophysal zone of the TSw unit. The test results can be used to understand large-scale flow and seepage processes across a tuff layer interface at the potential repository horizon.

2.2.2.2.4 Air-Permeability Tests and Potential Monitoring

Air-injection tests with multiple packers were conducted at all hydrological test sites to measure the air permeability and characterize the formation heterogeneity. With fast responses and a benign impact on the rock mass, air-injection tests are an effective method for site characterization. Air-permeability profiles were used for selecting liquid test intervals. Repeated air-injection tests were conducted before and after niche excavation to quantify the excavation-

induced permeability changes (Wang and Elsworth 1999, pp. 751–757; CRWMS M&O 2000, U0015, Section 6.1).

Air-injection testing is one of many examples where methods deployed in surface-based testing programs are successfully adopted, improved, and enhanced for underground studies. Other examples include neutron logging used for infiltration studies in the ESF boreholes to measure saturation changes associated with drying, heat-dissipation probes and psychrometers in boreholes used to monitor water-potential along drifts and into the walls, and relative humidity sensors from meteorological studies used to monitor the effects of ventilation on moisture monitoring. These methods, together with extensive mapping and sampling, enable the confirmation and verification of many site attributes, the improved evaluation of drift-scale processes, and the definition and quantification of interactions between natural barriers and engineered barriers.

2.2.3 Geochemical Data Collection

Geochemical and solute transport studies include major laboratory components to analyze samples collected in the field. Geochemical data collection is closely associated with hydrological data collection, especially with regard to the rock and water sample collection activities in recent years. The early efforts involved samples collected from surface mapping and analyses of drill-cuttings and cores of the rock samples (collected in the surface-based boreholes) to establish the mineralogic character of the tuff units. With the ESF access in the mid-1990s, sampling focused in the ESF drifts to elucidate the distributions of calcite, ^{36}Cl , and fracture fillings.

2.2.3.1 Mineral and Solubility Measurements

The mineral and petrologic studies identified the locations of altered zones, especially the presence of zeolites in the CHn units below the TSw potential repository units. The spatial distributions of vitric CHn (CHnv) and zeolitic CHn (CHnz), along with the characterization of the vitrophyre sublayer between the TSw and CHn units, are important for understanding the distribution of perched water bodies and determining potential flow paths for radionuclides.

The solubility and retardation factors of weakly sorbing radionuclides were measured extensively in the laboratory. Most of the UZ geochemical and transport property measurements performed in the laboratory used water from the well J-13 in the saturated zone (CRWMS M&O 2000, U0100). Dissolution and rock-water interaction parameters are determined in batch experiments with tuff fragments mixed with water. Column experiments are also conducted to determine various transport parameters. The transport test results form the basis of the minimum sorption coefficient approach used in radionuclide transport calculations.

2.2.3.2 Geochemical Measurements

In the boreholes and along the ESF drifts, samples have been collected for geochemical and isotopic measurements. Pore water is used for chemical analyses and age dating. The techniques to collect pore water from tight matrix evolved from mechanical squeeze (tri-axial compression) to ultracentrifuge spin. The total dissolved solids and chloride contents are mainly measured in nonwelded tuff samples that generally can yield sufficient amounts of water for chemical

analyses (Yang et al. 1998, pp. 6–7). Relatively high concentrations of dissolved-solid contents are used to indicate low infiltration fluxes. The total chloride distributions, especially along the ECRB Cross Drift, are shown to be an important data set for determining the percolation flux distribution (see Section 3.7 of this PMR).

The chemical composition and carbon dioxide concentrations are measured in pore-water samples to elucidate the saturation states, to determine the origin of pedogenic calcite and amorphous silica, and to measure the evolution of inorganic carbonate concentrations. Ion-exchange reactions along the flow paths generally cause an increase in the cation abundances in deep tuff units. Deviation from the general trend of geochemical evolution with depth may provide information about the effects of faults and other structural features. The calcite and opal studies along fracture surfaces (Paces et al. 1998b, pp. 36–39) and within lithophysal cavities (CRWMS M&O 2000, U0085, Section 6.5; see Section 3.9 of this PMR) are used to evaluate the alternation of flow paths and seepage into cavities, averaged over millions of years. Strontium participates in ion-exchange with zeolites, and concentrations may be significantly depleted in the CHnz unit (Sonnenthal and Bodvarsson 1999, pp. 143–147; see Section 3.8 of this PMR). Examples of geochemical studies of tuff samples are illustrated in Figure 2.2-10.

2.2.3.3 Isotopic Measurements

The environmental isotope data are used to infer the presence of fast flows from the ground surface into and through the UZ. High $^{36}\text{Cl}/\text{Cl}$ ratios well above background levels are related to global fallout from thermonuclear tests in the Pacific Ocean. The presence of greater-than-background concentrations of bomb-pulse ^{36}Cl therefore suggests travel times from the ground surface of 50 years or less. The ^{36}Cl signals, first observed in infiltration boreholes and later in the ESF at faults and other features, have received great attention and continue to be evaluated (Fabryka-Martin et al. 1993, pp. 58–68; CRWMS M&O 2000, U0085, Section 6.6). The $^{36}\text{Cl}/\text{Cl}$ data along the ESF are presented in Figure 2.2-4 in Section 2.2.2.2.1. Additional boreholes were recently drilled in the ESF around the Sundance fault and the Drillhole Wash fault for verification of the bomb pulse signals.

Other environmental isotope data are also collected. Bomb-pulse tritium (^3H) concentrations are also present at several locations at depth, associated with both liquid and pneumatic flow paths. The carbon-14 (^{14}C) age of the gas phase increases with depth in borehole UZ-1, with less obvious trends in other boreholes. The deuterium (^2H) and oxygen-18 (^{18}O) data reflect climatic conditions at time of groundwater recharge. Based on the analysis of these two isotopes, pore water in the CHn unit with lighter isotopic compositions is inferred to originate either during winter precipitation or during a time of colder climate. Perched water appears to be up to 11,000 years old, based on ^{14}C and ^{36}Cl ages. The perched water does not appear to have equilibrated with matrix water, based on major constituent concentrations and uranium isotope data (Paces et al. 1998a, pp. 185–188; CRWMS M&O 2000, U0085, Section 6.6). Examples of isotopic studies of tuff samples are illustrated in Figure 2.2-11.

2.2.3.4 UZ Transport Tests

Retardation of radionuclides can reduce the concentrations along the flow paths. Transport processes through the CHnv unit are currently under investigation at the Busted Butte

underground facility. This facility consists of a drift complex excavated 70 m below the ground surface. Tracer-injection tests, partial mine-out, and geophysical measurements (ground-penetrating radar, electric-resistivity tomography, neutron logging) were performed to map solute migration patterns, as illustrated in Figure 2.2-12. The available test results from the ongoing tests are documented in CRWMS M&O (2000, U0100, Section 6.8) (see Section 3.11 of this PMR).

The Phase 1A results indicated that the transport through the CHnv unit could be dominated by capillary-driven flow, with a well-defined plume developed following tracer injection (see Section 3.11). The plumes from the ongoing larger-scale Phase 2 test are tracked by sorbing pads in monitoring boreholes and by geophysical imaging techniques. Examples of a fluorescent plume photograph from Phase 1A test and a ground-penetrating radar tomograph from Phase 2 are illustrated in Figure 2.2-12. The results of transport tests with sorbing tracers that represent the sorbing radionuclides will indicate whether or not laboratory-measured retardation factors can be used to predict field-scale transport processes.

2.2.4 Thermal Testing

Thermal tests evaluate thermally induced effects on flow and transport. The thermal test is different from hydrological and geochemical tests that evaluate ambient conditions and UZ processes intrinsic to the system (see model discussion in Section 2.4). The waste heat represents an external perturbation to the system subjected to design and control. This section starts with a brief summary of the influence of modeling results on the design of thermal testing and waste loading in Section 2.2.4.1. The tests outside and inside the ESF are summarized in Sections 2.2.4.2 and 2.2.4.3, respectively.

2.2.4.1 Thermal-Hydrological Modeling

Early multiphase studies identified the importance of heat-pipe effects on TH conditions near the heaters. The heat pipe refers to the counter-flow mechanism with vapor flowing in one direction and liquid flowing in the opposite direction. The heat-pipe phenomenon is associated with regions under boiling conditions where the temperature is maintained at the nominal boiling point (approximately 97°C at Yucca Mountain). This can occur if sufficient liquid can be transported back toward the heat source to sustain the boiling (Pruess et al. 1990a, pp. 1235–1248).

After the rock becomes dry, temperature is determined by a heat-conduction mechanism and the thermal power of the heat source. The temperature can reach hundreds of degrees Celsius, if the heat load is high. If the heat load of the waste packages is high enough to keep the liquid away from the waste packages, it should in principle improve their performance (Buscheck and Nitao 1992, pp. 1003–1017; 1993, pp. 418–448).

The hot and dry potential repository concept has been a motivating factor in waste loading designs. YMP has designed large waste packages to contain multiple spent fuel assemblies. The large waste packaging with high thermal outputs is developed for drift-emplacement, as opposed to borehole-emplacement, as the basis for waste loading. With planar heat sources (used in early models) to represent a closely spaced drift configuration, large condensate zones are predicted

(Buscheck and Nitao 1992, pp. 1003–1017), with drainage occurring through shedding away from the high temperature regions, outside the boiling zones.

2.2.4.2 Thermal Characterization and Pre-ESF Testing

Concurrent with the thermal-modeling studies, the thermal properties of potential repository rock samples have been measured in the laboratory (Rautman and McKenna 1997, pp. 16–30). These data provide the basis for the development of thermal-mechanical (TM) stratigraphic descriptions and their comparison with geological and hydrological definitions of the tuff units.

Thermal test designs in the UZ have also benefited from the data from the prototype tests in the G-tunnel at Rainier Mesa at the NTS. The focus of the G-tunnel tests was on TM processes. However, measured temperature signatures could be interpreted as resulting from TH coupling. The thermal-hydrological-mechanical (THM) results of the G-tunnel tests are documented in reports by Zimmerman et al. (1986, Sections 6.0, 8.0, 9.0) and Ramirez et al. (1991).

The first heater test in the middle nonlithophysal zone of TSw was initiated to develop the testing approaches for TH and other coupled processes. The Large Block Test (LBT) is located in the large outcrop welded tuff at Fran Ridge (Lin et al. 1998, pp. 49–51). The LBT used five line heaters to represent a planer heat source. Sensors were emplaced to detect changes in temperature and water saturation above and below the heater plane. Temperatures were significantly affected by infiltration from the top of the block.

2.2.4.3 Underground Thermal Tests

Two underground thermal tests were conducted at Alcove 5 near the north end of the ESF Main Drift, in the top of the middle nonlithophysal zone of the TSw unit.

The Single Heater Test (SHT) was conducted near the entrance of Alcove 5 to evaluate the thermal-hydrological-chemical-mechanical (THCM) coupled processes in fractured tuff, as illustrated in Figure 2.2-13. Drainage of condensate to the region below the heater was observed (Tsang and Birkholzer 1999, pp. 411–415). Ambient percolation flux through the block was derived from the UZ site-scale evaluation. Condensate induced by heating was transported in the fractures and collected in packed borehole intervals. Cross-hole air-permeability tests, radar tomography, neutron logging, and electrical resistivity tomography were used to detect the changes in rock moisture content in the test block. Measurements showed that the dry-out zone extended about 1 m from the heater hole and that the condensate zone below the heater horizon was larger than above the heater. Cores collected from drill-back after the heating phase below the heater had higher saturation values than cores collected above the heater.

The DST, illustrated in Figure 2.2-14, is the largest test in the ESF. The testing methodologies developed in LBT and SHT were applied, improved, and expanded in the DST. Nine full-scale heaters are used to simulate waste packages emplaced in the potential repository. Two panels of wing heaters are used to simulate the thermal environments of multiple drifts. The heating phase is ongoing and has lasted for over two years, since December 1997, with the temperature at the drift wall reaching 190°C (see Section 3.10 of this PMR).

Nearly one hundred boreholes were drilled for thermal, hydrological, mechanical, and chemical measurements in the DST. Most of the boreholes are located within the middle nonlithophysal zone of the TSw, with the upper portions of some boreholes drilled into the upper lithophysal zone of TSw. The ongoing test results indicate that the heat-pipe signature is prominent in temperature measurements. Condensates increased the saturation below the wing heater early on. Air-permeability reduction from increased liquid saturation in fractures is measured by periodic cross-hole air-injection tests. Drying in rock matrix is monitored by geophysical imaging techniques.

Substantial increases of gas-phase CO₂ concentration are measured in large regions around the heaters in the DST. Chemical analyses of water collected in boreholes elucidate the interactions of calcite and silicate minerals with water. Temperature changes in the rocks and observations of dripping from condensation of hot air through the bulkhead indicate significant redistribution of moisture due to thermal effects. Various AMRs summarize data from the DST. The *Drift-Scale Coupled Processes (DST and THC Seepage Models)* (CRWMS M&O 2000, U0110/N0120, Section 6.2) evaluates changes in the chemistry of seepage and porosity arising from thermally induced precipitation. ESF and LBT TH thermal test results are summarized in an AMR for the Near Field Environment PMR. *Mountain-Scale TH Models* (CRWMS M&O 2000, U0105, Sections 6.10 and 6.11) assesses the temperature rises, saturation changes, and thermally induced fluxes toward the drifts and drainage between the drifts. See Sections 3.10 and 3.12 of this PMR for TH and THC analyses.

2.3 NATURAL ANALOGS AS CORROBORATIVE INFORMATION

Natural analogs with geological records can be used to support the long-time predictions of future performance of the potential repository. The ambient characterization of the UZ and the model prediction based on calibrations against short-term tests can greatly benefit from integration with natural-analog studies.

The AMR on *Natural Analogs for the Unsaturated Zone* (CRWMS M&O 2000, U0135) has evaluated analogs for the nuclear waste potential repository processes and Revision 1 of the YMSD will include a chapter on natural analogs. Winograd (1986) and ongoing studies use archeological artifacts preserved over thousands of years in underground structures as collaborative evidences for UZ potential repository performance. Table 2.3-1 lists the analog sites and the processes related to UZ flow and transport in the southwestern and western U.S., Mexico, and many geothermal, uranium deposit, and archeological sites worldwide. The sites in North America are listed first, followed by sites in the Pacific Rim, Asia, Europe, and Africa. Selected references are listed. Discussions of sites without cited references in the Table can be found in above-mentioned reports.

Table 2.3-1. Natural Analogs for Process Evaluation

Analog Site	Data and/or Process
Yucca Mountain as self-analog	Mineral reaction rates (Bish and Aronson 1993)
Rainier Mesa, NTS, Nevada	Seepage into drifts, discrete fractures, percolation, perched water (Thordarson 1965; Russell et al. 1987; Wang et al. 1993)
Papoose Lake sill, Paiute Ridge, NTS, Nevada	Magma intrusion, THC (Crowe et al. 1983; Matyskiela 1997; Lichtner et al. 1999)

Table 2.3-1. Natural Analogs for Process Evaluation

Analog Site	Data and/or Process
Caves and rock shelters, NTS and vicinity	Packrat midden preservation (Spaulding 1985)
Weapon tests, NTS, Nevada	Radionuclide transport (Hoffman and Daniels 1981; Buddemeier and Hunt 1988; Kersting et al. 1999)
Devils Hole, Nevada	Paleoclimate, calcite deposit (Winograd et al. 1992)
Beowawe, Nevada	Climate – glacial transition period lower bound analog (USGS 2000, U0005)
Uranium deposits in Northwestern Nevada and Southeastern Oregon - McDermitt caldera (Moonlight, Bretz, Opalite mines), Virgin Valley, Painted Hills	Uranium deposits, UZ radionuclide transport (Wallace and Roper 1981; Castor et al. 1996)
Archeological finds - preservation of cave arts in France and Germany, preserved seeds and Dead Sea Scrolls in Israel, wood, textiles, and plants in Peruvian cave, mummies in Chilean pits, manuscripts in Gobi desert, Chinese cave temples, etc.	Demonstrating the efficacy of an unsaturated environment in isolating nuclear wastes (Winograd 1986)
Caves, western North America	Biotic remains preservation (Davis 1990)
Ancient glass	Glass degradation (Kaplan and Mendel 1982; Miller and Chapman 1995)
Dixie Valley, Nevada	Geothermal, THC, preferential flow, fracture-matrix interaction, mineral precipitation and dissolution, mineral alteration
Apache Leap, Arizona	Seepage into drifts, discrete fractures, transient flow
Nogales, Arizona	Climate – monsoon period upper bound analog (USGS 2000, U0005)
Peña Blanca (Nopal I Mine), Mexico	Uranium ore deposits, secondary mineral formation and sequestration, plant uptake of radionuclides, seepage into drifts, discrete fractures, transient flow, sorption and matrix diffusion, (Percy et al. 1994, 1995; Pickett and Murphy 1997, 1999)
Cerro Prieto, Mexico	Geothermal, preferential flow, fracture network permeability, mineral reaction rates, self-sealing
Mitchell Caverns, California	Infiltration, dripping water deposits
Owens Lake, California	Paleoclimate (Forester et al. 1999)
East Mesa, California	Geothermal, preferential flow, mineral reaction rates
Heber, California	Geothermal (Lippmann and Bodvarsson 1985)
Long Valley, California	Geothermal, fracture-matrix interaction, mineral precipitation and dissolution
Geysers, California	Geothermal, preferential flow, fracture network permeability, heat pipes, boiling and condensation, self-sealing
Hobbs, New Mexico	Climate – monsoon period upper bound analog, (USGS 2000, U0005)
Valles Caldera, New Mexico	Magma intrusion, fossil hydrothermal reactions (Stockman et al. 1994)
Grants Ridge, New Mexico	Magma intrusion, fossil hydrothermal reactions (WoldeGabriel et al. 1999)
Fenton Hill, New Mexico	Geothermal, mineral precipitation and dissolution

Table 2.3-1. Natural Analogs for Process Evaluation

Analog Site	Data and/or Process
Delta, Utah	Climate (glacial transition period lower bound analog, USGS 2000, U0005)
Newberry Volcano, Oregon	Geothermal (Sammel et al. 1988)
INEEL Box Canyon, Idaho	Seepage, discrete fractures, transient flow (Faybishenko et al. 1998; CRWMS M&O 2000, U0135)
Yellowstone, Wyoming	Geothermal, fracture-matrix interaction, mineral alteration
Eldora stock and Alamosa River stock, Colorado	Deep hydrothermal intrusions (Brookins 1986; Wollenberg and Flexser 1986)
Spokane, Rosalia and St. John, Washington	Climate – glacial transition period upper bound analog (USGS 2000, U0005)
Wanapum basalt, Hanford, Washington	Basaltic glass (Jercinovic et al. 1986)
Hanford, Washington	Radionuclide migration (Barnett et al. 1997)
Alligator Rivers (Koongara deposit), Australia	Transient flow, uranium ore deposits (partially UZ) (Airey 1986; Isobe et al. 1992; Murakami et al. 1997)
Wairakei, New Zealand	Geothermal, hydrological properties, preferential flow, fracture network permeability, mineral precipitation and dissolution, mineral alteration, THM subsidence (Mercer and Faust 1979; Glassley and Christensen 1992; Bruton et al. 1993)
Broadlands, New Zealand	Geothermal, mineral precipitation and dissolution, mineral alteration
Kamojang, Indonesia	Geothermal, hydrological properties, fracture network permeability, heat pipes, boiling and condensation, self-sealing
Bulalo, Philippines	Geothermal, THM subsidence
Tianjin, China	Geothermal, hydrological properties
Oguni, Japan	Geothermal, hydrological properties
Sumikawa, Japan	Geothermal, hydrological properties, fracture network permeability
Matsukawa, Japan	Geothermal, fracture network permeability, heat pipes, boiling and condensation, self-sealing
Krasnoyarsk, Russia	Radionuclide transport at deep injection sites (Rybal'chenko et al. 1998)
Lake Karachai, Russia	Radionuclide contamination (Drozhko et al. 1997; Rumynin et al. 1998)
Chernobyl, Ukraine	Radionuclide contamination (Belyaev et al. 1997)
Negev Desert, Israel	Infiltration (Nativ et al. 1995)
Amman, Jordan	Seepage
Maqarin, Jordan	Alkaline water (Khoury et al. 1992)
Cappadocia, Turkey	Drift stability and insulation (Aydan et al. 1999)
Santorini, Greece	Trace-element transport (Murphy et al. 1998)
Larderello, Italy	Geothermal, fracture network permeability, heat pipes, boiling and condensation, mineral precipitation and dissolution, self-sealing

Table 2.3-1. Natural Analogs for Process Evaluation

Analog Site	Data and/or Process
Altamira, Spain	Cave seepage (Villar et al. 1985)
Chauvet, Cosquer, Lascaux, France	Cave painting preservation
Iceland	Basaltic glass (Jercinovic and Ewing 1987)
Krafla, Iceland	Geothermal, fracture network permeability, THM subsidence (Bodvarsson et al. 1984)
Reykjanes, Iceland	Geothermal, self-sealing
Oman	Alkaline plume, THC (McKinley et al. 1988)
Shinkolobwe mine, Zaire	Uranium oxidation (Finch and Ewing 1991)
Olkaria, Kenya	Geothermal, fracture network permeability, fracture-matrix interaction (Bodvarsson et al. 1987)
Angola	Rock shelter painting preservation
Bangombé, Gabon	Uranium ore deposits, secondary mineral formation and sequestration, criticality (Gauthier-Lafaye et al. 1989)

The YMP has used analogs for testing conceptual models and evaluating coupled processes. Yucca Mountain is viewed as a self-analog, using the past thermally driven hydrological-chemical processes of secondary mineral formation and alteration zones as a key to future alteration. Within the NTS, there are examples of waste emplacement in the Climax Stock; underground testing at G-tunnel; hydrological evaluations of seepage, percolation, perched water, and tunnel discharges at Rainier Mesa tunnel complexes; and a basalt intrusion study at Paiute Ridge. In Nevada and the surrounding southwestern/western states and Mexico, paleoclimatic analog, uranium ore deposit, and geothermal site evaluation have contributed to knowledge about hydrological and coupled processes.

The geothermal system at Wairakei, New Zealand, was endorsed by the YMP for study of THC processes. NRC sponsored the field studies at Apache Leap, Arizona, Las Cruces, New Mexico, and Peña Blanca, Mexico. Yucca Mountain, Apache Leap, and Las Cruces are test cases evaluated by the INTRAVAL project. Participation in international cooperative projects, such as the ongoing Development of Coupled models and their VALidation against EXperiments in nuclear waste isolation (DECOVALEX) for THCM coupled-processes modeling, is an effective forum for YMP to assemble useful information on nuclear waste potential repository studies. Geothermal reservoir studies address many thermally driven coupled processes and phenomena associated with nuclear waste disposal. The natural analog AMR (CRWMS M&O 2000, U0135) and Revision 1 of the YMSD also review analog information for waste package and waste form degradation. Some well-studied saturated zone sites are included for specific processes of interest.

The Peña Blanca site evaluation of uranium migration and the Idaho National Engineering and Environmental Laboratory (INEEL) infiltration test modeling are two examples of analog studies presented in the natural analog AMR (CRWMS M&O 2000, U0135, Section 6.5). For collecting corroborative evidences for radionuclide migration and drift seepage, YMP is conducting additional field sampling of borehole cores and assessing seepage into mine adits and migration from veins at the Nopal I mine at Peña Blanca. For the INEEL Box Canyon site, the modeling

approach used in the UZ Model for Yucca Mountain is used to interpret ponded-infiltration test results. These examples illustrate the approach for selecting and applying natural analog information for future use in SR and LA, and in performance confirmation. The confidence in the safe emplacement of nuclear wastes in the UZ can be greatly enhanced with natural analog studies to supplement field testing and UZ modeling at Yucca Mountain.

In addition to scientific/technical data and geological records from analog sites, archeological records can be more comprehensible to the public than hydrological/geochemical data and mathematical/numerical models (Winograd 1986). Paintings and tools preserved in caves, man-made opening and rock shelters (partial openings), structural integrity of underground dwellings, artifacts found in underground chambers, and even biotic remains from ancient animals can be used to demonstrate the possibility of preserving man-made materials surrounded by dry air over geological time scales. Model predictions and short-term experiments indicating flow diversion around openings can be demonstrated to be valid over very long time periods by archeological records.

2.4 EVOLUTION OF UZ AND TSPA MODELS

The conceptual model for the UZ flow at Yucca Mountain was first presented by Montazer and Wilson (1984, pp. 36–49). The basic geological framework with alternating welded and nonwelded tuff units, the hydrological perching and lateral flow diversions at tilted tuff interfaces, and the potential for flow and transport through faults were components of the model. Site characterization data were collected to modify, refine, and improve the understanding of the model of the UZ system. The evolution of the model was strongly influenced by the available data and information. The key parameters and processes included the magnitude of the infiltration flux, the partitioning between fast fracture-flow and slow matrix-flow components, and the redistribution of percolation flux over the potential repository horizon and at the water table.

Mathematical models were recognized at the onset of YMP as the tools needed to represent the system, interpret the observations and testing results, and make long-term predictions. Numerical modeling techniques developed within the context of geothermal reservoir research and in the petroleum industry were adopted and modified for the UZ at Yucca Mountain. The double-porosity, double-permeability model concepts evolved to describe fractured reservoirs with storage in the matrix and flow and transport through the fractures. The multiple interacting continuum formulation was developed for fractured medium representations (Pruess and Narasimhan 1985, pp. 14–26).

A description of the Yucca Mountain UZ utilizes many concepts developed in the field of soil physics. The water content (or saturation) and matrix densities are the first basic measurements in soil physics to characterize the unsaturated state. Water potential and permeability are the other essential parameters needed to characterize flow. The constitutive relationships between saturation and water potential, and between relative permeability and potential, are represented empirically with sets of functional relationships, also known as the characteristic curves. The van Genuchten functions are the most popular functions used in the scientific literature that treats flow through soil and tuffs. If the matrix continuum and the fracture continuum are in equilibrium, the fractured tuff can be represented by a composite characteristic curve (Montazer

and Wilson 1984, pp. 36–49; Peters and Klavater 1988, pp. 416–430; Pruess et al. 1990b, pp. 1249–1261). The composite-porosity model was first used by Rulon et al. (1986), the double-continuum model by Wittwer et al. (1995, p. 8), and the double-permeability model by Robinson et al. (1996, pp. 67–69) for site-scale models.

Montazer and Wilson (1984, pp. 36–49) suggested that the value of net infiltration ranged from 0.5 to 4.5 mm/yr, with the upper bound corresponding to 3% of precipitation. Weeks and Wilson (1984) estimated that downward flux in the matrix of the TSw unit was less than 0.2 mm/yr. It was suggested that most of the water (4 mm/yr) was diverted laterally within the PTn unit and flowed down the faults, with 0.5 mm/yr moving downward through the TSw. Sinnock et al. (1987) presented the first TSPA model and Klavetter and Peters (1986) and Peters and Klavetter (1988, pp. 416–430) presented numerical analyses to evaluate the conceptual model that consisted of low infiltration, lateral PTn flow and matrix-dominated flow. The transient transition from fracture-dominated flow to matrix dominated flow was theoretically evaluated by Wang and Narasimhan (1985, pp. 1861–1874) in a small fractured block, with fracture characteristic curves related to the fracture-matrix contact areas. Episodic pulse propagation and other alternative models to sustain fracture flow through unsaturated matrix blocks were presented by Pruess (1999, pp. 1039–1051) and Pruess et al. (1999, pp. 281–322).

One-dimensional column simulations for three different conceptual models are shown in Figure 2.4-1. The first 2-D site-scale model for Yucca Mountain was presented by Rulon et al. (1986). Using only the water-content profiles available at that time, multiple simulations were carried out for ranges of infiltration rates imposed on the surface boundary of the columns in the 2-D vertical cross section. The simulations indicated that as much as 50% of the infiltration was diverted for infiltration rates less than 1 mm/yr. For infiltration rates of 4.5 mm/yr, only 1 mm/yr of lateral flow was predicted. Because of the equilibrium constraint between matrix and fracture under steady-state conditions, water resided preferentially in the matrix. To keep the matrix unsaturated, only very small infiltration rates (< 1 mm/yr) could be accommodated through a tuff column (Figure 2.4-1a).

Because fractures are free to accept more water, the infiltration rate is believed to be much larger than the matrix flow component. High infiltration rates for short-term climate changes could be easily drained through high-permeability fractures, which would minimize the contact time between water and waste canisters (Roseboom 1983). Episodic pulses instead of steady infiltration rates were simulated to determine flow transmission in transient mode. The nonwelded tuff units had large damping capacities to smear the pulses. Instead of trying to transmit flows through the tuff layers, the TSPA-1991 (Barnard et al. 1992) used the weep model (Gauthier et al. 1992, pp. 891–898), which assumed that the fracture flows were decoupled from the matrix flow. The travel times of the weeps through the UZ were not modeled.

Using weep size and spacing as parameters, the extent of water contact with the waste packages was determined from geometrical considerations. The weep component could accommodate additional infiltration beyond the amount carried by the matrix. TSPA simulations from 1991 (Barnard et al. 1992) used six 1-D columns along the G-4 to H-5 transect and the weep model to accept 1 mm/yr infiltration (Figure 2.4-1b). In the TSPA-1993 (Wilson et al. 1994), the Infiltration Model was generalized to have a dry period and a wet period (Figure 2.4-1c). The

explicit representation of weeps contacting individual waste packages was accounted for in the eight areas covering the primary and secondary potential repository areas.

The first 3-D UZ model (UZ-1995) that faithfully honors the geology was presented by Wittwer et al. (1995). The nodal centers were aligned with major faults. Each major borehole was also located at the nodal center, as illustrated in Figure 2.4-2. Vertically, the layers were represented by fine gridding near layer interfaces. Fault offsets were accurately represented. Both fracture flow and matrix flow components were calculated with the effective-continuum model. With the 3-D model to redistribute the flow, percolation flux was no longer equivalent to infiltration on the surface boundary. The results of the 3-D flow field were used to select 1-D columns for TSPA-1995 (CRWMS M&O 1995). A five-fold increase (from 0.5 mm/yr to 2.5 mm/yr) was assumed to differentiate the dry years from the wet years. This ratio is probably conservative, although the magnitudes are not necessarily conservative.

Concurrently with the development of the UZ site scale flow models, UZ site-scale transport models were developed (Robinson et al. 1995, 1996, 1997). The UZ transport models took the outputs from the UZ site-scale flow models, transferred them to a finite-element mesh, and performed particle-tracking calculations for the transport of major radionuclides. The dual-porosity formulation was generalized to the dual-permeability formulation (Robinson et al. 1995, pp. 67–69; Zhou and Apted 1995, pp. 160–162). The first site-scale transport model with dual-permeability formulation is illustrated in Figure 2.4-3. The particle-tracking technique used is conservative in predicting early breakthrough. The AMR on *Analysis Comparing Advective-Dispersive Solution to Particle Tracking* (CRWMS M&O 2000, U0155) quantifies some of the differences in various approaches to modeling transport. The Flow Model and Transport Model were consolidated in 1999.

In TSPA-VA (DOE 1998), the flow fields from a further-refined UZ site-scale model (UZ-1997 model) were directly imported into the TSPA calculations. The refinement included a 100-fold increase in spatial resolution (from 10^3 nodes in UZ-1995 model to 10^5 nodes in UZ-1997 model), explicit gridding of the ESF drift, and incorporation of tilted faults, as illustrated in Figure 2.4-4. The UZ-1997 model was also expanded to incorporate a drift-scale model for the assessment of seepage into drifts. The preliminary test results of seepage at Niche 3650 in the ESF were used to confirm that the drift-scale model represents the capillary barrier mechanism well (Wang et al. 1999, pp. 323–347; Birkholzer et al. 1999, pp. 349–384). Thirty-nine calibrated flow fields were generated for inputs to TSPA. The corresponding drift-scale model results for each of the 39 flow fields were also provided to the TSPA.

Beside refinements and applications, the philosophy of the UZ Flow and Transport model to incorporate all available data was implemented in the UZ-1997 model (Bandurraga and Bodvarsson 1999, pp. 25–46; Wu et al. 1999a, pp. 185–215). Pneumatic responses were used to derive effective fracture and fault properties (Ahlers et al. 1999, pp. 47–68). Temperature profiles were used to derive the advective contribution to heat transfer. The perched water information at the interfaces within the CHn unit constrained the nature of flow field below the potential repository by diverting a large portion of flow away from the zeolitic tuff below the perched water bodies (Wu et al. 1999b, pp. 157–184). The infiltration models also evolved to using more accurate data and calculations to derive higher infiltration fluxes. The climate studies refined the future climate scenarios and designated three climate states (DOE 1998). The

infiltration ratios were 3 and 1/3 for the upper and lower bounds, respectively, for each of the climate periods. The effects of future climate and infiltration changes were modeled (Ritcey and Wu 1999, pp. 257–279). The UZ-1997 model was also used in thermal loading studies (Haukwa et al. 1999, pp. 217–255). TSPA-VA (DOE 1998) carried out systematic sensitivity analyses with probabilistic formulation for dose calculations. Compliance with regulations was more transparently presented.

The UZ PMR supporting the SR continues the refinement and improvement of modeling efforts with calibrations using traceable and verifiable data. The active fracture model (Liu et al. 1998, pp. 2633–2646; CWRMS M&O 2000, U0035), with saturation-dependent formulation for the fracture-matrix contact area, is used in model calibration. Validations against data from *in situ* tests and from new borehole data further establish the reasonableness of UZ models to represent the features, events, and processes (FEPs) in the UZ natural barriers. In addition to the AMRs, which analyze and model different UZ characteristics and processes, the abstraction of UZ model results for inputs to TSPA is an integral part of this UZ PMR. This UZ PMR, together with PMRs for other system components, lead to a more refined TSPA for SR and LA. Chapter 3 of this PMR describes the UZ model components in details.

2.5 KEY ISSUES FOR UNSATURATED ZONE FLOW AND TRANSPORT

This section discusses the key issues that have been identified by external peer reviews and oversight bodies and YMP workshops on unsaturated zone flow and transport. Section 2.5.1 summarizes major comments on the representation of unsaturated zone flow and transport in the TSPA-VA from the TSPA Peer Review Panel, the UZ Transport Panel (Independent Evaluation Panel), the Drift Seepage Peer Review, and others. NRC Key Technical Issues are discussed in Chapter 4 and not repeated in this Section 2.5.1. Section 2.5.2 summarizes key issues identified in the TSPA-VA (DOE 1998) and from YMP workshops on unsaturated zone flow and transport.

2.5.1 Summary of Key Issues from External Reviewers

This section summarizes comments from external reviewers of the representation of unsaturated zone flow and transport in the TSPA-VA and an expert elicitation completed during development of the TSPA-VA. Table 2.5-1 summarizes the key issues from these reviews and provides an explanation of how these issues are addressed in the UZ PMR. Because of NRC statutory role in the review of the technical basis for the SR, NRC issues are summarized separately in Chapter 4.

2.5.1.1 Summary of the TSPA Peer Review Panel

The YMP convened a peer-review panel to review the TSPA-VA (Budnitz et al. 1999). This panel recognized the importance of environmental tracers (^{36}Cl) as evidence of fast pathways and recommended their use in developing conceptual models of UZ flow. The existence of fast pathways in fractures was accounted for by using a dual-permeability model, and transport times between the surface and the repository were addressed in sensitivity analyses. The TSPA Peer Review Panel also recommended studies to improve the hydrologic characterization of the UZ and the understanding of fracture-matrix interactions. The TSPA Peer Review Panel also emphasized the need to better understand seepage into drifts, including the characterization of

heterogeneity and fracture capillary properties in the region around the drift wall. They also noted that many of the assumptions underlying the representation of seepage in the TSPA-VA, such as constant drift geometry, may not be valid.

The TSPA Peer Review Panel questioned the TSPA-VA assumption that the effects of THC processes will be short lived and can be neglected. They also recommended that the TH abstraction method be tested against real data, noting that the drift-scale heater test would provide a major step forward in understanding the thermal effects on the repository system. They were concerned with the uncertainties in the representation of water chemistry in the near-field environment.

With respect to transport in the UZ, the TSPA Peer Review Panel recommended validation of the assumption that flow is diverted around perched water zones. They also recommended obtaining field data that would support the modeling of colloid transport to assess the importance of processes such as colloid filtration and remobilization. They recommended a more careful analysis of the source term for radionuclides released from the potential repository. Additional issues raised by the Panel included the effect of grid scale on flow and sorption properties, upscaling in a fracture-matrix dual continuum, and the effect of episodic flow. They also recommended using the same approach to modeling transport in the unsaturated and saturated zones.

Table 2.5-1. Key External Issues for the Unsaturated Zone Flow and Transport Process Model Report

Issue	Source	PMR Approach
Climate and Infiltration		
The TSPA-VA model, using three distinct climate was simplistic and without a firm basis. A more robust justification for the duration of climate states would strengthen the analysis.	PARP ¹	Section 3.5.1 provides a more defensible justification for the duration of climate states, based on the paleoclimate record.
In the TSPA-VA, the justification for the range infiltration for each climate state was weak. A better justification of the range in infiltration under a given climate state would strengthen the analysis.	PARP	The Infiltration Model provides an improved justification for the range in net infiltration under a given climate state (Section 3.5.2). Infiltration for future climate states is based on analog climate sites.
The project could provide a stronger justification for 1-dimensional versus 3-dimensional infiltration modeling and grid resolution than was provided in TSPA-VA.	PARP	This issue is addressed in USGS (2000, U0010).
The TSPA-VA model for infiltration did not include the effects of processes such as runoff/run on, snowpack/snowmelt, seasonality, and cloudiness on infiltration. Addition of the effects of these processes in the Infiltration Model would improve estimates of infiltration.	PARP, DSPR ²	The Infiltration Model now includes effects of additional processes on infiltration, such as run-off/run-on, temperature, and vegetation (Section 3.5.2).
The YMP should study the hydrology of at least one drainage basin at Yucca Mountain.	UZEE ³ , DSPR	This proposed study is not planned. Eleven years of infiltration data are available from up to 98 boreholes and in at least five washes. It is not clear that additional field studies at new sites would improve the model significantly.

Table 2.5-1. Key External Issues for the Unsaturated Zone Flow and Transport Process Model Report

Issue	Source	PMR Approach
Unsaturated Zone Flow		
Alternative conceptual models for fracture/matrix interaction and perched water that were not considered in TSPA-VA should be evaluated.	PARP	The active fracture model (Section 3.3) provides a new, more defensible conceptual model for fracture/matrix interaction. Different conceptual models for perched water are being considered (Sections 3.7 and 3.11).
The YMP uses 1-dimensional (versus 3-dimensional) inversions for parameter estimation; The YMP should proceed with 3-dimensional inversions and incorporate additional measured data.	PARP	3-dimensional inversions are under consideration for future work; additional hydrologic data on flow and transport have been collected in the ECRB and the Busted Butte facility and are considered in current models (Section 3.7 and 3.11).
The TSPA-VA did not adequately evaluate episodic, transient percolation.	PARP, NWTRB ⁴	Model studies have shown that the PTn effectively damps episodic, transient flow (Doughty 1999).
More information is needed to analyze the spatial distribution and rate of percolation flux in fast pathways.	DSRP, NWTRB	Limited available data and model studies suggest that fast pathways carry only a small fraction of the total flow, so that fast pathways may have little effect on system performance (Section 3.7 and 3.8).
The YMP should implement subgrid modeling using different discretization and including re-calibration of properties on a smaller scale for comparison to base-case calibrated properties.	UZFTep ⁵	This modeling approach is under consideration for future study.
The YMP should complete comparisons of the single gridblock and multiple grid approaches with the standard grid discretization used in the UZ model.	UZFTep	These comparisons are under consideration for future study.
The YMP should study matrix flow within the PTn.	UZEE, DSRP	The proposed study is not planned. Percolation flux through the matrix has been estimated with a combination of integrated measures of total chloride content, geothermal gradient, and Darcy-flux estimations with borehole saturation data.
The YMP should complete focused investigations of site characteristics in the Cross Drift	NWTRB	Current data from focused investigations in the Cross Drift are summarized in Section 2.2.
The inversion process should account for appropriate ranges of parameters, given nonuniqueness of inverse method.	PARP	The Calibrated Properties Model (CPM) does specify an allowable range of parameters during the inversion process that is based upon the uncertainty of that specific parameter (Section 3.6).
Drift Seepage		
The TSPA-VA may have underestimated the amount of seepage into drifts, considering the recent results of testing in the ESF.	NC ⁶	The testing in the ESF was an artificial infiltration experiment in the Tiva Canyon. The results are not comparable to expected seepage below the PTn.
The TSPA-VA did not account for the effects of drift deformation, collapse, and backfill on seepage.	PARP, NWTRB	The effects of partial collapse of drifts have been evaluated (Section 3.9).

Table 2.5-1. Key External Issues for the Unsaturated Zone Flow and Transport Process Model Report

Issue	Source	PMR Approach
The YMP should analyze the effects of episodic, transient percolation on seepage.	PARP	This issue has only been partially addressed by repeated seepage tests (Section 2.2), and limited modeling studies (Section 3.9).
The YMP should evaluate the representativeness of continuum fracture flow model and should implement discrete fracture modeling.	PARP, UZFTEP	Partial evaluation of the continuum approach for seepage models has been completed; an active fracture model has been implemented (Section 3.9).
Additional work is needed to evaluate the effectiveness of the capillary barrier in diverting/preventing seepage.	DSPR	Seepage data (Section 2.2) and modeling studies (Section 3.9) have shown the effectiveness of the capillary barrier concept.
The YMP should plan experiments to measure amount of moisture diverted around drifts.	DSPR	Long-term drift-scale testing with wing slots to collect diverted water is one possible approach to measure the amount of water diverted around drifts. Geophysical techniques from surrounding boreholes can help to delineate the plume. These types of tests will be assessed as part of performance confirmation.
The YMP should consider fractures with a trace length of less than one meter in drift seepage analysis.	DSPR	Fractures with trace lengths of less than 1 m have been mapped in drift segments in the ESF. Drift seepage analyses use air-injection test results which capture the contributions from all fractures around test intervals, including fractures with a trace length of less than 1 meter. Seepage models do not rely on fracture mapping information. Microfractures are accounted for through the estimation of effective, seepage-specific formation parameters (Section 3.9). Although the impact of small-scale fractures is not likely to be great, the impact will be evaluated in future studies.
Unsaturated Zone Transport		
The YMP should refine EBS/UZ transport interface to appropriately treat localized releases of radionuclides.	PARP	Changes in radionuclide releases from the EBS over time are now directly input to the UZ transport model abstraction. Releases are assigned to individual blocks within the model.
The YMP has limited data from the Calico Hills directly beneath the potential repository at Yucca Mountain. The applicability of the results of testing in the Calico Hills at Busted Butte to the site has been questioned.	NC, NWTRB	Busted Butte provided readily accessible exposures of the hydrological units that are directly beneath the potential repository. The tests performed in the Calico Hills in the Busted Butte Test Facility generated data to evaluate flow and transport bounds in the Calico Hills.
The YMP should develop a more defensible colloid transport model, including irreversible capture of radionuclides by colloids.	NWTRB	The development of the colloid model continues with addition of irreversible capture of radionuclides by colloids (Section 3.11).
The YMP should continue testing to define the sorption characteristics to improve estimates of transport.	NC	Additional work on sorption in the Calico Hills is ongoing at Busted Butte.
The YMP should provide better documentation for basis of matrix sorption model.	PARP	Better documentation and model studies of matrix sorption have been completed (Section 3.11).

Table 2.5-1. Key External Issues for the Unsaturated Zone Flow and Transport Process Model Report

Issue	Source	PMR Approach
The YMP should consider thermal effects in radionuclide transport modeling.	UZFTPEP	Evaluation of the thermal effects in radionuclide transport modeling is under consideration for future study.
Complete benchmark tests to evaluate advection; advection and diffusion; advection and multiple diffusion; decay, advection, and multiple diffusion for model verification.	UZFTPEP	Benchmark tests are underway, but the results were not available for inclusion in the UZ PMR.
The YMP should complete comparisons of the single gridblock and multiple grid approaches for matrix diffusion.	UZFTPEP	This comparison is under consideration for future study.
Coupled Processes		
The YMP needs to consider the effects of thermal-hydrologic processes on UZ flow and transport in the early postclosure period, including how to treat transient flow during the first 10,000 years with respect UZ transport.	PARP	Thermohydrological effects on UZ flow have been quantified (Section 3.12). Thermal effects on flow were not found to be significant and were not included in UZ transport simulations (Section 3.11).
The YMP should consider the effects of THCM processes on post-thermal period geochemistry for drift seepage and radionuclide transport.	PARP, NWTRB, DSPR	Effect of THC processes on geochemistry of drift seepage has been addressed (Section 3.10). Effects of THC processes on porosity and permeability were small. THC effects on radionuclide transport were not analyzed (Section 3.10).
The YMP should complete coupled THC modeling.	UZFTPEP	Coupled THC modeling has been performed as summarized in Section 3.10.
The YMP should use a discrete fracture network model to evaluate coupled THC processes at smaller scales to improve the understanding of the repository system.	UZFTPEP	Work to address this issue is ongoing, but the results were not available for inclusion in the UZ PMR.
The YMP should complete bench mark tests for THC to evaluate a heat pipe with calcite/silica precipitation using a 1-D dual permeability approach for model verification.	UZFTPEP	The suggested bench mark tests are under consideration for future study.
The YMP should complete bench mark tests to evaluate chemical: microbial degradation and complexation of EDTA, copper leaching, and acid mine drainage for model verification.	UZFTPEP	The suggested bench mark tests are under consideration for future study.
The YMP should consider modeling small-scale THC processes.	UZFTPEP	The suggested modeling is under consideration for future study.

NOTES: ¹ PARP: Total System Performance Assessment Peer Review Panel (Budnitz et al. 1999)

² DSPR: Drift Scale Peer Review (Chandler et al. 1999)

³ UZEE: Unsaturated Zone Flow Expert Elicitation (CRWMS M&O 1997b)

⁴ NWTRB: Nuclear Waste Technical Review Board (NWTRB 1999, 2000)

⁵ UZFTPEP: Unsaturated Zone Flow and Transport Evaluation Panel (YMP 1999)

⁶ NC: Nye County (Bradshaw 1999)

Finally, the TSPA Peer Review Panel noted that there are two types of processes that should be analyzed in future TSPAs: those for which analytical models are available and those that may be essentially intractable, given current analytical capabilities or the Project's time constraints. They recommended the following approach to analyze these processes:

- Update models
- Increase the quality and quantity of data input to the analyses
- Use bounding analyses
- Implement design changes.

The TSPA Peer Review Panel also recommended using the defense-in-depth concept in conjunction with the approaches listed above to increase confidence that the potential repository system will meet regulatory requirements. This approach is being implemented as models are developed for the postclosure safety case as defined under the *Repository Safety Strategy* (CRWMS M&O 2000b).

2.5.1.2 Summary of the UZ Flow and Transport Model Independent Evaluation Panel

In 1999, the YMP convened an independent evaluation panel to review the UZ Flow and Transport Model using the TOUGH2 family of codes and determine the adequacy of this effort to meet the project goals within specified time frames. The panel's review (YMP 1999) focused on the conceptual model basis, water-flow capability, reactive-transport capability, and nuclide-transport capability. The panel concluded that the TOUGH2 models represent a capability at the leading edge of development in many areas. The panel also noted that the reactive-transport and nuclide-transport capabilities of the models are limited and have not yet been validated with site data. Accordingly, these capabilities should be primarily used for sensitivity studies. The panel also made several recommendations for future work to support the UZ flow and transport modeling effort. They noted that no proven best conceptual model for Yucca Mountain has been established, and a variety of methods using different conceptual perspectives, such as discrete fracture flow with particle tracking, could contribute to a better understanding of system performance. Key issues identified by the panel are listed in Table 2.5-1. The panel's report was issued after analyses supporting the UZ PMR had been initiated so some of their recommendations for new testing and analyses are not addressed in the UZ PMR; these recommendations are under consideration for future study.

2.5.1.3 Summary of the Drift-Scale Seepage Peer Review

In 1999, the YMP completed a peer review of the drift seepage studies (Chandler et al. 1999). The panel did not believe that it is realistic to develop models that predict current and future rates and locations of seepage into drifts. This panel also concluded that there is insufficient information and inadequate models to accurately predict the spatial and temporal distribution of moisture that will enter drifts in a potential repository at Yucca Mountain. Instead, they recommended that the project should develop models that provide reliable statistical bounds for estimating rates and locations of drift seepage. The panel recommended that the YMP develop a thorough plan for ongoing and future experimental and modeling work that is well integrated with developments in repository design and engineered barriers. The experiments should include a comprehensive program of drift seepage experiments in the ESF. The testing should include

acquisition of site data for a wide range of spatial scales, focusing on the rocks of the potential repository horizon, that can be used to develop multiscale relationships for geologic heterogeneity controlling movement of moisture through the rocks. Key issues are listed in Table 2.5-1.

2.5.1.4 Summary of the Unsaturated Zone Flow Expert Elicitation

In 1997, the YMP conducted a UZ Flow Model Expert Elicitation, in which project data and models were presented to a group of experts (mostly from outside YMP) so that they could provide assessments of uncertainties in key parameters and processes in the UZ (CRWMS M&O 1997b). Specific emphasis was placed on infiltration and deep percolation. Each expert estimated probability distribution functions for these processes. The panel also evaluated spatial and temporal variability in net infiltration and percolation flux, partitioning of fracture and matrix flow, seepage into drifts, modeling issues, and additional testing that might reduce uncertainty. The panel generally agreed that infiltration maps capture the general spatial variability of infiltration, but several experts suggested that more infiltration occurs beneath washes with thin alluvial cover. The experts also agreed that temporal variability in net infiltration was characterized by episodic events from major storms, but that most of the transient flux was attenuated within the system.

With regard to lateral diversion above the potential repository, most of the experts agreed that contrasts in hydrologic properties between units could cause lateral flow, particularly at the contact of the TCw with the PTn. However, they concluded that the distance of diversion would be limited to scales of several meters to tens of meters. This was consistent with the results of TSPA-VA UZ flow simulations showing nearly vertical flow above the repository. The experts did not address lateral diversion caused by perched water beneath the repository. The experts also estimated that the flow in the TSw was predominantly in fractures and that the fast-flow component likely represents only a small part of the total flux. This was consistent with simulated results in TSPA-VA.

With regard to seepage into drifts, the experts agreed that a capillary barrier would exist around the drifts and that it would likely divert the water flow in the matrix around the drifts. This behavior is also consistent with the results of TSPA-VA. Finally, the experts recommended a number of additional testing and modeling activities to address uncertainties in estimates of infiltration, percolation, and seepage. Their recommendations for additional testing were considered in planning tests in the ECRB. These recommendations included concerns with net infiltration, percolation flux in matrix and fractures at the repository horizon, temperature gradients, saturations and water potentials, chloride mass balance and isotopic evidence for fast paths, water balance, hydraulic properties of faults and fault zones, and fracture coating minerals (see Section 2.2). Two recommendations for additional testing have not been implemented (see Table 2.5-1)

2.5.1.5 Summary of Nuclear Waste Technical Review Board Issues

The Nuclear Waste Technical Review Board (NWTRB) has commented on the importance of understanding the spatial distribution and rate of percolation flux in fast pathways and the need to evaluate episodic, transient percolation. In recent meetings, the NWTRB has focused on the

importance of refining the understanding of seepage into drifts through the collection of site specific data and improving seepage models. They have emphasized the importance of focused testing in the lower lithophysal and lower nonlithophysal units of the Topopah Spring that may host the potential repository. They have encouraged the YMP to continue ongoing work in the Cross Drift, including systematic sampling, geologic mapping and small-scale fracture mapping, $^{36}\text{Cl}/\text{Cl}$ analyses, fracture mineralogy geochemistry and geochronology, and moisture monitoring. They have also expressed concern with extrapolating the results of testing at Busted Butte to the Calico Hills formation beneath the potential repository block, and the need to determine the thermal, hydrologic, mechanical, and chemical properties of the rock units that may host the potential repository (NWTRB 1999, 2000). These issues are summarized in Table 2.5-1.

2.5.1.6 Summary of Nye County Issues

In their review of the VA, Nye County provided some comments related to UZ flow and transport (Bradshaw 1999). They were concerned that seepage into drifts was underestimated in the VA, compared to the recent results of seepage testing in Alcove 1 in Tiva Canyon welded tuff in the ESF. The seepage model predicted the seepage observed in the Alcove 1 tests. However, the values determined are not directly applicable to the Topopah Spring welded tuff at the potential repository horizon. They also noted that there are limited data from the Calico Hills directly beneath the potential repository. They do not think that recent results from testing Busted Butte will resolve the lack of data because Busted Butte is not an analog for the Calico Hills beneath the potential repository. They believe that more data are needed from the Calico Hills at this location to confirm bounds on flow and transport in this formation. Finally, they noted that additional data are needed to define site-specific sorption characteristics. They believe that the treatment of sorption as a potential retardation mechanism may be underestimated in fractures and overestimated in the matrix. These issues are summarized in Table 2.5-1.

2.5.2 Summary of Key Project Issues

This section summarizes key findings identified in the TSPA-VA (DOE 1998) and at subsequent YMP workshops including the PA Workshop on UZ Flow and Transport (Houseworth and Ho 1999) and UZ Model Workshop (Cushey and Liu 1999). The issues identified in the TSPA-VA were further addressed in the PA Workshop and the UZ Model Workshop to identify direct strategies for addressing these and other issues.

2.5.2.1 TSPA-VA

The data and analyses in TSPA-VA (DOE 1998) provided an evaluation of repository performance, given the information available at that time. The analysis included an assessment of model enhancements and analyses that may improve future assessments of repository performance, including the representation of UZ flow and transport (DOE 1998, Section 6.5.1). The discussion below summarizes the key issues that were identified as having the potential to enhance the confidence in future assessments of UZ flow and transport. The manner in which these were incorporated or addressed in the UZ PMR is discussed in the sections on the PA and UZ Model Workshops.

Precipitation and infiltration. The TSPA-VA model evaluated three distinct climate states. This approach was simplistic and did not have a strong technical basis. The analysis of future climate states could have been improved by developing a more defensible basis for the number, timing, and duration of climate states. The timing of transitions from one climate to another is not known. Noninstantaneous climate transitions may lead to lower peak doses. Climate analogs were used as a basis for infiltration modeling; the analogs were defined simply by precipitation. Taking into account temperature and other factors would have provided a better definition of climate analogs. Section 3.5 summarizes the current evaluation of climate states; this evaluation provides a more defensible basis for the duration of each climate state and uses climate analog sites to define ranges of temperature and precipitation for infiltration modeling.

Percolation to depth. The adequacy of the TSPA-VA modeling using the continuum approach with coarse spatial discretization has not been fully established. The effect of localized channeling, or specifically the effect of flow in discrete fractures, is an important uncertainty in UZ flow modeling. Better integration of geochemical, isotopic, and temperature data could have improved the calibration procedure and provide insights into the importance of flow through fractures. Another uncertainty in the Flow Model is the role of perched water. The TSPA-VA model assumed that flow is diverted around water that is perched on an impermeable layer. Investigation of alternative models, such as mixing and flow through the perched zones, could have been analyzed. The effects of localized channeling and discrete fractures are evaluated in Section 3.9; an alternative model for perched water is presented in Section 3.7.

Effects of heat and excavation on flow. For the conceptual models of flow, differences had been noted between the dual-permeability flow model and the equivalent continuum model. The dual-permeability model provides for greater mobility of water in fractures, which has a great effect on the buildup of condensate and drainage. Current approaches to modeling UZ flow are described in Section 3.7. In addition, channelized flow, especially in fractures, could increase the spatial variability in the results by increasing the range of water-flow rates onto waste packages. These processes are addressed in Section 3.9. Coupling of TH and TC processes was not fully addressed in TSPA-VA. These processes are addressed in Section 3.10. In addition, TH effects could have been more closely coupled with mountain-scale UZ flow and transport. Section 3.12 summarizes TH effects on the mountain scale.

Almost all of the data on matrix hydrologic properties have been obtained from drying experiments. Data obtained from wetting experiments would be more appropriate for modeling the TH behavior during rewetting and condensate drainage in the potential repository. These data have not yet been obtained.

In situ thermal tests will continue to provide data to improve TH modeling. Ongoing tests are located in the Topopah Spring middle nonlithophysal hydrologic unit. In the current repository design, most of the drifts are in the Topopah Spring lower lithophysal unit with some drifts in the middle nonlithophysal unit and others in the lower nonlithophysal unit. Obtaining thermal-response data in these units could provide additional confidence in these models. These data have not yet been obtained.

Seepage. Several improvements to the approach to modeling seepage in TSPA-VA were suggested. The model could be tested by comparisons between field data and model predictions

to enhance the current confidence in the model. The number of waste packages that are contacted by seepage water relates to the average spacing of seeps along the drift, which is, in turn, related to parameters such as fracture spacing and permeability distribution. Field data that relate these parameters to the spacing of seeps could increase confidence in the seepage model. Seepage into drifts is also potentially strongly affected by channeling of flow and discrete-fracture effects. The adequacy of fracture-continuum models to represent these effects is uncertain. These improvements to the seepage models are summarized in Section 3.9.

For the TSPA-VA, seeps were assumed to occur at the same locations through time. Varying the location of seeps could result in more waste packages failing through time, but over a longer time. This effect had not been analyzed in TSPA-VA. Other effects that had not been analyzed in the seepage model include drift collapse and thermal alteration of hydrologic properties around the drifts. These effects could significantly impact seepage. Finally, the potential for episodic percolation at the repository and increases in seepage from drainage of thermally mobilized water were not considered. Section 3.9 summarizes the current seepage model that includes partial drift collapse; Section 3.10 summarizes TH effects on seepage.

UZ flow and transport. The TSPA-VA model did not account for the effects of thermal alteration of minerals, chemical interactions of repository materials, mineral dissolution and precipitation on UZ flow and transport. Development of a coupled, reactive transport representation would help assess these effects. The effect of colloid filtration was not included in TSPA-VA because there was insufficient information available to bound this mechanism. Colloid filtration is particularly important for the fraction of radionuclides that are irreversibly bound to colloids. The effects of higher infiltration evaluated in TSPA-VA imply that transport may be fracture-dominated in many units in the UZ. More data on the character and distribution of fracture materials would allow consideration of sorption onto fracture surfaces in future analyses. Radionuclide transport in the UZ may be sensitive to changes in matrix diffusion depending on the nature of the releases from the engineered barrier system. The current models for UZ flow and transport address thermal alteration of minerals, mineral dissolution and precipitation (Section 3.10) and colloid filtration (Section 3.11). Sorption on fractures is still conservatively neglected.

2.5.2.2 Summary of PA Workshop on UZ Flow and Transport

A YMP workshop to address the treatment of UZ flow and transport for TSPA-SR was held in December 1998. The participants developed work plans that address the remaining issues identified as requiring additional development in preparation for the TSPA-SR (Houseworth and Ho 1999). The workshop focused on the following topics: climate, infiltration, UZ flow, drift seepage, radionuclide transport, and thermal-hydrological-chemical-mechanical coupled processes. Issues considered included those from the NRC's Issue Resolution Status Reports, TSPA-VA and the TSPA Peer Review Panel (as discussed in previous sections), as well as comments from within the program. At the time of the workshop, the Issue Resolution Status Report on Radionuclide Transport was not available for review.

The issues presented at the workshop were discussed, modified, and agreed upon by the workshop participants. These issues are summarized below.

Climate and Infiltration. Issues centered on the justification for the results obtained in TSPA-VA. Improved justification for the magnitude and duration of climate states and changes in the water-table elevation were specifically identified as issues. For infiltration, improvements to the treatment of uncertainty, justification for the modeling approach, and explicit inclusion of additional processes were identified. Many of these processes have already been incorporated into the Infiltration Model. Stochastic simulations were identified as a more rigorous way to establish uncertainty in infiltration as compared to the TSPA-VA analyses based on observations of thermal gradients and water composition in the deep UZ.

UZ Flow. Issues included questions on physical processes such as alternative conceptual models for fracture-matrix interaction and perched water, transient flow, and coupled processes (THCM). Methodological issues were also identified, including parameter estimation from inverse methods, applicability of gas-phase measurements to hydraulic properties, and grid resolution. Uncertainty in the appropriate range of percolation flux was also raised as an issue.

Drift seepage. A mixture of issues on physical processes and methodology were identified. Specifically, drift collapse, which was not evaluated in TSPA-VA, was identified as an issue. Coupled processes (THCM) were identified as important to seepage. Additional physical processes of concern included episodic transient flow and the influence of matrix permeability. Methodological issues included representation of heterogeneity in models, coupling between the mountain-scale and drift-scale models, and continuum versus discrete representations of fractures.

UZ Transport. Documentation of existing work was raised as a key question for issues related to radionuclide sorption, radionuclide decay, matrix diffusion, and gas-phase radionuclides. Issues regarding physical processes were identified for colloid-facilitated radionuclide transport and THC coupled processes. Issues on methodology included interfacing of the engineered barrier system and the UZ, grid refinement, the abstraction of matrix diffusion, radionuclide screening, and particle tracking.

In conjunction with the technical issues, the workshop participants discussed issues related to the completeness and traceability of documentation, and quality assurance. These included the appropriate procedures to be followed for conducting and documenting work, qualification of existing data, tracking of existing data in technical reports, and software configuration management and verification.

The issues discussed above were addressed in work plans for the modeling and analyses that were completed for the UZ PMR.

2.5.2.3 Summary of the UZ Flow and Transport Model Workshop

In March 1999, the UZ Flow and Transport Model Workshop was held to discuss the current status of ongoing field studies at Yucca Mountain related to the UZ Flow and Transport Model and to discuss the model development strategies for TSPA-SR (Cushey and Liu 1999). The workshop included presentations of the recent work being performed by YMP scientists from LBNL, LANL, SNL, USGS, and PA. This work included the collection, analyses, and interpretation of field data, the development and use of conceptual models, the current and

planned use of calibration techniques, the interpretation of geochemical data, and the modeling of flow, transport, and coupled processes on the drift and mountain-scale. Each presentation was followed by discussions resulting in key decisions to direct the further development of the UZ Flow and Transport Model. The following summarizes these key decisions grouped by (1) those directed at the conceptual models that provide the framework for the UZ Flow and Transport Model and, (2) those related to the direct modeling approach, model inputs, and use of field data. For each key decision, a reference to the applicable section in this PMR and the AMR(s) that further discuss this information or approach is also provided.

1. Conceptual Models:

- The dual-continuum approach is the most appropriate for simulating flow and transport at the site or mountain scale for Yucca Mountain. Discrete fracture models are more appropriate for subscale analyses (alcove-, niche- or drift-scale) (see Sections 3.4.1.1, 3.4.1.2 and 3.4.1.3 and CRWMS M&O 2000, U0030, Section 6.4.1.1).
- There is adequate evidence that the van Genuchten model is applicable for welded tuffs and is defensible given the lack of better alternatives (see CRWMS M&O 2000, U0030, Sections 5 and 6.4.4).
- The active fracture model will be used for the UZ Flow and Transport Model and TSPA (see Section 3.4.1.4.1 and CRWMS M&O 2000, U0030, Section 6.4.5; U0035, Section 6; U0050, Section 6.1.2).
- It is not necessary to include film flow because it is most likely limited to active fractures and will only represent a small fraction of the total water flowing in the UZ (see CRWMS M&O 2000, U0030, Section 6.1.3).
- Alternative conceptual models for perched water (see Section 3.7.3.3 and CRWMS M&O 2000, U0050, Section 6.2.2) and distribution of percent zeolitic alteration in vitric zones (see Section 3.4.2.1 and 3.4.2.2 and CRWMS M&O 2000, U0000, Section 6.6.3) should be fully evaluated to determine their potential impact on performance.
- The percent alteration in the vitric zone within the CHn hydrogeological unit and the corresponding changes in permeability and sorption are primary components for understanding and modeling of radionuclide transport and evaluating repository performance. Once these data are available from Busted Butte test facility, the results will be used as an analog for the CHn hydrogeological unit below the repository.
- A consensus technical opinion on whether or not the perched water in G-2, UZ-14, SD-12, and SD-9 are the same chemically (i.e., do these form one continuous perched-water body) is needed.

2. Modeling Approach, Model Inputs and Use of Field Data:

- The 1999 infiltration map will be used for the UZ Model (see Section 3.5.2, 3.6.4, and 3.7.2 and, USGS 2000 U0010, Section 1; CRWMS M&O 2000 U0035, Section 4.1; U0050, Section 4.1).

- For the UZ Flow and Transport Model grid, the distribution of the percent zeolitic alteration for the CHn hydrogeological unit will be derived from the Rock Properties Model, a component of the Integrated Site Model (see Section 3.4.2.1 and 3.4.2.2 and CRWMS M&O 2000, U0000, Section 6.6.3).
- At the workshop, it was recommended that for a design drift spacing of 28 m that a grid spacing of 56 m x 56 m x 15 m, with 15 m being the maximum vertical height, be used. Subsequent to this workshop, the design drift spacing was changed to 81 m and, therefore, the grid spacing was changed. In addition, TSPA requested that a coarser, less computationally intensive grid be provided, resulting in a grid spacing of 81 m x 270 m x 5 m in the potential repository horizon and 81 m x 270 m x 20 m (or less) below the potential repository horizon (see Section 3.4.2.3 and CRWMS M&O 2000, U0000, Attachment VI).
- The fracture porosity used for the Tptpmn will be on the order of 0.01 (based on gas tracer data) rather than using calculated fracture porosities based only on fracture mapping data, which are on the order of 0.0001 (see Section 3.6.3.2 and CRWMS M&O 2000, U0090, Section 6.1.3).
- The proposal presented at this workshop for incorporating shorter trace length fractures (less than 1 m in length) will be utilized in determining the fracture properties for the UZ Model (see CRWMS M&O 2000, U0090, Section 6.1.2.3).
- Water potential measurements will be made in deep boreholes (approximately 5 m deep) in the ESF Main Drift and Cross Drift to provide additional data for comparison with the measurements already made from shallow boreholes (approximately 2 m deep).
- The calibrated mean properties (the layered approach) will be used in the UZ Flow and Transport Model and for the base-case flow fields (see Section 3.6.4 and CRWMS M&O 2000, U0035, Section 6). A geostatistical representation of matrix properties for the CHn hydrogeological unit will be evaluated as part of a sensitivity study in Revision 1 of the UZ PMR.
- Pneumatic data will continue to be used in performing calibration for the UZ Flow and Transport Model (see Section 3.6.4 and CRWMS M&O 2000, U0035, Sections 6.1, 6.2, and 6.3).
- Results from *in situ* field tests in the ESF provide bounds for several hydrological parameters, including fracture alpha and fracture porosities, and will be used to corroborate model values (see CRWMS M&O 2000, U0090, Section 6.5).
- Chloride data should be used for confirmation of the Infiltration Model, and bomb pulse data (^{36}Cl) should be used for determining the presence of fast flow paths (see Section 3.8.2 and 3.8.3 and CRWMS M&O 2000, U0050, Section 6.4).

These key decisions were used to direct the development of the UZ Flow and Transport Model and its supporting AMRs.

3. UZ FLOW AND TRANSPORT MODEL AND ABSTRACTIONS

3.1 INTRODUCTION

The Unsaturated Zone Process Model Report (UZ PMR) describes many models and analyses, all of which are aimed to gain a thorough understanding of flow and transport at Yucca Mountain. Some of these models are developed to explain certain specific data sets, others are used to evaluate parameter and process sensitivities, and the remainder provide TSPA with needed information. The UZ models developed for TSPA are the Calibrated Properties Model (CPM), the 3-D Flow Model (FM), the Seepage Model for Performance Assessment (SMPA), the Drift-Scale Thermal-Hydrological-Chemical Model (THCM), and the Transport Model (TM). The SMPA and TM directly evaluate the principal factors "Seepage into Drifts" and "UZ Transport" (see Section 1.2.2 for discussion of principal factors). Figure 1-2 shows the interrelation between the various UZ PMR models.

The term "model" is used throughout the UZ PMR as a generic term for a conceptualization or numerical analysis. However, the YMP distinguishes between *models* and *analyses* in implementing its quality-assurance program. In the terminology of the YMP, a *model* is "a representation of a process, system, or phenomenon, along with any hypotheses required to describe the process or system or explain the phenomenon, often mathematically" (AP-3.10Q, Section 3.13). An *analysis* is defined by the YMP to be a "scientific investigation that quantitatively or qualitatively describes, interprets, explains, or models a natural system, process, or phenomenon" (AP-3.10Q, Section 3.1). Analyses may be performed in constructing a model, in developing data sets for input to a model or an analysis, or in applying a model to generate output that, in turn, may be used as input to another model or analysis. Models and analyses are documented in Analysis/Model Reports (AMRs) that are prepared in accordance with the requirements set forth in AP-3.10Q. Different documentation requirements apply, depending on whether the purpose of an AMR is to document the development of a model or the performance of an analysis. The UZ PMR, on the other hand, is being prepared in accordance with AP-3.11Q and provides summary documentation of the models, submodels, and analyses that constitute the UZ Flow and Transport Model and its abstraction to support TSPA. The UZ PMR, in turn, provides reference to the individual supporting AMRs in which the detailed technical documentation of the models and analyses is presented.

This chapter is the main technical chapter of the UZ PMR and describes all of the models and analyses supporting the PMR. For each of the process models discussed, the following aspects of that particular model are addressed:

- Description of the model and submodels
- Relevant data and data uncertainties
- Assumptions and conceptual bases
- Model results (outputs)
- Abstraction of the model for TSPA (if applicable; see Table 1-1)
- Information on model validation
- Alternative models and interpretations

In addition, where appropriate, corroborative/supportive information is given, relevant journal articles are referenced, and natural analogs are discussed.

This chapter starts with sections on geology as it relates to flow and transport, descriptions of physical processes, and a discussion of numerical approaches and grid development. Then the various flow-related models are discussed, including those on climate and infiltration, calibrated properties, and 3-D flow fields. The ambient geochemistry model follows, describing modeling of geochemical data to ensure consistency between the flow fields and radionuclide transport models. Then the seepage models are discussed as well as THC models that evaluate seepage during the thermal period, chemistry of water entering drifts, and modifications of hydrological properties resulting from THC processes. Finally, the transport models and the mountain-scale TH models are described. The last section of Chapter 3 provides a high-level summary of the uncertainties of the various process models of the UZ Flow and Transport Model.

3.2 GEOLOGICAL CONSIDERATIONS FOR FLOW AND TRANSPORT

3.2.1 Overview

Located in southern Nevada, Yucca Mountain is composed of a thick sequence of volcanic rock units that were deposited as a result of a series of volcanic eruptions in the vicinity of Yucca Mountain during the Miocene Epoch (about 14 to 9.5 million years ago; Sawyer et al. 1994, pp. 1304–1318). Variations in lithostratigraphy within this sequence reflect the type of eruption, the rate of cooling and crystallization of the deposits, and the postdepositional processes of mineral alteration and tectonics. Sculpted by the slow but continual forces of erosion, Yucca Mountain is marked by washes and ridges that reflect the underlying structure of the mountain.

Situated in one of the most arid regions of the United States (see Section 3.5.1.4), Yucca Mountain is underlain by a thick unsaturated zone (UZ). Depth to the nearly flat water table ranges from approximately 500 to 750 meters (m) below ground surface. The current, potential repository design calls for waste emplacement at a depth ranging from 200 to 425 m below ground surface and from 175 to 365 m above the water table (DOE 1999, pp. S-9–S-10). Table 3.2-1 summarizes the key geological issues related to unsaturated flow and transport performance of the potential repository site.

Table 3.2-1. Geological Issues Related to Performance

Performance Aspect	Key Geological Issues
Liquid, Gas, and Heat Flow	<ul style="list-style-type: none"> • Fracture connectivity (fracture networks) in the welded units • Occurrence of fast pathways in the welded and nonwelded units • Layer continuity and heterogeneity • The occurrence and location of faults • Fault displacement and fault hydrological properties • Location of altered zones • Thermal properties of variably welded / fractured zones
Seepage	<ul style="list-style-type: none"> • Fracture connectivity • Breakouts and drift collapse due to rock stress, fracture orientation, and lithophysal zones • Location of major faults
Radionuclide Transport	<ul style="list-style-type: none"> • Tuff mineralogy (sorptive potential) • Effective surface area for matrix diffusion • Faulting and fracturing providing fast pathways • Groundwater travel times and focused flow below the potential repository
Repository Design	<ul style="list-style-type: none"> • Rock stability in fractured nonlithophysal and lithophysal zones • Location of major faults • Waste isolation/seepage into drifts

In the UZ, flow and transport phenomena—controlled by rock hydrogeological characteristics such as porosity, permeability, saturation, and moisture content—are closely linked to the depositional and postdepositional history of Yucca Mountain. It is important, therefore, to understand the distinguishing depositional characteristics of the volcanic rocks and any significant changes in rock properties resulting from hydrothermal and tectonic processes, as well as ongoing geochemical processes in variably saturated rocks.

The UZ at Yucca Mountain consists primarily of gently dipping pyroclastic flow and fall deposits (Figure 3.2-1). These tuffs grade from nonwelded to densely welded, reflecting differences in the rate of cooling and in the compressional stresses exerted on the tuffs during cooling caused by the weight of the overlying material. Typically, the degree of welding is inversely proportional to porosity and directly proportional to fracture frequency. The nonwelded tuffs usually have large porosities (typically 30 to 50%) and few fractures (less than 1 per meter), while the densely welded tuffs generally have greatly reduced pore space (generally less than 15 percent) and abundant fractures (approximately 1 to 4 per meter) (Flint 1998, p. 44, Table 7; CRWMS M&O 2000, U0090, p. 36). Fracturing within the stratigraphic layers that comprise Yucca Mountain is typically confined within each layer (i.e., most fractures terminate at layer boundaries) (Spengler et al. 1994, pp. 1-11; Rousseau et al. 1999, p. 23).

In some cases, gases trapped during the cooling process form cavities (lithophysae) of varying diameter, shape, and roughness within the welded tuff matrix, resulting in an increase in total porosity. Degree of welding and presence of lithophysal cavities govern fracture geometry and surface roughness. Fractures within densely welded tuffs have a more planar geometry and a smoother surface than less welded units. However, in lithophysal zones, fractures are less planar, and fracture surfaces are typically rougher than in nonlithophysal zones (Buesch et al. 1996, p. 15, Table 2 and Figure 5; Rousseau et al. 1999, p. 24) as shown in the photos and schematics in Figure 3.2-4. The occurrence of small fractures may be important in nonlithophysal zones because of the relative absence of abundant through-going or long-length fractures. Conceptually, small fractures may add to the bulk permeability of the rock.

Other important aspects of the geological setting at Yucca Mountain include layer continuity and heterogeneity. Layer thickness and lateral continuity initially depend on three principal factors: location of the source area, volume of deposited material, and shape of the pre-existing topographic surface (Rousseau et al. 1999, p. 30). On a regional scale, volcanic deposits thicken closer to the source area and pinch out in distal regions. Locally, layers thicken to fill existing topographic lows and thin (or even pinch out) around existing topographic highs. During volcanic deposition and cooling, variations in layer thickness, in addition to local moisture conditions, give rise to internal heterogeneity within the tuff layers. Margins of thick ash flows (including top, bottom, and lateral boundaries) cool quickly and under different pressures compared to the interior of the flow units, thus producing rock fabrics with different hydraulic characteristics. For instance, the upper and lower margins of the highly fractured, moderately to densely welded potential repository host rock, the Topopah Spring Tuff, grade into sparsely fractured, partially welded and nonwelded tuffs (Figure 3.2-2b and Figure 3.2-5). A similar trend is seen within the Paintbrush nonwelded unit (PTn), where two ash-flow members thin dramatically to the south across Yucca Mountain, with observed lateral and vertical increases in matrix porosity corresponding to reduced welding. These transitions between welded to

nonwelded intervals of rock can significantly impact vertical flow, leading to accumulation of water and focusing of flow.

Postdepositional processes such as mineral alteration, tectonics, and erosion further modify the hydrological characteristics and continuity of the tuffs beneath Yucca Mountain. The slow, continual process of mineral alteration resulting from prolonged rock-water interaction and weathering at the land surface (in addition to hydrothermally induced mineral changes that occurred during cooling of the welded tuffs) has led to the formation of clays, zeolites, and vapor-phase minerals in the rock layers (Bish and Chipera 1989, pp. 1–15; Bish and Aronson 1993, pp. 148–161). These alteration products are important because of their potential to reduce permeability and to sorb radionuclides. Also important to flow and transport are interruptions in layer continuity attributed to fault displacement and erosion. Faulting may further affect the hydrological properties of the tuffs by establishing a secondary high-permeability network through intense fracturing (Figure 3.2-5d), or, conversely, by reducing permeability through the formation of fault gouge (Figure 3.2-5e).

3.2.2 Major Hydrogeological Units

Tuffs occurring within the UZ beneath Yucca Mountain are identified by lithostratigraphic name and by major and detailed hydrogeological unit nomenclatures in Table 3.2-2. This table also provides the correlation between these units and UZ model layers. Most layers are laterally continuous across the site, except where eroded or interrupted by faults whose displacement exceeds layer thickness. The following discussion summarizes units of principal importance to flow and transport in the UZ at Yucca Mountain. Definition of major hydrogeological units comes from Montazer and Wilson (1984, pp. 9–19). Their abbreviation of each of the five major hydrogeological units (i.e., TC, P, TS, CH, and CF) has been modified slightly for use in this PMR. In order to be more descriptive, a lowercase letter has been added indicating whether the unit is welded (w), nonwelded (n), or undifferentiated (u).

Table 3.2-2. Major Hydrogeological Unit, Lithostratigraphic Unit, Detailed Hydrogeological Unit, and UZ Model Layer Nomenclatures (adapted from CRWMS M&O 2000, U0000, Table 10)

Major Hydrogeological Unit	Lithostratigraphic Unit		Detailed Hydrogeological Unit	UZ Model Layer
Tiva Canyon welded (TCw)	Tiva Canyon Tuff	Tpcr	CCR, CUC	tcw11
		Tpcp	CUL, CW	tcw12
		Tpcpv3	CMW	tcw13
		Tpcpv2		
Paintbrush nonwelded (PTn)		Tpcpv1	CNW	ptn21
	Bedded tuff	Tpbt4	BT4	ptn22
	Yucca Mountain Tuff	Tpy		TPY
	Bedded tuff	Tpbt3	BT3	ptn24
	Pah Canyon Tuff	Tpp	TPP	ptn25
	Bedded tuff	Tpbt2	BT2	ptn26
	Topopah Spring Tuff	Tptrv3		
Tptrv2				
Topopah Spring welded (TSw)		Tptrv1	TC	tsw31
		Tptm	TR	tsw32
		Tptrl	TUL	tsw33
		Tptpul		
		Tptpmn	TMN	tsw34
		Tptpll	TLL	tsw35
		Tptpin	TM2 (upper 2/3)	tsw36
			TM1 (lower 1/3)	tsw37
		Tptpv3	PV3	tsw38
		Tptpv2	PV2	tsw39
		Calico Hills nonwelded (CHn)		Tptpv1
Bedded tuff	Tpbt1			
Calico Hills Formation	Tac		CHV (vitric) or CHZ (zeolitic)	ch2 (vit, zeo)
				ch3 (vit, zeo)
				ch4 (vit, zeo)
				ch5 (vit, zeo)
Bedded tuff	Tacbt		BT	ch6
Prow Pass Tuff			Tcpuv	PP4 (zeolitic)
		Tcpuc	PP3 (devitrified)	pp3
		Tcpmd	PP2 (devitrified)	pp2

Major Hydrogeological Unit	Lithostratigraphic Unit		Detailed Hydrogeological Unit	UZ Model Layer
		Tcplc	PP1 (zeolitic)	pp1
		Tcplv		
	Bedded tuff	Tcpbt		
	Bullfrog Tuff	Tcbuv		
Crater Flat undifferentiated (CFu)		Tcbuc	BF3 (welded)	bf3
		Tcbmd		
		Tcblc		
		Tcblv		
	Bedded tuff	Tcbbt	BF2 (nonwelded)	bf2
	Tram Tuff	Tctuv		
		Tctuc		
		Tctmd		
		Tctlc		
		Tctlv & below	Not Available	tr2

3.2.2.1 Tiva Canyon Welded (TCw) Hydrogeological Unit

The TCw is the most prevalent hydrogeological unit exposed at the land surface. The unit is composed of moderately to densely welded, highly fractured pyroclastic flow deposits of the Tiva Canyon Tuff. The deposits are of variable thickness resulting from erosion. Within the potential repository area, the maximum thickness of the TCw is about 150 m along Yucca Crest (which runs along the western half of the potential repository footprint; see Figure 3.2-1), whereas in alluvial washes east of Yucca Crest, the TCw may be completely eroded (Montazer and Wilson 1984, p. 14; Rousseau et al. 1999, p. 30). Vapor-phase corrosion of volcanic glass and pumice in the lower TCw imparts a secondary porosity beneath central and northern Yucca Mountain (Buesch et al. 1996, pp. 35–36; Flint 1998, p. 21). The lower boundary of the TCw has been defined as the contact between the densely welded, vitric subzone (Tpcpv3) and the moderately welded, vitric subzone (Tpcpv2) of the Tiva Canyon Tuff. Because Tpcpv3 is typically very thin and only observed beneath southeastern Yucca Mountain, the base of Tpcpv2 is selected as the lower TCw boundary for the purpose of defining layers within the mountain-scale numerical grids discussed in this report.

TCw–PTn transition—Tuffs grade gently downward over a few tens of centimeters from densely welded (Tpcpv3, where present, otherwise the lower nonlithophysal zone of the TCw or the upper portion of Tpcpv2) to nonwelded (Tpcpv1), accompanied by an increase in matrix porosity and a decrease in fracture frequency (Figure 3.2-2a). Many fractures in the lower TCw terminate at the contact between TCw and PTn, or their apertures are greatly reduced across this boundary. Alteration to clay minerals is common at the base of the TCw (Moyer et al. 1996, pp. 1–2, 16–17, 88, Table 3; Buesch et al. 1996, pp. 35–36) and is correlated with observed increases in saturation (Flint 1998, p. 8 and Figures 6, 7). Changes in fracture characteristics and

the occurrence of alteration minerals at the TCw-PTn contact may have important implications for downward flow of water at this interface.

3.2.2.2 Paintbrush Nonwelded (PTn) Hydrogeological Unit

The PTn consists of layers of predominantly nonwelded and bedded tuffs (particularly in the potential repository footprint) with high matrix porosity and low fracture frequency (Moyer et al. 1996). The layers include the nonwelded vitric (i.e., glassy) subzone at the base of the Tiva Canyon Tuff (Tpcpv1), the bedded tuff Tpbt4, the Yucca Mountain Tuff (Tpy), the bedded tuff Tpbt3, the Pah Canyon Tuff (Tpp), the bedded tuff Tpbt2, and the non- to moderately welded vitric tuffs at the top of the Topopah Spring Tuff (Tpdrv3, Tpdrv2). Thickness of the PTn hydrogeological unit ranges from about 110 to 20 m (north to south) across the potential repository area and thickens to over 160 m beneath the northernmost part of Yucca Mountain (Figure 3.2-3a). Lateral variation in welding associated with the substantial thickening of two PTn units (Tpy and Tpp), in addition to the variable distribution of altered (e.g., smectitic and zeolitic) intervals, make rock-hydrological properties within the PTn highly heterogeneous. Through-going fracture networks are rare and are typically associated with faults (Rousseau et al. 1999, p. 54). The bottom of the PTn is defined as the contact between the moderately and densely welded, crystal-rich vitric subzones (Tpdrv2 and Tpdrv1, respectively). Given the overall large storage capacity of the highly porous rock matrix, the PTn unit may effectively dampen transient pulses of infiltration and more evenly distribute the downward flow of water.

PTn-TSw transition—A thin, but prevalent layer of argillic alteration is observed in the pre-Pah Canyon bedded tuff (Tpbt2), near the base of the PTn (Moyer et al. 1996; pp. 53, 80), and may behave as a capillary or permeability barrier to flow (Rousseau et al. 1999, p. 25). Below this horizon, crystal-rich vitric tuffs grade sharply downward from nonwelded (Tpdrv3) to densely welded (Tpdrv1), accompanied by a sharp decrease in matrix porosity and an increase in fracture frequency (Figure 3.2-2b). These changes in porosity and fracture characteristics may create saturated conditions above this contact that may reinitiate fracture flow into the TSw.

3.2.2.3 Topopah Spring Welded (TSw) Hydrogeological Unit

Sharing many characteristics of the TCw, the TSw is composed of moderately to densely welded, pyroclastic flow deposits with intense fracturing (Buesch et al. 1996, pp. 19–21). A key difference between the TSw and the TCw is the existence of a well-developed, densely welded, crystal-poor vitrophyre (i.e., rock with a glassy groundmass) near the base of the TSw (Buesch et al. 1996, p. 23; Rousseau et al. 1999, p. 22). (The densely welded, basal vitrophyre of the TCw is very thin and occurs only beneath southeastern Yucca Mountain.) Thickness of the TSw ranges from about 280 to 350 m in the potential repository area (Figure 3.2-3b). The base of the TSw is defined as the contact between the densely and moderately welded, crystal-poor vitric subzones (Tptpv3 and Tptpv2, respectively). In descending lithostratigraphic order (using the nomenclature of Buesch et al. 1996, Table 2), the key units within the TSw are (refer to Figure 3.2-4):

- **Tpdrv1 and/or uppermost Tptpn**—thin (~ 2 m thick), crystal-rich upper vitrophyre of the TSw, characterized by very low porosity and intense fracturing.

- **Tptrn**—crystal-rich nonlithophysal unit with well developed secondary porosity imparted by vapor-phase corrosion of volcanic glass and pumice clasts.
- **Tptrl & Ttpul**—crystal-rich and crystal-poor upper lithophysal units.
- **Ttpmn**—crystal-poor middle nonlithophysal unit (potential repository layer).
- **Ttpll**—crystal-poor lower lithophysal unit (potential repository layer).
- **Ttpln**—crystal-poor lower nonlithophysal unit; contains a highly fractured subzone and frequent clay alteration near base of unit (potential repository layer). Perched water is observed in several locations within the lower part of this unit.
- **Ttpv3**—crystal-poor basal vitrophyre, characterized by very low porosity and intense fracturing near unit top; alteration minerals (e.g., smectite, zeolite) commonly found at top of unit.

TSw-CHn transition—Tuffs grade downward from densely welded to nonwelded over several meters, accompanied by an increase in matrix porosity and a decrease in fracture frequency (Figure 3.2-5). Furthermore, much of the vitric material occurring above and below this boundary has been altered to clays or zeolites. Alteration occurs (although not ubiquitously) along fractures in the densely welded basal vitrophyre (Ttpv3) of the TSw as well as within the high porosity, nonwelded matrix of the CHn (Broxton et al. 1987, pp. 89–110; Bish and Chipera 1989, Appendix A; CRWMS M&O 2000, I0045, Section 6.3). Alteration near this contact has been linked to the occurrence of perched water and has important implications for transport and retardation of radionuclides.

3.2.2.4 Calico Hills Nonwelded (CHn) Hydrogeological Unit

Comprised of predominantly nonwelded pyroclastic flow and fall deposits, the CHn extends from the base of the crystal-poor, densely welded vitrophyre to the water table, except where units below the base of the upper vitric portion of the Bullfrog Tuff (Tcbuv) lie above the water table (which occurs in certain areas beneath Yucca Crest). The key units of the CHn include the moderately welded to nonwelded vitric subzones at the base of the Topopah Spring Tuff (Ttpv2 and Ttpv1, respectively), the bedded tuff Tpbt1, the Calico Hills Formation (Tac), the bedded tuff Tacbt, the entire Prow Pass Tuff (Tcupv—upper vitric, Tcupc—upper crystalline, Tcprd—moderate/densely welded, Tcplc—lower crystalline, Tcplv—lower vitric, and Tcplt—bedded tuff), and the upper vitric portion of the Bullfrog Tuff (Tcbuv). Within the potential repository footprint, the thickness of the CHn ranges from about 180 to 320 m, as shown in Figure 3.2-3c. Many different lithologies, distinguished by depositional history and degree of welding, by matrix color, and by the size, amount, and composition of pumice and lithic material, are contained within this interval. In a hydrogeological context, however, the most significant features in the CHn are the abundance and distribution of zeolites. The distribution of abundance of clays and zeolites beneath the potential repository horizon is difficult to determine because mineral data from only a small number of boreholes are available and because the degree of alteration is highly variable. Mineral alteration is discussed in greater detail in Section 3.2.4.

3.2.2.5 Crater Flat Undifferentiated (CFu) Hydrogeological Unit

The CFu consists of any units that occur above the water table and below the base of the upper vitric portion of the Bullfrog Tuff (Tcbuv). This includes portions of welded and nonwelded units from the Bullfrog and Tram tuffs. Within the potential repository area, the thickness of the CFu ranges from 0 (in the northern and eastern portions) to about 140 m (along the southwestern edge of the potential repository) (Figure 3.2-3d). Because of the limited number of deep boreholes, sufficient data are not available to fully characterize these tuffs. Nevertheless, the volume of CFu material is small and restricted to the southwestern area of Yucca Mountain.

3.2.2.6 Water Table Configuration

Several interpretations exist for the configuration of the water table beneath Yucca Mountain (Robison 1984; Wittwer et al. 1992; Ervin et al. 1994; Tucci and Burkhardt 1995). They range from an approximately flat interpretation (at an altitude of about 730 masl) to maps showing a steep hydraulic gradient linking observed water levels below southern Yucca Mountain (at about 730 masl in several boreholes) with water levels beneath northern Yucca Mountain (up to about 1,020 masl in borehole G-2). Given the limited amount of water level data in the north and the possibility that the few high altitudes observed represent perched water, either interpretation is valid.

Regardless of altitude, the potentiometric surface intersects many lithostratigraphic units because of faulting and the gentle eastward dip of the strata. Figure 3.2-6 shows the occurrence of the Topopah Spring Tuff, Calico Hills Formation, Prow Pass Tuff, Bullfrog Tuff, and Tram Tuff at the water table east of the Solitario Canyon fault.

3.2.3 Structural Setting

Major faults at Yucca Mountain are of two basic types: north-trending normal faults (whose principal direction of movement is vertical) and northwest-trending strike-slip faults (whose principal direction of movement is lateral). The Solitario Canyon and Bow Ridge faults are the two major block-bounding faults in the Yucca Mountain area (see Figure 3.2-6) (Day et al. 1998, p. 6). The volume of rock lying between these faults is referred to as the "central block." Both the Solitario Canyon and Bow Ridge faults are north-trending normal faults characterized by small (few meters) vertical displacement in the northern Yucca Mountain area and by large (several hundreds of meters) vertical displacement to the south. The zone of deformation along the western boundary of the central block associated with the Solitario Canyon fault is as much as 550 m wide (Day et al. 1998, p. 7). Numerous fault splays (three of which are shown in Figure 3.2-6) branch off from the main trace of the Solitario Canyon fault. Structural deformation associated with the Bow Ridge fault within the eastern part of the central block takes the form of a series of discontinuous, steeply-dipping normal faults, represented collectively as the "Imbricate" fault in Figure 3.2-6.

Located within the central block are other north-trending normal faults, including the Ghost Dance and Dune Wash faults. Currently, the potential repository footprint is located between the Solitario Canyon and Ghost Dance faults (Figure 3.2-6), in an area referred to as the Yucca Crest structural subdomain (Rousseau et al. 1999, p. 47). The Ghost Dance fault dips steeply to the

west and shows variable displacement and rock deformation along its trace (Day et al. 1998, pp. 9–10). Within the Yucca Crest structural subdomain lies a wide zone of minor northwest-trending faults referred to as the Sundance fault zone (represented by a single trace in Figure 3.2-6). The nature and continuity of the Sundance fault is described by Potter et al. 1999, pp. 1–15).

Northwest-trending strike-slip faults are the prevailing structures in the northern part of the central block. These include the Sever Wash, Pagany Wash, and Drill Hole Wash faults, whose surface expression/projection parallels elongated, northwest-trending alluvial washes. Vertical displacement along these faults is typically less than 10 m (Day et al. 1998, p. 8).

As described in the following section, faults may be important features in the UZ flow and transport regime given their potential role in the alteration history of Yucca Mountain. The effect faults may have on groundwater flow is also discussed in Section 3.3.5.

3.2.4 Mineral Alteration and the Vitric-Zeolitic Boundary

In the context of UZ flow and transport modeling, the abundance and distribution of clays and zeolites between the potential repository horizon and the water table are of particular interest because these alteration products can affect flow paths and sorb radionuclides. The potential for mineral alteration is affected by several factors: (1) rock fabric and composition, (2) proximity to structural features such as through-going fractures and faults, and (3) presence of water (rock-water interaction) (Broxton et al. 1987, pp. 89–110). The rock units at Yucca Mountain most susceptible to mineral alteration are vitric tuffs with high porosity and high permeability. High porosity and permeability provide a large surface area of particles for interaction with passing groundwater and can be established either through the process of deposition and subsequent cooling or through secondary fracturing.

Smectitic and zeolitic alteration has been observed in the highly porous nonwelded tuffs of the PTn and CHn, not only in the matrix, but along faults and well-connected fractures. Alteration to smectite and zeolite is also seen in fractures of the densely welded basal vitrophyre of the TSw and at the bottom of the lower nonlithophysal zone of the TSw, just above the contact with the basal vitrophyre (see schematic, Figure 3.2-5) (Broxton et al. 1987, p. 93).

Below the potential repository horizon, the most abundant type of alteration (and the most important to radionuclide transport and sorption) is zeolitic. The degree of zeolitic alteration of vitric material is highly variable between the potential repository horizon and the water table—large areas are considerably altered (zeolitic), while other areas remain unaltered (vitric) (Figure 3.2-7). Interpreted as an ancient water table (Broxton et al. 1987, p. 104; Bish and Aronson 1993, p. 150), the vitric-zeolitic boundary has been mapped as a three-dimensional surface that cross cuts several lithostratigraphic boundaries (Rousseau et al. 1999, pp. 40-43). This representation does not include the complex features of the vitric-zeolitic boundary such as transitions along fault zones and through-going fracture networks, local alteration associated with bodies of perched water, and areas of saturation transition, such as the capillary fringe of the water table.

Although many complexities in the vitric-zeolitic transition have been observed at Yucca Mountain (in outcrop mapping and borehole logging), limited amounts of data are available over the three-dimensional, site-scale domain of the UZ model to fully understand this transition and to numerically simulate its effects on flow and transport processes. Nevertheless, the general geometry of the vitric-zeolitic boundary has been identified using various types of data analyses, including mineralogic x-ray diffraction (XRD) analyses of core samples (CRWMS M&O 2000, I0045, Section 4.1.1) and rock property measurements of matrix porosity and matrix permeability (Flint 1998; CRWMS M&O 2000, I0040, Section 4.1). In most cases, rock hydrological measurements are consistent with mineralogic analyses and indicate a trend of increasing alteration to the north and east across the potential repository area, and with depth from the base of the TSw to the water table (Figure 3.2-7).

Within the welding transition from the base of the TSw into the upper CHn (Tptpv3 to Tptpv1), the occurrence of unaltered, vitric tuffs occupies much of the southern half of Yucca Mountain (Figure 3.2-7) (CRWMS M&O 2000, I0045, Section 6.3.2). A thin, vitric layer is observed in the area surrounding boreholes G-1, SD-9, G-4, and H-5 within the moderately welded, crystal-poor subzone (Tptpv2) at the base of the TSw. Given that this area is underlain by low-permeability zeolites (in layers Tptpv1 and Tpbt1), lateral diversion may occur within layer Tptpv2 beneath the northernmost part of the ESF.

Within the Calico Hills Formation (lithostratigraphic unit Tac which has been subdivided into four layers of equal thickness in the Integrated Site Model (ISM3.1) Mineralogy Model; CRWMS M&O 2000, I0045, Section 6.2.2), the areal extent of predominantly vitric material appears to diminish with depth as boreholes SD-12 and SD-7 show increased zeolite content (Figure 3.2-7). The transition into zeolitic material is not easily characterized and may be gradual or abrupt in vertical and lateral directions, with lenses or fingers of zeolitic material occurring in otherwise predominantly vitric zones, and vice versa.

The bedded tuff directly beneath the Tac is more pervasively altered to zeolites than the lithostratigraphic unit above it. The vitric area within the bedded tuff (Tacbt) appears limited in extent to an area surrounding boreholes SD-6, H-3, and G-3 (though an increase in smectite abundance is observed in borehole SD-6) (CRWMS M&O 2000, I0045, Section 6.3.2).

The upper vitric interval of the Prow Pass Tuff (Tcupv) has a distribution of zeolite abundance similar to layer Tacbt, with vitric material encountered in boreholes SD-6, H-3, and G-3. The remainder of the Prow Pass Tuff is moderately to densely welded, except at the base of the unit, which is nonwelded and pervasively zeolitized (CRWMS M&O 2000, I0045, Section 6.3.2). The maximum thickness of the largely unaltered, vitric rocks in the CHn is approximately 130 m and occurs just south of the potential repository footprint in an area surrounding borehole H-3 (Rousseau et al. 1999, p. 41, Figure 16).

Although not considered in the Mineralogy Model of ISM3.1, the location of and displacement along faults appear to affect the geometry of the vitric-zeolitic boundary. The Yucca Crest structural domain, within which lies the potential repository site, is bound in the west and east by two major faults: the Solitario Canyon and the Drill Hole Wash faults, respectively. Nearly all of the boreholes from which vitric samples in the CHn have been collected are located in the southern and western part of this structural domain. Boreholes intersecting predominantly

zeolitized tuffs within the CHn lie in the northern and eastern part of the Yucca Crest structural domain and beyond its boundaries. The lateral transition from predominantly altered tuffs to unaltered tuffs within the CHn occurs in an area cross cut by the Sundance fault. Though modeled in the ISM as a single fault plane, the Sundance fault is actually a system comprised of many small northwest-trending faults. It has been hypothesized that the Sundance and Ghost Dance fault systems may have acted as barriers to the alteration process by either ponding southward migrating zeolitizing waters (i.e., faults behaving as low-permeability barriers) or by diverting water downward through high-permeability fracture networks associated with the faulting (Buesch et al. 1995, pp. 800–804).

3.2.5 Summary

Potential repository performance is affected by key geological issues such as fracture connectivity in welded units, occurrence of fast flow pathways in nonwelded units, layer continuity and heterogeneity, distribution of mineralogically altered horizons and their sorptive potential, and rock stability in fractured nonlithophysal and lithophysal zones. Understanding the distinguishing depositional characteristics of the volcanic rocks, as well as any significant changes in rock properties resulting from postdepositional process (e.g., mineral alteration and tectonics), is the key to estimating rock hydrogeological characteristics (needed to simulate flow and transport phenomena) within the UZ at Yucca Mountain.

The UZ has been divided into five major hydrogeological units, whose primary characteristics are as follows (listed in order from land surface to water table):

1. TCw—variably eroded (0 to 150 m thick in the potential repository area), moderately to densely welded unit with high fracture frequencies.
2. PTn—predominantly nonwelded unit (20 to 110 m thick in the potential repository area) with large matrix porosity, low fracture frequency, and variable distribution of low-permeability clays and other alteration minerals.
3. TSw—moderately to densely welded unit (280 to 350 m thick in the potential repository area) with high fracture frequencies; contains potential repository horizon in the middle nonlithophysal, lower lithophysal, and lower nonlithophysal layers; perched water frequently occurs above the altered contact between the lower nonlithophysal unit and the densely welded, intensely fractured basal vitrophyre of the TSw.
4. CHn—mostly nonwelded tuffs (180 to 320 m thick in the potential repository area) with highly variable zeolite distribution; zeolite abundance increases to the north and east across the potential repository area, as well as with depth; major vitric (unaltered) areas in the CHn lie in the southern half of the potential repository area (maximum thickness of vitric material is about 130 m in an area just south of the potential repository footprint).
5. CFu—a relatively small volume of rock (up to about 140 m thick in the potential repository footprint) occurring just above the water table beneath the western-southwestern portion of the potential repository area; includes portions of welded and nonwelded units from the Bullfrog and Tram tuffs.

Subdivision of these five major hydrogeological units into detailed hydrogeological layers for the purpose of simulating flow and transport in the UZ is described in Section 3.4.2.2 of this report.

3.3 PHYSICAL PROCESSES

The UZ at Yucca Mountain is a complex system with a variety of flow and transport processes occurring at different scales. These processes include infiltration under different climate conditions, liquid and gas flow, chemical transport, and energy transport. The flow and transport processes occur within fracture networks, major faults, and the rock matrix. Fracture-matrix interactions, or the flow and transport between fractures and rock matrix, present additional process complexity. In addition, the potential repository for nuclear waste will introduce a large thermal perturbation (resulting from radioactive decay) that will drastically alter flow and transport processes. This section highlights some of these processes, which have relevance to Yucca Mountain UZ flow and transport modeling, with an emphasis on the current conceptual ideas. The discussion in this section is also closely related to some identified FEPs that could affect the potential repository performance (see Section 1.2.3). More detailed discussions on each process can be found in Sections 3.4 through 3.12 of this PMR that describe the relevant models and analyses.

3.3.1 Climate

Climate process refers to quantifying the precipitation rate and temperature at the surface of Yucca Mountain. This is used to determine the net infiltration into Yucca Mountain and hence water percolation at the repository horizon. These climate processes are used as indicators of climate change over the next 10,000 years at Yucca Mountain and are based upon paleoclimate reconstruction of an analogous time interval that occurred approximately 400,000 years ago. Three climates are forecast to occur within this time interval: the current modern climate, a monsoon climate and a glacial-transition climate. A range of precipitation rates and temperatures for each of these three climates is derived from analog meteorological stations within the contiguous US. Section 3.5.1 describes the Climate Model used to represent the climate process.

3.3.2 Infiltration

The infiltration process refers to the penetration of liquid water through the ground surface and to a depth where it can no longer be removed by evaporation or transpiration by plants. Net infiltration is the source of groundwater recharge and water percolation at the potential repository horizon and provides the water for flow and transport mechanisms that could move radionuclides from the potential repository to the water table.

The overall framework of the conceptual model for infiltration is based on the hydrological cycle. Important processes that affect net infiltration include precipitation (rain and snow), runoff and run-on (flow of surface water off one place and onto another), evaporation, transpiration, and moisture redistribution by flow in the shallow subsurface (USGS 2000, U0010, Section 5.1). As shown in Figure 3.3-1, infiltration is spatially and temporally variable because of the nature of the storm events that supply precipitation (Section 3.5.1 of this PMR) and variation in soil cover and topography (CRWMS M&O 2000, U0030, Section 6.1.1). Infiltration rates are believed to be high on sideslopes and ridgetops where bedrock crops are exposed, and fracture flow in the bedrock is able to move liquid water away from zones of active evaporation (Flint and Flint 1995, p. 15).

Significant infiltration occurs only every few years (USGS 2000, U0010, Section 5.3). In these years, the amount of infiltration still varies greatly, depending on storm amplitudes, durations, or frequencies. In very wet years, infiltration pulses into Yucca Mountain may occur over a relatively short time period. A detailed discussion of infiltration processes can be found in USGS (2000, U0010) and in Section 3.5, which describe the Infiltration Model.

3.3.3 Fracture and Matrix Flow Component

Figure 3.3-2 schematically shows the overall conceptualized water flow behavior in the UZ, including the relative importance of fracture and matrix flow components in the different hydrogeologic units, as defined in Section 3.2. Accurate determination of the flow components is especially important for chemical transport processes. Flow in fractures (fracture flow) is typically much faster than flow in the matrix (matrix flow), leading to much shorter travel times for radionuclides and other chemicals in fractures compared to the matrix. The characteristic flow behavior in each of the major hydrogeologic units is described in the following subsections.

3.3.3.1 Flow Through the TCw Unit

The high density of interconnected fractures and low matrix permeabilities in the TCw hydrogeologic unit (CRWMS M&O 2000, U0090, Sections 6.1 and 6.2) are considered to give rise to significant water flow in fractures and limited matrix imbibition (water flow from fractures to the matrix). Thus, episodic infiltration pulses are expected to move rapidly through the fracture system with little attenuation by the matrix. This is partially supported by pneumatic data in the TCw showing little attenuation of the barometric signal in monitoring boreholes relative to the barometric signal observed at the land surface (Rousseau et al. 1999, p. 89), as discussed in CRWMS M&O (2000, U0030, Section 6.1.2). The presence of relatively high fractional abundances of ^{36}Cl measured in TCw samples from boreholes (CRWMS M&O 2000, U0085, Section 6.6.3) also supports this conceptual model regarding water flow within the TCw. The source of the elevated (bomb-pulse) ^{36}Cl has been attributed to nuclear testing conducted in the 1950s, and its occurrence in the TCw indicates the presence of fast pathways for water flow within the unit (CRWMS M&O 2000, U0030, Section 6.1.2).

3.3.3.2 Flow Through the PTn Unit

The relatively high matrix permeabilities and porosities, and low fracture densities of the PTn unit (CRWMS M&O 2000, U0090, Sections 6.1 and 6.2) should convert the predominant fracture flow in the TCw to dominant matrix flow within the PTn (CRWMS M&O 2000, U0030, Section 6.1) (Figure 3.3-3). The dominance of matrix flow and the relatively large storage of the matrix resulting from its high porosity and low saturation give the PTn significant capacity to attenuate infiltration pulses. This will result in water flow below the PTn being approximately at steady state, as demonstrated by the modeling study of Wang and Narasimhan (1993, pp. 354–361).

In an early conceptual model of Yucca Mountain, Montazer and Wilson (1984, pp. 45–48) hypothesized that significant lateral flow occurs within and above the PTn unit. They argued that the contrast in hydraulic properties at the contact of the two units could cause lateral flow. Furthermore, the transient water flow from the TCw unit to the PTn promotes air entrapment,

which could further reduce the vertical liquid flux to the PTn. The current understanding is that local heterogeneities, vertical fractures in the upper portion of the PTn, and gradual transitions in hydraulic properties across the PTn/TCw interface may prevent lateral flow from occurring over extensive distances.

Montazer and Wilson (1984, p. 47) also showed that vertical heterogeneities within the PTn unit may result in a much larger effective permeability of the unit in the direction of dip, compared with the effective permeability in the direction normal to the bedding plane. They argued that combination of this factor and capillary barrier effects might introduce considerable lateral flow within the unit. Recent modeling studies (CRWMS M&O 2000, U0030, Section 6.1), however, indicate that lateral flow is reduced with increasing infiltration rate, and becomes significant only when infiltration rates are far lower than the current estimated values. This is because a lower infiltration rate corresponds to a larger capillary pressure gradient in the vertical direction, which enhances the strength of capillary barrier and limits vertical flow. Therefore, the current conceptual model is that lateral water flow above and within the PTn does occur, but is not significant.

An alternative conceptual model for water flow through the PTn is one which assumes pervasive fracture flow through this unit. While this conceptual model cannot be completely excluded, the pneumatic and the bomb-pulse ^{36}Cl data support the preferred conceptual model of predominately matrix flow through the PTn, as discussed above. A more detailed discussion of water flow within the PTn is given in Section 3.7.3.1.

3.3.3.3 Flow Through the TSw Unit

Unsaturated flow in the TSw hydrological unit is primarily through the fractures (Figure 3.3-2). One piece of supporting evidence for this comes from the magnitude of matrix hydraulic conductivity values of the TSw relative to the estimated average infiltration rate. The maximum matrix percolation rate is the same as the matrix hydraulic conductivity if the hydraulic gradient is assumed to be unity under unsaturated conditions. Because the matrix hydraulic conductivity is much lower than the average estimated infiltration rate (CRWMS M&O 2000, U0030, Section 6.1.2), the remainder of the flow must be distributed in the fracture network. The extensive fracture flow in this unit is also supported by other field observations (CRWMS M&O 2000, U0030, Section 6.1.2).

Other evidence for fracture flow comes from calcite-coating data, which are signatures of water flow history and indicate that most of the deposition is found within the fractures in the welded units (Paces et al. 1998b, p. 37). As discussed in CRWMS M&O (2000, U0030, Section 6.1.2), ^{14}C ages of the perched water bodies below the TSw unit also suggest fracture-dominant flow within the TSw. These ages approximately range from 3,500 to 11,000 years (Yang et al. 1996, p. 34), which is much younger than if the major path for water flow within the TSw was the matrix (CRWMS M&O 2000, U0030, Section 6.1.2). Therefore, fracture flow is considered as the dominant water flow mechanism within the TSw in the Flow Model.

3.3.3.4 Flow Below the Potential Repository

Flow behavior below the potential repository is especially important for modeling radionuclide transport from the repository to water table, because transport paths follow the water flow pattern. The main hydrogeologic units below the potential repository are the CHn and CFu. Both of these units have vitric and zeolitic components that differ by the degree of hydrothermal alteration and subsequent hydrological properties. The zeolitic rocks have low matrix permeabilities and some fracture permeability, and therefore a relatively small amount of water may flow through the zeolitic units, with most of the water flowing laterally in perched water bodies and then vertically down faults (Figure 3.3-2). On the other hand, similar to the PTn unit, the vitric units have relatively high matrix porosity and permeability, and therefore porous-medium-type flow dominates. This is supported by the test results within the CHn (defined in Table 3.2-2) at the Busted Butt underground facility, as discussed in Section 3.11.10.2 of this PMR. The results showed that water flow and tracer transport mainly occur within the matrix of the CHn. Fracture flow is believed to be limited in these units.

One distinctive feature below the potential repository is the existence of perched water zones, which have been reported from a number of boreholes at the lower portion of the TSw and the upper portion of the CHn (CRWMS M&O 2000, U0050, Section 6.2.2). The occurrence of perched water bodies indicates that the layers of the TSw basal vitrophyre and the CHn serve as barriers to vertical flow. Perched water is further discussed in Sections 3.3.8 and 3.7.3.3.

3.3.4 Fracture-Matrix Interaction

Fracture-matrix interaction refers to flow and transport between fractures and the matrix. Owing to their different hydrological properties, distinct flow and transport behavior occurs in each component. The extent of fracture-matrix interaction is therefore a key factor in modeling flow and transport processes in the UZ.

Modeling results and field observations show limited fracture-matrix interaction within welded units at Yucca Mountain (CRWMS M&O 2000, U0030, Section 6.1.3). The chloride concentration data indicate that perched water is recharged mainly from fracture water, with a small degree of interaction with matrix water (CRWMS M&O 2000, U0030, Section 6.1.3). The small degree of interaction between fractures and the matrix at locations associated with geologic features is also suggested by the presence of bomb-pulse ^{36}Cl (CRWMS M&O 2000, U0085, Section 6.6.3) at the potential repository level in the ESF. Studies by Ho (1997b, pp. 401–412) show that the match between simulations and observed matrix saturation and water potential data is improved by reducing the fracture-matrix interaction significantly.

The occurrence of limited fracture-matrix interaction is also supported by observations from Rainier Mesa and other sites. The Rainier Mesa site is characterized by thick sequences of alternating welded and nonwelded unsaturated tuffs and has been considered an analog to Yucca Mountain. Thordarson (1965, pp. 6–7 and pp. 75–80) noted that typically only portions of fractures carried water, and that the chemical composition of water obtained from fractures was substantially different from that of water samples extracted from the nearby rock matrix at that site. At a field site in the Negev Desert, Israel, man-made tracers were observed to migrate with velocities of several meters per year across a 20 to 60 m thick UZ of fractured chalk (Nativ et al.

1995, pp. 253–261). Such high velocities could only occur for conditions of limited fracture-matrix interaction.

The concept of limited fracture-matrix interaction at the Yucca Mountain site is also supported by many other independent laboratory tests as well as theoretical and numerical studies (CRWMS M&O 2000, U0030, Section 6.1.3). In a number of laboratory experiments without considering matrix imbibition, Glass et al. (1996, pp. 6–7) and Nicholl et al. (1994, pp. 2533–2546) demonstrated that gravity-driven fingering flow is a common flow mechanism in individual fractures. This can reduce the wetted area in a single fracture to fractions as low as 0.01 to 0.001 of the total fracture area (Glass et al. 1996, pp. 6–7), although the matrix imbibition can increase wetted areas of fingering flow patterns in individual fractures (Abdel-Salam and Chrysikopoulos 1996, pp. 1537–1538). A theoretical study by Wang and Narasimhan (1993, pp. 329–335) indicated that the wetted area in a fracture under unsaturated flow conditions is generally smaller than the geometric interface area between fractures and the matrix, even in the absence of fingering flow. This results from the consideration that liquid water in an unsaturated fracture occurs as saturated segments that cover only a portion of the fracture-matrix interface area. Liu et al. (1998, p. 2645) suggested that in unsaturated, fractured rocks, fingering flow occurs at both a single fracture scale and a connected fracture-network scale (Figure 3.3-4), which is supported by the field observations from the Rainier Mesa site, as discussed above, and by a numerical study of Kwicklis and Healy (1993, pp. 4097–4099). They found that a large portion of the connected fracture network played no role in conducting the flow. Studies have also shown that fracture coatings can either reduce or increase the extent of fracture-matrix interaction. Thoma et al. (1992, pp. 1357–1367) performed experiments on coated and uncoated tuff fractures and observed that the low-permeability coatings inhibited matrix imbibition considerably. In contrast, fracture coatings may in some cases increase the fracture-matrix interaction when microfractures develop in the coatings (Sharp et al. 1996, p. 1331).

Based on the above discussion, it is believed that fingering flow in fractures is a common flow mechanism in unsaturated fractured rocks and a major reason for limiting fracture-matrix interaction, although some other mechanisms exist. To incorporate the effects of fingering flow into modeling flow and transport in unsaturated fractured rocks, the active fracture model was developed by Liu et al. (1998, pp. 2633–2646) and documented in CRWMS M&O (2000, U0030, Section 6.4). In the model, only a portion of connected fractures are considered to actively conduct liquid water as a result of fingering flow at a fracture network scale.

Note that the active fracture model was developed to consider the average effects of subgrid channels within the context of the dual-continua approach, and could not be used to explicitly simulate individual subgrid channels (fingers or weeps) without additional channel-scale parameters. In addition to the active fracture model, several other models have been proposed to simulate the fracture-matrix interaction (Liu et al. 1998, p. 2635), with the fracture-matrix interface area reduction factor set empirically to a constant, to a power function of liquid saturation, or set equal to the liquid phase relative permeability. The relative permeability for the fracture continuum does not consider the fingering flow mechanism explicitly either.

The fracture-matrix interface area reduction factor from the active fracture model, together with fracture spacing, weep width, and fracture set dimensionality, can be used to estimate the weep spacing. The fracture-matrix interaction is one of the important factors for the TSPA abstractions

of flow focusing in the drift seepage abstraction (Section 3.9.6.3; CRWMS M&O 2000, U0120, Section 6.3.3). It also is taken into account in the radionuclide transport abstraction (CRWMS M&O 2000, U0065, Section 6.2.1). In addition to area, fracture coating distribution, matrix imbibition capacity and other flow path characteristics and transport processes control the spatial and temporal variations of the fracture-matrix interaction.

3.3.5 Effects of Major Faults

Different kinds of faults with varying amounts of displacements exist at Yucca Mountain, as discussed in Section 3.2.3. Fault properties are variable and generally controlled by rock type and stratigraphic displacement. Because major faults are important features of the UZ, they may have the potential to significantly affect the flow processes at Yucca Mountain.

A fault can act as a fast-flow conduit for liquid water (Figure 3.3-5). In this case, transient water flow may occur within the fault as a result of temporally variable infiltration. Note that major faults cut through the PTn, and therefore the attenuating effect of the PTn on water flow transience is significantly reduced within the faults. This is supported by the correlation of observed bomb-pulse ^{36}Cl data and localized geologic features in the depth of the UZ of Yucca Mountain (CRWMS M&O 2000, U0085, Section 6.6.3). However, this fast flow along the major faults is expected to carry only a small amount of water and may not contribute significantly to the liquid flow above the potential repository horizon in the UZ, as will be discussed in Section 3.3.7. Faults intercepting the perched water bodies, however, can correspond to significant vertical water flow as a result of lateral flow within perched water bodies to the faults (see Section 3.3.3.4).

Alternatively, a fault can act as a barrier for water flow (Figure 3.3-5b). Where a fault zone is highly fractured, the corresponding coarse openings will create a capillary barrier for lateral flow. On the other hand, a fault can displace the surrounding geologic units such that a unit with low permeability abuts one with relatively high permeability within the fault zone. In this case, the fault will act as a permeability barrier to lateral flow within the units with relatively high permeability. Montazer and Wilson (1984, p. 20) hypothesized that permeability would vary along faults, with higher permeability in the brittle, welded units and lower permeability in the nonwelded units where gouge or sealing material may be produced. While a fault sealed with gouge or other fine-grained material has much higher capillary suction (driving imbibition), it also has low permeability, retarding the movement of water.

Since lateral flow is considered to be small above the repository (Section 3.3.3.2) and focusing of infiltration near faults may not be significant (Section 3.3.7), it is assumed that faults will not significantly alter the percolation pattern from the surface to the repository level. Large lateral flow to the faults and/or focusing of infiltration near the fault zone on the ground surface are required to generate significant water flow in faults. Below the repository, low-permeability layers in the CHn channel some flow to faults that act as conduits to the water table. However, it is also possible that alteration of faulted rocks in the CHn and CFu causes them to be of low permeability, slowing water travel time from the TSw to the water table. The effects of major faults on flow processes are further discussed and analyzed in Section 3.7.3.2 within the context of the UZ flow submodels.

3.3.6 Transient Flow

Temporal variation in the infiltration rate drives the time-dependent or transient nature of flow in the UZ. The temporal variation of the infiltration may be short term due to weather fluctuations that drive episodic flow, or over much longer time periods corresponding to climate change. As discussed in Section 3.3.3, the PTn is believed to greatly attenuate episodic infiltration pulses such that water flow below the PTn is approximately steady. However, water flow in a relatively small area near the Solitario Canyon fault may be transient because the PTn is not present in that area. Some transience is also expected for liquid flow through isolated fast flow paths that cut through the PTn because of the lack of a significant attenuation mechanism. However, these isolated flow paths are believed to carry only a small amount of water, as will be discussed in Section 3.3.7. Based on these considerations, the FEP “Flow and Transport in the UZ from Episodic Infiltration” is believed to have low consequence, and therefore transient flow behavior is not considered in the UZ Model (Section 1.2.3).

3.3.7 Flow Focusing

Flow focusing refers to occurrence of significant water flow through a very small area and/or zone. Depending on geologic conditions and the magnitude of the flux, flow focusing leading to fast flow pathways across the PTn may occur. A number of samples obtained from the ESF show “bomb-pulse” signatures of ^{36}Cl (CRWMS M&O 2000, U0085, Section 6.6.3). They are generally associated with localized fault structures that cut through the PTn. These pathways are possibly responsible for the presence of high levels of ^{36}Cl within the TSw at the repository horizon. However, the Flow Model assumes for the following reasons that these fast and transient flow paths probably carry a small amount of water (CRWMS M&O 2000, U0030, Section 6.1): (1) bomb-pulse samples are found from only a few locations in the ESF, (2) no significant correlation between high matrix saturation and elevated ^{36}Cl has been reported, (3) these discrete fast paths are not associated with large catchment areas involving large volumes of infiltrating water, (4) bomb-pulse signatures of ^{36}Cl were not found in the perched water bodies (CRWMS M&O 2000, U0085, Section 6.6.3), and (5) post-bomb tritium was detected only in one sample from the perched water (in borehole NRG-7a), but not in any of the other samples (CRWMS M&O 2000, U0085, Section 6.6.2).

Fingering flow through the matrix is an alternative fast flow mechanism through the PTn (CRWMS M&O 2000, U0030, Section 6.1.7). Occurrence of fingering flow has been often reported for unsaturated soils (e.g., Yao and Hendrickx 1996, p. 20; Glass et al. 1991, pp. 1947–1956; Flury et al. 1994, pp. 1945–1954; Selker et al. 1992, pp. 1346–1350). However, fingering flow is a gravity-driven phenomenon and cannot occur when capillary forces are dominant (e.g., Yao and Hendricks 1996, p. 21). The tuff matrix at Yucca Mountain is subject to much greater capillary pressures, characterized by orders of magnitude higher absolute air-entry values than soils (Wang and Narasimhan 1993, pp. 374–377). Therefore, fingering flow through the matrix within the PTn is not considered to be a significant flow focusing mechanism.

While extensively fractured, observations indicate that the fracture water flow paths in the TSw are dispersed and not focused (CRWMS M&O 2000, U0030, Section 6.1.7; Bodvarsson et al. 1999, p. 13). Average measured matrix saturations suggest relatively uniform values for most of the units, and *in situ* water potential measurements also show little variability within the TSw for

different boreholes. It was also observed that temperature within the TSw unit is fairly uniform (CRWMS M&O 2000, U0030, Section 6.1.7). These observations are consistent with a conceptual model in which fracture flow is dispersed, resulting in relatively uniform conditions within the geologic formation.

3.3.8 Perched Water

Perched water is defined as saturated zones that are above or not directly connected to the groundwater table. It may occur when large permeability differences exist between geological units. Perched water zones at Yucca Mountain are reported from a number of boreholes (UZ-14, NRG-7a, SD-7, SD-9, SD-12 and G-2) at the lower portion of the TSw and the upper portion of the CHn (CRWMS M&O 2000, U0050, Sections 6.2.1 and 6.2.2). The hydraulic tests indicate that the perched water zones having very different water volumes exist at Yucca Mountain (CRWMS M&O 2000, U0030, Section 6.1.4).

The presence of perched water has important implications for the travel times and flow paths of water through the UZ of Yucca Mountain. First, perched water ^{14}C age data suggest dominant fracture flow in the TSw unit (see Section 3.3.3.3). Second, the occurrence of perched water bodies indicates that the layers of the TSw basal vitrophyre and the CHn serve as barriers to vertical flow and cause lateral flow (Figure 3.3-6).

3.3.9 Seepage into Drifts

Seepage refers to the flow of liquid water into emplacement drifts. The amount of water seeping into the drifts is crucial for the performance of the potential repository, since this affects the corrosion rates of the waste packages and the mobilization rate of radionuclides. While limited by the percolation flux occurring at the repository horizon, seepage into drifts is mainly determined by the capillary barrier effects of the underground openings to divert water around them. This condition is analogous to capillary barriers formed by fine-grained soils overlying coarse-grained soils (e.g., Frind et al. 1997, pp. 3133–3163; Ross 1990, pp. 2625–2629; Oldenburg and Pruess 1993, pp. 1045–1056). Here, the controlling physical mechanism is that the capillary pressure developed in the fine-grained material prevents water from entering the larger pores of the underlying coarse-grained material (Birkholzer et al. 1999, p. 350). If a drift is conceptualized as “very coarse-grained” with essentially zero capillarity, seepage into the drift can only occur if the capillary pressure in the rock close to the drift walls increases to positive values; i.e., the flow field becomes locally saturated. It can become locally saturated by either disturbance to the flow field caused by the drift opening (Philip et al. 1989, pp. 16–28) or spatial heterogeneities that create channelized flow and local ponding (Birkholzer et al. 1999, pp. 349–351). The capillary barrier effect has been tested in the ESF by niche tests in which water is injected above a niche (see Section 2). Results from the tests indicate that most of the water does not seep into niches, confirming the existence of the capillary barrier. A more detailed discussion of the seepage into drifts and associated modeling and analysis is given in Section 3.9.

3.3.10 Gas Flow Processes

Gas flow at Yucca Mountain depends primarily on the characteristics of fracture networks because fractures are generally much more permeable for the gas phase than the matrix. This is

particularly true for the welded units. However, in the nonwelded units, the matrix is also an important gas flow path because the gas permeability of the matrix continuum is much higher than that in the welded units, due to lower liquid saturation and larger pore sizes.

The ambient gas flow processes occurring at Yucca Mountain include barometric pumping, i.e., the response of subsurface pneumatic pressure to changes in atmospheric pressure. Because this is a transient process, both the permeability and storage of the media affect the subsurface response. In the welded units, this translates into little change in the pneumatic pressure signal with depth (CRWMS M&O 2000, U0030, Section 6.1.8). In the PTn, though, the high gas-filled porosity serves to attenuate and lag the response to barometric pumping between the top and the bottom of the unit. Ahlers et al. (1999, p. 58) showed a close correlation between the PTn thickness and pneumatic response below the PTn. They also showed that faults are fast pathways for gas flow but affect subsurface response only on a relatively local scale (Ahlers et al. 1999, p. 47; also see Sections 3.6.3.3 and 3.6.4.2). Gas flow also occurs under ambient conditions as a result of density- and wind-driven processes (Weeks 1987, pp. 165–170), while their effects on the overall flow and transport processes in UZ of Yucca Mountain are minor (CRWMS M&O 2000, U0030, Section 6.1). In general, under ambient conditions, it is believed that significant gas flow processes occur only in the shallow zone of the UZ, but not in the deep zone, as implied from the gas age data, showing that the rock gas is old at depth within the UZ, where its ^{14}C age is about 10,000 years (Yang et al. 1996, p. 47).

Thermal loading is expected to greatly impact gas flow processes. The modeling studies of Wu et al. (1995, p. 41) show that the average gas flux at the ground surface is increased by many orders of magnitude in response of the thermal loading, and that Solitario Canyon fault and Ghost Dance fault both serve as major pathways for heated gas. A more detailed discussion of the impact of thermal loading on gas flow is given in Section 3.12.3.

3.3.11 Radionuclide Transport Processes

Radionuclide transport processes are closely tied to water flow behavior, because liquid water is considered to be the principal medium in which solutes are transported through the UZ. Figure 3.3-7 schematically shows important radionuclide transport processes in the UZ, including advection, matrix diffusion, sorption, dispersion, and colloid-facilitated transport processes. Radionuclides also undergo radioactive decay, but this is not shown explicitly in Figure 3.3-7. These processes are briefly reviewed in this section, with a more detailed discussion given in Section 3.11.

Advection refers to the movement of dissolved or colloidal materials because of the bulk flow of fluid (Fetter 1993, p. 47). Transport is strongly related to water flow through advection, and advective transport pathways are consistent with the flow pathways discussed in Section 3.3.3.

Matrix diffusion refers to solute transport from fracture networks to surrounding matrix blocks resulting from molecular diffusion (Neretnieks 1993, pp. 47–48). Mass transfer between fractures and the tuff matrix plays an important role in transport within Yucca Mountain. Because flow velocity in the matrix is much slower than that in fractures, matrix diffusion and sorption (for sorbing radionuclides) can significantly retard the overall transport of radionuclides to the water table.

Dispersion is a transport mechanism that promotes dilution and spreading of the solute due to mixing caused by localized variations in flow velocity and heterogeneity (de Marsily 1986, pp. 234–235; p. 244). Dispersion is not expected to play an important role in UZ transport (CRWMS M&O 2000, U0030, Section 6.2). In the rock matrix, dispersion is also considered to be minor compared with diffusion because of low pore velocity in the matrix (de Marsily 1986, pp. 236–238).

Sorption describes a combination of chemical interactions between dissolved solutes and the solid phases (immobile rock matrix or colloids) (Fetter 1993, p. 117). Radionuclide sorption to the rock matrix can act to retard its movement relative to the bulk flow of the groundwater. Strongly sorbing radionuclides are relatively immobile.

Colloids, on the other hand, can facilitate the transport of radionuclides. Colloids are particles that are small enough to become suspended and transported in a liquid (Fetter 1993, p. 149). They can interact with radionuclides through sorption mechanisms (James and Chrysikopoulos 1999, p. 707). Unlike sorption of radionuclides to the rock matrix, however, radionuclides sorbed on colloids are potentially mobile. Therefore, colloids can facilitate radionuclide transport through the UZ at a faster rate than the aqueous phase alone (de Marsily 1986, pp. 270–271). Another form of colloidal movement occurs when the radionuclide is an integral component of the colloid structure. In this case, the radionuclide is irreversibly bounded to the colloid (Figure 3.3-7).

Radioactive decay affects the concentration of radionuclides during transport through the UZ. For simple decay, radionuclide concentration decreases exponentially with time (de Marsily 1986, p. 265), creating stable decay products. In chain-decay, radioactive daughters are produced from the decay of a parent radionuclide, with each daughter product having potentially different sorption and transport behavior.

3.3.12 Effects of Coupled Processes

Radioactive wastes potentially emit a significant amount of decay heat that can influence hydrological, mechanical, and chemical conditions in both the near field (drift scale) and far field (mountain scale) environments. Consequently, the corresponding coupled processes, including thermal-hydrological (TH), thermal-mechanical (TMe), and thermal-chemical (TC) processes, will affect flow and transport within the UZ of Yucca Mountain. TH, TMe and TC processes are also coupled among themselves, although they are discussed separately for simplicity. In this section, we briefly review these processes with an emphasis on their effects on flow and transport in the UZ. More detailed discussions of coupled processes are given in Sections 3.10 and 3.12 that describe the Drift-Scale THC and Mountain-Scale TH Models, respectively.

3.3.12.1 TH Processes

The TH response of the unsaturated fractured tuff to decay heat involves a number of processes (Tsang and Birkholzer 1999, pp. 389–390; Buscheck and Nitao 1993, pp. 418–448). As the formation temperatures are increased around the waste packages, pore water boils and vaporizes. Most of the generated vapor moves into the fractures, where it becomes highly mobile. The heated dry-out zone can prevent the infiltrating water from moving down through the potential

repository, resulting in a drop in the net water flux at the potential repository horizon. When the water vapor encounters cooler rock above and below the potential repository, it condenses, and the local fracture and matrix saturations increase, resulting in a liquid reflux toward the drier region. Between the dry-out and condensation zones, a heat-pipe zone may develop (Tsang and Birkholzer 1999, pp. 389–390). A heat-pipe is indicated by the persistence of liquid-vapor counter flow over a region of small temperature gradient, where temperatures are approximately at the nominal boiling point.

TH effects drive processes at two physical scales (CRWMS M&O 2000, U0030, Section 6.3), as indicated in Figure 3.3-8. At the drift scale (near-field scale), flow and transport is affected by decay-generated heat from each of the individual waste packages in an emplacement drift. Variability of heat output from waste packages could result in large variabilities in the extent of dry-out, rewetting, and of liquid-phase flux along drifts. Heat driven features at the mountain scale include thermally altered, large-scale water flow fields both above and below the potential repository, which may affect radionuclide transport. Thermal loading may also potentially alter the characteristics of perched water bodies (e.g., volume) because of the thermally induced vapor flow from the perched water bodies. However, the major effects of TH processes are expected to be near the emplacement drifts in the early part of the postclosure time period. Radionuclide releases will likely be after the main portion of the thermal pulse (after waste heat begins to dissipate), and a large part of the radionuclide transport process in the UZ will take place at locations outside the envelop of the main TH effects. Therefore, it is reasonable to assume for simplicity that the effects of TH processes on radionuclide transport are not significant. As discussed in Section 1.2.3, this reasoning is a basis for an assumption used in the FEPs exclusion arguments.

3.3.12.2 TMe Processes

Elevated temperatures of the host rock surrounding the potential repository will mechanically change the physical properties of the rock within the UZ (CRWMS M&O 2000, U0030, Section 6.3). Expansion of the rock matrix caused by heating will affect stress distribution in the rock and induce changes in the fracture apertures. These changes can affect the amount of flow through the fractures and subsequently through the entire system. Hydrological changes can, in turn, affect the thermal behavior, which governs the mechanical changes of the rock.

Thermal expansion of the matrix surrounding drifts tends to “close” fractures and reduce fracture aperture and permeability while increasing capillary forces. However, non-uniform deformation of heterogeneous matrix rock blocks will promote sliding or relative movement along two adjacent matrix block surfaces, which may lead to an increase in fracture permeability. During the cooling phase, the fracture apertures near the drifts would generally increase.

3.3.12.3 TC Processes

Chemical reactions in response to a high thermal load in the potential repository can alter hydrological properties of the rock matrix and fractures (CRWMS M&O 2000, U0030, Section 6.3; N0120/U0110). Above the potential repository horizon, the temperature is projected to be sufficiently high to vaporize water and cause the precipitation of minerals in fractures. Condensate may dissolve mineral phases from the walls of fractures and flow back to zones

where precipitation occurs. Mineral dissolution at one point in the fracture network, and redeposition at another, could lead to the formation of a precipitate cap over the potential repository. In the precipitate cap, porosities and permeabilities of fractures and portions of the matrix near the fractures will be reduced. The significance of this reduction depends on the abundance of readily dissolved fracture-lining minerals, relative to fracture porosity, and the dissolution and precipitation rates for the relevant minerals. Other potential effects of thermal loading include hydrothermal alteration of glasses in the PTn, Topopah Spring basal vitrophyre, and the CHn units. TC processes may also alter the chemical composition of seeping water and the sorption capacity of the formations below the potential repository. A more detailed discussion is given in Section 3.10. In general, as discussed in Section 1.2.3, the effects of TC and other coupled processes in the near-field are expected to be more severe than in the far-field. This is caused by the high temperatures that will occur near the waste emplacement drifts, including boiling of the rock-water and associated precipitation of the minerals and condensation of dilute water. This reasoning is a basis for an assumption used in the FEPs exclusion arguments (Section 1.2.3).

3.3.13 Current and Alternative Conceptual Models

Based on the above discussions of physical processes, the current conceptual model of flow in the UZ can be summarized as follows. Infiltration is spatially and temporally variable to a large extent. Infiltration pulses move rapidly through fractures in the TCw unit with little attenuation by the matrix. Because of the attenuative capacity of the PTn unit, water flow below this unit is approximately at steady-state under ambient conditions. Lateral flow in the PTn tends to be insignificant. Fracture flow dominates in the welded units and matrix flow in the nonwelded units. Fracture flow paths are dispersed. Isolated fast flow paths exist, but carry only a small amount of liquid water. Fracture-matrix interaction in the welded units is limited. Perched water bodies introduce three-dimensional, lateral flow. Flow through the major faults does not significantly alter the percolation pattern from the surface to the potential repository horizon. Below the potential repository, low-permeability layers in the CHn channel some flow to faults that act as conduits to the water table.

While the current conceptual model is largely based on the model originally presented by Montazer and Wilson (1984, pp. 36–49), the major difference between these two models are the roles of the PTn unit and structural features, or faults, in conducting water through the UZ. Montazer and Wilson (1984, pp. 50–51) hypothesized that the combination of dipping beds, permeability layering, and capillary-barrier effects results in significant lateral flow within the PTn toward the bounding structural features that transmit most of the infiltrated water downward to the water table. As discussed in Sections 3.3.3.2 and 3.3.5, more recent studies indicate that lateral flow in the PTn may not be as significant as previously thought, and faults are not likely to act as flow paths that significantly alter the flow pattern above the potential repository in the UZ.

Other conceptual models of flow in the UZ have been published in the literature. Since the mid-1980s, the prevailing view has held that under ambient conditions, water flow mainly occurs through the rock matrix, even in the welded, densely fractured TSw unit (Wang and Narasimhan 1993, pp. 327–339; Peters and Klavetter 1988, pp. 416–430; Nitao and Buscheck 1991, pp. 2099–2112; Rulon et al. 1986). It was believed that under unsaturated conditions, water

would essentially be excluded from fractures because of the strong capillarity in the matrix. However, as more site characterization data are available, it has become evident that unsaturated flow in the welded units is primarily through the fractures, as discussed in Section 3.3.3.3.

In a recent study, Pruess (1999, pp. 1040–1051) proposed a conceptual model for flow in thick, unsaturated, fractured rock zones. Key elements of the model are (Pruess 1999, p. 1041): (1) most water flow in thick UZs of fractured rock proceeds by way of episodic, transient, and localized flow through fractures, (2) water flow can remain localized even in the presence of dispersive effects that would tend to cause lateral spreading, and (3) several mechanisms combine to severely reduce the effects of matrix imbibition. While both the model of Pruess (1999, pp. 1040–1051) and the current conceptual model of flow in the UZ consider fracture-matrix interactions to be limited and that only a portion of fractures are active in conducting liquid water, they differ in the spatial distribution and time-dependent features of fracture flow. The former hypothesizes that fracture flow paths in unsaturated, fractured rocks are sparse (Pruess 1999, p. 1049) and transient (Pruess 1999, p. 1041). As discussed in Section 3.3.7, it is more likely that water flow below the PTn unit is approximately at steady state and that fracture flow paths are dispersed.

3.3.14 Summary and Conclusions

A variety of flow and transport processes are involved in the UZ at Yucca Mountain. Based on the discussions of physical processes in the UZ, a conceptual model of flow in the UZ has been developed, as summarized in Section 3.3.13. Because water is considered to be the principal medium in which solute is transported, solute transport is closely tied to flow processes. Major radionuclide transport processes include advection, matrix diffusion, sorption, radioactive decay and colloid-facilitated transport. Flow and transport will be affected by coupled TH, TMe and TC processes resulting from potential repository heat release.

INTENTIONALLY LEFT BLANK

3.4 NUMERICAL MODELS AND GRIDS

Based on available data, an understanding of the complex flow and transport processes occurring within the UZ at Yucca Mountain requires simplification of the real-world system. This is done by applying a set of numerical equations (believed to represent the behavior of the physical process under investigation) to a model volume that has been discretized into a finite number of nodes, or elements, for which certain rock properties are known or estimated.

Section 3.4.1 provides a general overview of numerical models for simulating flow and transport processes in the unsaturated, fractured porous media at Yucca Mountain. The process of numerical grid development and discretization, which is discussed at length in CRWMS M&O (2000, U0000), is summarized in Section 3.4.2.

3.4.1 Numerical Models for UZ Flow and Transport

A variety of numerical models have been proposed in the literature to deal with flow and transport processes in fractured media at the field scale. When classified according to the manner in which fracture networks are treated in the model structure, the models fall into one of three groups: continuum models, discrete fracture-network models, and other models. The other types of numerical models (e.g., Clemons and Smith 1997, pp. 1763–1783) can be considered as variations and/or combinations of the first two basic models. Excellent reviews on these models, which have been developed and used in different fields (including oil reservoir engineering, groundwater hydrology, geothermal engineering, and soil physics), can be found in Bear et al. (1993, pp. 267–320, 396–428) and the National Research Council (1996, pp. 307–394). The numerical models that can be used for unsaturated, fractured rocks will be briefly reviewed, and the rationale for determining the numerical models used in the UZ Flow and Transport Model PMR will be presented.

3.4.1.1 Continuum Models

In continuum models, fractures are considered to be sufficiently ubiquitous and distributed in such a manner that they can be described statistically in a meaningful way (Bear et al. 1993, pp. 395–396). The role of individual fractures in fractured media is considered to be similar to that of individual pores in porous media. Connected fractures and rock matrix are viewed as two or more overlapping interacting continua. In other words, at a “point,” two or more continua are considered to co-exist. In this case, the continuum-mechanics formulations, such as those used for porous media, can be used to describe flow and transport in each continuum. Coupling of processes between different continua is determined by interaction mechanisms at a subgrid scale (Figure 3.4-1). Depending on the number of continua and methodologies used to treat fracture-matrix interaction, continuum models can be classified further as effective-continuum (ECM), dual-continua, and multiple-interacting-continua (MINC) models.

In ECM models (Pruess et al. 1990b, pp. 1249–1261), fractures and rock matrix are replaced with a single effective continuum (Figure 3.4-1). Liquid saturation is partitioned into the matrix and fractures in accordance with the principle of local thermodynamic equilibrium, which requires capillary pressure in the matrix and fracture components of a gridblock to be equal. The ECM approach also assumes that fluids in the fractures and matrix have the same chemical

concentration and temperature (Doughty 1999, pp. 69–106). ECM models provide a substantial simplification for describing flow and transport in fractured porous media and is computationally efficient in handling a model with a large number of gridblocks ($>10^3$). However, the assumptions on which ECM models are based may break down when long times are needed to reach local equilibrium conditions between the fracture and matrix continua. This is especially true for a very tight and low-permeability rock matrix with rapid fracture flow (CRWMS M&O 2000, U0030, Section 6.4.4.1).

In the dual-continua models, fractures and matrix are treated as two separate, yet interacting continua, and each gridblock is subdivided into one fracture block and one matrix block (Doughty 1999, pp. 69–106) (Figure 3.4-1). The fracture-matrix flow and transport are approximated as quasi-steady. This treatment is the numerical equivalent of the Warren and Root (1963, pp. 245–255) formulation. If global flow occurs only between fracture gridblocks, the model is known as a dual-porosity model. If global flow occurs within both fracture and matrix continua, the model is known as a dual-permeability model (Doughty 1999, p. 76). Compared with ECM models, dual-continua models will more accurately predict flow and transport, because nonequilibrium is allowed between fracture and matrix continua. Since there is only one matrix block used for each gridblock and a quasi-steady fracture-matrix flow assumption is employed, gradients of matrix capillary pressures, temperature, and concentration near a fracture-matrix interface may be poorly predicted using dual-continua schemes. Under steady-state conditions, however, the gradients near the matrix surface become minimal, and the models are expected to generate acceptable solutions (CRWMS M&O 2000, U0030, Section 6.4.4.1).

Using a more general and rigorous approach, multiple interacting continua (MINC) models (Pruess and Narasimhan 1985, pp. 14–26), were developed to overcome the limitation of dual-continua models. Specifically, MINC models further subdivide the matrix into more than one matrix continuum to consider the nonequilibrium of flow and transport within the matrix. Compared with dual-continua models, MINC models can more accurately predict flow and transport in fractured media, but have larger computational requirements in both CPU times and storage space.

3.4.1.2 Discrete Fracture-Network Models

Discrete fracture-network models are based on an assumption that flow and transport behavior can be predicted from knowledge of the fracture geometry and data on hydraulic properties of individual fractures (National Research Council 1996, p. 332). These models involve computational generation of synthetic fracture networks and (subsequently) modeling of flow and transport in each individual fracture. These models have been extensively used for single-phase flow and transport, with deterministic, stochastic, artificial, or site-specific fracture networks in two or three dimensions (National Research Council 1996, pp. 333–350). Recently, the same models have also been applied to unsaturated conditions (e.g., Kwicklis and Healy 1993, pp. 4091–4102; Rasmussen 1991, pp. 67–76; Karasaki et al. 1994, pp. 2633–2638; Zimmerman and Bodvarsson 1996, pp. 433–438).

While discrete fracture-network models are useful as tools for concept evaluation or model-based process studies, they have several limitations. First, the models require geometric parameters that may strongly impact flow and transport, such as fracture apertures and conductivity, but typically

cannot be well constrained by field observations (Pruess et al. 1999, p. 308). Second, it is difficult to separate the conductive fracture geometry from the nonconductive fracture geometry (National Research Council 1996, p. 350). Third, flow and transport simulations with these models can be complex and computationally intensive for realistic fracture densities (National Research Council 1996, p. 350). Fourth, so far, the studies based on discrete fracture-network models have rarely considered fracture-matrix interaction because of computational complexity (Pruess et al. 1999, p. 308). The capability to simulate fracture-matrix interaction is essential because of its important effects on flow and transport in unsaturated, fractured rocks.

3.4.1.3 Numerical Models for UZ Flow and Transport at Yucca Mountain

Appropriateness of the currently available numerical models for the flow and transport simulations at Yucca Mountain depends on several important factors, including flow and transport behavior at the Yucca Mountain site, the scale of the problem, data availability, and computational feasibility.

The overall flow and transport behavior in the UZ at Yucca Mountain are characterized by two important features. The first feature is that the isolated fast flow paths only carry small amounts of water and do not significantly contribute to the overall flow and transport patterns in the UZ (see Section 3.3.7), and fracture flow paths are many and dispersed. This makes the continuum model a reasonable choice for simulations of flow and transport in the UZ at Yucca Mountain. The second feature is the coexistence of matrix-dominant flow and transport in nonwelded units and fracture-dominant flow and transport in welded units. This feature can be easily handled by continuum models, but not by other models, such as a fracture-network model. The scale of the problem is an important factor for assessing appropriateness of numerical schemes for flow and transport in the UZ. Because continuum models are relatively simple and straightforward to implement, they are preferred for most applications that are encountered in practice (National Research Council 1996, p. 331). Estimates of the number of potentially water-conducting fractures at Yucca Mountain are on the order of 10^9 (Doughty 1999, p. 77). Considering data availability and computational feasibility, it is practically impossible to construct and calibrate a discrete fracture-network site-scale model with so many fractures.

Based on the above considerations, continuum models are considered appropriate for use in the unsaturated flow and transport models at Yucca Mountain (CRWMS M&O 2000, U0030). As a compromise between accuracy and feasibility, dual-permeability models have become the main modeling approach currently used to simulate unsaturated water flow, heat transfer, and chemical transport at Yucca Mountain. Details of the numerical approaches utilized such as the use of upstream and downstream weighting are discussed in the individual AMRs documenting the particular model (e.g., CRWMS M&O 2000, U0050, Section 6.1 and CRWMS M&O, U0035, pp. 27–34).

3.4.1.4 Some Important Issues for Flow and Transport Modeling

While detailed discussions of dual-permeability models have been well documented in the literature (e.g., Doughty 1999, pp. 75–76), this section discusses some important issues specifically for modeling unsaturated flow and transport at Yucca Mountain.

3.4.1.4.1 Porous Medium Equivalence and Active Fracture Model

In dual-continua models, porous-medium equivalence has been used for describing water flow in the fracture continuum (National Research Council 1996, p. 380). Specifically, Darcy's law is used to determine water flux within the fracture continuum, and constitutive relations between relative permeability, capillary pressure, and saturation are employed for modeling water flow. The van Genuchten (1980, pp. 892–898) relations widely used for porous media are employed as approximate constitutive relations for water flow in the active fracture continuum. The active fracture continuum consists of fractures that actively conduct water. This represents only a portion of the whole fracture continuum because of fingering flow in fractures at different scales. Considering that fingering flow is a common flow mechanism in unsaturated fractures, its effects on overall flow and transport processes in the fracture continuum and between the fracture and matrix continua are considered by using the newly developed active fracture model (Liu et al. 1998, pp. 2633–2646). The active fracture model is documented in CRWMS M&O (2000, U0030, Section 6.4.5).

3.4.1.4.2 Particle Tracking and Conventional Algorithms for Transport Modeling

In general, two kinds of numerical algorithms are used for modeling chemical transport in the subsurface (Liu and Dane 1996, p. 359). One is the conventional algorithm based on finite-difference and/or finite-element methods, and the other is the particle-tracking algorithm. In the particle-tracking algorithm, chemical mass is divided into a large number of particles (Tompson and Gelhar 1990, pp. 2541–2562; LaBolle et al. 1996, pp. 583–593). Chemical transport is simulated by calculating particle movement, which is determined by velocity fields, dispersion/diffusion coefficients, and fracture-matrix interaction formulations. Particle tracking has the following two advantages, when compared with conventional approaches. First, it can significantly reduce or eliminate numerical dispersion, a common numerical problem for coarse grid simulations of chemical transport problems (artificially smearing concentration fronts in simulations). Second, the particle-tracking algorithms generally compute more efficiently. However, one shortcoming of particle-tracking algorithms is that they can only be used for chemical transport with simple chemical reactions (such as linear sorption and decay). Therefore, for unsaturated transport modeling at Yucca Mountain, particle-tracking algorithms are used for modeling chemical transport with simple reactions, and conventional algorithms are used for transport with complex reactions. A detailed comparison between the particle-tracking algorithms and a conventional approach is given in CRWMS M&O (2000, U0155).

3.4.1.4.3 Modeling the Dispersion Process in the Fracture Continuum

Although it is generally recognized that dispersion in a fractured medium is physically different than dispersion in a porous medium, the porous medium form of the dispersion tensor is generally used for lack of a more appropriate expression (Bear et al. 1993, p. 419). Since dispersion may not be a major transport mechanism for the UZ at Yucca Mountain (Section 3.3.11), it is believed that the use of the dispersion tensor is adequate for approximating dispersion processes in the fracture continuum.

3.4.1.4.4 Heterogeneity and Parameterization

Heterogeneities exist at different scales within both the fracture and matrix continua in the UZ at Yucca Mountain. Parameterization refers to the use of a number of parameters to represent the heterogeneous distribution. Treatment of subsurface heterogeneity and parameterization are important for modeling flow and transport processes. A variety of approaches are available for constructing subsurface heterogeneous property distributions, as reviewed by Koltermann and Gorelick (1996, pp. 2617–2658).

A geology-based, deterministic approach, in which an entire model layer is assigned uniform properties, is used mainly for characterizing subsurface heterogeneity and modeling flow and transport in the UZ. The justification for use of this approach is based on the following considerations (CRWMS M&O 2000, U0030, Section 6.4.3). First, it is expected that the overall behavior of site-scale flow and transport processes is determined mainly by relatively large-scale heterogeneities associated with the geologic stratification of the mountain. Stratification and faulting, which places units with highly different properties against each other, are the major heterogeneities within the UZ at Yucca Mountain. Within the same geologic unit, hydrological properties are relatively uniformly distributed because of the intra-strata homogenization induced by the tuff depositional environments (CRWMS M&O 2000, I0040, Section 6.3.1.1). In the geology-based, deterministic approach, subunits are defined within the major hydrogeologic units to capture variability in the vertical stratification. Within these subunits, important lateral heterogeneity can be accounted for by defining lateral boundaries, differentiating areas with significant differences in hydrological properties (Section 3.4.2.2). Second, the complexity of a heterogeneity model needs to be consistent with the availability of the data. More complicated models introduce larger degrees of uncertainties in rock property estimations when data are limited. Third, the layered approach is also supported by field observations, such as the relatively uniform matrix water saturations within a given layer. Fourth, flow and transport models based on a layered approach can be relatively easily calibrated with multiple data sets and provide a means to incorporate a significant amount of the available site data. Fifth, it is straightforward to upscale using inverse modeling when a layered approach is employed.

3.4.2 Development of Numerical Grids

Using the continuum approach (specifically, the dual-permeability method) described and justified above (Section 3.4.1.3), numerical grids of the UZ at Yucca Mountain were developed to simulate flow and transport processes. The following subsections discuss the process of numerical grid development, summarizing the input data, the key steps involved in data integration and grid generation, and the resulting numerical grids and their end uses. The flow of information is described schematically in Figure 3.4-2.

3.4.2.1 Input

Mountain-scale dual-permeability numerical grids of the UZ are developed using geologic and hydrogeologic data, including information from the Integrated Site Model (ISM) of Yucca Mountain as well as data describing fracture characteristics for each grid layer.

The ISM consists of three component models: the Geologic Framework Model (GFM), the Mineralogical Model (MM), and the Rock Properties Model (RPM). Several different versions

of the ISM have been developed, as new information allows for modification of the previous interpretation. ISM3.1 is the current version of the Integrated Site Model (containing GFM3.1, MM3.0, and RPM3.1). Details of this model and its components are given in the ISM Process Model Report (CRWMS M&O 1999, ISM PMR) and in CRWMS M&O (2000, I0035, I0045, I0040). During the development of numerical grids used in the UZ Flow and Transport Model PMR, the most recent ISM data consisted of GFM3.1, MM2.0, and RPM3.0. MM3.0 and RPM3.1 became available subsequent to numerical grid development, and the differences between these model versions and those used to generate the grids are discussed below.

The GFM describes the three-dimensional orientation of geologic layers and faults (CRWMS M&O 2000, I0035, Section 6). Layers explicitly defined within GFM3.1 correspond to lithostratigraphic units differentiated according to depositional history, to variations in degree of welding, crystallization, and alteration, and to fracture characteristics (see Section 3.2). The key difference between GFM3.1 (from ISM3.1) and its predecessor GFM3.0 (from ISM3.0) is the inclusion of new lithology data from boreholes SD-6 and WT-24. Data extracted from GFM3.1 form the basis of the numerical grids developed for the mountain-scale models described in this report. Of the 48 geologic units and 42 faults represented in GFM3.1, approximately 40 of these units and 18 faults (those that lie within the UZ mountain-scale domain) are incorporated into the model grids.

The MM provides three-dimensional interpretations of the distribution of mineral abundances, including smectite and zeolite (CRWMS M&O 2000, I0045, Section 6). Changes between MM2.0 (from ISM3.0) and MM3.0 (from ISM3.1) that may be important for unsaturated flow and transport include the incorporation of new data from boreholes SD-6 and WT-24, and the subdivision of an MM2.0 model layer (that combined geologic layers Tptpv3 and Tptpv2) into two layers of equal thickness to better represent a zone of intense smectitic and zeolitic alteration at the base of the TSw (CRWMS M&O 2000, I0045, Section 6.1). The procedure for modeling mineral abundance distributions was also improved in MM3.0. The deterministic inverse-distance-weighting function used to calculate the distribution of mineral abundances in MM2.0 produced certain point anomalies (centered at data point locations) determined inappropriate for use in defining vitric-zeolitic boundaries in the mountain-scale numerical grids described in this PMR (for more details, refer to CRWMS M&O 2000, U0000, Section 6.6.3). More recent mineral abundance distributions calculated for MM3.0 show more extensive regions of vitric material surrounding borehole SD-6 (Figure 3.4-3). The presence of more vitric material would lead to more matrix flow in the models and, consequently, slower radionuclide breakthrough times (beneficial to repository performance).

The RPM provides a three-dimensional geostatistical interpretation of the distribution of matrix porosity (CRWMS M&O 2000, I0040, Section 6). The model also describes the distribution of derivative properties (using porosity as a surrogate), including saturated hydraulic conductivity, bulk density, and thermal conductivity. Differences between RPM3.0 (from ISM3.0) and RPM3.1 (from ISM3.1) that may be important for unsaturated flow and transport include higher matrix permeabilities in the vitric areas in RPM3.1, although the overall pattern of the property distribution is similar in both versions (Figure 3.4-4). [Note that in light of the newer MM and RPM data, the current representation of the vitric-zeolitic boundary used in the flow and transport models can be considered conservative.]

RPM3.0 does not contain data from newly drilled boreholes SD-6 or WT-24 that suggest a greater extent of vitric material (corresponding to areas of higher matrix permeability) beneath the southern half of the potential repository footprint and a thin vitric interval within pervasively zeolitic tuffs beneath northern Yucca Mountain. Data used in numerical grid development discussed herein for defining "low permeability," zeolitic volumes of rock within certain model layers were obtained from the most current rock properties model available at the time, RPM3.0. The key assumption related to the use of these data was that matrix permeability could be correlated with sorptive alteration minerals (e.g., clays and zeolites). Sharp gradients between areas of high and low matrix permeability, calculated for the CHn hydrogeological unit in RPM3.0, were assumed to correspond to the boundary between unaltered (vitric) and altered (zeolitic) materials (see Section 3.2.4). Polygons were created along these sharp gradients within the CHn for five model layers in the mountain-scale numerical grids. The polygons were then used during grid development to distinguish between vitric and zeolitic areas in each of these five model layers.

The final data input, used to formulate the dual-permeability grids described in this PMR, is fracture hydrogeologic properties (CRWMS M&O 2000, U0000, Table 5). Fracture hydrogeologic properties consist of calculated fracture porosity, fracture frequency, and fracture-matrix interaction parameters for each model layer in the mountain-scale grids. Fracture hydrogeologic properties are summarized in Sections 3.6.3.2 and 3.6.5.1 of this PMR and are described in greater detail in CRWMS M&O (2000, U0090, Section 6.1).

3.4.2.2 Data Integration and Grid Generation

Data integration and numerical grid generation consist of three main steps:

1. Defining a hydrogeologic layering scheme appropriate for capturing important unsaturated flow and transport processes, and extracting relevant data from GFM3.1 based on this scheme.
2. Determining vitric-zeolitic boundaries within several model layers in the CHn hydrogeologic unit and incorporating these boundaries into the numerical grids.
3. Generating ECM and dual-permeability numerical grids using WinGridder software.

Although variations in rock hydrogeologic properties (such as porosity and permeability) often correspond to changes in lithostratigraphy, a strictly geologic model cannot adequately capture all of the important features that affect flow and transport processes in the UZ. For instance, materials with similar porosity but with highly contrasting saturations and matrix permeabilities, such as the nonwelded vitric and zeolitic tuffs, are found within the single GFM3.1 unit Tac (see Section 3.2.4). Similarly, hydrological property variations exist within lithostratigraphic unit Tpy (see Section 3.2.2.2), caused by porosity changes resulting from variations in the degree of welding. Hydrogeologic rock property data, therefore, were considered during the process of defining hydrogeologic layers for the mountain-scale numerical grids, as discussed in CRWMS M&O (2000, U0000, Section 4) and Chapter 2 of this PMR.

Based on hydrogeologic properties information presented in Flint (1998), certain GFM3.1 lithostratigraphic layers were combined, while others were subdivided for the purpose of developing a set of hydrogeologic model layers for the UZ Flow and Transport Model PMR (see Table 3.2-2). The details of these modifications are given in CRWMS M&O (2000, U0000, Section 6.4.1). The resulting scheme subdivides the TCw into 3 layers, the PTn into 6 layers, the TSw into 8 layers, the CHn (including the Prow Pass) into 11 layers, and the CFu into 4 layers. Data describing the thickness of each hydrogeologic layer (i.e., corresponding to a combined, subdivided, or unchanged GFM3.1 layer) retain the regular horizontal spacing of 61 m in both X and Y directions used in the GFM. Calibrated fracture and matrix hydrogeologic properties are determined for each of the 32 UZ model layers (see Sections 3.6.4 and 3.6.5). Fault gridblocks are identified by major hydrogeologic intervals (i.e., TCw, PTn, TSw, and CHn/CFu), and fault hydrogeologic properties are determined for each of these intervals (see Sections 3.6.4.2 and 3.6.5).

Because of the importance of mineral (especially zeolitic) alteration on flow and transport calculations, lateral boundaries between vitric and zeolitic areas are defined within model grid layers ch1 through ch5 (refer to Table 3.2-2). Zeolitic alteration reduces permeability (Loeven 1993, pp. 18–19, 22; Flint 1998, p. 32) and increases the rock's ability to sorb radionuclides (CRWMS M&O 2000, I0045, Section 1.2). As stated above, data used in numerical grid development for defining low-permeability, zeolitic volumes of rock are obtained from RPM3.0. The details of extracting permeability rock properties data in order to delineate the vitric-zeolitic boundary in model layers are provided in CRWMS M&O (2000, U0000, Section 6.6.3). Resulting distributions of vitric and zeolitic material in layers ch1 to ch5 of the mountain-scale numerical grids used in the UZ Flow and Transport Model PMR are shown in Figure 3.4-5.

The computer code WinGridder (WinGridder V1.0, STN: 10024-1.0-00) was used to generate the numerical grids for the model domain. WinGridder has the capability of designing complex, irregular grids with large numbers of gridblocks and connections, and can incorporate nonvertical faults and other embedded refinements, such as waste emplacement drift spacing within the potential repository area at Yucca Mountain.

Numerical grid development begins with the arrangement of node-centered gridblocks in map view (Figure 3.4-6). The map-view, nodal-point array establishes the location of vertical columns that comprise either 1-, 2-, or 3-D numerical grids. These columns either coincide with important calibration points (e.g., boreholes), or are aligned along the lateral trace of major faults, potential emplacement drifts, and/or the exploratory tunnels, or conform to specified boundaries (e.g., the repository outline). All columns within the grids are vertical, except within certain fault zones where the average slope of the fault plane is less than approximately 80 degrees (detailed criteria establishing vertical/nonvertical columns of gridblocks along faults are given in CRWMS M&O (2000, U0000, Section 6.3)). The vertical component of all grids contains the subdivision of the UZ into hydrogeologic layers according to their thickness and stratigraphic position.

Generation of the numerical grids requires specification of three reference horizons: an upper and lower model boundary (usually the bedrock surface and water table, respectively) and a structural reference horizon (in this case, the top of unit Tpbt4) that defines layer displacement along major fault traces and sets the elevation of the remaining layer interfaces (for 1-D grids,

fault displacement is irrelevant). Isochore maps (consisting of GFM3.1 data files that contain layer thickness data) are then added to or subtracted from the structural reference horizon to build the vertical component of the numerical grids.

The primary grid generated by WinGridder represents only a single (matrix) continuum and is, therefore, referred to as an ECM grid. The incorporation of fracture characteristics is determined from fracture data analyses summarized in Section 3.6.3.2 of this PMR. It allows for modification of the ECM grid to create a dual-permeability grid that distinguishes between fracture and matrix components of flow. Fracture characteristics include fracture porosity, frequency, aperture, and fracture-matrix interaction area. The details of dual-permeability grid generation are explained in CRWMS M&O (2000, U0000, Section 6.7).

3.4.2.3 Output

The resulting numerical grids include: (1) a set of 1-D, vertical columns of gridblocks centered at the location of boreholes used to calibrate rock hydrogeological properties that, in turn, are assigned to layers within the mountain-scale numerical models of the UZ; (2) a 2-D grid consisting of columns of gridblocks aligned along an east-west transect through borehole UZ-7a used for fault hydrogeologic property calibrations; (3) a 3-D grid used for mountain-scale model calibrations; and (4) a 3-D grid used to generate ambient and predictive flow fields for PA.

Table 3.4-1 summarizes the purpose, general description, and users of the four different numerical grids. CRWMS M&O (2000, U0000, Section 6) presents a detailed description of the steps involved in the generation of these grids.

Table 3.4-1. Summary of Grids Developed for UZ Flow and Transport Model PMR Activities (Adapted from CRWMS M&O 2000, U0000, Table 6)

Purpose	Grid Description	Grid User
1-D hydrogeologic property set inversions and calibrations	Consists of 1-D columns centered at borehole locations. Includes boreholes: SD-6, SD-7, SD-9, SD-12, NRG#5, NRG-6, NRG-7a, UZ#4, UZ-14, UZ#16, and WT-24.	Calibrated Properties Model
Fault hydrogeologic property calibration	East-west cross-sectional grid through borehole UZ-7a and the Ghost Dance fault.	Calibrated Properties Model (for faults)
3-D UZ Model calibration	Consists of a plan-view grid with discretization along major faults, the ESF, and the ECRB. Also contains columns of gridblocks centered at borehole locations. Vertical resolution in potential repository footprint is 5 m.	Flow Model Transport Model Ambient Geochemistry Model
Generation of 3-D flow fields for PA	Consists of a plan-view grid with repository refinement, but no ESF or ECRB discretization. Rows of gridblocks (width × length: 81 × 270 m) established along repository drift alignment. Vertical resolution in potential repository footprint is 5 m. Contains columns of gridblocks centered at certain borehole locations.	Flow Model Transport Model Mountain-Scale Thermal-Hydrological Model

Figures 3.4-7 through 3.4-9 show 2-D, cross-sectional grids extracted from the mountain-scale numerical grids. Cross sections from GFM3.1, corresponding to the approximate location of the grid profiles, are shown for comparison in each figure.

3.4.2.4 Grid Refinement Studies

Numerical grids must achieve a proper balance between desired numerical accuracy and computational time controlled by the total number of gridblocks. Gridblock size should reflect the scale of the process to be modeled and the availability of data. For reasons stated in Section 3.4.1.3, the mountain-scale models of Yucca Mountain do not attempt to capture isolated fast flow paths. Instead, the models focus on overall UZ characteristics and processes potentially affecting repository performance on a mountain scale.

Simulations of the UZ at Yucca Mountain with coarse and refined 2-D, cross-sectional grids have helped to determine the appropriate numerical grid resolution to be used in the mountain-scale numerical grids. Results of grid resolution sensitivity studies are described in CRWMS M&O (2000, U0000, Section 6.8). In summary, these results indicate that moisture flow is predominantly vertical, except where zeolites are present, suggesting that modeling results are less sensitive to lateral gridblock dimensions than to vertical changes in grid resolution, unless a sudden change in rock hydrogeologic properties occurs at a layer contact (resulting in significant lateral diversion). Below the repository horizon, lateral diversion is most likely to occur above zeolites in the CHn. Calculated saturation and percolation flux distribution can be adequately resolved by adding a few grid layers at the PTn-TSw interface and at the vitric-zeolitic interfaces within the CHn, since these are transitional areas where rock properties change rapidly over short vertical distances.

The current UZ mountain-scale models are vertically resolved with about 44 layers in the potential repository footprint; about 15 of these layers are above the repository horizon, 5 layers (each with 5 m vertical resolution) are within the repository horizon, and about 24 layers lie between the repository horizon and the water table. The transitional areas at the PTn-TSw interface and the TSw-CHn interface are generally captured by several thin model layers.

Also analyzed were results from tracer simulations at different grid resolutions and under different perched water scenarios. Results showed that differences in grid resolution were minimal, thus supporting the use of a relatively coarse numerical grid (CRWMS M&O 2000, U0000, Section 6.8).

3.4.3 Summary

Numerical simulation of performance-related flow and transport issues in the UZ at Yucca Mountain first requires an evaluation of numerical models and selection of the best approach based on the characteristic flow and transport behavior specific to the site, the scale of the problem, data availability, and computational feasibility. Dual-permeability (continuum) models have been determined to be the best approach for simulating flow and transport in the UZ at Yucca Mountain.

Geological and hydrogeological data, predominantly from the Integrated Site Model (ISM) of Yucca Mountain, are used to develop numerical grids of the UZ mountain-scale domain.

GFM3.1 provides key layer and fault-orientation data for establishing the structural and stratigraphic framework in the numerical grids of the UZ. Definition of detailed hydrogeologic units further refines the layering scheme used in the unsaturated flow and transport models. This hydrogeologic layering scheme subdivides the TCw into 3 layers, the PTn into 6 layers, the TSw into 8 layers, the CHn (including the Prow Pass) into 11 layers, and the CFu into 4 layers. Distribution of saturated hydraulic conductivity from RPM3.0 is used to differentiate between vitric and zeolitic regions within portions of the CHn hydrogeologic unit.

The resulting dual-permeability numerical grids include:

- A set of 1-D, vertical columns of gridblocks centered at the location of boreholes; used in the Calibrated Properties Model for determining calibrated fracture and matrix hydrogeologic properties.
- A 2-D grid consisting of columns of gridblocks aligned along an east-west transect through borehole UZ-7a; used in the Calibrated Properties Model for fault hydrogeologic property calibrations.
- A 3-D numerical grid for mountain-scale model calibrations; used in the Flow Model, Transport Model, and Ambient Geochemistry Model.
- A 3-D grid for generating ambient and predictive flow fields for PA; used in the Flow Model, Transport Model, and Mountain-Scale Thermal-Hydrological Model.

INTENTIONALLY LEFT BLANK

3.5 CLIMATE AND INFILTRATION

This section describes issues related to future climate states and resulting net infiltration for the Yucca Mountain region over the next 10,000 years. Issues, modeling methodology and data, and results are summarized in Figure 3.5-1 for both the climate and infiltration models to provide perspective within the entire Yucca Mountain Project. In Section 3.5.1, three potential future climates are identified: modern, monsoon, and glacial transition with durations of 600, 1,400, and 8,000 years, respectively. Estimates for lower-bound, mean, and upper-bound precipitation and temperature are determined using analog meteorological stations. These are used as input for the Infiltration Model discussed in Section 3.5.2, which includes the processes of precipitation, evapotranspiration, snowmelt, and surface water run-on. This model provides estimates of the net infiltration over the Yucca Mountain region for the future climate scenarios for input into the flow and transport process models for the unsaturated zone (UZ) which are presented in Sections 3.7 and 3.11, respectively. The abstraction of climate and infiltration, which quantifies uncertainty in output results from the Climate Model and Infiltration Model for the Viability Assessment, is described in Section 3.5.3. This work is supported by the AMRs *Future Climate Analysis* (USGS 2000, U0005), *Simulation of Net Infiltration for Modern and Potential Future Climates* (USGS 2000, U0010), and *Analysis of Infiltration Uncertainty* (CRWMS M&O 2000, U0095).

Anderson et al. (1998, pp. 12–15) provide a critical summary of the previous VA Climate Model. This model was constructed from three elements: the dry present-day climate (P-climate); the long-term average climate (LTA-climate) which is colder and wetter than the present; and the so-called “super pluvial” climate (SP-climate) which is wetter and colder still. The P-climate occurs once every 100,000 years, lasts for 10,000 years, and has a present-day precipitation rate of 170 mm/yr. The LTA-climate lasts for 80,000 to 90,000 years out of every 100,000 years and has twice the P-climate precipitation rate. The SP-climate occurs very infrequently—just twice per million years and lasts for 10,000 years—and has almost three times the P-climate precipitation rate. The infiltration rates from the corresponding TSPA base-case Infiltration Model were 8 mm/yr for the P-climate, 42 mm/yr for the LTA-climate, and 110 mm/yr for the SP-climate. They argue that the climate and infiltration models were overly conservative given evidence from precipitated secondary minerals in Yucca Mountain, regional shoreline and other geomorphic features, and lack of any past record of SP-climate. They further argue that evidence indicates that the Yucca Mountain region has become increasingly arid over the past million years. The Climate and Infiltration Models presented in this analysis provide an alternative methodology to that reviewed by Anderson et al. (1998, pp. 12–15). Precipitation and net-infiltration rates estimated by the previous VA Climate Model provide an upper bound to those estimated using the Climate and Infiltration Models in this work. Despite these differences, similarity in the precipitation and net-infiltration rates estimated by the two independent methodologies indicate that the Climate and Infiltration Models are conservative as well. In particular, the Climate Model is based on an analysis of natural analog sites intended to represent the Quaternary paleoclimate of the Southern Great Basin as requested by Anderson et al. (1998, p. 15).

3.5.1 Future Climate Analysis

3.5.1.1 Introduction

An analysis of potential future climate conditions for Yucca Mountain was conducted to estimate the timing and nature of climate change over the next 10,000 years. This is the imposed time interval appropriate for the analysis of future climates required for compliance with a regulatory standard as stated in NCR's proposed 10CFR63 (see Federal Register for February 22, 1999, 64FR8640). The approach involves estimating the upper and lower bounds for precipitation and air-temperature for each future climate scenario as well as estimated mean annual values. This analysis is documented in the USGS (2000, U0005) and is used to provide input for the Infiltration Model (USGS 2000, U0010) discussed in Section 3.5.2. Paleoclimate reconstruction was used to estimate future climate conditions. The timing and nature of climate change is primarily based on Devils Hole, Nevada, delta oxygen-18 ($\delta^{18}\text{O}$) and Owens Lake, California, microfossil data. Past climates were then used to select representative meteorological stations as future climate analogs.

Devils Hole is an active extensional fracture (located approximately 90 km south of Yucca Mountain) in the Paleozoic limestone that composes the regional Paleozoic aquifer. During the last 500,000 or more years, calcite has precipitated on the walls of the fracture leaving a $\delta^{18}\text{O}$ record of the precipitation-derived infiltrating water flowing through the fracture. The isotopic values of infiltration are related to the temperature of the source water (the tropical and subtropical Pacific Ocean), the path that the water vapor takes from the source to the recharge area (and the amount of precipitation that occurs along the path), and the temperature at which the precipitation in the recharge area forms. The Owens Lake Basin is located on the eastern side of the Sierra Nevada Mountain Range east of Los Angeles, California. Microfossil records of diatoms and ostracodes from cores drilled at Owens Lake are used to reconstruct the climate history. Ostracode and diatom species environmental tolerances provide a way to interpret the relative total dissolved solids (TDS) of the Owens paleolake, and the relative temperature of its water. The TDS and water-temperature information are then interpreted in climate terms. Thus the stratigraphic profiles of microfossil species provide a way to interpret regional climate history from their implied paleoenvironments, provide insight into glacial and interglacial climate change, and provide a means to compare past climates with each other.

The present-day earth climate system is illustrated in Figure 3.5-2a and consists of two active components, the tropical (Hadley Cell) and polar air masses, and one more passive component or mixing zone, the westerlies (Ferrell Cell). Yucca Mountain is currently dominated by the northern region of the tropical air masses, the Subtropical Highs. These consist of high-pressure descending air that creates a hot low-precipitation and high-evaporation climate. In general, the Subtropical Highs define the global desert belts. Specifically, in the late spring through early fall at Yucca Mountain, there is a northward movement and intensification of the Subtropical Highs that do not intensify to the point of creating monsoonal weather patterns as in southern Arizona, New Mexico, and Mexico. Typically, there are local thunderstorms and high evaporation. From late fall to early spring, the Subtropical Highs weaken and retreat south, leaving the region largely under the influence of the westerlies. The westerlies represent the mixing zone between the tropical and polar air masses and consist of both high- and low-pressure air masses. The precipitation and temperature in this zone are typically seasonal. The moisture potential of the

westerlies is greatly reduced by the Sierra Nevada Mountains and to a lesser extent by the Transverse Range. The wettest winters are attributed to El Niño years (USGS 2000, U0005, Section 6.2). The Subtropical Highs have dominated this region over the past 7,000 to 8,000 years. Figures 3.5-2b and 3.5-2c show the daily precipitation over a 15-year period and an aerial view of Yucca Mountain, respectively. Currently, Yucca Mountain is one of the more arid regions in the U.S.

The climate at Yucca Mountain for the last 8,000 years is not entirely representative of climate patterns that have existed for the past several hundred thousand years. Past climates exhibited a great deal of variability, alternating between glacial and interglacial periods. During glacial climates, winter seasons were longer and summers shorter, with the general climate conditions dominated by Polar Lows and Arctic Highs. Subtropical highs were less persistent and mean-annual temperature, summer temperature, and evaporation were lower. Polar Lows represent the southern region of the polar-air masses and consist of low-pressure rising air, resulting in cool temperatures and high precipitation and low evaporation climates. The average position of the Polar Lows roughly defines the current position of the Boreal Forests. Arctic Highs consist of cold dry air, low precipitation, and low evaporation climates that at times result in large continental ice sheets.

The following subsections provide a brief summary of the assumptions used in developing the future climate scenarios, the timing of future climate change, and the selection of analog meteorological stations (USGS 2000, U0005).

3.5.1.2 Analyses and Assumptions

The analysis of future climate change was based on examining paleoclimate records to find a past climate series that is expected to be repeated in the future. Four key assumptions are utilized (USGS 2000, U0005, Section 5) and described below.

The first assumption is that climate is cyclical with several alternating glacial and interglacial periods occurring during an approximate period of 400,000 years. Furthermore, this pattern is expected to continue into the future, so that future climates may repeat, or at least approximate, past climates. Analysis of $\delta^{18}\text{O}$ from Devils Hole, Nevada, is the basis for this assumption (USGS 2000, U0005, Section 6.3).

The second assumption is that a relationship exists between the timing of long-term past climates and timing of earth orbital parameters. Orbital parameters can be calculated from basic celestial mechanics, which can be used to estimate the timing of future climates once established. A correspondence was found between climate change chronology from Devils Hole and the earth orbital parameters of precession and eccentricity (USGS 2000, U0005, Section 6.4).

The third assumption is that there is a relationship between the characteristics of past climates and the sequence of those climates. Past climates are assumed to repeat in a systematic order. Thus the analysis can focus on this particular climate sequence rather than all past climates and need not take the conservative approach of using the climates that generate the highest infiltration as being those expected in the next 10,000 years. Therefore, the microfossil record

from cores drilled at Owens Lake, California, was used to reconstruct the projected climate history for the next 10,000 years.

The fourth assumption is that long-term earth-based climate-forcing functions, such as tectonic change, have remained relatively constant over the past 500,000 years or so and will remain constant for the next 10,000 or more years. This is important to climate forecasting because such forcing functions change climate in noncyclic ways, invalidating the first three assumptions. Furthermore, it is assumed that anthropogenic influences (global warming due to green house gases) and other natural catastrophic events (volcanic eruptions, meteorite impact etc.) will not significantly induce noncyclic climate change.

Using these four assumptions, which are intended to establish a defensible means for climate forecasting, the Owens Lake climate record is used to describe the climate conditions of the interval selected as the past/future climate analog. The past/future climate analog shows three distinct climates, each of which is described in terms of an upper-bound and a lower-bound climate value. The upper and lower bounds of each climate are described from what are believed to be representative meteorological stations, with the data at those stations then serving as input to the Infiltration Model.

3.5.1.3 Timing of Climate Change

The orbital clock as derived from the Devils Hole chronology (USGS 2000, U0005, Figures 7a, 7b, and 8) was used to approximately identify the past/present point in the Owens Lake record (USGS 2000, U0005, Figure 11). The past/present point is the point in the past climate series representing the equivalent to the present-day climate. The future climate analog is then defined as the paleoclimate reconstruction of a 10,000-year sedimentary record interval beginning at the past/present point. Chronological correlation between the Owens Lake sedimentary record and the Devils Hole $\delta^{18}\text{O}$ record is based on a sediment mass-accumulation curve that is a function of climate and is discussed in USGS (2000, U0005, Section 6.5.1)

From the past/present point at Owens Lake (about 400,000 years ago), the timing of the climate change intervals is further refined from the sediment mass-accumulation methodology on the basis of the abundance intervals for the ostracode species and the corresponding climatic conditions necessary to support these species (USGS 2000, U0005, Figure 14). The environmental tolerances of ostracode species provide a methodology to interpret the relative TDS of the Owens paleolake, and the relative temperature of the water. The TDS and water temperature are then interpreted in climatic terms. The time between the *Limnocythere sappaensis* abundance peak 403,970 years ago and the first appearance of *L. bradburyi* is about 600 years in Owens Lake time. This corresponds to the length of time before the transition occurs from the remaining modern-like climate into the enhanced monsoon climate at Yucca Mountain. The length of the *L. bradburyi* abundance interval representative of monsoon climate conditions is about 1,400 years. The monsoon interval is followed by more than 8,000 years of glacial transition climate as indicated by the *Candona caudata*. This completes a 10,000 year interval from the past/present point in the Owens Lake record for use as the future climate analog (USGS 2000, U0005, Section 6.6.1).

3.5.1.4 Nature of Future Climates

The nature of future climate and, in particular, the annual and seasonal precipitation and temperature provide the input terms for the Infiltration Model, discussed in Section 3.5.2. The nature of future climate, as discussed below, is forecast in terms of upper- and lower-bound precipitation rates and temperatures. The mean values of precipitation and temperature are obtained from these bounding values. The upper- and lower-bound values are quantified by selecting meteorological stations at locations that currently have similar climatic conditions to past climates observed in the Owens Lake chronological record. These analog stations are in areas with some or all of the common ostracodes and diatoms found in Owens Lake, thus potentially integrating the biology, hydrology, and climate linkages that were expressed in the past at Owens Lake. The selected stations are discussed below and listed in Table 3.5-1. Stations with complete and long records were given priority.

Table 3.5-1. Meteorological Stations Selected as Analogs for Future Climate States

Climate State	Duration	Representative Meteorological Stations	Locations of Meteorological Stations	
Modern Climate	600 years	Site and regional meteorological stations	Yucca Mountain region	
Monsoon Climate	1,400 years	Average Upper Bound:	North Latitude	West Longitude
		Nogales, Arizona	31° 21'	110° 55'
		Hobbs, New Mexico	32° 42'	103° 08'
		Average Lower Bound:	Yucca Mountain region	
		Site and regional meteorological stations		
Glacial Transition Climate	8,000 years	Average Upper Bound:	North Latitude	West Longitude
		Spokane, Washington	47° 38'	117° 32'
		Rosalia, Washington	47° 14'	117° 22'
		St. John, Washington	47° 06'	117° 35'
		Average Lower Bound:	North Latitude	West Longitude
		Beowawe, Nevada	40° 35' 25"	116° 28' 29"
		Delta, Utah	39° 20' 22"	112° 35' 45"

SOURCE: Adapted from USGS 2000, U0005, Table 6-1

Modern Climate

The modern-like climate interval consists of Owens Lake being supported by groundwater discharge and with Owens River predominately at base flow. Summers are warm to hot and very evaporative, with evaporation greatly exceeding precipitation at low elevations. Owens Lake remains saline and at a low lake level for long periods of time. The wettest years that are representative of the upper-bound present-day climate are characterized by Pacific airflow focused toward the high Sierra Nevada mountains. This results in an increase in snowpack and hence the seasonal duration of surface-water flow in the Owens River and its potential to dilute the salt content of Owens Lake. El Niño climates that have been common during the last couple of decades also focus Pacific moisture toward southern Nevada. Dry years representative of the lower-bound present-day climate are characterized by minimal winter precipitation when the polar front remains largely north of the region. Summer precipitation is dominated by subtropical high activity, but not to the degree necessary to generate a monsoon-type climate.

Meteorological data for the upper and lower bounds come from available stations in the region, including Yucca Mountain Project and non-Project data. Regional averaged meteorological data from the National Oceanic and Atmospheric Administration (NOAA) reported in USGS 2000 (U0005, Section 6.6.2) indicate that areas largely north of Yucca Mountain within central Nevada have had a range of mean annual precipitation from about 75 mm to one value as high as 360 mm for the period of record (about 100 years). Similarly, areas largely south of Yucca Mountain have had a range of mean annual precipitation from less than 50 mm to one value as high as 325 mm for the period of record. Notably, more low-precipitation years have occurred than extremely high ones (i.e., the typical value is in the lower half of the range). By contrast, the mean annual temperature in both regions falls into a smaller range, within 16–20°C for the area south of Yucca Mountain and about 8–12°C for the area north of Yucca Mountain.

Monsoon Climate

The second climate interval, the monsoon climate, is characterized in the Owens Lake record by a mixture of the ostracodes *Limnocythere bradburyi* and *L. sappausensis*. The existence of *L. bradburyi* in Owens Lake implies a relatively lower total dissolved solids (less than about 10,000 mg/L) and source water derived from expansion and intensification of the summer rain system, diluting surface flow in the Owens River.

Accordingly, an analog meteorological station for monsoon climate would be located to the south of Owens Lake in either Mexico or the southernmost U.S. to meet these conditions. The meteorological stations at Hobbs, New Mexico, and at Nogales, Arizona, with mean annual precipitations of 418 mm and 414 mm, respectively, were selected (USGS 2000, U0005, Section 6.6.2). Two stations were selected to minimize the influence of local meteorological phenomena. Meteorological stations in the Yucca Mountain region were selected as the lower bound for the monsoon climate.

Glacial Transition Climate

The change from the monsoon climate to the glacial transition climate in the Owens Lake record occurs rapidly within a time interval of 100 to 200 years. The glacial-transition climate in the

Owens Lake record is characterized by the appearance of *Candona caudata* as well as by the diatom *Stephanodiscus asteroides*, and diatom species belonging to *Campylodiscus* spp. and *Anomoeneis* spp. *Candona caudata* lives in the Owens Lake area today as well as in many places north of Owens Lake including sites within Canada and Alaska. In the Owens Lake area it lives in the Owens River as well as in freshwater lakes at higher elevation, and thus is tolerant of the region's seasonal temperature variability, but is not tolerant of saline water that would be typical for Owens Lake today under natural conditions. *Candona caudata* only enters Owens Lake when the TDS falls and remains below about 3,000 mg/L, and that typically implies that the lake is full and spilling. The presence of *Stephanodiscus asteroides*, a cool and freshwater planktic diatom, also implies a deep spilling lake. Conversely, the sporadic appearance of *Limnocythere sappaensis* as well as the diatoms *Campylodiscus* spp. and *Anomoeneis* spp imply that there were also episodes during this climate period that were relatively warm and dry, thus demonstrating some degree of climate variability.

Selecting analog meteorological stations for the glacial transition climate requires identifying sites with cool winter wet seasons, and warm to cool and dry summers. The analog sites should be in the semi-arid west and lie on the eastern side of large mountain ranges so that they are in the rain shadow. The absence of the *Cytherissa lacustris* ostracode within the Owens Lake record is indicative of a cold Canadian-like climate and implies that a suitable analog should lie within the contiguous U.S. Lastly, because the mean annual temperature at Yucca Mountain during the last full-glacial period was about 8°C (USGS 2000, U0005, Section 6.6.2), the analog for the glacial transition climate should have a mean annual temperature no colder than and preferably warmer than 8°C. This would support current ostracode populations (at the analog site) with identical temperature preferences to those that existed at the Owens paleolake.

Meteorological stations used to characterize an upper-bound analog for the glacial transition climate should be located in a region with a higher mean annual precipitation than observed during periods of high Owens Lake discharge. Given all of the conditions described above and the length and completeness of the record, the upper-bound glacial transition analog meteorological stations were selected from eastern Washington (namely Spokane, Rosalia, and St. John). The stations are all close to each other, but do not have identical records. Selecting multiple meteorological stations is intended to minimize local effects on the climate.

For the lower-bound glacial transition climate analog, the meteorological stations should be in a place where mean annual temperature is higher than for the upper bound and thus would be south of the upper-bound localities. The temperature should also be lower than that for the present-day Owens Lake Basin, so that effective moisture levels are higher and consistent with a fill-and-spill lake. The stations should have a lower mean annual precipitation than the upper-bound sites, because the record from the Owens Lake Basin shows episodes when either saline diatoms or ostracodes or both are present, implying less surface flow in the Owens River. Few meteorological sites meet all of these conditions. The one set of meteorological data that fits all of these criteria and also has a long and complete record of weather data are those at Delta, Utah. The site at Beowawe, Nevada meets most of the requirements noted above and was added as an additional lower-bound meteorological station to avoid using a single site for input (USGS 2000, U0005, Section 6.6.2).

3.5.1.5 Uncertainties

Uncertainty in climate impact is addressed by the use of upper and lower bounds for each climate state. These bounding climates provide a range of precipitation and temperature to the subsequent infiltration calculations. The other uncertainty of interest is in the timing of the climate changes.

Many uncertainties exist that may affect the timing of the three climate states. These include uncertainties in the Owens Lake sediment-accumulation rate, in Devils Hole age data, in the exact time when the Devils Hole record implies climate is changing, and in the exact location of the past/present point in the Owens Lake record (analog climate proxy record). In addition, the selection and timing of a particular past climatic sequence to forecast the future is problematic, given the chaotic nature of climate and the possibility that human activity may change the cyclical patterns.

A quantitative estimate has been made of the first uncertainty (the Owens Lake sediment-accumulation rate), leading to a range of 400–600 years for the duration of the modern climate and 900–1,400 years for the duration of the monsoon climate, with the glacial-transition climate extending for the balance of the 10,000-year period in each case (USGS 2000, U0005, Section 6.6.1). No simple or objective way of assessing the other uncertainties exists quantitatively. However, the impact of those uncertainties on TSPA results can be assessed by means of sensitivity analysis; see Section 3.5.3.

Both the monsoon and glacial-transition climate states are expected to be wetter than the present-day climate, and, as a result, the water table is expected to rise. However, uncertainty exists regarding the amount of water-table rise for each climate state. Therefore, as discussed in Section 3.7.5.2, a conservative water-table rise of 120 m is used for all flow fields using future climate states.

3.5.1.6 Alternative Conceptual Models

The analysis presented in USGS (2000, U0005) focused on predicting climate change over the next 10,000 years based upon paleoclimate reconstruction of an analogous time interval that occurred approximately 400,000 years ago. An alternative approach would be to focus instead on the paleoclimate record for the last 18,000 years since glaciation. The climate within this time interval is known with significantly greater confidence than that which occurred 400,000 years ago. Trends in climate change over the last 18,000 years could be used to extrapolate expected future climates for the next 10,000 years. Uncertainty in any predictions will increase dramatically by the end of the 10,000-year time period, and in fact predictions may become wholly unreliable. Global climate circulation models could be used to provide a physical basis for predicting climate change for the next 10,000 years, although their reliable use is currently restricted to short time periods given limitations in current knowledge of the mechanisms forcing climate change.

3.5.1.7 Corroborative Evidence

This analysis is based on meteorological data collected at natural analog sites for the monsoon and glacial-transition climates expected to occur at Yucca Mountain. These analogs provide

corroborative evidence for anticipated precipitation rates. Plant macrofossils recovered from packrat middens throughout the Yucca Mountain region, representing conditions since the last glacial climate (18,000 years), provide corroborative evidence for the glacial-transition climate predicted by the Climate Model (USGS 2000, U0005, Section 6.5.1).

3.5.1.8 Summary and Conclusions

The future climate at Yucca Mountain is treated as a sequence of three states whose timing and characteristics are described in detail in USGS (2000, U0005). Each climate state is defined in terms of climate analogs, with the monsoon and glacial-transition climates being bounded by a range of climate values that have wetter-than-modern upper-bound values and modern-like or wetter-than-modern lower-bound values. Tables 3.5-2 and 3.5-3 list the mean annual precipitation and temperature inferred from the lower- and upper-bound analog data for use in calculating infiltration over the area of the UZ Flow and Transport Model domain. Note that "lower" and "upper" refer to precipitation rate, not temperature.

The upper-bound precipitation values for the monsoon and glacial-transition climates exceed the upper bound of the region's present-day climate by about 150 mm/yr. The glacial-transition climate's lower bound exceeds the modern lower-bound values by about 15 mm/yr. Thus the future climate (based on this method of analysis) is wetter than the modern climate. Temperature, however, defines an important difference between the modern climate and the glacial-transition climate. The glacial-transition climate is cooler than the modern climate, so evaporation is substantially lower than during modern times. A lower level of evaporation means that precipitation will be more readily stored, and hence available for infiltration, than is true in today's climate.

Uncertainty in climate impact for use in the TSPA is addressed by the upper and lower precipitation and temperature values. The other uncertainty of interest is in the timing of the climate change with durations of 400–600 years for the modern climate, 900–1,400 years for the monsoon climate, and with the glacial-transition climate extending for the balance of the 10,000-year period in each case.

Table 3.5-2. Mean Annual Precipitation for Analogs for the Lower and Upper Bound of the Three Climate Scenarios

Climate	Lower Bound (mm/yr)	Mean (mm/yr)	Upper Bound (mm/yr)
Modern	186.8	190.6	268.6
Monsoon	190.6	302.7	414.8
Glacial Transition	202.2	317.8	433.5

SOURCE: Adapted from USGS 2000, U0010, Tables 7-3 (modern), 7-7 (monsoon), and 7-12 (glacial transition)

Table 3.5-3. Mean Annual Temperature for Analogs for the Lower and Upper Bound of the Three Climate Scenarios

Climate	Lower Bound (°C)	Mean (°C)	Upper Bound (°C)
Modern	(not provided)	(not provided)	(not provided)
Monsoon	17.3	17.2	17.0
Glacial Transition	10.2	9.8	9.4

SOURCE: Adapted from USGS 2000, U0010, Tables 7-6 (monsoon), and 7-11 (glacial transition)

3.5.2 Infiltration Model

3.5.2.1 Introduction

The Infiltration Model provides spatially distributed time-averaged estimates of net infiltration for defining the upper boundary of the UZ Flow and Transport Model and its associated site-scale process models. The approach used in this model is documented in USGS (2000, U0010) and its results are summarized here. Net infiltration is the component of infiltrated precipitation, snowmelt, or surface water run-on that has percolated below the zone of evapotranspiration as defined by the depth of the effective root zone. Estimates of net infiltration are based on the upper bound, mean and lower bound precipitation rates for the modern, monsoon and glacial-transition climates provided by USGS (2000, U0005) and given in Table 3.5-2. Field data were obtained at the Yucca Mountain site to monitor the transient response of infiltrating groundwater as well as overland and stream flow resulting from episodic precipitation events. These data are then used to calibrate a watershed-scale volume-balance model (i.e., the Infiltration Model) that simulates groundwater-surface water interaction on the slopes of Yucca Mountain. The scope of the model is limited to surficial hydrological processes, with estimates of net infiltration limited to depth of the root zone only. These estimates of net infiltration then provide direct input into the UZ Flow and Transport Model.

3.5.2.2 Analyses and Assumptions

The first assumption in USGS (2000, U0010, Section 5.1.2) involves the development of the conceptual model of net infiltration. Net infiltration is defined here as water that has percolated from the land surface through the entire thickness of the root zone. The root zone is defined as the zone from the ground surface to some variable depth in soil or bedrock from which infiltrated water is readily removed on an annual or seasonal basis by evapotranspiration. In the conceptual Infiltration Model, the hydrological cycle is used to identify, define, and separate the various field-scale components and controlling processes (see Figure 3.5-3a). The hypothetical starting point of the hydrological cycle is precipitation, which for the current (modern) climate at Yucca Mountain occurs primarily as rain but can also occur as snow. Precipitation can accumulate on the ground surface, infiltrate the soil or exposed bedrock surfaces, contribute to runoff, or accumulate as snow. The contribution of precipitation to runoff generation depends on precipitation intensity relative to soil and exposed bedrock permeability, as well as on the available storage capacity of soil and shallow bedrock with thin or no soil cover. Water

accumulated in the snowpack can sublime into the atmosphere or become snowmelt, which can then infiltrate, evaporate, or contribute to runoff. Rain or snowmelt that becomes runoff either accumulates in surface depressions and basins or contributes to surface water flow, which is routed to downstream locations as run-on. Note that runoff is defined here as the volume or depth of water accumulation on the ground surface prior to being routed as surface-water flow, whereas run-on is defined as the volume or depth of the routed surface flow. Run-on contributes to either infiltration or accumulated surface-water run-on at downstream locations. Infiltrated water percolates through the root zone as either saturated or unsaturated ground water and is subject to evapotranspiration. Water percolating through the root zone is available as potential net infiltration, but the actual net-infiltration rate is limited by the bulk (or field-scale) saturated permeability of the bedrock or soil underlying the root zone. When infiltration from rain, snowmelt, or surface-water run-on occurs at a rate greater than the bulk saturated hydraulic conductivity of a subsurface layer, water will begin to fill the available storage capacity of the overlying soil. When the total storage capacity is exceeded, runoff is generated.

The second assumption involves the numerical representation of the conceptual model. This involves simplifying physical processes while maintaining a sufficient level of accuracy in the mathematical approximation. In most cases, an exact mathematical formulation of the physical process being modeled is not required, and deference is given to computational efficiency and practical applicability.

The third assumption involves calibration and verification of the numerical model. This involves assuming that the model was adequately calibrated using a variety of data collected at Yucca Mountain. These data include soil and bedrock hydrological properties, vertical water-content profiles in soil and bedrock, meteorological data, and streamflow measurements and are described in detail in Section 3.5.2.3.

The fourth and final assumption is that climate conditions at Yucca Mountain as estimated in USGS (2000, U0005) are valid (USGS 2000, U0010, Section 5.4).

3.5.2.3 Hydrological Data Collected at Yucca Mountain

A significant body of hydrological data has been collected at Yucca Mountain to characterize the response of the hydrological system to precipitation events (USGS 2000, U0010, Section 5.3). These data include soil and bedrock hydrological properties, meteorological data, and streamflow measurements. Water-content profiles were measured using a network of 98 neutron-moisture probes at monthly or weekly intervals from 1984 through 1995. These data indicate that the episodic nature of precipitation events at Yucca Mountain with short periods of heavy precipitation (and/or snowmelt) result in highly transient surface run-on and stream flow events. Furthermore, thin soils and the fractured nature of the underlying tuff rock result in rapid percolation of infiltrated water below the root zone. In general, the average annual potential evapotranspiration rate is approximately six times greater than the average annual precipitation rate for the current climate, resulting in the arid condition of Yucca Mountain between episodic precipitation events.

3.5.2.4 Conceptual Model for Net Infiltration

Figure 3.5-3b provides a generalized illustration of the various model components required for simulating spatially distributed net-infiltration rates. In general, the main components of net infiltration are precipitation, evapotranspiration, and surface water run-on. These components are incorporated into a watershed-scale volume-balanced model using a snowpack submodel, an evaporation and net radiation submodel, one-dimensional (vertical) root-zone infiltration submodels, and a two-dimensional (plan view) surface-water flow-routing submodel. Precipitation rate is provided by the analog meteorological stations discussed in Section 3.5.1 and is spatially distributed based on an empirical precipitation-elevation correlation relationship. Evapotranspiration is the combined process of bare-soil evaporation and transpiration (excluding evaporation from open bodies), which is the uptake and transfer of water to the atmosphere by vegetation. The potential evapotranspiration is determined by an energy balance and is primarily dependent on net radiation, air temperature, ground heat flux, the saturation-specific humidity curve, and wind. Temperature is also spatially distributed for the model by using an empirical temperature-elevation correlation relationship. Net infiltration is modeled through soil layers of the root zone only. The change in root zone water content is calculated instantaneously as a total daily change in water content using a simple water balance approach. The amount of daily net infiltration is limited by the bulk saturated hydraulic conductivity of the soil and storm duration. Water that exceeds the infiltration capacity of a soil column is routed to lower elevation nodes for subsequent infiltration.

The modeling process is discussed in detail in USGS (2000, U0010, Section 6).

3.5.2.5 Net Infiltration for the Three Climate Scenarios

Results in USGS (2000, U0010) provide net-infiltration estimates over a 123.7 km² area, termed the infiltration model domain. Results are also discussed for the 38.7 km² area used as the modeling domain for the UZ Flow and Transport Model and the 4.7 km² area corresponding to the potential repository area. Results presented in this section focus on those for the UZ Flow and Transport Model only. Net-infiltration rates estimated by the Infiltration Model for the UZ Flow and Transport Model domain differ slightly from those actually implemented in the UZ Flow and Transport Model due to plan-view discretization effects in the UZ Flow and Transport Model and the need to spatially average net-infiltration rates over each node in the UZ Flow and Transport Model domain.

Modern climate

Figure 3.5-4 illustrates precipitation, surface run-on, and net infiltration for the mean modern climate scenario. For the model domain area of the UZ Flow and Transport Model, the average precipitation rate is 190.6 mm/yr; the average outflow rate is -0.2 mm/yr, and the average net-infiltration rate is 4.6 mm/yr (USGS 2000, U0010, Section 6.11.1). The negative outflow rate indicates that more surface water flows into the UZ Flow and Transport Model area than flows out (primarily because of inflow from Yucca Wash).

For the UZ Flow and Transport Model domain, the spatial distribution of estimated precipitation for the mean modern climate scenario indicates minimum values occurring along the eastern and

southern portions and the maxima occurring in the northwestern region (see Figure 3.5-4a). The minima and maxima for the Infiltration Model occur outside the UZ Flow and Transport Model domain. Estimated evapotranspiration rates in general reflect the distribution of precipitation, but also reflect local terrain and surface-water flow effects (see Figure 3.5-4b). Minimum evapotranspiration rates of less than 100 mm/yr occur for steep north-facing sideslopes and areas with minimal soil cover, such as the west-facing slope of Solitario Canyon and the rugged terrain in the northern part of Yucca Wash. On the other hand, maximum evapotranspiration rates of 240 mm/yr and higher are indicative of locations subject to a high volume or frequency of infiltrated surface-water run-on. This is particularly the case immediately downslope from areas receiving higher precipitation (as well as rugged terrain conducive to runoff generation) such as the northern part of Yucca Wash. Infiltrated surface-water run-on indicates the contribution of surface-water flow to potential net infiltration and evapotranspiration. Maximum infiltrated surface-water run-on rates of more than 100 mm/yr occur mostly along the Yucca Wash channel but also at more isolated locations in the upper sections of drainages, such as Drill Hole Wash, Solitario Canyon, Pagany Wash, and Abandoned Wash.

The spatial distribution of estimated net-infiltration rates for the mean modern climate indicates most net infiltration occurs in upland areas. Relatively high net-infiltration rates of 100 mm/yr and higher occur throughout the steep north, north-east facing slope of the Prow, caused by a combination of higher precipitation rates, reduced potential evapotranspiration, frequent surface-water run-on resulting from very thin soils, and high bedrock permeability associated with non-welded tuffs. Areas of relatively high net-infiltration rates also include the upper channel locations of Solitario Canyon, Drill Hole Wash, Pagany Wash, and Abandoned Wash. Variability in net infiltration caused by topographic effects on potential evapotranspiration are illustrated by the higher net-infiltration rates for the north slopes of washes compared to south facing slopes (this is well illustrated by the west-to-east drainages along the east slope of Yucca Mountain and bisected by the ESF main drift). Maximum net-infiltration rates of more than 100 mm/yr occur within the UZ Flow and Transport Model domain for isolated areas that include side-slope and channel locations with thin soils and high permeability bedrock. The contribution to the total net-infiltration volume over the area of the UZ Flow and Transport Model is dominated, however, by the lower rates of 1–20 mm/yr covering wider areas of sideslope and ridgetop locations because of a much greater total area of coverage.

The distribution of net infiltration for the upper-bound modern climate (USGS 2000, U0010, Figure 7-6) is similar to that of the mean but with an increase of net-infiltration rate directly over the proposed repository (along the ridge crest) from 10–20 mm/yr to 20–50 mm/yr. For the lower-bound modern climate (USGS 2000, U0010, Figure 7-5), the net-infiltration rate along the ridge crest decreases to 5–10 mm/yr without any net-infiltration over the majority of the potential repository and UZ Flow and Transport Model area.

Monsoon Climate

Net-infiltration results for the mean monsoon climate are shown in Figure 3.5-5a. For the UZ Flow and Transport Model area, results for the mean monsoon climate scenario include an average precipitation rate of 302.7 mm/yr, an average outflow rate of 4.6 mm/yr, and an average net-infiltration rate of 12.2 mm/yr (USGS 2000, U0010, Section 6.11.2). The maximum net-infiltration rate is 629 mm/yr. For the lower-bound monsoon climate scenario, average net

infiltration is 4.6 mm/yr for the UZ Flow and Transport Model area (the mean modern climate result). Estimation results for the upper-bound monsoon climate scenario include a precipitation rate of 414.8 mm/yr, a snowfall rate of 6.8 mm/yr, an average outflow rate of 9.5 mm/yr, and a net-infiltration rate of 19.8 mm/yr. The maximum net-infiltration rate for the upper-bound monsoon climate scenario is greater than 1,000 mm/yr. The minimum is no net infiltration for all three scenarios.

For the mean monsoon climate scenario, estimated net-infiltration rates along the crest of Yucca Mountain are in the range of 20–50 mm/yr. Within the potential repository area, maximum net-infiltration rates occur in the active channel of Drill Hole Wash and for outcrop locations of permeable, nonwelded tuffs in the middle section of the west-facing slope of Solitario Canyon. Relatively high net-infiltration rates (100–500 mm/yr) also occur at many steep side-slope locations in the northern part of the UZ Flow and Transport Model area. In contrast, net infiltration at upland locations with thin soils underlain by bedrock with low bulk permeability is less than 1 mm/yr.

The distribution of net infiltration for the upper-bound monsoon climate (USGS 2000, U0010, Figure 7-8) is almost identical to that of the mean but with a slight increase of net-infiltration rate directly over the proposed repository (along the ridge crest) and UZ Flow and Transport Model area. Results are not presented in USGS (2000, U0010) for the lower-bound monsoon climate and are not discussed here.

Glacial Transition Climate

Net-infiltration results for the mean glacial-transition climate are shown in Figure 3.5-5b. For the area of the UZ Flow and Transport Model domain, results for the mean glacial-transition climate scenario include an average precipitation rate of 317.8 mm/yr, an average annual infiltrated surface-water run-on depth of 15.6 mm/yr, an average outflow rate of –0.2 mm/yr, and an average net-infiltration rate of 17.8 mm/yr (USGS 2000, U0010, Section 6.11.3). For the lower- and upper-bound glacial-transition scenarios, the average net-infiltration rate is estimated to be 2.5 mm/yr and 33.0 mm/yr, respectively. The maximum net-infiltration rates are approximately 220 mm/yr, 1,280 mm/yr, and 2,560 mm/yr for the lower-bound, mean, and upper-bound scenarios, respectively, for the UZ Flow and Transport Model domain. The minimum is no net infiltration for all three scenarios.

For the mean glacial-transition climate scenario, the spatial distribution of net-infiltration rates is slightly greater than those of the mean monsoon climate, given their similar distribution of precipitation rates. Infiltration rates are slightly higher for the mean glacial-transition climate because annual temperatures are lower, resulting in reduced evapotranspiration. The net-infiltration rates along the crest of Yucca Mountain are also within 20–50 mm/yr.

The distribution of net infiltration for the upper-bound glacial-transition climate (USGS 2000, U0010, Figure 7-17) is similar to that of the mean but with an increase of net-infiltration rate directly over the potential repository (along the ridge crest) from 20–50 mm/yr to 50–100 mm/yr. For the lower-bound glacial-transition climate (USGS 2000, U0010, Figure 7-15), the net-infiltration rate along the ridge crest decreases to 0–20 mm/yr with the net-infiltration rate

predominantly in the lower range of this interval over the majority of the potential repository and UZ Flow and Transport Model area.

3.5.2.6 Uncertainties

A detailed analysis of infiltration uncertainty was conducted using the Monte Carlo method (CRWMS M&O 2000, U0095). This analysis shows that the lower-bound and upper-bound infiltration rates are not truly bounds when all uncertainties are taken into account, and the mean infiltration rate is not the statistical mean when the appropriate probabilistic weighting factors are applied. In the rest of this subsection the three infiltration cases will be referred to as “low”, “medium”, and “high” to simplify terminology.

The uncertainty in net-infiltration results from imperfect knowledge of input parameters used by the Infiltration Model. The uncertainty analysis focused on twelve key input parameters for which uncertainty distributions were developed. The key parameters include precipitation, bedrock and soil hydrological properties, and potential evapotranspiration. Latin Hypercube Sampling (LHS) was used to sample values from the twelve uncertainty distributions. LHS is a form of stratified sampling whereby the sampling interval is divided into a number of subintervals of equal probability. An equal number of samples is then drawn from each of these intervals. The result is greater confidence in the output distribution than would be obtained using the classical random-sampling approach.

The Infiltration Model was run with 100 realizations to sampling each of the twelve input parameters. The glacial-transition climate was used for the analysis because that climate state is in effect most of the time, and it is in effect at later times when radionuclide releases are more likely. The mean infiltration over the repository area (actually, over a rectangular area slightly larger than the loaded portion of the repository) was computed for each realization. The distribution of mean infiltration values has an approximately log-normal shape; a histogram of the log values is shown in Figure 3.5-6. Also shown on the plot are the logs of mean infiltration for the three reference infiltration cases that are actually used for subsequent process and TSPA modeling. Incorporation of this infiltration uncertainty distribution into TSPA simulations, including a discussion on the derivation of the weighting factors shown on Figure 3.5-6, is discussed in Section 3.5.3.

3.5.2.7 Alternative Conceptual Models

Fully coupled groundwater–surface water flow models have been developed to simulate the hydrological cycle within watersheds. They involve using Richards equation to simulate variably saturated groundwater flow and shallow water flow equations (i.e. Saint Venant equations of overland flow, such as a kinematic wave model using Manning’s equation) to simulate overland and stream flow. These models are designed to resolve spatial and temporal variations in net infiltration stemming from episodic precipitation events within a wide variety of watersheds. They could be used to simulate net infiltration on the slopes of Yucca Mountain in a manner physically identical to that used to simulate UZ flow. Specifically, the ability of precipitation to infiltrate the extremely dry soils on the slopes of Yucca Mountain is limited until they absorb sufficient water to become permeable enough to permit downward flow of the infiltrating water. Given the high intensity and short duration of storm events, a significant volume of water may

flow along the surface or within streams before finally infiltrating in the lower elevation reaches of a given watershed. Therefore, the transient nature of groundwater-surface water interaction may be a significant mechanism controlling net infiltration. The distribution of net infiltration may then appear dramatically different than that shown on Figures 3.5-4a and 3.5-5 where infiltration occurs predominantly at the higher elevation reaches of a given watershed. The temporal and spatial distribution of net-infiltration fronts observed in the neutron-moisture probe data along with the stream flow data would then help constrain the transient response of such a model to precipitation from storm events. Use of alternative models such as the one proposed may provide confidence in the applicability of the assumptions used to simulate net infiltration in USGS (2000, U0010) and generate the net-infiltration maps shown on Figures 3.5-4a and 3.5-5 for the UZ Flow and Transport Model and the TSPA.

3.5.2.8 Corroborative Evidence

Corroborative evidence that the mean modern net-infiltration rate of 4.6 mm/yr is a representative average value for the UZ Flow and Transport Model is provided by examining alternative approaches to estimating the net-infiltration rate. These include discharge (water balance), transfer function (based on variables such as precipitation), and geochemistry techniques. Winograd and Thordarson (1975, pp. 1–126) used discharge from springs at Ash Meadows (south of Yucca Mountain near the Nevada-California border) to estimate net infiltration for the lower carbonate aquifer. They estimated that 3% of the precipitation falling on carbonate-rock uplands within the boundaries of the Ash Meadows basin becomes infiltration. The Infiltration Model estimated that 2.4% of precipitation becomes net infiltration over the UZ Flow and Transport Model domain indicating excellent agreement with the water balance methodology. Watson et al. (1976, pp. 335–357) used a Maxey-Eakin transfer function approach to estimate net infiltration for basins in Nevada. They found that for precipitation rates between 0–300 mm/yr, approximately 0–3% becomes net infiltration further substantiating the Infiltration Model. Chloride concentrations measured in pore waters for the ESF and ECRB provided calibration targets for the UZ Flow and Transport Model by adjusting net-infiltration rates. Results on Figure 3.8-4 indicate a range of net-infiltration rates from 3–10 mm/yr. Furthermore, calcite abundances in the TSw were also used to estimate percolation fluxes (CRWMS M&O 2000, U0085) with a net-infiltration rate of 6 mm/yr capturing the approximate average abundances in the TSw. Therefore, the geochemistry data also supports the mean modern net-infiltration rate calculated by the Infiltration Model for the UZ Flow and Transport Model domain.

Long-term net-infiltration rates based upon analysis of sulfate and chloride data originating in water from the late Pleistocene to early Holocene epochs imply a spatially averaged infiltration rate of 21 mm/yr over the area of the UZ Flow and Transport Model (USGS 2000, U0010, Section 7). This value is similar to the upper-bound monsoon and glacial-transition climate values and provides qualitative validation of infiltration rates estimated by the Infiltration Model, assuming prevalence of these climates during the late Pleistocene to early Holocene epochs.

3.5.2.9 Model Validation

Validation of the Infiltration Model is supported by its ability to correctly estimate the top boundary condition for use in the calibration of the UZ Flow and Transport Model. Net-

infiltration rates comprising this boundary condition are integral to the successful calibration of the unsaturated zone flow parameter data set using one- and two-dimensional sections extracted from the UZ Models as described in Section 3.6. The unsaturated zone data set consists of water saturation as well as moisture tension measurements from all available boreholes. Calibration of the three-dimensional UZ Flow and Transport Model to the occurrence and distribution of perched water zones and the ambient temperature profile (see Section 3.7), and geochemistry data (chloride, strontium, calcite—see Section 3.8) further substantiate that the Infiltration Model is valid for its intended use.

3.5.2.10 Summary and Conclusions

Table 3.5-4 lists the average net-infiltration rates for the nine climate scenarios. As stated earlier, net-infiltration rates estimated by the Infiltration Model differ slightly from those actually implemented in the UZ Flow and Transport Model (see Table 3.7-1) due to plan-view discretization effects in the UZ Flow and Transport Model and the need to spatially average net-infiltration rates over each node in the UZ Flow and Transport Model domain. In general, the net-infiltration rates increase with time as climate changes from modern to monsoon to glacial transition. The exception is the lower bound of the glacial transition, where the estimated net infiltration decreases because of lower surface water run-on than in the lower-bound monsoon climate scenario. The highest net-infiltration rates occur on the steep north, north-east facing slope of the Prow, the upper channel locations of Solitario Canyon, Drill Hole Wash, Pagany Wash, and Abandoned Wash, and generally in the northern portion of the site.

Table 3.5-4. Average Net-Infiltration Rates over the UZ Flow and Transport Model Domain

Climate	Lower Bound (mm/yr)	Mean (mm/yr)	Upper Bound (mm/yr)
Modern	1.3	4.6	11.1
Monsoon	4.6	12.2	19.8
Glacial Transition	2.5	17.8	33.0

SOURCE: Adapted from USGS 2000, U0010, Tables 7-3 (modern), 7-7 (monsoon), and 7-12 (glacial transition)

The uncertainty in infiltration for use in the TSPA is determined by varying twelve key input parameters in the Infiltration Model and constructing a histogram of calculated infiltration rates for each climate. The resulting histogram yields the expected log-normal distribution of infiltration rates, combining the lower-bound, mean, and upper-bound climate and infiltration maps for the glacial transition climate only. This histogram is then used to incorporate infiltration uncertainty into TSPA simulations.

3.5.3 Abstraction of Climate and Infiltration

3.5.3.1 Climate

The abstraction of climate for use in TSPA simulations has largely been discussed already in Section 3.5.1. Future climate is represented as a sequence of three climate states: modern for

600 years, monsoon for 1,400 years (i.e., from 600 to 2,000 years in the future), and then glacial-transition for the balance of the 10,000-year period.

Climate-properties uncertainty (e.g., precipitation and temperature) within each climate state is included by use of upper- and lower-bound climate analogs. These climate properties are not, however, used directly in TSPA simulations but only indirectly through their effects on UZ flow and thermal hydrology. Uncertainty in the timing of climate changes is not included in the base TSPA simulations and in fact is not well understood (see Section 3.5.1.5). However, the impact of the uncertainty in climate-change times on TSPA results can be assessed by arbitrarily varying the climate-change times within a TSPA simulation to determine whether the TSPA results are sensitive to such changes. Based on sensitivity analyses performed for the Viability Assessment (DOE 1998, Volume 3, Section 5.1.1), it is anticipated that climate-change time will not be found to have significant impact on repository performance.

3.5.3.2 Infiltration

As with climate, infiltration is not included directly in TSPA simulations, but only indirectly through its use as a boundary condition for the UZ flow and thermal hydrology models. As described in Section 3.5.2, three infiltration maps were generated for each climate state. The three will be referred to here as the low, medium, and high infiltration cases. To conduct a probabilistic TSPA simulation, we must assign weighting factors, or probabilities, to the three infiltration cases. These weighting factors were derived from the results of the infiltration uncertainty analysis (see Section 3.5.2.6). The weighting factors were chosen so as to make the log mean and standard deviation of the three-point discrete distribution (that is, the distribution consisting of three infiltration cases with defined weights) equal to the log mean and standard deviation of the distribution from the Monte Carlo simulation (shown in Figure 3.5-6). Log values were used in deriving the weighting factors because the distribution has a more normal shape in log space than in linear space (CRWMS M&O 2000, U0095, Section 6.3). The weighting factors derived in this manner are 0.17, 0.48, and 0.35 for the low, medium, and high cases, respectively (CRWMS M&O 2000, U0095, Section 6.5). Those weights are used for sampling in TSPA simulations—that is, the low-infiltration case is used in approximately 17% of the TSPA realizations, the medium-infiltration case is used in 48% of the realizations, and the high-infiltration case is used in 35% of the realizations.

3.6 UZ PROPERTIES DEVELOPMENT

The development of hydrologic properties is a critical step for the UZ Flow and Transport Model. Property development integrates a large amount of data collected at Yucca Mountain (described in Section 2.2) with the conceptual model of UZ flow and transport (described in Sections 3.2, 3.3, and 3.4.1) to produce properties that are suitable for numerical simulations and predictions of present and future behavior of the UZ. Figure 3.6-1 shows the diverse data and models that are integrated for development of UZ properties. In addition to the raw data and the conceptual model, the Geologic Framework Model (GFM) (CRWMS M&O 2000, I0035), numerical grid (described in Section 3.4.2), and Infiltration Model (described in Section 3.5) are also used as input for the development process. The broad use, and therefore importance, of the developed UZ properties is indicated by the numerous analyses and models, also shown in Figure 3.6-1, to which the properties are input.

3.6.1 Introduction

Development of properties for the UZ Flow and Transport Model is a complex, multistep process. In this section, the framework for this process and the theory behind the process will be discussed. The process consists of two major steps. The first of these is the analysis of the hydrologic properties data, which is documented by CRWMS M&O (2000, U0090). In the second major step, in which the properties are calibrated as documented by CRWMS M&O (2000, U0035), the output of the first major step is integrated with other models and data, as shown in Figure 3.6-1, to produce properties that are suitable for numerical simulations and predictions of present and future behavior of the UZ.

Using input from the conceptual model and the GFM (CRWMS M&O 2000, I0035), the hydrologic properties data are analyzed to provide an initial estimate of properties that will be used by numerical models. The conceptual model specifies that properties may be characterized by dividing the mountain into essentially horizontal layers, based on geology, and assuming that the properties within each layer are homogeneous (see Section 3.4.1.4.4). The conceptual model and the GFM (CRWMS M&O 2000, I0035) give the framework for grouping the data by layer. The data are then analyzed to estimate effective properties for each layer. The data analysis considers, with input from the conceptual model, not only how best to statistically describe the data, but also whether upscaling is appropriate. *Upscaling* is an adjustment to the estimate of the effective property when the property data are collected on one support scale but the estimate is intended for use in simulations and predictions on a much larger scale. *Support scale* refers to the size of the rock volume on which measurements are made (e.g., for measurements made on borehole core, the support scale is the size of the core).

The hydrologic properties estimates are passed to the Calibrated Properties Model (CPM). The CPM integrates these estimates with a numerical model and data on the ambient conditions at Yucca Mountain using a technique called data inversion. The numerical model is used to attempt to simulate the ambient conditions. Input to the numerical model includes the Infiltration Model, which provides an estimate of the amount of water that is infiltrating into the UZ from the surface of the mountain; the numerical grid, which provides a representation of the geology for the numerical model; and hydrologic properties estimates. Data on the ambient conditions observed in the UZ are provided for comparison to the output of the numerical model. For the

inversion, some element or elements of the numerical model (e.g., selected hydrologic properties or net infiltration rates) must be selected to be varied, or calibrated, so that the output from the numerical model can be matched, as well as possible, to the ambient conditions data.

Here, it is appropriate to make the distinction between *properties* and *parameters*. *Properties* are those qualities of the real world that give rise to its behavior; in this case the real world may be confined to the UZ of Yucca Mountain. When this behavior is modeled, either analytically or numerically, the model is, by necessity, a simplification of the real world. So the *properties* of the real world are simplified to a limited set of *parameters* that are used to define the model. As much as possible, it is best to have a one-to-one correspondence between the properties and the model parameters because this simplifies the initial estimation of the parameters.

The choice of which elements, or parameters, of the numerical model are to be calibrated is governed by several criteria. Any of the elements of the numerical model can be selected for calibration. Some model parameters will have a larger impact on the match to the data than others. Without any other information, these would be the obvious choices for the model parameters to be calibrated. However, it must also be considered that some of the model parameters have been estimated with a low uncertainty. To retain the best correspondence possible between the model parameters and the actual properties of the UZ (here *properties* not only mean hydrologic properties but any element of the model, such as geologic information and net infiltration rates), it is best to select parameters that have been estimated with higher uncertainty. For this case, some of the hydrologic properties are selected as the model parameters to be calibrated. These model parameters have a relatively high uncertainty, but are also parameters that will have a significant impact on the match to the ambient conditions data. All other model parameters remain unchanged or fixed. The initial estimates of the model parameters being calibrated, called *prior information*, are another type of data to be included in the inversion.

When the selected model parameters are calibrated to the ambient conditions data and prior information, the changes to these parameters reflect biases in the initial estimates of the properties that the parameters represent, and they also reflect the inaccuracies that are inherent in the model because of simplifications. Additionally, biases in the property estimates for parameters that are fixed will also be compensated for by adjustments to the parameters being calibrated. In other words, biases, inaccuracies, and uncertainties in the fixed portion of the model will be compensated for by changes to the parameters that are being calibrated.

The parameter calibration is performed using iTOUGH2 V3.2 (see Section 1.3.2), a code that provides data inversion capabilities for the TOUGH2 V 1.4 (see Section 1.3.2) simulator. The misfit between the ambient conditions calculated by the models and the ambient conditions data, as well as the misfit between the prior information and the parameters being calibrated, is evaluated based on the least-squares objective function. The objective function is then minimized using the Levenberg Marquardt algorithm (Finsterle 1999, pp. 44-45). Sensitivity coefficients are evaluated by means of finite differences.

The end product is a calibrated set of model parameters that can be used to predict the present ambient conditions anywhere in the UZ at Yucca Mountain. These parameters can also be used

to predict future conditions that may arise because of climate changes and/or emplacement of heat generating radioactive waste as well as other potential future scenarios.

For simplification of the discussion in the remainder Section 3.6, the calibrated model parameters will be referred to as *calibrated properties* or *calibrated hydrologic properties*. The other model parameters are assumed to represent the real properties of the system. In the case of the GFM (CRWMS M&O 2000, I0035) and the numerical grid constructed from it as well as the conceptual and numerical model used to represent the processes at work in the UZ, this is probably a good assumption. In any case, uncertainties in these models are, as indicated above, incorporated into the calibrated hydrologic properties. Note that the uncertainties in other model parameters have been incorporated into the calibrated hydrologic properties. Thus, they are only appropriate for predicting present and future behavior when the other elements of the model are applied in the same way (e.g., the scale on which the processes are being represented must not be changed dramatically). In the case of the Infiltration Model, uncertainty is incorporated by estimating calibrated hydrologic properties for the mean, or expected, infiltration rates as well as for upper and lower bounds of expected infiltration.

3.6.2 Issues

Several important issues arise with regard to developing properties for the downstream models shown in Figure 3.6-1. These issues are summarized in Figure 3.6-2.

- Calibrated hydrologic properties are required for two types of models. The first type, the mountain-scale model, is used to predict mountain-scale (or site-scale) behavior under ambient and future conditions. The second type, the drift-scale model, is used to predict system behavior within the potential repository horizon at the scale of the emplacement drifts. As discussed in Section 3.6.1, the models used to calibrate properties for use at these two different scales must be carefully chosen to properly represent the processes at those scales.
- *In situ* water potential data have shown that water potential data from core may indicate drier or stronger matrix water potentials than actually exist in the UZ. Flint (1998, pp. 18–19) also believes that the core data may have reflected drier than actual conditions and proposes a correction to the data. Flint (1998, p. 19) also states that the laboratory water potential and saturation data give a lower bound estimate of the matrix van Genuchten α parameter. The combination of these two situations gave rise to calibrated estimates of the α parameter for VA (CRWMS M&O 1998g, Chapter 2) that were probably too low.
- The conceptual model of flow in the UZ indicates that water flow will occur mainly in the fractures in the welded units and mainly in the matrix in the unaltered nonwelded units (see Section 3.3.3). In addition to the ambient conditions data and the prior information, this element of the conceptual model must be considered in the property calibration.

- The uncertainty of the calibrated properties is important for downstream analysis of the models that use the calibrated properties, particularly TSPA. However, estimating the uncertainty of the 196 independent calibrated properties is at best a difficult task.

3.6.3 Analysis of Hydrologic Properties Data

Hydrologic properties are estimated from measurements made on core and from *in situ* measurements. These estimates are either used directly for modeling flow and transport or are used as initial estimates of properties to be calibrated. For those properties to be calibrated, statistical data about the estimate are also calculated to provide a basis for evaluating the uncertainty of the initial estimate. Development of hydrologic properties data for input to the Calibrated Properties Model and numerical grids is summarized here and fully documented by CRWMS M&O (2000, U0090).

The dual-permeability conceptual and numerical model is used for simulations (see Section 3.4.1.3), so hydrologic properties are developed for the matrix and for the fractures. Permeability and porosity are the primary hydrologic properties necessary for simulations of flow and transport. In the UZ, partially saturated flow processes are important. Relative permeability and water potential are described as a function of saturation using the van Genuchten (1980) relationships (see Section 3.4.1.4.1). Two additional hydrologic properties are necessary to describe the frequency of the fractures (which also describes the average size of the matrix blocks) and the geometrical interface area between the fractures and the matrix (which can also be thought of as the surface area of the matrix blocks). One set of thermal properties is developed for the rock itself. All of these properties are developed for the formation rock, and a second set is developed for the rock in fault zones.

3.6.3.1 Matrix Property Data

Matrix properties estimates are based on data from laboratory analysis of core recovered from nine deep boreholes, which penetrate to at least the bottom of the TSw, and 33 relatively shallow boreholes, which generally penetrate only to the top of the TSw. Collection, processing, and preliminary analysis of the core data are described by Flint (1998). Additional data from *in situ* water potential measurements are used to estimate the α parameter of the van Genuchten relationship. Collection and preliminary analysis of these data are described by Rousseau et al. (1997, pp. 39–45; 1999, pp. 143–151).

Several other sources of data were considered but not included in the analysis. The bulk properties data (i.e., porosity and grain density) from the 42 boreholes indicated above are numerous and considered sufficient to describe those properties, so it was not necessary to include more recent data from the tunnels and recently drilled boreholes. Geophysical data characterizing porosity were not used because they include both the inter-grain porosity and porosity resulting from lithophysal cavities. The core data only represent the inter-grain porosity, and this is the property that is important for the downstream models. Data from samples collected at the surface of the mountain were not used because weathering of the rock can alter the properties so that they are not representative of properties deep in the mountain.

Data from the Busted Butte test site, which significantly adds to the permeability characterization for the top of the vitric portion of the Calico Hills Formation, were not yet available at the time the analysis was done. Preliminary review of these data (DTN: GS990708312242.008) indicate that they are consistent with the calibrated permeability for this layer, shown in Figure 3.6-6.

The data are divided by stratigraphic location corresponding to the 29 detailed hydrogeologic units shown in Table 3.2-2. Effective properties are calculated for each of these layers. Data from core are not available for Tram tuff layers (model layers tr3 and tr2), so the overlying Bullfrog tuff layers (model layers bf3 and bf2, respectively) are used as analogs.

Permeability is commonly accepted to be a log-normally distributed property (de Marsily 1986, p. 80; Domenico and Schwartz 1990, p. 66; Freeze and Cherry 1979, p. 31). But it must also be considered that the core samples on which permeability is measured are much smaller than the average size of matrix blocks *in situ*, so an upscaling factor proposed by Paleologos et al. (1996, p. 1336) is used to correct for the size discrepancy. Thus the effective permeability is estimated as an upscaled geometric mean. Several layers include samples with permeability that is below the detection limit of the permeameters; these data are also considered when estimating the effective permeability. Figure 3.6-6 shows the initial estimates of matrix permeability that are input to the calibration process described below in Section 3.6.4. Note that while the PTn and vitric CHn have very high matrix permeability, the welded and zeolitic layers have much lower permeability. In some welded or zeolitic layers, the matrix permeability is insufficient to carry the estimated site average net infiltration which is 4.6 mm/yr (see Section 3.5.2.5). This net infiltration value is approximately equal to a permeability of $1.5 \times 10^{-17} \text{ m}^2$ under vertical percolation conditions. In these layers, a portion of the percolation must be carried by the fractures.

Porosity is measured twice on each sample, once after drying in a low-temperature, humidity-controlled oven that does not remove bound water or water hydrating clays and again after drying in an above-boiling oven that removes all water. Total porosity is estimated as the arithmetic average of data from the second measurement. Residual water content is estimated as the total porosity minus the arithmetic average of porosity data from the first measurement. Residual saturation is residual water content divided by total porosity.

The parameters of the van Genuchten relationship, α , m , residual saturation, and saturated saturation, are estimated using both core and *in situ* data. Residual saturation, in the context of the van Genuchten relationship, is the amount of water that remains after the pores are fully drained under ambient conditions, and is calculated as indicated above. Saturated saturation, or the amount of water present in the matrix when zero water potential and full relative permeability are reached, is not measured and is assumed to be equal to full saturation. The other two parameters, α and m , are estimated by first fitting them to drainage data measured on core. These data are obtained by measuring the water potential at several points, starting with a fully saturated sample and gradually reducing the saturation. This gives a lower bound estimate for α . Second, *in situ* water potential data are used to give a better effective estimate of α . Figure 3.6-7 shows that the initial estimate of the α parameter for the welded and zeolitic layers, like permeability, is generally lower than that of the unaltered, nonwelded layers, though there is not as marked a difference. Note that model layer ptn23, analogous to the detailed hydrogeologic unit Tpy, while in the generally nonwelded PTn, represents the partially to moderately welded

interior of the Yucca Mountain tuff (Tpy) lithostratigraphic unit (Flint 1998, p. 27), and this is reflected in the value of the α parameter (i.e., it is lower than the other α parameter values in the PTn and similar to values in the TCw and TSw).

3.6.3.2 Fracture Property Data

Fracture properties estimates are based on permeability data from *in situ* air-injection tests conducted in four surface based boreholes and boreholes in alcoves of the ESF, porosity data from gas tracer tests in boreholes in Alcove 5, and fracture mapping from the ESF, ECRB, and surface based boreholes. Air-injection testing is described by LeCain (1997; 1998) and Rousseau et al. (1999) and in CRWMS M&O (2000, U0015).

As with the matrix property data, some fracture property data were considered but not used. In particular, fracture frequency data from the surface of the mountain, measured on outcrops and at the Large Block Test area, are not considered representative of fracture frequencies in the deep subsurface because unloading, or the absence of overburden at the surface, is likely to have enhanced fracturing. Permeability data from air-injection testing in the Main Drift Niches (1-4) were not used because the support scale is 0.3 meters (one foot), and thus the data may not be representative of the fracture permeability at the scale of interest. The support scale of the air-injection test data that were used is from 1 to 12 meters (CRWMS M&O 2000, U0090, Section 6.1.1.1)

There are also two new data sets that have become available since the analysis was performed. First, small-scale fracture data (DTN: GS990908314224.009) (data on fractures shorter than the 0.3 and 1.0 meter cutoff lengths of Detailed Line Survey fracture data) are likely to significantly affect only the estimate of the interfacial area between the fractures and matrix. If the interfacial area is underestimated, the calibrated active fracture parameter (see Section 3.3.4 for discussion the active fracture model for which this is the parameter) will be affected and will correct for it. Inclusion of these data may also affect the estimate of the van Genuchten α parameter, but it will not be a very large change because the van Genuchten α parameter is proportional to the cube root of fracture frequency (CRWMS M&O 2000, U0090, Section 6.1.2). Second, air injection data from Niche 5 in the ECRB Cross Drift (DTN: LB002181233124.001) show larger permeabilities for the Ttp11 than previously measured in tests with a larger support scale. Reevaluation of the decision to exclude these small support-scale data is appropriate, though, preliminary evaluation of these data indicate that the impact on the calibrated properties is not likely to be large.

Air injection and gas tracer test intervals are grouped by lithostratigraphic unit (see Table 3.2-2) for analysis. Similarly the fracture mapping data are divided at lithostratigraphic unit contacts. Data are only available to the top of the CHn. Fracture properties in this unit and below are assigned on the basis of analogous layers.

Like matrix permeability, fracture permeability is estimated as the geometric mean of the data. Figure 3.6-6 shows that the initial estimates of fracture permeability are much higher than the initial estimates of matrix permeability in the welded layers, but in the nonwelded layers they are nearly equal to and sometimes lower than the matrix permeability. The deeper, nonwelded layers

have the lowest permeability, but the initial estimates of fracture permeability only cover a range of about three orders of magnitude, which is much less than the range of matrix permeability.

Fracture frequency and intensity and the interfacial area between fractures and matrix are estimated using fracture mapping data from the tunnels and boreholes. Fracture intensity is the length of fractures per unit area, while frequency is the number of fractures per unit length. Intensity is the better number to use because it accounts for both the number of fractures and the length of those fractures, but it is only available where a tunnel is present. For deeper layers, borehole data, which only give frequency, are used. The intensity or frequency data are used to estimate the interfacial area between the fractures and matrix, which can also be thought of as the surface area of the matrix blocks.

Analysis of gas tracer tests in the Tptpmn suggests that the fracture porosity in this layer is 1% (CRWMS M&O 2000, U0090, Section 6.1.3). This porosity datum is extrapolated to other layers using the cubic law (CRWMS M&O 2000, U0090, Section 6.1.3) to relate porosity, fracture intensity or frequency, and permeability. This method was chosen so that all possibly relevant fracture data were considered when estimating fracture porosity. An alternative approach would have been to use the gas tracer estimate of fracture porosity in the Tptpmn directly for at least the TSw if not all layers. This would ignore any information about fracture porosity contained in the fracture intensity (and/or frequency) and permeability data. CRWMS M&O (2000, U0090, Section 6.1.4) further discusses the defensibility of the approach used.

No water potential or relative permeability data are available for fractures at Yucca Mountain, so these relationships are based on theory. The van Genuchten relationships are used for the fractures as they are for the matrix. The van Genuchten m parameter is estimated from fracture permeability and intensity data for the Tptpmn, and capillary theory (CRWMS M&O 2000, U0090, Section 6.1.2). The van Genuchten α parameter is assumed to be equal to the inverse of the air-entry pressure, again calculated using fracture permeability and frequency or intensity data and capillary theory (CRWMS M&O 2000, U0090, Section 6.1.2). Figure 3.6-7 shows that like fracture permeability, the estimate of the α parameter for the fractures has much less variability than in the matrix. Unlike permeability, the α parameter for the fractures is consistently higher than that of the matrix. The impact of assumptions used to estimate fracture van Genuchten parameters is insignificant because any estimation biases due to these assumptions are corrected for during the calibration phase of property development described in Section 3.6.4.

3.6.3.3 Fault Property Data

As discussed in Section 3.4.2.2, faults are divided into just four layers, corresponding to the major units (CHn and CFu are combined into one major unit for the faults). Very few property data specifically about faults exist. A small number of permeability measurements from air-injection tests have been performed and are described by LeCain (1998). These data indicate that, at least within the welded units, the fractures in the faults are more permeable and porous than the fractures in the formation (or nonfaulted rock).

Matrix properties for faults are estimated by calculating the layer thickness weighted averages for each major unit from the matrix properties estimated for the formation. As appropriate to

flow perpendicular to bedding, the harmonic mean is used to estimate the effective permeability and thermal conductivity. The effective α parameter is also estimated using the harmonic mean. All other matrix properties except specific heat for faults are estimated using the arithmetic mean. Specific heat is estimated as documented by CRWMS M&O (2000, U0090, Section 6.3).

Fracture permeability estimates for faults are based on cross-hole air-injection tests performed in Alcoves 2 and 6. However, these estimates are only available for the TCw and TSw major hydrogeologic units. For the PTn and CHn/CFu major hydrogeologic units, the fault fracture permeability is estimated by assuming that the permeability structure of the major hydrogeologic units is the same in the faults and in the formation (outside faults). Permeability structure can be reasonably assumed to be correlated to rock type (i.e., welded or nonwelded). The impact of this assumption is minimized by the subsequent property calibration.

Fracture frequency is estimated as the inverse of the layer thickness weighted average spacing. Fracture aperture is then calculated in the same manner as for the formation, using the cubic law. The increase in the fault fracture aperture as compared to the formation fracture aperture is applied to the major unit average fracture porosity to estimate fracture porosity for faults.

3.6.3.4 Thermal Property Data

Rock thermal properties, wet and dry conductivity and specific heat, are estimated from thermal measurements made on core (Brodsky et al. 1997) and porosity and grain density estimates made by Flint (1998). Unlike the hydrologic properties, these properties are not calibrated and are used directly by the downstream models.

3.6.4 Calibrated Properties Model

The Calibrated Properties Model incorporates many different data from analyses and models into one model to develop calibrated properties for the UZ Flow and Transport Model that are consistent with all these sources. Figure 3.6-1 shows the inputs to the Calibrated Properties Model (CPM). At the heart of the calibrated properties model is the conceptual and numerical model of Yucca Mountain. This specifies how it is thought that the system behaves under ambient conditions and how to simulate that behavior with a numerical model. The numerical grids provide a model of the geologic layering on which the simulations are performed. The Infiltration Model provides the infiltration rates for the upper boundary condition. Hydrologic properties data, described above, are used to specify properties for each of these layers. The model is calibrated to saturation, water potential, and pneumatic pressure data by varying some of the properties. Initial estimates of these properties are included as prior information (Carrera and Neuman 1986, pp. 199–210).

The properties that are calibrated are fracture and matrix permeability (k_f and k_m), the fracture and matrix van Genuchten α and m parameters (α_f , α_m , m_f , and m_m), and the active fracture parameter (γ) (see Section 3.3.4 for discussion the active fracture model for which this is the parameter). Except for γ , these are also the properties for which prior information is provided. All other properties are used unchanged from the initial hydrologic properties estimates described in Section 3.6.3.

Figure 3.6-3 shows the sequence of numerical grids and data that is used to produce the calibrated properties. The 1-D model, which is actually a collection of 1-D columns, is used to first calibrate some of the formation properties to saturation and water potential data. The same model, with the updated properties, is then used to calibrate the remaining formation properties (fracture permeabilities from the surface to the bottom of the TSw) to pneumatic data. The fully updated properties are then again checked against the saturation and water potential data, and any further calibration that is needed is performed. If the properties are updated, they are checked against the pneumatic data and refined if needed. In general, this process is iterated until no further property changes are needed to maintain the match to all the data. The use of this type of iterative process for model calibration is not limited to the YMP. Bullivant and O'Sullivan (1998, pp. 53–58) have followed a similar iterative procedure for calibrating a geothermal reservoir model to data gathered prior to and during reservoir development. They have then successfully used the calibrated model in a predictive mode.

These calibrated mountain-scale formation properties are then used as input to the 2-D model, which is used to calibrate the fault properties. The 2-D model is also alternately calibrated to saturation and water potential data and then to pneumatic data until a final fault property set is produced. The combination of the mountain-scale formation properties and the fault properties gives a comprehensive, mountain-scale calibrated property set.

The calibrated mountain-scale formation properties are also used as input for development of drift-scale properties. These are developed by recalibrating fracture permeabilities to the small-scale (drift-scale) saturation and water potential data and air permeability prior information.

Calibrated properties, both mountain scale and drift scale, are produced for three different present-day infiltration scenarios. As described in Section 3.5, the base case infiltration scenario provides the most likely estimate of present-day infiltration. The upper and lower bound infiltration scenarios are intended to provide reasonable bounds of possible present-day infiltration. By providing property sets calibrated using each of these scenarios, the impact of future climate variability on flow and transport can be evaluated in light of the uncertainty of present-day infiltration.

Development of saturation, water potential, and pneumatic data; prior information; and 1-D and 2-D inversions are documented by CRWMS M&O (2000, U0035). The misfit between the ambient conditions calculated by the models and the ambient conditions data as well as the misfit between the prior information and the parameters being calibrated all contribute to the objective function, which is the quantitative measure that the inversion code, iTOUGH2 V3.2, attempts to minimize. Saturation and water potential data are evaluated after steady-state conditions are reached. Pneumatic data are evaluated after a 30-day, barometric pumping initialization period. During the inversion of saturation and water potential data for the mountain-scale formation property calibration, the parameter selection feature of iTOUGH2 V3.2 is used. When this feature is used parameters (hydrologic properties being calibrated) that have an insignificant impact on the objective function are automatically deselected for a short period during the inversion. The inversion can then be performed more quickly because the complete set of hydrologic properties being calibrated is not being continuously evaluated.

3.6.4.1 1-D Inversions

The 1-D submodel is used for the calibration of formation properties because there are 173 separate formation properties to be calibrated. This requires numerous forward simulations, and a 1-D model provides the most efficient way to perform them. The 1-D submodel consists of 11 vertical columns, shown schematically in Figure 3.6-4, that reflect the stratigraphy at the 11 boreholes for which there are saturation, water potential, and/or pneumatic data suitable for inversion.

The use of a 1-D, vertical model implicitly assumes that flow can be adequately approximated as one-dimensional and vertical, i.e., that lateral flow is not important. In the TCw, PTn, and TSw, this assumption is substantiated by the lack of perched water. The presence of perched water is an indicator of potential lateral flow in the UZ (see Sections 3.3.2 and 3.7.3.3). It is believed that in the PTn, small amounts of lateral flow may occur because of capillary gradients from areas under high infiltration to areas under low infiltration. To compensate for this, the source term at the upper boundary, representing infiltration, is calculated as an average of the infiltration rates within 200 m of the borehole. At the bottom of the TSw and below, perched water does exist in some areas, especially to the north. However, the presence of perched water and the potential for lateral flow is ignored while calibrating properties using a 1-D model. Perched water is investigated with the 3-D model (see Section 3.7.3.3).

Saturation data measured on core from seven boreholes are included in the inversion. The saturation data are much more numerous than the model layers, so the data are averaged for each model layer before being included in the inversion. Water potential data measured *in situ* in four boreholes and pneumatic data measured *in situ* in five boreholes are included in the inversion.

Several other sources of data were considered but not included in the inversion. Water potential data measured on core are not used. Core recovered from boreholes undergo a small amount of drying due to drilling with air and handling at the surface. While this drying is not significant for the saturation data and can be easily quantified and accounted for in the data uncertainty, it appears to be more significant for the water potential data. More importantly, it is not easily quantified. Saturation data from shallow boreholes were not used because they generally represent only the upper layers and would give only marginal improvement to the calibrated properties for a significantly increased computational burden. Geophysical saturation data are not used because lithophysal porosity cannot be easily separated out of the measurement.

3.6.4.1.1 Calibrated, Mountain-Scale Properties

As discussed above, the saturation and water potential data are inverted first. Additionally, a subjective criterion is used to evaluate the adequacy of the calibrated, mountain-scale properties to honor the conceptual model of flow partitioning between the fracture and matrix. Water flow is required by the conceptual model to be predominantly in the fracture continuum in the welded and zeolitic layers and predominantly in the matrix in the nonwelded layers (see Section 3.3.3).

After a suitable initial match is obtained between the simulation and the saturation and water potential data, the pneumatic data are inverted to calibrate the fracture permeability. Pneumatic data inversion is itself a two-step process. First, the permeabilities of each layer in the TCw and

PTn are calibrated. Then the permeabilities of layers tsw31 through tsw37 are calibrated as a whole. One factor is estimated to modify all the initial fracture permeabilities. This is done because the pneumatic data show insignificant attenuation and lag between sensors in the TSw. This means that inversion of these data can at best provide a minimum permeability necessary to match the data. The permeabilities are modified by a single factor to retain the permeability structure of the TSw indicated by the initial estimates.

The calibrated properties are rechecked against the saturation and water potential data, and any adjustments to the calibrated properties that are necessary are made (e.g., to keep the water flow in the matrix through the unaltered, nonwelded layers). The new properties are then checked against the pneumatic data. For all three property sets, corresponding to the three infiltration scenarios, this check showed that no further calibration was necessary. Figure 3.6-4 shows the match between the final calibrated simulations and the saturation, water potential, and pneumatic data for the base case infiltration scenario.

3.6.4.1.2 Calibrated, Drift-Scale Properties

The calibrated properties produced using mountain-scale data are not appropriate for simulation of processes at the drift scale such as the seepage models (Section 3.9) or the THC Seepage Model (Section 3.10). Specifically, the use of pneumatic data that represent the mountain-scale process of barometric pumping of the UZ produces fracture permeabilities for the potential repository horizon and neighboring layers that are larger than appropriate for drift-scale modeling.

To provide drift-scale properties, the fracture permeabilities for model layers tsw32 through tsw37 are recalibrated to saturation and water potential data and to air-injection derived fracture permeability prior information. The calibrated mountain-scale formation properties are used for all other properties. With the pneumatic data taken out of the inversion, the fracture permeabilities return to near their initial estimate values (i.e., prior information values).

3.6.4.2 2-D Inversions

Fault properties are calibrated using a 2-D model of an east-west cross section at borehole USW UZ-7a, shown schematically in Figure 3.6-5. Use of a 2-D model implies that flow constrained to the vertical and east-west directions adequately approximates ambient conditions. The dip of the bedding is approximately parallel to the cross section, and since bedding is most likely to control lateral flow, the assumption is reasonable. It is also reasonable to assume that flow in the fault, which strikes perpendicular to the cross section and dips nearly vertical, is adequately represented by a 2-D model.

Borehole USW UZ-7a penetrates the Ghost Dance fault, and data from it represent ambient conditions in a fault at Yucca Mountain. This is the only borehole that provides a range of data with respect to faults. Data are available only from the upper portion of the TSw to the surface. Because of the lack of data for the lower layers, properties for faults in the CHn/CFu major unit are not included in the calibration.

The same property types as were calibrated for the mountain-scale formation properties are calibrated for the faults. The same approach is also followed, with the exception that the

proportion of flow in the fractures and matrix is not a criterion for an acceptable calibration because this criterion is only applicable to the formation. Figure 3.6-5 shows the match between the calibrated simulation and the saturation, water potential, and pneumatic data for base case infiltration.

Note that Figure 3.6-5 shows that even though a single set of properties is used for each of the major hydrogeologic units, the results of the simulation still vary significantly. This is because the fault is narrow and the simulated conditions are controlled by the properties of the surrounding formation. Because this is the case, the calibrated fault properties for the base case infiltration are evaluated for the upper and lower bound infiltration scenarios and are found to be suitable for all three infiltration scenarios.

3.6.5 Results and Discussion

3.6.5.1 Results

Simulations using the calibrated properties show a significant improvement in the match between the simulated ambient conditions and the data. In general, there is less than an order of magnitude difference between the calibrated properties and the prior information. The calibrated matrix permeability shows nearly the same structure as the initial estimates as shown in Figure 3.6-6. The most pronounced changes are those of more than an order of magnitude. At the top of the PTn and again at the top of the CHn, the matrix permeability increases approximately one and a half orders of magnitude. These changes result from the criterion discussed above for matrix dominated flow in the PTn and vitric CHn layers. For flow to transition from the fractures in the welded TCw and TSw, the respective underlying layers must have a high permeability, so that percolating water can be imbibed quickly. The matrix permeability of layers tsw36 and tsw37 near the bottom of the TSw also increases more than one order of magnitude. In these layers, as well as tsw34, the initial estimate is extremely low and causes nearly fully saturated conditions to develop in the simulations. The increased permeability allows the saturations to be reduced to match the data, as shown above in Figure 3.6-4.

The most widespread exception to the generally small property changes are the calibrated mountain-scale fracture permeabilities in the TCw and TSw, which are increased significantly over the initial estimates. These high permeabilities are necessary to reproduce the pneumatic pressure data that show little or no attenuation or lag of the barometric signal as it crosses these units. This increase can be attributed to upscaling. The scale of the data from which the initial estimates of fracture permeability were made is on the order of 10 meters (the scale of the drifts). The scale on which the process of barometric pumping of the thick unsaturated zone occurs is hundreds of meters (the scale of the mountain). Note that for the drift-scale properties, the pneumatic data are not considered so that the calibrated fracture permeabilities reflect the scale of the initial estimate.

Like the calibrated matrix permeabilities, generally only small differences appear between the initial estimates and the calibrated mountain-scale fracture and matrix van Genuchten α parameter values, as shown in Figure 3.6-7. The larger changes are observed in the same layers and for the same reasons as stated above for the matrix permeabilities. Matrix α at the top of the PTn is reduced, increasing the suction into the matrix, so that water will be imbibed into the

matrix as it percolates into the PTn. At the bottom of the PTn and top of the TSw, fracture α is reduced so that flow will transition into the fractures through the TSw. Near the bottom of the TSw, matrix α is increased to reduce suction and consequently reduce the nearly saturated conditions initially predicted by the simulations.

The difference between the fracture and matrix van Genuchten α parameter is approximately two orders of magnitude, where previous calibrated property sets (e.g., for VA (CRWMS M&O 1998g, Chapter 2)) indicated approximately three orders of magnitude difference. This is a direct result of using only *in situ* water potential data for both the initial estimate of the matrix van Genuchten α parameter and in the data inversion, whereas the previous models had included core data. Use of the current calibrated properties produces thermal-hydrologic simulation results that closely match the expected performance (CRWMS M&O 2000, N0120/U0110, Section 6.2).

The calibrated mountain-scale properties for the upper and lower bound infiltration scenarios are similar to those shown and discussed here (CRWMS M&O 2000, U0035, Section 6.1).

3.6.5.2 Uncertainty

With a total of 194 calibrated properties (all calibrated formation and fault properties), determining estimation uncertainty is conceptually and numerically difficult. Cross-correlations between the properties make the uncertainties of individual properties very large. Furthermore, the linearity and normality assumption underlying the error analysis implemented in iTOUGH2 V3.2 is invalid if the estimation uncertainties become very large as a result of cross-correlations. However, as shown above, the calibrated properties generally do not vary much from their initial estimates. Where the calibrated properties have changed significantly with respect to the prior information, the data influencing the change reflect processes not completely accounted for in the initial model setup. For example, water flow transition from fractures to matrix at welded to nonwelded interfaces is likely a result of processes which occur at a subgrid scale, so the changes of calibrated properties at these interfaces incorporate the effects of these processes. Because the initial and calibrated properties are generally similar, the uncertainty of the initial property estimates is assumed to be an approximate surrogate for the uncertainty of the calibrated properties. Further confirmation of the appropriateness of this approach is warranted and can be achieved with sensitivity studies and/or Monte Carlo simulations. However, either of these confirmation approaches will still be of a limited nature because of the extremely large number of properties calibrated.

3.6.5.3 Validation

Validation of the Calibrated Properties Model, in the strict sense of validation being comparison to data not used for calibration, is performed by using the 3-D model. This is documented by CRWMS M&O (2000, U0050, Section 6.8). *In situ* water potential data measured in boreholes off the ECRB Cross Drift compare well with the predicted water potentials as shown in Figure 3.6-8. Although the predicted water potentials are generally lower, the difference is only a few tenths of a bar (1 bar = 10^5 Pa). The difference is exaggerated by the logarithmic scale because the water potentials are so close to zero. Pneumatic pressure data also compare well to the predicted pneumatic pressures as shown in Figure 3.6-8. These data partially show that the calibrated properties are valid for predicting ambient conditions and that the assumptions of one-

and two-dimensional flow are suitable for use in the calibration process. That the Calibrated Properties Model works for ambient thermal simulations (Section 3.12), drift heating simulations (Section 3.10.4), and ambient geochemistry simulations (Section 3.8) also builds confidence in the validity of the model under a wider range of conditions. However, these simulations also allow other elements of their models to vary in order to match data, which might hide inaccuracies in the Calibrated Properties Model.

Validation of the Calibrated Properties Model, in the regulatory sense of building confidence that the model is appropriate for its intended use, is also partially satisfied by meeting the following criteria.

- The model is calibrated within experimental data sets.
- The calibrated properties are reviewed for reasonableness and consistency with respect to the prior information. For large differences between the calibrated properties and the prior information, consistency with respect to other data is necessary (see Section 3.6.5.1).
- Calibration exercises for previous incarnations of calibrated properties for the UZ at Yucca Mountain have been published in open literature (i.e., Bandurraga and Bodvarsson 1999, pp. 25–46; Ahlers et al. 1999, pp. 47–68).

Meeting these criteria builds confidence that the Calibrated Properties Model is appropriate for its intended use, in particular for predicting ambient conditions in the UZ for the present-day climate. The appropriateness for the other intended uses of predicting conditions under possible future scenarios, including changed climate and potential repository heating, is not as certain. This is because the properties were calibrated using present-day net infiltration estimates and were checked against present-day thermal and geochemical conditions. The drift-scale calibrated properties have also been checked against thermally perturbed conditions. Because there is less data about conditions under possible future scenarios (which is one of the reasons that predictions are necessary), and because the properties cannot be calibrated to these data, the confidence in the appropriateness of the calibrated properties for predictions of conditions under possible future scenarios is necessarily less than the confidence in the appropriateness of the calibrated properties for predictions of conditions under the present-day scenario. However, the calibrated properties do represent the best estimate of properties that are valid for all intended uses.

3.6.5.4 Alternative Conceptual Models

The main element of the conceptual model for the properties of Yucca Mountain developed as documented here is that the thermal-hydrologic system can be described by homogeneous layers. An alternative to this conceptual model is that the properties are heterogeneous and distributed three-dimensionally within the UZ. The Rock Properties Model (CRWMS M&O 2000, I0040) documents properties developed in such a way. The spatial variability of matrix porosity, the most numerous data available, is calculated and used to predict the spatial distribution not only of matrix porosity, but also matrix permeability, bulk density, and thermal conductivity. The

distributions of these three other properties are predicted by developing correlations between them and porosity.

The advantage of this type of model is that properties vary not only from layer to layer but also within layers. It is thus a more accurate representation of the properties data. However, several disadvantages arise from using this type of model as opposed to the homogeneous layer model. Distributed properties models need numerous data points to develop and support the choice of the spatial distribution. When data are sparse, correlations are necessary, but these correlations are simplifications of complex relationships between properties, which may lead to misrepresentation of the distribution. For example, the Rock Properties Model develops a correlation between porosity data, which are very numerous, and permeability data, which are not nearly as numerous (CRWMS M&O 2000, I0040, Section 6.4.5). While this correlation captures the trend of the relationship between the two properties, the data do not show an exact one-to-one correlation. Thus the distributed model of permeability that is produced has lost some of the original information about the distribution of permeability. Distributed properties models are also difficult to calibrate to other data (e.g., saturation, water potential, and pneumatic pressure data). Several approaches can be used to calibrate distributed properties models, but each has its pitfalls. In one approach, only the properties in the local area of a data point are varied, but this will have no effect on predictions where there are no data because the properties there are not changed. This approach also involves calibration of many more properties than the approach used for producing calibrated properties for the current UZ Flow and Transport Model. A second approach, which is a variant on the first approach, is to use the calibrated properties to re-estimate the property distributions iteratively during the data inversion, but this has the disadvantage of being a very computationally intensive approach. A third approach is to group the properties together, such as by layer, so that the mean of the group can be varied to match a set of data. However, this is very much like the approach used here and is not likely to be a significant improvement.

A distributed properties model is an important alternative conceptual model to consider especially where a homogeneous boundary condition, such as potential repository heating or release of radionuclides from the potential repository horizon is applied. Work is currently being performed to address evaluation of this model.

Deterministic models of the hydrologic properties are also an alternative, but are not favored because they only use properties data and do not incorporate other data, such as ambient conditions data. Related to the deterministic model would be the alternative of using Monte Carlo simulations based on parameter distributions developed from the properties data. In addition to having the same disadvantage of not using as much data as possible, Monte Carlo simulations evaluate unlikely parameter combinations with the same weight as more likely ones, and they are computationally intensive.

3.6.6 Summary and Conclusions

The UZ properties are developed for use in flow, seepage, transport, and coupled process simulations. Figure 3.6-9 shows the resolution of the important issues to property development raised at the beginning of this section. Mountain-scale and drift-scale properties are developed for use in flow, transport, and coupled process simulations at mountain-scales and drift-scales,

respectively. The key difference between the two scales is in the fracture permeabilities and only those of the TSw are of interest for the drift-scale calibrated properties. Fracture permeabilities of 10 to 70×10^{-12} in the TSw are estimated for the mountain-scale calibrated properties, while for the drift-scale calibrated properties, the TSw fracture permeabilities are close to their initial estimate range of 0.1 to 1×10^{-12} .

The use of only *in situ* water potential data has significantly improved results compared to previous calibrations that included core data. Predicted water potentials in the TSw are approximately -10^5 Pa (-1.0 bar). Calibrated van Genuchten α parameter values for the TSw fractures and matrix differ by approximately two orders of magnitude. These results are a large change from results reported for VA (CRWMS M&O 1998g, Chapter 2) and provide calibrated properties for thermal-hydrologic simulations such that they are in better agreement with expected and observed results.

The conceptual model of water flow that is dominantly in the matrix in the unaltered, nonwelded layers and dominantly in the fractures in the welded layers is satisfied by the calibrated properties.

Calibrated properties uncertainties are difficult to estimate. In general, the calibrated properties do not change significantly with respect to the initial estimates, except where the calibrated properties must compensate for model simplifications, such as those required to obtain flow repartitioning between fractures and matrix. The assumption that the uncertainty of the calibrated properties equals the uncertainty of the initial estimates of those properties is based on the small changes in the calibrated properties relative to the prior information, but further substantiation of this assumption is necessary.

The calibration of hydrologic properties for the UZ Flow and Transport Model is an important step in the model's development. This is true not only because of the number of users of these properties but also because it allows the large amount of data from the UZ at Yucca Mountain to be combined. With the calibrated properties that result from these combined data, the UZ Flow and Transport Model can provide the best estimates of present and future conditions in the UZ at Yucca Mountain.

3.7 FLOW MODEL

The Flow Model for the UZ, as described in this section, is divided into two categories: (1) UZ flow submodels (Section 3.7.3) and (2) site-scale flow analysis (Section 3.7.4). The submodels consist of studies of PTn, CHn/perched water, and major fault effects developed for specific studies and analyses. The site-scale flow analysis includes the results of modeled percolation fluxes and flow fields, and fracture and matrix flow components.

3.7.1 Introduction

The Flow Model and its submodels have been developed to simulate past, present, and future hydrological, geothermal and geochemical conditions in the UZ of Yucca Mountain. Over the past decade, Yucca Mountain has been studied extensively, and many types of data have been collected. These data have been used to develop conceptual and numerical models for the hydrological, geothermal and geochemical behavior of the site. These models have been used to simulate ambient conditions and perform predictive studies of changes in the mountain caused by climate-related, thermal, and geochemical perturbations. The comprehensive model that integrates all pertinent data from the UZ at Yucca Mountain is the 3-D, site-scale UZ Flow and Transport Model (e.g., Bodvarsson et al. 1999, pp. 3–24; Wu et al. 1999a, pp. 185–215).

3.7.1.1 Objectives

The primary objectives in developing the Flow Model for the UZ are:

- To integrate the available data from the UZ system into a single, comprehensive, and calibrated 3-D model for simulating the ambient hydrological, thermal, and geochemical conditions and predicting system response to future climate conditions
- To develop a number of submodels with representative boundary and initial conditions specifically for detailed studies of perched water, percolation through the PTn, flow through CHn zeolitic units, and thermal effects from the potential repository heat after waste emplacement
- To quantify the flow of moisture, heat, and gas through the UZ, under present-day and estimated future climate scenarios
- To predict groundwater flow patterns from the potential repository to the water table
- To contribute model parameters and model conditions for other specific studies, such as seepage into drifts
- To provide Performance Assessment and Repository Design with a defensible and credible model that accounts for relevant UZ flow processes.

3.7.1.2 UZ Flow Issues

The Flow Model is an integrated process model for the YMP's Repository Safety Strategy and for support of the License Application (LA). The Total System Performance Assessment for Site Recommendation (TSPA-SR) will use the UZ flow simulations to provide input to other models such as ambient and thermal drift-scale models, the Mountain-Scale Thermal-Hydrological (TH) model, and the Transport Model. The Flow Model and its submodels provide estimates of important processes relevant to UZ flow regarding the performance of the potential repository, all of which contribute to the TSPA-SR and TSPA-LA.

The important issues regarding UZ flow and transport are illustrated in Figure 3.7-1, including the following:

- The spatially and temporally averaged values of the percolation flux at the potential repository horizon
- The components of fracture and matrix flow and interactions within and below the potential repository horizon
- The effects of observed perched water zones, and associated flow barriers and lateral flow diversion
- The probable flow paths from the potential repository to the water table
- The effects of faults on flow and transport processes
- The role played by the PTn unit in lateral flow diversion and damping of infiltration pulses
- Groundwater flow and potential radionuclide migration paths from the potential repository to the water table or from the land surface to the repository level, and breakthrough curves and collection areas at the water table.

In developing the Flow Model, much emphasis has been placed on addressing these issues and preparing a defensible and credible UZ model for Yucca Mountain to evaluate its potential as an underground radioactive waste repository. Major activities, as discussed in this report, include the model calibration studies of 3-D UZ flow, perched water, geochemistry, and geothermal conditions, and model validation efforts.

3.7.2 Description of the Flow Model

The fundamental goal of developing the Flow Model is to conceptualize and represent the UZ system of Yucca Mountain using a computer model. The Yucca Mountain is a complex, heterogeneous hydrogeological system and is subject to many physical and geochemical processes. The Flow Model and its submodels are designed to capture these processes. The development of the Flow Model and its submodels consists of the following steps:

- Development of a conceptual hydrogeological model for moisture, gas and heat flow, and tracer/chemical transport processes in the UZ system
- Representation of the hydrogeological system using a 3-D computer model
- Integration and incorporation of available field and laboratory observations and data into the model
- Model calibration and sensitivity studies, including both inverse and direct modeling efforts, to estimate model input parameters and conditions and evaluate different conceptual models
- Model applications including predictive and sensitivity studies.

Geological Model and Numerical Grids—The Flow Model and its submodels are built on the current geological conceptual model of the GFM 3.1 and ISM 3.0, as discussed in Section 3.2 of this PMR. The development and features of the 3-D model grids with the geological model are discussed and documented in the *AMR Development of Numerical Grids for UZ Flow and Transport Modeling* (CRWMS M&O 2000, U0000, Section 6.1). In this geological model and the associated numerical grids, the geologic formations within the UZ have been reorganized into layered hydrogeologic units, based primarily on the degree of welding of the Yucca Mountain tuffs (see Section 3.2.2). These are the Tiva Canyon welded (TCw) hydrogeologic unit, the Paintbrush nonwelded unit (PTn) (consisting primarily of the Yucca Mountain and Pah Canyon Tuffs and their bedded tuffs), the Topopah Spring welded (TSw) unit, the Calico Hills nonwelded (CHn) unit, and the Crater Flat undifferentiated (CFu) unit (see Figure 3.7-2a).

The 3-D UZ Flow Model domain (Figure 3.7-2a) is represented using a 3-D numerical grid, as shown in Figure 3.7-2b (CRWMS M&O 2000, U0000, Section 6.7). The plan view of the model grid (as well as represented model domain) is given in Figure 3.7-3. The 3-D UZ model grid, designed for simulations of 3-D flow fields delivered for use in TSPA-SR calculations, uses relatively refined meshes in the vicinity of the proposed repository, located near the center of the model domain. Also, shown in Figure 3.7-3 are the locations of several boreholes, used in model calibrations and analyses. The model domain is selected to focus on studies at and near the potential repository area and to investigate effects of different infiltration scenarios and major faults on fluid and heat flow and radionuclide migration around and below the potential repository.

Modeling Approach—The numerical modeling approach used in the Flow Model, as discussed in details in Section 3.4.1, is based on a mathematical formulation of the TOUGH2 code V1.4 (STN:10007-1.4-01) (Pruess 1991) for coupled multiphase, multicomponent fluid and heat flow through porous and fractured rock. The numerical scheme of the TOUGH2 family of codes is based on the integral finite-difference method. The mass conservation equations for air, water and chemical constituents and thermal energy equations are discretized in space using the integral finite-difference method, without any reference to a global system of coordinates. This offers the advantage of being applicable to regular and irregular geometries of gridding in one, two, and three dimensions. The method also makes it possible, by means of simple preprocessing of geometric data, to implement double- and multiple-porosity, or dual-permeability methods for treatment of flow in fractured porous media. In the TOUGH2 formulation, time discretization is fully implicit using a first-order backward finite-difference scheme. The resulting discretized finite-difference equations for mass and energy balances are nonlinear and are solved simultaneously using the Newton/Raphson iterative scheme.

Fracture-Matrix Interaction—Fracture and matrix flow in the UZ model and its submodels is treated using the dual-permeability conceptual model. In this dual-continua modeling approach, as discussed in Section 3.4.1.1, flow and transport processes at Yucca Mountain are simulated by two overlapping fracture-matrix systems with interactions between them. The dual-permeability concept represents each grid block by a fracture and matrix element. Because each fracture grid block is associated with only one matrix element, fracture-matrix flow must be approximated as quasi-steady state (Warren and Root, 1963, pp. 245–255). Global flow occurs within both fracture and matrix continua. When applied to the Flow Model, the traditional dual-permeability concept is further modified using the active fracture model (Liu et al. 1998, pp. 2633–2646) to represent effects of liquid flow channeling and fingering through fractures, which may limit flow into the matrix system (CRWMS M&O 2000, U0030, Section 6.4.5).

Model Conditions—In the Flow Model, the UZ system is represented by a multilayer sequence of hydrogeologic units, with rock properties estimated from field measurements and modeling studies (Section 3.5). The UZ model domain (Figure 3.7-2 and 3.7-3) covers a total area of approximately 40 km². Boundary conditions for the Flow Model are discussed in the AMR *UZ Flow Models and Submodels* (CRWMS M&O 2000, U0050, Section 6.1.3). The ground surface of the mountain (or the tuff-alluvium contact in areas of significant alluvial cover) is defined as the top model boundary, and the water table is treated as the bottom model boundary. Both the top and bottom boundaries of the model are described as Dirichlet-type boundaries with temperature, gas pressure, and liquid saturation values specified along these surfaces. Surface infiltration of different climatic scenarios is applied using a source term in the gridblocks within the second grid layer from the top. All the lateral boundaries, as shown in Figure 3.7-3 are treated as no-flow (closed) boundaries. The constant temperatures and their spatially distributed values, along the top and bottom boundaries, were based on field observation. The pressure conditions at the bottom boundary of the model are calculated using observed gas-pressure values. The water table, which is the bottom boundary of the site-scale model, is treated as a flat, stable surface (CRWMS M&O 2000, U0000, Section 6.4). East of the Solitario Canyon fault, the water table elevation is about 730 meters above sea level (masl); however, the water table elevation increases by 46 meters when it crosses the Solitario Canyon fault to the west. The gas pressures are approximated by the atmospheric pressure of 0.92 bars at an elevation of 730 m.

Infiltration Scenarios—Net infiltration of water, resulting from precipitation that penetrates the top-soil layer of the mountain, is the most important factor affecting the overall hydrological behavior of the UZ. Net infiltration is the ultimate source of groundwater recharge and percolation through the UZ and provides water as a transport medium for potential advective transport of radionuclides from the repository to the water table. A total of nine net infiltration maps (Section 3.5.2) are implemented by the UZ model and its submodels (USGS 2000, U0010; CRWMS M&O 2000, U0050, Section 6.1.3). The nine infiltration scenarios include present-day, monsoon, and glacial transition—three climates, each of which consists of lower-, mean, and upper-bound maps. The statistics of the nine infiltration rates are summarized in Table 3.7-1 for average values over the model domain. These values (as well as the infiltration rates listed in Tables 3.7-3 and 3.7-4) are slightly different from what are estimated in Table 3.5-4 and Figure 3.5-1 of Section 3.5, due to using different grids. The flux distributions of the three mean infiltration maps over the model domain are shown in Figure 3.7-4.

Table 3.7-1. The Average Value (mm/yr) of Infiltration Rates over the UZ Model Domain (Adapted from CRWMS M&O 2000, U0050, Table 6-3)

Climate Scenario	Lower Infiltration	Mean Infiltration	Upper Infiltration
Present-day	1.2	4.6	11.2
Monsoon	4.6	12.4	20.1
Glacial transition	2.4	18.0	33.5

Model Parameters and Rock Properties—The key input parameters for rock and fluid flow used in UZ model development include (1) fracture properties (frequency, permeability, van Genuchten α and m parameters, aperture, porosity, and interface area) for each UZ model layer; (2) matrix properties (porosity, permeability, and the van Genuchten α and m parameters) for each UZ model layer; (3) thermal and transport properties (grain density, wet and dry thermal conductivity, grain specific heat, and tortuosity coefficients) for each UZ model layer; and (4) fault properties (matrix and fracture parameters) for each of the major hydrogeologic units—TCw, PTn, TSw, and CHn. The development and estimation of these parameters are presented in the AMRs *Calibrated Properties Model* (CRWMS M&O 2000, U0035, Sections 6.1, 6.2 and 6.3), *Analysis of Hydrologic Properties Data* (CRWMS M&O, 2000, U0090, Section 6), and *UZ Flow Models and Submodels* (CRWMS M&O, 2000, U0050, Section 6.1.4) as well as in Section 3.6 of this PMR.

The rock parameter specification in the Flow Model and its submodels is, in general, by layer averages, but certain parts of grid layers in the CHn unit are altered to vitric or zeolitic regions. In these property-altered layers, zeolitic and vitric tuff properties are specified to correspond to actual geologic properties according to the alterations, instead of layers (CRWMS M&O 2000, U0000, Section 6.6.3). All the geological units, including fault zones, are treated as fracture-matrix systems using the dual-permeability approach described above. The van Genuchten relative permeability and capillary pressure functions (van Genuchten 1980, pp. 892–898) are used to describe unsaturated flow in both fractures and matrix.

UZ Flow Model Input and Output—The key input data to (CRWMS M&O 2000, U0050, Section 6.1), and output models from, the UZ Flow Model are illustrated in Figure 3.7-5. As shown in this diagram, the Flow Model uses input from the perched water and matrix properties, calibrated properties models, the conceptual model, the geological and numerical grid model, and the climatic/infiltration model, as well as the geochemistry model. The output of the Flow Model directly feeds many process models, such as the TSPA UZ Flow Model, the Transport Model, the Ambient Geochemistry Model, the Mountain-Scale TH Model, the Seepage Model for PA, and the Drift-Scale THC Model.

3.7.3 UZ Flow Submodels

The submodels of the Flow Model, described in this section, include the studies of the PTn, effects of major faults submodel, and the CHn and perched water occurrence. These investigations are made to specifically study the effects of these geological units or features on flow and transport in the UZ system. In addition to the submodels of the Flow Model of this section, the Seepage Calibration Model is discussed in Section 3.9.4 and the Seepage Model for PA is presented in Section 3.9.5.

3.7.3.1 PTn Flow Studies

The PTn studies of this section are based mainly on the site-scale, 3-D UZ modeling efforts of the AMR *UZ Flow Models and Submodels* (CRWMS M&O 2000, U0050, Section 6.6). The focus of this investigation is on understanding the flow behavior through the Paintbrush Tuff nonwelded (PTn) unit. The role of the PTn in altering the pattern of percolation into the underlying Topopah Spring welded (TSw) unit is of great significance in assessing repository performance. A key issue is whether the PTn effectively damps pulses of transient infiltration, resulting in a generally uniform percolation flux into the underlying repository rocks of the TSw, or whether preferential flow paths within the PTn serve to focus flow above or around potential repository drifts.

The present conceptual model for UZ flow at Yucca Mountain, as discussed in Section 3.3.3, considers that net infiltration at the bedrock surface (top of the TCw unit) is episodic, with significant pulses probably occurring only once every few years. These spatially and temporally variable pulses of moisture percolate rapidly through the highly fractured tuffs of the TCw, as indicated by the numerous bomb-pulse ^{36}Cl signatures measured within the TCw (CRWMS M&O 2000, U0085, Section 6.6.3). However, at the TCw-PTn interface, where welded tuffs grade sharply into nonwelded tuffs, flow behavior changes from fracture-dominated to matrix-dominated flow. The highly porous PTn matrix significantly attenuates the episodic infiltration flux; however, in localized areas such as around faults and zones with high infiltration rates, fracture flow within the PTn may predominate. In general, the high storage capacity of the PTn matrix damps moisture flow through the unit so that percolation flux across the bottom of the PTn into the TSw is more uniformly distributed spatially and temporally. Therefore, the net episodic surface infiltration, once crossing the PTn, may be effectively approximated as steady-state and the alternative view that the episodic flow through the TSw unit is pervasive is unlikely, except along the major faults.

Figure 3.7-6 presents two vertical cross sections along the south-north and west-east of the UZ model domain, showing lithostratigraphic horizons and geological unit thicknesses. The PTn unit consists of non- to partially welded tuffs, and it extends from the base of the densely welded and devitrified portion of the Tiva Canyon Tuff to the top of the densely welded portion of the TSw (Section 3.2.2). The combined thickness of these layers exceeds 150 m at the northern end of Yucca Mountain, while at the southern end, the PTn thins to less than 30 m. Above the potential repository area, the PTn thickness ranges from approximately 30 to 60 m.

The PTn unit displays significantly different hydrogeological properties from the TCw and TSw units that bound it. Both the TCw and the TSw are characterized by dense welding and intense fracturing. Where exposed at the land surface, the TCw plays an important role in controlling surface infiltration, since fracturing through the low-porosity matrix may initiate rapid vertical percolation. During percolation through the PTn, the flow pattern changes from fracture-dominated flow in the TCw, to matrix-dominated flow within the PTn, to the initiation of significant fracture flow in the upper layers of the TSw.

In the Flow Model, the PTn unit is represented using six model layers, in general, using the 3-D TSPA grid (see Section 3.4.2). Calibrated parameters for the present-day, mean infiltration scenario and perched water conceptual model #1 (flow-through model), described in Section 3.7.3.3 are used in the PTn modeling studies. The infiltration maps incorporated are the three mean infiltration scenarios of the present-day, monsoon, and glacial transition climates.

The distribution of simulated vertical percolation fluxes at the interface between the PTn and TSw units is demonstrated in Figure 3.7-7 for the mean, present-day infiltration scenario. In this and subsequent figures, the total flux is defined as total vertical liquid mass flux per year through both fractures and matrix, divided by a constant water density, converted to mm/yr, which is the commonly used unit for surface infiltration. Comparison of Figures 3.7-7 and 3.7-4a (corresponding surface infiltration map) shows that simulated percolation fluxes at the PTn-TSw interface are similar, in distribution patterns, to the surface infiltration map for the present-day case. The high percolation areas, located at the northern part and along the Solitario Canyon fault in the middle portion of the model domain, are especially preserved. The similarity between surface infiltration maps and percolation fluxes simulated at the bottom of the PTn unit, as shown in Figure 3.7-7, indicates that there may be only small lateral diversion of infiltrated water flowing through the PTn unit. A close look at the figure reveals that some lateral movement does occur in several areas when crossing the PTn. In particular, the percolation fluxes simulated under the high infiltration areas along the north-south mountain crest (east of the Solitario Canyon fault), at the middle portion of the model domain, show obvious differences from the infiltration maps.

The simulations reveal two types of lateral flow diversion through the PTn: (1) up to a hundred meters movement to the east in the areas above the potential repository and (2) lateral diversion into major faults (e.g., Solitario Canyon and Ghost Dance). In general, high infiltration zones of the mountain crest along the middle, north-south model domain are damped and spread into larger areas after crossing the PTn.

Table 3.7-2 compares the fraction of vertical fracture and matrix flow at the middle of the PTn with that at the repository horizon below. Note that on the ground surface, infiltration is introduced into fractures only; therefore, it is 100% fracture flow at the top of model domain. The statistics in Table 3.7-2 show that matrix flow is dominant in the PTn unit, taking nearly 90% of the total flow, with little variation among the three climate scenarios. This indicates that a dramatic transition takes place from fracture-dominant flow within the TCw to matrix-dominant flow in the PTn crossing the interface between the TCw and PTn units. While flowing down across the PTn and TSw interface, percolation flux changes back from matrix-dominated to fracture-dominated flow into the TSw, as indicated by the statistics in the table.

Table 3.7-2. Comparison of the Water Flux through Matrix and Fractures as a Percentage of the Total Flux at the Middle PTn and at the Potential Repository (CRWMS M&O 2000, U0050, Section 6.6.3)

Climate	Flux at middle PTn (%)		Flux at Potential Repository (%)	
	Fracture	Matrix	Fracture	Matrix
Present-day	11.6	88.4	83.7	16.3
Monsoon	12.1	87.9	89.5	10.5
Glacial Transition	11.8	88.2	91.4	8.6

Summary—The 3-D simulations with three climate scenarios have provided some key insights into the flow pattern alteration by the predominantly nonwelded PTn formation. The PTn studies indicate the following:

- Percolation through the PTn is predominantly matrix flow, comprising nearly 90% of the total flow. This conclusion is consistent with the field-observed pneumatic responses, which are controlled by the porous-medium-like PTn unit (Ahlers et al. 1999, pp. 47–66). Therefore, the alternative view that fracture flow is dominated crossing the PTn unit is a very unlikely scenario.
- In general, the model predicted insignificant lateral flow diversion by the PTn over the entire UZ model domain. However, some lateral, east-bound flow (up to 100 m) is predicted in the areas above the potential repository along the mountain crest. Occurrence of large-scale or significant lateral flow in the PTn, however, is unlikely due to existence of a large amount of faults in the PTn and these faults will intersect the lateral flow and provide downward flow paths.
- Some flow is to be diverted into nearby faults when crossing the PTn unit.

3.7.3.2 Effects of Major Faults

Introduction—Major faults may significantly affect the ambient hydrogeologic system and flow and transport processes at Yucca Mountain. Compared to the surrounding rock, the larger

fracture apertures and higher fracture densities generally lead to increased permeability and reduced capillarity within and near faults and fault zones. Flow is also affected by the amount of offset at the fault, which can range from meters to hundreds of meters (see discussion in Sections 3.2.3 and 3.3.5). Figure 3.7-6b presents a vertical cross section along the east-west UZ model domain (EW-S on Figure 3.7-3), showing several vertical and inclined faults and fault displacements as well as lithostratigraphic horizons and geologic unit thicknesses.

Faults may provide a direct path from the potential repository horizon to the water table. This is particularly significant to the problem of waste isolation because radionuclides released from the potential repository could bypass altered, zeolitic, or vitric layers within the CHn hydrogeologic unit, where they could be retarded by sorption. Consequently, dissolved radionuclides could enter the saturated zone where hydrologically significant faults and the water table intersect. Alternatively, faults might be considered a positive feature of the site if they divert water around waste emplacement drifts or prevent laterally flowing water from focusing at the area of waste emplacement.

In this section, the site-scale, 3-D TSPA UZ model, as documented the AMR *UZ Flow Models and Submodels* (CRWMS M&O 2000, U0050, Sections 6.1 and 6.6), is used for analyzing effects of major faults on the UZ flow processes at Yucca Mountain.

Conceptual Model—As discussed in Section 3.2, Yucca Mountain is a structurally complex system of Tertiary volcanic rock. Faults at Yucca Mountain fall into three types: (1) north-striking block-bounding faults such as the Solitario Canyon and Bow Ridge faults, (2) northwest-striking faults such as Drill Hole Wash, Sever Wash and Pagany Wash faults, and (3) intrablock faults (Day et al. 1998). Block-bounding faults are key structural features that dip steeply to the west and have large cumulative displacements of up to 500 m. Intrablock faults tend to be shorter and more discontinuous than block-bounding faults, and, with the exception of the Ghost Dance fault, generally have minor displacements of 5 to 10 meters (Day et al. 1998). Displacement along northwest-striking faults varies from small to moderate (30 m).

Permeability is expected to vary along faults, with higher values in the brittle, welded units and lower values in the nonwelded units, where gouge or sealing material may exist (Montazer and Wilson 1984). Highly brecciated fault zones may act as capillary barriers to flow, as indicated by high pneumatic permeability measurements in portions of the faults, which suggest large fracture apertures and correspondingly low air entry pressure. However, if water does enter this type of zone, its high permeability could facilitate rapid transport to the water table (Wang and Narasimhan, 1988).

The observed data show that the conceptual model for the effects of major faults on flow should depend upon the type of rock, the proximity of portions of the fault zone to the surface and/or to the water table, and the degree of offset along the fault. These factors affect the impact of the faults on fluid flow in the following ways (Sections 3.2.3 and 3.3.5):

- Fault zones in the TCw are intensely fractured and therefore provide a major conduit for gas flow and high liquid flux or transient percolation.

- Fault zones in the PTn are less likely to be intensely fractured because of the more plastic (non- to partially welded) character of the rock, but fracturing is more intense than in unfaulted areas of the PTn. PTn fracture zones may provide a conduit for gas and liquid flow.
- The TSw, like the TCw, is intensely fractured within and around faults, mainly as a result of the brittle character of the rock. Fault zones in the TSw are major conduits for gas flow and may provide preferential water flow in certain areas.
- Faults within the CHn behave like the PTn. The more plastic character of the CHn reduces the intensity of fracturing in comparison to the densely welded TCw and TSw. In addition, hydrothermal alteration may have reduced permeability of the fault zone. However, the fault zones are likely to be more permeable than the surrounding altered rock and thus are still the main drain from perched water or low-permeability zeolitic zones.

In this section, the conceptual model of fault influence on the hydrogeologic system is investigated using the Flow Model, in which faults are represented using vertical or inclined walls 30 m thick. Vertically, faults are subdivided into four hydrogeologic units, according to their connections to the neighboring nonfaulting rocks, in the four major hydrogeologic units of TCw, PTn, TSw, and CHn. Therefore, each fault, as shown in Figures 3.7-3 and 3.7-8, is represented in the model as a vertical or inclined 3-D sheet of gridblocks. Fracture-matrix flow and interactions with fault elements are also treated using the dual-permeability approach. The fault properties are estimated using a two-dimensional inversion of saturation, water potential, and pneumatic data from borehole USW UZ-7a (CRWMS M&O 2000, U0035, Section 6.3).

Model Results and Analyses of Effects of Major Faults on UZ Flow—An example of the effects of faults on UZ flow is presented in Figures 3.7-8 (a and b), using the simulation results with the present-day, mean infiltration map, showing (a) percolation flux at the water table and (b) vertical fracture flow along an east-west cross section. A comparison of the flux pattern between surface infiltration (Figure 3.7-4a) and the water table map (Figure 3.7-8a) clearly indicates that flow has been significantly converged to the faults after penetrating the UZ system. At the top boundary, infiltration rates or distributions, as shown in Figure 3.7-4a, are located independently of faults. However, on arriving at the water table, a large fraction of the water has been diverted to the Solitario Canyon, Ghost Dance, and the other faults in the model domain.

The effects of faults on the UZ flow under the current conceptual model can be analyzed using vertical flow path plots. Figure 3.7-8b displays such results, showing flow fields through fractures (flow through matrix is similar) along a west-east cross section. The flow path results shown along the 2-D cross section are extracted from the 3-D flow fields and the background contours show liquid saturation in the matrix. Figure 3.7-8b shows that flow paths for particles released in the surface areas close to faults either converge downward along or parallel to faults. No flow lines are seen to cross faults laterally. This indicates that faults can serve as either capillary barriers or downward flow conduits for UZ percolation. In addition, some lateral flow diversion can also be seen in the figure at the PTn in both matrix and fracture continua and at the CHn in the matrix continuum along this cross section.

Analysis of the simulation results reveals that the fraction of flow occurring through the faults, as a percentage of the total flow (through the fractures, matrix and faults), increases with depth. Table 3.7-3 lists these percentages at four different horizons and for the three climate scenarios. At the ground surface, 4% of the total flow occurs through the faults. This percentage increases to 10 - 15% for flow through the PTn. At the water table, fracture flow accounts for 35 - 44% of the total flow. The percentage of fracture flow at the water table is the most sensitive to climate scenario as compared to the other horizons. It increases from 35% to 42% to 44% for the present-day, monsoon and glacial transition climates, respectively. In addition, Table 3.7-3 shows that flow percentages through faults at the water table are very different in the southern (through vitric zones) and northern (through zeolitic zones) part of the model domain. Fault flow consists of 42, 51 and 54% of the total flow in the northern model domain versus only 16, 22 and 24% in the south for the three infiltration scenarios. This indicates more lateral flow diversion occurring in the north when crossing the zeolitic zones.

Table 3.7-3. Comparison of the Water Flux through Faults as a Percentage of the Total Flux at Four Different Horizons (1) on Ground Surface; (2) Interface between PTn and TSw; (3) at the Potential Repository; and (4) at the Water Table (Data from CRWMS M&O 2000, U0050, Section 6.6.3)

Climate Scenarios	Fraction of Total Flow through Faults (%)												
	Mean Infiltration (mm/yr)	Ground surface			PTn-TSw interface			Potential Repository level			Water table		
		Total	South	North	Total	South	North	Total	South	North	Total	South	North
Present-day 4.6	3.8	3.6	3.9	14.3	18.9	12.7	14.6	19.8	12.7	34.9	15.9	42.0	
Monsoon 12.4	4.1	3.8	4.2	10.5	13.0	9.6	10.5	13.3	9.5	42.4	21.9	51.3	
Glacial Transition 18.0	4.0	3.7	4.1	9.1	10.8	8.4	9.1	11.0	8.2	44.4	24.3	54.2	

NOTE: "Total" denotes flow over the entire model domain, "South" denotes flow over the southern part/half of the model domain; and "North" denotes flow over the northern part/half of the model domain.

Summary—Overall, percolation fluxes in the UZ system of Yucca Mountain are predicted to converge into the faults as water flows downward through the geologic units. Faults serve as major focusing conduits for the downward unsaturated liquid flow in the UZ system. Lateral diversions of water into faults occur mainly in the CHn and some in the PTn unit. In addition, the percentage of fault flow increases as mean infiltration rates increases.

3.7.3.3 Investigations of Calico Hills and Perched Water Occurrence

In terms of groundwater flow paths, as well as radionuclide transport from the repository level, the CHn hydrogeologic unit may play a crucial role in the assessment of geologic repository performance. This unit separates the potential repository horizon from the saturated zone. The

predominantly nonwelded nature of the CHn makes these initially high-porosity, vitric tuffs susceptible to hydrothermal alteration. Hydrothermal alteration produces low-permeability clays and zeolites that create complex, heterogeneous flow paths within the CHn (see Section 3.2.4). The observed, widespread alteration within the CHn has important implications for perched water, for groundwater flow paths, and for radionuclide transport because of the reduced permeability and the sorption potential associated with zeolitic and vitric rocks.

The presence of perched water within the UZ, which is associated with the densely welded basal vitrophyre of the Topopah Spring Tuff or with zeolitic intervals of the CHn, has important ramifications for flow patterns. In perched water locations, vertical percolation flux locally exceeds the saturated hydraulic conductivity of the perching layers. Perched water bodies suggest that flow paths may not be completely vertical through the CHn unit to the water table. Instead, the water may be partially diverted laterally to a fault zone or another high-permeability channel that may serve to focus flow downward to the water table. The diverted flow may bypass zeolitic layers, reducing the potential sorption of radionuclides.

CHn Geological Model—Within the Flow Model, the CHn is represented with 14 model layers based on lithostratigraphy and available hydrogeologic properties, as discussed in CRWMS M&O (2000, U0000, Sections 6.1 and 6.3) and Section 3.2.2. The CHn unit extends from the base of the lower welded vitrophyre of the TSw to the top of the welded portion of the Bullfrog Tuff. The CHn consists of the non- to partially welded vitric subzone of the lower TSw (Ttpv1), the pre-Topopah Spring bedded tuffs (Tpbt1), the Calico Hills Formation (Tac), the pre-Calico Hills bedded tuffs (Tact), the entire Prow Pass Tuff (Tcp), and the upper nonwelded, vitric portions of the Bullfrog Tuff. More detailed description on the hydrogeological units can be found in Table 3.2-2 of Section 3.2 of this PMR.

The cumulative, unsaturated thickness of the CHn ranges from about 400 m at the northern end of Yucca Mountain to approximately 200 m near the southern end. Figure 3.7-6a presents a north-south cross section through the UZ near borehole UZ-14, showing the major grouping of layers into hydrogeologic units. Governed by the water table elevation, the location of major faults, and the gentle eastward dip of the strata, the thickness of the CHn at Yucca Mountain, in general, increases to the east of the Solitario Canyon fault (Figure 3.7-6b).

Perched Water Conceptual Model—Conceptual models involving perched water occurrence in the UZ below the repository horizon are of particular interest in assessing the natural geologic system performance of the potential repository. The extent of radionuclide sorption within the zeolitically altered CHn and groundwater flow patterns between the repository horizon and the water table may be altered by perched water. The genesis of perched water at Yucca Mountain is much debated among Yucca Mountain project scientists, and several conceptual models have been proposed (e.g., Wu et al. 1999b, pp. 157–184).

Perched water may occur where percolation flux exceeds the capacity of the geologic media to transmit vertical flux in the UZ. At Yucca Mountain, perched water has been encountered in a number of boreholes, including UZ-14, SD-7, SD-9, SD-12, NRG-7a, G-2, and WT-24 (Figure 3.7-3) (CRWMS M&O 2000, U0050, Sections 6.2 and 6.6). These perched water occurrences are found to be associated with low-permeability zeolites in the CHn or the densely welded basal

vitrophyre of the TSw unit. It should be noted that the perched water body found at SD-7 is very small, as inferred from pumping tests and is not believed to impact the performance of the potential repository. Possible mechanisms of water perching in the UZ of Yucca Mountain may be permeability and/or capillary barrier effects.

A permeability barrier conceptual model for perched water occurrence (model #1) has been used in the UZ flow modeling studies since 1996 (Wu et al. 1999b). The major assumptions of the permeability barrier conceptual model are: (1) no large-scale vertically connected fractures transect the underlying low-permeability units, (2) both vertical and horizontal permeabilities within and below the perched water zone are small compared with permeabilities outside perching zones, and (3) sufficient percolation flux (>1 mm/yr) exists. Previous modeling studies (Wu et al. 1999b, pp. 157–184) concluded that this conceptual model is able to match the observed data of perched water in the UZ of Yucca Mountain.

Another conceptual perched water model is an unfractured zeolite model (model #2). Similar to the permeability barrier model discussed above, this model presumes that the occurrence of perched water at Yucca Mountain results mainly from the lack of globally connected fractures within zeolitic units. This model can be considered a special case of the permeability barrier model, in which a water-perching mechanism is controlled by the low-permeability zeolitic matrix only, i.e., the existence of fractures in zeolites is ignored. In the present Flow Model, the occurrence of perched water is assumed to follow either model #1 or model #2. In other words, a perched water body is formed mainly as a result of permeability barrier effects.

There are other alternative conceptual models for explaining perched water occurrence at Yucca Mountain. One of the alternative views considers that the perched water zones in the northern part of the model domain may have resulted from elevated water tables or steep water gradients there. Another alternative explanation is that water sources of perched water bodies have been supplied from the recharge in the Solitario Canyon area and then lateral flow along low permeability units, such as the basal vitrophyre of the TSw. The current perched water conceptual models have not included these two alternative concepts because they are not strongly supported neither by field-observed data nor by modeling results.

To calibrate the Flow Model against observed perched-water conditions at Yucca Mountain, some local modification of rock properties is necessary. In general, permeability was adjusted only within the model layers associated with the perching zones (CRWMS M&O 2000, U0050, Section 6.2). For perched water conceptual model #1, calibrated parameters of fracture and matrix permeabilities within perched zones are results from a series of modeling studies of 3-D simulations. Matrix permeabilities of potential perched layers/zones are based on average values of the measured matrix permeabilities, while fracture permeabilities were manually calibrated so that modeled perched water results matched observed data. For perched water conceptual model #2, rock properties of all the fractures within the zeolitic layers/zones were replaced by the corresponding matrix properties of the same units.

Model Results and Analyses—Simulations using the two conceptual perched water models incorporate all three climate scenarios (present-day, monsoon and glacial transition) and their associated mean or upper-bound infiltration maps (CRWMS M&O 2000, U0050, Section 6.6).

Both perched water conceptual models can generally match the water perching conditions, as observed in Yucca Mountain. Figure 3.7-9 presents a simulated perspective view of 3-D perched water bodies and their volumetric extensions. This figure shows fracture-water saturations, simulated along the bottom of the TSw or the low basal vitrophyre layer for perched water model #1. The blue isosurfaces on the figure reflect the regions of 100% liquid saturations, or perched water zones, within fractures along the model layer, while the green isosurface represents a portion of the model layer with fracture liquid saturations less than 100%. Figure 3.7-9 clearly shows several extensive perched water bodies, separated by faults, predicted in the northern part of the model domain.

Effects of perched water zones on flow processes in the CHn unit is best explained by comparing percolation fluxes simulated at the repository level and the water table. Figure 3.7-10 presents three map views of the simulated percolation fluxes (a) at the repository horizon with model #1; (b) at the water table with Conceptual Model #1; and (c) at the water table with model #2. The map at the potential repository horizon is only shown for model #1 because model #2 is applied only to the zeolites in the CHn unit and consequently has minimal effect on flow at the repository and higher-elevation horizons.

Figure 3.7-10 reveals large differences in the magnitude and distribution of percolation fluxes or their distributions at the water table and the repository horizon. This confirms significant lateral flow or diversion occurring above or within the CHn for both perched water models. Comparing the flux distribution in the northern part of the model domain in Figure 3.7-10a, b, and c shows that there is a large amount of the percolation flux at the water table, which is focused along the major faults. The water table flux maps, compared to the flow patterns at the repository level, show significantly lower fluxes (red zone) in the northern part of the potential repository area, directly below the perched water bodies and bounded by the Solitario Canyon and the Drillhole Wash faults. A large amount of water is diverted laterally to the east, along layer slopes, and intersects faults that focus flow downward to the water table.

In the southern part below the potential repository area of the model domain, the majority of percolation flux at the water table is found to be contributed by high-permeability matrix flow in vitric zones. The analyses of the simulated fracture and matrix flow (e.g., near borehole SD-7) indicate that matrix flow dominates in those vitric zones, as predicted by both perched water conceptual models. Even in these areas, however, water is laterally diverted to the east and intercepted by faults along the thin zeolitic layers, when one compares the repository fluxes with the water table fluxes of Figure 3.7-10.

Summary—The CHn hydrological unit could play a critical role in controlling groundwater flow patterns and radionuclide transport pathways from the potential repository horizon to the saturated zone. One specific issue related to flow below the potential repository horizon is perched water. Its presence implies that vertical percolation flux locally exceeds the saturated hydraulic conductivity of the perching layer. Thus, predominant flow paths may not be vertical through the CHn from the potential repository horizon to the water table. Instead, water may be diverted laterally to a fault zone, fracture network, or relatively high-permeability vitric zone that focuses flow to the water table.

The modeling results show that the flow patterns, or pathways, through the CHn are controlled mainly by fracture and matrix parameters in the CHn unit and by the presence of high-permeability flow channels, such as faults, that cross-cut the unit. All modeling scenarios, based on the two perched water conceptual models, indicate significant lateral flow diversion (40-50% of the total flow) at the CHn resulting from the presence of perched water or thick zeolitic layers. In addition, faults act as major flow paths in the northern part of the model domain under the current conceptualization. In the southern part of the model domain, flow through the vitric zone of the CHn is matrix flow dominated because of the high matrix permeability.

3.7.4 Site-Scale Flow Analysis

This section presents an in-depth analysis of site-scale 3-D UZ flow using the Flow Model for the UZ. The results, as discussed in the following subsections, represent the best estimates and the current understanding of the Yucca Mountain UZ flow system.

3.7.4.1 Percolation Flux at the Potential Repository Horizon

Percolation flux through the UZ is one of the most critical factors affecting the potential repository performance of the natural waste storage system as well as TSPA calculations. The quantity and spatial and temporal variations in percolation flux directly affect: (1) the amount of water flowing into waste emplacement drifts; (2) moisture conditions and corrosion environment of canisters within the drifts; (3) waste mobilization from the potential repository; (4) thermal-hydrological behavior of the potential repository; and (5) radionuclide migration from the UZ to the saturated zone. However, because percolation fluxes of unsaturated flow cannot be readily measured in the field, we must rely on indirect data and model results to estimate these fluxes.

The past modeling studies (Wu et al. 1999a, pp. 185–215 and Wu et al. 1999b, pp. 157–184) indicate that accurate model predictions of percolation fluxes at Yucca Mountain depend on many factors. The most important are (1) net infiltration rates over the surface boundary; (2) representative geological and conceptual models; (3) reliable distributed rock property values for fractures and matrix blocks; and (4) treatment of fracture-matrix flow and interactions. Percolation fluxes at the repository horizon, as predicted by the UZ Flow Model, have been analyzed using 28 3-D UZ flow simulation results, with nine infiltration maps and different perched water conceptual models (CRWMS M&O 2000, U0050, Section 6.6.3).

Figures 3.7-11a, b, and c show samples of percolation fluxes simulated at the repository level for the three mean infiltration rates of mean present-day, monsoon and glacial-transition climate scenarios. As discussed for the perched water studies, percolation fluxes at the potential repository are nearly the same for the same infiltration map, regardless of the specific perched water conceptual models. Figure 3.7-11 displays a highly nonuniform pattern of flux distributions (the darker blue spots on the figure indicates the higher modeled percolation fluxes). The high percolation fluxes are located primarily at the northern part, but also along the Solitario Canyon fault in the middle portion of the model domain. A comparison of the modeled percolation fluxes to their corresponding surface infiltration maps (Figure 3.7-4) indicates very similar flux patterns, and therefore minimal lateral flow diversion between the surface and potential repository level.

Percolation fluxes at the level of the potential repository horizon are largely a reflection of surface infiltration rates. Areas of higher infiltration rates (i.e., in the northern portion of the model domain and along the Yucca Mountain crest) have the highest percolation fluxes, and the low infiltration areas have correspondingly lower percolation. Beneath the potential repository horizon, the distribution of percolation fluxes is more diffuse and generally spread to the east as a function of lateral flow.

The statistics of the averaged percolation fluxes within the potential repository footprint, extracted from the 3-D UZ model results for the three mean infiltration scenarios, are listed in Table 3.7-4. Table 3.7-4 indicates that the total percolation flux within the potential repository horizon is very similar to the average surface infiltration rate over the model domain of Table 3.7-1. The only exception is the glacial-transition scenario, which predicts a higher average percolation flux within the potential repository footprint than the average value over the entire model domain.

Table 3.7-4. Average Percolation Fluxes Simulated within the Potential Repository Footprint for the Three Mean Infiltration Scenarios (Data from CRWMS M&O 2000, U0050, Section 6.6.3)

Climate Scenario Mean Infiltration over the UZ Model Domain (mm/yr)	Average Percolation Flux within Potential Repository (mm/yr)		
	Fracture	Matrix	Total
Present-day 4.6	4.0	0.5	4.5
Monsoon 12.4	12.1	0.8	12.9
Glacial Transition 18.0	19.5	0.9	20.5

3.7.4.2 Repository Percolation Flux Frequency Distribution

Percolation fluxes within the potential repository footprint can be further analyzed using a frequency distribution plot, which displays the average percentage of the potential repository area subject to a particular percolation flux. This information is useful to drift-scale modeling studies of flow and transport at drifts. Figure 3.7-12 shows the frequency distribution of percolation flux within the potential repository horizon for the three mean infiltration scenarios of present-day, monsoon, and glacial-transition climates. The frequencies are generated by grouping the vertical flux results for the repository model nodal areas, counting the total area found in each flux group, and then calculating the percent contribution relative to the total potential repository area in each category. On the plots, a node in the 1 mm/yr category has a flux in the 0.0 to 1.0 mm/yr range.

Figure 3.7-12a indicates that the highest flux frequencies have fluxes within the 1.0 to 4.0 mm/yr range and occur over about 50% of the potential repository area. The nodal area with percolation

fluxes greater than 20.0 mm/yr comprises only about 1% of the total repository area. For the monsoon scenario, Figure 3.7-12b shows that the highest frequency of percolation fluxes is in a range of about 6 to 7 mm/yr, occurring over 18% of the total repository area. Less than 1% of the repository area is subject to 50 mm/yr or higher percolation rates. For the high-infiltration rates of the glacial-transition climate, the highest areal frequency of percolation fluxes is in the range of 8 to 13 mm/yr (Figure 3.7-12c), 25% of the total repository area, and less than 3% of the repository area is subject to 60 mm/yr or higher percolation flux.

The areal frequency distributions of percolation fluxes at the potential repository are approximately log normal (see Figure 3.7-12) for the three base-case infiltration scenarios. The percolation flux with highest areal frequencies is lower than the average values of corresponding average infiltration rates.

3.7.4.3 Fracture and Matrix Flow Components

This subsection presents a modeling analysis of steady-state fracture and matrix flow components using the Flow Model. The objective of this section is to examine the effect of various climate scenarios and perched water conceptual models on fracture and matrix flow, especially at the repository level of the TSw unit. Fracture flow is predicted to control percolation where flux exceeds the hydraulic conductivity of the matrix. This is most likely to occur within the densely welded units, such as in the TSw. Fracture flow has important implications for flow into emplacement drifts and therefore may directly impact the long-term performance of the potential repository. In addition, fractures provide preferential fast flow paths from the ground surface to the repository level and from the repository level to the water table. For these reasons, the conceptual model of fracture flow is of major concern for TSPA-SR calculations of radionuclide releases from the potential repository.

Similar to percolation fluxes, fracture and matrix flow components are difficult to measure directly at the site. The partitioning of flow between fractures and matrix must, therefore, be inferred from modeling results. Examples of simulated fracture and matrix flow at the repository horizon are shown in Figure 3.7-13. The terms "fracture flow" and "matrix flow" are defined as mass flux of water through fractures or matrix, respectively. Units are also given in mm/yr per unit area, a commonly used measurement for infiltration and percolation rates. Summation of fracture and matrix flows gives total percolation flux.

Figure 3.7-13a and b shows that fracture flow is predominant, as compared to matrix flow for the same climate scenario at the level of the potential repository. Table 3.7-5 lists the percentage of fracture-matrix flow components at the potential repository horizon and the water table as a percentage of the total flux. These statistics were predicted using the 18 simulation results of nine infiltration maps and two perched water conceptual models. They show that fracture flow is dominant both at the potential repository horizon and at the water table in all the 18 flow fields. Specific predictions are as follows:

- For three present-day climate scenarios, at the potential repository level, fracture flow consists of 84-94% of the total flow; at the water table, it consists of 70-95% of the total flow.

- For two future climate scenarios, the percentage of fracture flow increases relative to the present-day case at both the potential repository (87–96%) and water table level (71–97%).
- Perched water conceptual model #2 predicts consistently lower fracture flow components at the water table (by 10% or more) for all three climate scenarios.

Table 3.7-5. Comparison of the Water Flux through Fractures as a Percentage of the Total Flux at Two Different Horizons (1) at the Potential Repository and (2) at the Water Table, Using the Nine Infiltration Scenarios and Two Perched Water Conceptual Models (Data from CRWMS M&O 2000, U0050, Section 6.6.3)

Climate		Present-Day		Monsoon		Glacial Transition	
Perched Model	Infiltration	Potential Repository (%)	Water Table (%)	Potential Repository (%)	Water Table (%)	Potential Repository (%)	Water Table (%)
#1	Lower	86.6	84.7	90.0	90.1	86.9	87.2
#2	Lower	86.4	69.4	89.9	76.6	86.8	71.4
#1	Mean	83.7	86.7	89.5	90.2	91.4	90.5
#2	Mean	83.7	71.2	89.5	80.9	91.4	83.4
#1	Upper	94.5	95.4	95.6	96.5	96.5	96.9
#2	Upper	94.3	82.1	95.5	83.9	96.4	89.0

In addition, the Flow Model can also predict moisture conditions in fracture and matrix systems, respectively. In terms of moisture contents or liquid saturations of fracture and matrix continua, the modeled results of liquid saturations in matrix matched well with observations in all the units. For fractures, the Flow Model estimates fracture saturation at 1-2% at the potential repository level, which is lower than the previous estimates (Haukwa et al. 1999, pp.236). This is because the new values of van Genuchten's alpha for fractures, calibrated using newly measured in-situ water potentials, are higher than before.

3.7.4.4 Model Validation and Confidence Building

Validating the Flow Model and its submodels and confidence building for these models have been the top priority in the development of the UZ model over the past decade. The comprehensive model calibration and validation studies have been carried out and the main results and conclusions of these model validation efforts are summarized as follows.

Previous Model Validation Efforts- As a critical step in developing the 3-D UZ Flow Model, borehole-measured saturation, water potential and temperature data were compared with the model predictions (Wu et al. 1999a, pp. 199–206). This has been part of the important iterative processes of model calibration and verification to increase confidence in model predictions of the site condition. Liquid saturation data taken from five boreholes UZ-14, UZ#16, SD-7, SD-9 and SD-12 (Figure 3.7-3) were used to calibrate the 3-D simulation results. The modeling results

indicated that the UZ Flow Model could generally reproduce the moisture condition in the UZ at Yucca Mountain.

Temperature and heat flow calibrations with the Flow Model have also been carried out, in which the 3-D simulation results were compared with temperature profiles measured from 25 boreholes within and near the potential repository area (Wu et al 1999a, pp. 203–206). The model results were found to match temperature data from the 25 boreholes and therefore the geothermal conditions were incorporated in the model.

Another important step of model calibration is to match perched water occurrence at Yucca Mountain. Perched water data observed from boreholes UZ-14, NRG-7a, SD-7, SD-9, SD-12 and G-2 were compared with the UZ model predictions (Wu et al. 1999b, pp. 168–174). It has been concluded that the simulation results were generally in good agreement with water perching locations at these boreholes and the pumping tests at boreholes UZ-14 and G-2 (Wu et al. 1999b, pp. 178–180).

In addition, calibrations using pneumatic and geochemical data have been performed, showing that the UZ model provides a good representation of gas flow and geochemical conditions at Yucca Mountain. The results have been documented (Ahlers et al. 1999, pp. 54–64; Sonnenthal and Bodvarsson 1999, pp. 125–150).

Current, Continual Model Validation Results—During its continual development, as discussed in this section and documented in CRWMS M&O (2000, U0050, Sections 6 and 6.8.1), the Flow Model has been further calibrated and validated using all available, updated observation data. These updated model validation studies have further confirmed and enhanced the capability of the Flow Model.

The first example of the current model validation efforts is based on the water infiltration test at the ESF Alcove 1 (CRWMS M&O 2000, U0050, Section 6.8.1). The test was conducted by applying water at the ground surface directly above Alcove 1 and measuring the amount of water flowing into the alcove with time. The experimental observations are directly related to the flow and transport processes in the unsaturated fractured rocks, and have been used for evaluating the continuum approaches used in the Flow and Transport Model. Comparisons between observed seepage data and the simulation results show fair agreement and indicate that the continuum approach, as used in the Flow Model, is valid for capturing the complex flow and transport processes in an unsaturated fractured porous medium.

The Flow Model has been further examined against water-potential data collected along the wall of ECRB tunnel (CRWMS M&O 2000, U0050, Section 6.8.2) as well as liquid-saturation and water-potential data from the two new boreholes, WT-26 and SD-6 (CRWMS M&O 2000, U0050, Section 6.8.3). The modeling results were compared to these field observation data to check the accuracy of the modeling predictions. Even though the data available at the ECRB drift and the two boreholes are limited, the comparisons indicate that the Flow Model matches those from *in situ* measurements and accurately predicts the location of perched water occurrence at borehole WT-24.

Furthermore, all the 3-D flow fields, as generated for TSPA calculations using the Flow Model, have been calibrated against the field observed data of matrix liquid saturations, water potentials, and perched water. One example of the calibrations is given in Figure 3.7-14, for comparisons at UZ-14 of the results using the three mean infiltration rates of the three climatic scenarios of the present-day, monsoon, and glacial transition with perched water conceptual model #1. The figure shows a good match between simulated and observed saturation and perched water data at this location from the three simulations. Overall, all the simulation results are generally consistent with the observed saturation, water potential and perched water data.

As part of the model validation efforts, the 3-D pneumatic predictions using the Flow Model have been compared to pneumatic data from six boreholes, namely NRG#5, NRG-6, NRG-7a, SD-7, SD-12, and UZ-7a (CRWMS M&O 2000, U0050, Section 6.8.4). In these comparisons, the first 30 days of each data record are used for the inversion as documented in the AMR, *Calibrated Properties Model* (CRWMS M&O 2000, U0035, pp. 41 and 62), and the second 30 days are compared to the prediction for validation. Comparisons of the 3-D prediction and the data for borehole UZ-7a are shown in Figure 3.7-15. The figure shows a good match between the prediction and the data. This validates the base-case infiltration-scenario calibrated properties for use in gas-flow simulations.

Finally, geochemical modeling of Cl and calcite deposition has been used to build some constraints on hydrological parameters such as infiltration/percolation flux. These geochemical studies provide additional evidence for validation of flow and transport model (CRWMS M&O 2000, U0050, Sections 6.4 and 6.5).

In all these model calibration studies and validation efforts, it has been shown that the results of the Flow Model can match different types of data, such as water potentials, liquid saturation, seepage rate, breakthrough and *in situ* concentrations, and pneumatic pressures, as observed for the mountain. These modeling investigations and results have provided sufficient confidence in the Flow Model for its accuracy and reliability for its intended use in describing and predicting flow and transport processes in the UZ system of Yucca Mountain.

3.7.4.5 Bounds on Percolation and Uncertainties/Limitations

Upper-Bound of Net Infiltration Rate—Bounds or upper limits of percolation fluxes or infiltration rates at the site can be estimated based on the studies of the AMR *UZ Flow Models and Submodels* (CRWMS M&O 2000, U0050, Section 6.2, 6.4, 6.5 and 6.6). The analysis of chloride data in the AMR indicates that the average percolation rate is about 4.6 mm/yr over the UZ model domain, which is further confirmed by the temperature analysis by matching steady-state temperature profiles in the UZ. Analysis of calcite deposition also gives us some estimates on infiltration near WT-24, which are 2 to 20 mm/yr.

In the 3-D model calibrations using the perched water data, the average infiltration rate should be 1 mm/yr or higher. Otherwise the model cannot match perched water occurrence, e.g., as observed in borehole UZ-14. Therefore, the upper limit of the average infiltration rate at Yucca Mountain is no more than three times the average base-case infiltration rate or less than 15

mm/yr. This needs to be further investigated and verified, using the updated field data and understanding of the mountain system.

Uncertainties/Limitations—The Flow Model and its submodels are comprehensive and complex. These models have played an important role in characterizing flow and transport processes at Yucca Mountain. Limitations and uncertainties associated with these models should be recognized for their successful applications. The accuracy and reliability of the Flow Model predictions are critically dependent on the accuracy of estimated model properties, other types of input data, and hydrogeological conceptual models. These models are limited mainly by the current characterization of the mountain system, including the geological and conceptual models, the volume-average modeling approach, steady-state moisture flow, and available field and laboratory data.

The past site investigations have shown that large variability exists in the flow and transport parameters over the spatial and temporal scales of the mountain. Even though considerable progress has been made in this area, the major remaining uncertainties in model parameters are: (1) accuracy in estimated current, past, and future net-infiltration rates over the mountain; (2) quantitative descriptions of welded and nonwelded tuff heterogeneity, their flow properties, and detailed spatial distributions within the mountain, especially below the potential repository; (3) sufficiency of field studies, especially for fracture properties in zeolitic units and faults; (4) alternative conceptual models of major-fault water-flow transmission; (5) evidence of lateral diversion due to zeolites in the CHn units; and (6) transport properties (e.g., adsorption or K_d coefficients in different rock types, matrix molecular diffusion coefficients in different units for different radionuclides, dispersivities in fracture and matrix systems). All of these uncertainties have been addressed in this report.

3.7.4.6 Corroborative Evidence and Natural Analog

The variably saturated fractured basalt at Box Canyon, Idaho, was used as a natural analog to Yucca Mountain to examine the applicability of conceptual and numerical modeling methodologies developed to represent preferential flow paths in variably saturated, fractured rock (CRWMS M&O 2000, U0135, Section 6.5.1). A dual-permeability model was constructed using TOUGH2 V1.4 representing both the matrix and fracture continua of the upper basalt flow at the Box Canyon site. A consistent set of hydrogeological parameters was obtained by calibrating the model to predict infiltration-front arrival times in the fracture continuum. These times were inferred from bromide samples collected from fracture/borehole intersections that were observed to conduct the infiltrating water. Parameters included the permeability of the fracture and matrix continua, the interfacial area between the fracture and matrix continua, and the porosity of the fracture continuum. The interfacial area was decreased by a factor of 0.01 during calibration to reduce imbibition of water from the fracture continuum into the matrix continuum during the infiltration pulses. Furthermore, the porosity of the fracture continuum, as calculated using the fracture aperture inferred from pneumatic-test permeabilities, was increased by a factor of 50. The fracture-continuum porosity was a highly sensitive parameter controlling the arrival times of the simulated infiltration fronts. Although the dual-permeability approach is also applied to explain groundwater flow at Yucca Mountain, the vastly different scales of Box Canyon and Yucca Mountain mean that upscaling is an issue when comparing parameter values.

3.7.4.7 Alternative Conceptual Models

The Flow Model, as summarized in this section, represents our current understanding of the UZ flow system of Yucca Mountain. The simulation results and the sensitivity analyses conducted in the Flow Model are based primarily on the conceptual hydrogeological model, the calibrated rock properties, the dual-permeability approach for fracture-matrix interactions, and the infiltration maps for present-day and two future climates. Many alternative conceptual models have been investigated and tested for describing the UZ flow processes at Yucca Mountain. Other alternative conceptual models are also possible and make the current model more uncertain, especially with regard to their impact on radionuclide transport from the repository to the water table. These alternative conceptual models include:

1. Different conceptualization and numerical representation of faults
2. Different numerical approaches for handling fracture and matrix interactions in different hydrogeological units or in faults
3. Hybrid grid conceptual numerical models of a combination of dual-permeability, MINC, single- or double-porosity, ECM, and explicit-fracture models to represent the UZ system
4. Transient infiltration rate model
5. Alternative models of lateral flow diversion and perched water beneath the repository.

3.7.5 UZ Flow Abstractions for TSPA-SR

The previous sections have described the development, use, and results of the conceptual and process models for UZ flow. The Flow Model forms the basis for the model that is used (or “abstracted”) for TSPA-SR. This section summarizes the products of the UZ flow models and the abstractions that are carried forward to the TSPA-SR calculations.

3.7.5.1 Abstraction of Flow Fields

A total of 18 flow fields were originally defined for the base-case TSPA-SR calculations. These consisted of three infiltration cases (lower, mean, and upper) within each of the three climate states (present-day, monsoon, and glacial transition), along with two different perched water conceptual models. As discussed in Section 3.7.5.3, only one perched water model was selected for conservatism, so nine flow fields are carried forward to TSPA-SR. Each of the nine flow fields are used directly for TSPA-SR calculations, but the files are postprocessed so that the code used for transport simulations in TSPA-SR (FEHM V2.1, STN: 10086-2.10-00) can interpret the files (CRWMS M&O 2000, U0125; Section 6.1). This method maintains consistency with the three-dimensional UZ site-scale flow fields that have been calibrated using TOUGH2 V1.4.

As discussed in Section 3.5, the three infiltration cases are weighted based on Monte Carlo analyses of the uncertainty in the infiltration input parameters. The flow fields that correspond to

each of the three infiltration cases are assigned the same weightings (i.e., 0.17, 0.48, and 0.35 for the lower, mean, and upper infiltration cases, respectively). These weightings are the same for each climate state, and the infiltration cases are consistent among all three climates. For example, if the low-infiltration case were selected for a present-day climate realization, the low-infiltration case would also be used for the monsoon and glacial-transition climates for that realization.

3.7.5.2 Abstraction of Water-Table Rise

The two future climate states (monsoon and glacial transition) are expected to be wetter than the present-day climate, and, as a result, the water table is expected to rise. However, uncertainty exists regarding the amount of water-table rise for each climate state. Therefore, as discussed in CRWMS M&O (2000, U0125, Section 6.2), a conservative water-table rise of 120 m is used for all flow fields using future climate states. All elements (nodes) located at or beneath an elevation of 850 m are modified by changing the liquid saturation to a value of one and applying a large mass-flow "sink," which effectively removes particles from the UZ in FEHM V2.1 (for use as a source term for the SZ model).

The impact of the water-table rise on groundwater flow and transport beneath the potential repository was evaluated in CRWMS M&O (2000, U0160, Section 6.2.4). Results of that analysis showed that the majority of particle paths between ~730 m and ~850 m were primarily vertical, and the higher water-table elevation decreased the median breakthrough time for a sorbing tracker (Np) by nearly a thousand years for the mean-infiltration case using perched water model #1. At ten thousand years, the cumulative breakthrough of particles increases from ~70% to ~80%.

3.7.5.3 Abstraction of Perched Water Models

Section 3.7.3.3 introduced two perched water models: (1) a permeability-barrier model with reduced permeability in both fracture and matrix elements in the vicinity of the perched water and (2) an unfractured zeolite model that eliminated fractures in all zeolitic units. Figure 3.7-17 shows that the breakthrough curves resulting from the two perched-water models are similar. As a result, only one of the two models is carried forward to TSPA-SR, and a PA analysis was performed to determine the most conservative model.

In the analysis performed by PA (CRWMS M&O 2000, U0160 Sections 6.2.1 and 6.2.2), FEHM V2.1 was used to assess the particle breakthrough locations and flow patterns resulting from the two perched water models. Figure 3.7-16 shows the particle-breakthrough locations at the water table for an advective tracer (no diffusion, sorption, or dispersion) released uniformly as a pulse in the outlined repository region using the mean infiltration case, glacial-transition climate, and both perched water models. Both perched-water models show a significant amount of lateral diversion of particles in the northern part of the repository, but perched water model #2 shows more diversion in the southern portion. Many of the diverted particles are concentrated in faults, which act as a conduit to the water table.

Figure 3.7-17 shows the breakthrough curve for a nonsorbing tracer (Tc) released uniformly as a pulse in the repository region using the mean-infiltration case, glacial-transition climate, and both perched-water models (CRWMS M&O 2000, U0160, Section 6.2.2). Results of the two perched water models are similar, although perched water model #1 yields slightly more conservative results, especially for early breakthrough times (via fracture transport). Perched water model #1 also yielded slightly more conservative results for the other flow fields as well. Therefore, only perched water model #1 is used in TSPA-SR.

The difference in the calculated groundwater flow patterns using the PA model may be a consequence of the shorter travel paths in the southern portion of the repository, where more particles experience vertical flow rather than lateral diversion as in perched water model #2. As a result, particles may be experiencing less opportunity for matrix diffusion and subsequent matrix sorption in those vertical pathways. Although significant matrix flow can occur in the Calico Hills vitric unit (Section 3.7.3.3), it appears that at least some of the flow may still occur in the fractures, especially at higher infiltration rates during future climates, which results in faster and more direct travel paths in perched water model #1.

3.7.5.4 Abstraction of Groundwater Flow Patterns

The arrival at the water table of a nonsorbing tracer (Tc) released uniformly in the repository region is simulated using FEHM V2.1 to gain insight into the range of possible groundwater flow patterns that can result based on the different possible infiltration cases for the present-day climate. Breakthrough curves for future climates are also presented in CRWMS M&O (2000, U0160, Section 6.2.6), but they are not presented here.

Figure 3.7-18 shows the breakthrough curves for Tc using the present-day climate and three infiltration cases. The median arrivals at the water table are approximately 400 years, 2,000 years, and 600,000 years for the upper, mean, and lower infiltration cases, respectively. As expected, the higher infiltration rates yield shorter breakthrough times relative to lower infiltration rates. As a result, the range of median breakthrough times among the three different infiltration cases is large (nearly 600,000 years).

3.7.6 Summary and Conclusions

The Flow Model and its submodels are developed to simulate past, present, and future hydrogeologic, geothermal and geochemical conditions at the UZ of Yucca Mountain for supporting various TSPA activities, including the current TSPA-SR calculations. This section has presented the Flow Model and its submodels in terms of the methodology and key model results, summarized as follows (as well as in Figure 3.7-19).

Model Calibration and Validation—Model calibration is part of the important iterative processes of the UZ model development to build and enhance the confidence in model predictions of the site condition. The Flow Model has been calibrated using the available data observed and measured from the site, including field-measured saturation, water potential and perched water data, temperature profiles, and geochemical data. These model-calibration efforts conclude that the Flow Model can accurately reproduce moisture conditions in the UZ of Yucca

Mountain in terms of liquid saturations, water potentials, and perched water occurrence, as well as temperature conditions.

Role of the PTn Unit—The 3-D PTn submodel (Section 3.7.3.1) has provided some important insights into the role played by the PTn unit to alter the flow pattern of the incoming moisture flux after the flux has traversed through the welded TCw unit and encounters the predominantly nonwelded PTn unit. The PTn submodel results indicate that (1) percolation flux at the middle of the PTn is predominantly matrix flow, comprising nearly 90% of the total flow; (2) the model predicted that lateral flow diversion by the PTn is insignificant over the entire UZ model domain. However, certain east-bound lateral flow (up to 100 m) is predicted in the areas above the potential repository from the mountain crest; and some flow is predicted to be diverted into nearby faults when crossing the PTn unit.

Effects of Major Faults—Faults serve as major focusing conduits for and as a capillary barrier to the downward unsaturated liquid flow in the UZ system (Section 3.7.3.2). Lateral diversion of water into faults occurs mainly in the CHn and PTn units. Percentage of fault flow versus total percolation fluxes increases as mean infiltration rates increases. Under the present-day, mean infiltration scenario, the Flow Model predicts that fault flow will increase from 4% at the ground surface to 15% at the repository level and to 35% at the water table.

CHn and Perched Water Occurrence—The CHn hydrological unit plays a critical role in controlling groundwater flow patterns and radionuclide transport pathways from the potential repository horizon to the saturated zone (Section 3.7.3.3). The presence of perched water zones implies that vertical percolation flux locally exceeds the saturated hydraulic conductivity of the perching layer. Thus, the Flow Model predicts that water is significantly diverted laterally, when crossing the CHn to a fault zone, fracture network, or relatively high-permeability vitric zone that focuses flow to the water table. As indicated by modeling results, the flow patterns, or pathways, across the CHn, are controlled mainly by fracture and matrix parameters and their distributions in the CHn unit, and by the presence of high-permeability flow channels, such as faults. All modeling scenarios indicate significant lateral flow diversion at the CHn resulting from the presence of perched water or thick low-permeability zeolitic layers. In addition, the model indicates that faults act as major flow paths through the CHn in the northern part of the model domain under the current conceptualization. In the southern part of the model domain, flow through the vitric zone of the CHn is dominated by matrix flow.

Percolation Fluxes at the Potential Repository Horizon—Repository percolation fluxes (Section 3.7.4.1) are predicted largely as a reflection of surface infiltration rates, with areas of higher surface infiltration in the northern portion of the model domain and along the Yucca Mountain crest and with other areas having correspondingly lower fluxes. These percolation fluxes and their distributions indicate little large-scale lateral flow or diversion by the PTn unit and flow focusing into faults in the vicinity of the potential repository.

The statistics of the averaged percolation fluxes within the potential repository footprint indicate that the total percolation fluxes within the repository are very similar to the average surface infiltration rates over the model domain, except for the glacial-transition scenario, which predicts higher average repository fluxes than the average over the entire model domain.

Percolation Flux Frequency Distribution at the Potential Repository Level—The areal frequency distributions of simulated percolation fluxes at the potential repository horizon are approximately log normal, and the fluxes with the highest areal frequency are lower than the average values of infiltration rates (Section 3.7.4.2). For the present-day, mean infiltration rate of 4.6 mm/yr, the highest flux frequencies over 50% of the repository area have fluxes within the range of 1.0 to 4.0 mm/yr.

Fracture-Matrix Flow Components—The model shows that fracture flow is dominant in the welded tuff, both at the potential repository horizon and at the water table in all the UZ flow fields generated for TSPA-SR calculations (Section 3.7.4.3). For three present-day infiltration scenarios, fracture flow consists of 85 to 95% of the simulated fracture-matrix flow components at the potential repository level. At the water table fracture flow makes up 70 to 95% of the total flow. For two future climate scenarios, a higher percentage of fracture flow occurs, at both the potential repository (87–96%) and water table level (71–97%), than for the case with of the present-day infiltration scenario.

UZ Flow Abstractions for TSPA-SR—Nine flow fields are being used in the base-case TSPA-SR calculations (Section 3.7.5). These consist of the three infiltration cases (low, mean, and high) in each of the three climate states (present-day, monsoon, and glacial-transition), using a permeability-barrier perched water model (model #1, Section 3.7.3.3). (A second perched-water model was not used because it produced similar results.) In addition, the model selected produced slightly more conservative results in terms of calculated breakthrough times using the TSPA transport model. For the two future climate states, a conservative water-table rise of 120 m is implemented (water-table elevation = 850 m). Results showed that the increased water table decreases the duration of groundwater flow and transport beneath the repository, but it is not expected to be significant for TSPA calculations. Finally, an evaluation of the breakthrough times of a nonsorbing tracer revealed that the median present-day groundwater breakthrough time ranges from 400 years to 600,000 years, depending on the infiltration scenario.

3.8 AMBIENT GEOCHEMISTRY ANALYSIS AND MODELS

3.8.1 Introduction

This section gives an overview of the modeling and analysis of the geochemistry of the Yucca Mountain unsaturated-zone (UZ) as it pertains to flow and transport modeling. The conceptual models and analyses are here grouped together as the Ambient Geochemistry Model (AGM). The major emphasis of this work has been to quantitatively describe geochemical processes relevant to the task of refining bounds on infiltration rates and percolation fluxes to the potential repository. The data used for validation and calibration in this overview are pore-water chloride concentrations, $^{36}\text{Cl}/\text{Cl}$ isotopic ratios in pore waters (or extracted salts), and calcite abundances. The measured geochemical data described in this section are considered to be the best understood and characterized within a much larger and more diverse body of information. Detailed descriptions and analysis of geochemical data in the UZ and other relevant data (e.g., precipitation and runoff water chemistry) are given in the Analysis/Model Report (AMR) *Analysis of Geochemical Data for the Unsaturated Zone* (CRWMS M&O 2000, U0085). More complete discussion of the modeling results is presented in the AMR *UZ Flow Models and Submodels* (CRWMS M&O 2000, U0050, Sections 6.4 and 6.5).

Variations in water chemistry in the UZ can be quite large because of processes such as evapotranspiration, water-rock interaction, and climatic changes. Secondary mineral distributions and assemblages are also useful for testing hydrological models of the UZ because of their sensitivity to infiltration rate, percolation flux, and fracture-matrix interaction. The following discussion in the introduction presents the conceptual models for the analysis and modeling of Cl , $^{36}\text{Cl}/\text{Cl}$, and calcite. Sections 3.8.2 and 3.8.3 present discussion of modeling results and data for Cl and $^{36}\text{Cl}/\text{Cl}$, and Section 3.8.4 is focused on modeling of calcite abundances. Following these subsections, several aspects related to model uncertainties, limitations, validation, and corroborating evidence are discussed.

The sensitivity of natural conservative tracers such as chloride (Cl) to infiltration rate is well-known, i.e., the "chloride mass-balance method" (Phillips 1994, pp. 15–24). For such constituents, the flux is related to the precipitation rate and additions from other sources such as windblown dust (Plummer et al. 1997, pp. 538–541). The extent of evapotranspiration in the shallow soil zone then controls the concentration in infiltrating water. In arid environments, with significant topographic and soil cover thickness variations, the infiltration rate can vary by orders of magnitude over short distances (USGS 2000, U0010). Thus, it is expected that spatial distributions of a conservative tracer in the subsurface could also vary over a similar range. In contrast to using a method such as chloride mass balance and making assumptions about the absence of diffusion and lateral flow, limiting the system to one-dimensional piston-flow, it is preferable to incorporate such tracers directly into the calibrated flow model. One uncertainty concerns the actual scale of variability of net infiltration, because this determines the scale of concentration variations.

A conceptual model illustrating the variations in Cl and $^{36}\text{Cl}/\text{Cl}$ in the subsurface and the processes thought to control their distributions is shown in Figure 3.8-1. This diagram also relates the major issues to the available data that can be used to address these issues. This schematic diagram is based on geochemical data described in CRWMS M&O (2000, U0085).

Hydrogenic calcite deposits in fractures and cavities at Yucca Mountain have been studied to estimate past percolation fluxes, flow pathways, and hydrological processes in the (CRWMS M&O 2000, U0085, Section 6.10). These deposits can provide an important understanding of the current and future UZ percolation, because direct measurements of infiltration fluxes over thousands of years are not possible. Using reaction-transport modeling, several factors were investigated that influenced calcite deposition (CRWMS M&O 2000, U0050, Section 6.5). Calcite deposition in the unsaturated fractured rock occurs through a complex interplay of fluid flow, chemical transport, and reaction processes. The following major processes were considered in the simulations presented in Section 3.8.4: (1) fracture-matrix interaction (dual permeability) for water flow and chemical constituents, (2) gaseous CO₂ diffusive transport and partitioning in liquid and gas phases, (3) effect of temperature (geothermal gradient) on geochemical reactions, and (4) kinetics of fluid-rock chemical interaction.

The flow of information between various models and data sources and the Ambient Geochemistry Model is presented in Figure 3.8-2. The Ambient Geochemistry Model takes its inputs from the UZ Flow Model (FM), the Calibrated Properties Model (CPM), and numerous sources of geochemical data (Geochemical Data). The results of geochemical modeling are also used for testing conceptual models of flow and transport and calibration of percolation fluxes and therefore feed back into the UZ FM. This information is then abstracted for use in Total System Performance Assessment (TSPA).

Other geochemical data, such as Sr, isotopic ratios of Sr and U, and stable isotopes of carbon, oxygen, and hydrogen, ¹⁴C, and tritium, are also important for evaluation of UZ processes. However, the more limited number of samples, analytical uncertainties (in particular, tritium), and the more complex geochemical behavior (carbon) limit their direct use in a transport model at this time. Once the reaction-transport models are shown to capture the important mineralogical and geochemical aspects of the UZ, then the modeling of the Sr, U, and C isotopic systems will have a much stronger basis, because they are controlled by the nature and magnitude of water-rock reactions.

3.8.2 Chloride and ³⁶Cl/Cl Data and Analysis

This subsection gives an overview of Cl data from pore waters in the UZ and the relations employed to model the concentration variations. The observed distribution of Cl is of moderately high values at the base of the TCw (> 100 mg/L) and near the top of the PTn, with a range of values in the bulk of the PTn and TSw units of approximately 10 to 120 mg/L (CRWMS M&O 2000, U0085, Table 4). Chloride concentrations of several thousand mg/L have been reported in the alluvial pore waters; the highest value found in pore waters from rocks in the UZ was 245 mg/L (CRWMS M&O 2000, U0085, Table 4). Chloride concentrations in the perched water bodies average around 7 mg/L (Sonnenthal and Bodvarsson 1999, p. 142) and reach values as low as 4 mg/L in borehole SD-7 (CRWMS M&O 2000, U0085, Table 7). Although some pore water in the TSw from the ECRB (Enhanced Characterization of Repository Block) have Cl concentrations of around 10 mg/L, most are in the 15 to 30 mg/L range, which are distinctly higher than that in the perched water (CRWMS M&O 2000, U0085, Table 5). There are differing interpretations to explain the difference between Cl concentrations in perched and pore waters. One explanation is that the perched water was derived from fracture water that is more dilute than that traveling through the matrix. Another explanation is that the perched water was

derived from areas of higher infiltration (and lower Cl), which are found generally to the north of the potential repository area. A third explanation is that the perched water only forms during relatively short periods (thousands of years) of high infiltration associated with wetter glacial cycles. These hypotheses for the origin are not mutually exclusive, though. A fourth hypothesis (p.16 of this PMR) suggests that the perched water in the north is actually SZ water. However, the chemistry of perched water in UZ-14 and WT-24 (northern region) is unlike SZ water because it does not show the effect of cation exchange with zeolites (Sonnenthal and Bodvarsson 1999, p. 119).

The model used for the simulation of Cl considers that its source is the precipitation reaching the surface. The Cl concentration in precipitation is taken as 0.62 mg/L (Sonnenthal and Bodvarsson 1999, p. 113) and is assumed to be spatially and temporally constant. The model must also consider runoff and runon because these processes can result in large changes in the local chloride flux. Although runoff may carry some Cl from the surface, the amounts are likely to be variable and difficult to quantify. Measurements of surface runoff have typically exhibited Cl concentrations of a few mg/L (CRWMS M&O 2000, U0085, Section 6.4), not much higher than the estimated effective concentration in precipitation. Therefore, it is assumed that runoff and runon are given the same Cl concentration as precipitation. The chloride flux can then be expressed as:

$$\text{Cl Flux} = \text{Concentration Cl (in precipitation)} \times (\text{Precipitation Flux} - \text{Runoff Flux} + \text{Runon Flux})$$

The model boundary condition is therefore the chloride flux and is not derived from measurements of chloride in pore waters from Yucca Mountain. Therefore, this boundary condition is independent of the measured pore water Cl concentrations to which the model simulations are compared.

Pore-water chloride, $^{36}\text{Cl}/\text{Cl}$, and sulfate concentrations were analyzed using 3-D transport simulations and analytical methods. Water infiltration rate calibrations were performed by calculating infiltration rates with the measured pore-water Cl concentrations. As a result, modeled Cl and $^{36}\text{Cl}/\text{Cl}$ concentrations compared more favorably with measured concentrations using the calibrated infiltration rates. An analytical method was applied to the transient transport analysis for Cl and $^{36}\text{Cl}/\text{Cl}$. This method, verified by the 3-D simulations under the same flow and transport conditions, was able to capture major Cl and background $^{36}\text{Cl}/\text{Cl}$ trends under conditions of transient Cl input (CRWMS M&O 2000, U0050, Section 6.4).

A base-case simulation was conducted using the present-day (modern), mean infiltration rate to compare the base-case model with observed Cl data. Chloride concentrations from the steady-state transport simulation were compared with measured pore-water Cl concentration data (CRWMS 2000, U0085, Section 6.5). Simulated and measured concentrations along the stations in the ESF and ECRB are shown in Figure 3.8-3; see also Figure 2.1-4 for locations. In comparison to the measured Cl concentrations, the simulated concentrations are higher in the North (0 to 2,000 m) and South (6,400 m to 8,000 m) ramps, and in the northeast side of the ECRB (left side of the figure); and are lower at the southwest end of the ECRB. At the entrance of the ECRB, higher simulated Cl concentrations correspond to very low infiltration rates, whereas near the western end of the ECRB, higher infiltration leads to lower simulated values of Cl concentrations. The results indicate that measured Cl concentrations show a smaller range

than would be predicted by the modern infiltration rates under steady-state conditions. However, because many measured Cl concentrations are fit closely by the model results, it appears that the mean infiltration rate is approximately correct.

Differences between measured and modeled Cl concentration in the high and low infiltration regions suggest that the time-averaged infiltration rates may be more uniform. Therefore, applying the simple chloride mass-balance approach, using the measured pore-water Cl concentration data, we developed a modified water percolation flux map, as shown in Figure 3.8-4. The domain was divided into nine regions based on measured Cl concentrations, and by inspection of the modern infiltration map. In those regions where pore-water data were unavailable (Regions I, II and VIII), the rate was approximated using an average value of the present-day, mean infiltration in that area of the map. This was done very coarsely, only to capture the mean percolation flux for a large area. The percolation fluxes obtained from this analysis are then assumed to be the infiltration rates. Note that this approach is in part an alternative interpretation of the distribution of percolation fluxes to that of USGS (2000, U0010). Because results from that AMR were used to guide the analysis, it cannot be considered completely independent. These percolation fluxes may represent more appropriate time-averaged values. The infiltration rates estimated by chloride mass balance are actually very close to the mean infiltration rates obtained by averaging the rates over the same area (CRWMS M&O 2000, U0050). Cl concentrations modeled using this distribution of infiltration rates are shown in Figure 3.8-3, compared to the measured concentrations and the simulated concentrations using the base-case infiltration map.

The distribution of Cl concentrations in the ESF and the ECRB are closer to the mean of the measured data with the modified percolation flux map, as would be expected. If a smoother distribution of infiltration rates is qualitatively correct, then the modified percolation fluxes would have a positive impact on performance because of the lower maximum percolation fluxes near the crest of Yucca Mountain.

To more efficiently assess the effect of the change in Cl and background $^{36}\text{Cl}/\text{Cl}$ due to climate changes, a 1-D analytical solution was derived that approximates transport to the potential repository horizon. $^{36}\text{Cl}/\text{Cl}$ ratios can be used as an approximate indicator of age if the samples can be shown to have had no bomb pulse ^{36}Cl additions. The $^{36}\text{Cl}/\text{Cl}$ ratio during the late Pleistocene (10-20 ka) was about 50 to 100% higher than present-day (pre-bomb) ratio of about 500×10^{-15} . This latter modern ratio has been approximately constant for the past 10,000 years. Correlation of higher than modern $^{36}\text{Cl}/\text{Cl}$ ratios with early Holocene ages determined by ^{14}C and a lack of bomb-pulse tritium is good evidence for the older ages of the perched waters. Chloride and ^{36}Cl concentrations at ESF and ECRB stations were calculated using a 1-D analytical solution to each column of the 3-D calibration grid over the model domain. An assumed glacial maximum infiltration rate, corresponding Cl and ^{36}Cl fluxes, and zero initial Cl and ^{36}Cl concentrations were first used to estimate a glacial steady-state distribution of Cl and ^{36}Cl concentrations. Chloride concentrations and $^{36}\text{Cl}/\text{Cl}$ ratios at different times after changing to a modern climate were then computed using the calibrated present-day infiltration rates and modern Cl and ^{36}Cl fluxes, with the glacial steady-state Cl and ^{36}Cl results as initial concentrations. Results of Cl simulations, including climate changes, are presented in CRWMS M&O (2000, U0050, Section 6.4), and do not change the overall conclusions presented in the

preceding paragraph. Analytical results of $^{36}\text{Cl}/\text{Cl}$ ratios, with a climate change, are discussed in the following paragraph.

Travel times to the potential repository horizon in the UZ are dependent on the thickness of little-fractured PTn units (leading to longer times), and the infiltration rate that is dependent on climate. Models of $^{36}\text{Cl}/\text{Cl}$ were used to explore these aspects for the UZ Flow and Transport Model. Modeled background $^{36}\text{Cl}/\text{Cl}$ ratios for different simulation times are plotted in Figure 3.8-5 and show that after 18,000 years, the ratios in the South Ramp are much lower than the $^{36}\text{Cl}/\text{Cl}$ ratios in the North Ramp. Measured background $^{36}\text{Cl}/\text{Cl}$ ratios in extracted pore salts/waters (CRWMS M&O 2000, U0085, Table 13) are plotted in Figure 3.8-5 and, while highly variable, show uniformly low values over much of the South Ramp compared to those measured from the North Ramp (see Figure 2.1-3, also). This analysis supports the interpretation that the difference in the ratios is primarily a result of the thinner PTn in the South, which more than counteracts the lower infiltration rate in this area. Therefore, travel times to the potential repository horizon are expected to be greater in the northern region, relative to the southern region. The times for equilibration of pore waters (between Pleistocene and modern) at the potential repository horizon depend on many factors, including the initial $^{36}\text{Cl}/\text{Cl}$ ratio during the Pleistocene, and the rate of transition to a modern $^{36}\text{Cl}/\text{Cl}$ ratio (500×10^{-15}). The $^{36}\text{Cl}/\text{Cl}$ ratio of $1,000 \times 10^{-15}$ is close to a peak value for the last 20,000 years (CRWMS M&O 2000, U0085, Figure 31) and therefore the time of 18,000 years is probably overestimated, compared to what would be obtained with a time-varying $^{36}\text{Cl}/\text{Cl}$ ratio in infiltrating water.

3.8.3 Evidence for Fast Flow Paths and Transport from $^{36}\text{Cl}/\text{Cl}$ and Tritium

The magnitude and spatial distribution of flow through fast pathways is a critical question for the performance of the potential repository. Because flow through fast pathways may be prevalent only under transient infiltration events, that may be spaced in time by years or longer, it is difficult, if not impossible, to quantify the flux associated with fast flow paths through hydrological measurements. Several lines of geochemical evidence can be brought to bear on this question. The most recent fast flow path (within the last 50 years) can be investigated by the study of isotopes produced by the atmospheric testing of nuclear weapons during the 1950s and 1960s. The most studied bomb-pulse isotopes at Yucca Mountain are ^{36}Cl and ^3H (tritium). Data collected from the ESF, ECRB, and surface-based boreholes are described in detail in CRWMS M&O (2000, U0085, Section 6.6).

Locations of fast path flow at the depth of the potential repository in the ESF and ECRB, as evidenced by elevated $^{36}\text{Cl}/\text{Cl}$ and tritium in pore waters, are generally limited to regions in and close to faults (CRWMS M&O 2000, U0085, Section 6.6). In samples collected in the tunnels, no evidence has been found for pervasive fast flow path water not associated with faults or fracture zones. At locations in the tunnels where bomb-pulse ratios of $^{36}\text{Cl}/\text{Cl}$ were found (i.e., ratios greater than $1,250 \times 10^{-15}$), there are also samples with lower ratios, indicating that the effect of fast flow path water has been limited in spatial extent. The latter observation could be interpreted as either a very limited degree of fracture-matrix interaction, resulting in highly confined transport pathways, or very small fluxes such that Cl has not diffused significantly into the matrix or dispersed widely through the fracture system. Locally higher pore-water Cl concentrations, however, could mask a bomb-pulse signature (Sonnenthal and Bodvarsson 1999, p. 150). However, in the ESF tritium values over the cutoff for bomb-pulse values of 25 TU

(tritium units) are only found in the Bow Ridge fault zone (CRWMS M&O 2000, U0085, Table 10). Although waters having tritium below 25TU may have a bomb-pulse component, they have uncertainties that make them suspect. This observation validates the conceptual model of generally slow matrix flow through the PTn where it is undisturbed by faulting.

Tritium values above 25 TU have been found in the TSw in some surface-based boreholes (UZ#16, NRG-7a, UZ-1, WT-24, and SD-6), as reported in CRWMS M&O (2000, U0085, Table 10). Because inversions in tritium abundances with depth were found in samples collected from the surface-based boreholes, it has been suggested that fracture and lateral flow are important for fast flow path transport (CRWMS M&O 2000, U0085, Section 6.6.2.2). In the five boreholes in which perched waters were analyzed for tritium, the maximum tritium abundance was 10 TU found in NRG-7a in 1994 (CRWMS M&O 2000, U0085, Table 9). Because many UZ pore waters have over 100 TU in the PTn and TCw units (CRWMS M&O 2000, U0085, Table 11), the very low tritium abundances in the perched waters suggests that they are unlikely to have a significant component of very recent fast-path water. However, because of the short half-life of tritium (approximately 12 years) and the change in tritium abundances in precipitation to as low as 10 TU by the early 1990s (CRWMS M&O 2000, U0085, Section 6.6.2.2) it is not possible to calculate a maximum proportion of recent fast flow path water (i.e., very recent fast-path water could be lower in tritium). Pore waters in NRG-7a had up to 46.8 TU in the TSw (CRWMS M&O 2000, U0085, Table 11), indicating that the fast flow path waters could have raised the perched water tritium abundances significantly from their pre-bomb values that were most likely less than 1 TU. Because the $^{36}\text{Cl}/\text{Cl}$ ratio in perched water from NRG-7a is approximately 500×10^{-15} and the calculated ^{14}C age is over 3,000 years, it is highly unlikely that there is a significant proportion ($> 10\%$) of recent fast path water in NRG-7a perched water. However, it is also possible that the perched water consists of older fast path water emplaced under much wetter conditions or more intense storm events than has occurred over the past 30 years.

$^{36}\text{Cl}/\text{Cl}$ ratios in perched waters are elevated above modern ratios in several boreholes, but are consistent with calculated ages based on ^{14}C measurements. The highest $^{36}\text{Cl}/\text{Cl}$ ratio in the perched water was found in UZ-1 (999×10^{-15}) and had a tritium value of only 1.0 TU (CRWMS M&O 2000, U0085, Table 9). In fact, tritium abundances in perched water samples collected from UZ-14 over time decreased to 0 TU from a maximum of 3.1 TU, with the $^{36}\text{Cl}/\text{Cl}$ ratios increasing to 690×10^{-15} , which is well above the modern pre-bomb ratio of 500×10^{-15} . In the latter sample the age calculated from ^{14}C was over 10,000 years. If the $^{36}\text{Cl}/\text{Cl}$ ratios in the perched waters were the result of mixing with fast path water, then the relationship between tritium would be opposite to what is observed. In summary, the perched waters could have no more than a small fraction of fast path water from flow in the past 50 years (probably less than a few percent, and certainly less than 10%).

3.8.4 Calcite Simulation Results and Data

The purpose of this study was to investigate the relationship between percolation flux and measured calcite abundances. Other factors that may be important in relating calcite abundance to the percolation flux were also considered, such as the infiltrating water chemistry, partial pressure of carbon dioxide, reactive surface areas of minerals, and the relevant model mineral assemblage. In CRWMS M&O (2000, U0050, Section 6.5), several simulations were performed using a range of infiltration rates, water, and gas chemistry (at the top boundary), and effective

reaction rates. Two sets of initial mineralogical conditions were considered, so that the effect of uncertainties in thermodynamic and kinetic data for more complex minerals, such as zeolites and clay minerals, can be assessed.

Two 1-D columns (representing boreholes NRG-7A and WT-24) were used for analysis of the calcite deposition in the Yucca Mountain UZ. There are no calcite data for NRG-7A, so these runs cannot be compared with measured data. Analyses of total calcite abundances (ppm by mass) in borehole WT-24 were recently reported (CRWMS M&O 2000, U0085, Figure 53) and made possible the refinement of the model parameters to better match the profile. The active fracture model (Liu et al. 1998, pp. 2633–2646) was used to describe gravity-dominated and preferential liquid flow in fractures. Because a constant infiltration and steady-state water flow were considered, percolation through the entire column is equal to net infiltration. Two types of water chemical compositions were used for the top boundary of the hydrochemical transport simulations. The first water in Table 3.8-1 is a calculated, average Topopah Spring tuff water (CRWMS M&O 2000, U0050, Table 6-14). The second water type is a pore water extracted from a core from Alcove 5 in the Tptpmn (CRWMS M&O 2000, N0120/U0110, Table 3.10-1). This pore water has a higher Ca concentration than the average TSw water. The initial water chemical composition used was uniform throughout the column for both the fracture and matrix blocks, and was adopted from the average TSw water (Type 1).

In addition to aqueous species transport and reaction in water, diffusive transport of CO₂ in the gas phase and equilibration with pore water were considered. The CO₂ gas partial pressure used for initial and top boundary conditions is in equilibrium with the corresponding aqueous chemical composition (the bottom row of Table 3.8-1). These CO₂ partial pressures were calculated based on the measured pH and calculated HCO₃ concentration (by charge balance). Water Types 1 and 2 are slightly oversaturated with respect to calcite. The water chemical composition, especially pH, is controlled primarily by the CO₂ partial pressure. Therefore, the boundary water type is also denoted by the characteristic CO₂ partial pressure, meaning that the CO₂ partial pressure is used to indicate the corresponding equilibrated water type as listed in Table 3.8-1.

Table 3.8-1. Aqueous and Gaseous Chemical Concentrations (mg/L) Used for Initial and Boundary Conditions of Hydrochemical Transport Simulations (CRWMS M&O 2000, U0050, Table 6-14)

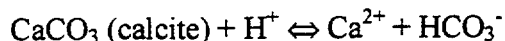
Water type	1	2
Component	Average TSw water	Measured TSw water
Ca ²⁺	27	101
Mg ²⁺	5	17
Na ⁺	91	61.3
K ⁺	4	8
SiO ₂ (aq)	60	70.5
Al ³⁺	9.92×10 ⁻⁷ (5)	9.92×10 ⁻⁷ (1)
HCO ₃ ⁻ (3)	219	200
Cl ⁻	41	117
SO ₄ ²⁻	40	116
F ⁻	0.86	0.86
Fe ³⁺	6.46×10 ⁻⁸ (5)	6.46×10 ⁻⁸ (2)
pH	8.2 (6)	8.32
P _{CO2} (bar) (4)	1.322×10 ⁻³	8.565×10 ⁻³

- NOTES: (1) Calculated by equilibrating with Ca-smectite at 25°C
 (2) Calculated by equilibrating with hematite at 25°C
 (3) Total aqueous carbonate as HCO₃⁻, calculated from charge balance
 (4) Calculated at equilibrium with the solution at 25°C
 (5) Total aqueous Al and Fe are set equal to those of Type 2 water
 (6) Measured

A series of simulations examining the sensitivity of calcite deposition to infiltration (percolation) rate, boundary water and gas chemistry, and reaction rate are described in CRWMS M&O (2000, U0050, Section 6.5). Simulations were carried out for 10 million years based on mineral growth having remained approximately constant over the past eight million years (Ma) and the age of the rocks being over 12 Ma. This record of growth has been indicated by radiocarbon, ²³⁰Th/U, and U-Pb ages (CRWMS M&O 2000, U0085, Section 6.10.3.8).

To compare with measured calcite abundances in WT-24 borehole cuttings and in the ESF, simulated calcite abundances (ppmV) were expressed as the average among the matrix and the fractures (calculated by calcite volume in the matrix and fractures divided by the total matrix and fracture solid volume). Difference in volume and mass abundances are slight for these rocks and would imperceptibly change the plots.

Calcite precipitation generally increased as infiltration rate increased, especially in the TSw unit. An increased infiltration rate results in a slight change in the amount of calcite at the bottom of the PTn unit. Calcite precipitation is sensitive to the boundary water chemical composition and the CO₂ partial pressure. Higher CO₂ partial pressure results in lower pH and calcite dissolution or less calcite precipitation (Type 1 water with a partial pressure of 1.322×10^{-3} bar over Type 2 water with a partial pressure of 8.565×10^{-4} bar). The decrease in pH (increase in H⁺) destabilizes calcite, as in the following reaction:



The Type 1 water with a partial pressure of 1.322×10^{-3} bar may represent the average water chemical composition and was used for most sensitivity simulations.

The calcite distribution is also dependent on reaction rate. Sensitivity studies were performed by modification of the reactive surface area for all of the units by a constant factor (CRWMS M&O 2000, U0050, Section 6.5.4). Close to the land surface in the TCw unit, the higher the reaction rate, the more calcite precipitation there was. For simulations using larger reactive surface areas, the results show less calcite precipitation in the deeper welded TSw unit because of more rapid calcite precipitation at shallower depths, such as in the TCw. Reactive surface areas reduced by one order of magnitude from the initial estimated data yielded calcite abundances closest to those measured in the TSw unit.

The following analysis considers the effect of a different mineralogy on calcite deposition, based on the WT-24 column. A base-case infiltration rate of 5.92 mm/yr, and estimated bounding values of 2 mm/yr and 20 mm/yr at WT-24, respectively, were used in these simulations (CRWMS M&O 2000, U0035, Table 9), for consistency other UZ flow simulations. Two top boundary water chemical compositions, average TSw water and measured TSw water (Types 1 and 2, respectively, in Table 3.8-1) were employed. Changes in calcite volume fraction are presented in Figure 3.8-6, together with measured calcite deposition data in the WT-24 well cuttings (CRWMS M&O 2000, U0085, Section 6.10).

Modeled calcite abundances in the welded TCw unit are closer to the measured data (in terms of curve shape and range of values) with the calcite-silica system and the average TSw water (Type 1) than the abundances obtained with a more complex mineralogy (including aluminosilicates) and the measured TSw water. The simulations using the calcite-silica system also reproduce the calcite deposition in the nonwelded PTn unit more closely, except for the bottom layer. The improved agreement for the PTn unit is achieved by reducing the reactive surface area, which is consistent with the fact that fewer fractures occur in this unit. The simulated abundances at the bottom of the PTn unit are higher than those measured in the WT-24 column, especially the values from the complex-mineralogy simulation. However, bulk rock analyses by X-ray diffraction in the USW G-2 borehole core have high calcite abundances at the base of the PTn, suggesting that high values are possible. Results for the middle nonlithophysal TSw unit and below for both mineralogy conditions generally fall in the wide range of measured calcite data. Between 1200 m and the PTn boundary there is a large discrepancy that cannot be explained.

The simulated results are sensitive to the net infiltration rate (percolation flux). Modeled calcite abundances obtained from the highest net infiltration rate (20 mm/yr) are close to the highest of the measurements. Those from the base-case (5.92 mm/yr) and lower infiltration rate (2 mm/yr) fall in the middle of the TSw measured data range. This may imply that the 20 mm/yr percolation flux is an upper bound for the WT-24 location, whereas the base-case net infiltration rate (5.92 mm/yr) used in the flow model may be close to a mean value. The reactive surface area for calcite, reduced by one order of magnitude from the initial estimate, provides the most favorable condition for calcite formation in the deeper welded TSw unit. Therefore, the simulated values may be slightly overestimated.

Calcite abundances provide constraints on percolation fluxes, but cannot give a definite value or even a narrow range of values. This is because calcite precipitation depends not only on the percolation flux, but also on the water and gas chemistry, reaction rate, geothermal gradient, and mineralogy considered. In addition, the uncertainty could rise from climate and infiltration variations over time, transient water flow condition, and possible lateral water recharge.

Over a range of 2 to 20 mm/yr infiltration rates, the simulated calcite distributions using the simpler mineralogy (most relevant to calcite precipitation) agree reasonably well with the measured data from the WT-24 well cuttings. The amount of calcite precipitation generally increases as infiltration rate increases. The simulated calcite abundances are also sensitive to the model water and gas chemistry, reaction kinetics, and mineralogy. The analysis provides some constraints on hydrological parameters and the percolation flux, and additional evidence for validation of the flow and transport model. However, this analysis cannot give a definite value or a narrow range of values because of the dependence of calcite deposition on the other factors. The main reason for calcite precipitation with depth is its inverse solubility with temperature. However, the partial pressure of CO₂ and Ca concentration in percolating water controls the abundances of calcite and its stability. The reaction rate, and therefore the reactive surface area, controls its distribution with depth.

Measured calcite abundances vary significantly in the ESF as well as in the WT-24 borehole. According to the findings in CRWMS M&O (2000, U0085, Section 6.10.1.1), calcite abundances decrease with depth in the TSw unit in the ESF, which is not the case in WT-24. However, the mean calcite abundance in the ESF is 0.034% (CRWMS M&O 2000, U0085, Section 6.10.1.1), which is close to the lower bound of calcite observed in WT-24 borehole cuttings. Therefore, the ESF data are consistent with the overall rate of deposition on the UZ, as indicated by the WT-24 calcite abundances. The specific trends with depth may be more difficult to compare, because the ESF data are obtained over a large lateral distance that encompasses areas that may have experienced different percolation fluxes.

3.8.5 Uncertainties and Limitations

The use of chloride to estimate infiltration rates or percolation fluxes is directly related to the initial estimate of the effective Cl concentration in precipitation, its spatial variations and changes over time (Ginn and Murphy 1997, pp. 2065–2066). If the effective chloride concentration is twice the estimated value, then the infiltration rate necessary to produce a given subsurface Cl concentration would be twice as high. Studies on the range in chemistry of precipitation are given in CRWMS M&O (2000, U0085, Section 6.3). The spatial and temporal

patterns of precipitation are also uncertain because they have been measured for less than one hundred years, which is short compared to the time period over which the chloride concentrations have developed in the UZ (tens of thousands of years; Sonnenthal and Bodvarsson 1999, p. 107). Therefore, given these uncertainties, the model can only be used to provide ranges in the infiltration rate. The percolation flux at the potential repository horizon is also influenced by lateral flow in the PTn or at unit boundaries, as well as diffusion and dispersion, and thus may not directly reflect the spatial distribution of infiltration.

As has been investigated in CRWMS M&O (2000, U0050, Section 6.5), the amount of calcite precipitated over time is sensitive to the water and gas composition, the reactive surface area, and the thermodynamic and kinetic parameters used in the model. Because calcite abundances are highly variable within a single unit in the WT-24 borehole and in the ESF (CRWMS M&O 2000, U0085, Section 6.10.1.1 and Figure 53), it is only possible to estimate a range of percolation fluxes (~2–20 mm/yr).

3.8.6 Alternative Conceptual Models

There are no clearly defined alternative conceptual models for the evolution of Cl abundances in the UZ. The problems with the model generally reflect the uncertainties and limitations described above. Elevated $^{36}\text{Cl}/\text{Cl}$ values that are below the bomb-pulse cast-off could easily be mixtures of prebomb and postbomb fast path waters. ^{14}C ages of the waters could help discriminate between these models; however, dilution with “dead” carbon from interaction with calcite could make the ages appear older.

An alternative conceptual model for calcite deposition would consider its formation as an episodic rather than as steady-state process. Because of the kinetics of calcite precipitation, an episodic fluid pulse would tend to change the distribution of calcite with depth, possibly resulting in near-surface dissolution and deeper calcite deposition. During more typical smaller infiltration events, more precipitation might take place near the surface and little at depth. This does not necessarily change the underlying conceptual model for calcite precipitation (kinetic rate law), but would change the modeling method and the modification of parameters to match measured abundances.

3.8.7 Corroborating Evidence

The chloride model can be corroborated, in part, by the study of other conservative and also reactive species. Strontium (Sr) was used by Sonnenthal and Bodvarsson (1999, p. 146) similarly to Cl, except for undergoing exchange in deeper zeolitic units. The rough match of Sr in a few PTn samples and in perched waters is corroborating evidence, but much more data are needed to attempt a more quantitative modeling study. Sulfate (SO_4) behaves similarly to Cl; however, calcium sulfate precipitation in soils may cause some shifts in the SO_4/Cl ratio in infiltrating water. Differences in atmospheric contributions over time and space may also affect the initial SO_4/Cl ratio in infiltrating waters (see CRWMS M&O (2000, U0085, Section 6.3) for a detailed discussion on precipitation chemistry).

3.8.8 Analogs

Other areas of similar climate and rock types provide the best analogs to the ambient geochemical system at Yucca Mountain. Analyses of Cl and $^{36}\text{Cl}/\text{Cl}$ in thick alluvium elsewhere in the Nevada Test Site (Tyler et al. 1996, pp. 1481–1499) have been studied in detail and have been interpreted to represent a long climatic history (over 100,000 years). Chloride profiles from the base of the TCw through the PTn at Yucca Mountain and elsewhere in the Nevada Test Site (profiles in thick alluvium) show some similarities (Sonnenthal and Bodvarsson 1999, pp. 115–116).

The rate of stalagmite growth in caves, tunnels and mines around the world have been investigated for the purpose of correlating water supply rate and chemistry to calcite precipitation rate (Baker et al. 1998). Theoretically predicted growth rates (using calcite reaction kinetics) and calculated rates (based on calcite thickness and C-14 ages) compared favorably (Baker et al. 1998, p. 393).

3.8.9 Model Validation

The model for chloride concentrations can be tested on the basis of a prediction done in early 1998 before the excavation of the ECRB (Sonnenthal and Bodvarsson 1999, Figure 14). The model used for the prediction differed little from the current Cl model. The predictive model used earlier estimates of infiltration rates and hydrologic properties but used the same initial Cl concentration in precipitation. It also did not consider runoff and runoff. The main similarities between the models are the governing boundary condition of Cl fluxes at the surface, the scale of the model grids, and the rates of flow and mixing in the subsurface which are controlled by the hydrogeological properties. A comparison of the predicted concentrations and those measured in pore waters (CRWMS M&O 2000, U0085, Section 6.5) is shown in Figure 3.8-7. The measured concentrations generally fall within the range of those predicted for a glacial climate and for the modern climate, except in the western part of the ECRB where the model slightly underestimates the concentrations, and in the eastern part where they are overestimated. Compared to the range of Cl concentrations measured in the UZ (about 4 to 245 mg/L; CRWMS M&O 2000, U0085, Section 6.5), the range observed in the ECRB (about 13 to 38 mg/L, CRWMS M&O 2000, U0085, Section 6.5) is quite narrow. Given that the ECRB shows substantially lower average concentrations than were previously observed in the ESF and in boreholes (Sonnenthal and Bodvarsson, 1999, pp. 107–156; CRWMS M&O 2000, U0085, Section 6.5), the model predictions capture the difference between this area and the other areas where Cl concentrations were measured. Differences in concentrations for fracture and matrix in transient climate change simulations, and in the matrix for the different climate scenarios, illustrates the sensitivity of chloride concentrations to changing boundary conditions. Because sufficiently detailed climate records and spatial variations of precipitation and its chemistry will never be obtainable, the model results can only be used to provide a range of infiltration rates or percolation fluxes. Thus, predictions using estimated glacial maximum precipitation and infiltration rates could have also have been similar conditions during the early Holocene. Given these uncertainties, the model can be considered validated for its intended use.

The calcite model (AMR U0050, 2000) incorporated the important processes in the UZ that are thought to control calcite precipitation. The model is therefore adequate for its intended use.

Validation of the calcite model for a quantitative estimate of percolation flux can only be done once significantly more data are available as a function of depth, such as at WT-24. This is because the reactive surface areas were modified to better match the data. The major uncertainty is the unknown effective reactive surface area for calcite, as well as uncertainties in the input thermodynamic and kinetic data, and the unknown water chemistry as a function of time for the several million years over which the calcite was precipitated. Thus, the parameters used to estimate calcite abundances in WT-24 have been modified somewhat to match these data and are nonunique because of the many parameters that could be modified simultaneously. Another complicating factor is that the development over time of the calcite abundances from WT-24 is unknown. Therefore, the model treats the system as at steady state, whereas calcite precipitation could have formed during many short transient events. However, the trends and absolute abundances of calcite were captured using reasonable modifications to the reactive surface areas, which gives confidence in the conceptual model and the range of values of the parameters used in the analysis.

3.8.10 Summary and Conclusions

Chloride concentrations measured in pore waters from the ESF and the ECRB can be roughly matched using the 3-D UZ FM using the base-case, present-day infiltration rates. However, a better match to the data is achieved by modifying the infiltration rates so that the percolation fluxes are more uniform. This results in lower infiltration rates in those areas over the potential repository footprint that are currently estimated to have significantly higher rates, yet maintaining roughly the same average rate as the Infiltration Model predicts. Differences in background $^{36}\text{Cl}/\text{Cl}$ ratios in the ESF may be explained by the thinner PTn section above the South Ramp compared to the section above the North Ramp, even though infiltration rates are lower in the South Ramp. The higher $^{36}\text{Cl}/\text{Cl}$ ratios in the North Ramp could therefore reflect a larger proportion of late Pleistocene/early Holocene water or it could be a result of mixing of bomb-pulse water and matrix pore water. Although bomb-pulse ratios of $^{36}\text{Cl}/\text{Cl}$, indicating fast flow paths, are found in several locations in the ESF and ECRB, they are confined to the immediate vicinity of faults and other structural discontinuities, strongly suggesting that large areas of the potential repository are unaffected by fast path flow. The lack of bomb-pulse levels of ^{36}Cl and tritium in the perched waters supports this position. The results of the analyses are summarized in Figure 3.8-8.

Calcite abundances and ages in the UZ have been used as a tool for estimating percolation fluxes (CRWMS M&O 2000, U0085, Section 6.10). Modeling studies, incorporating reaction-transport in UZ flow simulations, were used to investigate the relationship of calcite deposition to infiltration rate, water and gas compositions, and reactive surface area (CRWMS M&O 2000, U0050, Section 6.5). With some modification of the reactive surface area, the model results indicated that a range in infiltration rate from about 2 mm/yr to 20 mm/yr could bound the spread in calcite abundances, with approximately 6 mm/yr capturing the approximate average abundances in the TS_w.

INTENTIONALLY LEFT BLANK

3.9 DRIFT SEEPAGE MODELS

3.9.1 Introduction

This section summarizes modeling studies performed to estimate seepage of liquid water into waste emplacement drifts. These seepage-related studies are discussed in detail in three AMRs: (1) the development of a seepage process model and its calibration, described in AMR *Seepage Calibration Model and Seepage Testing Data* (CRWMS M&O 2000, U0080), (2) the application of the model to predict seepage under a variety of conditions, described in AMR *Seepage Model for PA* (CRWMS M&O 2000, U0075), and (3) the seepage abstraction process, described in AMR *Abstraction of Drift Seepage* (CRWMS M&O 2000, U0120).

Potential seepage of water into waste emplacement drifts has been identified by YMP as a principal factor that may affect the overall performance of the potential high-level nuclear-waste repository at Yucca Mountain, Nevada (Section 1.2.2). The number of waste packages contacted by water, the corrosion rate of drip shields and waste packages, the dissolution and mobilization of radioactive contaminants, and their release and migration towards the accessible environment all depend on the rate, the chemical composition, and the spatial and temporal distribution of water seeping into the waste emplacement drifts. Consequently, the design requirements of the engineered barriers (CRWMS M&O, 1998h) are affected by the presence or absence, rate, and distribution of drift seepage.

Seepage is defined here as flow of liquid water into an underground opening such as a niche, alcove, or waste emplacement drift. According to this definition, seepage does not include vapor diffusion into the opening or condensation of water vapor within the drift. *Seepage flux* is defined as the rate of seepage per unit area. *Seepage percentage* is defined as the ratio of seepage flux divided by percolation flux. In the context of liquid-release tests, seepage percentage is the ratio of the amount of water that seeped into the niche divided by the total amount of water released. *Seepage threshold* is defined as a critical percolation flux below which no seepage occurs. *Seepage fraction* is defined as the fraction of waste packages affected by seepage. This is equivalent to the number of 5 m drift sections that exhibit a nonzero seepage percentage.

Estimating seepage into underground openings excavated from an unsaturated fractured formation requires process understanding on a wide range of scales, from the mountain-scale distribution of percolation flux to the intermediate-scale channeling or dispersion of flow in an unsaturated fracture network, to the small-scale capillary-barrier effect, to the micro-scale phenomena within fractures and specifically at the drift wall. Moreover, the thermodynamic environment in the drift (temperature, relative humidity, ventilation regime, etc.) must be considered.

The schematic in Figure 3.9-1 illustrates some of the seepage-relevant phenomena and processes. The factors affecting drift seepage can be described as follows:

1. *Capillary-Barrier Effect, Flow Diversion:* Under unsaturated conditions, the rate of water dripping into the opening is expected to be less than the downward percolation rate because the cavity acts as a capillary barrier (Philip et al. 1989, pp. 16–28). (A capillary barrier is sometimes also referred to as a Richards barrier

or cavity effect.) If percolating water encounters the cavity, the relatively strong capillary forces in the formation retain the water, preventing it from seeping into the drift. Water accumulates at the drift ceiling, where the increase in saturation leads to capillary pressures that are locally less negative than in the surrounding rock, allowing water to be diverted around the drift. If the lateral hydraulic conductivity is insufficient to divert the water, fully saturated conditions are reached locally, and seepage occurs as the capillary barrier fails. In an anisotropic fracture network, the orientation of an individual fracture determines which of its hydraulic properties affects seepage most. The effectiveness of the capillary barrier is determined by the capillarity of the vertical fractures and by the permeability and connectivity laterally within the fractures. Note that even though the capillary barrier fails and seepage occurs, the seepage flux is (perhaps significantly) lower than the percolation flux. The seepage threshold and the seepage rate are strongly affected by the drift geometry and formation properties, especially the capillary-pressure and unsaturated hydraulic-conductivity functions. The capillary-barrier effect generally leads to a saturation increase at the apex (crown) of the drift. Flow rates and liquid saturations below the drift are usually lower as a result of the capillary barrier effect, but may be locally increased depending on the drainage system.

2. *Distribution of Percolation Flux, Flow Channeling:* As water percolates through the layered, unsaturated, fractured porous system at Yucca Mountain, it is likely to be redirected and focused into flow channels, which may again be dispersed at fracture intersections. The distribution of flow channels, their frequency, width, and hydrologic properties determine the seepage probability and thus the number of emplacement drifts and waste packages affected by seepage. The spatial distribution of flow channels may change with average percolation flux and potentially with time. Note that calcite deposits suggest that flow channels do not change significantly with time (CRWMS M&O 2000, U0085, Section 6.10.3). Flow focusing is estimated based on the active fracture concept (CRWMS M&O 2000, U0120, Section 6.3.3); these estimates are consistent with an observation of a damped feature in Niche 3566 (Section 2.2.2.2.1). Depending on the flux within an individual flow channel, the seepage threshold may or may not be exceeded locally. A general discussion of channeling effects under unsaturated flow conditions can be found in Birkholzer and Tsang (1997, pp. 2221–2238). Flow focusing occurs and must be accounted for on a variety of scales, as discussed in Section 3.9.3.1.
3. *Hierarchical Fracture Network:* The geometric and hydrologic characteristics of the fracture network affect seepage as they determine the flux distribution and the effectiveness of the capillary barrier. The intermediate-scale (between mountain and drift scale) characteristics of the fracture network affect seep development, potential compartmentalization of the flow field, and effective anisotropy. All these factors determine the spatial distribution of flow channels and the flux within one of those channels. Heterogeneities of the fracture network on different scales and within individual fractures affect local percolation fluxes, and therefore seepage. The capillary-barrier effect is governed by the connectivity of the

fracture network and its capillary strength. Small fractures and microfractures, if interconnected, have the potential to reduce seepage because they have sufficient capillary strength to hold the water, preventing it from freely seeping into the opening. At the same time they have—unlike the matrix—sufficient permeability to facilitate flow diversion around the drift. The question arises whether seepage-relevant fracture properties can be derived from fracture-trace maps, considering that the mapped geometric characteristics and hydraulic properties are not necessarily related. Model calibration is the approach relied upon to determine effective parameters that include the potential effects of individual fractures and microfractures on seepage. Simulations with multiple realizations of a heterogeneous property field are performed to account for the random nature of the fracture network (CRWMS M&O 2000, U0075).

4. *Drift Geometry, Roughness, Breakouts* The geometry (shape, size) of the underground opening (waste emplacement drift, alcove, niche) determines the likelihood of encountering seeps and the ease with which water can be diverted around it as a result of the capillary barrier effect. Analytical solutions examining the impact of drift geometry on seepage threshold were developed by Philip et al. (1989, pp. 16–28). The geometry of drift-wall roughness and the characteristics of the surface (wettability, micro-roughness, dust, and coating) partially control local water accumulation, droplet formation, the potential for film flow along the drift wall, and eventually dripping locations. The frequency, location, size, and geometry of breakouts (locations with a cavity in the drift wall because rock has fallen out) and partial drift collapse affect the integrity of the capillary barrier. Breakouts may lead to distinct topographic lows, which increase seepage, or they make the drift more cone-shaped, which promotes flow diversion and thus decreases seepage.
5. *Ventilation, Evaporation/Condensation:* The temperature and humidity conditions in the drift and their regulation by ventilation determine evaporation and condensation effects. Evaporation at the drift wall generally reduces drop formation and dripping (Ho 1997a, pp. 2665–2671), and creates a dry-out zone around the drift. If relative humidity in the drift is kept below 100% by ventilation, seepage of liquid water is reduced, whereas vapor diffusion into the drift is increased. The moisture from the increased vapor influx is effectively removed by ventilation. Nevertheless, local differences or temporal changes in drift temperature may lead to condensation of vapor, causing droplet formation at the drift wall and other surfaces within the drift. Accumulation of condensate may lead to dripping.
6. *Excavation-Disturbed Zone, Dry-Out Zone:* The properties of the fractured rock in the immediate vicinity of the drift wall control the capillary-barrier effect, which occurs within a relatively small region around the opening. The extent of this zone is approximately given by the height to which water rises on account of capillarity. The zone governing seepage is likely to be smaller than the zone affected by excavation-induced stress redistribution and related rock deformations (opening and closing of existing fractures, generation of new microfractures and

cracks) resulting from drift excavation. Moreover, drift ventilation and/or heating lead to a dry-out zone with associated dissolution and precipitation of minerals (CRWMS M&O 2000, N0120/U0110). The hydrologic properties of this zone, its extent, and the characteristics of its transition to the undisturbed formation potentially impact seepage.

7. *Design:* The layout and design of the potential repository and the engineered barrier system affect the probability of seepage water contacting waste packages.

The complex physical processes affecting drift seepage cannot be addressed comprehensively in an analytical or numerical model, mainly because it is impossible to obtain sufficient characterization data over many scales to describe all the relevant geometric features and hydrologic properties. The characterization and modeling approach presented here focuses on obtaining effective parameters based on seepage-relevant hydraulic data. The abstraction of seepage for Total System Performance Assessment (TSPA) aims at yielding robust, conservative seepage estimates over a wide range of hydrologic conditions (CRWMS M&O 2000, U0120).

3.9.2 Objectives and General Modeling Approach

Seepage predictions are based on and provide information for a suite of models and analyses:

- Site-Scale UZ Flow Model (UZFM) (CRWMS M&O 2000, U0050)
- Calibrated Properties Model (CPM) (CRWMS M&O 2000, U0035)
- Seepage Calibration Model (SCM) (CRWMS M&O 2000, U0080)
- Thermal-Hydrological-Chemical Seepage Model (THC Seepage Model) (CRWMS M&O 2000, N0120/U0110)
- Seepage Model for Performance Assessment (SMPA) (CRWMS M&O 2000, U0075)
- Seepage abstraction (CRWMS M&O 2000, U0120)
- TSPA

The site-scale UZ Flow Model provides (among other quantities) the large-scale distribution of percolation fluxes at the potential repository horizon (Sections 3.7.4.1 through 3.7.4.3). The Calibrated Properties Model (Section 3.6) provides estimates for some of the parameters input to the drift-scale seepage process models. The purpose of the Seepage Calibration Model (SCM) is to present a methodology for the subsequent development of seepage process models (Section 3.9.4). The purpose of the Seepage Model for PA (SMPA) is to provide seepage estimates for a variety of hydrologic properties and drift shapes (Section 3.9.5). The purpose of the THC Seepage Model (Section 3.10) is to analyze the impact of thermal and chemical effects on seepage and to predict the chemical composition of water and gas that may seep into waste emplacement drifts. The purpose of the seepage abstraction is to provide the framework for evaluating seepage into potential repository emplacement drifts for TSPA simulations and to

generate probability distributions that represent the uncertainty and spatial variability of seepage (Section 3.9.6). This information is then used in TSPA calculations for SR.

Figure 3.9-2 schematically shows the relationships between the different seepage models as well as data input and the exchange of information. Air-permeability and liquid-release-test data enter the development and calibration of the SCM, which also uses parameters developed by the CPM. The modeling approach and some of the seepage-relevant parameters from the SCM are used to develop the SMPA, which also evaluates various drift-degradation scenarios. The seepage data calculated with the SMPA enter the seepage abstraction process, which incorporates results from the mountain-scale percolation flux modeling as well as drift-scale THC modeling to arrive at defensible seepage values to be used in the TSPA calculation. This section of the PMR describes the SCM and SMPA as well as the seepage abstraction.

Given the objectives outlined above, the current seepage models are not expected to accurately predict individual seepage events or the precise spatial distribution along the emplacement-drift axis or the drift ceiling. Instead, the seepage models are intended to provide estimates of the seepage flux averaged over a 5 m drift segment (the approximate length of a waste package) as a function of the percolation flux on the drift scale. Once seepage rates are known deterministically for a wide range of conditions, a probabilistic analysis is performed to include uncertainty and spatial variability. In addition, the seepage models improve our understanding of seepage in fractured formations and the relative importance of certain factors (such as drift deformation, variability in the permeability field, and the correlation between permeability and capillary strength).

Seepage models are simplifications and abstractions of the recognized seepage-relevant processes and features summarized in Section 3.9.1. The selection of processes being included in a specific seepage model is guided by their expected significance. Experiments are designed to identify, understand, and characterize significant processes and parameters. Remaining uncertainties and property variabilities are considered either by stochastic simulations and uncertainty propagation analyses, or by assuming large parameter uncertainties in the TSPA calculations. Conservative assumptions are made for effects that cannot be accounted for because of a lack of characterization data.

The following premises guide the seepage modeling approach:

1. Seepage amounts and seepage locations are sensitive to magnitude and local distribution of percolation flux as well as the heterogeneity in fracture properties around the drifts. The heterogeneity cannot be captured deterministically, but rather through geostatistical description, stochastic simulations, and the estimation of effective parameters.
2. Parameters affecting seepage are best derived from tests that reveal seepage-relevant processes. The effective parameters determined in such a manner are process specific, scale dependent, and model related.

3. Uncertainties in the parameters defining the geostatistical model and mean hydrogeologic properties are accounted for in a probabilistic uncertainty propagation analysis.
4. The seepage models must be consistent and compatible with the suite of UZ flow and transport models.

Finally, independent evidence from analog sites is examined and alternative conceptual models are studied to guard against potential flaws in the conceptual models.

As mentioned in Section 3.9.1, seepage is affected by features and processes occurring on a multitude of scales, which cannot be captured in a single model. The model hierarchy presented here assures that each scale is appropriately represented. The site-scale UZ Flow Model provides the large-scale distribution of percolation fluxes (Sections 3.7.4.1 through 3.7.4.3). Flow focusing factors are calculated (Section 3.9.6.3) to account for channeling effects occurring on the drift scale. The heterogeneity in the seepage process models (Sections 3.9.4 and 3.9.5) leads to further flow focusing down to the sub-meter scale. Finally, the estimation of effective parameters through calibration against seepage-relevant data (Section 3.9.4) takes into account the effects of sub-grid-block channeling and other small-scale flow phenomena.

3.9.3 Key Issues and Corresponding Modeling Assumptions

The following is a discussion of key issues pertaining to seepage (see Figure 3.9-3); their relevance (given the objectives described in Section 3.9.2) is discussed, and the simplifying assumptions made in the seepage process models and seepage abstraction are presented in the remainder of this subsection.

3.9.3.1 Percolation Flux and Channeling Effects

Flux and spatial distribution of downward percolating water is the most important factor affecting seepage rates and locations. Water movement is controlled by net infiltration at the surface and subsequent multiscale moisture redistribution either by channeling (flow focusing) or bifurcation (flow dispersion). Large-scale geological units and features such as the PTn and faults lead to a redistribution of percolation fluxes. On an intermediate scale, flow through the fracture network may be focused as a result of flow channeling effects. This leads to zones of locally higher percolation fluxes and (in between them) areas of reduced water flow. Water within such a high-flux zone (weep) may be further channeled by small-scale heterogeneities of the fracture network. Finally, heterogeneity and flow instabilities within individual fractures lead to small-scale flow channels (rivulets or fingers). Since flow diversion and average seepage flux are determined by the characteristics of these rivulets as they encounter the drift wall, it is important to estimate channeling effects on all scales.

A single numerical model cannot possibly account for multiscale heterogeneity and channeling effects—from large-scale flow redistributions to small-scale rivulet formation. Therefore, a series of models was developed, each addressing flow channeling on its assigned scale. The model hierarchy can be described as follows:

1. Flow redistribution on account of large-scale features is considered in the site-scale UZ Flow Model (Section 3.7.2). This model provides average percolation fluxes on the scale of hundreds of meters (CRWMS M&O 2000, U0050).
2. Potential concentration of flow from the large-scale averages to the scale of an individual drift segment (an area of tens of square meters) is accounted for by multiplying the average flux with a stochastic flow-focusing factor, taking into account the fact that flow is reduced in other areas. These flow-focusing factors are estimated using the active fracture concept of Liu et al. (1998, pp. 2633–2646) and geometric arguments. The approach is described in Section 3.9.6.3 and CRWMS M&O (2000, U0120, Section 6.3.3).
3. Flow redistribution on the scale of a few meters or less is simulated in the drift-scale seepage process models (Sections 3.9.4 and 3.9.5), in which heterogeneities in the fracture continuum are explicitly represented based on geostatistical analysis of air-permeability values (Sections 3.9.4.4 and 3.9.5.2). Seepage is then calculated for multiple realizations of stochastically generated property fields.
4. Phenomena and processes that occur on a scale smaller than the gridblock size of the numerical model are accounted for by estimating effective parameters through inverse modeling. The impact of rivulets on seepage and other small-scale effects are not modeled explicitly, but are implicitly considered by estimating seepage-relevant parameters. Specifically, if water from a small-scale rivulet or through film flow seeps into the opening during a liquid-release test, it is reflected in the corresponding seepage data point. By adjusting parameters during the calibration process to match these data points, the small-scale effects are automatically accounted for in an integrated way.

In summary, percolation flux used in the seepage process models is taken to be the large-scale average flux multiplied by flow-focusing factors. This increased flux is applied uniformly at the top boundary of the model, and additional focusing occurs as water percolates through the heterogeneous property field of the model. The calculated seepage fraction is finally determined based on property values determined in an inversion of seepage-relevant data that include small-scale effects.

3.9.3.2 Episodic Flow

Percolation flux is not expected to be constant with time, but may increase episodically as a result of high-infiltration events, seasonal variations, and climate changes (Section 3.7.2). Episodic flow events may affect seepage in two ways:

1. Episodic flow events lead to periods when percolation fluxes (and thus seepage rates) are greater than the corresponding average values.
2. Episodic flow events lead to transient effects (such as storage and hysteresis).

Temporally increased percolation fluxes can be handled by applying episodic-flow factors in a way similar to the flow-focusing factors discussed in Section 3.9.3.1 (see also CRWMS M&O

(2000, U0120, Section 6.3.4)). Currently, there is no evidence that high-frequency fluctuations (a few years or shorter) penetrate to the depth of the potential repository. Flow simulations have shown that the PTn effectively damps out flow transients (Section 3.7.3.1). Note that increased percolation from long-term transients (climate change) is explicitly accounted for in the TSPA analysis (CRWMS M&O 2000, U0120).

Seepage is controlled by the properties of a small zone surrounding the drift. Consequently, storage effects as a result of episodic flow events are negligible if the event is longer than the time required to change the saturation in the available pore space in that zone. High-frequency, large-amplitude net infiltration events are damped as they travel through the mountain to the extent that they arrive as diffuse fronts of small amplitude at the potential repository horizon, making storage effects in the seepage-controlling zone negligible. An episodic-flow scenario is discussed in CRWMS M&O (2000, U0075, Section 6.6.7). Additional documentation on the implications of episodic flow for seepage is presented in CRWMS M&O (2000, U0170, FEP number 2.2.07.05.00).

The parameters of the capillary pressure curve are determined by inversion of liquid-release tests (Section 3.9.4). These tests are imbibition experiments, yielding a wetting branch of a hysteretic capillary pressure curve. If hysteresis were important, this approach would lead to a conservative estimate of capillary strength. Potential hysteresis effects, however, are neglected because these effects are considered to be small in comparison to the uncertainty inherent in the empirically determined capillary pressure relations.

3.9.3.3 Ventilation, Evaporation, and Condensation Effects

Ventilation leads to reduced relative humidity in the drift and forced advective removal of water vapor. The potential impact on seepage and seepage experiments are as follows:

1. Water evaporates at the drift wall, reducing the rate of liquid water seeping into the opening.
2. Diffusive vapor transport into the drift increases, potentially creating a dry-out zone around the opening.
3. Water collected in the capture system during liquid-release tests evaporates, leading to apparently smaller seepage rates.
4. Spatial or temporal temperature changes may lead to condensation of water at the drift wall.

Evaporation of water at the drift wall reduces seepage. This effect may be significant during ventilation periods, when the evaporation rate exceeds the potential seepage rate, preventing the development of liquid droplets that drip into the opening. Ho (1997a, pp. 2665–2671) provides a detailed description of evaporation mechanisms on the scale of individual water droplets within or emerging from fractures. The fact that no natural seepage is currently observed in the ESF could be attributed to ventilation effects. (Note that, because of the capillary-barrier effect, zero seepage may result even if the relative humidity in the ESF were 100%.) Neglecting ventilation and evaporation effects in a numerical seepage prediction is conservative because omitting them

increases predicted seepage of liquid water. Therefore, the assumption is made that the relative humidity in the drift is 100% (i.e., there is a zero-capillary-pressure boundary condition applied at the drift wall). In a ventilated drift, the development of a dry-out zone increases the capillary pressure and local storage volume and thus reduces the risk of reaching seepage conditions; the assumption of 100% relative humidity in the drift is again conservative. The assumption is also reasonable for the time when ventilation is stopped and the drift is closed.

The reduced relative humidity in a ventilated drift increases diffusive vapor flow from the rock into the opening. However, the underestimation of diffusive vapor flow in a model with 100% relative humidity is irrelevant, because the assumption already implies that the moisture content in the drift environment is at its maximum. The assumption of 100% relative humidity is conservative since it maximizes the amount of moisture that can condense within the drift. While condensation is a potentially important effect, no estimates of drip formation as a result of condensation due to temperature variations or in-drift movement of moist air are presented here.

Evaporation of water collected in the seepage-test capture system leads to an underestimation of seepage rates during a liquid-release test and is therefore not conservative. Parameters are adjusted during the inversion such that the model reproduces the observed seepage percentage, which is likely to be too small. This issue is currently addressed by monitoring relative humidity in the niche and directly measuring evaporation rates. Moreover, the estimation of seepage-relevant parameters is predominantly based on data from short-term liquid-release tests that were performed at rates significantly higher than the potential evaporation rate.

For these reasons, drift ventilation effects are neglected in the current seepage process models. Note that evaporation and condensation in the rock as a result of waste-generated heat is accounted for in the THC Seepage Model (Section 3.10.5; CRWMS M&O 2000, N0120/U0110). In-drift evaporation and condensation effects are not considered here.

3.9.3.4 Excavation Effects, Surface Roughness, and Drift Degradation

Drift excavation induces mechanical disturbance and stress redistribution in the surrounding rock, creating a zone with altered formation properties. Surface roughness at the drift wall, breakouts and rock fall from the drift ceiling, and changes in drift geometry as a result of partial drift collapse may result in local topographic lows along the drift ceiling, where water tends to accumulate. These features have the following impact on seepage:

1. Increased fracturing, fracture dilatation, and fracture compression affect the hydrologic properties of the excavation-disturbed zone (EDZ), and may increase or decrease seepage.
2. Small-scale roughness increases local ponding probability and thus increases seepage.
3. Depending on the location of rock fall along the drift perimeter and the geometry of the breakouts, these intermediate-scale changes in drift-wall geometry tend to promote seepage as water may be channeled into rock wedges from which it

cannot escape. The frequency, location, and geometry of breakouts determine their overall impact on total seepage.

4. Depending on the final shape of the drift, partial or complete drift collapse may either increase or decrease seepage into the remnants of the opening. Since breakouts tend to produce local topographic lows along the drift wall, it is more likely that drift collapse leads to an increase in seepage.

Existing fractures may be opened or compressed as a result of drift excavation. The mechanism leading to either opening or closing of fractures depends on the location of the drift in relation to major geologic features, the position along the drift circumference (crown, spring line, invert), the local stress condition, the fracture orientation and fracture network characteristics, the rock-mechanical properties of the fractures and the matrix, and the rock-mechanical behavior during the deformation (elastic, inelastic). Fracture dilatation leads to an increase in permeability, which tends to reduce seepage, and at the same time to a decrease in capillary strength, which tends to increase seepage. Conversely, reduced permeability as a result of fracture compression tends to promote seepage, but at the same time the increased capillary strength enhances the water retention capability, reducing seepage. This counteracting effects reduce the overall impact of fracture deformation on seepage. A detailed analysis of the coupled hydrologic-mechanical behavior as a result of drift excavation and its effect on seepage is difficult to perform. Note that the approach described in this section relies on the calibration of data from seepage experiments that were performed in the excavation-disturbed zone. The data thus reflect potential effects of fracture dilatation or compression on seepage. Matching these data through inverse modeling yields effective parameters that include potential excavation effects.

The extent of the EDZ is likely to exceed the thickness of the zone that determines seepage. This is confirmed by modeling (Bidaux and Tsang 1991, pp. 2993–3008) and experimentation (Wang and Elsworth 1999, pp. 751–757). The seepage-relevant properties of this zone are determined by calibration against liquid-release-test data. As a result of this approach, the potential impact of the EDZ on seepage is automatically accounted for in a calibrated seepage process model. Note that excavation-induced (micro-) fracturing around the drift increases permeability without significantly reducing the effective capillary strength. This reduces seepage by promoting flow diversion. On the other hand, dilatation of existing fractures is accompanied by a reduction in capillary strength, offsetting the advantage of increased permeability by a reduced strength of the capillary barrier.

If the amplitude of small-scale surface roughness reaches a significant fraction of the capillary head, small-scale lateral flow diversion is impeded and saturation in the troughs of the wavy or jagged surface is elevated, leading to increased seepage. The impact of small-scale, sub-gridblock surface roughness is automatically accounted for through the estimation of effective seepage parameters.

A breakout can be described as an intermediate-scale surface roughness. Water is accumulated in topographic lows created by the breakout, leading to increased local seepage if no opportunities or insufficient opportunities for flow diversion exist. The impact of breakouts on seepage depends on block size and rock fall frequency, which in turn is functions of fracturing and stress

conditions. Examples of 3-D seepage simulations with discrete breakouts are presented by CRWMS M&O (2000, U0075, Sections 6.4.2 and 6.6.5).

Extended rock failure and partial drift collapse may change the shape of the opening in a way that promotes or reduces seepage. One example yielding increased seepage is shown in Section 6.4.3 and CRWMS M&O (2000, U0075, Sections 6.4.3 and 6.6.5). The composite effects of drift degradation are accounted for in the seepage abstraction (Section 3.9.6) through application of a seepage-rate enhancement factor (CRWMS M&O 2000, U0120, Section 6.3.1).

3.9.3.5 Capillary Barrier and Seepage Threshold

The capillary-barrier effect has been described in Section 3.9.1, Point 1. While the development of a capillary barrier and the existence of a seepage threshold are the result of the fundamental behavior of fluids in unsaturated media and are well-understood features of a hydrogeologic system (see, for example, Frind et al. (1977, pp. 3133–3163); Philip et al. (1989, pp. 16–28); Oldenburg and Pruess (1993, pp. 1045–1056); Birkholzer et al. (1999, pp. 349–384)), the effectiveness of the capillary barrier at a specific location is difficult to determine. It specifically depends on the permeability and capillary strength near the opening. Moreover, the performance of a capillary barrier must be assessed as a total system (here on the scale of the cross section of a waste emplacement drift) that considers all the factors discussed in Sections 3.9.3.1 through 3.9.3.4.

A detailed characterization of seepage-relevant, small-scale hydrogeologic properties near the drift wall appears unfeasible. Fracture-trace maps are likely to be biased because they exclude small fractures and microfractures, which may be crucial for the performance of the capillary barrier. In addition, it is difficult to relate the mapped geometric characteristics to the hydraulic properties governing seepage. For these reasons, no use of geometric fracture network information is made, because it would require making numerous simplifying assumptions to arrive at the hydrogeologic properties controlling seepage. Instead, seepage-relevant properties are determined, and the overall performance of the drift as a capillary barrier is assessed by conducting and analyzing liquid-release tests. As water injected from a borehole reaches the opening at the drift crown, the capillary barrier comes into effect. Some of the water may seep into the opening, whereas the rest is diverted laterally, eventually flowing around the drift. Analyzing data from this experiment ensures that the capillary barrier is tested on the appropriate scale, in the relevant zone, and using the pertinent physical processes such as water retention and pressure build-up in the fractures, flow diversion through microfractures, local failing of the capillary barrier in discrete fracture segments intersected by the opening, and seepage as a result of film flow. Nevertheless, numerical modeling is required to estimate seepage under changed conditions, namely lower percolation fluxes. Currently, the validity of such an extrapolation cannot be assessed experimentally. The synthetic modeling study presented in CRWMS M&O (2000, U0080, Section 5.3) suggests that reasonable predictions of seepage for lower percolation fluxes can be obtained when following the approach described here and in Section 3.9.4 below. It should be realized that applying a numerical model to conditions and time scales different from those encountered during model calibration always bears a risk, because the underlying mechanisms significant to seepage may change.

The seepage threshold may be considered a characteristic point describing the performance of a capillary barrier. It indicates whether or not water seeps into the opening for a given local percolation flux. However, performance assessment requires predicting seepage rates over the entire range of expected percolation fluxes. Even if seepage-threshold estimates remain uncertain, the reduction of drift influx at percolation fluxes above the seepage threshold is an important aspect of the seepage problem. The relative difficulty of accurately determining the seepage threshold does not invalidate the calculation of seepage fluxes.

3.9.4 Seepage Calibration Model

3.9.4.1 Objectives and General Approach

In this section the development, calibration, and validation of the Seepage Calibration Model is described. The purpose of the SCM is to present a methodology for the subsequent development of seepage process models such as the Seepage Model for Performance Assessment (Section 3.9.5). The SCM is a template, heterogeneous fracture-continuum model that is developed based on air-permeability and liquid-release-test data from the experiments performed in Niche 3650 of the ESF at Yucca Mountain. The steps involved in the development of the SCM are schematically shown in Figure 3.9-4. A geostatistical analysis of post-excavation air-permeability data provides the basis for the generation of a heterogeneous property field, which is mapped onto the model grid. Liquid-release tests are simulated to calibrate the model against measured cumulative-seepage data. The calibrated SCM is then validated using data from additional liquid-release tests. The development of the SCM is documented in CRWMS M&O (2000, U0080).

The scope of this modeling study is limited to an analysis of seepage data from Niche 3650. The parameters estimated by the SCM are thus only representative for isothermal seepage into an uncollapsed opening excavated in the middle nonlithophysal zone of the Topopah Spring welded tuffs at Yucca Mountain.

3.9.4.2 Air-Permeability and Liquid-Release-Test Data

Air-injection tests were performed in boreholes drilled above Niche 3650, and air-permeability values were determined (CRWMS M&O 2000, U0015, Section 6.1). A geostatistical analysis of these post-excavation air permeabilities provided a measure of statistical variability and spatial correlation (see variogram in the top panel of Figure 3.9-4). The air-permeability field is essentially random, without a noticeable spatial correlation.

A series of short-duration liquid-release tests was performed at Niche 3650. The seepage tests were conducted after niche excavation by introducing water into select test intervals in boreholes located above the niche. The tests were performed by sealing a short section of borehole (using an inflatable packer system) and then releasing water at a constant rate into the isolated test interval. Any water that migrated from the borehole to the niche ceiling and dripped into the opening was captured and weighed. The seepage percentage, defined as the mass of water that dripped into the capture system divided by the mass of water released into the borehole interval, was used to quantify seepage into the drift from a localized water source of known duration and

flow rate. Details about the liquid-release tests can be found in CRWMS M&O (2000, U0015, Section 6.2).

The heterogeneous property field of the SCM was developed based on the geostatistical characteristics of the air-permeability data (Section 3.9.4.4). The seepage-relevant hydrologic properties were determined by calibrating the SCM against the liquid-release-test data (Section 3.9.4.5).

3.9.4.3 Model Assumptions

The basic assumptions of the SCM are consistent with those of other submodels of the UZ Flow and Transport Model (see Section 1 for list of submodels; see CRWMS M&O (2000, U0050, Sections 5 and 6.1.2) for assumptions and modeling approach); the submodel of specific concern is the SMPA described in Section 3.9.5. Consistency and compatibility are essential requirements because the concepts and parameters derived with the SCM are only valid and useful for subsequent seepage calculations if they refer to similar conceptual models. The key assumptions are summarized below; additional assumptions and a more detailed discussion of why they are considered valid or reasonable can be found in CRWMS M&O (2000, U0080, Section 5).

It is assumed that the continuum approach is a valid concept to calculate percolation flux and drift seepage at Yucca Mountain. This assumption is based on the observation that the fracture network in the Topopah Spring middle nonlithophysal unit at Yucca Mountain is well connected (CRWMS M&O 2000, U0075, Section 6.7). In addition, the synthetic study presented in CRWMS M&O (2000, U0080, Section 5.3) demonstrates that simulating seepage into underground openings excavated from a highly fractured formation can be performed using a model that is based on the continuum assumption, provided that the model is calibrated against seepage-relevant data such as data from a liquid-release test. Synthetically generated data from a model that exhibits discrete flow and seepage behavior were used to calibrate a simplified fracture-continuum model. Seepage predictions for low percolation fluxes made with the calibrated fracture-continuum model were consistent with the synthetically generated data from the discrete-feature model. The appropriateness of using the continuum approach to simulate flow through fractured rock was also studied by Jackson et al. (2000, pp. 189–202) using synthetic and actual field data. They concluded that heterogeneous continuum representations of fractured media are self-consistent, i.e., appropriately estimated effective continuum parameters are able to represent the underlying fracture network characteristics.

Adopting the continuum approach, water flow under unsaturated conditions is assumed to be governed by Richards' equation (Richards 1931, pp. 318–333). Relative permeability and capillary pressure are described as continuous functions of effective liquid saturation according to the expressions given by the van Genuchten-Mualem model (Luckner et al. 1989, pp. 2191–2192). Within the heterogeneous property field, capillary strength is correlated to absolute permeability according to the Leverett scaling rule (Leverett 1941, p. 159).

3.9.4.4 Model Development

Because the SCM was to be calibrated against liquid-release-test data obtained in Niche 3650, the model was discretized to include the approximate geometry of the niche and its boreholes. A permeability field was generated, conditioned on and following the geostatistical properties of the post-excavation air-permeability data measured in various intervals of the three boreholes drilled above the niche. The resulting permeability field was mapped onto the numerical grid of the SCM, and the capillary-strength parameter was correlated to the permeability in each grid block according to Leverett's scaling rule (Leverett 1941, p. 159). The location of Niche 3650, its layout, and the corresponding numerical grid and log-permeability field of the 3-D heterogeneous SCM are shown in Figure 3.9-5. Simplified versions of the SCM include a 2-D X-Z cross section and homogeneous versions of the model in two and three dimensions.

A free-drainage boundary condition was applied at the bottom of the model. The niche itself was set at a reference pressure of 1 bar. No capillary suction was applied in the niche, i.e., it was assumed that the air at the niche wall was of 100% relative humidity (see discussion in Section 3.9.3.3). Water was allowed to enter, but was prevented from exiting the niche. Thus, the temporal change of water in the niche element represented the cumulative seepage collected in the capture system installed during the liquid-release tests in Niche 3650. No-flow boundary conditions were specified at the left, right, back, and front sides of the model. Initial parameter estimates were obtained from the Calibrated Properties Model (CRWMS M&O 2000, U0035), and a steady-state simulation was performed to obtain the initial saturation distribution. More details about the development of the SCM can be found in Section 6.3 of CRWMS M&O (2000, U0080).

3.9.4.5 Model Calibration

Data from five liquid-release tests (CRWMS M&O 2000, U0080, Table 6) were selected for calibration of the seepage model by means of inverse modeling. The five tests were conducted in 30 cm long borehole intervals at various injection rates (ranging from approximately 120 ml/min for the first test to 1 ml/min for the last test), revealing the dependence of seepage on flux. Approximately 1 liter of water was injected in each test. The inactive time between individual test events ranged from approximately 2 hours between the second and third test, to 20 days between the first and the second test. This reveals potential memory effects such as the increased seepage percentage in the third test, which is a result of reduced storage because the pore space is occupied by water injected during the previous test. The seepage percentages observed at the end of each test (ranging from approximately 56% for the third test to 0% for the last test) are thus expected to reveal a number of seepage-relevant processes, including storage effects and rates below and above the seepage threshold.

Using the measured amount of water collected during the five seepage tests, two parameters were determined by inverse modeling. The two parameters are the porosity (ϕ) and the reference capillary-strength parameter ($1/\alpha$). These parameters were selected because of their sensitivity to the observed data and their correlation to other parameters. In a transient seepage experiment with only a small volume released, the amount of water seeping into the niche depends mainly on the following three factors:

1. The ability of the formation to hold the water by capillary forces, here expressed through an effective van Genuchten parameter α
2. The ability of the formation to store the finite amount of water released, here expressed through an effective porosity ϕ , which may include effects of matrix imbibition
3. The ability of the formation to divert water around the opening, here expressed through an effective permeability k .

The simulated seepage mass can be increased by decreasing either capillary strength, $1/\alpha$, porosity, ϕ , or permeability, k . Consequently, all possible parameter pairs are negatively correlated if inversely determined from seepage data. Because only seepage-mass data are available for calibration, the parameter correlations are expected to be strong; that is, it is unlikely that they can be determined independently from one another and with a reasonably low estimation uncertainty. The parameters to be determined are the porosity (ϕ) and the reference capillary-strength parameter ($1/\alpha$) while permeability (k) is fixed at the value estimated from the air-injection tests. A joint inversion of all five tests using iTOUGH2 V4.0 (STN: 10003-4.0-00) (Section 1.3.3.2) yielded a good match and reasonable parameter estimates. As shown in Figure 3.9-6, the heterogeneous three-dimensional SCM matches the observed seepage-mass data well and better than the two-dimensional or homogeneous alternatives.

The estimated reference capillary-strength parameter of $1/\alpha = 66$ Pa is low relative to values derived from calibration against saturation and water-potential data (CRWMS M&O 2000, U0035, Section 6.1.2). This is mainly because the injected water preferentially flowed through the relatively large fractures, which exhibit weak capillarity. In addition, the apertures of these fractures are likely to be larger in the excavation-disturbed zone as opposed to the undisturbed rock, leading to weaker capillarity. Moreover, the low estimate results from the fractures not being modeled as discrete features but as a continuum. Discrete fractures intersecting the niche promote seepage (i.e., for some flow paths, diversion around the drift is not possible). Consequently, the absence of discrete fractures in the model is partly compensated by a reduction of the estimated $1/\alpha$ value, which has the effect of weakening the capillary barrier and thus increasing seepage. The porosity estimate of $\phi = 0.0013$ seems reasonable (CRWMS M&O 2000, U0090, Section 6.1); it comprises all fractures involved in the flow and seepage process, including microfractures and the pore space affected by matrix imbibition. Note that porosity is of no importance for the prediction of long-term, near-steady-state seepage. More details about the calibration of the SCM can be found in CRWMS M&O (2000, U0080, Section 6.4).

3.9.4.6 Model Validation

The purpose of the SCM is to provide a general modeling approach that can be used for the subsequent development of process models for seepage predictions. These predictions are performed with the Seepage Model for Performance Assessment (SMPA), which develops the data basis for the seepage abstraction. Confidence into the SCM and the modeling approach can be gained by demonstrating that seepage-relevant processes and seepage-relevant parameters are identified to the degree required by the objectives of the downstream models. The SMPA evaluates seepage over a wide range of parameter values to accommodate spatial variability and

uncertainty (Section 3.9.5). Moreover, uncertainty is accounted for during the abstraction process by choosing appropriate distribution functions for the input parameters and by applying safety factors based on conservative assumptions (Section 3.9.6).

Given the objectives of the downstream models, the following testing of the SCM was considered sufficient and appropriate. The calibrated SCM was used to make predictions of observed seepage percentages from liquid-release tests that were performed in a different borehole interval using different injection rates and varying inactive time periods in between the individual test events. The uncertainty of the model predictions was evaluated using linear error propagation analysis and Monte Carlo simulations. This approach reflects the intended use of the downstream models, in which seepage is treated as a stochastic process. The observed seepage percentages lay within the uncertainty range of the model predictions, i.e., a correct probabilistic statement would have been made regarding the predicted seepage value. This favorable result increased confidence in the appropriateness of the chosen approach to seepage modeling. The relevant processes are understood and the key factors affecting seepage are identified. The proposed modeling approach, which includes the conceptual model development and the calibration against seepage-relevant data, is appropriate for evaluating seepage into waste emplacement drifts. The model is thus validated for its intended use. More details about the testing of the SCM can be found in CRWMS M&O (2000, U0080, Section 6.5).

3.9.4.7 Seepage Threshold Prediction

Steady-state seepage simulations were performed with the calibrated SCM (CRWMS M&O 2000, U0080, Section 6.6). The percolation flux applied at the top of the model was varied over a large range. Starting from a small value yielding zero seepage, the percolation flux was increased stepwise until seepage occurred, at which point the seepage threshold was identified. Further increasing the flux at the top model boundary provided estimates of seepage percentage as a function of percolation flux. A seepage threshold of approximately 200 mm/yr was obtained for the middle nonlithophysal unit of the Topopah Spring tuff. Note that this value applies to an opening of the size and geometry of Niche 3650; thus, the estimate cannot be directly applied to seepage into waste emplacement drifts because they are of a different geometry and—more importantly—are predominantly located in a different stratigraphic unit. Furthermore, seepage threshold predictions are expected to be highly uncertain and variable with location. Conservatively estimated distributions of seepage thresholds for the potential repository horizon are presented in Section 3.9.6.4. The preliminary seepage-threshold prediction obtained for Niche 3650 suggests that a potentially significant amount of water percolating under natural flow conditions is diverted around the drift.

3.9.4.8 Summary

The calibration and validation of the SCM demonstrate that simulations of seepage into underground openings excavated from a highly fractured formation can be performed using a heterogeneous fracture-continuum model, provided that the model is calibrated against seepage-relevant data. The calibration process yields scale-dependent, seepage-specific, and model-related effective parameters that partly reflect the discreteness of the fracture network. The modeling and calibration approach was successfully applied to seepage data from liquid-release

tests performed in Niche 3650 in the ESF. The calibrated model can be used to predict seepage threshold and seepage percentages for different percolation fluxes, as described in Section 3.9.5.

3.9.5 Seepage Model for PA

3.9.5.1 Objectives and General Approach

This section contains a description of the simulations performed with the Seepage Model or Performance Assessment (SMPA) and its submodel, the Disturbed Drift Seepage Model (DDSM). The main purpose of the SMPA is to evaluate long-term drift seepage over a large range of hydrogeologic parameters and for a variety of percolation fluxes. In addition to these parameter sensitivity studies, the SMPA is also used to examine certain scenarios described below (Section 3.9.5.3). The SMPA is run for multiple realizations of heterogeneous rock properties. Effects of episodic flow events and changed drift geometry on account of drift degradation are also evaluated. The results of these simulations are to be used by TSPA to develop the probability distributions of water seepage into waste emplacement drifts (Section 3.9.6). The SMPA is documented in CRWMS M&O (2000, U0075).

The SMPA simulations are based on the current repository design, using hydrogeologic information and seepage-related data from the middle nonlithophysal unit of the Topopah Spring tuff. Moreover, it only considers seepage under ambient thermal conditions. These limitations require the use of relatively large uncertainties in the subsequent TSPA calculations (Section 3.9.6).

3.9.5.2 Model Development

The SMPA follows the approach of the SCM (see Section 3.9.4 and CRWMS M&O (2000, U0080)) and the modeling framework described in Birkholzer et al. (1999, pp. 358–362) (CRWMS M&O 2000, U0075, Section 5). The model is based on the same assumptions already discussed in Section 3.9.4.3. The SMPA is a three-dimensional, heterogeneous fracture-continuum model 5.23 m long (corresponding to the waste package length plus 0.1 m spacing), 15 m wide (drift diameter is 5.5 m), and 20 m high. Gridblock size is 0.5 m × 0.5 m × 0.5 m. Additional information about the development of the SMPA can be found in CRWMS M&O (2000, U0075, Section 6.3).

3.9.5.3 Selection of Parameter Ranges and Case Studies

Table 3.9-1 shows four parameters identified as being relevant for long-term seepage predictions. Seepage is evaluated for each parameter combination at discrete points within the ranges indicated; three realizations of the heterogeneous property field were generated for each point in the four-dimensional parameter space. This can be considered an extensive sensitivity analysis. No probability distributions or parameter correlations need to be specified here; during the seepage abstraction (Section 3.9.6) and TSPA calculations, correlations are identified, and the seepage rates developed here are sampled following the probability distributions of the input parameters.

Table 3.9-1. Parameter Ranges for Which Seepage Is Evaluated Using the SMPA (Adapted from CRWMS M&O 2000, U0075, Section 6.3)

Parameter	Minimum	Maximum	Parameter Description
k, m^2	0.9×10^{-14}	0.9×10^{-11}	Mean permeability of fracture-continuum
$1/\alpha, Pa$	30	1000	van Genuchten's capillary-strength parameter
$\sigma_{\ln(k)}$	1.66	2.50	Standard deviation of log-permeability field
$Q_p, mm/yr$	5	500	Percolation flux

The permeability range is based on a review of air-permeability data from the niche studies (CRWMS M&O 2000, U0015, Section 6.1), the Single Heater Test area (Tsang and Birkholzer 1999, p. 393), pneumatic pressure signal analyses (Ahlers et al. 1999, pp. 47–68), and air-injection tests in four surface-based boreholes (LeCain 1997, pp. 2, 11–14) (CRWMS M&O 2000, U0075, Section 6.3.2).

The range of the capillary-strength parameter $1/\alpha$ covers the values obtained with the SCM (CRWMS M&O 2000, U0080, Table 10) and previously published values by Birkholzer et al. (1999, p. 354) (CRWMS M&O 2000, U0075, Section 6.3.4). The lower bound for the $\sigma_{\ln(k)}$ parameter, which reflects the degree of heterogeneity, is taken from the geostatistical analysis of post-excavation air-permeability data at Niche 3650 (CRWMS M&O 2000, U0080, Section 6.2.3).

Seepage is expected to increase with increasing variability in the heterogeneous permeability field, because local channeling effects and ponding probabilities are increased. Consequently, the range of $\sigma_{\ln(k)}$, which is a measure of heterogeneity, is examined for values higher than that obtained from the geostatistical analysis of the air-permeability data (CRWMS M&O 2000, U0075, Section 6.3.5).

Finally, seepage is evaluated for percolation fluxes as low as 5 mm/yr and as high as 500 mm/yr (CRWMS M&O 2000, U0075, Section 6.3.6). The latter accounts for a pluvial climate scenario as well as spatial and temporal focusing effects (Sections 3.9.3.1, 3.9.3.2, and 3.9.6.4). The rationale for selecting the parameter ranges shown in Table 3.9-1 is further discussed in Sections 6.3.2 through 6.3.4 of the AMR CRWMS M&O (2000, U0075).

Two parameter combinations were singled out for additional sensitivity studies. Parameter Set A is close to the base-case set given in Birkholzer et al. (1999, Table 1); Set B is close to the best-estimate parameter set obtained with the SCM, reflecting parameters of the EDZ (CRWMS M&O 2000, U0075, Section 6.3.5). Sensitivity studies were performed to examine the following parameters, processes, and features:

- The correlation length of the heterogeneous permeability field (three λ values).
- The van Genuchten parameter n (two n values).
- Correlation between capillary-strength parameter and permeability (Leverett scaling).
- Drift degradation (four scenarios).
- Episodic flow events.

Details about the different scenarios can be found in CRWMS M&O (2000, U0075, Sections 4.1, 6.3.5, 6.4, and 6.5).

3.9.5.4 Results

The seepage percentage—defined as the seepage flux divided by the average percolation flux over the drift footprint—is evaluated for three realizations of the permeability field at 240 points in the four-dimensional parameter space described in Section 3.9.5.3. The results confirm the expected behavior where seepage increases with decreasing permeability, decreasing capillary strength, and increasing percolation flux. The seepage flux is high and approaches the percolation flux only if the capillary barrier is weak (i.e., $1/\alpha$ is small), permeability is relatively low (smaller than 10^{-12} m²), or percolation flux is high. In all other cases, the capillary barrier effect results in seepage fluxes that are substantially lower than the corresponding percolation fluxes. Zero seepage is obtained for a relatively large portion of the examined parameter space.

The various sensitivity studies indicate the following trends:

- Seepage increases with increasing correlation length λ (CRWMS M&O 2000, U0075, Section 6.6.2). Note that the geostatistical analysis of the post-excavation air-permeability data (CRWMS M&O 2000, U0080, Section 6.2.2) support the choice of the base-case value with the smallest correlation length.
- Seepage is relatively insensitive to the van Genuchten parameter n (CRWMS M&O 2000, U0075, Section 6.6.3).
- Seepage tends to be higher if the capillary strength is correlated to permeability according to the Leverett scaling rule (CRWMS M&O 2000, U0075, Section 6.6.4).
- Drift degradation leads to increased seepage (CRWMS M&O 2000, U0075, Section 6.6.5).
- Episodic flow events result in averaged seepage fluxes that are higher than those obtained with constant percolation flux. However, transient effects from episodic flow events are not expected to be significant over most of the potential repository.

The detailed results can be obtained from Tables 6 through 8 of the report CRWMS M&O (2000, U0075). They are summarized and condensed as part of the PA seepage abstraction (see CRWMS M&O (2000, U0120) and Section 3.9.6 below).

3.9.6 Abstraction of Seepage into Drifts

3.9.6.1 Introduction and Objectives

Evaluating the impact of drift seepage on repository performance is complex because many of the effects previously discussed counteract one another. For example, seepage is more likely to occur (and seepage rate is generally higher) if the water percolating through the rock is focused into discrete flow channels. On the other hand, the stronger the focusing effect, the fewer

channels are developed, reducing the number of waste packages being affected by seepage. Similarly, the ability of the capillary barrier forming at the drift wall to divert some of the water around the opening is reduced if permeability is low, leading to higher seepage rates. At the same time, low-permeability rocks tend to exhibit stronger capillary forces, which increase the capillary-barrier effect, leading to reduced seepage rates. Because of this negative correlation, it is difficult to predict whether competent rock with few fractures leads to higher or lower seepage than less competent rock with a high fracture density or larger fracture apertures.

The situation is further complicated by the fact that the relationships between the degree of channeling and flow rate within an individual channel, the flow rate in a channel and seepage, seepage and corrosive damage, and finally corrosive damage and contaminant release are strongly nonlinear. Moreover, each of these relationships exhibits conceptual and parametric uncertainties.

Figure 3.9-7 shows schematically the relationships between some of the major seepage-relevant factors and their impact on repository performance. For example, if a given percolation flux is focused into a few flow channels (i.e., low seep frequency) the flux in each flow channel is relatively high (Figure 3.9-7a). This has the following two effects: (1) the number of waste packages affected by seepage is relatively small (Figure 3.9-7b), potentially reducing the negative impact of seepage; on the other hand, (2) the seepage threshold is likely to be exceeded and seepage fluxes in the affected area are relatively high (Figure 3.9-7c). High seepage rates can promote corrosion of engineered barriers, waste dissolution, and contaminant release from the affected waste package (Figure 3.9-7d). The total release of radionuclides is the product of the relatively high release rate and the relatively small number of waste packages being affected by seepage.

On the other hand, flow dispersion lead to relatively small local percolation fluxes that are potentially below the seepage threshold. As a result, seep flow rates can be expected to be low, and—depending on the distribution of percolation flux and seepage threshold—the seepage fraction is smaller or larger compared to the scenario with strong flow focusing. A detailed performance-assessment calculation must determine which of these factors dominate. Moreover, local conditions, uncertainties, and spatial variabilities must be propagated through these models to arrive at seepage probabilities and distributions for use in downstream TSPA models.

The seepage models discussed in Sections 3.9.4 and 3.9.5 focus on the determination of the seepage threshold and seepage rates for a given percolation flux (i.e., the relationship schematically shown in Figure 3.9-7c). Flow focusing and seep frequency (Figure 3.9-7a) and their impact on seepage fraction (Figure 3.9-7b) are accounted for in the abstraction (Section 3.9.6.4).

The presumption that seepage events are not localized and occur everywhere in the waste emplacement drifts (i.e., all waste packages encounter seepage), and that the seepage rate is equal to the percolation rate (i.e., no capillary-barrier effect exists, leading to maximum seepage rates), would be overly conservative. Consideration of a seepage threshold is beneficial for TSPA even if the seepage threshold value remains highly uncertain. Essentially, the occurrence of seepage is the product of two probabilities, namely the probability of experiencing high local percolation fluxes and the probability of encountering a drift segment with a low seepage

threshold. The situation is schematically shown in Figure 3.9-8. Given a certain percolation flux, the conditional probability for the capillary barrier to fail is indicated by the shaded area. While the failure probability increases with increasing percolation flux, the probability for reaching such high percolation fluxes decreases. The probability that the capillary barrier fails and seepage occurs can be determined by independently sampling from both the percolation-flux and seepage-threshold distribution, and by counting the number of realizations in which the percolation flux exceeded the seepage threshold. Even assuming a large uncertainty in the seepage threshold, the resulting seepage fraction will be less than one (the seepage fraction obtained by neglecting capillary-barrier effects).

A good understanding of seepage processes, an accurate determination of seepage-relevant formation parameters, and a careful estimation of seepage rates and seepage distribution are therefore some of the main objectives of the experimental, numerical, and analytical UZ studies at Yucca Mountain. A more detailed discussion of PA-related aspects of seepage can be found in CRWMS M&O (2000, U0120).

The purpose of the seepage abstraction is to put the information generated by the seepage process modeling in a form appropriate for use in TSPA for SR. The abstraction method is an extension of that employed for the TSPA for VA (DOE 1998, Sections 3.1.1.4, 3.1.2.4, and 3.1.3.3; CRWMS M&O 1998g, Sections 2.2.4, 2.4.4, and 2.5.2). The objective is to develop the framework for evaluating the amount of seepage of liquid water into potential repository emplacement drifts for TSPA simulations. Seepage is treated as a stochastic quantity in TSPA simulations by sampling values from generated probability distributions that represent the uncertainty and spatial variability of seepage. The process is schematically shown in Figure 3.9-9. Seepage has been evaluated as a function of percolation flux and k/α , a lumped parameter capturing the effectiveness of the capillary barrier. Probability density functions are prescribed for each of the two parameters. During a TSPA simulation, a large number of random values are generated based on these distributions. The seepage rate corresponding to each pair of random parameter values yields the probability density function of seepage into waste emplacement drifts. Note that the actual sampling procedure is more complicated as the potential repository is located in multiple units, and additional constraints and correlations must be observed.

The Monte Carlo simulation is basically an uncertainty analysis: each realization is taken to be equally likely, so any one of the realizations could be the "correct" one. The differences between one realization and another are within the range of uncertainty about each parameter that is varied. Some parameters, like fracture permeability or α parameter, are uncertain, so they vary from one TSPA realization to another; but they are also spatially variable, so they vary from location to location within each TSPA realization. TSPA calculations thus account for both uncertainty and spatial variability.

In Section 3.9.6.2, probability distributions of seepage are developed, combining the results of the SMPA with information about the relative likelihood of the various parameter combinations. In Section 3.9.6.3, adjustments for several perturbing physical processes are introduced. In Section 3.9.6.4, the results of the abstraction of drift seepage are summarized.

3.9.6.2 Initial Abstraction of Seepage Results

The SMPA was used to simulate seepage for a large number of parameter combinations (Section 3.9.5). Examination of the results reveals that seepage percentages are not strongly dependent on the standard deviation of the heterogeneous permeability field. In addition, similar seepage percentages were obtained for simulations with the same value of k/α (and common values of other parameters). Thus, for the abstraction analysis, seepage is treated as a function of k/α rather than of k and α separately. With these simplifications, seepage can be treated as a function of just two variables, namely k/α and percolation flux q .

The abstraction analysis focuses on two quantities: (1) the *seepage fraction*, f_s , which is the fraction of waste-package locations (model simulations) that have seepage (i.e., that have nonzero seepage percentage); and (2) the *seep flow rate*, Q_s , which is the volumetric flow rate of seepage in a drift segment. The seep flow rate is obtained from the seepage percentage by multiplying by the percolation flux and the area of a drift segment. For each modeled percolation flux q , and for all simulations with a common value of k/α , the seepage fraction and the mean and standard deviation of the seep flow rate are calculated.

The next step in the abstraction is to assign probabilities, or weights, to the two parameters. The distribution for k/α is obtained from the means and standard deviations of k (based on air-injection data) and α (based on SCM calibration results). Details of this procedure can be found in CRWMS M&O (2000, U0120, Section 6.2.2). The mean of k/α was determined to be $6 \times 10^{-11} \text{ m}^2 \text{ Pa}$. To account for uncertainty, a range of values is considered. The available information indicates that our uncertainty increases at higher values of k/α , so the range considered is skewed to higher values: values of k/α from one-half order of magnitude lower to one order of magnitude higher than $6 \times 10^{-11} \text{ m}^2 \text{ Pa}$ are considered. This is the range of values for the geometric mean of the distribution of k/α from location to location; in each case the standard deviation of the distribution of $\log(k/\alpha)$ from location to location is taken to be 0.32. As is implied by the use of logs, the spatial distribution of k/α values is taken to be log-normal.

Percolation flux q is not weighted at this stage. Percolation information is supplied with the appropriate spatial and temporal distribution during the actual TSPA simulations. All the results are thus given as a function of percolation flux. Given a distribution for k/α , a corresponding distribution can be developed for seepage. When the seepage information from the Seepage Model for PA is combined with the discrete distribution of k/α , weighted seepage statistics are obtained, representing the distribution of spatial variability of seepage within a TSPA realization.

3.9.6.3 Adjustments

The following adjustment are made to account for certain effects:

1. Distributions for the amount of seepage as a function of percolation flux are derived directly from seepage process-model results (CRWMS M&O 2000, U0075) and are constrained by measurements of permeability around three niches in the ESF (CRWMS M&O 2000, U0015, Section 6.1) and calibration of seepage tests conducted in one niche in the ESF (CRWMS M&O 2000, U0080,

Section 6.4). The derived distributions are summarized in Section 3.9.6.4; more details can be found in CRWMS M&O (2000, U0120, Section 6.2.4).

2. Seepage calculations for drifts with breakouts in the drift wall were performed with the SMPA (CRWMS M&O 2000, U0075, Section 6.4.3). These simulations suggested a moderate increase of drift seepage as a result of partial drift degradation. In the abstraction, seep flow rates calculated with the SMPA were increased by a conservative factor of 1.55 to account for the effects from partial drift degradation and rock bolts (CRWMS M&O 2000, U0120, Section 6.3.1).
3. The impact of the correlation between permeability and capillary strength on seepage was evaluated by the SMPA (CRWMS M&O 2000, U0075, Section 6.6.4). Using the Leverett scaling rule (Leverett 1941, p. 159) to relate capillary strength to local permeability variations yielded slightly higher seepage rates as compared to the rates obtained with a spatially constant α value. Seep flow rates calculated with the SMPA were therefore increased by 10% as an adjustment for the potential correlation of k and α (CRWMS M&O 2000, U0120, Section 6.3.2).
4. Distributions of the degree of flow focusing above the drifts are determined based on estimates of “weep” spacings implied by the active fracture model of UZ flow. Weep spacings were calculated by two methods to estimate lower and upper bounds for three net infiltration levels (mean, lower, and upper; see CRWMS M&O (2000, U0120, Section 6.3.3.1)). Both methods generate weep spacings that are approximately log-normally distributed. The distributions of weep spacings are used to define distributions of the flow-focusing factor, which is a multiplicative factor describing how much percolation flux might be increased over its average value at any given location. The flow-focusing factor is used to scale the percolation flux and the seepage fraction; it is log-uniformly distributed, with minimum of 1 in each case and maximum of 47 for the low-infiltration case, 22 for the base-infiltration case, and 9.7 for the high-infiltration case. This distribution of flow-focusing factors is an uncertainty distribution, which means that one value of it is sampled for each TSPA realization. That value is then applied to modify the spatial variability of seepage within the realization. Details can be found in CRWMS M&O (2000, U0120, Section 6.3.3.2).
5. Episodic flow could be accounted for through application of temporally varying percolation fluxes during the TSPA calculations in analogy to the use of spatial flow focusing factors. Since episodic flow events are damped by the PTn and are not expected to penetrate to the potential repository horizon, no adjustment is currently made.
6. Coupled processes (thermal-hydrologic, thermal-hydrologic-mechanical, and thermal-hydrologic-chemical) have generally been found to have limited impact (in terms of magnitude and time scale) on seepage or are beneficial. Currently, no adjustments are being made (see Section 4.2.1.1 and CRWMS M&O (2000, U0120, Sections 5 and 6.3.5)).

3.9.6.4 Abstraction Results

As discussed in Section 3.9.6.2, seepage is mainly a function of the ratio of geometric-mean fracture permeability k to fracture α parameter, k/α , and the uncertainty in this ratio is taken to be one order of magnitude above and one-half order of magnitude below the best-estimate value, which is $6 \times 10^{-11} \text{ m}^2 \text{ Pa}$. A triangular shape is chosen for the seepage uncertainty distributions. This distribution appropriately represents the key features desired, which are that seepage values for $k/\alpha = 6 \times 10^{-11} \text{ m}^2 \text{ Pa}$ are most likely and that k/α could be higher or lower, but those values are less likely to be representative of potential repository conditions.

Table 3.9-2 summarizes the seepage distributions as they vary with percolation flux. A seepage threshold of approximately 200 mm/yr, 15 mm/yr, and 5 mm/yr was found for minimum, peak, and maximum k/α values, respectively. Note that these values are the abstracted, conservatively estimated seepage rates, seepage fractions, and seepage thresholds for a waste emplacement drift with a 5.5 m diameter, taking into account uncertainty and spatial variability of the entire potential repository horizon. This has to be distinguished from the previously reported seepage-threshold estimate of 200 mm/yr (Section 3.9.4.7), which referred to a single location in the middle nonlithophysal zone and for an opening smaller than a waste emplacement drift. Additional details on the derivation of the values in this table and their interpretation may be found in CRWMS M&O (2000, U0120, Section 6.4). For values of percolation flux not in the table, linear interpolation or extrapolation was used.

Table 3.9-2. Uncertainty in Seepage Parameters as Function of Percolation (Table from CRWMS M&O 2000, U0120, Table 11)

q (mm/yr)	Minimum Value of k/α			Peak Value of k/α			Maximum Value of k/α		
	f_s	Mean $Q_s \text{ (m}^3\text{/yr)}$	Std. Dev. $Q_s \text{ (m}^3\text{/yr)}$	f_s	Mean $Q_s \text{ (m}^3\text{/yr)}$	Std. Dev. $Q_s \text{ (m}^3\text{/yr)}$	f_s	Mean $Q_s \text{ (m}^3\text{/yr)}$	Std. Dev. $Q_s \text{ (m}^3\text{/yr)}$
5	0	0	0	0	0	0	1.97×10^{-3}	3.21×10^{-3}	3.16×10^{-3}
14.6	0	0	0	2.45×10^{-3}	7.95×10^{-3}	7.09×10^{-3}	5.75×10^{-2}	2.26×10^{-2}	2.45×10^{-2}
73.2	0	0	0	0.250	0.106	0.198	0.744	0.404	0.409
213	4.91×10^{-3}	0.284	0.188	0.487	1.51	1.15	0.944	3.31	2.24
500	6.01×10^{-2}	0.992	1.05	0.925	5.50	4.48	0.999	13.0	5.74

NOTE: q is percolation flux, f_s is seepage fraction, and Q_s is seep flow rate.

The standard deviations of seep flow rate in Table 3.9-2 are relatively large. These large standard deviations result from the large differences in seepage from one set of simulations to another. For example, the weighted mean and standard deviation for $k/\alpha = 6 \times 10^{-11} \text{ m}^2 \text{ Pa}$ are a combination of the results for k/α values from 9×10^{-12} to $2.7 \times 10^{-10} \text{ m}^2 \text{ Pa}$ and over that range of k/α the mean seep flow rate at 73.2 mm/yr goes from zero to $0.408 \text{ m}^3\text{/yr}$. Thus, an amount of spatial variability in k/α corresponding to a log standard deviation of 0.32 (Section 3.9.6.2) translates into a relatively large spatial variability of seepage. This is consistent with the concept of seepage as a random process.

The effect of flow focusing is illustrated in Figures 3.9-10 and 3.9-11 for seepage fraction and mean seep flow rate, respectively. Each plot has four curves, for the flow-focusing factor F equal to 1 (no flow focusing), 5, 15, and 45. The $F = 1$ curves are based on the mean of the respective uncertainty distributions (for a triangular distribution, the mean is $(\text{min} + \text{peak} + \text{max})/3$, with min, peak, and max as listed in Table 3.9-2). The curves with higher values of F are generated from the $F = 1$ curves as described in CRWMS M&O (2000, U0120, Section 6.3.3.2). Increased flow focusing results in lower seepage fractions and higher seep flow rates. Note, however, that at very low percolation fluxes the seepage fraction is higher for higher focusing factors, because a percolation flux below the threshold for seepage can be boosted above the threshold by the focusing multiplier (CRWMS M&O (2000, U0120, Section 6.3.4)

3.9.7 Corroborative Evidence and Analog Studies

3.9.7.1 Calcite Depositions in Lithophysal Cavities

Observations of calcite and opal in lithophysal cavities in the Topopah Spring tuff were used to estimate long-term seepage rates into these small openings (CWRMS M&O 2000, U0085, Section 6.10.3). Calcite is assumed to precipitate from downward-percolating meteoric water because of (1) evaporation, (2) CO_2 outgassing as a result of the geothermal gradient, and (3) interaction with a gas phase containing less CO_2 than the gas with which the water was last equilibrated. Considering these calcite-precipitation mechanisms and assuming certain water-to-calcite ratios, seepage into lithophysal cavities was estimated from calcite-deposition data. This analysis shows that (1) not all lithophysal cavities encountered seepage and (2) seepage flux is a very small fraction of percolation flux. Both conclusions corroborate the general concept and the findings of the drift-seepage studies discussed in Sections 3.9.1 through 3.9.5. Specifically, they support the concept of a capillary barrier reducing seepage over percolation flux. Note that the seepage threshold for small cavities may be significantly higher than for a large waste emplacement drift.

The presence of lithophysal cavities does not directly impact seepage into a waste emplacement drift. However, there is a second-order, indirect effect. On account of the capillary barrier effect, lithophysal cavities are partial obstacles to downward flow of water. Consequently, their presence may lead to local, small-scale flow channeling, which could induce increased seepage. Lithophysal cavities also increase the roughness of the drift wall. Both effects are accounted for through the use of conservative flow focusing factors and safety factors for drift roughness.

3.9.7.2 Rainier Mesa

Rainier Mesa, located approximately 30 km northeast of Yucca Mountain, is underlain by a sequence of welded and nonwelded tuffs similar to those that underlie Yucca Mountain. Precipitation is about double the mean at Yucca Mountain, and percolation is estimated to be about eight percent of precipitation (Wang et al. 1993, p. 676). Most of the Rainier Mesa tunnels were constructed in the zeolitic tuffs, which are believed to be near full saturation. Faults and joints are abundant in these zeolitic-bedded tuffs. When intersected by tunnels, some of these joints and especially through-going faults have yielded significant amounts of water. The seeping features are thought to be pathways for flow from a perched water zone above the zeolitic horizon. Seepage water is geochemically similar to meteoric water and is associated with fast-

flow paths. Seepage at Rainier Mesa occurs only in tunnels constructed in the zeolites; no seepage is observed in the tunnel intersecting the vitric tuff units. These observations suggest that seepage into tunnels may be localized and restricted to certain flow paths and units. This corroborates the modeling results, which indicate that the seepage fractions are less than one. More details can be found in CRWMS M&O (2000, U0135, Section 6.5.1.2) and Wang et al. (1993, pp. 675–681).

3.9.7.3 Altamira

Seepage into caves can be used as a natural analog for seepage into waste emplacement drifts. Unfortunately, most caves are part of a karst system found in limestone formations in the saturated zone or in zones of significantly higher percolation fluxes than those expected at Yucca Mountain. The caves near Altamira, Spain are located in the unsaturated zone of a fractured limestone bedrock with clay-rich layers. Precipitation is approximately ten times higher than at Yucca Mountain. Nevertheless, seepage rates into the caves are estimated to be a small fraction of the expected percolation flux. Moreover, there are essentially no fluctuations in the observed seepage rates despite the fact that the unsaturated zone is only about 7 m thick and evapotranspiration is expected to exceed precipitation for a few months out of the year. More details can be found in Villar et al. (1985, pp. 21–24).

3.9.7.4 Absence of Seepage into Sealed Drift Segments

Currently, no natural seepage into the ESF has been observed. Furthermore, no construction water was observed to seep into the ESF Main Drift as the tunnel boring machine passed the cross-over point during the excavation of the ECRB Cross Drift. However, evaporation and moisture removal through ventilation of the ESF is likely to be larger than potential seepage rates, preventing direct observation of liquid water dripping into the drift.

As described in Section 2.2.2.2.1, an approximately 100 m long segment of Alcove 7 and an approximately 1,000 m long segment of the ECRB Cross Drift have been sealed by bulkheads to isolate them from ventilation. No seepage has been observed so far in either of these two drift segments. The absence of visible seepage in sealed-off drift segments corroborates the modeling results which estimate that present-day percolation fluxes are likely to be smaller than the prevailing seepage thresholds.

3.9.8 Alternative Conceptual Models

3.9.8.1 Discrete Fracture Network Model

A discrete fracture network model (DFNM) is an alternative conceptual model to the heterogeneous fracture continuum model (Pruess et al. 1999, pp. 307–309). The DFNM has the advantage of being intuitively more appealing for seepage predictions. A high-resolution DFNM model is capable of generating channelized flow and discrete seepage events. The development of a defensible DFNM requires collecting a very large amount of geometric and unsaturated hydrologic property data. While part of the required geometric information can be obtained from fracture mappings, the description of the network remains incomplete and potentially biased. Moreover, unsaturated hydrologic parameters on the scale of individual fractures are required, along with conceptual models and simplifying assumptions regarding unsaturated flow within

fractures and across fracture intersections. These databases required to develop a DFNM are currently not available. As a result, the cumulative effect of all the input uncertainties is likely to outweigh the apparent advantage of a detailed representation of the fracture network.

In general, the choice of a conceptual model for seepage predictions should be based on a careful consideration of the study objectives, the available database in comparison with the data needs, the uncertainties in the input parameters, and the corresponding prediction uncertainties, as well as computational aspects. The appropriateness of using a fracture-continuum model for the prediction of effective seepage quantities was demonstrated in CRWMS M&O (2000, U0080, Section 5.3).

3.9.8.2 Seepage Governed by Ponding Probability

As an alternative conceptual model to a seepage process model, Birkholzer et al. (1999, pp. 372–379) related seepage to the local ponding probability, which was derived from the variability of the permeability field. Their approach assumed that in strongly heterogeneous formations, seepage is predominantly affected by pressure variations governed by local heterogeneity rather than the presence and geometry of the capillary barrier. This is different from the behavior in a homogeneous system, where the geometry of the capillary barrier has a strong impact on seepage (Philip et al. 1989, pp. 16–28). Strong medium- to small-scale heterogeneities tend to increase seepage as they increase channeling and local ponding. This effect is included in the current seepage process models through the estimation of effective, seepage-specific parameters. While the approach presented by Birkholzer et al. (1999, pp. 372–379) and discussed in CRWMS M&O (2000, U0075, Section 6.7) may provide guidelines for how to extrapolate seepage predictions to other units or drift geometries, it nonetheless requires a calibration step similar to that described in Section 3.9.4.

3.9.9 Summary and Conclusions

Seepage into waste emplacement drifts is considered a key factor affecting the performance of a potential high-level nuclear waste repository at Yucca Mountain, Nevada. Theoretical analyses, numerical modeling studies, field testing, and observations at analog sites suggest that seepage into underground openings excavated in unsaturated formations is smaller than the local percolation flux. This is mainly a result of capillary pressure holding water in the formation, diverting it around and preventing it from entering the openings. The effectiveness of this capillary barrier depends on the percolation flux itself, the hydrogeologic properties of the formation, and the geometry of the drift.

A sequence of models was used to predict seepage fraction, seepage threshold, and seep flow rate for waste emplacement drifts. A seepage process model was calibrated against seepage-relevant data from liquid-release tests. Seepage rates were then calculated over a wide range of parameter values and compiled in an abstraction process. Finally, probability distributions of the key parameters were introduced and conservative assumptions were made to arrive at probabilities for seepage into waste emplacement drifts.

These analyses indicate that seepage fluxes are lower than percolation fluxes, even under conservative assumptions, and that only a fraction of the waste packages will encounter seepage. However, seepage predictions remain uncertain.

Figure 3.9-12 summarizes qualitative and quantitative results pertaining to the issues discussed in Section 3.9.3. The results reflect the values obtained after the TSPA abstraction.

3.10 DRIFT-SCALE THERMAL-HYDROLOGICAL-CHEMICAL PROCESSES AND MODELS

3.10.1 Introduction

The purpose of this section is to describe (1) the conceptual model and input data for coupled thermal, hydrological, and chemical (THC) processes; (2) the Drift Scale Test (DST) THC Model; (3) the THC Seepage Model; and (4) the abstractions done by Performance Assessment on the results of the THC Seepage Model. The conceptual model for THC processes provides a comprehensive basis for modeling the pertinent mineral-water-gas reactions in the host rock under thermal loading conditions, as they influence the water and gas chemistry that may enter drifts over 100,000 years. The purpose of the DST THC Model is to validate the conceptual model and input data by comparison of measured gas and water chemistry from the DST to the results of simulations. The purpose of the THC Seepage Model is to evaluate the effects of THC processes in the rock around emplacement drifts on the possible seepage-water chemistry, gas-phase composition, and the potential effects of THC processes on unsaturated zone (UZ) flow and transport. This model was used to evaluate the effects of mineral dissolution and precipitation, the effects of CO₂ exsolution and transport in the region surrounding the drift, the potential for forming zones of calcite, silica, or other minerals, the resulting changes to porosity, permeability, and the potential effects on seepage. The THC Seepage Model and validation of the data and processes using the DST are treated in the Analysis/Model Report (AMR) *Drift-Scale Coupled Processes (DST and THC Seepage) Models* (CRWMS M&O 2000, N0120/U0110).

3.10.2 Thermal-Hydrological-Chemical Conceptual Model

The THC conceptual model underlies the numerical simulations of THC processes in the DST THC Model and in the THC Seepage Model. The conceptual model must be able to describe processes involving liquid and vapor flow, heat transport, and thermal effects resulting from boiling and condensation, transport of aqueous and gaseous species, mineralogical characteristics and changes, and aqueous and gaseous chemistry. A conceptual model of reaction-transport processes in the fractured welded tuffs of the potential repository host rock must also account for the different rates of transport in very permeable fractures compared to the much less permeable rock matrix (see for example, Steefel and Lichtner 1998, pp. 186–187).

In addition to the unsaturated hydrological properties required to simulate THC processes in the UZ, the data necessary for the evaluation of THC processes include the initial and boundary water and gas chemistry, the initial mineralogy, mineral volume fractions, reactive surface areas, equilibrium thermodynamic data for minerals, aqueous and gaseous species, kinetic data for mineral-water reactions, and diffusion coefficients for aqueous and gaseous species. The following subsections describe the conceptual model for thermal-hydrological (TH), geochemical, and coupled THC processes in the fractured tuffs.

3.10.2.1 TH Processes

TH processes in the fractured welded tuffs at Yucca Mountain have been examined theoretically and experimentally since the early 1980s (Pruess et al. 1984; Pruess et al. 1990a, pp. 1235–1248;

Buscheck and Nitao 1993, pp. 418–448; Pruess 1997, pp. 335–372; Tsang and Birkholzer 1999, pp. 385–425; Kneafsey and Pruess 1998, pp. 3349–3367). A conceptual model showing the important TH processes occurring around a drift (as derived through these studies and through observations of the Single Heater Test and the DST) is shown in Figure 3.10-1. To summarize the processes as depicted in the figure, heat conduction from the drift wall into the rock matrix results in vaporization and boiling, with vapor migration out of matrix blocks into fractures. The vapor moves away from the drift through the permeable fracture network by bouyancy, by the increased vapor pressure caused by heating and boiling, and through local convection. In cooler regions, the vapor condenses on fracture walls, where it drains through the fracture network either down toward the heat source from above or away from the drift into the zone underlying the heat source. Slow imbibition of water from fractures into the matrix gradually leads to increases in the liquid saturation in the rock matrix. Under conditions of continuous heat loading, a dryout zone may develop closest to the heat source separated from the condensation zone by a nearly isothermal zone maintained at about the boiling temperature. Where this nearly isothermal zone is characterized by a continuous process of boiling, vapor transport, condensation, and migration of water back to the heat source (either by capillary forces or gravity drainage), this zone may be termed a heat pipe (Pruess et al. 1990a, pp. 1235–1248).

The design shown in Figure 3.10-1 includes backfill; however, this conceptual model is not dependent on the presence of backfill. A design change was made in January 2000 that removed backfill from the reference design. Qualitatively, this change does not affect the TH processes occurring in the rock around the drifts; however, the absence of backfill may result in a different temperature distribution at the drift wall and different times of maximum drift-wall temperature, maximum dryout and rewetting. These different rates of heating would affect the time variation of water and gas chemistry around the drifts.

3.10.2.2 Effects of TH Processes (Boiling, Condensation, and Drainage) on Water and Gas Chemistry and Mineral Evolution

The chemical evolution of waters, gases, and minerals is intimately coupled to the TH processes discussed in the previous section. The distribution of condensate in the fracture system determines where mineral dissolution and precipitation can occur in the fractures and where there can be direct interaction (via diffusion) between matrix pore waters and fracture waters. Figure 3.10-2 shows schematically the relationships between TH and geochemical processes in the zones of boiling, condensation, and drainage in the rock mass outside of the drift and above the heat source.

One important aspect of the system is the exsolution of CO_2 out of the liquid phase as temperature increases. The exsolution and transport of CO_2 out of the boiling zone results in a local increase in pH and a decrease in pH in the condensation zone into which the vapor enriched in CO_2 is transported. The extent to which the pH is shifted depends strongly on the rates of mineral-water reactions, which can buffer the change in pH. Because the diffusivities of gaseous species are several orders of magnitude greater than those of aqueous species, and because the advective transport of gases can be more rapid than that of liquids, the region where CO_2 degassing affects water and gas chemistry could be much larger than the region affected by transport of aqueous species.

Effects of TH processes on water chemistry are varied and depend on the behavior of the dissolved species and their relation to mineral-water reactions. Conservative species (i.e., those that are unreactive and nonvolatile), such as chloride (Cl^-), become concentrated in waters undergoing vaporization or boiling, but are absent from the vapor condensing in the fractures. Therefore, the concentration in the draining condensate waters is determined by mixing with fracture pore waters and interaction with matrix pore waters via diffusion. Concentrations of aqueous species, such as Ca^{+2} , are also affected by calcite dissolution or precipitation as well as reactions involving Ca-bearing zeolites, clays, and plagioclase feldspar.

Zonation in the distribution of mineral species may occur as a result of varied temperature effects on mineral solubility. The inverse relation between temperature and calcite solubility (as opposed to the silica phases, which are much more soluble at higher temperatures) may cause zonation in the distribution of these phases in the condensation and boiling zones (Figure 3.10-2). Precipitation of amorphous silica or another silica phase is likely to be confined to a narrower zone where evaporative concentration from boiling exceeds its solubility. Hence, calcite may precipitate in fractures over a broad zone of elevated temperature and where CO_2 has exsolved due to temperature increases or boiling. Alteration of feldspars to clays and zeolites is likely to be most rapid in the boiling zone because of their increased solubility (as well as dissolution and precipitation rates) at higher temperatures (Lasaga 1998, p. 66). In drainage zones, there may also be zonation in mineral alteration within the rock matrix adjacent to the fracture similar to that observed as a function of distance along the transport path (Steefel and Lichtner 1998, pp. 186–199).

3.10.2.3 Effects of Infiltration and Climate Changes on THC Processes

Early in the thermal history of the potential repository, much of the chemistry of the UZ around drifts will be constrained by the chemistry of ambient fracture and matrix pore water, which may change the concentration as a result of boiling, by dilution with condensate water, or by mineral-water-gas reactions. Once the peak thermal period has subsided, percolating water mixes with the condensate water above the potential repository and eventually rewets the dryout zone. The composition of the percolating waters (before mixing) may be similar to that presently found above the potential repository as matrix pore water, or it may reflect more dilute water, from a wetter climate, that has traveled through fractures. Changes in the percolation flux also affect the extent of mineral deposition and dissolution, because of the changes in the flux of dissolved species to the region around drifts. For example, the greater the flux of Ca, the more calcite would be precipitated, at a given concentration. Higher percolation fluxes could increase the dissolution rates of minerals that are undersaturated in the fluid, because it can increase the degree to which the mineral is undersaturated.

3.10.2.4 Hydrologic Property Changes in Fractures and Matrix

Mineral precipitation and dissolution in fractures and matrix have the potential for modifying the porosity, permeability, and unsaturated hydrologic properties of the system. Because the molar volumes of minerals created by hydrolysis reactions (i.e., anhydrous phases, such as feldspars, reacting with aqueous fluids to form hydrous minerals, such as zeolites or clays) are often larger than the molar volumes of the primary reactant minerals, dissolution-precipitation reactions can often lead to porosity reductions. The extent of mineral-water reactions is controlled by the

surface areas of the mineral phases in contact with the aqueous fluid, and the distribution of minerals in the fractures is heterogeneous. Therefore, changes in porosity and permeability caused by these processes may also be heterogeneously distributed. Other factors that may lead to heterogeneity in property changes are the distribution of liquid saturation in fractures, the proportion of fractures having actively flowing water, and the rates of evaporative concentration due to boiling, which may change the dominant mechanisms of crystal growth and nucleation.

As summarized in the preceding subsection, the conceptual model for THC processes incorporates a wide range of coupled physical and chemical processes. The following subsection deals with the implementation of this conceptual framework into a quantitative numerical model.

3.10.3 Modeling Approach, Assumptions, Inputs and Outputs

The flow of information between various models and data sources and the DST THC Model and THC Seepage Model is presented in Figure 3.10-3. The DST THC Model takes its inputs from the DST TH Model, the Calibrated Properties Model (CPM; CRWMS M&O 2000, U0035), and numerous sources of geochemical data (Geochemical Data) as discussed in CRWMS M&O (2000, N0120/U0110). Geochemical Data include mineral abundances and compositions, and water and gas chemistry. The THC Seepage Model obtains its inputs from the Calibrated Properties Model (CPM), Geochemical Data, and also Repository Design (CRWMS M&O 1999e; CRWMS M&O, EBS PMR, Section 2.5) and the UZ Flow and Transport Model (Flow and Transport; CRWMS M&O 2000, U0050). Repository Design provides the data on in-drift geometry and drift spacing, and the thermal and hydrological properties of Engineered Barrier System components. The UZ Flow and Transport Model provides the hydrogeologic layer boundaries and pressure and temperature boundary conditions. Results of sensitivity studies on mineral assemblages and conceptual model validation in the DST are used to guide the development and analysis of the THC Seepage Model. However, direct numerical output from the DST THC Model is not used in the THC Seepage Model. Output data from the THC Seepage Model are abstracted for use in Total System Performance Assessment (TSPA) and discussed further in Section 3.10.11.

The following subsections describe in more detail the implementation of the conceptual model as a mathematical description of THC processes in the fractured tuffs. Data that form the basis of the DST THC and THC Seepage models are also discussed.

3.10.3.1 Dual-Permeability Model For Reaction-Transport Processes

To handle separate yet interacting processes in fractures and matrix, the dual-permeability method was adopted for all aspects of the system (flow, transport, and reaction). Transport rates greater than the rate of chemical equilibration via diffusion necessarily lead to disequilibrium in water chemistry between fractures and matrix. This can lead to differences in dissolution/precipitation rates and therefore the rate of change in porosity and permeability between the two media. Because the system is unsaturated and undergoes boiling, the transport of gaseous species is an important consideration. The model must also capture the differences between initial mineralogy in fractures and matrix and their evolution. In the dual-permeability method, each gridblock is separated into a matrix and fracture continuum, each of which is

characterized by its own pressure, temperature, liquid saturation, water and gas chemistry, and mineralogy.

The fracture continuum is considered as separate from but interacting with the matrix continuum, in terms of the flow of heat, water, and vapor through advection and conduction. Aqueous and gaseous species are transported via advection and molecular diffusion between fractures and matrix. It is assumed that the dual-permeability approach, with appropriate material and fracture properties and an appropriate discretization of time and space, is a sufficiently accurate approximation of the real world for the spatial scales of interest. The dual-permeability approach for modeling hydrologic processes in fractured porous media is also discussed in Section 3.4. This approach is validated by the comparison of measured geochemical data to results of simulations presented in CRWMS M&O (2000, N0120/U0110), and as discussed in Section 3.10.4.

3.10.3.2 Active Fracture Model For Reaction-Transport Processes

The active fracture model (Liu et al. 1998; CRWMS M&O 2000, U0030, Section 6.4.5) has been used in many of the modeling studies described in this report. Because a major intent of the method is to modify the fracture-matrix area for the liquid phase as a function of the liquid saturation, for consistency the active fracture model should also be used for the calculation of the surface area of minerals on fracture walls in contact with the liquid phase. The reference saturation for the active fracture model is the residual liquid saturation, below which flow is considered to be absent. However, mineral-water reactions are expected to occur at all saturations above zero. Therefore, a modification of the active fracture model was implemented for mineral-water reactions, such that the reference saturation was taken as a small value (1×10^{-4}), consistent with that implemented for mineral-water reactions and transport near conditions of complete dryout. This value is approximately a cutoff at which evaporative concentration increases the ionic strength of the residual porewater to values outside the range of the validity of thermodynamic relationships for dilute systems.

3.10.3.3 Equilibrium and Kinetic Models for Mineral–Water–Gas Reactions

Mineral-water reactions are considered to take place under kinetic or equilibrium conditions. The methods used to express the kinetic and equilibrium reactions are described in CRWMS M&O (2000, N0120/U0110) and are similar to those described in Reed (1982, pp. 513–528) and Steefel and Lasaga (1994, pp. 529–592). Because the dissolution rates of many mineral-water reactions are quite slow, most phases were treated using pseudo-first-order reaction kinetics. Data for kinetic mineral-water reactions were derived from published experimental data. Gas species, such as CO_2 , were treated as ideal mixtures of gases in equilibrium with the aqueous solution.

3.10.3.4 Initial and Infiltrating Water and Gas Chemistry and Mineralogy

The initial water chemistry for the DST THC Model and the THC Seepage Model was an average of measurements made of pore waters from Alcove 5, near the Drift Scale Test (CRWMS M&O 2000, N0120/U0110, Section 6.1.2). The chemistry of this water is given in Table 3.10-1.

Table 3.10-1. TSw Porewater Composition and CO₂ Partial Pressure (CRWMS M&O 2000, N0120/U0110, Table 3)

Parameter	Units	Concentration
pH (at 25°C)	pH Units	8.32
Na	mg/L	61.3
SiO ₂ (aq)	mg/L	70.5
Ca	mg/L	101
K	mg/L	8.0
Mg	mg/L	17
Al	mg/L	9.92x10 ⁻⁷ (1)
Fe	mg/L	6.46x10 ⁻⁸ (2)
HCO ₃ ⁻ (3)	mg/L	200
Cl	mg/L	117
SO ₄	mg/L	116
F	mg/L	0.86
CO ₂ (gas) (4)	Pa	85.2

NOTES: (1) Calculated by equilibrating with Ca-smectite at 25°C.
 (2) Calculated by equilibrating with hematite at 25°C.
 (3) Total aqueous carbonate as HCO₃⁻, calculated from charge balance.
 (4) Calculated at equilibrium with the solution at 25°C.

The infiltrating water chemistry could be chosen from either the porewater chemistry in the UZ at or above the potential repository horizon or from a more dilute composition found in the perched water or saturated zone (e.g., J-13 water). The perched waters are much more dilute than UZ pore waters (CRWMS M&O 2000, U0085, Tables 6 and 8), and isotopic compositions (³⁶Cl/Cl, ¹⁸O/¹⁶O, D/H, ¹⁴C) and Cl concentrations also suggest the presence of a large proportion of late Pleistocene/early Holocene water (Levy et al. 1997, p. 906; Sonnenthal and Bodvarsson 1999, pp. 107–108; CRWMS M&O 2000, U0085, Table 9). Consequently, we assume that the infiltrating water and the water in the fractures have the same chemical composition as the matrix pore water. The sample chosen was collected from Alcove 5 near the DST and is listed in Table 3.10-1. Analyses of PTn pore waters (and some at the top of the TSw) and many Cl analyses of TSw pore waters are consistent with this interpretation (Sonnenthal and Bodvarsson 1999, pp. 140–141; CRWMS M&O 2000, U0085, Table 6).

The minerals, aqueous and gaseous species shown in Table 3.10-2 include the major phases found in fractures and the matrix in the TSw and others that are likely to occur under thermally perturbed conditions, based on their occurrence in deeper zeolitized units (denoted Case 1). Two sets of geochemical species were chosen, so that the sensitivity to the mineral assemblage could be evaluated, and additional information could be obtained for PA abstractions. Case 2 represents a smaller set of species and minerals (calcite, gypsum, silica phases) that captures

many basic aspects of the DST water and gas chemical evolution, such as the pH and gas-phase CO₂ concentrations, but neglects Al, Fe, and F-bearing aqueous species and minerals. Simulations of the DST and the THC Seepage Model considered both geochemical cases.

Table 3.10-2. Model Mineral Assemblage, Aqueous and Gas Species (Full Geochemical System; CRWMS M&O 2000, N0120/U0110, Table 7)

Species	Minerals
Aqueous:	
H ₂ O	Calcite
H ⁺	Tridymite
Na ⁺	α-Cristobalite
K ⁺	Quartz
Ca ⁺²	Amorphous Silica
Mg ⁺²	Hematite
SiO ₂	Fluorite
AlO ₂ ⁻	Gypsum
HFeO ₂ ⁺³	Goethite
HCO ₃ ⁻	Albite
Cl ⁻	Microcline
SO ₄ ⁻²	Anorthite
F ⁻	Ca-Smectite
	Mg-Smectite
Species	Minerals
Gas:	Na-Smectite
CO ₂	K-Smectite
	Illite
	Kaolinite
	Sepiolite
	Stellerite
	Heulandite
	Mordenite
	Clinoptilolite
	Volcanic Glass

3.10.3.5 Relations for Mineral Reactive Surface Areas

Reactive surface areas of minerals on fracture walls were calculated from the fracture-matrix interface area/volume ratio, the fracture porosity, and the derived mineral volume fractions (CRWMS M&O 2000, N0120/U0110, Section 6.1.5.1). The fracture-matrix interface areas and

fracture porosities for each unit were taken from the drift-scale calibrated properties set (CRWMS M&O 2000, U0050, Section 6.2). These areas were based on the fracture densities, fracture porosities, and mean fracture diameter. The wall of the fracture is treated as a surface covered by mineral grains having the form of uniform hemispheres.

Mineral surface areas in the rock matrix were calculated using the geometric area of a cubic array of truncated spheres that make up the framework of the rock (CRWMS M&O 2000, N0120/U0110, Section 6.1.5.2). Clay minerals are considered as coatings of plate-like grains. The grains forming the framework of the rock matrix are considered to be the primary high-temperature phases of the tuff (i.e., quartz, cristobalite, tridymite, and feldspars). The abundance of secondary phases (i.e., those that formed as alteration products or low-temperature coatings on the primary assemblage), such as clay minerals, is used to reduce the free surface area of the framework grains.

3.10.3.6 Relations for Hydrological Property Changes

Changes in porosity, permeability, and capillary pressure as a result of mineral precipitation and dissolution are treated in CRWMS M&O (2000, N0120/U0110, Sections 6.1.6.2–6.1.6.3). Porosity changes in matrix and fractures are directly tied to the volume changes resulting from mineral precipitation and dissolution. Fracture-permeability changes are approximated using the porosity change and an assumption of plane parallel, fractures of uniform aperture (cubic law; Steefel and Lasaga 1994, p. 556). Although this is a gross simplification of the fracture geometry, it is not possible to predict the actual form and distribution of mineral precipitates at a very small scale. This is because of the many complexities of the fracture geometry and the very complex nature of mineral nucleation and growth under changing physical and chemical conditions. Thus, the permeability changes are only approximate. Matrix permeability changes are calculated from changes in porosity using ratios of permeabilities calculated from the Carmen-Kozeny relation (Bear 1988, p. 166) and ignoring changes in grain size, tortuosity, and specific surface area. Because of the exceedingly small initial matrix permeabilities of the welded Topopah Spring tuff, simplification in the matrix relations is immaterial. If mineral precipitation caused very substantial changes in permeability, or the permeability of the fracture system was already very low, then it would be necessary to treat the relations between permeability changes and porosity changes more rigorously. Changing permeability and porosity also induces changes in the unsaturated flow properties of the rock. Therefore, the capillary pressure is modified using the Leverett scaling relation (Slider 1976, p. 280).

3.10.3.7 Basis for Numerical Code TOUGHREACT V2.2

The geochemical module incorporated in TOUGHREACT V2.2 (described in Section 1.3.2.3) simultaneously solves a set of chemical mass-action, kinetic-rate expressions for mineral dissolution/precipitation, and mass-balance equations. Implementation of multiphase flow and heat transport for dual-permeability media is equivalent to TOUGH2 V1.4, which was used for other UZ flow calculations and TH calculations (CRWMS M&O 2000, U0050) and for TH calculations of the DST. TOUGHREACT V2.2 provides the extent of reaction and mass transfer between a set of given aqueous species, minerals, and gases at each gridblock of the flow model (Xu and Pruess 1998; Xu et al. 1998). Equations for heat, liquid and gas flow, aqueous and gaseous species transport, chemical reactions, and permeability/porosity changes are solved

sequentially (e.g., Steefel and Lasaga 1994, p. 550). It is assumed that the physical properties of the gas phase are unaffected by changes in the partial pressure of CO₂ resulting from heating, calcite reactions, and gas-phase transport. This assumption is justified by the results of the DST and THC Seepage Model runs, which show that the volume fraction of CO₂ is generally less than 5% and always less than 10% (CRWMS M&O 2000, N0120/U0110).

3.10.4 DST THC Model Results and Validation

The DST is the second underground thermal test being carried out in the Exploratory Studies Facility (ESF) at Yucca Mountain, Nevada. The purpose of the test is to evaluate the coupled thermal, hydrological, chemical and mechanical processes that take place in unsaturated fractured tuff over a range of temperatures from approximately 25°C to 200°C. The heaters were activated in December 1997 and are planned to run for 4 years followed by a 4 year cooling period.

Simulation of DST THC processes provides an important validation test for the THC conceptual models and input data used in the THC Seepage Model (Figure 3.10-3) for a much longer time scale. Geochemical input parameters have not been calibrated to measured data collected during the DST and therefore the DST THC Model simulations are an independent test of the conceptual model and input data used also in the THC Seepage Model. Detailed analysis of THC processes in the DST and validation tests are presented in CRWMS M&O (2000, N0120/U0110). This validation process involves examination of areas of modeled fracture drainage compared to the locations where water was collected during the test, the comparison of CO₂ concentrations collected from sampled gases, and comparison of the chemistry of waters collected from boreholes over time. These validation exercises are continuing as more data are collected from the DST and the models are improved to represent the physical and chemical processes more accurately. The following subsection compares modeling results to measured CO₂ concentrations collected from boreholes. Brief descriptions of the evolution of the water chemistry and mineralogy follow.

3.10.4.1 Gas-Phase CO₂ Evolution

In the first test, CO₂ concentrations measured in gas samples taken from boreholes during the DST are compared to simulation results using the DST THC Model. It is very important to capture changes in gas-phase CO₂ concentrations because they strongly control the pH of condensate waters, they are sensitive to temperature, and CO₂ transport is sensitive to the fracture hydrologic properties. CO₂ also affects HCO₃⁻ concentrations in fracture waters, which are important for the in-drift geochemical environment. Modeled distributions of CO₂ concentrations and temperature in fractures and matrix are shown after 6 and 20 months of heating (which are also times for which CO₂ measurements are available) in Figure 3.10-4 for the calcite-silica-gypsum geochemical system (Case 2). At both times, and in both fractures and matrix, a halo of increased CO₂ concentrations appears centered approximately at the 60°C isotherm. Over the 14-month period, between 6 months and 20 months, the halo increases considerably in extent and magnitude.

To evaluate how the model predicts the time evolution of CO₂ concentrations in the gas phase, measured CO₂ concentrations from intervals that were repeatedly sampled from February 1998

to August 1999 (20 months) are compared to model results for the same times. Figure 3.10-5 shows the time evolution of CO₂ concentrations in borehole intervals 74-3, 75-3, 76-3, and 78-3 (see Figure 3.10-4 for locations of borehole intervals). In borehole interval 74-3, there were only grid nodes above (cooler side) and below (hotter side) the interval, and therefore results from both nodes are plotted to see if they bracket the measured compositions. In borehole interval 78-3, two locations (center and end) were chosen, because of the strong thermal gradient across this region. The comparison shows that the simulations generally follow the trends in measured CO₂ concentrations. Two exceptions are when a known heater power loss occurred (around 19 months; see slope change in 74-3 and 75-3 at 20 months) or when the samples were at boiling temperatures and were nearly all water vapor (instead of air) and had much of the water condensed out during sampling (76-3 and 78-3, largest peaks). In the latter case, the modeling results should diverge from the measured data, because they reflect the CO₂ concentration for the full water vapor-air mixture. This effect is discussed in CRWMS M&O (2000, N0120/U0110, Section 6.2.7.2).

3.10.4.2 Water Chemistry Evolution

The modeled chemistry of waters in fractures is shifted from an initial pH of about 8.3 to 6.5, and is captured as changes in time and space. The lowest modeled pH values are in the region of highest gas-phase CO₂ concentrations. The shift in pH in the modeled fracture water is similar to that observed in the water collected from hydrology boreholes at the same times and in the expected regions during the DST (CRWMS M&O 2000, N0120/U0110), which were also areas of high gas-phase CO₂ concentrations. Chloride concentrations in waters collected from hydrology boreholes are considerably more dilute (a factor of 5 to 10) than the matrix pore water, which was also predicted by the modeling. Other species such as Ca and Si show similar trends in the modeled fracture water compositions compared to measured water compositions. Additional information on water chemistry can be found in CRWMS M&O (2000, N0120/U0110).

3.10.4.3 Mineralogical Changes

In the model simulations, calcite is the major phase forming in the zone above the heaters, although the abundances are exceedingly small. Secondly, amorphous silica also precipitates, but is much less abundant compared to calcite. No direct observation of the precipitation or dissolution of calcite has been found because the DST is ongoing; however, trends such as decreasing Ca in water found in boreholes with increasing temperature, pH and silica concentrations are strongly suggestive of calcite precipitation (CRWMS M&O 2000, N0120/U0110, Table 9). Fracture porosity changes in the DST simulations are very small after 20 months of simulation (on the order of 0.01%) and follow closely the area of calcite precipitation (CRWMS M&O 2000, N0120/U0110, Figure 17). Such small changes likely have no measurable effect on the hydrologic properties of the rock. More data are being collected from the DST, including ¹⁴C concentrations in gas-phase CO₂ and hydrogen, carbon, oxygen, strontium, and uranium isotopic measurements that will allow for more careful testing of the DST THC Model.

3.10.5 THC Seepage Model

This subsection describes the THC Seepage Model and the results of predictions of water and gas chemistry that may seep into drifts over the next 100,000 years. This model also considers any changes in the hydrological properties as a result of mineral precipitation and dissolution.

3.10.5.1 THC Seepage Model Description

A THC Seepage Model incorporates the elements of the EDA II (Enhanced Design Alternatives; Wilkins and Heath 1999, Enclosure 2) to represent waste package heating over time, changes in heat load due to ventilation, the effective heat transfer within the drift, the addition of backfill after 50 years, and THC processes. This two-dimensional model incorporated the initial layering in hydrologic and thermal properties and mineralogy from the surface to the Calico Hills zeolitic unit, along with different initial mineralogy and reactive surface areas in fractures and matrix (Figure 3.10-6). A number of cases were evaluated for different calibrated property sets, climate change scenarios, and geochemical systems. The climate scenarios were constructed from average values of the present-day infiltration, monsoon and glacial transition climates along with the upper and lower bounds. These averages were calculated from about 30 TH chimney models in the potential repository footprint. Predictions were presented of the water and gas chemistry that may enter the drifts for a period of 100,000 years, including a preclosure period of 50 years with 70% heat removal by ventilation.

3.10.5.2 TH Effects

TH effects on liquid saturation and flow around drifts were investigated in CRWMS M&O (2000, N0120/U0110). The TH effects on liquid saturation and temperature around drifts are a function of the infiltration rate and the initial liquid saturations calculated from steady-state simulations using specific calibrated property sets (CRWMS M&O 2000, U0035). Liquid saturations and temperature are shown around the drifts at 600 years, which is approximately the time of maximum dryout extent for the three climate cases investigated (Figure 3.10-7). These climate cases considered three time periods (0–600, 600–2,000, and 2,000–100,000 years) and different infiltration rates for each period (0.6/6/3, 6/16/25, and 15/26/47 mm/yr) for a lower, mean, and upper bound, respectively (CRWMS M&O 2000, N0120/U0110). The dryout zone is asymmetric around the drift as a result of the position of the waste package and backfill, and the effect of infiltration above the drift. The smaller dryout zone in the lowest infiltration case compared to the mean infiltration case is apparently the result of the differing property sets rather than differences in the infiltration rate. Higher liquid saturations in the pillar region are a result of water being diverted around the drift.

3.10.5.3 Gas-Phase CO₂ Evolution

The CO₂ evolution in the gas phase is a controlling factor for the pH and mineral-water reactions. Time profiles for gas-phase CO₂ concentrations at three locations around the drift are shown in Figure 3.10-8 for the Case 2 (calcite-silica-gypsum) geochemical system. Carbon dioxide concentrations in fractures drop significantly during dryout and increase again during rewetting. The increase in CO₂ concentrations in the gas phase during rewetting is likely a result of heating of these waters as they approach the drift wall, as suggested by the high-infiltration

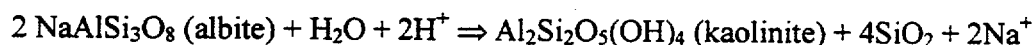
case showing the largest CO₂ concentration after rewetting (near 12,000 ppmV). The highest concentrations are similar to those observed during the DST, although rewetting has not taken place in the DST because it is still in the heating phase.

3.10.5.4 Water Chemistry Evolution

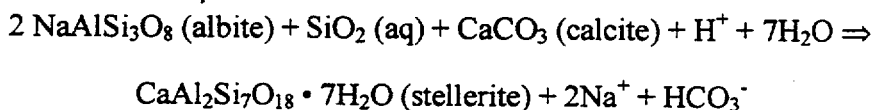
Chloride is a useful indicator of the extent of boiling or dilution, and interaction of condensate waters in fractures that are low in Cl with matrix pore waters having much higher chloride concentrations. Chloride concentrations are plotted in Figure 3.10-9 as a function of time at three locations around the drift. The gap in concentrations between about 75 and 1,000 years reflects the dryout period when no aqueous phase is present at the drift wall. Upon rewetting, chloride concentrations drop relatively quickly below 400 mg/L toward ambient values near 110 mg/L. There is no evidence of water with high concentrations of chloride at liquid saturations above residual saturation during the reflux period (after about 1,000 years). Therefore, waters that are most likely to seep into drifts will not be significantly more concentrated in chloride than the ambient pore water.

Predicted pH and total aqueous carbonate concentrations (as HCO₃⁻) in fracture pore water are shown in Figures 3.10-10 and 3.10-11 for the calcite-silica-gypsum system. The calculated pH is generally higher for the full geochemical system results (approximate range 8.5 to 9.8; shown in CRWMS M&O 2000, N0120/U0110, Figure 30) than for the calcite-silica-gypsum system (approximate range 7 to 8.5). The composition of waters reaching the drift wall during rewetting were roughly neutral in pH (7.2 to 8.3) for the smaller system, and approximately 8.6 to 9.0 for the full geochemical system. Total aqueous carbonate concentrations are higher in the full system at the drift crown (maximum, after rewetting, near 10,000 mg/L for the low infiltration case) than in the calcite-silica-gypsum system (near ambient values of 200 mg/L after rewetting).

The pH-carbonate-CO₂ data show different trends when aluminosilicates in the mineral assemblage are considered. The aluminosilicate reactions are sensitive to competing effects of infiltration rate and gas phase CO₂ diffusion relative to calcite dissolution/precipitation, feldspar dissolution, and calcium-zeolite precipitation. The dissolution of feldspars to form zeolites and clays directly affects the pH. For example, the dissolution of albite (Na-feldspar) to form kaolinite (clay) results in an increase in pH, as follows:



Feldspar dissolution also indirectly causes an increase in pH when Ca-rich zeolites precipitate, depleting calcium from solution and destabilizing calcite, as in the following reaction:



As a result, simulations that consider aluminosilicate reactions generally yield higher pH and total aqueous carbonate concentrations and generally lower CO₂ partial pressures than simulations with the simpler calcite-silica-gypsum system. Simulations of the DST show that results from the calcite-silica-gypsum system matches the observed pH, bicarbonate, and calcium

more closely than the more complex system. However, over longer and more stable periods of reflux and boiling, the system may trend toward the chemistry of the more complex system.

3.10.5.5 Porosity and Permeability Changes and Assessment of Precipitation Cap Formation

The calculated change in fracture porosity in the vicinity of the drift, at a simulation of 10,000 years, is shown in Figure 3.10-12 for the three climate scenarios and the calcite-silica-gypsum system. The maximum porosity reduction (negative in the plots) occurs for the high-infiltration case and is predominantly above the drift, adjacent to the tsw33 and tsw34 hydrogeologic unit contact. In all cases, the porosity change is relatively small (less than 1% of the initial porosity) and mostly to smaller values. The porosity decrease results primarily from calcite precipitation (as in the DST simulations). In the full geochemical system, the fracture porosity change is similarly small, but is dominated by zeolite reactions. Because the fracture porosity changes are exceedingly small, and permeability changes are negligible, TH processes are not significantly affected by mineral precipitation or dissolution.

3.10.6 Uncertainties and Limitations

Many uncertainties exist in the thermodynamic and kinetic parameters used to describe mineral precipitation and dissolution. Limitations also arise under specific geochemical and/or physical conditions. For example, as the concentrations of dissolved solutes increase during boiling of porewater, the activity coefficients of the dissolved species may deviate significantly from unity, and the ionic strength at which the models yield reasonable results is exceeded. Rapid boiling can also lead to mineral supersaturation outside the range of the pseudo-first-order kinetic models employed, which are generally reasonable under near-equilibrium conditions. Mineral precipitation may then be controlled by nucleation kinetics and other surface-energy-related phenomena. These uncertainties and limitations are generally difficult to quantify, because the models also introduce simplifications in the process of using these data, and the physical regimes under which the model breaks down may not be important for the overall dynamics of the system. Geochemical reactions are a strong function of temperature and the presence of water, which are better constrained than the rates of reaction and may control the spatial distribution of mineral precipitation, even if the exact quantities of the minerals at a given time are uncertain.

Relations between permeability changes and porosity changes are also highly uncertain. These uncertainties are difficult to quantify because they depend on the detailed geometry of the pore space and throats; however, some methods have succeeded in quantifying this effect in diagenetically altered rocks (Ehrlich et al. 1991, pp. 1579–1592). The effect of porosity reductions in fractures on the fracture permeability is even more uncertain.

The model is also limited to the middle nonlithophysal unit of the Topopah Spring tuff. Lithophysal units may exhibit different TH behavior that would change the interaction of fracture and matrix waters. Differences in the mineralogy of fractures and lithophysae could change the chemistry of the system somewhat, although the bulk rock chemistry is very similar for all of the welded TSw units. More important than small differences in mineral abundances is the effective reactive surface area which could be larger in lithophysal units because of the

greater abundance of vapor-phase minerals and as result of the interaction of waters flowing between fractures and lithophysae.

These uncertainties do not, in general, limit the applicability of the models because of the ability to calibrate effective reaction rates to fit the results of laboratory and in-situ experiments (i.e., thermal tests). Some of the uncertainties inherent in the thermodynamic and kinetic data have been addressed by the consideration of a simplified and a more complex mineral assemblage. Validation of the model by comparison to geochemical data from the DST provides the best degree of confidence building, and these comparisons have shown that the model is reasonable. Differences in the model results between the two geochemical systems, showing that the pH and CO₂ concentration in the gas phase for the simpler system compare more favorably to data from the DST shows that the model does provide important bounds on reaction rates. Results from the more complete system yield a higher pH than in the measured waters from the DST, which is due to a greater calculated reaction rate for feldspars. Therefore, porosity reductions as a result of feldspars altering to clays and zeolites likely take place at rates less than that given by model, giving an important upper bound.

3.10.7 Alternative Conceptual Models

A model proposed by Matyskiela (1997, pp. 1115–1118) suggests that silica precipitation in the rock matrix adjoining fractures will strongly reduce the permeability of the matrix, resulting in significantly decreased imbibition of percolating waters. The times for strong silica sealing of the matrix wall for a vitric tuff were 5 years for a solution having 350 ppm SiO₂ and 105 years for a solution having 125 ppm SiO₂. For a devitrified tuff, it was estimated that cristobalite dissolution followed by quartz precipitation would lead to a 1 mm thick quartz margin in about 30 years. It is clear that several factors would immediately reduce the magnitude of the effects described. First, the potential repository would be located in a devitrified tuff where the rates of reaction are orders of magnitude slower than for volcanic glasses. Second, the proposed model considered the system as fully saturated, maximizing the reactive surface area, the water available for reaction, and the diffusion coefficient. In an unsaturated system, only a part of the fracture area would be contacted by water, so that the process would have to take place for much longer periods to actually affect a large part of the fracture surfaces. Third, it is considered that the fracture water will have higher silica concentrations than a matrix porewater, thus leading to a diffusion gradient into the matrix. However, no clear reason exists why the fracture water should have a higher silica concentration, because it originated as pure condensate (zero SiO₂) that has drained back toward the heat source, increasing its silica content through wall rock reactions. Because the system is unsaturated, there is little driving force for convection as in a single-phase hydrothermal system. A quantitative analysis of this problem was explored by Lichtner et al. (1999) which also questioned the interpretations and conclusions presented in the Matyskiela (1997, pp. 1115–1118) paper (see CRWMS M&O 2000, U0135) and in Section 3.10.9 below.

3.10.8 Corroborative Evidence

Water and gas chemistry collected from the ongoing DST has been invaluable in the testing of the models developed for the prediction of potential long-term repository performance. No other data can be used to directly corroborate the model because of the uniqueness of the system.

However studies from natural geothermal analogs has been used as corroborative evidence, as discussed in Section 3.10.9.

3.10.9 Analogs

THC processes are better constrained through analysis of selected intrusive complexes hosted in unsaturated tuffaceous rock. The ideal intrusion to serve as a natural analog to THC processes anticipated at a potential Yucca Mountain repository should have been emplaced above the water table, should be of sufficient size to have produced enough heat to sustain boiling conditions for times on the order of several thousand years (~30 m width), and should occur in host rock of similar composition and characteristics to the Topopah Spring tuff.

An analogy for understanding future behavior of a potential repository is the fossil hydrothermal system at Yucca Mountain itself (Bish and Aronson 1993, pp. 148–161). After formation of the major zeolitic horizons (13–11.6 Ma), deep-seated hydrothermal activity persisted until about 10 million years ago (Ma). This activity was limited to temperatures of 90–100°C, the zeolite stability limit. Conceptual models for mineral evolution at Yucca Mountain (CRWMS M&O 2000, I0045, Section 6.3) suggest that the most likely mineralogical reactions caused by potential repository heating would include dissolution of volcanic glass and precipitation of clinoptilolite, clay, and opal-CT; dissolution and precipitation of silica polymorphs (cristobalite, opal-CT, tridymite, and quartz); alteration of feldspars to clays; and, finally, reactions involving calcite and zeolites. Present-day temperatures in borehole G-3, within the potential repository block, compare closely to inferred paleotemperatures. In contrast, increasingly higher paleotemperatures are inferred for boreholes G-1 and G-2, which are closer to the center of the Timber Mountain caldera source of eruption (G-2 being the farthest north). Mineral abundances in G-1 and G-2 cores indicate a northward progression of an increasing abundance of clays and zeolites along with decreased abundance of glass. This is consistent with the reactions stated above.

In addition to considering Yucca Mountain as a self-analog, contacts between igneous intrusions and host rock may provide useful information as coupled-process analogs. The Banco Bonito obsidian flow filled a steep-walled canyon cut in the Battleship Rock tuff on the southwest rim of the Valles Caldera, New Mexico, about 400,000 years ago. The obsidian, initially at temperatures of 850°C, heated the porous tuff in the canyon walls to 150–350°C for decades, and, according to models, vaporized much of the pore water, and caused refluxing of water (Stockman et al. 1994). Contact effects include a reddish “baked” zone extending several meters into the tuffs. No evidence of hydrothermal alteration was noted, suggesting that the area was unsaturated at the time of contact. Apart from devitrification, the principal mineralogic change in tuff near the contact was the development of feldspar-silica linings on voids in the pumiceous tuff matrix; no significant development of zeolites was found. Stockman et al. (1994) concluded that overall, the effects of heating in this unsaturated environment appeared to have been slight and were limited to the tuff nearest the contact.

At Grants Ridge, New Mexico, a 2.6 Ma basalt plug intruded into 3.3 Ma non-welded, pumice-rich, compositionally homogeneous, rhyolitic tuff and volcanoclastic sediments (WoldeGabriel et al. 1999, pp. 389–411). A 10 m wide aureole characterized by color variation, contact welding, brecciation, partial melting, and stoping developed around the 150 m wide basalt plug. Despite

the high-temperature ($> 700^{\circ}\text{C}$) basaltic intrusion, there was no evidence of pervasive hydrothermal circulation and alteration of the country rock. WoldeGabriel et al. (1999, pp. 389–411) postulated that vapor-phase expulsion of elemental species could have been responsible for the minor depletion of elements at the contact during devitrification of the silicic glass at near-solidus temperature related to the basaltic intrusion. Because devitrification is generally enhanced by the presence of aqueous fluids, the abundance of volcanic glass within a short distance (~ 10 m) from the plug is consistent with the inference of WoldeGabriel et al. (1999, pp. 389–411) that the plug intruded into an unsaturated environment.

In the Paiute Ridge area of the Nevada Test Site, late Miocene basaltic magma intruded a sequence of 22 to 11 Ma tuffs in a single magmatic pulse as dikes, sills, and lopoliths (Lichtner et al. 1999). A contact aureole ~ 3 m wide surrounds the intrusions. Matyskiela (1997, pp. 1115–1118) studied alteration surrounding one intrusion, the 50 m wide Papoose Lake sill. His major finding was alteration of glass shards to cristobalite and clinoptilolite within 60 m of the intrusion, which he interpreted as resulting from emplacement of the intrusion. Most significant was his observation of complete filling of pore spaces with silica at fracture-matrix interfaces, thus reducing fracture-matrix interaction and facing infiltrating water to flow within fractures. Matyskiela (1997) estimated enhanced fracture flow to be as much as five times ambient conditions. This is the opposite behavior to formation of a silica cap, as predicted by recent simulations conducted for Yucca Mountain (Nitao 1998) in which fractures would become filled with quartz or chalcedony, thus inhibiting further flow. An issue is the extent to which a fracture can be filled by the silica contained in matrix pore water. Lichtner et al. (1999) shows that for a given matrix porosity, the degree of sealing of the fracture depends on the fracture porosity and the particular silica polymorph that precipitates. The two-phase numerical simulation results of Lichtner et al. (1999) suggest that at distances of tens of meters from the larger Paiute Ridge intrusion in their study (width ≥ 39 m), prolonged boiling conditions were established for times on the order of several thousands of years. Amorphous silica, with its higher solubility, gives the largest fracture filling, followed by chalcedony and quartz. For complete sealing of the fracture, a very small fracture porosity is necessary.

Some other questions arise regarding the effect of the sill on the host rocks. First, it is stated that the basaltic magma was particularly dry because hydrous phases (such as amphibole) were not found and because it was nonvesiculated (Matyskiela 1997, p. 1115). However, the absence of amphibole in this sill is not evidence for a lack of water in the melt because amphiboles are not stable phases at low pressures in basaltic melts (Ehlers 1972, p. 161). Also, this igneous body is a sill and not a flow; the slower cooling allows water degassing without obvious vesiculation (as in a lava flow). Basaltic magmas also can exsolve significant quantities of CO_2 in addition to H_2O , and therefore the geochemical environment was not clearly analogous to that around a potential repository drift.

In summary, in both the Banco Bonito flow and the Grants Ridge basaltic intrusion, the effects of high temperature on unsaturated environments appeared to have been slight, were limited to within about 10 m of the contact, and showed no evidence of fluid-driven convective heat transfer or pervasive hydrothermal alteration of the country rock. These field studies provide a limiting-case natural analog for evaluating effects of heat from decay of radioactive waste in an unsaturated environment.

3.10.10 Model Validation

The drift-scale THC models have been extensively validated by comparison of gas and water geochemical data collected during the DST, as discussed in Section 3.10.4 and described in detail in CRWMS M&O (2000, N0120/U0110). These comparisons include gas-phase CO₂ concentrations as a function of time and space, the pH of waters collected in boreholes, and general observations on changes in concentrations of Cl and other aqueous species. The model can be considered validated for its intended use.

The thermal tests provide the only field-scale experiments that have produced seepage under thermally perturbed conditions. Numerous samples of water have been collected from several borehole intervals during the DST, and previously a few samples were collected in the Single Heater Test.

Prediction and comparison to data from thermal tests and experimental studies have allowed for validation of the models describing coupled THC processes. However, it is not possible to validate all aspects of the model over a 100,000 year period. Yet reasonable bounds on the system behavior were made based on validation over relatively short time scales using the DST as described in this section and in CRWMS M&O 2000, N0120/U0110. The model has provided bounds on the gas and water chemistry over time (i.e., CO₂ and pH) as well as changes in porosity, as discussed in Section 3.10.6. For example, the composition of waters reaching the drift wall during rewetting was roughly neutral in pH (7–8.5) for the smaller geochemical system (without aluminosilicates) and had a pH of approximately 8.6–9.0 for the more complete geochemical system.

3.10.11 Abstraction of Drift-Scale THC Modeling for TSPA-SR

The THC water chemistry and gas-phase composition abstraction represents the fracture waters impinging at the crown and sides of the potential emplacement drifts. The abstraction uses the detailed time-history results of the process-level THC model and discretizes them into four distinct geochemical periods for which compositional boundary conditions are provided for the potential in-drift geochemical environment for TSPA models. The abstraction compositional boundary conditions include constituents represented by five cations, six anions, and pH. In addition, this abstraction includes the partial pressure of carbon dioxide in the gas phase in fractures adjacent to the potential drifts (and, during the abstraction boiling period, the equilibration temperature used for that gas with the condensate water composition). These boundary conditions to the potential drifts allow incorporation of time varying, thermally perturbed water and gas compositions within the assessment of chemical interactions of the in-drift environment.

The abstracted use of the THC process model results from the Case 2 mineralogy is based on the fact that it reproduces more accurately the observed changes to water and gas compositions in the drift-scale heater test (CRWMS M&O 2000, N0120/U0110; Sections 6.1.7 and 6.2.7). This corresponds to using the mineralogic phase constraints represented in Case 2 to set the major element composition of the water and gas. This decision is supported by the THC process-level model validation with the DST results, for which the Case 2 results provide closer description of the ambient and thermally perturbed geochemical system (CRWMS M&O 2000, N0120/U0110;

Sections 6.1.7, 6.2.7 and 6.3.5). Therefore, the abstraction of aqueous water chemistry of the major chemical species (which are contained in both Case 1 and Case 2 representations) is from Case 2 only.

For the constituents included in both those chemical systems, the major differences between results (for PA purposes this is defined as a factor of 10—or one log unit—or more) are limited to Ca^{2+} , Na^+ , and HCO_3^- . These represent differences that result primarily from the more uncertain kinetic representation of the more complex chemical system (CRWMS M&O 2000, N0120/U0110; Sections 6.1.7, 6.2.7, and 6.3.5). As discussed therein, the uncertain precipitation rates of the alumino-silicates create a feedback to the carbonate system by removing Ca from solution, impacting the carbonate system through the changes in calcite saturation state. However, estimates of the additional constituents included only within the Case 1 results should be reasonably obtained from those results. This is because the primary differences in the systems are those constituents listed above and the variations in pH, that may impact mineral equilibria in the more complex chemical system, are of lesser magnitude. The process model Case 1 results for F^- are assessed to be relatively insensitive to the possible changes (CRWMS M&O 2000, N0120/U0110; Section 6.3.5). The phase constraints applied within the Case 1 representation for these additional constituents should be largely unchanged (although more accurate kinetic parameter sets should prevent them from impacting the carbonate subsystem) and these are all trace constituents compared to the major constituents included within both Case 1 and Case 2. Given this, the values for the additional constituents from the Case 1 representation should provide at least order-of-magnitude estimates for incorporating abstracted first approximations for these constituents. In the abstraction these values are combined with the constituents from the Case 2 results to describe a more comprehensive water composition (Table 3.10.3). Addition of these values to these abstracted water compositions should have only minor effects on charge balance, because these additional aqueous species are trace constituents compared to the major elements given within the Case 2 representation.

Table 3.10.3 represents the THC abstraction of water and gas compositions for the THC boundary conditions adjacent to the drift wall. Each of the time periods defined below has a defined composition of gas and water that represent those constituents that can enter the drift during those times based on the process-level THC models for the thermally perturbed geosphere. Four periods were defined based on the examination of the process-level results. Each of these periods was evaluated to define constant representative values (as discussed above) for all constituents during that period with step (i.e., instantaneous) changes between the periods. The first period defined goes from 0 to 50 years and is the entire preclosure period. This is followed by the defined boiling period 2, during which the fractures are calculated to have zero saturation. The water that may enter the drift through these fractures would be that moving rapidly down from the condensate zone. This boiling period is followed by a transitional cooldown period from 1000 to 2000 years during which the temperature is still high, but below boiling. Finally an extended cool-down period 4 is defined from 2000 to 100,000 years, over which the temperatures return to ambient and water compositions change gradually.

Although the preclosure period (50 years) is included in the process models, the postclosure performance assessment starts at the end of this initial period. Abstracted results for Period 1 preclosure are included only for complete coverage of the time of the process-level results. The process model results do not include the chemical effects of pre-closure ventilation, so the gas

composition and water chemistry within this period may not be very representative of those that could enter the drifts. These abstracted values for Period 1 preclosure are not used within the performance assessment analyses. Because the preclosure period is not being used within the performance assessment, the values for the 0-50 year period are more coarsely abstracted and chosen to be roughly representative of the first 50 years. This period will not be used further in this abstraction. The abstracted boiling period 2 directly follows the preclosure abstraction period 1. During the second abstraction period, the boiling period, the fracture saturation around the drifts is calculated to be zero in the THC process model results. The chemical composition of the condensate water, calculated to be in the zone of highest saturation above the fracture dryout, is used to represent the water that may flow rapidly through the fractures during the boiling period. The values for such water are given below in Table 3.10.3 with the value of the partial pressure of CO_2 in the gas surrounding the drift wall during that dryout time. The flux of such water would be at a minimum during this period, so that the fracture gas composition at the drift wall during the dryout period should be the appropriate composition with which to equilibrate the condensate liquid. This value ($\log \text{CO}_2$, volume fraction = -6.5) is given in Table 3.10.3 below. This gas composition, and associated boiling temperature, should be used to equilibrate with the abstracted condensate water composition shown for this period in Table 3.10.3. This represents the abstracted water that may flow rapidly down fractures into the dryout zone from the overlying condensate zone.

It is re-emphasized that during the abstracted boiling period (50-1000 years), denoted as period 2 in Table 3.10.3, the abstracted aqueous concentrations and pH are obtained from the process-level model results from `satmax_summary.xls` (DTN: LB991200DSTTHC.002), not the results for locations at the drift wall. These latter water compositions are artifacts of the point at which the water chemistry representation was shut off either due to high ionic strength or low saturations. However, the gas composition (CO_2 , gas) is obtained from the appropriate results for the crown fractures at the drift wall because the process-level THC gas chemistry calculation is continuous through this period (see Figure 29, CRWMS M&O 2000, N0120/U0110). The boiling period abstracted water composition is based on the condensate water chemistry above the dryout zone, representing water that would flow rapidly down the fracture if possible.

The remaining two THC periods, the transitional and extended cool-down periods, are abstractions of the chemistry results obtained from the process-level THC model in the same manner as that for the pre-closure period (0-50 years). However, because the changes are more gradual for most constituents in these time periods, it was possible to identify a result at a specific time given by the process model that corresponded to a reasonable representation for the compositional parameters needed in the abstraction. Using specific calculated results from the THC process model ensures that issues of charge balance and phase equilibria are maintained completely consistently within the abstracted representation.

It is noted that the abstracted temperatures listed in Table 3.10.3 are given for use as a guide only, especially in Period 4 in which the temperature changes gradually from about 90°C to 25°C over 98,000 years. Only the temperature in the Boiling Period 2 should be used in process models to calculate re-equilibration of the condensate-zone water composition with the abstracted CO_2 gas composition in the fractures at the drift crown for that period of time. For further Performance Assessment model abstractions, the temperatures given in Table 3.10.3 can be used as the representative values for the temperature of the abstracted compositions, but

should be tied to the thermal variation of the repository system as abstracted for the total system performance assessment.

The following should be noted for the abstraction shown in Table 3.10.3:

- The first 50 years represents the repository preclosure period with 70% heat removal via ventilation. However, because the Performance Assessment only starts at closure, these values are not used there and are only provided for completeness of the time span. It is emphasized that the values probably would not be representative of preclosure conditions because the potential chemical effects of ventilation are not included in the process model.
- The values for abstraction period 3, correspond to the process-level model results at 2000 years after initial waste emplacement. This is because as soon as the drift wall rock resaturates, the CO_2 very rapidly approaches about 1×10^{-3} bars and the pH and water composition are taken consistently with this gas chemistry.
- The 10,000-year process-level model results are used for the abstraction values in the last period as a reasonable approximation of the water composition average for that whole period.
- The additional constituents taken from the results of the more detailed chemical system are, in general, trace constituents compared to those taken from the less detailed chemical system. Even though combination of these results may lead to discrepancies of the trace constituents that could be large in a relative sense, their contributions to the absolute uncertainties will remain small because of their trace abundances. Only potassium approaches the concentrations of the constituents taken from the less detailed chemical system, and even it is one to two orders of magnitude lower in concentration than the major cation species Ca^{+2} and Na^{+} included in Case 2 results.

Table 3.10-3. THC Abstraction for the Mean Infiltration Rate Case with Climate Change (CRWMS M&O 2000, N0125, Table 3)

Constituents from Simplified Chemical System (Calcite-Silica-Gypsum)				
	Preclosure	Boiling	Transitional Cool-Down	Extended Cool-Down
	Period 1	Period 2	Period 3	Period 4
Parameter	Abstracted Values	Abstracted Values	Abstracted Values	Abstracted Values
Time	0 - 50 years	50 - 1,000 years	1,000 - 2,000 years	2,000 - 100,000 years
Temperature, °C	80	96	90	50
log CO ₂ , vol. frac.	-2.8	-6.5	-3.0	-2.0
pH	8.2	8.1	7.8	7.3
Ca ²⁺ , molal	1.7E-03	6.4E-04	1.0E-03	1.8E-03
Na ⁺ , molal	3.0E-03	1.4E-03	2.6E-03	2.6E-03
SiO ₂ , molal	1.5E-03	1.5E-03	2.1E-03	1.2E-03
Cl ⁻ , molal	3.7E-03	1.8E-03	3.2E-03	3.3E-03
HCO ₃ ⁻ , molal	1.3E-03	1.9E-04	3.0E-04	2.1E-03
SO ₄ ²⁻ , molal	1.3E-03	6.6E-04	1.2E-03	1.2E-03
Additional Constituents from Full Chemical System				
Mg ²⁺ , molal	4.0E-06	3.2E-07	1.6E-06	7.8E-06
K ⁺ , molal	5.5E-05	8.5E-05	3.1E-04	1.0E-04
AlO ₂ ⁻ , molal	1.0E-10	2.7E-07	6.8E-08	2.0E-09
HFeO ₂ ⁻ , molal	1.1E-10	7.9E-10	4.1E-10	2.4E-11
F ⁻ , molal	5.0E-05	2.5E-05	4.5E-05	4.5E-05

3.10.12 Summary and Conclusions

The conceptual model for THC processes provides a comprehensive basis for modeling the pertinent mineral-water-gas reactions in the host rock, under thermal loading conditions, as they influence the water and gas chemistry that may enter drifts over 100,000 years. Data are incorporated from the drift-scale calibrated property sets, the UZ Flow and Transport Model, geochemical data (fracture and matrix mineralogy, aqueous geochemistry, and gas chemistry), thermodynamic data (minerals, gases, and aqueous species), data for mineral-water reaction kinetics, and transport data. Simulations of THC processes included coupling between heat, water, and vapor flow, aqueous and gaseous species transport, kinetic and equilibrium mineral-water reactions, and feedback of mineral precipitation/dissolution on porosity, permeability, and capillary pressure (hydrologic properties) for a dual-permeability (fracture-matrix) system. The effect of these coupled THC processes on the time evolution of flow fields in the UZ around drifts has been investigated for different climate change scenarios, calibrated property sets, and initial mineralogy. Validation of the model was done by comparison of measured gas and water chemistry from the Drift Scale Test (DST) to the results of simulations using the DST THC

Model. In particular, simulation results were compared to measured gas-phase CO₂ concentrations and the chemistry of waters collected from hydrology boreholes collected during the test.

Comparisons of water chemistry (pH) and CO₂ concentrations in the gas phase from the DST indicate that a smaller set of aqueous species and minerals (calcite, silica phases, gypsum), but including gaseous CO₂, can describe the general evolution of DST water quite closely. Including a wide range of aluminosilicates, such as feldspars, clays, and zeolites yields information on additional species (i.e., Al, Fe, F), but their inclusion causes shifts in the water and gas chemistry that are more rapid than observed. These effects may be more important over longer time periods, leading to similar but less rapid changes (i.e., a slightly closer approach to equilibrium). However, over the time scale of the DST, the effective reaction rates and/or thermodynamic properties of these phases will clearly require some refinement.

The THC Seepage Model incorporates the elements of the EDA II design to represent waste package heating over time, changes in heat load due to ventilation, the effective heat transfer within the drift, the addition of backfill after 50 years, and THC processes in the unsaturated zone. A number of cases were evaluated for different calibrated property sets, climate-change scenarios, and geochemical systems. The THC seepage simulations indicate that there may be an increase in the CO₂ gas and aqueous carbonate concentrations around the drift during rewetting. The extent of the dryout zone and the time of rewetting were different for each climate history and calibrated property set, although the general character was unchanged. As in the Drift Scale Test THC simulations, some notable differences in the pH and CO₂ concentrations appeared in the two geochemical systems. The composition of waters reaching the drift wall during rewetting were roughly neutral in pH (7–8.5) for the smaller geochemical system (without aluminosilicates) and approximately 8.6–9.0 for the more complete geochemical system. Predicted pH and HCO₃⁻ concentrations in the smaller geochemical system simulations are supported by the data from the DST; however, the long term evolution could trend in the direction of the more complex system chemistry, if the slow reaction rates of the aluminosilicates limit the changes in water chemistry that can be observed over the short heating time of the DST.

Even with the apparently overestimated reaction rates for the full mineral assemblage, the changes in porosity and permeability around drifts over 100,000 years were small (less than 1% of the total fracture porosity), and therefore effects on flow and transport are considered negligible. A summary of important results as related to the conceptual model of drift-scale THC processes is shown in Figure 3.10-13.

In the abstraction for TSPA-SR calculations, the transient water and gas compositions are averaged over four discrete time periods from 0 to 100,000 years. Only the mean infiltration cases are selected because the results of the low and high infiltration cases showed similar behavior in general. The results that are passed to the in-drift geochemical models in TSPA are aqueous concentrations for five cations and six anions, pH, and partial pressure of carbon dioxide during the four discrete periods. These results are used to determine the in-drift environment and the corrosion of the drip shields and waste packages over time.

3.11 UZ TRANSPORT MODEL

3.11.1 Introduction

The evaluation of possible radionuclide transport from the potential repository horizon to the groundwater in the saturated zone is key to assessing the performance of the potential repository. This section describes the issues, approach, assumptions, and understanding of the relevant physical processes, and input parameters used to develop the Transport Model in the UZ. The Transport Model utilizes the understanding of the complex flow processes from the Flow Model (Section 3.7) and accounts for the transport of aqueous/colloidal radionuclide species in both the fracture and matrix continua, with exchange between continua resulting from advective and/or diffusive processes, as well as sorption in the matrix. Results of 2-D vertical cross sections, 3-D site-scale simulations of the important radionuclides and daughter products, and 3-D simulations of tracer breakthrough at the water table are presented for different climate scenarios developed in Section 3.5. These results are analyzed to identify the major transport mechanisms and breakthrough times through the different hydrogeologic units and the effects of the major hydrogeologic features (faults and perched water). Model validation using the results of the ESF Alcove 1 and Busted Butte tracer tests is summarized. Review of known analog sites for UZ transport indicates that unsaturated systems in arid environments may provide favorable sites for geologic disposal of radioactive waste. The abstraction of the Transport Model used for calculations of radionuclide transport in TSPA is then discussed. Finally, this section ends with conclusions regarding the important issues identified for radionuclide transport at Yucca Mountain.

3.11.1.1 Issues

The Transport Model evaluates a suite of factors that control potential radionuclide transport to determine their effects on radionuclide breakthrough times and concentrations at the groundwater table. A schematic representation of the key issues for the Transport Model is shown in Figure 3.11-1. The flow of water from the potential repository horizon to the groundwater table can transport both aqueous and colloidal phase radionuclides. The concentration of radionuclides and their daughter products are diminished according to their radioactive decay rates, dilution due to mixing (i.e., dispersion), and the extent of sorption onto the solid phase. The flow pathways are determined by the characteristics of the faults, hydrogeologic units, and the presence of perched water. These characteristics control the extent of downward versus lateral flow, fracture-matrix interaction, and the partitioning of flow between fractures and rock matrix. Fractures and faults can be fast flow paths, where fluid contact time and surface area are small relative to the matrix and limit the extent of rock-water interaction relative to the slower-moving matrix flow. Fracture properties, such as aperture, frequency, mineralogy and saturation, affect fracture-matrix interactions, dispersion, sorption and the transport of aqueous and colloidal species. Matrix porosity, saturation, and mineralogy affect the extent of diffusion and sorption of species. The transport of colloidal species is further affected by their size, which determines the nature of pore exclusion, and filtration processes. More detailed discussions of these issues follow in Section 3.11.2.

3.11.1.2 Approach

Transport modeling studies of representative radionuclide and colloids are conducted in 2-D vertical cross sections and 3-D site-scale models of the UZ to:

- Evaluate the effectiveness of matrix diffusion and sorption/filtration as retardation mechanisms in the various hydrogeologic units
- Determine the dominant transport features and mechanisms
- Estimate transport breakthrough from the potential repository to the water table
- Evaluate the importance of decay daughter products on transport.

Relationships of other models and data feeds to the Transport Model are schematically shown in Figure 3.11-2.

3.11.1.3 Assumptions

The key assumptions for the Transport Model in the UZ are listed here. The complete list of assumptions for the Transport Model and the discussion of the supporting rationale are in CRWMS M&O (2000, U0060, Section 5).

- Flow component assumptions are the same as for the Flow Model described in Section 3.7 (e.g., isothermal water flow, dual continuum, active fracture concept, van Genuchten-Mualem model for relative permeability and capillary-pressure constitutive relationships).
- The processes governing the transport of dissolved and/or colloidal species include advection, molecular and surface diffusion, hydrodynamic dispersion, sorption, radioactive decay, colloid filtration, and colloid-assisted solute transport.
- Colloid filtration does not affect the medium's porosity and permeability on account of the anticipated low colloid concentrations.
- The initial radionuclide (solute or colloidal species) concentrations are constant in the gridblocks corresponding to the potential repository and zero throughout the rest of the UZ model domain.

Section 3.11.2 provides a detailed discussion of the transport processes and other major factors affecting UZ transport.

3.11.2 Physical Processes

3.11.2.1 Flow Processes

Transport is closely tied to water flow. A detailed discussion about hydrology in the UZ is presented in Section 3.3, and transport modeling is based on the Flow Model discussed in Section 3.7. In addition to the advective flow processes, transport of radioactive solutes and/or colloids involves hydrodynamic dispersion, sorption (solutes) or filtration (colloids), matrix diffusion, and radioactive decay. The effects of these processes on UZ transport are discussed below.

3.11.2.2 Advection

Advection is the movement of dissolved or colloidal species resulting from the bulk flow of fluid (Fetter 1993, p. 47). In advective transport, the flowing water carries contaminants, and transport pathways coincide with flow pathways determined by the characteristics of the faults, hydrogeologic units, and perched water (Section 3.3). As flow in Yucca Mountain is predominately downward because of gravity, so is advective transport. The presence of perched water bodies may result in lateral flow and subsequent transport of the radionuclides.

Advection is probably the most important mechanism for fast radionuclide transport through the UZ to the water table. Advection through fractures is expected to dominate transport behavior in welded units because water flows largely through fracture networks. Dominant fracture flow in the zeolitic portions of the CHn and CFu also provides relatively short transport times to the water table, whereas the dominant matrix flow in the vitric CHn leads to much longer transport times.

3.11.2.3 Hydrodynamic Dispersion

Hydrodynamic dispersion includes both mechanical dispersion arising from local velocity variations and molecular diffusion driven by concentration gradients. Dispersion of the radionuclides occurs both along (longitudinal) and transverse to the average flow direction. Hydrodynamic dispersion dilutes and smears sharp concentration gradients and reduces the breakthrough time of radionuclides to the water table. The dispersion coefficient is a function of dispersivity and flow velocity.

Values of dispersivity are difficult to determine without site-specific measurements. Dispersivity has been shown to increase as a function of observation scale, attributed mainly to mixing as more heterogeneities are sampled at larger scales (e.g., Gelhar et al. 1992, pp. 1955–1974; Fetter 1993, pp. 65–66). Furthermore, the reported field measurements of transverse dispersivity show it to be significantly less than longitudinal dispersivity (Fetter 1993, pp. 65–66).

Hydrodynamic dispersion is not expected to play an important role in UZ transport. First, dispersion effects are implicitly accounted for by the fracture–matrix dual-continuum approach, which explicitly models local velocity variations. Second, the potential repository emplacement area is very broad (relative to the distance to the water table), which tends to suppress dispersion effects (CRWMS M&O 2000, U0030, Section 6.2).

3.11.2.4 Sorption

Sorption is a general term to describe the binding of a solute (radionuclide) onto the sorbent (either the immobile rock matrix or colloids). As a result of sorption onto the rock matrix, the advancing rate of sorbing radionuclides is retarded. On the other hand, the attachment of sorbing radionuclides onto colloids can potentially facilitate their transport, which is to be discussed in Section 3.11.2.7.

In Yucca Mountain studies, the effective sorption distribution coefficient (K_d) approach is employed to quantify the extent of radionuclide-sorbent interactions. This approach does not require identifying the specific underlying processes of sorption, such as surface adsorption, precipitation, and ion exchange. While the use of K_d to describe the complex radionuclide-sorbent interactions in a flowing fluid of variable chemistry is a simplification, the results from numerous laboratory batch and column experiments have not produced recommendations to abandon the K_d approach for modeling radionuclide retardation in the YMP (CRWMS M&O 2000, U0100, Sections 6.4 to 6.6).

Experimentally determined K_d values have been predominantly derived from batch experiments using crushed tuff (with the sample size of 75–500 μm) under water-saturated conditions for a variety of rock types and radionuclides (K_d values are listed in Table 3.11-1 in Section 3.11.3.2). There are concerns that this experimental approach may overestimate the K_d values in UZ transport, as discussed in more detail in Section 3.11.10.2.

Sorption onto fracture surfaces will retard radionuclide migration. The minerals coating the fracture surfaces generally differ from the host-rock mineralogy as a result of different exposure to precipitation of hydrothermal or meteoric waters, or alteration of the pre-existing minerals (CRWMS M&O 2000, U0100, Section 6.5.3). Laboratory sorption experiments showed that trace minerals might be quite effective at retarding ^{237}Np (neptunium) transport when they are concentrated on fracture surfaces (CRWMS M&O 2000, U0100, Section 6.5.3). Numerical simulations also showed that the limited sorption on the fracture walls is sufficiently important to retard transport of strongly sorbing radionuclides [e.g., ^{239}Pu (plutonium)] (CRWMS M&O 2000, U0060, Section 6.17.1). However, sorption in the fractures is not considered in the TSPA transport evaluations because of the limited data and conservative nature of this assumption regarding the radionuclide transport to the water table.

3.11.2.5 Matrix Diffusion

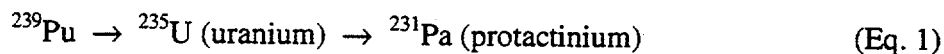
Matrix diffusion can play an important role in radionuclide exchange between the fractures and the rock matrix. Radionuclide diffusion into the rock matrix and away from the fracture surface is driven by a concentration gradient, and it will slow the advance of radionuclides by removing them from the faster flowing fractures. The significance of matrix diffusion depends mainly on factors such as effective contact area between fracture and matrix, the diffusion coefficient of the species, and characteristics of fracture networks (CRWMS M&O 2000, U0030, Section 6.2). The presence of inactive and relatively dry fractures, accounted for with the active fracture model (Section 3.4), could serve as barriers for matrix diffusion.

The effective diffusion coefficient, which is the product of the molecular diffusion coefficient, tortuosity, porosity, and water saturation, is used to account for rock geometry and saturation effects on matrix diffusion. Laboratory diffusion studies in porous geologic materials show that tortuosity values between about 0.5 and 0.01 are commonly observed (Fetter 1993, p. 44). Very limited experimental data exist on the tortuosity distribution in the various Yucca Mountain hydrogeologic units. CRWMS M&O (2000, U0060, Section 6.1.2) employed the approach of using the porosity value to approximate tortuosity, as suggested from the literature (Farrell et al. 1994, p. 64; Grathwohl 1998, pp. 28–35). Tortuosity measurements on devitrified tuffs showed good agreements with this approximation, thereby validating the approach (CRWMS M&O 2000, U0060, Section 6.1.2).

3.11.2.6 Radioactive Decay and Daughter Products

The decay of the radioactive species of interest and their half-lives are completely predictable and well documented. The production of daughter products from chain-decay adds complexity because transport simulations must compute the total radioactivity distribution, i.e., the sum of the concentrations of all the members of the radioactive decay chain. This is especially significant if the daughters have long half-lives. Daughter products with short half-lives relative to the simulation periods may not need to be considered.

The daughter products may have significantly different transport behavior than the parent radionuclide. Equation (1), for example, shows the ^{239}Pu decay chain.



This equation includes only the most important radioactive chain members and omits daughters with short half-lives. The daughter ^{235}U has significantly smaller K_d values compared to its parent ^{239}Pu (see Table 3.11-1).

3.11.2.7 Colloidal Transport

Colloids are very fine particles such as clay minerals, metal oxides, viruses, bacteria, and organic macromolecules that range in size from 1 to 10,000 nm (McCarthy and Zachara 1989, pp. 496–502). Generation and mobilization of colloids has become an important issue in the facilitated transport of radionuclides as intrinsic colloids [e.g., colloidal Pu (IV) and colloidal Pu (V)], or as radionuclide-bearing pseudocolloids for ^{239}Pu and ^{243}Am (americium). Colloidal transport differs from solute transport because of colloidal particle interactions (e.g., flocculation), pore exclusion, and surface reactions (e.g., deposition or attachment).

There is some field evidence of colloid-facilitated transport of radionuclides. In one case, the rapid migration of Pu and Am, attributed to colloidal transport, was found more than 30 m downward through unsaturated tuff over the course of approximately 30 years from a low-level waste site at Los Alamos National Laboratory (Buddemeier and Hunt 1988, p. 536). In a saturated zone study at the Nevada Test Site (NTS), 240Pu/239Pu isotope ratio “fingerprints” of the source of Pu in groundwater showed that it had been transported more than 1.3 km over a 30-year period, although Pu is strongly sorbing at the NTS and assumed to be immobile (Kersting et al. 1999, pp. 56–59). There was a direct finding that Pu was on colloidal material in samples

taken from the NTS through filtration of the groundwater samples. Note that the Pu observed at the NTS originated from an underground nuclear bomb test and that the effects of the underground blast on Pu transport are not fully understood. Microspheres are used as a colloidal tracer at the saturated C-Wells tests (CRWMS M&O 2000, AMR U0100, Section 6.9) and at the Busted Butte transport test in the unsaturated vitric Calico Hills Formation (CRWMS M&O 2000, AMR U0100, Section 6.8).

Colloid concentrations have been measured in several groundwater samples from Yucca Mountain and from other areas at the Nevada Test Site. The measured particle concentrations vary between 1.05×10^6 and 2.72×10^{10} particles/mL, with the lowest being for water from well J-13 and the highest for water from well U19q on Pahute Mesa (CRWMS M&O 2000, U0070, Section 6.2.2.2). These values are consistent with what has been reported in the literature for various groundwaters around the world.

In addition to natural colloids, anthropogenic colloids may be produced from the waste itself or from potential repository construction and sealing materials. This was demonstrated in a 50-month-duration experiment on simulated weathering of a high-level nuclear waste glass, where the amounts of Pu and Am released from waste forms were orders of magnitude greater than their respective concentrations in the dissolved phase (Bates et. al 1992, pp. 649–651). Constraints on these types of colloids are treated in the Waste Form Degradation (WFD) PMR (CRWMS M&O 2000, WFD PMR, Section 3.8).

3.11.3 Transport Properties

This section describes the transport properties used for the abstraction of UZ transport for TSPA evaluations, which is discussed in Section 3.11.13. Matrix diffusion and dispersivity values used for UZ transport modeling and validation, discussed in Sections 3.11.5–10, are different from those used for TSPA abstraction and will be explicitly identified.

3.11.3.1 Dispersion

No data are available to determine dispersivity in the UZ over the travel distance between the potential repository and the water table. In a transport simulation longitudinal dispersion results in earlier arrivals, but generally lower concentrations. Given this behavior, no simple conservative bound exists for the longitudinal dispersion. However, a dispersivity value of 20 m over the approximately 300 m UZ travel distance (in TSPA calculations) is consistent with the dispersivity versus scale correlation of Neuman (1990, pp. 1749–1758). Furthermore, the longitudinal dispersivity (primarily in the vertical direction) is not expected to have a large effect on radionuclide transport processes in the UZ because of the strong dispersive effects of fracture-matrix interactions that are explicitly captured in the Finite Element Heat and Mass Transfer (FEHM) particle-tracking calculation (see Section 3.11.13). Transverse dispersion acts only to reduce concentrations, with generally little effect on breakthrough time. Therefore, a conservative value of zero for transverse dispersivity is used. The base-case distribution for longitudinal dispersivity has been selected to be normal, with a mean of 20 m and a standard deviation of 5 m, which captures a range of 7.5 m to 32.5 m within the 99 percent probability limits. This dispersivity distribution applies to transport in all model units for both the fracture

and matrix continua, but values for fracture and matrix are sampled independently for TSPA calculations.

3.11.3.2 Sorption Coefficients

The main experimental program for sorption was carried out using batch sorption experiments. Table 3.11-1 gives the sorption distribution coefficients recommended for TSPA (CRWMS M&O 2000, U0100, Table 2a). For some radionuclides, specific sorption measurements using rock and water samples from Yucca Mountain have not been performed. For these radionuclides, sorption behavior has been evaluated on a theoretical basis.

Three assumptions were made to develop values of K_d for use in performance assessment (CRWMS M&O 2000, U0100, Section 5). First, the water compositions from wells J-13 and UE-25 p#1 are assumed to provide an adequate range of compositions to capture the influence of water compositional variability on sorption in the UZ. Potentially perturbed fluid compositions moving as plumes out of the potential drifts are not included in the evaluation of this assumption. Second, the effects of mineral variations on sorption in the UZ may be approximated using three rock types: devitrified tuff, vitric tuff, and zeolitic tuff. Finally, the effects of temperature are bounded by measurements of sorption at ambient temperature. However, the effects of mineral alteration because of thermal history are not included in the evaluation of this assumption.

The use of a linear, infinite-capacity sorption model is important for both describing sorption and for modeling the transport of sorbing radionuclides (see Section 3.11.13). Sorption of uranium shows nonlinear sorption behavior, in which the sorbed concentration is reduced from that of a linear model at higher concentrations (see CRWMS M&O 2000, U0100, Section 6.4.4.1.4.4). Linear sorption behavior is expected for the lower concentration levels that will constitute the earliest releases. At higher concentrations, nonlinear effects will act to "self-sharpen" the solute fronts (i.e., longitudinal dispersion is decreased). A linear sorption model may still be used for predicting radionuclide movements and breakthrough times in general, provided appropriate values of K_d are selected that account for the range of K_d s represented by the data at different solute concentrations. In this case, the range of K_d s as a function of concentration is incorporated as part of the frequency distribution defining the overall uncertainty in K_d .

Table 3.11-1. Sorption Coefficient Distributions for UZ Units (Adapted from CRWMS M&O 2000, U0100, Table 2a)

Element	Rock type	Min K_d (mL g ⁻¹)	Max K_d (mL g ⁻¹)	E[x]*	COV*	Distribution type
Americium (also Actinium, Samarium, Thorium, Zirconium)	Devitrified	100	2000	—	—	Uniform
	Vitric	100	1000	400	0.20	Beta
	Zeolitic	100	1000	—	—	Uniform
	Iron oxide	1000	5000	—	—	Uniform
Plutonium	Devitrified	5	70	—	—	Uniform
	Vitric	30	200	100	0.25	Beta
	Zeolitic	30	200	100	0.25	Beta
	Iron oxide	1000	5000	—	—	Uniform
Uranium	Devitrified	0	2.0	0.5	0.3	Beta
	Vitric	0	1.0	0.5	0.3	Beta
	Zeolitic	0	10.0	4.0	1.0	Beta (exp)
	Iron oxide	100	1000	—	—	Uniform
Neptunium	Devitrified	0	1.0	0.3	0.3	Beta
	Vitric	0	1.0	0.3	1.0	Beta (exp)
	Zeolitic	0	3.0	0.5	0.25	Beta
	Iron oxide	500	1000	—	—	Uniform
Radium	Devitrified	70	300	—	—	Uniform
	Vitric	50	100	—	—	Uniform
	Zeolitic	800	2000	—	—	Uniform
	Iron oxide	0	500	30	1.0	Beta (exp)
Cesium	Devitrified	10	700	—	—	Uniform
	Vitric	10	100	—	—	Uniform
	Zeolitic	300	3000	—	—	Uniform
	Iron oxide	0	300	30	1.0	Beta (exp)
Strontium	Devitrified	5	30	—	—	Uniform
	Vitric	0	20	—	—	Uniform
	Zeolitic	200	2000	—	—	Uniform
	Iron oxide	0	20	10	0.25	Beta
Nickel	Devitrified	0	200	50	0.33	Beta
	Vitric	0	50	30	0.33	Beta
	Zeolitic	0	200	50	0.33	Beta
	Iron oxide	0	500	—	—	Uniform
Lead	Devitrified	100	500	—	—	Uniform
	Vitric	100	500	—	—	Uniform
	Zeolitic	100	500	—	—	Uniform
	Iron oxide	100	1000	—	—	Uniform
Tin	Devitrified	20	200	—	—	Uniform
	Vitric	20	200	—	—	Uniform
	Zeolitic	100	300	—	—	Uniform
	Iron oxide	0	5000	—	—	Uniform
Protactinium	Devitrified	0	100	—	—	Uniform
	Vitric	0	100	—	—	Uniform
	Zeolitic	0	100	—	—	Uniform
	Iron oxide	500	1000	—	—	Uniform
Selenium	Devitrified	0	1	0.1	1.0	Beta (exp)
	Vitric	0	1	0.1	1.0	Beta (exp)
	Zeolitic	0	1	0.2	1.0	Beta (exp)
	Iron oxide	0	200	30	1.0	Beta (exp)
Carbon	Iron oxide	10	100	—	—	Uniform
Chlorine, Technetium, Iodine		0	0	—	—	—

NOTE: *Coefficient of variation: $COV = \sigma[x]/E[x]$; $E[x]$ is the expected value of K_d (mL g⁻¹).
 "—" means this parameter is not applicable.

3.11.3.3 Matrix Diffusion Coefficients

The matrix diffusion values for radionuclides are based on measured diffusion coefficients of tritium and Tc (technetium) (CRWMS M&O 2000, U0100, Section 6.6.1). The measurements (in water-saturated rock) showed that tritium diffused at a rate between $1 \times 10^{-10} \text{ m}^2/\text{s}$ and $3.5 \times 10^{-10} \text{ m}^2/\text{s}$ in several samples of devitrified tuff. For Tc, the matrix diffusion coefficient varied between $1 \times 10^{-11} \text{ m}^2/\text{s}$ and $4.9 \times 10^{-11} \text{ m}^2/\text{s}$, which is lower than that of tritium (CRWMS M&O 2000, U0100, Table 16). The lower diffusion rate is believed to be caused by exclusion from some matrix pores caused by the larger ion size and negative charge of the pertechnetate anion (TcO_4^- , the predominant aqueous species of Tc).

A distribution for Tc diffusion coefficients has been assigned to account for variations in rock type and water content. Using the measured Tc diffusion coefficients as a rough guide to the variability in the diffusion coefficient for different rock types, the overall range is estimated to be about a factor of 10. This range is roughly captured by the distribution shown in Table 3.11-2 for anionic radionuclides.

Predictions of radionuclide transport for cationic radionuclides (Np, barium, strontium, Am, cesium) using the diffusion coefficient for tritium and measured batch sorption coefficients were found to be conservative (i.e., faster than) relative to measured diffusion behavior (CRWMS M&O 2000, U0100, Section 6.6.1.3). Diffusion coefficient measured for tritium has been assigned to cationic radionuclides, and the combination of using a batch-sorption K_d value and the tritium diffusion coefficient provides a conservative model. As described above, the variations in rock type and water content are expected to result in variations in the diffusion coefficient of about one order of magnitude. This range is roughly captured by the distribution shown in Table 3.11-2 for cationic radionuclides.

Table 3.11-2. Summary of Diffusion Coefficient Data (CRWMS M&O 2000, U0100, Section 6.6.3)

Radionuclide Type	Mean (m^2/s)	Standard Deviation (m^2/s)	Maximum (m^2/s)	Minimum (m^2/s)	Distribution Type
Anionic	3.2×10^{-11}	1.0×10^{-11}	1×10^{-9}	0	Beta
Cationic	1.6×10^{-10}	0.5×10^{-10}	1×10^{-9}	0	Beta

3.11.3.4 Fracture Aperture and Spacing

Fracture aperture and spacing affect flow and transport between fractures and matrix. For a continuous, parallel fracture pattern, the inverse of the fracture aperture is half the area of contact between the fracture and matrix continua per unit volume of fracture pore space. Therefore, the larger the aperture, the less the diffusion (in a saturated system). For an unsaturated fracture the relevant volume (per unit matrix area) is not the fracture pore volume itself but the volume of water. In either case (saturated or unsaturated), specification of the aperture is necessary. Fracture spacing also affects the diffusion process because it sets the boundary for the depth of penetration from matrix diffusion.

The fracture apertures are derived from the fracture porosity and fracture-matrix connection area (see CRWMS M&O 2000, U0065, Section 6.2.1). Aperture distributions are described using a log-normal distribution of apertures for all the model layers beneath the potential repository. Apertures are sampled stochastically in the transport calculations for TSPA. The sensitivity of transport to fracture spacing is low, so a constant value for each layer is used.

3.11.3.5 Parameters for Colloid-Facilitated Radionuclide Transport

The association of radionuclides with colloids is modeled using two end-member representations: reversible equilibrium exchange with the aqueous phase and irreversible attachment. Radionuclides associated with colloids in either condition (reversible or irreversible) may be subject to size exclusion for fracture-matrix exchange. Colloids are excluded from moving from a fracture into matrix pores smaller than the colloid diameter. This tends to keep colloids (and the associated radionuclides) in the fractures, which leads to more rapid transport of the radionuclide. The chance of exclusion of a colloid from the matrix during fracture-matrix exchange is computed using a probabilistic method that considers different colloid sizes and pore size distribution (CRWMS M&O 2000, U0070, Section 6.1.2).

The description of reversible, colloid-facilitated radionuclide transport for the particle-tracking transport model used in performance assessment is quantified through two parameters (CRWMS M&O 2000, U0065, Section 6.1.4). One parameter, K_c , defines the equilibrium partitioning of radionuclides between the aqueous phase and colloids. The other parameter, R_c , is a retardation factor that captures the details of an equilibrium balance between colloid deposition and resuspension. The retardation factor in the colloid model abstraction applies to the transport through fractures. The distribution of retardation factors used is derived from C-Wells data for saturated-zone colloid transport (CRWMS M&O 2000, U0065, Section 6.2.5).

3.11.4 Geological Layers below the Potential Repository

The subsurface at Yucca Mountain consists of heterogeneous layers of anisotropic, fractured rocks consisting of alternating layers of welded and nonwelded ash flow and air fall tuffs. A more detailed discussion about the UZ geology is presented in Section 3.2; this section focuses on the effects of geological layers on transport.

The potential repository will be located in the TSw. The fractures in the TSw typically have permeabilities several orders of magnitude larger than the matrix permeabilities. Unsaturated flow in the TSw is primarily through the fractures, because the matrix permeability in many of the TSw subunits can support flows of only a few millimeters per year (Bodvarsson et al. 1999, p. 13).

The geological complexity of the underlying CHn results in heterogeneous distributions of fracture and matrix hydrological properties. These properties are expected to have pronounced effects on flow and transport of radionuclides in the UZ. The permeability of nonwelded tuffs is strongly dependent on the degree of alteration of the rock minerals into zeolites. The zeolitic alteration in the CHn (a common occurrence in its lower portions) can reduce the matrix permeability by orders of magnitude to the welded tuff permeability level (see Section 3.6).

Flow in the zeolitic portions of the Calico Hills Formation and surrounding bedded tuffs (CH) (CHz) (see Table 3.2-2) is dominated by fracture flow (similar to that in the TSw layers), although the fracture density is smaller in the CHz than that in TSw layers. In vitric portions of the Calico Hills Formation and overlying bedded tuff (CHv), the matrix and fracture permeabilities are on the same order. Thus, these layers behave as porous (rather than fractured) media, and flow is matrix-dominated, as confirmed from the Busted Butte field test results (discussed in more detail in Section 3.11.11.2). Below the potential repository horizon, both vitric and/or zeolitic layers are present. The existence of CHv layers below the repository has important implications in radionuclide transport because fracture flow originating in the TSw will be strongly attenuated, transport velocities significantly reduced, and contact of dissolved radionuclides with the rock matrix enhanced (which leads to more retardation for sorbing radionuclides).

Information about the zeolitic alteration of the Prow Pass Tuff and the underlying bedded tuffs (PP) is limited. Current understanding is that the model layers pp4 and pp1 are zeolitic and that pp3 and pp2 are devitrified and unaltered. Layers of pp4 and pp1, similar to the CHz layers, have small matrix permeabilities that are several orders of magnitude smaller than the fracture permeabilities (see Section 3.6). Permeability contrast between matrix and fracture in layers of pp3 and pp2 is small, similar to the CHv layers. Therefore, fracture flow may be dominant in pp4 and pp1 layers, while pp3 and pp2 behave like nonfractured porous media.

At some locations in the UZ (e.g., near borehole SD-6), Bullfrog Tuff layers may be present above the water table. There is limited information about the flow and transport behavior in these layers. Current understanding is that the bf3 model layer is devitrified and unaltered while the bf2 layer is zeolitic. According to the Calibrated Properties Model in Section 3.6, the permeability contrast between matrix and fracture in the bf3 layer is small; the bf3 layer might behave like a nonfractured porous medium. The bf2 layer has small matrix permeabilities that are several orders of magnitude smaller than the fracture permeabilities, and fracture flow may be dominant in the bf2 layer.

Based on the above discussions, conceptual schematics of flow and transport in two representative hydrogeologic sections are shown in Figure 3.11-3 to illustrate the effect of geologic layers on radionuclide migration below the potential repository. Borehole UZ-14 is located in the northern part of the potential repository site, while borehole SD-6 is located in the southern part. As radionuclides leave the potential repository, they could migrate through the TSw layers quickly, with limited matrix diffusion and sorption. CHv layers could be very effective in retarding migration because of the matrix-dominated flow in these layers. On the other hand, radionuclides could pass through CHz and zeolitic layers quickly, owing to the fracture-dominated flow. Devitrified layers pp3, pp2, and bf3 could also act as porous media and retard radionuclide migration effectively.

3.11.5 2-D Radionuclide Transport Simulations

Two vertical cross sections, representative of the geologic and mineralogical variability below the potential repository horizon, are used to study radionuclide transport from the potential repository to the groundwater of Yucca Mountain. These cross sections are located in the vicinity of the SD-6 and UZ-14 boreholes. The purpose of the transport simulations is to

evaluate the integrated transport performance of the complete geologic system as well as the individual important hydrogeologic units (i.e., TSw, CHv, CHz, and PP) beneath the potential repository. The simulations account for fracture aperture, fracture frequency, active fracture spacing, and saturation distribution (in the fractures and the matrix) across geologic formation interfaces.

3.11.5.1 2-D Semi-Analytical Code FRACL

FRACL V1.0 (see Table 1.3-1) can analyze transport of reactive solutes and colloids through layers of fractured and porous media. The transport equations in the matrix account for molecular and surface diffusion, mass transfer between the mobile and immobile water fractions, and physical, chemical, or combined sorption following a linear equilibrium, kinetic or irreversible isotherm. Radioactive decay, first order chemical reactions, and tracking of up to five products of radioactive decay or chemical reactions are also included in the solution. The transport equations in the fractures account for the same processes, in addition to advection and hydrodynamic dispersion. FRACL V1.0 accounts for the effects of different fracture spacing and it can accommodate layers of fractured rocks or a combination of fractured rock and nonfractured strata (CRWMS M&O 2000, U0060, Section 6.3.2).

3.11.5.2 Simulation Approach

Three representative radionuclides are considered: ^{99}Tc (nonsorbing), ^{237}Np (moderately sorbing), and ^{239}Pu (strongly sorbing). The radionuclides are released continuously at the top of the domain (which coincides with the location of the potential repository or the individual unit of interest), and the contaminant distribution is monitored over time. When occurring, sorption is assumed to follow a linear equilibrium isotherm (CRWMS M&O 2000, U0060, Section 6.5.2). Percolation rate is 6 mm/year, i.e., close to the mean present-day rate.

It is assumed that advection occurs only in fractures with the longitudinal dispersivity of 1 m (CRWMS M&O 2000, U0060, Table 6.7). The only mechanism of radionuclide transport from the fracture to the matrix is by matrix diffusion. In the transition between layers with nonaligned fractures and/or different fracture spacing, it is assumed that transport in the fracture continuum is continuous. Thus, the results represent the worst-case scenario, yielding the shortest possible breakthrough times of radionuclide transport (CRWMS M&O 2000, U0060, Section 6.5.4).

3.11.5.3 Transport in the Individual Hydrogeologic Unit

The TSw does not effectively retard radionuclide transport because of the dominance of fracture flow that reduces matrix diffusion and sorption (see Section 3.11.4). The breakthrough time for the radionuclides is in the order of $^{99}\text{Tc} < ^{237}\text{Np} < ^{239}\text{Pu}$, which corresponds to their difference in sorptive strength, K_d . In borehole SD-6, for example, breakthrough of the nonsorbing ^{99}Tc at the lower boundary of the TSw occurs in about 1 year. Breakthrough of the moderately sorbing ^{237}Np takes about 35 years, while for ^{239}Pu it occurs at about 300 years (CRWMS M&O 2000, U0060, Section 6.6).

Flow in the CHv is primarily matrix flow, and the unit behaves similarly to a nonfractured porous medium. The reduced flow velocity and increased contact time for matrix diffusion and sorption make the CHv an effective transport barrier (see Section 3.11.4). The CH in borehole

SD-6 consists of five vitric layers (i.e., ch1v, ch2v, ch3v, ch4v, and ch5v) and one zeolitic layer (ch6z) at the bottom. The ^{99}Tc front reaches the bottom of the ch5v in a few hundred years, while the ^{237}Np takes several thousand years. Advancement of ^{239}Pu is limited to the uppermost ch1v layer because of its strong sorptive tendency (CRWMS M&O 2000, U0060, Section 6.7).

Flow in the CHz is dominated by the fractures, and radionuclide transport through the unit is expected to be rapid, similar to that in TSw (see Section 3.11.4). The CH in borehole UZ-14 consists of six zeolitic layers (i.e., ch1z, ch2z, ch3z, ch4z, ch5z, and ch6z). The simulation results are consistent with the expected transport behavior. Both ^{99}Tc and ^{237}Np reach the bottom boundary in less than 10 years. Note that the value of K_d for ^{237}Np is 4 mL/g in the zeolitic tuffs as compared to 1 mL/g in the vitrified tuffs. The larger K_d value does not lead to more retardation in the CHz than the CHv, since the contact time for ^{237}Np with the tuffs is much shorter in the CHz because fracture flow is dominant. The strongly sorbing ^{239}Pu needs several thousands years to cover this distance (CRWMS M&O 2000, U0060, Section 6.7).

Within the PP, fracture flow may be dominant in pp4 and pp1 layers, while pp3 and pp2 layers behave like nonfractured porous media (Section 3.11.4). The top pp4 layer near SD-6 is breached in a short time, and then radionuclide transport is controlled by layers pp3 and pp2. These layers are quite efficient in retarding transport even for the nonsorbing ^{99}Tc , which takes more than 1,000 years. It takes several thousand years for ^{237}Np to reach the pp1 layer. The ^{239}Pu front does not cross the pp3 even after 10^5 years (CRWMS M&O 2000, U0060, Section 6.8).

3.11.5.4 Transport Simulations below the Potential Repository

Migration of radionuclides in borehole SD-6 is slow because of the presence of the CHv (see discussions in Section 3.11.4). The ^{99}Tc front takes several thousand years to reach the water table. The ^{237}Np breakthrough takes longer than 10^4 (but $<10^5$) years to reach the water table because of the moderate sorption (shown in Figure 3.11-4, where the right-side of the X-axis coincides with the location of water table). The strongly sorbing ^{239}Pu does not advance past the ch1v layer, less than 60 m from the point of release, even after 10^5 years (CRWMS M&O 2000, U0060, Section 6.9.2).

The ^{99}Tc transport in borehole UZ-14 shows a drastically different profile from that of SD-6. The extensive zeolitic zones of the CH at this location, where fracture flow is dominant, result in very rapid transport with a significant amount of ^{99}Tc reaching the water table in less than 10^3 years. Similarly, the ^{237}Np breakthrough at the water table takes substantially less than 10^4 years. Figure 3.11-4 compares the effects of the CHv and CHz on transport. The large portions of near-constant concentrations indicate the substantial impact of fracture-flow dominated CHz layers on transport (Figure 3.11-4). Even the strongly sorbing ^{239}Pu shows drastically enhanced migration by reaching a distance of about 255 m from the release point, yet it has not migrated past the pp3 layer after 10^5 years (CRWMS M&O 2000, U0060, Section 6.9.6).

3.11.6 3-D Site-Scale Radionuclide Transport

Modeling of radionuclide transport using large-scale 3-D grids was documented by CRWMS M&O (2000, U0060, Sections 6.10 to 6.14). The release rate of radionuclides at the potential repository was considered constant over time. Radionuclides of ^{99}Tc , ^{237}Np , and ^{239}Pu were

investigated, as well as the important members in the decay chains of ^{237}Np and ^{239}Pu . The grids and flow fields used for present-day infiltration and perched water model #1 were identical to those discussed by CRWMS M&O (2000, U0065, Section 6.2). The longitudinal dispersivity used was 1 m in the fractures and 0.1 m in the matrix as there is advective-dispersive transport through the matrix block (CRWMS M&O 2000, U0060, Table 6.14).

3.11.6.1 EOS9nT Code

EOS9nT V1.0 (see Section 1.3.2) is a TOUGH2 (V1.11) module for the simulation of an arbitrary number of solutes and/or colloids in the subsurface. The tracer transport equations account for advection, hydrodynamic dispersion, molecular diffusion, mass transfer between the mobile and immobile water fractions, sorption, radioactive decay, filtration (for colloids only), first-order chemical reactions, and colloid-facilitated transport. EOS9nT V1.0 considers equilibrium (linear, Freundlich, or Langmuir) sorption and kinetic sorption (linear, Freundlich, or Langmuir). Daughter products of radioactive decay can also be tracked.

EOS9nT V1.0 offers the option of a Laplace space formulation of the transport equations (in addition to conventional time-stepping) after the flow field becomes time-invariant. The Laplace transform formulation eliminates the need for time discretization, and an unlimited time-step size is thus possible without loss of accuracy or stability. It also completely linearizes all the kinetic transport equations and, thus, does not increase the order of the matrix to be solved. Additionally, the Laplace transform alleviates accuracy problems that may arise from the inaccurate weighting of the radioactive decay (CRWMS M&O 2000, U0060, Section 6.3.1). All the 3-D transport simulations are conducted by using the DeHoog implementation of the Laplace transform formulation of EOS9nT V1.0. Simulations are very fast and efficient, requiring 1,800–2,200 seconds of execution time to cover a simulation period of 10^6 years (CRWMS M&O 2000, U0060, Section 6.11.5).

3.11.6.2 Transport Simulation of ^{99}Tc

Breakthrough is described by the normalized release rate R , i.e., the ratio of radionuclide mass release rates at the groundwater versus that at the potential repository. The normalized release rate in Figure 3.11-5 shows a very strong dependence of ^{99}Tc transport on the infiltration regime. As the infiltration rate increases from lower bound to mean present-day level, the t_{10} time, defined as the time at which $R = 0.1$, decreases from about 10^4 years to about 300 years. The t_{50} , the time at which $R = 0.5$, decreases from about 45,000 years to about 4,000 years. Upper bound infiltration rate further reduces t_{10} (see Table 3.11-3). Figure 3.11-5 also shows that the maximum attainable R decreases with the infiltration rate, because lower bound infiltration results in lower velocities and longer times for transport, thus higher radioactive decay.

3.11.6.3 Transport Simulations of ^{237}Np and its Daughters

The sorption of ^{237}Np retards its transport through the UZ system, as compared to ^{99}Tc (Figure 3.11-5). From the values of t_{10} and t_{50} , the moderate sorption of ^{237}Np is sufficient to increase the time to reach the water table by a factor of about 40 (Table 3.11-3). Because of significant retardation, the maximum attainable R varies over a large range, and $R = 1.0$ is not achieved

within the simulation period. At $t = 10^6$ years, R is 0.98, 0.86, and 0.42 for the three infiltration rates, respectively (Figure 3.11-5).

Table 3.11-3. Breakthrough Time of Radionuclides at the Water Table (Years) (CRWMS M&O 2000, U0060, Table 6.15)

		Present-Day Infiltration		
		Lower Bound	Mean	Upper Bound
⁹⁹ Tc	t_{10}	10,000	300	45
	t_{50}	45,000	4,000	1,000
²³⁷ Np	t_{10}	220,000	10,000	1,700
	t_{50}	>1,000,000	120,000	22,000
²³⁹ Pu + ²³⁵ U + ²³¹ Pa	t_{10}	600,000	40,000	12,000
	t_{50}	>1,000,000	250,000	90,000

Important members in the ²³⁷Np decay chain are shown in Equation 2. The relative flux fraction M_R of each member of the chain, defined as the fraction of each radionuclide in the sum of the mass fluxes at the water table, shows that the daughter contribution only reaches a maximum of 2% at 10^6 years (CRWMS M&O 2000, U0060, Section 6.13.1.2). As such, daughter contributions to the ²³⁷Np transport are rather insignificant and could be safely ignored.



3.11.6.4 Transport Simulations of ²³⁹Pu and its Daughters

The value of R for ²³⁹Pu never reaches the 0.1 level even after 10^6 years of continuous release because of the strong sorption of ²³⁹Pu (Figure 3.11-5). The picture changes dramatically, however, if the daughter contributions to the release rate at the water table are accounted for in the computations. Given the half-life of ²³⁹Pu and the much longer one of ²³⁵U, the daughter contributions can become significant under the upper bound infiltration regime (Table 3.11-3).

The relative flux fractions M_R are also shown in Figure 3.11-5. The Pu contribution to the release rate starts declining rapidly after 100 years, and ²³⁵U is by far the dominant species after $t = 20,000$ years. Earlier emergence of ²³⁵U is associated with the lower bound infiltration rates because less ²³⁹Pu reaches the water table owing to strong sorption. Thus, after 1,000 years, the release at the water table consists mostly (over 95%) of ²³⁵U under lower bound present-day infiltration conditions. The ²³¹Pa contribution is negligible because of the very long half-life of ²³⁵U.

3.11.6.5 Transport-Controlling Features

The simulation results reveal that transport is controlled by the faults, especially at the early times. Splay G of the Solitario Canyon fault is the main transport-facilitating feature, as shown from the ^{99}Tc distribution of the fracture mass fraction (normalized to that at the point of release in the potential repository) at the bottom of the TSw at $t = 100$ years (Figure 3.11-6). Once contaminants reach the TSw-CHn interface, they move in an easterly direction, moving with the draining water that hugs the downward sloping low-permeability interface (CRWMS M&O 2000, U0060, Section 6.12).

The Ghost Dance fault splay is the next most important transport-facilitating feature (Figure 3.11-6). Though it facilitates downward migration, this fault appears to act as a barrier to the lateral migration of radionuclides, as evidenced both at the bottom of the TSw and at the water table. The Sundance fault and the Drill Hole Wash fault are also important. The Drill Hole Wash fault appears to act as a barrier to radionuclide migration laterally across it, while providing pathways for relatively fast transport to the water table (Figure 3.11-6). The main Ghost Dance fault does not play an important role in transport at the bottom of the TSw, as the ^{99}Tc does not reach the fault at this level even after 10^5 years (CRWMS M&O 2000, U0060, Section 6.12.2.2). This fault is more important at the water table, where it acts as a barrier to lateral transport while facilitating downward migration into the groundwater (Figure 3.11-6).

As time progresses, contributions of fractures and matrix become important. Fractures act as the important pathways of transport, and diffusion from the fractures into the matrix is the main retardation process in radionuclide transport. By sorbing onto the matrix into which they diffuse, the migration of radionuclides is retarded (CRWMS M&O 2000, U0060, Section 7.2).

The emerging transport pattern indicates that radionuclide transport to the groundwater is faster in the southern part of the potential repository block, where it is also areally concentrated. There are several reasons for this transport pattern (CRWMS M&O 2000, U0060, Section 6.12.2.3). First, the water flow pattern dictates the advective transport pattern, and the maximum water flow within the footprint of the potential repository is in its southern part in the Perched water model #1 (see Section 3.7.3.3). Second, the presence of the highly conductive faults (e.g., Splay G of the Solitario Canyon fault and the Ghost Dance fault splay) act as the venue for fast transport, despite the fact that the vitric CHn behaves as a porous medium (with relatively lower water velocities). This may be facilitated by flow focusing in the vitric CHn, whose vertical distribution shows a funnel-type structure in the south. Third, the low-permeability zones at the TSw-CHn interface in the northern part of the potential repository act as barriers to water drainage, and lead to low water velocities and presence of perched water bodies. Radionuclides move slowly through the perched water before reaching the underlying conductive zeolitic CHn, hence the delay in transport.

3.11.7 3-D Site-Scale Transport of Pu True Colloids

EOS9nT V1.0 is used for colloidal transport simulations, and the flow field and 3-D grid are identical to the ones discussed in Section 3.11.6.

3.11.7.1 Colloidal Forms, Properties, and Filtration Model

As concluded in CRWMS M&O 2000 (U0070, Section 7), the waste-form colloids (i.e., true colloids) will play a more significant role than natural colloids. True colloids are taken to have the properties of PuO_2 and are subject to radioactive decay. Four colloids of different sizes (450 nm, 200 nm, 100 nm, and 6 nm) are considered, with their accessibility factors into the geological units taken from CRWMS M&O (2000, U0070, Table 1). As reported by CRWMS M&O (2000, U0060, Section 6.16), the linear kinetic model of colloid filtration was used, with the forward kinetic coefficient, κ^+ , directly computed. There is no information on the kinetic declogging (reverse) coefficient, κ^- , which was entered as a fraction of κ^+ to examine the sensitivity of this parameter on colloidal transport.

3.11.7.2 Colloid Transport Simulations

For a given κ^+ , the transport of radioactive true colloids is strongly influenced by the κ^- . When no declogging is allowed, no colloids reach the groundwater (CRWMS M&O 2000, U0060, Section 6.16). Smaller values of κ^- (i.e., slow declogging) lead to significant retardation of colloids and longer times to reach the water table. In this case, t_{10} is more than 10^4 years, and t_{50} cannot be reached because the maximum attainable R at the water table never exceeds 0.3 (Figure 3.11-7). Larger values of κ^- (i.e., fast declogging) lead to dramatically different behavior, with very fast transport for the radioactive colloids to the water table. In this case, t_{10} can be as low as 15 years (Figure 3.11-7). The extreme sensitivity of colloid filtration on κ^- and the dearth of any representative information on this value in the various UZ geologic units underline the need for attention to this subject.

For a given κ^- , the colloid size has a significant effect on transport (Figure 3.11-7). Given the fact that fractures are the main transport conduit at Yucca Mountain, the inability of larger colloids to diffuse into the matrix, because of smaller diffusion coefficient values and size exclusion, result in fast transport to the groundwater. Smaller colloidal particles can diffuse more easily into the matrix, and their transport is thus more retarded. Size exclusion at the interfaces of different geologic units leads to colloid concentrations that can be significantly higher than that in the water released from the potential repository. These high concentrations are observed behind (i.e., they do not penetrate) the straining interfaces and are due to colloid accumulation because of their inability to move across these interfaces. This phenomenon is more pronounced for larger colloids (CRWMS M&O 2000, U0060, Section 6.16).

3.11.8 Estimates of Mass Breakthrough

This section summarizes the studies of tracer (conservative and reactive) transport using more than 20 3-D UZ flow fields and the T2R3D code V1.4 (see Section 1.3.2). The results provide insight to flow and transport processes from the repository to the water table (saturated zone) or from the land surface to the repository level and consider the potential effects of the major faults, different perched water conceptual models, infiltration scenarios, and sorption onto rocks.

Estimates of breakthrough are based on calculations of a conservative (nonsorbing) tracer, using the properties of ^{99}Tc and chloride-36 (^{36}Cl), and a reactive (adsorbing) tracer, using the properties of ^{237}Np (CRWMS M&O 2000, U0050, Section 6.7). Except for ^{36}Cl , the mechanical

dispersion effects through the fracture-matrix system are ignored, because sensitivity analyses show little effects of mechanical dispersion on cumulative tracer breakthrough curves at the water table. All transport simulations are run to 1 million years under steady-state flow and an initial, constant source concentration or constant mass flux conditions at the repository or surface fracture blocks. This assumes that all of the tracer is released instantaneously from the starting time of a simulation at the repository or land surface, while the radionuclides and/or colloids are released continuously at the potential repository for transport simulations discussed in Sections 3.11.6 and 3.11.7.

The fractional mass breakthrough is shown in Figures 3.11-8 and 3.11-9 and is defined as the cumulative mass of a tracer arrived at the water table or at the repository level over the entire bottom model boundary or the entire repository layer at the time, normalized by the total initial mass of the component at the source. Fifty percent mass breakthrough times for transport from the repository to the water table, estimated using 36 simulations are summarized in Figure 3.11-8. The figure correlates average infiltration rates with 50% cumulative mass-breakthrough, including all the infiltration scenarios and two perched water conceptual models discussed in Section 3.7. As shown in Figure 3.11-8, the predominant factors are (1) infiltration rates or net water recharge and (2) adsorption effects. In addition, perched water conceptual models also affect transport. However, the overall impact of the perched water conceptual models on tracer breakthrough at the water table is insignificant compared to infiltration and adsorption effects.

Analyses of mass breakthrough estimates at the water table indicate that:

- Times for 50% mass breakthrough are inversely proportional to the average infiltration (net water recharge) rate over the model domain. When an average infiltration rate increases from 5 to 35 mm/yr, the time for 50% mass breakthrough decreases by one to two orders of magnitude.
- Nonsorbing tracers migrate about one to two orders of magnitude faster than sorbing tracer when travelling from the repository to the water table under the same infiltration condition.

The transport of ^{36}Cl from the ground surface to the potential repository is also estimated using a fractional breakthrough curve, as shown in Figure 3.11-9, under the present-day, mean infiltration scenario. The figure shows a similar range of tracer transport times from the simulations with different surface source conditions (CRWMS M&O 2000, U0050, Section 6.7). Simulations 3 and 4 apply the ^{36}Cl source over the entire upper boundary while simulations 1 and 2 apply the source over the central area only to avoid lateral boundary effects. Simulations 1 and 3 apply all the ^{36}Cl at time = 0 while simulations 2 and 4 apply it as a constant mass fraction of the infiltrating water. There is about 1% or less total mass breakthrough during 10 to 100 years after tracer release on the ground. This indicates the existence of possible fast flow pathways with a transport time of 50 years, travelling from the ground surface to the repository level, under the steady-state UZ flow condition. However, the cumulative mass breakthrough is small (~1% of the total mass released on the ground) for the early breakthrough at 50 years. The average transport time from the surface to the repository level is estimated between 5,000 to 20,000 years using the 50% mass breakthrough curves of Figure 3.11-9 from the four simulation results.

Simulated tracer concentration distributions along vertical cross sections, and the ESF and ECRB tunnels show that earlier breakthrough of the tracer at the repository level is associated only with high-permeability faults.

3.11.9 Alternative Models

As discussed above in Sections 3.11.6 and 3.11.7, the main mechanism of radionuclide retardation in the UZ is diffusion from the fractures into the matrix. This process transfers radionuclides from the fast pathways to the matrix, where their transport is retarded because of the much slower water velocities and matrix sorption for sorbing radionuclides. An alternative conceptual model that does not allow diffusion (but still allows advection) into the matrix was investigated by CRWMS M&O 2000 (U0060, Section 6.17); the results of the investigation are discussed below.

3.11.9.1 Effects of Matrix Diffusion on Radionuclide Transport

For the no-diffusion alternative model using mean present-day infiltration, the nonsorbing ^{99}Tc and the moderately sorbing ^{237}Np move unhindered in the fractures, with their t_{10} and t_{50} about 5 and 30 years, respectively. A characteristic plateau at $t = 50$ years marks their arrival at the water table from fracture flow (Figure 3.11-10). The effects of the matrix flow become evident for $t > 100$ years, when matrix flow and contaminant transport begin to arrive at the water table. The nonsorbing ^{99}Tc arrives at the water table earlier than the moderately sorbing ^{237}Np . The phase of ^{237}Np release from fracture flow lasts from 50 to about 2,000 years, after which time the matrix flow (and the ^{237}Np it transports) arrives at the water table (Figure 3.11-10).

The limited sorption on the fracture walls is, however, sufficiently important to retard transport of strongly sorbing ^{239}Pu in the fractures (CRWMS M&O 2000, U0060, Section 6.17). If only ^{239}Pu is considered, the fracture release rate reaches a plateau at about 300 years, i.e., a very short time considering its half-life. There is no matrix flow contribution to the groundwater release of ^{239}Pu in the first 10^6 years. Accounting for the daughter products leads to matrix contributions to the water table after 10^4 years. These result (almost) exclusively from the release of the ^{235}U daughter, which sorbs less strongly than ^{239}Pu (Figure 3.11-10).

3.11.9.2 Colloidal Transport Simulation

Analysis of the alternative model indicates that diffusion is less significant in colloid transport than in solute transport, because (a) colloid diffusion is smaller than solute molecular diffusion because of the larger colloid size, and (b) size-exclusion effects at the interfaces of different geologic units further limit entry through diffusion into the matrix (especially for larger colloids) (CRWMS M&O 2000, U0060, Section 6.17). Its effect, however, becomes increasingly important for a decreasing colloid size (Figure 3.11-10).

The colloid breakthrough curves do not exhibit the plateaus (denoting pure fracture transport with no matrix contribution) of the solute curves, but rather a section of milder slope (Figure 3.11-10). This is attributed to the slower transport in the fractures (as a result of straining at the geologic unit interfaces) and the resulting evolution of concentrations larger than the one in the water released from the potential repository. Hence, the colloid concentration gradients across

straining interfaces keep increasing over time (because of colloid accumulation behind them), and they do not reach a steady state as in solutes (CRWMS M&O 2000, U0060, Section 6.17.2).

3.11.10 Uncertainty and Limitations

This section discusses the uncertainties and limitations related to radionuclide transport analysis in the UZ.

3.11.10.1 Assumptions

The soundness of radionuclide transport analysis depends upon the validity of the assumptions discussed in Section 3.11.1.3.

3.11.10.2 Sorption

Experimentally determined K_d values in Yucca Mountain studies have been predominantly derived from batch experiments using crushed tuff (with the sample size of 75–500 μm) under saturated conditions. There are concerns that this experimental approach may overestimate the K_d values (CRWMS M&O 2000, U0060, Section 6.1.3.1). This is because:

1. Batch experiment conditions may not be representative of the unsaturated conditions in the UZ. Little work has been reported for radionuclide sorption and transport in unsaturated rocks. Values of K_d may be invariant with respect to the water content, *if* similar experimental conditions (e.g., sample size, water chemistry, contact time) are employed. Experimental measurement of radionuclide sorption in unsaturated tuffs, however, deserves more attention. Laboratory studies of tracer penetration were presented to generate K_d values for core-sized samples under unsaturated conditions (CRWMS M&O 2000, U0015, Section 6.4). This approach could be adopted to generate K_d values of radionuclides in unsaturated solid tuff samples.
2. Crushing of tuff may create new surfaces and also increase the accessibility of pores that may not be contributing to radionuclide sorption in the intact rocks. Using smaller-sized samples could likely generate larger K_d values. Some studies have compared the K_d values obtained from batch sorption with diffusion-sorption experiments that use multimillimeter scale samples. The results consistently show little agreement between K_d values from these two methods, which could be largely attributable to the difference in sample sizes used (CRWMS M&O 2000, U0060, Section 6.1.3.1). Removal of fines (particle sizes less than 75 μm) is a routine step used in the standard batch-sorption procedures of the YMP; however, this could serve as a compensating factor for this issue.

Rate-limited sorption could be important, especially for fluid-radionuclide-rock systems with large sorption potential. Breakthrough curves for ^{237}Np transport in tuffs from the column experiments cannot be analyzed without considering rate-limited sorption (Viswanathan et al. 1998, p. 267). This result indicates the existence of rate-limited sorption under flowing conditions, possibly resulting from the slow diffusion of radionuclides into tuff pores. Rate-limited sorption may have a substantial effect on transport in fast fracture flow because it reduces

the extent of sorption in the matrix, thus allowing larger radionuclide concentrations and longer migration in the fractures. Nonlinear and irreversible sorption are also evident from the diffusion and transport studies by CRWMS M&O (2000 U0100, Sections 6.5 and 6.6). Overall, rate-limited and nonlinear sorption can insert an element of uncertainty into the validity of the linear equilibrium isotherm assumed in UZ transport studies.

There is limited information on sorption onto the fracture surfaces, which will retard migration of sorbing radionuclides. However, sorption in the fractures is not considered in the TSPA transport evaluations because of the limited data and conservative nature of this assumption.

3.11.10.3 Matrix Diffusion

Very limited experimental data exist on the tortuosity distribution in the various Yucca Mountain geologic units. In CRWMS M&O (2000, U0060), tortuosity is approximated by the value of porosity, an approach validated by the available, yet limited, experimental data (Section 3.11.2.5). Even less information exists on the effect of water content on effective diffusion coefficient, and the dependence could be much stronger than what could be expected from a linear relationship. This subject deserves more attention, because it could significantly affect transport estimates.

No information exists on whether the UZ media support surface diffusion (a possibility in zeolites). Surface diffusion can be important in radionuclides that exhibit strong sorption (e.g., Pu). A larger K_d clearly indicates stronger sorption, but this does not mean immobilization of the dissolved species when the fractured porous medium supports surface diffusion (Moridis 1999, pp. 1729–1740).

Different approaches to represent matrix diffusion could yield different transport behavior. Comparisons between FEHM V2.10 (see Section 1.3.2) particle-tracker and DCPT (see Section 1.3.2) were performed by CRWMS M&O (2000, U0155, Section 6.4.3). The two particle-tracking routines agree only if diffusion and dispersion are neglected. For the cases that include diffusion and dispersion, the median breakthrough for FEHM V2.10 occurs at times more than one or two orders of magnitude earlier. The difference is more pronounced for radionuclides undergoing sorption in the matrix. These differences stem from different implementations of the diffusive mass flow between fractures and the matrix in the two codes (CRWMS M&O, 2000, U0155, Section 7).

3.11.10.4 Radioactive Decay and Daughter Products

The ζ factor defines the fraction of the mass of the decayed sorbed parent that remains sorbed as a daughter ($0 \leq \zeta \leq 1$). The term ζ is introduced to account for the different sorption behavior of parents and daughters, and the fact that daughters can be ejected from grain surfaces because of recoil (CRWMS M&O 2000, U0060, Section 6.2.8.1). The ζ factor is a function of the decay type as well as of the chemical form of the sorbed cation. In alpha decay (e.g., ^{237}Np , ^{239}Pu), $\zeta = 0$ (CRWMS M&O 2000, U0060, Section 6.2.8.2). There is no information on the behavior of ζ for other types of decay. This issue can have significant implications for the transport behavior of daughters if (a) the large sorbed masses of strongly sorbing parents are ejected back

into the aqueous phase after decay, (b) the daughter is a much weaker sorber, or (c) its sorption follows a kinetic isotherm (CRWMS M&O 2000, U0060, Section 6.2.8.2).

3.11.10.5 Radionuclide Transport Simulations

The importance of faults and perched water bodies in transport depends directly upon the underlying geologic and perched water conceptual models. In the simulations discussed in Section 3.11.6, the geological model discussed in Section 3.2 and implemented in Section 3.4.2 and Perched water model #1 (see Section 3.7.3.3) were assumed. Changing geologic and perched water models may very well lead to different results (CRWMS M&O 2000, U0060, Section 6.11).

3.11.10.6 Colloidal Transport

Caution should be exercised in the interpretation of the colloid simulation results of Figure 3.11-7 because substantial knowledge gaps exist. The tremendous variation in behavior with the change in the kinetic declogging coefficient should only serve as an indication of the sensitivity of this parameter and to underline the need for more reliable information on this subject. The limits of the equations for the prediction of the forward kinetic filtration (clogging coefficient) have not been tested under the UZ conditions, and the subject of kinetic declogging coefficient has barely been raised (let alone studied). Additionally, it is unclear how representative the current size exclusion models are, because they are not based on laboratory measurements of filtered colloid suspension through rock samples but rather on predicted values obtained from retention curves and theoretical soil physics equations. The affinity of colloids for air-water interfaces could also have a potential effect on their transport (CRWMS M&O 2000, U0060, Section 6.15.8). The TSPA model only uses simple size exclusion filtering at fracture-matrix interfaces (Section 3.11.3.5).

3.11.11 Model Validation

This subsection discusses the validation of the Transport Model utilizing the results from Alcove 1 and Busted Butte tracer tests, and it shows that the model can be considered valid for its intended use.

3.11.11.1 Alcove Tracer Test

This section is based on Section 6.8.1 of CRWMS M&O (2000, U0050), which includes more detailed discussions and references for data sources. An infiltration and tracer transport test was performed in Alcove 1, located near the North Portal of the ESF in the upper lithophysal zone of the Tiva Canyon Tuff (Tpcpul). The crown of Alcove 1 is approximately 30 m below the ground surface. The infiltration test at Alcove 1 involved applying water at the ground surface. At a late stage of the test, a conservative tracer, bromide, was introduced into the infiltrating water. The seepage into the alcove and the tracer arrival time were recorded. The tracer test was carried out over a 51-day period, beginning on May 18, 1999. First detection of the tracer within the seepage occurred after 28 days.

Hydrological properties calibrated to earlier seepage data were used in the tracer simulation. The simulated breakthrough curve closely matches the tracer concentration data for a tortuosity value

of 0.75, which is close to the value of 0.7 given by Francis (1997, p. 5). This relatively high tortuosity value (see Section 3.11.2.5) is possibly related to the nearly saturated conditions in the test. The results indicate that the continuum approach is valid for modeling flow and transport in unsaturated fractured rock. The use of an active fracture model can capture the major features of fingering flow and transport in fractures. The matrix diffusion has a significant effect on the overall transport behavior in unsaturated fractured rock, while the dispersion in fractures does not.

3.11.11.2 Busted Butte Tracer Test

3.11.11.2.1 Laboratory K_d Measurements

The Busted Butte test facility was chosen based on the presence of a readily accessible exposure of the TSw and CHn and the similarity of these units at this location to their occurrence beneath the potential repository horizon (CRWMS M&O 2000, U0100, Section 6.8.1). Table 3.11-4 presents the K_d results obtained on rock samples collected from the TSw and CHn at Busted Butte. Values of K_d for Np and Am in Table 3.11-4 are similar to these in Table 3.11-1. However, the sorption values for Pu are significantly larger.

Table 3.11-4. Summary of Radionuclide Sorption Results from Busted Butte Tests (adapted from CRWMS M&O 2000, U0100, Tables 27-28)

Sample Source	Geologic Unit (Model Layer)	Approximate Average K_d (mL g ⁻¹)		
		Np	Am	Pu
Phase 1A, BH 3	Tptpv1 (ch1v)	0.3	380	19
Phase 1A, BH 4	Tac (ch2v)	1.4	470	2500
Phase 1B, BH 7	Tptpv2 (tsw39)	1.1	460	1100

3.11.11.2.2 Field Tracer Tests

The Busted Butte Unsaturated Zone Transport Test is a long-term experiment conducted by the YMP. Numerical simulations were conducted for two components of the first phase (Phases 1A and 1B) by CRWMS M&O (2000, U0060, Section 6.10). The field work of the first phase has been completed, but the analysis of the experimental results is not yet complete.

3.11.11.2.2.1 Phase 1A Test

The location of Phase 1A test was the vitric CHn (i.e., layers ch1v and ch2v; CRWMS M&O 2000, U0060, Figure VI.1). It involved injection rates of 10 mL/hr into boreholes 1 and 3, with borehole 3 located above and near the ch1v-ch2v interface and borehole 1 farther away from the interface. Injections were conducted continuously for 285 days, starting from April 2, 1998. At the end of the test, digital photographs were taken to evaluate tracer distribution, and rock samples were collected for moisture and tracer analysis. A 3-D modeling study, using the Calibrated Properties Model (Section 3.6) and hydraulic property measurements from field-collected samples, was conducted to predict the concentration of a nonreactive tracer and water saturation distributions (CRWMS M&O 2000, U0060, Section 6.10).

The simulated Br distribution in borehole 1 exhibits symmetric, near-circular patterns, and indicates the dominance of capillary over gravitational forces in the vitric CHn. This is consistent with the experimental results and the expected flow and transport behavior in the vitric CHv discussed in Section 3.11.4. Borehole 3 simulations using the Calibrated Properties Model show that the flattening of tracer distribution occurs as the tracer moves preferentially laterally along the chl_v-ch_{2v} interface. Experimental results also show the flattening behavior for borehole 3. When the hydraulic property measurements from field-collected samples are used, the Br distribution follows a more uniform pattern, which exhibits little flattening. This indicates that the permeability contrast from the limited number of core measurements is smaller than that suggested from the Calibrated Properties Model.

3.11.11.2.2.2 Phase 1B Test

In the Phase 1B field test, the tracers were injected into the lower portion of the TSw basal vitrophyre, which is a relatively low-permeability fractured rock. The tracer solution was injected at a rate of 10 mL/hr at the location $x = 1.30$ m from the rock surface into borehole 5. Injections began on May 12, 1998, and ceased on November 9, 1998. Liquid samples from collection borehole 6 were regularly collected and analyzed. For the 3-D numerical studies, the geologic model treated the domain as a homogeneous, unfractured rock matrix. Although this geologic layer is known to have fractures, the use of unfractured rock matrix as the domain model in the simulation was made possible by the system behavior during the injections, which did not show evidence of fracture flow.

Experimental breakthrough data for both the nonsorbing and sorbing tracers can be found in CRWMS M&O (2000, U0100, Section 6.8.5.3.2). Peak concentrations are observed directly beneath the injection point of borehole 5. The measured concentrations indicate transport consistent with flow in the matrix (rather than in the fractures), which appears to quickly imbibe the injected solution.

Visual inspection of the predicted breakthrough curves for nonsorbing tracer at several sampling locations indicates that the predictions are in good agreement with the measured data (CRWMS M&O 2000, U0060, Section 6.10). The breakthrough curves of sorbing tracer Li⁺ (lithium) follow a distinctively different pattern. Sorption of Li⁺ results in maximum relative concentrations significantly lower than the ones observed in the nonsorbing tracers. Predictions based on the laboratory-derived $K_d = 1$ mL/g are higher than the measured concentrations in CRWMS M&O (2000, U0100, Section 6.8.5.3.2). When K_d is increased to 2 mL/g, predictions are consistent with the measured Li⁺ concentrations (CRWMS M&O 2000, U0060, Section 6.10).

3.11.12 Analogs to Radionuclide Transport in the UZ

This section is based on Section 6.5.2.1 of CRWMS M&O (2000, U0135), which includes more detailed discussions and references for data sources. Three UZ analogs are considered: (1) the Nopal I uranium deposit at Peña Blanca, Chihuahua, Mexico, (2) the collective northwestern Nevada-Southeastern Oregon uranium deposits, and (3) the trace metal migration study at Santorini, Greece.

3.11.12.1 Natural Analog Studies at Peña Blanca, Mexico

From the 1980s, the Nopal I uranium deposit at Peña Blanca has been recognized as a natural analog for the potential repository at Yucca Mountain. Transport of U-series nuclides at Peña Blanca has occurred over a range of time scales. From the U-Th (thorium) age data, it appears that the primary transport of U to the fractures occurred more than 300 ka (thousand years) ago. Subsequently, there has not been significant ^{238}U or ^{235}U redistribution. The 300 ka stability of uranium (235, 238), thorium, and protactinium in the fracture-filling minerals has apparently survived even recent hydrological disturbances from surface water infiltration of the fractures, as well as the infiltration of rainwater.

Recent data obtained from U-series thermal ionization mass spectrometry indicate that the geochemical system at Nopal I restricts actinide mobility in the unsaturated environment. By analog, the tuffs at Yucca Mountain should have similar retentive properties to impede oxidized uranium mobility. The accumulation of natural analog data from Peña Blanca and similar sites would be of particular importance if such data demonstrated the general validity (or lack thereof) of low actinide mobility in unsaturated silicious tuffs under semi-arid climate conditions.

3.11.12.2 Uranium Deposits in Northwestern Nevada/Southeastern Oregon

The McDermitt Caldera uranium deposits and other uranium deposits in northwestern Nevada and southeastern Oregon have also been mentioned as possible analogs. Some of the uranium mineralization at these sites may constitute good analogs to aspects of radionuclide transport at Yucca Mountain, but this is questionable for several reasons. One reason is that the host volcanic rocks for these deposits are somewhat different. Another is that the uranium mineralization is fine-grained and low in concentration in these deposits. Also, age of deposition is poorly constrained for most of the deposits, and source-term information needed for models is lacking. Furthermore, hydrological data are sparse. Hence, in spite of their appealing proximity to Yucca Mountain for ease of study, these uranium deposits would require extensive additional characterization to build confidence in flow and transport process models.

3.11.12.3 Akrotiri Archeological Site, Santorini, Greece

Akrotiri is similar to Yucca Mountain in its silicic volcanic rocks, dry climate, and oxidizing, hydrologically unsaturated subsurface conditions. Bronze and lead artifacts were buried under 1.5 to 2.0 meters of volcanic ash 3,600 years ago. Evidence for a plume of Cu (copper), Sn (tin), and Pb (lead) was investigated through selective leaching of packed earth and bedrock samples collected directly beneath the site where bronze and lead artifacts were excavated. Field data indicated that little of the bronze material had been transported away from its primary location. The total amount of Cu predicted to have been removed from the artifacts is roughly three orders of magnitude smaller than the volume of the artifacts. Neither Cu nor Pb was detected below a depth of 45 cm. The Akrotiri study shows preservation of artifacts for a long period of time in an oxidizing environment, indicating that unsaturated systems in arid environments may provide favorable sites for geologic disposal of radioactive waste.

3.11.13 Abstraction of Transport Model

3.11.13.1 Introduction

An abstraction of Transport Model in the UZ is used for calculations of radionuclide transport in performance assessment. In this case, the abstraction is also a process model in which simplified mathematical representations of the physical processes are used. The reason for using a model abstraction for performance assessment is that computational requirements for the process model are too demanding for performance assessment calculations that require a large number of calculations to address different scenarios and encompass the desired parameter ranges. Therefore, the transport model abstraction is computationally streamlined to allow for more rapid calculations. As a more streamlined computational tool, the transport model abstraction can be run concurrently with the TSPA model. Changes in radionuclide releases from the engineered barrier system over time are directly input to the transport model abstraction, which then determines the spatial and temporal distributions of the radionuclides at the water table.

The transport model abstraction is a 3-D, dual-permeability, particle-tracking method (CRWMS M&O 2000, U0065). Flow fields derived using the 3-D site-scale flow model are input directly to the particle-tracking method and are used to compute transport velocities. The method explicitly accounts for transport in both the fracture and matrix continua, with exchange between continua resulting from advective or diffusive processes. The velocity fields from the flow model are also used for advective transport exchange between the fracture and matrix continua. The various aspects of the transport process—advection, diffusion, dispersion, sorption, radionuclide decay, and colloid-facilitated transport—are all explicitly modeled.

3.11.13.2 Assumptions

As for any mathematical model of a physical process, there are assumptions associated with the model. These assumptions represent simplifications or idealizations that allow a specific mathematical treatment.

Assumption 1: Sorption can be adequately represented by a linear model.

Basis: The basis for this assumption is discussed in Section 3.11.3.2.

Assumption 2: The effects of flow in the matrix are negligible with respect to radionuclide exchange between fractures and matrix through matrix diffusion.

Basis: This is a simplifying assumption that allows for rapid computation of the effects of matrix diffusion on transport while including the specific effects of the radionuclide concentration gradients in the matrix (normal to the fracture planes). The details of this fracture to matrix concentration gradient are difficult to capture in a numerical model because of the fine spatial resolution of the grid required. This assumption allows for the treatment of this process with an analytical or semi-analytical model that captures the effects of this gradient without requiring the numerical gridding. Results from comparison calculations between the model abstraction and the process-level model suggest that this assumption is conservative for predictions of radionuclide transport (CRWMS M&O 2000, U0065, Section 6.3; CRWMS M&O 2000, U0160, Section 6.2.5).

Assumption 3: Colloid-facilitated radionuclide transport can be approximated by two end-member representations for colloid-radionuclide associations: equilibrium, reversible exchange of radionuclides between colloids and the aqueous-phase radionuclides, and irreversible association of radionuclides with colloids.

Basis: Any radionuclide/colloid association would lie somewhere between the bounds established by this assumption. Because transport behavior is expected to be conservatively bounded by radionuclides irreversibly attached to colloids, the effects of colloid transport can be conservatively bounded with a mixture of these end-member models.

Assumption 4: Colloid filtration/resuspension processes can be represented as an equilibrium process in which colloids are partitioned between mobile and immobile conditions.

Basis: Any opposing first-order rate reactions can be expressed in terms of an equivalent, equilibrium partitioning coefficient that is proportional to the ratio of the forward and reverse rate constants — if the process can be averaged over a sufficiently long time. The rate constants identified by CRWMS M&O (2000, U0070, Section 6.2.3) indicate that filtration/resuspension time scales are on the order of tens of days. Given typical UZ transport times of years to thousands of years, the use of an equilibrium-partitioning coefficient is reasonable.

Assumption 5: Dispersive transport is small in comparison with advective transport.

Basis: The criterion for applicability is based on the grid Peclet number $Pe_g = \Delta x / \alpha$, where Δx is the characteristic length scale of the computational cell and α is the dispersivity, or dispersion length scale, associated with transport across the cell (Fetter 1993, pp. 49–52). Dispersive transport over a computational cell in the numerical model is expected to be scale dependent, i.e., the appropriate value of dispersivity is proportional to the size of the computational cell. This Pe_g ratio is expected to be greater than 10 for a scale-dependent dispersivity, indicating advection-dominated transport.

3.11.13.3 Approach

The particle-tracking abstraction model follows particles through an interconnected network of computational cells that constitutes the computational domain. Particle locations are identified by the computational cell coordinates, which is the lower limit of spatial resolution in the model. This cell-to-cell particle tracking method is similar to that described by Desbarats (1990, pp. 153–163). The basis for the method is described by CRWMS M&O (2000, U0065, Section 6.1.1). Briefly, particles are assigned a residence time randomly from a residence time distribution that is computed from the processes that affect residence time (e.g., advection, sorption, and matrix diffusion). For a cumulative probability distribution function of particle residence times, we compute the residence time of a particle in a cell by generating a random number between 0 and 1 to determine the corresponding residence time from the distribution function in Figure 3.11-11. The advection-dispersion equation was used to generate the schematic residence time transfer function (RTTF) curve, but other transport mechanisms can be incorporated as well. The particle moves from the resident cell to an adjoining cell randomly, with the probability of entering an adjoining cell set according to the proportion of efflux from the resident cell into each of the adjoining cells.

This same methodology is extended to a dual-permeability grid with residence time distributions in a single cell determined through mathematical models for advection, sorption, matrix diffusion, dispersion, radionuclide decay, and colloid-facilitated transport. The dual-permeability transport model includes advective and diffusive transfers between the fracture and matrix continua.

Colloid transport is included in the abstraction through two end-member representations of radionuclide/colloid associations (Assumption 3 in Section 3.11.13.2). Radionuclides that reversibly exchange between the aqueous phase and a sorbed phase on colloids are included in the transport abstraction as a separate aqueous "species". It is shown in CRWMS M&O 2000 (U0065, Section 6.1.4) that this type of colloid-facilitated radionuclide transport is mathematically equivalent to aqueous transport with appropriately modified transport coefficients. This approach assumes a linear partition coefficient between the mass concentration of radionuclide in the aqueous phase and the mass concentration of radionuclide attached to any given type of colloid. Colloids may be temporarily "detained" at the fracture/matrix interfaces, and this interaction is captured in the colloid transport model as a retardation factor for colloid transport in the fracture system. Finally, colloids are subject to size exclusion for entering the matrix from the fractures. This is represented by a size exclusion factor that multiplies the probability for a colloid to enter the matrix from the fractures. The size exclusion factor is computed based on the colloid sizes and matrix pore size distribution.

Colloids that have a fixed radionuclide content represent the other end-member representation for colloid-facilitated radionuclide transport. In this case, the radionuclides may be considered permanently fixed in the colloid structure and do not partition with the aqueous phase. Radionuclides permanently attached to colloids are also tracked as separate species in the particle-tracking model. This colloid type is subject to retardation in the fracture system and size exclusion, as described above. In addition, this colloid type is subject to permanent filtration for cases in which the colloids are making a transition from one matrix unit to another. Permanent filtration is computed in a manner similar to the way colloid size exclusion is computed for movement between fractures and matrix. The colloid filtration is expressed as a factor that multiplies the probability for colloid movement between matrix units, which is again a function of the colloid size and matrix pore size distribution. It should be noted that this filtration mechanism is not applied to colloids with radionuclides that reversibly exchange with the aqueous phase because a permanently filtered colloid in this case will not remove the radionuclide from subsequent transport.

3.11.13.4 Results

The particle-tracking method has been compared to alternate solution methods for a variety of problems. Results for 1-D transport with diffusion and sorption are found to agree with well-established analytical solutions (CRWMS M&O 2000, U0065, Section 6.2.1). A good match is also obtained for transport in a dual-porosity system including matrix diffusion (CRWMS M&O 2000, U0065, Section 6.2.2).

Comparisons with numerical models for transport in a 1-D, dual-permeability model have also been performed (CRWMS M&O 2000, U0065, Section 6.3). The comparisons shown here are for a simplified, 1-D, dual-permeability flow model for the UZ of Yucca Mountain. The flow

system consists of three significant hydrological units between the solute release point (the potential repository elevation) and the water table. Figure 3.11-12 shows the ability of the particle-tracking abstraction to match the full numerical solution for a dual-permeability model. The Y-axis is labeled the Cumulative RTD, which stands for Cumulative Residence Time Distribution. This is the fraction of particles that have traversed the UZ (between the potential repository and the water table) at any given time. This case, without matrix diffusion, shows how the model is able to capture advection and dispersion (the solid black line is the full dual-permeability numerical solution and the dashed red line is for dispersion with no diffusion using the particle-tracking algorithm). The dashed black line in Figure 3.11-12 shows that the particle-tracking algorithm is also able to produce sharp breakthrough curves when dispersion is zero, something that is difficult to do in a conventional numerical solution.

Figure 3.11-13 shows comparisons for a 1-D dual-permeability solution when matrix diffusion is included. Here there is a discrepancy at early time, in which the conventional numerical simulation predicts an early breakthrough in the case where the matrix diffusion is nonzero. The conventional solution uses a single cell to represent the matrix adjacent to a fracture cell. Thus the concentration gradient in the matrix (in a direction normal to the fracture plane) is only roughly represented in the conventional model. This discrepancy results in an early breakthrough because the exact representation of this gradient can represent a steep but narrow gradient in the matrix near the fracture plane and therefore gives a larger fracture to matrix diffusive flux. This reduced diffusive flux into the matrix leads to an earlier breakthrough.

Matrix diffusion in the particle-tracking algorithm is only exact if matrix advection is zero (see Assumption 2). To test this assumption, we performed calculations (CRWMS M&O 2000, U0160) using a particle-tracking method that does not use this assumption. The results shown in Figures 3.11-14 and 3.11-15 are for a 3-D simulation using the dual-permeability site-scale flow model. Transport is calculated for the 3-D, dual-permeability system using the model abstraction (FEHM V2.10) and a second particle-tracking routine, DCPT V1.0. The DCPT V1.0 code uses a Lagrangian approach that interpolates the velocity field onto a continuous space in which particles can travel. This routine simultaneously accounts for the effects of matrix diffusion and matrix advection. The breakthrough for the nonsorbing Tc is shown in Figure 3.11-14. The reason for the delayed breakthrough curve for DCPT V1.0 is thought to be a result of the inclusion of matrix advection in the treatment of matrix diffusion. Advective flow from the fractures to the matrix will reduce the flux of radionuclides from matrix to fractures through diffusion. Thus, radionuclides will tend to be retained for longer times in the matrix, leading to slower breakthrough.

A similar comparison is also made for the sorbing Np in Figure 3.11-16. The differences in the two solution methods found in Figure 3.11-14 are accentuated for sorbing radionuclides. In these comparisons, we find that in the model abstraction solution FEHM V2.10 predicts radionuclide movement to the water table that is significantly faster than that predicted by the DCPT V1.0 solution. Although the differences can be large, the model abstraction solution is found to be conservative. These two particle tracking methodologies and the advective-dispersive approach utilized in T2R3D V1.4 are further compared in CRWMS M&O (2000, U0155).

3.11.14 Summary and Conclusions

Figure 3.11-16 corresponds to Figure 3.11-1, which shows key issues related to radionuclide transport in the UZ. The following conclusions can be drawn from this section:

1. Two-dimensional simulations show that transport in the CHn is strongly dependent on the distribution of the vitric and zeolitic tuffs at the different locations. Occurrence of the zeolitic CHn leads to fast transport; on the other hand, the vitric CHn acts as an effective barrier to radionuclide transport, and its effectiveness increases with the sorptive tendencies of the radionuclides.
2. Three-dimensional site-scale simulations indicate that radionuclide transport is both dominated and controlled by the faults (especially at early times). Faults provide fast pathways to downward migration to the water table, but also limit lateral transport across them.
3. Fractures are also the main pathway of transport. Diffusion from the fractures into the matrix is the main retardation mechanism in radionuclide transport. By sorbing onto the matrix into which they diffuse, the migration of radionuclides is retarded.
4. Three-dimensional site-scale simulations show that radionuclide breakthrough at the water table occurs early and over a large area in the southern part of the potential repository block. The maximum water flow within the footprint of the potential repository in the southern part in the Perched water model #1 contributes to this transport pattern. Also the low-permeability zones at the TSw-CHn interface in the northern part of the potential repository are barriers to water drainage and lead to low water velocities and formation of perched water bodies. The presence of the highly conductive Solitario Canyon Splay G and Ghost Dance fault splay also contributes to the dominance of the southern part as the main pathway.
5. The members of the decay chain (^{239}Pu , ^{235}U , and ^{231}Pa) must be considered in the transport of ^{239}Pu . Uranium-235 will become the main contributor in the release at the water table after 10,000 years (at most) because of its weaker sorption onto the matrix and longer half-life. The contributions of ^{231}Pa are not important.
6. Colloidal transport is very sensitive to filtration parameters, and for the given parameters, the colloid size has a significant effect on transport.
7. More than 40 tracer transport simulations indicate a wide range of time for mass breakthrough depending on infiltration rates, type of tracers/radionuclides, and perched water conceptual models. The most important of these factors for transport times are (1) surface infiltration rates and (2) adsorption effects in the CHn. Compared with the effects of infiltration and adsorption, perched water conceptual models are of secondary importance to the overall impact on transport,

but have primary impact on determining breakthrough areas of tracers/radionuclides at the water table.

8. The modeling results of tracer (^{36}Cl) transport from the land surface to the repository level indicate the existence of possible fast flow pathways with transport times of 50 years. However, the cumulative mass breakthrough carried by the fast flow is relative small (about 1%) for the early times of 50 to 100 years. The 50% mass breakthrough times to the repository level since release from the surface is estimated between 5,000 to 20,000 years under the present-day, mean infiltration scenario. The fast flow breakthrough at the earlier time occurs mainly along faults.
9. Available tracer transport results of the ESF Alcove 1 and Busted Butte tests are analyzed for model validation as a confidence-building process. The Alcove 1 analyses indicate that the continuum approach is valid for modeling flow and transport in unsaturated fractured rock, an active fracture model can capture the major features of fingering flow and transport in fractures, and matrix diffusion has a significant effect on the overall transport behavior. Busted Butte tracer tests and simulations of the vitric CHn show that the unit behaves as a porous medium, which is consistent with the expected behavior.
10. Known analog sites for UZ transport are reviewed as additional corroborative analyses with respect to radionuclide transport at Yucca Mountain. Analyses of the Nopal I uranium deposit in Mexico and the trace metal migration study in Greece indicate that unsaturated systems in arid environments may provide favorable sites for geologic disposal of radioactive waste.
11. An efficient particle-tracking model abstraction for 3-D site-scale simulations of radionuclide transport in the UZ has been developed for TSPA analysis. This model abstraction utilizes simplified mathematical representations of advection, dispersion, sorption, matrix diffusion, colloid transport, and radionuclide chain decay in a dual-permeability system. Comparisons show that the TSPA particle-tracker will yield conservative transport calculations.

INTENTIONALLY LEFT BLANK

3.12 MOUNTAIN-SCALE TH MODEL

3.12.1 Introduction

Unsaturated zone (UZ) flow and transport will be affected by the heat released from the decay of radioactive waste in emplacement drifts of the potential repository at Yucca Mountain. The Analysis/Model Report for mountain-scale coupled processes (CRWMS M&O 2000, U0105), documents the development of the Mountain-Scale Thermal-Hydrological (TH) Model. This model evaluates the effects of heat on UZ flow and the distribution of liquid and temperature over a period of 100,000 years and provides the necessary framework to test conceptual hypotheses of coupled heat and fluid flow in the UZ. This model can then be used to predict future behavior in the UZ under thermal loading. This section summarizes the results of the TH Model, identifies the performance issues addressed and provides resolutions of the issues in terms of input for Performance Assessment (PA).

The Mountain-Scale UZ TH model complements the EBS MultiScale TH (MSTH) (CRWMS M&O 2000, E0120) model in the evaluation of the impact of thermal loading on the NFE TH conditions and the EBS system, at the potential repository. The MSTH model samples TH conditions at several locations at the potential repository and includes influence of alternative waste package configurations. The model is a localized alternative to a fully coupled 3-D drift-scale and Mountain-Scale TH model, that provides detailed drift-scale processes at the repository under thermal loading, from a sampling of mountain-scale locations. The Mountain-Scale UZ TH model on the other hand provides an estimate of mountain-scale evolution of the flow field coupled to a simplified representation of the drift-scale processes. Detailed drift-scale TH and THC processes are modeled and discussed in CRWMS M&O (2000, N0120/U0110).

Figure 3.12-1 presents design issues modeled by heating the volume of UZ rock surrounding the potential repository. The issues provide for qualitative and quantitative evaluation of the impact of potential repository heat on the UZ and include the following:

- Extent of the two-phase zone
- Liquid and gas flux in near field and far field
- Moisture redistribution in the UZ
- Temperature at drift walls and in pillars in between drifts
- Potential for flow and transport property changes in the PTn and CHn
- TH effects on water table and perched water bodies
- Influence of climate and ventilation.

The thermal load and the resulting temperature changes have a large influence on many related processes, which directly impact the performance of the potential repository. The emplacement of heat-generating high-level waste will elevate temperatures and cause the redistribution of the *in situ* moisture in the unsaturated zone. For example, if the temperature of the rocks near the emplacement drifts approaches or exceeds the boiling point of water (97°C at ambient pressure), boiling of formation water will take place, with the associated increase in vapor pressure and overall gas-phase pressure. This will result in forced convection of the gas phase, that is accompanied by large latent heat effects. Phase transformation and gas-phase flow will perturb the *in situ* fluid distribution in the fractures and matrix, thereby changing capillary pressure gradients, relative

permeability and liquid-phase flow rates. The impact of heat on the TH processes will depend on the thermal load as well as its distribution in the emplacement drifts.

The Mountain-Scale TH Model numerically simulates the potential impact of the heat that is released by radioactive decay on the natural hydrogeological system, including a representation of heat-driven processes occurring in regions far away from the potential repository (the far field). The simulations provide predictions for thermally affected liquid saturation, gas- and liquid-phase flux (together referred to as flow fields), and the distribution of temperature and saturation in the UZ. Of particular interest is the impact of thermal loading imposed by waste emplacement on water percolation at and near the potential repository host rock and the flow barrier effects in the basal vitrophyre of the Topopah Springs and the Calico Hills zeolites underlying the potential repository horizon. These rock units impede the transport of radionuclides from the potential repository to the water table due to their low permeability and high sorptivity. When heated for long periods of time at temperatures exceeding 90°C, the flow and transport properties of these rocks can be altered, thus directly impacting their ability to impede transport of radionuclides.

The Mountain-Scale TH Model is developed based on the UZ Flow Model. This model uses input parameters based on the calibrated property set (CRWMS M&O 2000, U0035), a spatially varying mean infiltration rate, with varying climates during the thermal-loading period. The simulations were performed using the average initial thermal load of 72.7 kW/acre, scaled down by the natural decay curve over a total simulation period of 100,000 years. To account for ventilation, only 30% of this heat is used during the first 50 years.

Prediction of the thermal-loading effect in such models in turn requires establishment and acceptance of mathematical models that accurately represent the physics of coupled heat and fluid flow in the UZ. The TH Model uses the mathematical formulation employed in the TOUGH2 family of codes (Pruess 1987, pp. 2–11; Pruess 1991), the dual-continua approach (Section 3.4) and the van Genuchten capillary pressure and relative permeability parameter values obtained from the calibrated properties data (CRWMS M&O 2000, U0035) to describe the behavior of the UZ under thermal-loading conditions. This formulation is based on the traditional energy- and mass-conservation relationships.

During the development of the TH Model (CRWMS M&O 2000, U0105), the accuracy and validity of the model results were evaluated based on current understanding of fracture-matrix interactions, heat transfer, and two-phase flow in unsaturated subsurface systems. Calibration of modeled temperature against the measured temperature profiles in boreholes (CRWMS M&O 2000, U0050, Section 6.3) provides a basis for assessing the effectiveness of the model to capture the ambient, mountain-scale temperature distribution, which is used as the initial temperature for TH modeling.

3.12.2 Modeling Approach

The TH Model is used to model the nonisothermal TH processes due to heat generated by the emplaced heat source. Figure 3.12-2 shows the relationship between the TH Model, the input data, and the models supporting its development. This section presents a brief discussion of the

development of the TH conceptual model and numerical grids, as well as the selection of input data and the model boundary and initial conditions.

3.12.2.1 Conceptual Model

The conceptual model for describing the TH processes at Yucca Mountain is based on the conceptual model used for the UZ Flow Model, as discussed in Sections 3.3 and 3.7. In this hydrogeological conceptual model, the UZ system consists of multi-layered hydrogeologic units, with flow behavior determined primarily by the degree of welding of the Yucca Mountain tuffs (Sections 3.2 and 3.4). The heat transfer within the UZ system is fully coupled with other processes, such as liquid percolation and air circulation.

The numerical approaches (Section 3.4) involve volume averaging and the continuum concept for modeling coupled fluid and heat flow and fracture-matrix interaction. The dual-permeability formulation described in Section 3.4 and CRWMS M&O (2000, U0000, Section 6.7) with a single fracture element and single matrix element representing each continuum is used in all the TH simulations. This dual-continua method allows for global flow through both the fracture and matrix continua. The fracture-matrix interaction is modeled using the active fracture concept (Liu et al. 1998, pp. 2633–2646) for liquid flow in dual-continua.

The TH simulations were conducted using TOUGH2 V1.4 (Section 1.3), with the equation-of-state module EOS3 (water, air and heat). The EOS3 module contains the constitutive relationships that describe the thermodynamic properties of water (enthalpy, density, viscosity) as functions of temperature and pressure. In all simulated cases the relationships between relative permeability and capillary pressure for unsaturated rock are estimated using documented relations of Brooks and Corey (1966, pp. 61–88) and van Genuchten (1980, pp. 892–898).

3.12.2.2 Numerical Grids

Several numerical grids were used for TH simulations, including (1) a 3-D submodel grid of the UZ 3-D grid and (2) two 2-D cross-section grids (NS#1 and NS#2). All the numerical grids are based on the Geologic Framework Model (GFM 3.1). Figure 3.12-3 shows a plan view of the UZ 3-D grid and the location of the potential repository submodel grid and the 2-D cross-section grids NS#1 and NS#2. The numerical grid resolution and layers along the NS#2 cross section are shown in Figure 3.12-4. Most of the results presented in this section utilize this cross section, with the lateral grid spacing equal to 1/4 of the drift spacing. A detailed discussion of numerical grids is presented in Section 3.4 and in CRWMS M&O (2000, U0000) and CRWMS M&O (2000, U0105, Section 6.2).

The design of the lateral grid spacing within the potential repository domain includes the proposed spacing and orientation of the drifts. For the 3-D grid, the lateral spacing over the potential repository domain is equal to the spacing between the drifts (81 meters). The vertical grid design uses a 5 m thick grid layer to represent the potential repository horizon, at the elevation of the proposed repository. This layer is bounded above and below by 5 m thick layers CRWMS M&O (2000, U0000, Section 6.6.2). This type of grid, although sufficient to resolve mountain-scale processes, does not provide sufficient resolution for detailed evaluation of TH conditions around and between drifts.

In the 3-D grids discussed above and in CRWMS M&O (2000, U0000 and 2000, U0105), each potential repository drift is represented by elements aligned along the direction of drifts. For the 2-D cross-section grids, each drift is represented by a single element (with both matrix and fracture continua). In the design for the potential repository, the heat-generating radioactive waste will be stored in widely spaced drifts (up to 81 m spacing) at the repository horizon. This physical separation of the drifts in the real world can be lost in numerical grids if large grid spacing is used. If the grid spacing within the potential repository is equal to the drift spacing, then although the drifts are physically separated, they are in fact numerically adjacent. This results in a laterally continuous (smeared) heat source across the potential repository. Such a numerical grid (although sufficient for resolution of UZ Mountain-Scale ambient flow processes) cannot provide adequate resolution to study TH processes in terms of temperature, saturation, and flux between the drifts. The discrete (drift-by-drift) grid provides a model in which such phenomena can be investigated and the effect on the mountain-scale TH processes to be documented. In the 3-D grids this requires development of a new, locally refined grid, with a large number of elements, which greatly increases numerical computation time. In the cross-section grids, locally refined drift elements can be added at the potential repository horizon, without a substantial increase in the total number of elements.

To develop TH models that provide a detailed resolution of the ambient flux and resolve the TH conditions near and between the drifts, the locally refined grid NS#2 described in CRWMS M&O (2000, U0105, Section 6.2.2) was used. This grid incorporates individual drifts, and provides several nodes between the drifts so that evolution of TH conditions at the drifts and within the pillars can be modeled. Detailed discussion of the development of this numerical grid that provides a physically more accurate representation of the heat distribution at the potential repository is presented in CRWMS M&O (2000, U0105 Sections 6.2 and 6.3).

3.12.2.3 Potential Repository Thermal Load

Mountain-scale thermal-loading data, which include the initial thermal load and the natural radioactive decay rate, were used in all the TH models. The total initial thermal load for the base-case scenario is 72.7 kW/acre (18.0 W/m²), based on a potential repository area of 1,050 acres (4.25×10⁶ m²). In the cross-section grids, the amount of heat to be applied to individual drifts was computed based on this initial thermal load, the decay curve, and the lateral spacing between the drifts. This thermal load was then applied as a heat source to the matrix continuum of the discrete drift elements at the potential repository, beginning with the maximum thermal load at time zero and scaling it down according to the tabulated decay curve at subsequent times. This thermal load is included in the TOUGH2 input as a tabulated lookup of time versus heat for matrix elements representing the potential repository drifts. To include the effects of a 50 year pre closure period of ventilation, this heat load is further scaled down. In the ventilated drift thermal-loading scenario, 70% of the heat generated by the radioactive is removed by the ventilation system. Therefore, only 30% of the computed heat is included in the input during this period. After 50 years, the "no-ventilation" heat input is used. Since the practical and logistical details of ventilation and its efficiency have not been ascertained both the "no-ventilation" and "ventilation" scenarios were modeled in order to quantify the impact of ventilation.

3.12.2.4 Boundary and Initial Conditions

The UZ numerical grids (Section 3.4 and CRWMS M&O 2000, U0000) consider the top of Tiva Canyon (TCw) hydrogeological unit as the top boundary. This coincides with the ground surface in most areas, except in areas with thick alluvium cover, where the top of the model is at the alluvium-TCw contact. All TH numerical grids also use this surface as the reference top boundary. Fixed temperature, gas saturation and gas pressure corresponding to the near surface conditions are assigned along this boundary.

The water table is used as the bottom boundary for fluid flow with a fixed liquid saturation and gas pressure prescribed. These conditions represent estimated gas pressure and capillary fringe saturation at the water table. Temperature changes at the water table are modeled by extending the bottom temperature boundary to 1,000 meters below the water table. The temperature at the extended boundary is then fixed at 65°C. A simulation of nonisothermal UZ flow under the fixed top temperature and saturation conditions, and fixed bottom temperature, pressure, and saturation boundary conditions, was conducted to obtain mountain-scale ambient conditions using the present-day mean infiltration. This simulation shows that the average temperature at the water table (730 masl) is between 30 to 33°C over the potential repository domain, which is in agreement with the calibrated temperature distribution at the water table (CRWMS M&O 2000, U0050, Section 6.3). The average temperature at the repository horizon is about 23°C. These mountain-scale ambient conditions are the initial conditions for the TH simulations.

3.12.2.5 Input Data and Parameters

Key input data used in the TH model development are summarized in CRWMS M&O (2000, U0105, Section 4) and include the following:

- Fracture properties (frequency, permeability, van Genuchten α and m , and aperture, porosity, and surface area) for each UZ model layer.
- Matrix properties (porosity, permeability, van Genuchten α and m) for each UZ model layer.
- Thermal properties (grain density, wet and dry thermal conductivity, grain specific heat, and tortuosity coefficients) for each UZ model layer.
- Fault properties (matrix and fracture) for each hydrogeologic unit.
- Repository thermal-load and ventilation scenarios.
- Present-day infiltration and temporal changes in infiltration due to long-term climate changes.

In the TH models, three infiltration rates based on three climate scenarios were used over the thermal loading period. These are discussed in detail in Sections 3.3 and 3.5, and in USGS (2000, U0010, Section 5.1). Net infiltration maps corresponding to the following climates were used for TH modeling:

Present Day: The mean present-day climate was used. In the 3-D models and the 2-D model NS#1, this climate was used for the entire simulation period. For the refined 2-D cross-section NS#2 model, this climate was used for the period from 0 to 600 years.

Monsoon: The mean monsoon climate was used for the 2-D NS#2 model and was applied for the period 600 to 2,000 years.

Glacial Transition: The mean glacial transition climate was used for the rest of the simulation period beyond 2,000 years in the 2-D NS#2 models. Although models of climate only cover a period of 10,000 years, the glacial-transition climate is assumed to extend up to the total modeled period of 100,000 years.

The average net infiltration rate along the NS#2 cross-section is 4.8 mm/yr for the mean present-day infiltration rate, 11.3 mm/yr for the mean monsoon climate average infiltration, and 16.9 mm/yr for the mean glacial transition climate. These rates compare well with the net infiltration rates over the entire UZ model domain, as presented in Section 3.5, Table 3.5-4.

3.12.3 Results of TH Simulations

Table 3.12-1 summarizes the cases simulated to characterize the TH processes on the Mountain-Scale under thermal loading. The simulations of the non-isothermal fluid and heat flow were conducted for a thermal-loading period of 100,000 years. The simulations start at time zero using the ambient conditions of the UZ Flow Model as initial conditions. The simulations were stopped at 600 years and at 2,000 years to change the infiltration to that of the corresponding climate.

The main purpose of the Mountain-Scale TH Model is to predict the extent of the thermally disturbed zone, i.e., the mountain-scale changes in temperature, saturation, and liquid and gas flux. In particular, attention is given the TH Model results that directly impact performance issues, as outlined in the introduction. This section presents a detailed discussion of the results only for the fine grid simulations (Cases 5 and 6). The reader is referred to CRWMS M&O (2000, U0105, Sections 6.10 and 6.11) for detailed discussions of the other cases.

Table 3.12-1. Summary of Numerical Model Cases for Mountain-Scale TH.

Case No.	Numerical Grid	Infiltration	Thermal Load	Temperature Boundary
1	3-D Submodel, no drifts	Mean present day	72.7 kW/acre; no ventilation	1,000 m below the water table
2	3-D Submodel, no drifts	Mean present day	72.7 kW/acre; no ventilation	At the water table
3	2-D Cross-Section (NS#1), no drifts	Mean present day	72.7 kW/acre; no ventilation	1,000 m below water table
4	2-D Cross-Section (NS#1) with locally refined drifts	Mean present day	72.7 kW/acre; no ventilation	1,000 m below water table
5	2-D Cross-Section (NS#2) with locally refined drifts	0-600 years, mean present day; 600-2,000 years, mean monsoon; 2,000+ years, glacial transition	72.7 kW/acre; no ventilation	1,000 m below water table
6	2-D Cross-Section (NS#2) with locally refined drifts	0-600 years, mean present day; 600-2,000 years, mean monsoon; 2,000+ years, glacial transition	72.7 kW/acre; with ventilation: use 30% of the total heat for 50 years	1,000 m below water table

SOURCE: Adapted from CRWMS M&O 2000, U0105, Table 5)

3.12.3.1 Temperature

The evolution of the temperature distribution provides an estimate of the volume and lateral extent the UZ that is affected by the heat at the potential repository, as well as the temperature in the drifts and in the pillars. The numerical model can provide the predicted distribution at any desired time during the thermal loading period. The average ambient temperature at the potential repository horizon is about 23 °C (CRWMS M&O 2000, U0105, Section 6.9). Figure 3.12-5 shows the distribution of temperature along the cross-section NS#2 after 1,000 years of thermal load (a) without ventilation, and (b) with ventilation (for the first 50 years). The variations in net infiltration across the model strongly influence the evolution of temperature in both cases. Higher temperatures are predicted in the low infiltration areas. The plots show extensive boiling only in the area immediately above and at the potential repository horizon. At a lateral distance of 100 meters or more from the potential repository, no substantial increases in temperature are predicted. For example, the predicted maximum temperature is 37°C at 100 meters north of the potential repository and about 40°C at 100 meters south. The temperatures at 200 meters away from the potential repository remain near ambient conditions throughout the simulation. This response suggests that the convection mode of heat transfer, driven by extensive boiling and rapid fracture flow, is dominant near the potential repository. The ambient infiltration flux (predominantly vertical) controls the temperature changes outside the potential repository boundaries.

A detailed evaluation of temperatures changes can be obtained by plotting the evolution of temperature profiles in a column within the potential repository domain. The plots of vertical temperature profiles in a column at the center of the potential repository (location #1, see Figure 3.12-4) are shown in Figure 3.12-6. The figure shows that TH processes at and near the potential repository are controlled by convection. Without ventilation (Figure 3.12-6a), the model predicts that temperature at the drift wall could rise to 250°C after both the matrix and the fracture elements of the drifts become completely dry. In this case, a two-phase boiling zone at 97°C develops above the potential repository and extends out to 50 meters after 500 years. This zone expands to 200 meters after 1,000 years. With ventilation (Figure 3.12-6b) the two-phase boiling zone is small and is confined to within 20 meters above the potential repository drifts. In this case the average temperature within the drifts rises to boiling conditions (97°C), although in a few locations, temperatures rise to about 110°C (CRWMS M&O 2000, U0105, Section 6.11).

A plot of the evolution of temperature along the middle section of the potential repository horizon is presented in Figure 3.12-7 (a) without ventilation, and (b) with ventilation. The peaks correspond to the individual drifts that are spaced about 21.4 m along this cross section. The maximum temperatures occur in the drifts and minimum temperatures occur in the pillars. Without ventilation, the temperatures at the potential repository horizon rise to above boiling conditions (97°C) between 5 and 10 years. At ten years, most of the drifts are at a temperature of 100°C as shown in Figure 3.12-7a. However, at this time the temperatures rise to 260–300°C in the completely dried out zone at the northern end of the potential repository, where the surface infiltration rate is nearly zero (CRWM M&O 2000, U0105, Section 6.11). At 50 years, the temperatures in most drifts decline to 210–235°C. After 50 years, the temperatures in the drifts decline rapidly due to re-wetting, driven by strong capillary suction in the near-field environment. At 100 years, temperature within the drifts is 160–180°C but continues to decline. After 500 years, the temperature range of the drifts is 120–135°C and after 1,000 years the average temperature is about 97°C at the center of the pillars with peaks of 100°C to 110°C within the drifts. After 10,000 years the average is about 65°C between the pillars, but rises to about 70°C at the drifts. Therefore, even without ventilation, the predicted maximum temperatures at the center of the pillars between the drifts do not exceed boiling temperature.

Figure 3.12-7b shows the temperatures in the middle section of the potential repository horizon with ventilation. Even with ventilation, the models predict the development of a small zone of two-phase counter-current flow of liquid towards the drifts and vapor away from the drifts (heat-pipe) at the potential repository horizon. The model predicts much lower elevated temperatures within the drifts due to ventilation cooling. When the ventilation system is shut-off after 50 years, the temperatures at the drift wall are predicted to rise. The models predict that maximum temperatures at most locations along the potential repository horizon will not exceed boiling temperature (Figure 3.12-7b), although at localized areas with low ambient infiltration the temperature may rise to 110°C after these zones dry out (CRWM M&O 2000, U0105, Section 6.11). In this case, the temperatures in the central pillars rise to a maximum of 85°C after 1,000 years. After 10,000 years this temperature drops to about 65°C at the center of the pillars and to about 70°C at the drifts. Similar temperature conditions are predicted at 10,000 years without ventilation (Figure 3.12-7a), showing that the long-term temperature response is not affected by the 50 years of ventilation.

At the top of the Calico Hills nonwelded hydrogeological unit (CHn), at an elevation of 907 masl (at location #1), the models predict a maximum temperature of 70–75°C between 2,000 and 7,000 years. This temperature range suggests minimal potential for temperature-induced mineralogical changes to occur within the zeolites of nonwelded hydrogeological Calico Hills unit. Therefore, the sorptive properties of these zeolites will not be altered significantly as a result of thermal load at the potential repository. At the water table the models predict a maximum temperature of 65–70°C compared to the average ambient temperature of 30°C. Without ventilation, temperatures at the base of the PTn may rise to boiling conditions at an elevation of 1,250–1,270 masl (Figure 3.12-5) and induce property changes within the low infiltration areas. Temperatures within the PTn are predicted to rise to a maximum of 70–75°C. With ventilation, temperatures in the PTn are predicted to rise by 20–25°C from the ambient condition to an average of 40–45°C. The numerical simulations show that there is minimal potential for temperature induced property changes within the PTn.

The elevated temperature at the drift wall during thermal loading may lead to significant changes in thermal-mechanical stresses that may alter permeability and other properties of the host rock in the vicinity of the drifts. The extent of permeability changes as a result of thermally induced stresses are not addressed in the Mountain-Scale TH Model, because the thermal-mechanical effects are expected to occur on smaller scale. In addition, there are few site-specific studies or data available for describing thermal-hydrological-mechanical processes at Yucca Mountain.

3.12.3.2 Saturation

Changes in liquid saturation are important for several reasons. First, they indicate how long the dryout period at the potential repository will be. Secondly, they are used to assess the potential desaturation-induced changes in porosity and hydraulic conductivity (for example, in the zeolitic units). Finally, they help identify the onset of re-wetting processes and the subsequent potential for corrosion at the potential repository horizon. The TH simulations begin with the ambient liquid saturation obtained by a steady-state simulation using the present day mean infiltration and the boundary conditions discussed in Section 3.12.2.4. The heat leads to mobilization of liquid and gas in both the matrix and fracture continua.

Figure 3.12-8 shows contour plots of matrix liquid saturation at 1,000 years (a) without ventilation, and (b) with ventilation. The plots show large decreases in matrix liquid saturation only near the drifts. In both models all fractures in the drifts at the potential repository horizon are completely dry within the first few years of thermal loading and do not rewet until 1,000 years after thermal loading begins. Figure 3.12-9 shows the matrix liquid saturation at location #1 whereas Figure 3.12-10 shows the corresponding matrix saturation along the entire repository horizon. Without ventilation, the models predict completely dry matrix conditions (Figures 3.12-9a and 3.12-10a) for all the drifts between 10 and 50 years, and an area of reduced matrix liquid saturation below and above the potential repository. This area of reduced matrix liquid saturation extends up to 100 m below and above the potential repository horizon without ventilation. In this case, the matrix liquid saturation in the pillars drops to a minimum of 0.4 after 500 years. The fracture liquid saturation in pillars adjacent to drifts rises above ambient saturation at 10 years (CRWMS M&O 2000, U0105, Section 6.11) due to condensing of water vapor. After 10 years the fracture liquid saturation reduces to and remains at near ambient saturation controlled by the climate.

With ventilation (Figures 3.12-9b and 3.12-10b), completely dry matrix conditions are predicted only at a few isolated locations having low percolation flux. Vertically (Figure 3.12-9b) the zone of reduced matrix saturation extends to about 50 m above and below the drifts. The matrix saturation in several drifts with high percolation flux recovers to above 0.9 at 1,000 years (Figure 3.12-10b). After 5,000 years the matrix liquid saturation is almost fully recovered to the liquid saturation controlled primarily by the prevailing climate. In this case the fracture and matrix liquid saturation within the pillars remains at near-ambient conditions and is controlled primarily by the changes in climate throughout the simulated period. With and without ventilation the simulations predict that the liquid saturation at a lateral distance more than 50 meters away from the repository remains at near-ambient conditions.

3.12.3.3 Water Flux

Analysis of the liquid flux gives an estimate of the quantity and duration of enhanced liquid flux that may potentially contact the waste canisters (near-field environment) under thermal load. Flow at the potential horizon can be enhanced by a decrease in saturation, which leads to an increase the capillary suction. The liquid flux can also be enhanced by an increase in saturation due to drainage of condensate that leads to an increased liquid relative permeability. The suction-induced increase in liquid flux is due to the intense boiling and vaporization of both fracture and matrix liquid at the potential repository drifts because the temperatures reach or exceed boiling conditions (about 97°C) even with ventilation. The liquid vaporization results in increased gas flow at the potential repository, which dries up the fractures first and reduces matrix liquid saturation at the potential repository horizon. The dry-out of fractures and lower matrix saturation at the potential repository drifts creates a large capillary pressure gradient between the continua at the potential repository horizon and the adjacent formations. This promotes liquid flow toward the potential repository, i.e., enhances percolation flux. This liquid flux is directed toward the repository drifts, but there is ample heat to vaporize all the liquid, particularly at early times. The vaporization leads to increased gas flux, which may cause localized condensation and drainage through the fractures in the pillars and the drifts. Details of such processes are better resolved by the refined NS#2 grid, which is described Section 3.12.2.2 and used for the TH simulations described here.

Figure 3.12-11 shows the evolution of predicted liquid flux through the fractures at location #1 at the center of the potential repository with and without ventilation. Because of an extensive low-saturation zone within the drifts, both models predict high percolation fluxes near the drifts. Figure 3.12-11a, shows a plot the vertical liquid flux at this location without ventilation (the plots here show liquid flux scale of up to 200 mm/yr for clarity). The predicted maximum liquid flux rises 360 mm/yr at 10 years (CRWMS M&O 2000, U0105, Section 6.11), but declines to less than 30 mm/yr at 500 years. With ventilation (Figure 3.12-11b) the average vertical flux near the potential repository rises to only 60 mm/yr at 10 year. When ventilation is turned off at 50 years, the increase in the available heat within the drifts leads to further decrease in matrix liquid saturation and increase in capillary pressure gradients. This in turn increases liquid flow toward the drier drifts. After 500 years the liquid flux is has only declined about 40 mm/yr.

Figure 3.12-12a (the figures here show liquid flux scale of up to 100 mm/yr for clarity) shows the liquid flux through the fractures at the potential repository horizon, without ventilation. Note that vertical liquid flux at location #1 (Figure 3.12-11) is calculated based on the entire column

area. In the locally refined NS#2 grid, 5 m drifts plus two equal elements represent the columns at the potential repository horizon in which drifts are located (CRWMS M&O 2000, U0105, Section 6.3.3.2). The liquid flux through an entire column above the drift is thus funneled toward the narrower drift by the high capillary gradients, because heat is applied only to the drift element. The figure shows that without ventilation, the liquid flux through the fractures toward the drifts, calculated based on this smaller drift area, rises to between 1,250–1,600 mm/yr (CRWMS M&O 2000, U0105, Section 6.11) after 10 years. This liquid flux drops to zero, as the fractures in the drifts become completely dry (between 10 and 50 years). As the fractures begin to rewet between 500 and 1,000 years (see Figure 3.12-10a), the fracture liquid flux recovers (Figure 3.12-12a). Around 1,000 years, fracture liquid flux at several locations increases to 20–50 mm/yr (2 to 5 times mean infiltration rate for the monsoon climate), controlled by the infiltration rate, capillary-pressure and the liquid-saturation gradients. This is the liquid flux that can potentially contact the canisters. The simulations also show increased fracture liquid flux in the pillars between the drifts. At around 500 years the average fracture flux between drifts is about 20 mm/yr, about 5 times higher than the infiltration rate. This is because the predicted boiling within the pillars in the no-ventilation case leads to a decrease in saturation and increased capillary suction.

Although ventilation lasts only 50 years, it results in changes in flux patterns that last for several hundred years. This is because the heat removed by ventilation results in a delay in the dry-out of the matrix, and decreased gas flux at the potential repository horizon. Ventilation leads to much lower induced liquid and gas flux because the effective thermal load is only 30% of the total load during the period in which the heat yield of the emplaced waste is highest. With ventilation (Figure 3.12-12b, plot shows scale of up to 100 mm/yr for clarity) the predicted fracture flux at the potential repository horizon rises to maximum of 270–300 mm/yr at 10 years, but subsequently declines due to decreased vaporization. When ventilation is shut off at 50 years, the retained heat leads to increased drying of the matrix and an increase liquid flux. However, this process is delayed because first the temperature of the rock-mass at the potential repository must rise to boiling conditions before liquid can be vaporized to create the large capillary pressure gradients. At 100 years (50 years after end of ventilation) the liquid flux is 10 mm/yr. However, flux recovers to over 150 mm/yr at 500 years (Figure 3.12-12b) as a result of increased heating, drying of matrix and re-wetting of the fractures. Because of the general decline in the heat released from the emplaced nuclear waste and the increased infiltration due to climate change, the fracture continuum at the potential repository horizon is almost completely re-wetted after 5,000 years, and the fracture liquid flux recovers to the ambient percolation flux. With ventilation, the fracture flux through the pillars between the drifts remains at or above ambient conditions throughout the thermal-loading period. This is because temperatures do not rise to boiling conditions and condensation of liquid vapor gives rise to localized increase in fracture liquid saturation and a corresponding increase in liquid relative permeability. For example, the liquid flux between the drifts is 15 to 20 mm/yr, (about 2 to 3 times the ambient infiltration rate), at 500 years. Beyond 500 years the fracture liquid flux in the pillars is controlled primarily by the changes in ambient infiltration due to changes in the ambient climate, monsoon climate at 600 to 2,000 years and glacial transition climate thereafter.

Analysis of the liquid flux through the matrix gives an indication of the liquid that flows toward the potential repository primarily through the matrix during thermal loading. Figure 3.12-13 shows the matrix liquid flux at the potential repository (a) without ventilation, and (b) with

ventilation. Without ventilation (Figure 3.12-13a, plot shows scale of up to 100 mm/yr for clarity) the matrix liquid flux rises to a maximum of 400–450 mm/yr after 500 years at the drifts, but stays at ambient conditions between the drifts. As the matrix continuum of the drifts becomes completely dry, this flux also drops to near zero between 500 to 1,000 years. With ventilation (Figure 3.12-13b) the matrix liquid flux rises to a maximum of 20 to 30 mm/yr at the drifts after 500 years but remains at ambient conditions (about 0.25 mm/yr which is less than 6% of total liquid flux) between the drifts throughout the thermal-loading period.

3.12.4 Model Validation

Model validation here is discussed in terms of confidence building for the validity of the numerical and mathematical approaches used to model TH processes. There is no data for direct validation of the Mountain-Scale response to thermal loading. Validation data for a Mountain-Scale TH Model can only be obtained by monitoring the response of a fully operational repository. Numerical modeling of Mountain-Scale TH processes can provide a prediction of the performance of the potential repository under thermal loading. Such a model can then provide quantitative and qualitative evaluation of the issues discussed in Section 3.12.1, which are used to evaluate alternative designs for the potential repository. The validation process then becomes one of assuring that the numerical model adequately represents the physical processes, and that the results of such a model provide reliable data for decisions on the design of the potential repository.

The problem to be modeled here is essentially that of coupled two-phase fluid and heat flow in a fractured geological medium. Approaches for the development of the numerical models for the simulation of the two-phase processes in such systems are generally based on geothermal and petroleum reservoir simulation methods. Numerical models of geothermal and petroleum systems can be validated from a wealth of field-scale tests and production data. The validity of model predictions based on this modeling approach is demonstrated using corroborative results from the modeling of these natural analog systems (Table 3.2-1), from the previously published UZ numerical modeling studies, and from small-scale underground thermal tests in the ESF discussed in Section 2.2.4.

Validation of the TH Model, although incorporating results of the small-scale TH tests, relies mainly on the conceptual and mathematical validity of the models, the validity of flow and thermal properties, and the associated numerical grids. Performance Assessment of the effect of heat on the UZ flow, based on numerical simulation of fluid and heat flow, can include the physical processes affecting repository and host-rock behavior. The TH models explicitly represent the relevant thermal-hydrological conditions at the potential repository over the applicable time and space scale. These TH numerical models can then provide model predictions of the mountain-scale responses to thermal loading under the proposed design conditions. For example, the numerical models can be used to determine the effect of thermal loading on mountain-scale liquid and gas flux, temperature, and moisture distribution in the UZ. This coupled flow of heat and fluid in the UZ is modeled using TOUGH2 V1.4 (STN: 10007-1.4-0). Previous versions of this code have been used in the modeling of several natural analogs discussed in CRWMS M&O (2000, U0105, Section 6.12) and presented in Table 2.3-1 of this PMR. The table also documents the similarity between these natural analog systems and the UZ at Yucca Mountain that is modeled here. Applications include detailed studies, production

history and future performance of geothermal fields. The justification for the modeling approaches employed in the TH Model and the validity of the TH predictions rely upon the successful modeling of fluid and heat transport in large natural sub-surface systems (for example geothermal systems) for which an extensive volume of field data is available for model validation. These natural analog models are validated by field measurements in several operating geothermal fields as discussed in Section 2.2.4.

The predicted heat-pipe mode of heat transfer near the drifts in the Mountain-Scale TH Model, and its influence on temperature distribution agrees with the observations from the SHT results and the interim results of the thermal DST, discussed in Section 2.4 and documented in CRWMS M&O (2000, N0000). In addition, the modeled drift-scale THC response discussed in Section 3.10 shows similar heat-pipe signatures and condensation in fractures. This response is validated by comparison to measured temperature at several observation points, by repeat air-injection tests, neutron logs and electrical-conductivity logs, which measure changes in liquid in liquid saturation. Both the results of the heater tests and the TH Model suggest no major adverse conditions in terms of temperature changes, moisture redistribution near the drifts, as well as liquid drainage towards the drifts and within the pillars. The TH Model shows no major moisture redistribution in the UZ except near the heated drifts. The simulations also show only moderate temperature increase within the zeolites and at the water table. We consider the TH Model developed here validated for the intended use because of this good agreement with the heater test models, the validity of the geothermal analog models, and the documented theoretical and physical validity of similar unsaturated flow studies with and without heat.

3.12.5 Summary and Conclusions

The TH modeling study investigates the effects of thermal loading on the UZ of Yucca Mountain. This study uses both 3-D and 2-D dual-permeability submodels of the 3-D UZ Flow Model and incorporates the calibrated model properties. Detailed investigation of the UZ response to thermal loading discussed in this PMR is conducted using refined 2-D cross-section models that include explicit representation of the drifts at the potential repository.

These models simulate the mountain-scale TH response under the design base-case thermal load scenario. The models include expected future climatic changes in infiltration rate and the effects of drift ventilation. The numerical grids are sufficiently refined to determine Mountain-Scale, long-term TH behavior resulting from thermal load within the drifts, but do not explicitly include detailed heat transfer processes within the drifts. This is because such processes affect only small distances around the drift (a few meters) and at early times (less than 500 years) relative to the Mountain-Scale model spatial domain and the modeled temporal scale. Figure 3.12-14 summarizes the results of the TH modeling in terms of the issues discussed in Section 3.12.1. The figure provides qualitative and quantitative data primarily based on the results of the detailed NS#2 cross-section UZ model. This study indicates that the available heat source and its distribution as well as the infiltration rates are the determining factors for boiling and re-wetting TH processes at the potential repository.

With or without ventilation, heat-pipe conditions are developed in a region above the potential repository in the period of 10 to 100 years after thermal loading starts. Without ventilation, the TH models predict drift temperatures exceeding 100°C for hundreds of years. The results show

that temperatures may be elevated to more than 250°C within the completely dry drift zone, when no ventilation is implemented. In this case, temperature within the pillars may rise to boiling temperature (about 97°C) after 1,000 years of heating. With ventilation, temperatures only rise to boiling conditions in the immediate vicinity of the drifts, but may reach 110°C at drifts with low ambient liquid flux. In this case the temperatures in the pillars are predicted to rise to an average of 80–85°C. In both cases the models predict a nearly 30–35°C temperature increase at the water table to an average of 60–65°C. At the top of the CHn stratigraphic unit, the predicted maximum temperature rises to 70–75°C and occurs between 2,000 and 7,000 years. This suggests that temperature-induced property changes will be insignificant in the CHn because such changes are expected to occur if CHn zeolite temperatures remain above 90°C for prolonged periods of time. Without ventilation, temperatures within the PTn are predicted to rise to a maximum of 70–75°C. With ventilation, temperatures within the PTn are predicted to rise by 20–25°C from the ambient condition to an average of 40–45°C, indicating minimal potential for temperature-induced property changes within the PTn. In both cases, temperatures at a lateral distance of more than 100 m outside the potential repository are expected to remain at near ambient conditions.

Therefore, thermal loading at the potential repository results in significant changes in the temperature conditions particularly near the drifts. The models predict that heating of the potential repository drifts will result in hot and dry conditions within the drifts that last for hundreds of years in the fractures with and without ventilation. Two-phase heat-pipe conditions will develop in a region above the potential repository. In areas with low surface infiltration this region may extend to the base of the PTn stratigraphic unit if no ventilation is implemented.

Without ventilation most of the rock mass surrounding the drifts is predicted to become completely dry and remain so for over 1,000 years. With ventilation, although the TH Model does not predict completely dry conditions near all the drifts, the walls of the drifts are expected to remain dry for hundreds of years. In both cases the fractures at the potential repository drifts are predicted to completely dry and remain so for hundreds of years. With and without ventilation the matrix and fracture liquid saturation within the pillars remains high, and at several locations increases to above the ambient liquid saturation because of vapor condensation. Vertically, the zone of substantially reduced matrix liquid saturation extends to 50 m directly above and below the drifts with ventilation, and up to 100 m without ventilation, except in areas of high ambient liquid infiltration.

With and without ventilation, large liquid and gas flow rates are predicted, primarily through the fractures. These flow rates are two to three orders of magnitude higher than the ambient flux at the repository drifts and are primarily driven by capillary pressure gradients due to drying of both the matrix and the fractures at the drifts. However, these large fluxes are confined to a period of less than 100 years. The liquid flux through the fractures towards the drifts may exceed 1,250–1,600 mm/yr without ventilation, and 270–300 mm/yr with ventilation, particularly in the low infiltration areas due to these high capillary pressure gradients. However, in both cases there is ample heat within the potential repository drifts that immediately vaporizes this liquid flux, at this early period. Therefore, this liquid does not directly seep into the drifts and has little impact on the waste canisters in the drifts. The liquid flow through matrix towards the drifts rises to maximum of 400–450 mm/yr without ventilation but is only 20–30 mm/yr with ventilation. This liquid flux is also vaporized by the repository heat. The TH Model predicts continued liquid

flow through the pillars, at a rate close to the ambient percolation flux for most of the thermal-loading period. In some locations the flow may be enhanced by condensate drainage for several hundred years. The models predict little impact on liquid and gas flux outside the potential repository domain.

INTENTIONALLY LEFT BLANK

3.13 OVERVIEW OF UNCERTAINTIES IN UZ FLOW AND TRANSPORT MODELS

The models and components that comprise the UZ Flow and Transport Model contain inherent uncertainties. The identification and propagation of these uncertainties is important for the appropriate treatment of the models used in TSPA-SR calculations. Table 3.13-1 lists the major model components described in the UZ PMR and the uncertainties in the model inputs and outputs. Uncertainties in conceptual models are also identified. It is important to note that input and output parameters have both variability and uncertainty. For example, infiltration is spatially variable at the surface of Yucca Mountain, and there is also uncertainty in the rates that are simulated because of uncertainty in the input parameters such as precipitation, soil depth, and evapotranspiration. Spatial and temporal variability and uncertainty are included in the models where they are important and could potentially have a significant effect on TSPA calculations for repository performance.

Table 3.13-1. Uncertainty in Major Model Components of the UZ Flow and Transport Model

Model Component	Input Parameter Uncertainty & Variability	Conceptual and Numerical Model Uncertainty	Output Parameter Uncertainty & Variability
Climate (USGS, 2000, U0005; Section 3.5 this PMR)	Uncertainty in Owens Lake sediment-accumulation rate, Devils Hole age data, time when Devils Hole record implies climate has changed, exact location of the past/present point in the Owens Lake record (analog climate proxy record)	Uncertainty in use of orbital cycles, interpretation of climate analogs	Upper and lower bounds for precipitation and temperature using different meteorological stations as analogs; duration of climate periods
Infiltration (USGS 2000, U0010; CRWMS M&O 2000, U0095; Section 3.5 this PMR)	Uncertainty in precipitation, bedrock permeability, soil depth, evapotranspiration, etc.; variability in precipitation, temperature, etc. at surface	Deterministic use of surface mass balance model	Spatial and temporal variability of infiltration (USGS 2000, U0010); uncertainty in infiltration rates based on input parameters (CRWMS M&O 2000, U0095)
UZ Properties (CRWMS M&O 2000, U0035; CRWMS M&O 2000, U0090; Section 3.6 this PMR)	Uncertainty in measured core data parameters and cross-correlation; spatial variability in properties	Uncertainty in calibration method (non-uniqueness); initial estimates; upscaling	Spatial variability in calibrated parameters; parameter calibration for different infiltration cases
UZ Flow (CRWMS M&O 2000, U0050; CRWMS M&O 2000, U0125; CRWMS M&O 2000, U0000; Section 3.7 this PMR)	Uncertainty and variability in hydrologic parameters (CRWMS M&O 2000, U0035); infiltration uncertainty (CRWMS M&O 2000, U0095)	Uncertainty in dual-permeability model (Doughty, 1999); active fracture model (Liu et al. 1998); perched water models, fault models (CRWMS M&O 2000, U0030; CRWMS M&O 2000, U0050); water table rise (CRWMS M&O 2000, U0125); refinement of mesh (CRWMS M&O (2000, U0000)	Spatial and temporal variability and uncertainty in flow fields

Unsaturated Zone Flow and Transport Model Process Model Report

Model Component	Input Parameter Uncertainty & Variability	Conceptual and Numerical Model Uncertainty	Output Parameter Uncertainty & Variability
Ambient Geochemistry (CRWMS M&O 2000, U0085; Section 3.8 this PMR)	Uncertainty and spatial variability in precipitation (chloride concentrations); reactive surface area; kinetic and thermodynamic parameters	Uncertainty in thermodynamic and kinetic relationships; same conceptual uncertainties as UZ Flow Model	Spatial prediction of percolation; uncertainty in estimate of infiltration rates
Drift Seepage (CRWMS M&O 2000, U0075; CRWMS M&O 2000, U0080; CRWMS M&O 2000, U0120; Section 3.9 this PMR)	Spatial variability of fracture permeability (CRWMS M&O 2000, U0080); spatial variability and uncertainty in fracture permeability and van Genuchten α (CRWMS M&O 2000, U0075; CRWMS M&O 2000, U0080)	Uncertainty in heterogeneous fracture continuum model (CRWMS M&O 2000, U0080); effects of drift degradation (CRWMS M&O 2000, U0075); episodic flow (CRWMS M&O 2000, U0075); refinement of mesh; correlation of k and α	Variability and uncertainty in seepage distributions (seepage fraction, mean seep flow rate, standard deviation of seep flow rate, flow focusing factor) (CRWMS M&O 2000, U0120)
Drift-Scale THC (CRWMS M&O 2000, N0120/U0110; Section 3.10 this PMR)	Variability in hydrologic parameters—use of calibrated parameters (CRWMS M&O 2000, U0035); uncertainty in chemistry data (thermodynamic and kinetic data, chemistry of infiltrating water) (CRWMS M&O 2000, U0085)	Uncertainty in dual-permeability model to capture THC changes in matrix at fracture wall; use of middle-nonlithophysal parameters instead of lower-lithophysal parameters; refinement of mesh to capture THC changes in matrix at fracture wall	Temporal and spatial variability of water and gas composition, as well as uncertainty from different infiltration cases (CRWMS M&O 2000, N0120/U0110); temporal variability in water and gas composition for TSPA-SR
UZ Transport (CRWMS M&O 2000, U0060; CRWMS M&O 2000, U0065; CRWMS M&O 2000, U0160; Section 3.11 this PMR)	Uncertainty and variability in transport parameters (CRWMS M&O 2000, U0100); spatial and temporal variability and uncertainty in flow fields (CRWMS M&O 2000, U0050; CRWMS M&O 2000, U0125)	Uncertainty in matrix-diffusion model and particle tracking model (CRWMS M&O 2000, U0060; CRWMS M&O 2000, U0065; CRWMS M&O 2000, U0155; CRWMS M&O 2000, U0160); colloidal transport model (CRWMS M&O 2000, U0070); discretization of gradient for matrix diffusion (CRWMS M&O 2000, U0065); number of particles (CRWMS M&O 2000, U0160)	Spatial and temporal radionuclide mass flux at water table (CRWMS M&O 2000, U0065)
Mountain-Scale Thermal Hydrology (CRWMS M&O 2000, U0105; Section 3.12 this PMR)	Variability in hydrologic and thermal properties for different units (CRWMS M&O 2000, U0105)	Uncertainty in dual-permeability model for transient TH simulations (Doughty, 1999); active fracture model (Liu et al., 1998); perched water models, fault models (CRWMS M&O 2000, U0030; CRWMS M&O 2000, U0050); water table rise (CRWMS M&O 2000, U0125); Refinement of mesh (CRWMS M&O (2000, U0000)	Spatial and temporal variations in temperature and hydrologic conditions (CRWMS M&O 2000, U0105)

Table 3.13-2 provides a distilled list of uncertainties that are carried forward to TSPA calculations. The uncertainty in the parameters and models is included in TSPA calculations through the use of multiple realizations (statistically equivalent simulations) and stochastic sampling of parameters (i.e., a Monte Carlo approach). Each realization samples a set of parameters and/or models from given distributions for use in the TSPA calculation. The simulation of multiple realizations produces a range of performance results, with each outcome having a probability corresponding to its likelihood of occurrence. Thus, the uncertainty of the parameters and models leads to uncertainty in system performance. In the TSPA, the uncertainty in performance is analyzed, both in terms of its importance (i.e., is the uncertainty so great that it casts doubt on the safety of the repository?) and in terms of sensitivities (i.e., which parameter and submodel uncertainties have the greatest impact on the uncertainty in performance?).

In addition, uncertainties in the process-model outputs can also be addressed in abstracted TSPA models and analyses that use conservative assumptions. If insufficient evidence exists to provide a defensible range of values for a given parameter, values that bound the physical behavior or provide conservative estimates of the range of physical behavior are used. For example, a conservative factor that increases the seep flow rate by over 50% is used in the TSPA seepage-abstraction model to account for the uncertain impacts of drift degradation and rock bolts. For future climates, the water table is assumed to rise by a conservative amount in the abstracted UZ Flow Model, which will reduce travel times in the UZ. These conservative assumptions are intended to increase the defensibility of the models used in TSPA calculations given the inherent uncertainties in the actual system.

The uncertainty and variability in the model parameters are due, in part, to the natural variability and heterogeneity in the geological, hydrological, chemical, and mechanical systems that are difficult to characterize in situ, such as the precise fracture network in the UZ. Uncertainties in models may also be due to conditions that are difficult to predict, such as future climate states. Nevertheless, the previous sections in this PMR have provided the basis and confidence (through data collection, field tests, and calibration exercises) for using these parameters and models. In addition, the models and analyses that are used in TSPA calculations address remaining uncertainties through probabilistic simulations or appropriate conservative bounding assumptions.

Table 3.13-2. Uncertainties in UZ Flow and Transport Products for TSPA-SR

Model Component	Treatment of Uncertainty in Abstracted Product for TSPA-SR
Climate	<ul style="list-style-type: none"> • Future climates: three climates are assumed with uncertainty in precipitation and temperature (Section 3.5), which provide ranges of infiltration. • Duration of climates: Duration of the three climate states is assumed to be fixed and transitions are assumed to be instantaneous. Sensitivity studies of different climate durations are required.
Infiltration	<ul style="list-style-type: none"> • Three spatially variable infiltration maps (low, mean, and high) are used for each of the three climates (Section 3.5). • Monte Carlo simulations produced weightings for three infiltration cases used in each climate (Section 3.5).
UZ Flow	<ul style="list-style-type: none"> • Nine flow fields are used that correspond to low, mean, and high infiltration cases for each of the three climates (Section 3.7). • Assessment of uncertainty in the two perched water models revealed that both are similar. Only perched water model #1 is used for TSPA (Section 3.7). • Conservative estimate for water-table rise is used for future climates (Section 3.5 and CRWMS M&O 2000, U0125). • Weightings for three infiltration cases are used for each corresponding flow field.
Drift Seepage	<ul style="list-style-type: none"> • Distributions are developed for seepage fraction, mean seep flow rate, standard deviation of seep flow rate, and flow focusing factor based on process model results (Section 3.9). • A conservative factor is applied to increase seepage due to drift degradation and rock-bolt effects. • A conservative factor is applied to increase seepage to account for potential parameter correlations not included in process models.
Drift-Scale THC	<ul style="list-style-type: none"> • Water and gas compositions are abstracted and prescribed at four discrete time periods following emplacement based on drift-scale THC process model results (Section 3.10). Sensitivity studies may be required.
UZ Transport	<ul style="list-style-type: none"> • Distributions of K_d and K_c (for reversible colloids), colloid filtration parameter, aperture parameter, and diffusion coefficient are used to capture uncertainty (CRWMS M&O 2000, U0100; CRWMS M&O 2000, U0065). • Weightings for three infiltration cases are used for each corresponding flow field during transport simulations. • Uncertainty in location of source term is implemented through random nodal release within bins in the repository region that are consistent with bins used in the near-field environment. • Uncertainty in dispersion of radionuclides within the UZ is treated conservatively by collecting mass flux at the water table in the UZ and releasing it at "point locations" at the water table in the SZ model.
Mountain-Scale TH	<ul style="list-style-type: none"> • Based on results of the process model (Section 3.12 and CRWMS M&O 2000, U0105), TH effects on far-field flow and transport are not considered. Sensitivity studies may be required. Note that thermal impacts on the near-field environment are considered in the Near-Field Environment PMR.

4. RELATIONSHIP TO NRC ISSUE RESOLUTION STATUS REPORTS

4.1 SUMMARY OF THE KEY TECHNICAL ISSUES

As part of the review of site characterization activities, the Nuclear Regulatory Commission (NRC) has undertaken an ongoing review of information on Yucca Mountain site characterization activities to allow early identification and resolution of potential licensing issues. The principal means of achieving this goal is through informal, prelicensing consultation with the DOE. This approach attempts to reduce the number of, and to better define, issues that may be in dispute during the NRC licensing review, by obtaining input and striving for consensus from the technical community, interested parties, and other groups on such issues.

The NRC has focused prelicensing issue resolution on those topics most critical to the post-closure performance of the potential geologic repository. These topics are called Key Technical Issues (KTIs). Each KTI is subdivided into a number of subissues. The KTIs are:

- Activities Related to Development of the EPA Standard
- Container Lifetime and Source Term
- Evolution of the Near-field Environment
- Igneous Activity
- Radionuclide Transport
- Repository Design and Thermal Mechanical Effects
- Structural Deformation and Seismicity
- Thermal Effects on Flow (TEF)
- Total System Performance Assessment (TSPA) and Integration
- Unsaturated Zone (UZ) and Saturated Zone (SZ) Flow under Isothermal Conditions

Identifying KTIs, integrating their activities into a risk informed approach, and evaluating their significance for postclosure performance helps ensure that NRC's attention is focused on technical uncertainties that will have the greatest affect on the assessment of repository safety.

Early feedback among all parties is essential to define what is known, what is not known, and where additional information is likely to make a significant difference in the understanding of future repository safety. The Issue Resolution Status Reports (IRSRs) are the primary mechanism that the NRC staff uses to provide feedback to the DOE on the status of the KTI subissues. IRSRs focus on NRC acceptance criteria for issue resolution and the status of issue resolution, including areas of agreement or when the staff has comments or questions. Open meetings and technical exchanges between NRC and DOE provide additional opportunities to discuss issue resolution, identify areas of agreement and disagreement, and develop plans to resolve any disagreements.

KTIs are subdivided into a number of subissues. For most subissues, the NRC staff has identified technical acceptance criteria that the NRC may use to evaluate the adequacy of information related to the KTIs. The NRC has also identified two cross-cutting programmatic criteria that apply to all IRSRs related to the implementation of the Quality Assurance Program and the use of

expert elicitation. The following sections provide a summary level discussion of the KTIs by subissues (Section 4.2) and a discussion of the specific NRC acceptance criteria (Section 4.3).

4.2 RELATIONSHIP OF THE UZ FLOW AND TRANSPORT PMR TO THE KTIS

The UZ PMR provides technical analyses that relate to six of the KTIs and their associated IRSRs. Table 4.2-1 shows these KTIs and their subissues; subissues that relate directly to this PMR, hereafter referred to as the UZ PMR, are shown in *italics*. The KTIs and subissues that relate directly to the UZ PMR are discussed in the following sections.

4.2.1 Evolution of the Near-Field Environment

The near field is considered to be the part of the site for which changes in the physical and chemical properties (that result from construction of the underground facility or from heat generated by the emplaced radioactive waste) affect performance of the repository (NRC 1999a). Evolution of the near field is expected to include coupling of thermal, hydrological, and chemical (THC) processes that could affect parts of the mountain. These coupled processes could affect components of the natural and engineered barrier system (EBS) and thereby affect repository system performance. The introduction of repository construction material and waste package materials may also perturb the near-field environment.

The resolution of each of the subissues of this KTI (see Table 4.2-1) must adequately address four aspects of coupled processes:

- Identify the potential effects of coupled processes on performance
- Determine how the natural system will influence, and be influenced by, coupled processes
- Evaluate how the engineered materials will influence, and be influenced by, coupled processes
- Determine the adequacy of any representation of the effects of coupled processes in performance assessment.

Two of the subissues for the near-field environment KTI relate to the UZ PMR (see Table 4.2-1), as described in the following subsections. PMRs on the EBS, the near-field environment, and waste-form degradation also provide information relevant to the evolution of the near-field environment.

4.2.1.1 Effects of Coupled THC Processes on Seepage and Flow

The NRC notes that previous performance assessments have included limited analyses of the effects of coupled processes for the representation of seepage and groundwater flow (NRC 1999a, p. 15). For example, coupled THC processes that affect seepage and flow were not explicitly addressed in the Total System Performance Assessment (TSPA) that was completed

for the Viability Assessment (VA) (DOE 1998). There was no abstraction of the effect of coupled THC on seepage and flow and no corresponding sensitivity and uncertainty analysis to evaluate the need for additional data (NRC 1999a, p. 107). The NRC also notes that use of homogeneous hydrological properties in modeling coupled processes did not account for the spatial and temporal variability in fracture flow.

Table 4.2-1. Issue Resolution Status Report/Key Technical Issues (IRSR/KTI) Related to the UZ PMR

NRC Key Technical Issues	Subissues
Evolution of the Near-field Environment	<i>Coupled thermal-hydrological-chemical (THC) processes effects on seepage and flow</i> Coupled THC effects on the waste package chemical environment Coupled THC effects on the chemical environment for radionuclide release <i>Coupled THC processes effects on radionuclide transport</i> Coupled THC processes effects on potential nuclear criticality in the near field
Radionuclide Transport	<i>Radionuclide transport through porous rock</i> Radionuclide transport through alluvium <i>Radionuclide transport through fractured rock</i> Nuclear criticality
Structural Deformation and Seismicity	Faulting Seismic hazard <i>Fracturing and structural framework of the geologic setting</i> Tectonics and crustal conditions
Thermal Effects on Flow (TEF)	Is DOE's thermal testing program, including performance confirmation, sufficient to evaluate the potential for thermal reflux to occur in the near field? <i>Is DOE's thermal modeling approach sufficient to predict the nature and bounds of TEF in the near field?</i> <i>Does DOE's total system performance assessment (TSPA) adequately account for TEF?</i>
Total System Performance Assessment (TSPA) and Integration	System Description and demonstration of multiple barriers <i>Scenario analysis</i> <i>Model abstraction</i> Demonstration of the Overall Performance Objection
UZ and SZ Flow Under Isothermal Conditions	<i>Future climates</i> <i>Hydrological effects of climate change</i> <i>Shallow infiltration</i> <i>Deep percolation</i> Saturated zone <i>Matrix diffusion UZ/SZ</i>

NOTE: Italicized subissues are addressed in the UZ PMR

Analyses have been completed to evaluate the effects of various coupled processes on seepage into drifts, including coupled THC processes (see Section 3.10). A fully coupled drift-scale THC model has been developed. Simulations using this model show only very small changes in hydrological properties, suggesting that thermal-chemical effects on seepage do not need to be represented in the abstraction of seepage.

4.2.1.2 Effects of Coupled THC Processes on Radionuclide Transport

The evolution of the near-field environment influences two abstractions of UZ flow and transport processes that are important to this subissue. These are (1) the distribution of mass flux between fracture and matrix and (2) radionuclide retardation in fractures in the UZ. The NRC staff has no major concerns with DOE's analyses of the distribution of mass flux between fracture and matrix and retardation in fractures in the UZ (NRC 1999a, p. 140).

Section 3.13 summarizes modeling studies of transport in the UZ (see Section 4.2.2). Note that current transport models do not take credit for retardation in fractures because of relatively rapid travel times and limited data on the details of fracture mineralogy. This approach is conservative.

4.2.2 Radionuclide Transport

The primary objective of the Radionuclide Transport KTI is to evaluate the processes that may affect radionuclide transport from the repository to the biosphere (NRC 1999b). Transport in the near-field environment is considered in the IRSR/KTI for evolution of the near-field environment (Section 4.2.1). The key elements of the Radionuclide Transport KTI are retardation of radionuclides in fractures and the matrix in the UZ and retardation in the saturated zone (NRC 1999b, p. 5). The IRSR focuses on sorption and other chemical processes that affect transport and colloid-facilitated transport. Two mechanisms that can reduce radionuclide concentrations along flow paths, matrix diffusion and dilution, are evaluated separately in the IRSR/KTI for UZ and SZ Flow under Isothermal Conditions (Section 4.2.6). Resolution of the KTI for radionuclide transport requires adequate characterization of the physical and chemical processes that affect radionuclide transport (NRC 1999b, p. 3).

Two of the subissues for this KTI relate to the UZ PMR, as described in the following subsections. The PMR on SZ flow and transport also provides information relevant to radionuclide transport.

4.2.2.1 Radionuclide Transport through Porous Rock

This subissue focuses on the extent to which radionuclides can sorb onto minerals in the porous matrix and filtration of colloidal and particulate contaminants (NRC 1999b, p. 3). It addresses physical transport processes, chemical processes, and heterogeneities (NRC 1999b, p. 12). Issues related to physical transport processes include the appropriate conceptual models for fracture-matrix interaction, the range and dependencies of parameters associated with fracture-matrix interactions, the effects of both long and short term transient flow conditions, and the expected magnitude of lateral and longitudinal dispersion. Chemical issues include the appropriateness of the minimum K_d approach, the amount of sorption expected in fractures, and the contribution of

colloids to radionuclide flux. Issues related to heterogeneities in the UZ include the spatial distribution of infiltration, areal variations in amounts and compositions of zeolites, and the appropriate scale of heterogeneities.

The NRC indicates that methods proposed to treat sorption are generally acceptable (NRC 1999b, p. 80). In some cases, particularly for neptunium, adequate investigations have been completed. Additional work may be needed, such as batch sorption experiments for a few radionuclides, crushed tuff and intact rock column experiments for some radionuclides, and analyses using theoretical models and experimental data to demonstrate that sorption coefficients are compatible with the range of geochemical conditions expected in the postclosure time-frame.

This PMR documents the current representation of UZ transport (see Section 3.11). It includes the following improvements to the UZ Transport Model:

- Enhancement of the UZ/EBS transport interface and refinement of the UZ grid between the repository and the water table
- A matrix diffusion algorithm that recognizes finite fracture spacing effects and an improved model for colloid transport
- Improved justification for the treatment of sorption, chain decay, radionuclide screening, and gas-phase radionuclide transport.

Current modeling provides better justification for coupling with the EBS transport at the potential repository and SZ transport at the water table, with releases spread over a more realistic area compared to the VA analysis. The effects of repository heating have also been considered in the UZ transport model. The improved colloid transport model was developed in conjunction with modeling conducted for the Nevada Test Site (NTS) (Section 3.11), using data from the NTS to calibrate the colloid model.

The issue of heterogeneity requires proper scaling from laboratory-derived parameters; this has been evaluated with respect to the Calico Hills vitric unit (Section 3.8).

4.2.2.2 Radionuclide Transport through Fractured Rock

This subissue evaluates radionuclide transport in fractured rock where there is a potential for preferential pathways for transport and limited radionuclide-rock interactions. For the UZ, important factors include percolation rate, partitioning of flow between fractures and matrix, and sorption coefficients (NRC 1999b, p. 11). Many of the process parameters considered in this subissue are the same as those identified for the subissue on radionuclide transport through porous rock (Section 4.2.2.1). The NRC notes that preliminary experiments suggest that some sorption does occur in fractures (NRC 1999b, p. 94).

Current transport models (Section 3.11) do not take credit for retardation in fractures because of relatively rapid travel times and limited data on the details of fracture mineralogy. This is a conservative assumption.

4.2.3 Structural Deformation and Seismicity

The objective of this KTI is to evaluate the tectonic features, events, and processes (FEPs) that may affect performance of the potential repository (NRC 1999c). One of the subissues for this KTI relates to the UZ PMR. The PMR on disruptive events provides information relevant to the remaining subissues.

4.2.3.1 Fracturing and Structural Framework of the Geologic Setting

The NRC will evaluate alternative modeling approaches for distribution and properties of fractures that are consistent with current data and geologic understanding. They will review representations of fracture data and properties in the UZ models and their abstractions to evaluate the degree to which data on fracture variability are honored, the justification for excluding data, and the degree to which there is adequate integration of fracture data into the UZ models (NRC 1999c, p. 51).

The NRC did not consider the values assigned to fracture-continuum hydraulic properties in the TSPA-VA (DOE 1998) parameter sets justified by the distribution of apertures in the model-grid scale. They were concerned with the limited fracture characterization in key stratigraphic units in the UZ, the potential bias in ESF fracture measurements by the one-meter cut-off, and low-angle fractures not being properly represented (NRC 1999c, pp. 113–114). Thus, uncertainties in the representation of fractures and their properties were not reasonably bounded. Data used in the abstractions were not representative, and alternative modeling approaches were not adequately considered (NRC 1999c, p. 117). The NRC also states that the assumption of spatial homogeneity in fracture distribution in the UZ is not supported by sufficient field evidence (NRC 1999c, p. 107).

Section 2.2 of the UZ PMR documents current data and analyses from ambient field testing in the ESF. These data and analyses provide an enhanced framework in which to refine the conceptual model of matrix and fracture processes in the UZ. Fracture property estimates are based on permeability data from *in situ* air-injection tests conducted in four surface boreholes and boreholes in alcoves of the ESF, porosity data from gas-tracer tests in boreholes in Alcove 5, and fracture mapping from the ESF, the ECRB, and surface boreholes. The YMP is considering reevaluating the decision to exclude small-scale data, although the impact on the mountain-scale and the drift-scale calibrated properties is not likely to be large.

4.2.4 Thermal Effects on Flow (TEF)

This KTI focuses on the estimation of temperature, moisture content, and humidity at the waste package surface and estimation of temperature and thermally driven water flux with respect to transport of radionuclides away from failed waste packages (NRC 1999d, p. 3). This includes evaluating the redistribution of moisture driven by heat that may result in periods of dryness in the potential repository and in channeling of moisture towards waste packages. The UZ PMR evaluates parameters and processes that are key to understanding the TH behavior of the potential repository, such as percolation flux, seepage into drifts, and the effect of coupled TH processes

on seepage. Other technical concerns related to this KTI are addressed in the Near-Field Environment and EBS PMRs.

Two of the KTI subissues apply to this PMR, as discussed in the following subsections. The PMRs on the near-field environment and the EBS provide additional information related to these subissues and the remaining subissues.

4.2.4.1 Is DOE's Thermal Modeling Approach Sufficient to Predict the Nature and Bounds of TEF in the Near Field?

This subissue addresses the ability of the DOE's TH process models to represent thermally driven flow in the near field. For example, these models should adequately account for the effects of heterogeneities in the models (including focused recharge) and discrete geologic features (NRC 1999d, pp. 66–67). The models do not adequately account for the effects of spatially variable infiltration coupled with the effect of variable heat load at the repository edge, seepage into drifts, and capillary diversion (NRC 1999d, pp. 68–70).

As discussed in Section 4.2.1.1, analyses have been completed to evaluate the effects of various coupled processes on seepage into drifts, including coupled THC processes (see Section 3.10). Current analyses consider the effects of mineral dissolution and precipitation, CO₂ exsolution and transport in the region surrounding the drift, the potential for forming zones of calcite, silica, or other minerals, the resulting changes to porosity, and permeability, and the potential effects on seepage.

4.2.4.2 Does DOE's TSPA Adequately Account for TEF?

This subissue addresses adequate representation of TH processes in the TSPA. Model abstraction should conservatively bound the predictions from the process models. Process models in TSPA-VA do not adequately incorporate processes such as seepage into drifts under ambient conditions and refluxing into drifts during and after the thermal period (NRC 1999d, p. 77). When these processes have been adequately represented in the process models and abstraction, sensitivity analyses should be completed to assess the need for additional data with respect to TEF (NRC 1999d, p. 78).

The UZ PMR summarizes a systematic modeling study that evaluates the effects of TH processes in the UZ (Section 3.12). The model provides mountain-scale thermal response (based on infiltration rate), thermal load, numerical discretization, and the effects of ventilation. It simulates the potential impact of thermal perturbations from emplaced waste on the natural hydrological system, including a representation of heat-driven processes in the far field.

The seepage abstraction has been enhanced to include additional effects, such as changes in drift shape, preferential pathways resulting from degraded rock bolts, and focusing of flow. THC processes have been found to have little effect on seepage (Section 3.10.12).

4.2.5 TSPA and Integration

The objective of this KTI is to describe an acceptable methodology for conducting performance assessments of repository performance and using these assessments to demonstrate compliance with the overall performance objective and requirements for multiple barriers (NRC 2000, p.3). Three of the subissues for this KTI relate to the UZ PMR, as described in the following subsections.

4.2.5.1 System Description and Demonstration of Multiple Barriers

This subissue addresses the demonstration of multiple barriers. This includes the identification of natural and engineered barriers important to isolation, the capability of these barriers to isolate waste, and the identification of processes that may degrade the engineered barriers and thus adversely affect performance of the natural barriers (NRC 2000, p. 4). DOE's TSPA, including scenario analysis (Section 4.2.5.2), model abstractions (Section 4.2.5.3) and transparency and traceability (this section) will support the demonstration of multiple barriers (NRC 2000, p. 17). Specific technical acceptance criteria have not yet been developed for the demonstration of multiple barriers.

This subissue also addresses the NRC's staff expectation on the contents of DOE's TSPA and supporting documents (NRC 2000, p. 4). It provides criteria to evaluate the transparency and traceability of the DOE's TSPA, of the identification and classification of features, events, and processes (FEPs), and of the abstractions for TSPA. Finally, this subissue focuses on the transparency, traceability and validity of data used to support TSPA and of code design and the flow of data in the TSPA (NRC 2000, pp. 10-17).

With respect to transparency and traceability, the YMP is committed to improving the documentation of the technical analyses that support the TSPA. The development of this PMR, and the associated AMRs, focused on improving the transparency and traceability from initial data collection through the analysis and incorporation of data and analyses into the process model for UZ flow and transport to the abstraction of the process models for use in the TSPA. Attachment 1 to the UZ PMR summarizes the data used in the UZ PMR, including the major inputs and outputs with specific references to the technical data bases that store the data. Section 1.3 summarizes the quality assurance status of data and software.

4.2.5.2 Scenario Analysis

This subissue focuses on the process of identifying, screening, and selecting FEPs for inclusion in the TSPA. FEPs that could affect future system performance are used to formulate scenarios. This includes construction of scenario classes, assignment of probabilities to scenario classes, and their incorporation into the TSPA. This is a key factor in ensuring the completeness of the TSPA (NRC 2000, p. 4).

A systematic method was applied to identify and screen FEPs for UZ flow and transport phenomena. One hundred and fifteen FEPs have been identified and grouped into two broad categories of primary and secondary FEPs. The primary FEPs capture the issues associated with

the secondary FEPs. The FEPs are further divided into "included" and "excluded" FEPs. Included FEPs are those directly represented in TSPA models and process models that support the TSPA. Analyses have focused on the identification and screening of FEPs; this work partially addresses this subissue (see Section 1.2.3). The construction and evaluation of scenario classes will be documented in TSPA-SR.

4.2.5.3 Model Abstraction

This subissue focuses on the information and technical approaches needed to develop defensible model abstractions and their integration into TSPA. The following aspects of model abstraction are addressed under this subissue: data used in the development of conceptual approaches or process models, the abstracted models, and estimates of system performance (NRC 2000, p. 4). Specifically, this subissue requires documentation of data used to develop conceptual or process models for model abstractions, verification of the consistency of the abstractions, and explanation of their integration (such as coupling and dependencies) into the TSPA.

For each model abstraction for unsaturated zone flow and transport models, this PMR addresses the NRC's five general principles underlying the technical acceptance criteria: data and model justification, data uncertainty and verification, model uncertainty, model verification, and integration (NRC 2000, p. 32). The PMR summarizes: 1) data available to support the conceptual basis of process models and abstractions, 2) the basis for bounding assumptions and representations of uncertainties and parameter variabilities, 3) alternative conceptual models, 4) abstractions based on and consistent with the underlying process models, and 5) incorporation of design features, physical phenomena, and couplings and use of consistent assumptions throughout the abstraction process. To address consistency in assumptions, the AMRs that document assumptions have been subjected to interdisciplinary review to help ensure that assumptions are applied consistently to the extent practicable. In addition, the PMRs have been reviewed by a single team whose main objective was to identify inconsistencies among the PMRs. These measures provide confidence that consistent assumptions are used in the abstraction process, as appropriate.

4.2.6 UZ and SZ Flow under Isothermal Conditions

The main objective of this KTI is to evaluate all aspects of the ambient hydrological regime at Yucca Mountain that may adversely impact the performance of a potential repository (NRC 1999e). Another objective is to assess the adequacy of the characterization of key hydrological processes and features at the site and in the region that may adversely affect performance.

Four of the subissues for this KTI relate to the UZ PMR, as described in the following subsections. The PMR on SZ flow and transport provides information on the subissue for the SZ.

4.2.6.1 Future Climates and Hydrological Effects on Climate Change: What Is the Likely Range of Future Climates at Yucca Mountain and What Are the Likely Hydrological Effects of Climate Change?

The NRC considers all acceptance criteria for these subissues (NRC 1999e, pp. 170–174) closed with the exception of the programmatic criterion on adequacy of the quality assurance program. This PMR summarizes improvements to the representation of future climate for the Yucca Mountain site since the VA. Section 3.5 provides a more defensible climate model that is focused on 10,000 years and includes upper- and lower-bound climate analogs as compared to TSPA-VA.

4.2.6.2 Present-Day Shallow Infiltration: What Is the Estimated Amount and Spatial Distribution of Present-Day Shallow Infiltration?

The NRC staff agrees with the use of multipliers of the mean annual infiltration (MAI) to incorporate the uncertainty of MAI estimates into the abstraction of the infiltration model (NRC 1999e, p. 176). They note that the infiltration model does not account for surface runoff and shallow lateral flow, potentially impacting calculations of MAI. The NRC is also concerned that the methodology used to assign probabilities to the MAI multipliers is biased towards producing low values for the MAI. All other technical acceptance criteria are considered closed.

The Infiltration Model (Section 3.5) has been refined to provide an improved surface water model and to enhance the ability to model future climate states by considering temperature dependence, vegetation dependence, and snow pack. These improvements provide a better representation of infiltration under future climates and a more defensible basis for the uncertainty in the Infiltration Model to address the NRC concerns. The methodology for assigning probabilities to the MAI multipliers has been enhanced to address the bias towards producing low values for the MAI.

4.2.6.3 Deep Percolation: What Is the Estimated Amount and Spatial Distribution of Percolation through the Proposed Repository Horizon (Present Day and through the Period of Repository Performance)?

The NRC has several concerns with respect to the representation of deep percolation in the UZ. The analyses do not provide a reasonable bound on the uncertainty in the distribution of UZ flow between fractures and the rock matrix (NRC 1999e, p. 181). In addition, fast-path contributions to flow are not adequately represented in the UZ Flow Model (NRC 1999e, p. 179). The effects of climate-induced change (temperature, soil, and vegetation) have not been addressed in defining the bounds on percolation flux and seepage. Uncertainty in flow paths below the repository needs to be addressed and incorporated into the TSPA.

A new active fracture model for fracture-matrix interaction has been used to provide an improved theoretical basis for fracture-matrix interaction as compared to TSPA-VA (DOE 1998). The model describes gravity-dominated, nonequilibrium, preferential liquid-water flow through fractures, including a reduction factor for the interface area that conducts flow between fractures and matrix. As noted in Section 4.2.6.1, improvements have been made to the representation of climate states to address NRC concerns.

The NRC is also concerned that the drift-scale seepage model in the VA did not incorporate several potentially important processes, such as multiple scales of heterogeneity in the hydraulic properties around the drift, modifications to drift geometry from rock fall, thermally induced geochemical changes, and episodic percolation flux (NRC 1999e, p. 180). This PMR summarizes the current seepage model (Section 3.9). This model has been enhanced to incorporate data from niche testing, establish a range of flux values for the upper boundary of the model, and provide a simplified representation of partial collapse of a drift. The model evaluates drift seepage under long-term, steady-state, and episodic conditions for a range of parameters and conditions. Alternative models of flow and transport around and through the perched water beneath the repository have been analyzed (Section 3.7).

4.2.6.4 Matrix Diffusion: To what Degree Does Matrix Diffusion Occur in the UZ and SZ?

If the DOE takes credit for matrix diffusion in the UZ, then the NRC will expect predictions of transport to be consistent with geochemical and isotopic data for the site (NRC 1999e, p. 191). The NRC is concerned about the application of matrix diffusion in the residence-time transfer function (RTTF) approach to modeling transport. This approach has a bias towards predicting faster diffusion from fractures into the matrix. If matrix diffusion is incorporated into UZ transport models, the DOE should (NRC 1999e, p. 192):

- Implement small-scale discrete-fracture models to verify the RTTF approach
- Scale the assumed value for the matrix diffusion coefficient for radionuclide diffusion to account for diminished transport resulting from reduced matrix saturation and reduced fracture-matrix interface area.

The UZ PMR summarizes the current approach to modeling matrix diffusion in the UZ. The former model for matrix diffusion was based on the assumption that fracture spacing is large relative to the average diffusion penetration depth from fractures into the matrix. The matrix-diffusion model has been enhanced to account for the effects of finite fracture spacing. UZ transport modeling assumes that the active fracture model appropriately accounts for reduced fracture-matrix interaction. The current model also assumes that effects of flow in the matrix are negligible with respect to exchange between fractures and matrix through matrix diffusion.

4.3 NRC ACCEPTANCE CRITERIA

Specific technical acceptance criteria for each subissue that relates to this PMR are summarized in Table 4.3-1, along with the approach to addressing the criteria and sections of the PMR that describe these approaches.

The UZ PMR also addresses the NRC's programmatic criteria for quality assurance and the use of expert elicitation. These programmatic criteria apply to all subissues and are not repeated under each subissue in Table 4.3-1.

The acceptance criteria for quality assurance addresses DOE's implementation of an adequate quality assurance program. The UZ PMR was developed in accordance with project procedures

for documenting data, analyses, models, and/or computer codes and preparing and reviewing technical reports (see Section 1.3). The programmatic criterion for expert elicitation specifies that expert elicitation should be conducted in accordance with NUREG-1563 (Kotra et al. 1996) or other acceptable approaches. An expert elicitation on the UZ flow model was completed in 1997 (see Section 1.2). This elicitation was conducted and documented following the NRC guidance on the use of expert elicitation (Kotra et al. 1996). No additional expert elicitations have been completed for the UZ PMR.

Table 4.3-1. Issue Resolution Status Reports, Subissues, Technical Acceptance Criteria, and PMR Approach (NRC 1997, 1999a-e, 2000)

NRC Technical Acceptance Criteria	PMR Approach and Section Reference
IRSR: Evolution of the Near-field Environment	
Subissue 1 - Effects of coupled THC processes on seepage and flow	
Data and model justification acceptance criteria for Subissue 1	
1 - Available data relevant to both temporal and spatial variations in conditions affecting coupled THC effects on seepage and flow were considered.	The TSPA-VA did not explicitly consider the effects of coupled THC processes; the evaluation of coupled THC effects is documented in this PMR. Attachment I summarizes available site data. Section 3.10 documents the abstraction of coupled THC effects for TSPA, based on the process modeling results presented in the same section.
2 - DOE's evaluation of coupled THC processes properly considered site characteristics in establishing initial and boundary conditions for conceptual models and simulations of coupled processes that may affect seepage and flow.	Attachment I summarizes available data. These data on the site characteristics were used to establish initial and boundary conditions for the evaluation of THC effects on seepage and flow in the near field (Section 3.10).
3 - Sufficient data were collected on the characteristics of the natural system and engineered materials, such as the type, quantity, and reactivity of material, to establish initial and boundary conditions for conceptual models and simulations of THC coupled processes that affect seepage and flow.	Attachment I summarizes available data. The THC model incorporates site data to establish initial and boundary conditions and incorporates specific aspects of the design, including in-drift geometry, drift spacing, and the TH properties of the components of the EBS, such as waste packages and invert (Section 3.10). The current design does not include concrete liners in the emplacement drifts limiting the potential effects of interactions between concrete and tuff on seepage and flow.
4 - Sensitivity and uncertainty analyses (including consideration of alternative conceptual models) were used to determine whether additional new data are needed to better define ranges of input parameters.	Sensitivity and uncertainty analyses will be included in TSPA-SR.
5 - If the testing program for coupled THC processes on seepage and flow is not complete at the time of license application, or if sensitivity and uncertainty analyses indicate additional data are needed, DOE will identify specific plans to acquire the necessary information as part of the performance confirmation program.	The performance confirmation plan addresses coupled THC effects on seepage and flow. Rock mass cooling response, coupled process testing, and seepage testing under heated environments are planned for the pre-emplacement period. Longer term testing for seepage and near-field THC testing and monitoring around selected emplacement drifts and under simulated postclosure conditions is also addressed (CRWMS M&O 2000c, Appendix G).
Data uncertainty and verification acceptance criteria for Subissue 1	
1 - Reasonable or conservative ranges of parameters or functional relations were used to determine effects of coupled THC processes on seepage and flow. Parameter values, assumed ranges, probability distributions, and bounding assumptions are technically defensible and reasonably account for uncertainties.	The TSPA-VA did not explicitly consider the effects of coupled THC processes; the evaluation of the effects of coupled THC processes is documented in this PMR. Section 3.10.3 discusses ranges in the characteristics of the natural system that were used to evaluate the effects of THC processes on seepage and flow and the rationale for these ranges.

NRC Technical Acceptance Criteria	PMR Approach and Section Reference
Data uncertainty and verification acceptance criterion for Subissue 1, continued	
2 - Uncertainty in data due to both temporal and spatial variations in conditions affecting coupled THC effects on seepage and flow were considered.	Section 3.10.6 discusses the uncertainty in data affecting THC coupled processes on seepage and flow.
3 - DOE's evaluation of coupled THC processes properly considered the uncertainties in the characteristics of the natural system and engineered materials, such as type, quantity, and reactivity of material, in establishing initial and boundary conditions for conceptual models and simulations of THC coupled processes that affect seepage and flow.	Section 3.10.6 discusses uncertainties in the characteristics of the natural system. Engineered materials are discussed in the PMR on the engineered barrier system.
4 - The initial conditions, boundary conditions, and computational domain used in sensitivity analyses involving coupled THC effects on seepage and flow were consistent with available data.	Sensitivity analyses will be included in TSPA-SR.
5 - DOE's performance confirmation program should assess whether the natural system and engineered materials are functioning as intended and anticipated with regard to coupled THC effects on seepage and flow.	The performance confirmation plan addresses coupled THC effects on seepage and flow. Rock mass cooling response, coupled process testing, and seepage testing under heated environments are planned for the pre-emplacement period. Longer term testing for seepage and near-field THC testing and monitoring around selected emplacement drifts and under simulated postclosure conditions is also addressed (CRWMS M&O 2000c, Appendix G).
Model uncertainty acceptance criteria for Subissue 1	
1 - Appropriate models, tests, and analyses were used that are sensitive to the THC couplings under consideration for both natural and engineered systems, as described in the following examples. The natural setting data indicate processes that should be evaluated include: (i) zeolitization of volcanic glass, which could affect flow pathways; (ii) precipitation of calcite and opal on the footwall of fracture surfaces and the bottoms of lithophysal cavities, which indicates gravity-driven flow in open fractures that could affect permeability and porosity; and (iii) potential dehydration of zeolites and vitrophyre glass, which could release water affecting heat and fluid flow. The effects of THC coupled processes that may occur due to interactions with engineered materials or their alteration products include: (i) changes in water chemistry that may result from interactions between cementitious materials and groundwater, which, in turn, may affect seepage and flow; (ii) dissolution of the geologic barrier (e.g. tuff) by a hyperalkaline fluid that could lead to changes in the hydraulic properties of the geologic barrier; and (iii) precipitation of calcite or calcium-silica-hydrate phases along fracture surfaces as a result of migration of a hyperalkaline fluid that could affect hydraulic properties.	Attachment I summarizes available site data. Section 3.10 summarizes data, analyses, and models that were used to evaluate THC processes on the natural system. The purpose of the THC seepage model is to evaluate the effects of THC processes in the rock around the emplacement drift on seepage water chemistry, gas-phase composition, and the potential effects of THC processes on UZ flow and transport. This model evaluates the effects of mineral dissolution and precipitation, the effects of CO ₂ exsolution and transport in the region surrounding the drift, the potential for forming zones of calcite, silica or other minerals, the resulting changes in porosity and permeability, and the potential effects on seepage. See also the PMR on the near field environment.

NRC Technical Acceptance Criteria	PMR Approach and Section Reference
2 - Given the current design of the repository, it will be acceptable to ignore the potential effects of microbial processes on seepage and flow.	The DOE agrees that the potential effects of microbial processes on seepage and flow are not significant, given the current design (Section 1.2.3, Assumption 3) (CRWMS M&O 2000, EBS PMR; CRWMS M&O 2000, WFD PMR).
Model uncertainty acceptance criteria for Subissue 1, continued	
3 - Alternative modeling approaches consistent with available data and current scientific understanding were investigated, and their results and limitations were appropriately considered.	Section 3.10.7 addresses the alternative conceptual model proposed by Matyskiela (1997).
4 - DOE provided a reasonable description of the mathematical models included in its analyses of coupled effects on seepage and flow. The description should include a discussion of alternative modeling approaches not considered its final analysis and the limitations and uncertainties of the chosen model.	Section 3.10 summarizes the mathematical models used; an alternative conceptual model is discussed in Section 3.10.7.
Model verification acceptance criteria for Subissue 1	
1 - The mathematical models for coupled THC effects on seepage and flow are consistent with conceptual models based on inferences about near-field environment, field data and natural alteration observed at the site, and expected engineered materials.	Section 3.10 summarizes the mathematical models used to evaluate coupled THC effects on seepage and flow.
2 - DOE appropriately adopted accepted and well-documented procedures to construct and test the numerical models used to simulate coupled THC effects on seepage and flow.	Procedures were followed, consistent with the governing quality assurance requirements (see Chapter 1).
3 - Abstracted models for coupled THC effects on seepage and flow were based on the same assumptions and approximations shown to be appropriate for closely analogous natural or experimental systems. Abstracted model results were verified through comparison to outputs of detailed process models and empirical observations. Abstracted model results are compared with different mathematical models to judge robustness of results.	Abstractions in Section 3.10 were derived from the underlying process models described in the UZ PMR.
Integration acceptance criteria for Subissue 1	
1 - DOE has considered all the relevant features, events, and processes. The abstracted models adequately incorporated design features, physical phenomena, and couplings, and used consistent and appropriate assumptions throughout.	Section 1.2.3 discusses the relevant features, processes and events. Included FEPS are directly represented in the process models and abstractions that support TSPA and discussed in other sections of the PMR corresponding to the specific models.
2 - Models reasonably accounted for known temporal and spatial variations in conditions affecting coupled THC effects on seepage and flow.	Section 3.10 summarizes the parameter ranges used in the THC model and provides a rationale for these ranges. Section 3.10.4 describes the process of validating the THC model with results from the drift scale test.

NRC Technical Acceptance Criteria	PMR Approach and Section Reference
Integration acceptance criteria for Subissue 1, continued	
3 - Not all THC couplings may be determined to be important to performance, and DOE may adopt assumptions to simplify PA analyses. If potentially important couplings are neglected, DOE should provide a technical basis for doing so. The technical basis could include activities, such as independent modeling, laboratory or field data, or sensitivity studies.	The DOE agrees that simplifying assumptions may be appropriate if not all the THC couplings are determined to be important to performance and will provide the technical basis for the simplifying assumptions.
4 - Where simplifications for modeling coupled THC effects on seepage and flow were used for PA analyses instead of detailed process models, the bases used for modeling assumptions and approximations were documents and justified.	Section 3.10 11 documents the basis for the abstraction of coupled THC effects on seepage and flow.
Subissue 2 - Waste package chemical environment (Waste Package Degradation PMR)	
Subissue 3 - Effects of THC processes on the chemical environment for radionuclide release (Waste Form /Engineered Barrier System PMRs)	
Subissue 4 - Effects of coupled THC processes on the radionuclide transport through engineered and natural barriers	
Data and model justification acceptance criteria for Subissue 4	
1 - Available data relevant to both temporal and spatial variations in conditions affecting coupled THC effects on transport of radionuclides in the near field were considered.	The TSPA-VA did not explicitly consider the effects of coupled THC processes; the evaluation of coupled THC effects are documented in this PMR. Attachment I summarizes available data; Section 3.10 describes how relevant data were incorporated into the modeling.
2 - DOE's evaluation of coupled THC processes properly considered site characteristics in establishing initial and boundary conditions for conceptual models and simulations of coupled processes that may affect radionuclide transport in the near field.	The evaluation of coupled THC processes in Section 3.10 considered site characteristics in establishing initial and boundary conditions for conceptual models and simulation of coupled processes. See also the PMRs on near field environment and EBS.
3 - Sufficient data were collected on the characteristics of natural system and engineered materials, such as the type, quantity, and reactivity of material, in establishing initial and boundary conditions for conceptual models and simulations of THC coupled processes that affect transport of radionuclides in the near field.	Attachment I summarizes available site data. The THC model incorporates site data to establish initial and boundary conditions and incorporates specific aspects of the design, including in-drift geometry, drift spacing, and the TH properties of the components of the EBS, such as waste packages and invert (Section 3.10). The current design does not include concrete liners in the emplacement drifts limiting the potential effects of interactions between concrete and tuff on seepage and flow (CRWMS M&O 2000, EBS PMR; CRWMS M&O 2000, WFD PMR).
4 - A nutrient and energy inventory calculation should be used to determine the potential for microbial activity that could adversely affect radionuclide transport through engineered and natural barriers.	The potential effects of microbial processes on transport away from a drift are not considered significant, given the current design (Section 1.2.3, Assumption 3). See the PMRs on the engineered barrier system and waste form.

NRC Technical Acceptance Criteria	PMR Approach and Section Reference
Data and model justification acceptance criteria for Subissue 4, continued	
5 - Should microbial activity be sufficient to allow microbial effects on transport of radionuclides through engineered and natural barriers, then the time-history of temperature, humidity, and water saturation in engineered and natural materials should be used to constrain the probability for these effects.	See the PMRs on the engineered barrier system and waste form.
6 - Sensitivity and uncertainty analyses (including consideration of alternative conceptual models) were used to determine whether additional new data are needed to better define ranges of input parameters.	Sensitivity and uncertainty analyses will be included in TSPA-SR.
7 - If the testing program for coupled THC processes on the chemical environment for radionuclide release from the engineered barrier system is not complete at the time of license application, or if sensitivity and uncertainty analyses indicate additional data are needed, DOE has identified specific plans to acquire the necessary information as part of the performance confirmation program.	Although THC effects on radionuclide transport have been determined not to be important to performance, the performance confirmation plan contains testing during the pre-placement period to confirm this assumption (CRWMS M&O 2000c, Appendix G).
Data uncertainty and verification acceptance criteria for Subissue 4	
1 - Reasonable or conservative ranges of parameters or functional relations were used to determine effects of coupled THC processes on transport of radionuclides in the near field. Parameter values, assumed ranges, probability distributions, and bounding assumptions are technically defensible and reasonably account for uncertainties.	The TSPA-VA did not explicitly consider the effects of THC processes; the evaluation of coupled THC effects is documented in this PMR. Attachment 1 summarizes available site data. Section 3.10 discusses the range of parameters in the characteristics of the natural system that were used to evaluate the effects of coupled processes along with the rationale for the range of parameters.
2 - Uncertainty in data due to both temporal and spatial variations in conditions affecting coupled THC effects on radionuclide transport in the near field were considered.	Section 3.10.6 discusses uncertainties in data due to temporal and spatial variations in conditions affecting THC processes.
3 - DOE's evaluation of coupled THC processes properly considered the uncertainties in the characteristics of the natural system and engineered materials, such as type, quantity, and reactivity of material, in establishing initial and boundary conditions for conceptual models and simulations of THC coupled processes that affect transport of radionuclides in the near field.	Section 3.10.6 discusses uncertainties in the characteristics of the natural system. See also the PMR on the engineered barrier system.
4 - The initial conditions, boundary conditions, and computational domain used in sensitivity analyses involving coupled THC effects on radionuclide transport in the near field were consistent with available data.	Sensitivity analyses will be included in the TSPA-SR.
5 - DOE's performance confirmation program should assess whether the natural system and engineered materials are functioning as intended and anticipated with regard to coupled THC effects on transport of radionuclides in the near field.	Although THC effects on radionuclide transport have been determined not to be important to performance, the performance confirmation plan contains testing during the pre-placement period to confirm this assumption (CRWMS M&O 2000c, Appendix G).

NRC Technical Acceptance Criteria	PMR Approach and Section Reference
Model uncertainty acceptance criteria for Subissue 4	
<p>1 - Appropriate models, tests, and analyses were used that are sensitive to the THC couplings under consideration for both natural and engineered systems, as described in the following examples. The effects of THC coupled processes that may occur in the natural setting or due to interactions with engineered materials or their alteration products include: (i) TH effects on gas and water chemistry in the unsaturated zone and saturated zone; (ii) precipitation of calcite and opal on the footwall of fracture surfaces and the bottoms of lithophysal cavities, which indicates gravity-driven flow in open fractures, and isolation of transport pathways from sorption sites in the rock matrix; (iii) zeolitization of volcanic glass, that could affect transport pathways; (iv) precipitation and dissolution of oxides and hydroxides on fracture surfaces, illitization of smectite, and recrystallization of zeolites to analcime, which could affect sorption characteristics; (v) effects of microbial processes; (vi) effects of corrosion products of container materials and waste forms on transport of radionuclides in the near field; and (vii) changes in hydraulic and sorptive properties of the natural system resulting from interactions between cementitious materials and groundwater.</p>	<p>Attachment I summarizes available site data. Section 3.10 summarizes data, analyses, and models that were used to evaluate THC processes on the natural system. The purpose of the THC seepage model is to evaluate the effects of THC processes in the rock around the emplacement drift on seepage water chemistry, gas-phase composition, and the potential effects of THC processes on UZ flow and transport. This model evaluates the effects of mineral dissolution and precipitation, the effects of CO₂ exsolution and transport in the region surrounding the drift, the potential for forming zones of calcite, silica or other minerals, the resulting changes in porosity and permeability, and the potential effects on seepage. See also the PMR on the near field environment.</p>
<p>2 - Alternative modeling approaches consistent with available data and current scientific understanding were investigated, and their results and limitations were appropriately considered.</p>	<p>Section 3.10.7 addresses the alternative conceptual model proposed by Matyskiela (1997).</p>
<p>3 - DOE provided a reasonable description of the mathematical models included in its analyses of coupled effects on radionuclide transport in the near field. The description should include a discussion of alternative modeling approaches not considered its final analysis and the limitations and uncertainties of the chosen model.</p>	<p>Section 3.10 summarizes the relevant mathematical models.</p>
Model verification acceptance criteria for Subissue 4	
<p>1 - The mathematical models for coupled THC effects on radionuclide transport in the near field are consistent with conceptual models based on inferences about near-field environment, field data and natural alteration observed at the site, and expected engineered materials.</p>	<p>Section 3.10 summarizes the basis for the mathematical models used to evaluate coupled THC effects.</p>
<p>2 - DOE appropriately adopted accepted and well-documented procedures to construct and test the numerical models used to simulate coupled THC effects on transport of radionuclides in the near field.</p>	<p>Procedures were followed, consistent with the governing quality assurance requirements (See Section 1).</p>

NRC Technical Acceptance Criteria	PMR Approach and Section Reference
Model verification acceptance criteria for Subissue 4, continued	
3 - Abstracted models for coupled THC effects on radionuclide transport in the near field were based on the same assumptions and approximations shown to be appropriate for closely analogous natural or experimental systems. Abstracted model results were verified through comparison to outputs of detailed process models and empirical observations. Abstracted model results are compared with different mathematical models to judge robustness of results.	Thermal effects on flow were not found to be significant and will not be included in UZ transport simulations for TSPA-SR (Sections 3.11.1.3, 3.11.2, and 5.2.4).
Integration acceptance criteria for Subissue 4	
1 - DOE has considered all the relevant features, events, and processes. The abstracted models adequately incorporated design features, physical phenomena, and couplings, and used consistent and appropriate assumptions throughout.	Section 1.2.3 discusses the relevant features, processes and events. Included FEPs are directly represented in the process models and abstractions that support TSPA and are discussed in sections of the PMR corresponding to the specific models.
2 - Models reasonably accounted for known temporal and spatial variations in conditions affecting coupled THC effects on transport of radionuclides in the near field.	Section 3.10 discusses temporal and spatial variations in conditions affecting THC effects.
3 - Not all THC couplings may be determined to be important to performance, and DOE may adopt assumptions to simplify PA analyses. If potentially important couplings are neglected, DOE should provide a technical basis for doing so. The technical bases could include activities, such as independent modeling, laboratory or field data, or sensitivity studies.	The DOE agrees that simplifying assumptions may be appropriate if not all the THC couplings are determined to be important to performance and will provide the technical basis for the simplifying assumptions.
4 - The bases used for modeling assumptions and approximations were documented and justified, where simplifications for modeling coupled THC effects on radionuclide transport in the near field were used for performance assessment analyses instead of detailed process models.	In general, the PMR documents the basis for modeling assumptions and approximations in the specific sections addressing the UZ flow and transport models. Also see Assumption 4 in Section 1.2.3.
Subissue 5 - Coupled THC processes affecting potential nuclear criticality in the near field (covered in a topical report and supporting documents)	
IRSR: Radionuclide Transport	
Subissue 1 - Estimation of radionuclide transport through porous rock	
1 - For the estimation of radionuclide transport through porous rock DOE has:	
1.a - Determined, through PA calculations, whether radionuclide attenuation process such as sorption, precipitation, radioactive decay, and colloidal filtration are important to performance.	Section 3.11.2 evaluates the effect of processes such as hydrodynamic dispersion, matrix diffusion, sorption (solutes), filtration (colloids), and radioactive decay. These processes are considered important to performance and are all explicitly modeled in the transport model abstraction (3.11.12).

NRC Technical Acceptance Criteria	PMR Approach and Section Reference
Subissue 1 - Estimation of radionuclide transport through porous rock, continued	
1.b - (i) Assumed K_d is zero and radionuclides travel at the rate of groundwater flow, if it has been found that radionuclide attenuation is unimportant to performance and it can be demonstrated that this assumption is conservative, in which case Acceptance Criteria 2 and 3 do not have to be met, or (ii) demonstrated that Criterion 2 or 3 has been met, if radionuclide attenuation in porous rock is important to performance, or if an assumption that K is zero in porous rock is not conservative	This PMR uses an assumed K_d of zero, therefore acceptance criteria 2 and 3 need to be evaluated.
2 - For the valid application of the constant K_d approach, using equation (1) $R_r = 1 + \rho_b K_d/n$, DOE has:	
2.a - Demonstrated that the flow path acts as a single continuum porous medium. If the flow can not be shown to be a single continuum porous medium, then the Acceptance Criteria for radionuclide transport in fractured rock apply.	Section 3.4 summarizes numerical approaches for modeling UZ hydrology; transport modeling is based on the UZ flow model summarized in Section 3.7.2.
2.b - Demonstrated that appropriate values for the parameters. K_d , n or θ , and ρ_b have been adequately considered (e.g., experimentally determined or measured).	Details of the experimental program are provided in the Yucca Mountain Site Description.
2.c - Demonstrated that the three implicit assumptions (i.e. linear isotherm, fast reversible sorption reaction, and constant bulk chemistry) are valid.	Section 3.11 discusses these assumptions; the AMR on radionuclide transport models under ambient conditions provides the supporting rationale.
3 - For the valid application of process models affecting radionuclide transport such as surface complexation, ion exchange, precipitation/dissolution, and processes involving colloidal material	
3.a - Demonstrated that the flow path acts as a single-continuum porous medium. See Subissue 4, page 312 of this PMR.	Transport modeling is based on the UZ flow models discussed in Section 3.7.
3.b - Demonstrated that values for the parameters used in process models are appropriate and sufficient.	Transport parameters are summarized in Section 3.11.2.
3.c - (i) Demonstrated that the three implicit assumptions (see 2c) are valid, if process models are intended to yield a constant K_d for use in the retardation equation (equation 1); or (ii) determined transport in a dynamic reactive transport system mode (e.g., PHREEQC, MULTIFLO, HYDROGEOCHEM, etc.).	See 2 c) above.
Subissue 2 - For the estimation of radionuclide transport through alluvium (covered in Saturated Zone Flow and Transport PMR)	
Subissue 3 - Radionuclide transport through fractured rock	
1 - For estimation of radionuclide transport through fractured rock, DOE has continued	

NRC Technical Acceptance Criteria	PMR Approach and Section Reference
1a - Determined, through PA calculations, whether radionuclide attenuation processes such as sorption, precipitation, and radioactive decay, and colloidal transport are important to performance.	Section 3.11 summarizes attenuation processes, such as sorption, precipitation, radioactive decay, and colloidal transport. These processes are considered important to performance.
1b - Assumed K_d (or K_a) is zero and that radionuclides travel at the velocity of groundwater flow through fractures, if it has been found that radionuclide attenuation in fractures is unimportant to performance, and it can be demonstrated that this assumption is conservative. In this case, Acceptance Criterion 2 does not have to be met.	There is limited information on sorption onto the fracture surfaces, which will retard migration of sorbing radionuclides. However, sorption in the fractures is neglected in the PA transport evaluations because of limited data and the conservative nature of the assumption.
1c - Justified the length of flow path to which these fracture transport conditions apply	There is limited information on sorption onto the fracture surfaces, which will retard migration of sorbing radionuclides. However, sorption in the fractures is neglected in the PA transport evaluations because of limited data and the conservative nature of the assumption (Section 3.11.10.2.).
2 - If credit is taken for radionuclide attenuation in fractured rock, DOE has:	There is limited information on sorption onto the fracture surfaces, which will retard migration of sorbing radionuclides. However, sorption in the fractures is neglected in the PA transport evaluations because of limited data and the conservative nature of the assumption (Section 3.11.10.2.).
2a - Demonstrated capability to predict breakthrough curves or reactive, nonreactive, and colloidal tracers in field tests.	There is limited information on sorption onto the fracture surfaces, which will retard migration of sorbing radionuclides. However, sorption in the fractures is neglected in the PA transport evaluations because of limited data and the conservative nature of the assumption (Section 3.11.10.2.).
2b - Demonstrated nonradioactive tracers used in field tests are appropriate homologues for radioelements.	There is limited information on sorption onto the fracture surfaces, which will retard migration of sorbing radionuclides. However, sorption in the fractures is neglected in the PA transport evaluations because of limited data and the conservative nature of the assumption (Section 3.11.10.2.).
2c - Justified the length of flowpath to which these fracture transport conditions apply.	There is limited information on sorption onto the fracture surfaces, which will retard migration of sorbing radionuclides. However, sorption in the fractures is neglected in the PA transport evaluations because of limited data and the conservative nature of the assumption (Section 3.11.10.2.).
Subissue 4 - Nuclear criticality in the far field (covered in a topical report and supporting documents)	
IRSR: Structural Deformation and Seismicity	
Subissue 1 - Fault displacement hazard (covered in Disruptive Events PMR)	
Subissue 2 - Seismic hazard (covered in Disruptive Events PMR)	

NRC Technical Acceptance Criteria	PMR Approach and Section Reference
Subissue 3 - Fracturing and structural framework of the geologic setting	
1 - Data and model justification: Adequate field, borehole, and underground excavation data are acquired to sufficiently support conceptual models, assumptions, and boundary conditions of numerical abstractions of fracture data and fracture models of ambient and perturbed conditions.	This information is provided in the Yucca Mountain Site Description. Attachment I summarizes data on the properties of fractures. Fracture property estimates are based on permeability data from <i>in situ</i> air injection tests conducted in four surface boreholes and boreholes in alcoves in the ESF, porosity data from gas tracer tests in boreholes in Alcove 5, and fracture mapping from the ESF, ECRB, and surface based boreholes (Section 3.6.3.2).
2 - Data and uncertainty verification: Parameter values, assumed ranges, probability distributions, and bounding assumptions used to determine fracture distributions and properties reasonably account for uncertainties and variabilities.	See above. Small-scale fracture data from detailed line surveys have become available since the analysis in this PMR was performed. Although the impact of small-scale fracture data on mountain-scale and drift-scale calibrated properties is not likely to be large, the impact will be evaluated in the future (Section 3.6.3.2).
3 - Model uncertainty: Alternative modeling approaches for fracture distribution and properties of fractures consistent with available data and current geologic understanding are investigated and results and limitations are appropriately considered in process, TSPA, or both models of ambient and perturbed repository conditions	Physical processes, including a discussion of the fracture and matrix flow component for each major unit, are discussed in Section 3.3. Alternative numerical approaches for modeling are summarized in section 3.4. The representation of fractures in the UZ model is discussed in Section 3.7. Section 3.7.3.2 analyzes the effects of major faults on UZ flow. The results indicate that faults serve as major focusing conduits for downward liquid flow in the UZ. For the seepage model (Section 3.9.) model calibration is used to determine the effective parameters, including potential effects of individual fractures and microfractures on seepage. Simulations with multiple realizations of a heterogeneous property field are completed to account for the random nature of the fracture field.
4 - Model verification: Results of fracture data analyses and fracture models are verified by comparison with output of sensitivity studies, detailed process level models, natural analogs, and empirical observations, as appropriate.	Physical processes, including a discussion of fracture and matrix flow component for each major unit, are discussed in Section 3.3. The representation of fractures in the UZ model is discussed in Section 3.7.
5 - Integration: Results of abstractions of fracture data are consistent with physical and geological phenomena and coupled processes.	Abstractions are based on available site fracture characteristics (Section 3.7).
Subissue 4 - Tectonic framework of the geologic setting (covered in Disruptive Events PMR and the Yucca Mountain Site Description)	
IRSR: Thermal Effects on flow	
Subissue 1 - Is the U.S. Department of Energy TH testing program, including performance confirmation testing, sufficient to evaluate the potential for thermal reflux to occur in the near field? (covered in Near Field Environment PMR)	

NRC Technical Acceptance Criteria	PMR Approach and Section Reference
Subissue 2 - Is the thermohydrologic modeling approach sufficient to predict the nature and bounds of thermal effects on flow in the near field?	
1 - Sufficient data are available to adequately define relevant parameters, parameter values, and conceptual models. Demonstrate that:	
1.1 - Uncertainties and variabilities in parameter values are accounted for using defensible methods. The technical bases for parameter ranges, probability distributions or bounding values used are provided. Parameter values (single values, ranges, probability distributions, or bounding values) are derived from site-specific data or an analysis is included to show the assumed parameter values lead to a conservative effect on performance.	Section 3.10 summarizes the parameter ranges and the technical basis for these ranges. Parameter values derived from site data are specified.
1.1.- Analyses are consistent with site characteristics in establishing initial conditions, boundary conditions, and computational domains for conceptual models evaluated.	Analyses in Section 3.10 considered site characteristics in establishing initial conditions, boundary conditions, and computational domains. In addition to the required UZ hydrologic properties, the model includes initial and boundary water and gas chemistry, initial mineralogy, mineral volume fractions, reactive surface areas, equilibrium thermodynamic data for minerals, aqueous and gaseous species, kinetic data for mineral-water reactions, and diffusion coefficients for aqueous and gaseous species (Section 3.10.2).
2 - Descriptions of process-level conceptual and mathematical models used in the analyses are reasonably complete. Demonstrate that:	
2.1 - Models are based on well-accepted principles of heat and mass transfer applicable to unsaturated geologic media.	Sections 3.10 and 3.12 summarize TH models that are based on accepted principles of heat and mass transfer.
2.2 - Models include, at a minimum, the processes of evaporation and condensation and the effects of discrete geologic features.	Current models (Section 3.10.2) include processes of evaporation and condensation. Figure 3.10-2 shows schematically the relationships between TH and geochemical processes in zones of boiling, condensation, and drainage in the rock mass outside of the drift and above the heat source. Seepage models (Section 3.9) now include an active fracture model to describe fracture-matrix interactions.

NRC Technical Acceptance Criteria	PMR Approach and Section Reference
Subissue 2 - Is the thermohydrologic modeling approach sufficient to predict the nature and bounds of thermal effects on flow in the near field?, continued	
2.3 - Models include, at a minimum, an evaluation of important thermohydrological phenomena, such as: (i) multidrift dry-out zone coalescence, (ii) lateral movement of condensate, (iii) cold-trap effect, (iv) repository edge effects, and (v) condensate drainage through fractures.	The current design has a lower thermal load than the VA design to eliminate dryout zone coalescence. Section 3.10 evaluates the extent of the dryout zone and time of rewetting for different calibrated property sets and climate scenarios. Section 3.12 summarizes TH mountain scale models of the effects of temperature changes over the mountain, including effects on flow around the drift.
2.4 - Models include all significant repository design features.	Sections 3.10 and 3.12 summarize the design features included in the TH model. For example, the THC model uses in-drift geometry and drift spacing, and the thermal and hydrologic properties of the EBS components, such as waste package and invert, from the current design.
2.5 - Models are capable of accommodating variation in infiltration.	The TH model incorporates variation in infiltration (Sections 3.10 and 3.12).
2.6 - Conceptual model uncertainties have been defined and documented and effects on conclusions regarding performance assessed.	Sections 3.10 and 3.12 summarize conceptual uncertainties.
2.7 - Mathematical models are consistent with conceptual models, based on consideration of site characteristics.	Sections 3.10 and 3.12 discuss mathematical models used to represent conceptual models and are based on site characteristics.
2.8 - Alternative models and modeling approaches, which are consistent with available data and current scientific understanding, have been investigated, limitations defined, and results appropriately considered.	Section 3.10.7 discusses an alternative model proposed by Matyskiela (1997).
2.9 - Results from different mathematical models have been compared to judge robustness of results.	Numerical approaches that can be used for unsaturated, fractured rock have been reviewed in the AMR on conceptual and numerical models for UZ flow and transport.
2.10 - Models used to predict shedding around emplacement drifts are shown to contain an adequate level of heterogeneity in media properties.	Sections 3.10 and 3.12 summarize the approach to evaluating heterogeneities in TH models.
2.11 - TH models have been demonstrated to be appropriate for the temperature regime expected at the repository.	TH models incorporated the anticipated thermal load for the current design (Sections 3.10 and 3.12).
2.12 - Models include radiative heat transport unless it is shown that radioactive heat loss by a WP is not significant.	TH models include radiative heat transfer at the drift scale (Section 3.10.5.1).
2.13 - Models include the effect of ventilation particularly if ventilation could result in deposition or condensation of moisture on a WP surface.	Effects of ventilation are included (Sections 3.10.5.1 and 3.12.1).

NRC Technical Acceptance Criteria	PMR Approach and Section Reference
Subissue 2 - Is the thermohydrologic modeling approach sufficient to predict the nature and bounds of thermal effects on flow in the near field?, continued	
2.14 - The media properties of a model contain an adequate level of heterogeneity so that mechanisms such as dripping are not neglected or misrepresented.	The drift seepage model has been enhanced to account for heterogeneities (Section 3.9.3).
2.15 - Drift wall representations in models contain sufficient physical detail so that processes predicted using a continuum model, such as capillary diversion, are appropriate for the geologic media at the proposed repository horizon.	Models predicting seepage include partial drift collapse and multiple realizations of heterogeneous rock properties (Sections 3.9.3.4 and 3.9.4.5). See also the PMR on near field environment.
2.16 - Physical mechanisms such as penetration of the boiling isotherm by flow down a fracture are not omitted from model predictions due to over simplification or the physical medium or the conceptual model.	Section 3.9 summarizes the drift seepage models, including enhancements such as the evaluation of partial drift collapse and episodic percolation flux. Section 3.10 describes the seepage THC models.
3 - Coupling of processes has been evaluated using a methodology in accordance with NUREG-1466 (Nataraja and Brandshaug, 1992) or other acceptable methodology. Coupled processes may be uncoupled, if it is shown that the uncoupled model results bound the predictions of the fully coupled model results.	NUREG-1466 provides logical steps for the development of predictive models and their numerical representation of thermally induced TMHC behavior of the host rock. Models of coupled processes in Sections 3.10 and 3.12 present the current approach to modeling drift scale and mountain scale TH effects. The DOE agrees that coupled processes may be uncoupled if the models bound the effects of fully coupled processes.
4 - The dimensionality of models, which include heterogeneity at appropriate scales and significant process couplings, may be reduced, if shown that the reduced dimension model bounds the predictions of the full dimension model.	The DOE agrees with this approach, and has implemented a modeling approach with models of different dimensions and scales. See for example Section 3.10, Drift-Scale THC Processes and Models, and Section 3.12, Mountain-Scale TH Model.
5 - Equivalent continuum models are acceptable for the rock matrix and small discrete features, if it can be demonstrated that water in small discrete features is in continuous hydraulic equilibrium with matrix water. Significant discrete features, such as fault zones, should be represented separately unless it can be shown that inclusion in the equivalent continuum model (ECM) produces a conservative effect on calculated overall performance.	Section 3.10.3 summarizes the approach to modeling thermal-hydrologic processes.
6 - Accepted and well-documented procedures have been adopted to construct and calibrate numerical models used.	Procedures were followed, consistent with the governing quality assurance requirements (see Section 1).
7 - Results of process-level models have been verified by demonstrated consistency with results/observations from field-scale, thermohydrologic tests. In particular, sufficient physical evidence should exist to support the conceptual models used to predict thermally driven flow in the near field.	Process level models have been calibrated against field data and observations (Sections 3.9.4.5, 3.10.4, 3.12.4).

NRC Technical Acceptance Criteria	PMR Approach and Section Reference
Subissue 3: Does the DOE's TSPA adequately account for thermal effects on flow?	
1 - Abstractions of process-level models may be used if predictions from the abstracted model are shown to conservatively bound process-level predictions. In particular, DOE may use an abstracted model to predict water influx into an emplacement drift if the abstracted model is shown to bound process-level model predictions of the influx of water as liquid or vapor into an emplacement drift.	Section 3.9 summarizes the abstraction of seepage into drifts. As noted in Section 3.9.6.3, distributions for the amount of seepage as a function of percolation flux are derived directly from process-model results and constrained by measurements of permeability around three niches in the ESF and calibration of seepage tests conducted in one niche in the ESF.
2 - Sufficient data are available to adequately define relevant parameter values and conceptual models. Demonstrate that:	
2.1 - Uncertainties and variabilities in parameter values are accounted for using defensible methods. The technical bases for parameter ranges, probability distributions or bounding values used are provided. Parameter values (single values, ranges, probability distributions, or bounding values) are derived from site-specific data or an analysis is included to show the assumed parameter values lead to conservative effect on performance.	The THC abstraction of the mean infiltration rate (with climate changes) includes both geochemical systems (full and calcite-silica-gypsum) considered in the THC process model (Section 3.10.11).
2.2 - Analysis are consistent with site characteristics in establishing initial conditions, boundary conditions, and computational domains for conceptual models evaluated.	Site characteristics have been considered in establishing initial conditions, boundary conditions, and computational domains (Sections 3.10 and 3.12).
3 - Descriptions of conceptual and mathematical models used in DOE's TSPA are reasonably complete.	
3.1 - Performance affecting heat and mass transfer mechanisms, including processes observed in available thermohydrologic tests and experiments, have been identified and incorporated into the TSPA. Specifically, it is necessary to either demonstrate that liquid water will not reflux into the underground facility or incorporate refluxing water into the TSPA and bound the potential adverse effects of: (i) corrosion of the WP; (ii) accelerated transport of radionuclides; and (iii) alteration of hydraulic and transport pathways that result from refluxing water.	Section 3.12 summarizes the evaluation of flow changes close to drifts and drainage in the pillars.
3.2 - Significant Geologic Repository Operations Area underground facility design features, such as the addition of backfill of drip shields, that can result in changes in TSP have been identified and incorporated in to the TSPA.	See the PMR for the engineered barrier system.
3.3 - Conceptual model uncertainties have been defined and documented, and their effects on conclusions regarding TSP have been assessed.	Section 3.12 summarizes the evaluation of flux into drifts during and after the thermal period.
3.4 - Mathematical models are consistent with conceptual models, based on consideration of site characteristics.	Modeling approaches for thermal effects are summarized in Sections 3.10 and 3.12.

NRC Technical Acceptance Criteria	PMR Approach and Section Reference
Subissue 3: Does the DOE's TSPA adequately account for thermal effects on flow?, continued	
3.5 - Alternative models and modeling approaches, consistent with available data and current scientific understanding, are investigated; limitations defined; and results appropriately considered.	Alternative modeling approaches are discussed in Section 3.10.7.
3.6 - Results from different mathematical models have been compared to judge robustness of results.	Sensitivity analyses will be included in TSPA-SR.
4 - Coupling of thermal processes has been evaluated using a methodology in accordance with NUREG-1466 (Nataraja and Brandshaug, 1992) or other acceptable methodology. Coupled processes may be uncoupled, if it is shown that the uncoupled model results bound the predictions of the fully-coupled model results.	NUREG-1466 provides logical steps for the development of predictive models and their numerical representation of thermally induced THMC behavior of the host rock. Sections 3.10 and 3.12 summarize the approach to evaluating coupled processes at the drift-scale and mountain-scale. The DOE agrees that coupled processes may be uncoupled if the models bound the effects of fully coupled processes.
5 - The dimensionality of models used to assess the importance of refluxing water on repository performance may be reduced if it is shown that the reduced dimension model bounds the predictions of the full dimension model in performance.	The DOE agrees with this approach. Section 3.4.2.4 summarizes studies of grid refinement; Section 3.12.2.2 summarizes numerical grids for TH simulations.
6 - Results of the TSPA related to TEF have been verified by demonstrating consistency with results of process-level models.	TSPA analyses related to TEF were based on the process level models.
7 - Sensitivity and importance analyses were conducted to assess the need for additional data or information with respect to TEF.	Sensitivity analyses will be included in TSPA-SR.
IRSR: Total System Performance Assessment and Integration	
Subissue 1 - System description and demonstration of multiple barriers	
Total system performance assessment documentation style, structure, and organization	
DoE's approach to document structure and organization will be acceptable if:	
1 - Documents and reports are complete, clear, and consistent.	The UZ PMR was carefully structured to be complete, clear, and consistent. The review of the draft document included checks for completeness, clarity and consistency.
2 - Information is amply cross-referenced	The UZ PMR contains ample references to data sources, codes, assumptions, and conclusions.
Features, Events, and Processes Identification and Screening	
1 - The screening process by which FEPs were included or excluded from the TSPA is fully described.	Section 1.2.3 summarizes excluded and included FEPs along with the rationale for these decisions.
2. Relationships between relevant FEPs are fully documented.	Section 1.2.3 describes the relationship between primary and secondary FEPs based on the overlap that exists among the FEPs for UZ flow and transport.

NRC Technical Acceptance Criteria	PMR Approach and Section Reference
Abstraction Methodology	
1- The levels and method(s) of abstraction are described starting from assumptions defining the scope of the assessment down to assumptions concerning specific processes and the validity of given data.	For each model in the UZ PMR, the relevant chapter summarizes the data used to construction the process model, the process model, and the abstraction of that model, if the model is abstracted for TSPA.
2 - A mapping (e.g., a road map diagram, a traceability matrix, a cross-reference matrix) is provided to show what conceptual features (e.g., patterns of volcanic events) and processes are represented in the abstracted models, and by what algorithms.	The UZ PMR provides a sufficient basis for the decisions and assumptions that were made during the abstraction process.
3 - An explicit discussion of uncertainty is provided to identify which issues and factors are of most concern or are key sources of disagreement among experts.	The UZ PRM provides a discussion of uncertainties and limitations for the major process models included in the report.
Data Use and Validity	
1 - The pedigree of data from laboratory tests, natural analogs, and the site is clearly identified.	Section 1.3 summarizes the quality assurance status of the data and software used in the component models.
2 - Input parameter development and basis for their selection is described.	The UZ PMR discusses input parameter development and the basis for using the parameters. For example, Section 3.6 summarizes the development of UZ properties, model calibration, and the results.
3 - A thorough description of the methods used to identify performance confirmation program parameters.	The DOE is developing a plan that will define the performance confirmation program. Performance confirmation testing is not covered in this PMR.
Assessment results	
1 - PA results (i.e., the peak expected annual dose within the compliance period) can be traced back to applicable analyses that identify the FEPs, assumptions, input parameters, and models in the PA.	The TSPA-SR will summarize UZ flow and transport features, processes and the conceptual model, and their implementation into the TSPA. This discussion will be based on the UZ PMR.
2 - The PA results include a presentation of intermediate results that provide insight into the assessment (e.g., results of intermediate calculations of the behavior of individual barriers).	Intermediate results for PA are not discussed in the UZ PMR. The TSPA-SR is planned to include sensitivity analysis, including uncertainty importance analyses, one-off analyses, and robustness analyses.
Code design and data flow	
1 - The flow of information (input and output) between the various modules is clearly described.	The flow of information (input and output) is documented in accordance with QA procedures to ensure traceability.
2 - Supporting documentation (e.g., user's manuals, design documents) clearly describes code structure and relations between modules.	The codes used in the UZ PMR were documented in accordance with software QA procedures that include requirements for appropriate documentation.
Demonstration of multiple barriers (acceptance criteria have not been included in this revision of the IRSR).	

NRC Technical Acceptance Criteria	PMR Approach and Section Reference
Subissue 2 – Scenario Analysis	
Identification of an initial set of processes and events	
1 - DOE has identified a comprehensive list of processes and events that: (i) are present or might occur in the Yucca Mountain region and (ii) includes those processes and events that have the potential to influence repository performance.	Section 1.2.3 discusses the relevant FEPs for unsaturated zone flow and transport. Included FEPs are directly represented in the process models and abstractions that support TSPA, and discussed in sections of the PMR corresponding to the specific models.
Classification of Processes and events	
1 - DOE has provided adequate documentation identifying how its initial list of processes and events has been grouped into categories.	Section 1.2.3 discusses the identification and categories of relevant FEPs for unsaturated zone flow and transport.
2 - Categorization of processes and events is compatible with the use of categories during the screening of processes and events.	Section 1.2.3 discusses categories of relevant FEPs for unsaturated zone flow and transport and their use.
Subissue 2 – Scenario Analysis, continued	
Screening of processes and events	
1 - Categories of processes and events that are not credible for the Yucca Mountain repository because of waste characteristics, repository design, or site characteristics are identified and sufficient justification is provided for DOE's conclusions.	Sections 1.2.3 discusses excluded FEPs and the rationale for exclusion. The exclusion of FEPs from TSPA is based on arguments of low probability or low consequence.
2 - The probability assigned to each category of processes and events not screened based on criterion T1 or criterion T2 is consistent with site information, well documented, and appropriately considers uncertainty.	Section 1.2.3 provides the rationale for excluding FEPs.
3 - DOE has demonstrated that processes and events screened from the PA on the basis of their probability of occurrence, have a probability of less than one chance in 10,000 years of occurring over 10,000 years.	Section 1.2.3 provides the rationale for excluding FEPs.
4 - DOE has demonstrated that categories of processes and events omitted from the PA on the basis that their omission would not significantly change the calculated expected annual dose, do not significantly change the calculated annual dose.	Section 1.2.3 summarizes information on FEPs that are directly and the rationale for their exclusion.
Formation of scenarios (covered in TSPA-SR)	
Screening of scenario classes (covered in TSPA-SR)	
Subissue 3 - Model abstraction	
Engineered barrier system	
Engineered barrier degradation (to be covered in the Waste Package Degradation PMR)	
Mechanical disruption of engineered barriers (to be covered in the Disruptive Events PMR)	
Quantity and quality of water contacting waste packages and waste forms	

NRC Technical Acceptance Criteria	PMR Approach and Section Reference
1 - Sufficient data (field, laboratory, and/or natural analog data) are available to adequately define relevant parameters and conceptual models necessary for developing the quantity and chemistry of water contacting WPs and waste forms abstraction in TSPA. Where adequate data do not exist, other information sources such as expert elicitation have been appropriately incorporated into the TSPA.	Section 3.9 summarizes the available data and conceptual models for seepage into drifts.
2 - Parameter values, assumed ranges, probability distributions, and bounding assumptions used in the quantity and chemistry of water contacting WPs and waste forms abstraction, such as pH, chloride concentration, and amount of water flowing in and out of the breached WP, are technically defensible and reasonably account for uncertainties and variability.	See the PMRs on waste package degradation and waste form.
3 - Alternative modeling approaches consistent with available data and current scientific understanding are investigated and results and limitations appropriately factored into the quantity and chemistry of water contacting WPs and waste forms abstraction.	See the PMRs on waste package degradation and waste form.
4 - Output of quantity and chemistry of water contacting WPs and waste forms abstraction are verified through comparison to output of detailed process models and/or empirical observations (laboratory testing or natural analogs, or both).	See the PMRs on waste package degradation and waste form.
5 - Important design features, physical phenomena and couplings, and consistent and appropriate assumptions are incorporated into the mechanical disruption of WPs abstraction.	See the PMR for waste package degradation.
Radionuclide release rates and solubility limits (to be covered in Waste Form PMR)	
Geosphere	
Unsaturated zone flow and transport	
Spatial and temporal distribution of flow	
1 - Sufficient data (field, laboratory, and/or natural analog data) are available to adequately define relevant parameters and conceptual models necessary for developing the spatial and temporal distribution of flow abstraction in TSPA. Where adequate data do not exist, other information sources such as expert elicitation have been appropriately incorporated into the TSPA.	Attachment I summarizes available data used to define relevant parameters and conceptual models. Section 3.7.5 summarizes the abstraction of flow fields for TSPA-SR. The UZ flow model forms the basis for the model that is abstracted for TSPA-SR.

NRC Technical Acceptance Criteria	PMR Approach and Section Reference
2 - Parameter values, assumed ranges, probability distributions, and/or bounding assumptions used in the spatial and temporal distribution of flow abstraction, such as the effects of climate change on infiltration, near surface influences (e.g., evapotranspiration and runoff) on infiltration, structural controls on the spatial distribution of deep percolation, and thermal reflux owing to repository heat load, are technically defensible and reasonably account for uncertainties and variabilities.	Sections 3.7.2 through 3.7.4 summarize UZ flow models and Section 3.7.5 summarizes the results of abstractions of UZ flow. The abstraction considers three infiltration cases (low, mean, and high) within each of the three climate states (present-day, monsoon, and glacial transition). For the abstraction of TH processes, only the mean infiltration cases were selected since the results of the low and high infiltration cases showed similar behavior in general.
3 - Alternative modeling approaches consistent with available data and current scientific understanding are investigated and results and limitations appropriately factored into the spatial and temporal distribution of flow abstraction.	Section 3.7.4 summarizes alternative conceptual models.
4 - Spatial and temporal distribution of flow abstraction output is justified through comparison to output of detailed process models, and/or empirical observations (laboratory testing or natural analogs, or both).	The abstraction of flow was based on detailed process models (Section 3.7.5).
5 - Important design features, physical phenomena and couplings, and consistent and appropriate assumptions are incorporated into the spatial and temporal distribution of flow abstraction.	The abstraction of UZ flow is summarized in Section 3.7.5.
Flow paths in the unsaturated zone	
1 - Sufficient data (field, laboratory and/or natural analog data) are available to adequately define relevant parameters and conceptual models necessary for developing the distribution of mass flux between fracture and matrix in the abstraction in TSPA. Where adequate data cannot be readily obtained, other information such as expert elicitation or bounding values have been appropriately incorporated in the TSPA.	Attachment I describes available data used to define relevant parameters and conceptual models. The abstraction in Section 3.7.5. was based on available data and conceptual models.
2 - Parameter values, assumed ranges, probability distributions, and bounding assumptions used in the flow paths in the UZ in the abstraction, such as hydrologic properties, stratigraphy, and infiltration rate, are technically defensible and reasonably account for uncertainties and variability.	Abstraction results are summarized in Section 3.7.5. The abstraction considers three infiltration cases (low, mean, and high) within each of the three climate states (present-day, monsoon, and glacial transition), based on the process-model results.
3 - Alternative modeling approaches consistent with available data and current scientific understanding are investigated and results and limitations appropriately factored into the distribution of mass flux between fracture and matrix in the abstraction.	Abstraction results are summarized in Section 3.7.5.

NRC Technical Acceptance Criteria	PMR Approach and Section Reference
4 - Flow paths in the UZ abstraction output is verified through comparison to output of detailed flow process models, or empirical observations (laboratory testing or natural analogs, or both).	The abstraction was based on detailed process models (Sections 3.7.2 through 3.7.4).
5 - Important design features, physical phenomena and couplings, and consistent and appropriate assumptions are incorporated into the flow paths in the UZ abstraction.	The results of the abstraction are summarized in Section 3.7.5.
Radionuclide transport in the unsaturated zone	
1 - Sufficient data (field, laboratory and/or natural analog data) are available to adequately define relevant parameters and conceptual models necessary for developing the RT in the UZ abstraction in TSPA. Where adequate data do not exist, other information sources such as expert elicitation have been appropriately incorporated in the TSPA. Alternatively, The parameters or models lacking sufficient data have been replaced by bounding parameter values.	Section 3.11.3 summarizes the transport properties that are used for the abstraction of radionuclide transport in the UZ. The AMR on UZ and SZ transport properties provides additional detail on transport properties for the UZ.
2 - Parameter values, assumed ranges, probability distributions, and bounding assumptions used in the RT in the UZ in the abstraction, such as sorption on fracture surfaces, and K_d for the matrix, are technically defensible and reasonably account for uncertainties and variability.	Section 3.11.3 summarizes parameter values, ranges, distributions, and bounding assumptions for the abstraction of radionuclide transport, as applicable.
3 - Alternative modeling approaches consistent with available data and current scientific understanding are investigated and results and limitations appropriately factored into the RT in the UZ abstraction.	Section 3.11.9 summarizes an alternative conceptual model for transport in the UZ.
4 - RT in the UZ abstraction output is justified through comparison to output of detailed process models, or empirical observations (laboratory testing or natural analogs, or both).	The abstraction of radionuclide transport is based on process models and compared to alternate solutions methods.
5 - Important physical phenomena and couplings and consistent and appropriate assumptions are incorporated into the consideration of radionuclide transport in the UZ abstraction.	Section 3.11.13 discusses the abstraction of radionuclide transport, including physical phenomena, couplings, and assumptions.
Saturated zone flow and transport (to be covered in Saturated Zone Flow and Transport PMR)	
Radionuclide transport in the saturated zone (to be covered in Saturated Zone Flow and Transport PMR)	
Direct release and transport (to be covered in Disruptive Events PMR)	
Biosphere (to be covered in the Biosphere PMR)	

NRC Technical Acceptance Criteria	PMR Approach and Section Reference
Subissue 4 – Demonstration of the overall performance objective (acceptance criteria not included in the IRSR)	
IRSR: Unsaturated and Saturated Zone Flow Under Isothermal Conditions	
Subissue 1 - Climate change	
1 - Climate projections used in performance assessments of the YM region are based on paleoclimate data, considering, at a minimum, information contained in Forester et al. (1996); Winograd et. al. (1992); Szabo et al. (1994)	Climate projections are based on paleoclimate data (Section 3.5.1). The Yucca Mountain Site Description provides contains a detailed discussion of the paleoclimate data, including references to Forester, et al. (1996) and Szabo, et al. (1994) in Section 4 (Climatology and Meteorology). Winograd et al. (1992) is referenced in Section 5 (Hydrologic System).
2 - DOE has evaluated long-term climate change based on known patterns of climatic cycles during the Quaternary, especially the last 500 k.y.	Long term climate change is based on an analogous climate cycle that occurred approximately 400,000 years ago (Section 3.5.1).
3 - If used, numerical climate models are calibrated with paleoclimate data and their use suitably simulates the historical record, before being used for projection of future climate.	Numerical models of climate are not used in this PMR.
4 - Climate-affected parameters (e.g., onset times for climate change, MAP, and MAT) used in YM performance assessment models include, as bounding condition, a return to full pluvial climate (higher precipitation and lower temperatures) for at least a part of the first 10-k.y. period, using parameter values that are supported by scientific data and analyses.	The future climate at Yucca Mountain is treated as a sequence of three climate states, including a glacial transition at 1400 years (Section 3.5.1). Analog climate sites are used define the three climate states, including low, mean, and upper bound annual precipitation and temperature.
Subissue 2 - Hydrologic effects of climate change	
1 - If bounding analyses are used to predict climate-induced effects (water table rise, for example), the analysis are based on a reasonably complete search of paleoclimate data pertinent to water-table rise and other effects (for example, changes in precipitation and geochemistry), including, at a minimum, information contained in Paces et al. (1996), Szabo et al. (1994), Forester et al. (1996).	A comprehensive literature search of the paleoclimate data has been completed and documented in the Yucca Mountain Site Description. This description references Paces et al. (1996) in Section 5 (Hydrologic System). Szabo et al. (1994) and Forester et al. (1996) are referenced in Section 4 (Climatology and Meteorology).
2 - Regional and sub-regional models for the SZ that are used to predict climate-induced consequences are calibrated with the paleohydrology data, and are consistent with evidence that the water-table rise during the late Pleistocene was up to 120 m.	This acceptance criterion is addressed in the Saturated Zone PMR.

NRC Technical Acceptance Criteria	PMR Approach and Section Reference
3 - DOE has incorporated future climate changes and associated effects in its performance assessments. For example, available information does not support an assumption that present-day climate will persist unchanged for 10 k.y. or more.	Future climate changes and associated effects have been incorporated into TSPA (Section 3.5). Three climate states are expected to occur over the next 10,000 years: the current modern climate, a monsoon climate, and a glacial transition climate.
Subissue 3 - Present day shallow infiltration	
1 - DOE has estimated present-day shallow infiltration at YM for use in TSPA using mathematical models that are reasonably verified with site-specific climatic, surface, and subsurface information, and the fundamental effects of heterogeneities, time-varying boundary conditions, evapotranspiration, depth of soil cover, and surface-water runoff have been considered in ways that do not underestimate infiltration.	Section 3.5.2 summarizes models of present day infiltration and the site-specific parameters that are incorporated into the model. Important processes considered include precipitation, runoff and run-on, evapotranspiration, transpiration, and moisture redistribution in the shallow subsurface.
2- DOE has analyzed infiltration at appropriate time and space scales for performance assessment, and has tested the abstracted model against more detailed models to assure that it produces reasonable results.	The infiltration model in Section 3.5.2 evaluates time and space scales for infiltration.
3 - DOE has characterized shallow infiltration in the form of either probability distributions or deterministic upper-bound values for performance assessment, and provided sufficient data and analyses to justify the chosen probability distribution or bounding value.	The methodology for assigning probabilities to the mean annual infiltration multipliers has been enhanced to address the NRC concern that the method used to assign probabilities to the mean annual infiltration multipliers is biased toward lower values of mean annual infiltration (Section 3.5.1).
4 - If DOE can show through TSPA and associated sensitivity analyses that refinements of shallow infiltration estimates will not significantly alter performance predictions, no further refinement will be necessary.	Sensitivity studies will be included in TSPA-SR.
Subissue 4 - Deep percolation	
1 - Estimates of deep percolation flux rates and the fraction of flux that occurs in fractures will be acceptable provided that they are: (i) shown to constitute a conservative upper bound, or (ii) based on a technically defensible UZ flow model that reasonable represents the physical system, including flow in fracture systems and matrix-fracture interaction. The flow model has been calibrated using site-specific hydrologic, geologic, and geochemical data.	The UZ flow model has been calibrated with available site data (Section 3.6). The representation of flow in the UZ is summarized in Section 3.7, including a discussion of fracture-matrix interaction.
2 - To estimate deep-percolation flux, spatial and temporal variability of model parameters and boundary conditions must be considered. Model parameters must be averaged over appropriate time and space scales. DOE must also consider climate-induced change in soil depth and vegetation.	Section 3.7 summarizes the UZ flow model, including the treatment of spatial and temporal variability of model parameters and boundary conditions. The infiltration model has been enhanced to include an improved surface-water model.

NRC Technical Acceptance Criteria	PMR Approach and Section Reference
Subissue 4 - Deep percolation, continued	
<p>3 - For estimates of the amount of water that may contact waste packages DOE must (i) demonstrate that coupled thermal-mechanical-chemical changes in rock mass properties will not focus deep percolation into the drifts; and (ii) rigorously justify estimated diversion of deep percolation away from the waste package footprints. This must include direct observations of dripping in test drifts or tunnels under ambient (unventilated) conditions in the repository horizon, or in an analog horizon with similar characteristics. Also needed are model calculations that account for the effects of backfill (if used), drift collapse, and coupled thermal-mechanical-chemical changes to rock properties. The models have been calibrated to niche studies and tracer tests in the ESF, or using an analog with characteristics similar to the repository horizon.</p>	<p>Seepage models (Sections 3.9 and 3.10) evaluate partial drift collapse and coupled THM changes. These models have been calibrated to available data from the ESF and the cross drift. Direct observation of an unventilated segment of the ECRB is ongoing and dripping has not been observed.</p>
<p>4 - In predicting likely flow and transport pathways beneath the proposed repository horizon, DOE must either (i) conservatively assume that all deep percolation below the repository level bypasses the bulk of the non-welded units, either by lateral movement above the units or through vertical flow through fractures and faults; or (ii) demonstrate that the estimated fraction of deep percolation that flows vertically through the matrix of the non-welded units is supported by (a) characterization data and (b) two-dimensional or three-dimensional modeling that accounts for spatial and temporal variability that may result in lateral diversion of flow, and uses model parameter values appropriate for the scale of model discretization.</p>	<p>Section 3.7 summarizes the approach to modeling flow through each of the major units below the repository horizon. Modeling results show that fracture flow is dominant both at the potential repository horizon and at the water table. The model uses input from perched water and matrix properties, calibrated properties model, the geologic and numerical grid model, the climate/infiltration model, and the geochemistry model.</p>
Subissue 5 - Saturated zone ambient flow (covered in Saturated Zone PMR)	
Subissue 6 - Matrix diffusion	
<p>1 - If credit for matrix diffusion in the UZ is taken, then transport predictions must be consistent with site geochemical and isotopic data.</p>	<p>The matrix diffusion model has been enhanced to account for the effects of finite fracture spacing (Section 3.11.3).</p>
<p>2 - If credit for matrix diffusion in the SZ is take, rock matrix and solute diffusion parameters must be (i) based on a SZ transport model that reasonably matches the results of the field tracer tests that are conducted over different distance scales and flow rates with multiple tracers of different diffusive properties, and (ii) consistent with laboratory data.</p>	<p>This acceptance criterion is addressed in the Saturated Zone PMR.</p>

INTENTIONALLY LEFT BLANK

5. SUMMARY AND CONCLUSIONS

The Unsaturated Zone Flow and Transport Process Model Report (UZ PMR) documents the approach, development, and basis for the models and analyses that are used to understand and predict flow and transport processes in the unsaturated zone at Yucca Mountain. The models and analyses are supported by data collection, experiments, field tests, and calibration efforts that have been performed by project scientists for many years. The extensive studies provide confidence in the models and tools that will be used in Total System Performance Assessments for Site Recommendation and License Application. The following two sections provide a general summary of the contents of this PMR (Section 5.1), as well as a more detailed summary of the models and abstractions that will be used in TSPA-SR calculations (Section 5.2).

5.1 SUMMARY OF THE UZ FLOW AND TRANSPORT PMR

This section provides a concise summary and review of the contents of this PMR. More detailed summaries and conclusions can be found at the end of each chapter, as well as at the end of major subsections describing the process models.

Chapter 1 provides an introduction to the scope and objectives of this PMR. Identification of key issues and FEPs (features, events, and processes) are presented to provide the motivation and requirements for this document. A summary of the quality assurance (QA) requirements for the data, software, models, and analyses in this PMR are also presented, and relationships to other relevant PMRs are discussed.

Chapter 2 presents historical background on the evolution of site characterization and data collection at Yucca Mountain that support this PMR. This includes early surface-based testing and more recent underground testing and monitoring activities in the Exploratory Studies Facility (ESF). These characterization studies provide the basis for the geological, hydrological, geochemical, and thermal models presented in this PMR. Natural analogs to the processes and events at Yucca Mountain are also presented in Chapter 2, and an overview of the evolution of the conceptual and mathematical UZ Flow and Transport Model is given.

Chapter 3 includes a description of the relevant process models and their underlying basis. Applicable abstractions for TSPA-SR are also presented. Section 3.2 begins with geological considerations for flow and transport. Geological issues important to repository performance (e.g., fracture characterization, mineralogy, and location of major faults) are listed and discussed. The hydrogeologic units at Yucca Mountain are identified, and their major features and impact to hydrology are presented. Mineralogy and locations of altered rock that may be important for UZ transport are also presented.

Section 3.3 provides a summary of the physical processes and conceptual models relevant to UZ flow and transport. The components and processes that are described include climate, infiltration, flow through fractures and matrix in various hydrogeologic units, fracture-matrix interaction, effects of major faults, transient flow, focusing of flow, perched water, seepage into drifts, gas flow processes, radionuclide transport processes, and the effects of coupled processes. These process and component conceptualizations comprise the UZ Flow and Transport Model

described in this PMR. Alternative conceptual models that are not used in this PMR are also presented.

Section 3.4 documents the development of the numerical approaches and grids that are used in the development of the UZ Flow and Transport Model. Numerical modeling approaches that are discussed include continuum vs. discrete fracture-network modeling for flow through fractured rock, and a description of the current numerical approach is presented. Other numerical approaches that are discussed include the active fracture model, particle tracking, and methods for modeling dispersion and heterogeneities. The development of the numerical grids is then presented, starting with the required inputs and data for grid generation. The outputs are described, which include one-, two-, and three-dimensional grids for various aspects of the development of the UZ Flow and Transport Model. Grid-refinement studies were also performed that showed the refinement of the current grid used in the UZ Flow and Transport Model was adequate.

Section 3.5 summarizes the development of the Climate and Infiltration Models, which provide the upper boundary condition (net infiltration) for the UZ Flow and Transport Model. The results and abstraction of the Climate Model reveal that a modern-like climate will persist for approximately 600 years, followed by a warmer and wetter monsoon climate for another ~1,400 years. A cooler and wetter glacial-transition climate follows the monsoon climate for the remaining duration of the 10,000-year period analyzed in TSPA-SR. For each of these climates, three infiltration scenarios ranging from low to high are generated using different values for precipitation and temperature, as well as surface infiltration parameters such as soil depth, and evapotranspiration. The three infiltration cases are denoted as low, mean, and high (or upper); Section 3.5 provides a summary of how weightings are assigned to each case for TSPA-SR calculations.

Section 3.6 documents the available hydrologic parameter data and the development of the calibrated hydrologic property sets for the UZ Flow and Transport Model. The data that were evaluated and used for property calibrations include information on measured matrix, fracture, and fault parameters. The calibration process is then presented to obtain calibrated parameter sets for mountain-scale and drift-scale applications. One- and two-dimensional numerical inversions were performed to estimate parameters that optimize the match between predicted results and measured data. Results and uncertainties of the calibration process are presented, and comparisons to additional data and alternative models are discussed.

Section 3.7 provides a description of the site-scale UZ Flow Model, which simulates three-dimensional flow fields that are used in transport calculations. This section begins with a summary of the inputs that are subsequently used in the Flow Model, which include the infiltration boundary conditions, the numerical grids, calibrated properties, and conceptual models of flow and fracture-matrix interaction. A description of the Flow Model and its submodels is provided, which include flow through the PTn, effects of major faults, flow through the Calico Hills, and the effects of perched water. Results of the site-scale Flow Model are then presented, which describe the flow fields for the nine infiltration scenarios (three infiltration cases for each of the three climates) and different perched water models. Flow predominantly occurs in the fractures in the welded units and in the matrix in the nonwelded units. Significant lateral diversion exists, especially in the northern portion of the potential repository, where

perched water is simulated over zeolitized units. Abstractions include assessment of perched water models and water-table rise.

Section 3.8 presents an analysis of the Ambient Geochemistry Model and its use in testing various components of the site-scale UZ Flow Model. The features and processes that can be analyzed using the Ambient Geochemistry Model include infiltration rate, percolation flux, partitioning between matrix and fracture flow, flow pathways, and travel times in the UZ. This section summarizes the geochemical data that are available for the analyses, and it describes the development of the model, which uses the calibrated properties (see Section 3.6) and available geochemical data as input. Results indicate that chloride concentrations in the ESF and ECRB can be qualitatively predicted by the model using the mean present-day infiltration rates. Modeling studies that investigated the relationship of calcite deposition to infiltration rate, water and gas compositions, and reactive surface area also revealed that the range of net infiltration rates used in the model could capture the calcite abundance in the TSw.

Section 3.9 documents the development of the drift seepage models that are used to estimate the fraction of waste packages contacted by water and the amount of water that enters the drift as a function of several hydrologic parameters and boundary conditions. The relevant processes that impact drift seepage are detailed along with the inputs required for the model. Then, a sequence of seepage models is presented, beginning with the Seepage Calibration Model that provides seepage-related calibrated parameters. The Seepage Model for Performance Assessment is used to perform a wide range of seepage simulations using a combination of input parameters. Finally, seepage abstraction creates distributions for four seepage parameters that are sampled in TSPA-SR. Results indicate that seepage fluxes are likely to be significantly lower than percolation fluxes even under conservative assumptions, and that only a fraction of the waste packages will encounter seepage.

Section 3.10 describes the thermal-hydrological-chemical drift-scale model, which is used to simulate the composition of the water and gas in the vicinity of the heated repository as well as any mineralogical alterations that result from precipitation and dissolution processes. A description of the conceptual model for coupled processes is provided, along with a complete description of the numerical approach, which is consistent with the approach taken by the Flow Model. The results of the drift-scale THC Model reveal that the water seeping into the drifts is likely to be neutral, and the concentration of chloride in the water will not be more than four times the concentration in ambient pore water. The fracture porosity decreases by less than 1% (e.g., from 0.01 to 0.0099) in the vicinity of the drifts, which suggests that the impacts of THC effects on fracture and matrix properties (and subsequently on UZ flow) are negligible. In the abstraction for TSPA-SR calculations, the transient water and gas compositions are averaged over four discrete time periods from 0 to 100,000 years. These results are used to determine the in-drift environment and the corrosion of the drip shields and waste packages over time.

Section 3.11 presents the UZ Transport Model that is used to investigate radionuclide transport between the potential repository and the water table. This section presents two distinct transport models. The first is a process-oriented model used to investigate the importance of several features and processes that include advection, matrix diffusion, sorption, flow through faults, radioactive decay, colloidal transport, and perched water. Results of the process modeling indicate that (1) fast transport is controlled by faults at early times; (2) matrix diffusion and

sorption can be effective retardation mechanisms; (3) the vitric Calico Hills layers can provide effective retardation via flow through the matrix; (4) decay products may be important for radionuclide transport; and (5) colloidal transport is very sensitive to filtration. The second model is the particle-tracking method that is used in TSPA-SR to simulate radionuclide transport, which also includes the same processes considered in the first model. The benefit of the particle-tracking method is its computationally efficiency, which is essential for TSPA calculations.

Section 3.12 presents the mountain-scale Thermal-Hydrological (TH) Model, which is used to assess the importance of TH effects on far-field flow and transport. A description of the mountain-scale TH Model is presented, which consists of the conceptual model, input parameters, design configuration for heat load, and boundary conditions. The numerical approach for flow is consistent with that used in the Flow Model. Results are provided regarding the hydrologic and thermal behavior throughout the simulated two- and three-dimensional domains. The refined 2-D model predicts that vertical liquid flow crossing the interval between the drifts continues at a rate close to the ambient percolation flow for most of the thermal-loading period, although at some locations enhanced flow may occur as a result of condensate drainage for early times (less than a few hundred years). Based on these results, the effects of TH on far-field flow and transport are assumed negligible for TSPA-SR calculations, which simulate performance over a 10,000-year period.

Section 3.13 summarizes the uncertainties associated with the UZ flow and transport models and components. A brief description of the uncertainties in the model inputs and outputs is presented, along with the uncertainties that are carried forward to TSPA-SR. A description of how uncertainties are treated in TSPA calculations is also summarized.

Finally, Chapter 4 presents a detailed summary of the Key Technical Issues (KTIs) issued by the Nuclear Regulatory Commission that are relevant to this PMR. The six KTIs relevant to UZ flow and transport are the following: (1) Evolution of the Near-Field Environment; (2) Radionuclide Transport; (3) Structural Deformation and Seismicity; (4) Thermal Effects on Flow; (5) Total System Performance Assessment and Integration; and (6) Unsaturated Zone and Saturated Zone Flow Under Isothermal Conditions. Chapter 4 provides pointers to sections in this PMR that address each of these KTIs.

5.2 SUMMARY OF MODELS AND ABSTRACTIONS FOR TSPA-SR

This section summarizes the major components that comprise the UZ Flow and Transport Model for TSPA-SR. An overview of the process models is presented that highlights the primary inputs, outputs, and basis for each model. The subset of products that are actually used in TSPA-SR are also discussed along with a summary of the abstraction methodology. The reader is referred to the model sections (Section 3.5–3.12) for a more thorough discussion of the major conclusions from each process model component.

The integrated UZ Flow and Transport Model for TSPA-SR is comprised of four major components: (1) UZ flow, (2) drift seepage, (3) drift-scale coupled thermal-hydrologic-chemical (THC) processes, and (4) UZ transport. Figure 5.2-1 shows the icons that represent these components along with a conceptual sketch of the UZ at Yucca Mountain. Additional sub-

components (e.g., infiltration, thermal-hydrology) are described within the four major components.

5.2.1 UZ Flow

The UZ Flow Model is a three-dimensional, site-scale numerical model that simulates groundwater flow from the surface of the mountain to the water table using a dual-permeability formulation to capture flow through fracture and matrix materials (see Section 3.7). The model is generated based on information from the Geologic Framework Model, Rock Properties Model, and Mineralogical Model. It is calibrated and tested against relevant data that include perched-water data, matrix saturation, moisture potential, pneumatic data, air-permeability data, temperature data, and ambient geochemistry data. The 3-D Flow Model is also validated through percolation tests performed in Alcove 1 and comparisons to data from the ECRB, SD-6 and WT-24.

Additional submodels that provide input to the Flow Model include climate and Infiltration Models (see Section 3.5). The Climate Model provides upper and lower bounds for precipitation and temperature for modern and future climates. The temperature and precipitation records are obtained through selected meteorological stations that are chosen based on interpretation of climate analogs and orbital cycles. In the TSPA-SR base-case calculations, the timing of the climate states following post-closure are deterministically prescribed and assumed to be as follows: (1) a modern climate lasting for 600 years; (2) a monsoon climate from 600 years to 2,000 years; and (3) a glacial-transition climate for the remainder of the simulated 10,000-year period. Planned sensitivity studies using a different duration of the climate states are not expected to reveal a significant impact on performance.

The Infiltration Model uses the precipitation and temperature data from the Climate Model, along with other inputs such as hydraulic permeability and soil depth, to determine the amount of net infiltration that penetrates beneath the surface of the mountain. The Infiltration Model implements a mass balance among flow processes at the surface such as precipitation, evapotranspiration, run-on, run-off, and net infiltration. The resulting products are maps of spatially variable infiltration rates that serve as the upper boundary condition for the 3-D Flow Model. Three infiltration maps, representing low, mean, and high infiltration cases, are produced for each of the three climates to capture the uncertainty in the infiltration parameters. Therefore, a total of nine infiltration maps are used in the Flow Model.

The nine infiltration maps are used in the simulation of steady-state flow fields that are used in TSPA-SR calculations. Additional flow fields are generated for an alternative conceptual model of perched water. The alternative is a flow-through model (perched water model #1; Section 3.7) that allowed more water to percolate downward through the northern portion of the repository rather than being diverted above the basal vitrophyre. A comparison of the different perched water models revealed that the models produced similar results, although the flow-through model was slightly more conservative. As a result, only the flow-through perched water model was carried through to TSPA-SR, and the final product consisted of nine three-dimensional flow fields in the UZ (i.e., three infiltration cases for each of the three climate states).

The flow fields are used directly in TSPA-SR calculations of transport. As part of the post-processing of the flow fields, the water-table elevation is increased for the two future climate states, which are wetter than the modern climate. A conservative water-table elevation of 850 m is implemented by changing the liquid saturation of all elements (nodes) below 850 m to a value of one and adding a large sink to those nodes, effectively removing particles from the UZ. The cumulative mass of these particles leaving the UZ system are used as the source term for SZ modeling.

To weight the three infiltration cases (low, mean, and high) within each climate for TSPA-SR calculations, a Monte Carlo analysis was performed using distributions for the input parameters (e.g., hydraulic permeability, soil depth, precipitation). The results of the uncertainty analysis yielded statistical weightings of 0.17, 0.48, and 0.35 for the low, mean, and high infiltration cases, respectively (see Section 3.5.3). The weightings are used to select a flow field (corresponding to one of the three infiltration cases) within each realization of the TSPA-SR calculation. In other words, for each realization, there is a 17% chance that the low infiltration case will be selected, a 48% chance that the mean infiltration case will be selected, and a 35% chance that the high infiltration case will be selected. A given realization uses the same infiltration case for all climate states (e.g., if a realization uses a high infiltration case for the modern climate, then a high infiltration case is used for the monsoon and glacial-transition climates as well).

A final submodel that complements the ambient, steady-state flow simulations is the mountain-scale Thermal-Hydrological Model (see Section 3.12). This model consists of two- and three-dimensional submodels of the UZ Flow Model that include refinement around the repository to accommodate thermal loading. Temperatures and hydrologic conditions are simulated to determine the impact of repository heating on far-field flow. Currently, the impact of thermal effects on far-field transport remains to be rigorously tested, but based on results of the TH Model regarding increased flow through fractures due to condensate drainage, the changes to the far-field flow during the 10,000 period are not expected to be significant.

A schematic of major inputs to and outputs from the UZ Flow Model and its submodels is shown in Figure 5.2-2.

5.2.2 Drift Seepage

The drift-scale seepage models consist of a sequence of models that are used to estimate the amount of water that can enter the waste emplacement drifts under a variety of conditions (see Section 3.9). The first model in the sequence of seepage models is the Seepage Calibration Model (SCM). The SCM is a three-dimensional heterogeneous fracture-continuum numerical model that contains small-scale variability and correlation structure in the hydrologic properties. The input parameters include permeabilities from air-injection tests and other hydrologic parameters from the Calibrated Properties Model. The SCM is calibrated to seepage data obtained from liquid-release tests in the ESF to produce model-related, seepage-relevant flow parameters. The calibrated model is then used to predict the behavior of additional liquid-release tests to validate the model. Results of the SCM include a conceptual seepage process model and calibrated parameters that are relevant to the seepage processes.

The second model in the sequence of seepage models is the Seepage Model for Performance Assessment (SMPA). The SMPA is a three-dimensional, heterogeneous fracture-continuum numerical model that uses the conceptual model from the SCM as its basis. It implements a broader range of parameters from available data as well as drift-degradation scenarios. The SMPA considers variations in percolation flux, permeability, and capillarity (van Genuchten α). Results from the SMPA indicate that seepage decreases with increasing capillary strength and increasing permeability, which are conducive to greater capillary diversion around the drifts. The results also show that seepage increases with increasing permeability correlation length and drift degradation.

The wide range of seepage rates calculated from the SMPA are then used in a PA abstraction model that creates distributions for seepage fraction, mean seep flow rate, standard deviation of seep flow rate, and a flow-focusing factor. The flow-focusing factor is based on estimates of discrete "weep" spacings implied by the active fracture model and percolation fluxes calculated by the Flow Model. It is used to scale the percolation flux and the seepage fraction. Greater amounts of flow focusing yield increased seep flow rates (where seepage exists) but lower seepage fractions. Additional effects of drift degradation, rock bolts, and possible correlation between hydrologic parameters are accounted for in the abstracted model by increasing the seep flow rates. The PA seepage abstraction also has provisions for episodicity, but because the PTn overlies the entire potential repository, transient effects of precipitation and infiltration are effectively dampened at the potential repository horizon.

A schematic of major inputs to and outputs from the drift seepage models is shown in Figure 5.2-3.

5.2.3 Drift-Scale THC

The Drift-Scale THC Model is a two-dimensional dual-permeability "chimney" model that extends from the surface to the water table. It includes geologic layering consistent with the Flow Model. The model is more refined in and around the drift region, where it captures the features of the waste package, invert, and backfill (after 50 years; note that a design change was made in January 2000 that removed backfill from the reference design). It predicts transient water and gas chemistry, mineralogy, porosity, and permeability for 100,000 years (see Section 3.10). A 50-year ventilation period is simulated, as well as three infiltration scenarios corresponding to the three climate states. The model is validated through predictions and comparisons to the measured gas and water chemistry from the Drift Scale Test.

The results of the drift-scale THC process model reveal that the water seeping into the drifts is likely to be neutral (pH between 7 and 9), and the concentration of chloride in the water will not be more than a factor of four times the concentration in ambient pore water. The carbon dioxide concentrations increase with time in the drift, and the aqueous carbonate concentrations increase up to a few thousand mg/l. However, the fracture porosity decreases by less than 1% (e.g., from 0.01 to 0.0099) in the vicinity of the drifts, which suggests that the impacts of THC effects on fracture and matrix properties (and subsequently on UZ flow) are negligible.

In the abstraction for TSPA-SR calculations, the transient water and gas compositions are averaged over four discrete time periods from 0 to 100,000 years. Only the mean infiltration

cases are selected since the results of the low and high infiltration cases showed similar behavior in general. The results that are passed to the in-drift geochemical models in TSPA are aqueous concentrations for five cations and six anions, pH, and partial pressure of carbon dioxide during the four discrete periods. These results are used to determine the in-drift environment and the corrosion of the drip shields and waste packages over time.

A schematic of major inputs to and outputs from the drift-scale THC Model is shown in Figure 5.2-4.

5.2.4 UZ Transport

There are two distinct UZ transport modeling approaches: (1) a process model that tests and evaluates various transport processes and mechanisms, and (2) a TSPA particle-tracking model that incorporates the tested transport processes and mechanisms (see Section 3.11). The process model is used to gain confidence in understanding the impacts of various processes such as matrix diffusion, sorption, colloid filtration, and decay. It also serves as a basis for comparison to the TSPA model, which incorporates the same features and processes, but which uses an efficient particle-tracking algorithm that can be run in a few minutes for each TSPA realization.

The UZ transport process model includes advection, dispersion, sorption, matrix diffusion, radioactive decay and daughter products, and colloid transport. The model uses geologic and hydrologic parameters from the Flow Model and transport parameters from CRWMS M&O (2000, U0100) and CRWMS M&O (2000, U0070). The model consists of 2-D and 3-D numerical simulations that can efficiently simulate radionuclide transport. Results of the process modeling indicate that (1) fast transport is controlled by faults at early times; (2) matrix diffusion and sorption can be effective retardation mechanisms; (3) the vitric Calico Hills layers can provide effective retardation via flow through the matrix; (4) the ^{239}Pu daughter products are important to transport (at least for this subsystem analysis; full TSPA calculations must be performed to determine the overall importance to performance); and (5) colloidal transport is very sensitive to filtration.

The TSPA transport model uses the FEHM particle-tracking algorithm. It also considers advection, dispersion, matrix diffusion, sorption, and colloidal transport. It uses the flow fields generated from the Flow Model, so the dual-permeability nature of flow through fractures and matrix is preserved. The individual components and processes of the FEHM particle-tracking algorithm have been compared to other process models and analytical solutions, and the basis for the particle-tracking method is substantiated. A notable discrepancy has been identified in the conceptualization for matrix diffusion. The FEHM particle-tracking method uses a dual-porosity semi-analytical solution for retardation due to matrix diffusion (i.e., no flow occurs in the matrix in the matrix diffusion model). Studies evaluating the use of a dual-permeability matrix diffusion model have shown that significantly longer travel times can result when particles that diffuse into the matrix are allowed to subsequently transport through the matrix. Thus, the dual-porosity matrix diffusion model is considered to be a conservative choice.

As presented earlier, the thermal effects on flow are not expected to be significant, so thermal effects are neglected in the UZ transport simulations for TSPA-SR. The influence of increased temperatures on transport parameters such as distribution coefficients are also neglected.

Uncertainty in the radionuclide source-term location is implemented by using discretized zones in the repository region. The zones are currently based on ranges of infiltration (0–3, 3–10, 10–20, 20–60, and > 60 mm/yr). The release of radionuclides occurs at a random location within one of these five zones depending on the zone in which the release occurs in the engineered barrier system (EBS) models. Four zones are also defined at the water table, where radionuclide mass is collected for release at a random point in the SZ model.

A schematic of major inputs to and outputs from the UZ transport models is shown in Figure 5.2-5.

5.2.5 Treatment of Uncertainties

As discussed in Section 3.13, the models that comprise the UZ Flow and Transport Model for TSPA-SR contain inherent uncertainty and variability. The uncertainty and variability in the parameters are due, in part, to the natural variability and heterogeneity in the geological, hydrological, chemical, and mechanical systems that are difficult to characterize *in situ*, such as the precise fracture network in the UZ. Uncertainties in models may also be due to conditions that are difficult to predict, such as future climate states.

This PMR presented the bases (data collection, field tests, and calibration exercises) for using these parameters and process models. In addition, the models and analyses that are used in TSPA calculations address remaining uncertainties through probabilistic simulations or appropriate conservative assumptions.

The probabilistic simulations used in TSPA calculations consist of multiple realizations (statistically equivalent simulations) and stochastic sampling of parameters (i.e., a Monte Carlo approach). Each realization samples a set of parameters and/or models from given distributions for use in the TSPA calculation. The simulation of multiple realizations produces a range of performance results, with each outcome having a probability corresponding to its likelihood of occurrence. Thus, the uncertainty of the parameters and models leads to uncertainty in system performance. In the TSPA, the uncertainty in performance is analyzed, both in terms of its importance (i.e., is the uncertainty so great that it casts doubt on the safety of the potential repository?) and in terms of sensitivities (i.e., which parameter and submodel uncertainties have the greatest impact on the uncertainty in performance?). The probability distributions used in the TSPA uncertainty analyses reflect the degree of confidence in the input parameters and model assumptions. The resulting output distributions show whether input uncertainties have an acceptable or unacceptable impact on the calculated repository performance. The actual results of the TSPA calculations and uncertainty analyses will be included in the documentation for TSPA-SR.

In addition to probabilistic analyses, uncertainties in the process-model outputs can be addressed in abstracted TSPA models and analyses that use conservative assumptions. If insufficient evidence exists to provide a defensible range of values for a given parameter, values that bound the physical behavior or provide conservative estimates are used. These conservative assumptions are intended to increase the defensibility of the models used in TSPA calculations given the inherent uncertainties in the actual system.

In summary, as detailed in this report, the confidence in the models and parameters is built on rigorous experimental and numerical studies; remaining uncertainties are addressed in the TSPA models and analyses through probabilistic simulations or appropriate conservative assumptions.

6. REFERENCES AND INPUTS

6.1 CITED DOCUMENTS

- Abdel-Salam, A. and Chrysikopoulos, C.V. 1996. "Unsaturated Flow in a Quasi-Three-Dimensional Fractured Medium with Spatially Variable Aperture." *Water Resources Research*, 32, (6), 1531-1540. Washington, D.C.: American Geophysical Union. TIC: 239861.
- Ahlers, C.F.; Finsterle, S.; and Bodvarsson, G.S. 1999. "Characterization and Prediction of Subsurface Pneumatic Response at Yucca Mountain, Nevada." *Journal of Contaminant Hydrology*, 38, (1-3), 47-68. New York, New York: Elsevier. TIC: 244160.
- Airey, P.L. 1986. "Radionuclide Migration Around Uranium Ore Bodies in the Alligator Rivers Region of the Northern Territory of Australia: Analogue of Radioactive Waste Repositories - A Review." *Chemical Geology*, 55, (3/4), 255-268. Amsterdam, The Netherlands: Elsevier. TIC: 246691.
- Albin, A.L.; Singleton, W.L.; Moyer, T.C.; Lee, A.C.; Lung, R.C.; Eatman, G.L.W.; and Barr, D.L. 1997. *Geology of the Main Drift—Station 28+00 to 55+00, Exploratory Studies Facility, Yucca Mountain Project, Yucca Mountain, Nevada*. Denver, Colorado: Bureau of Reclamation and U.S. Geological Survey. ACC: MOL.19970625.0096.
- Anderson, R.E.; Hanks, T.C.; Reilly, T.E.; Weeks, E.P.; and Winograd, I.J. 1998. *Viability Assessment of a Repository at Yucca Mountain*. A Report to the Director, U.S. Geological Survey. Reston, Virginia: U.S. Geological Survey. ACC: HQO.19990205.0013.
- Aydan, O.; Ulusay, R.; Yuzer, E.; and Erdogan, M. 1999. "Man-made Rock Structures in Cappadocia, Turkey and Their Implications in Rock Mechanics and Rock Engineering." *International Society for Rock Mechanics News Journal*, 6, (1), 63-73. Orebro, Sweden: International Society for Rock Mechanics. TIC: 247253.
- Baker, A.; Genty, D.; Dreybrodt, W.; Barnes, W.L.; Mockler, N.J.; and Grapes, J. 1998. "Testing Theoretically Predicted Stalagmite Growth Rate with Recent Annually Laminated Samples: Implications for Past Stalagmite Deposition." *Geochimica et Cosmochimica Acta*, 62, (3), 393-404. Amsterdam, The Netherlands: Elsevier Science. TIC: 247408.
- Bandurraga, T.M. and Bodvarsson, G.S. 1999. "Calibrating Hydrogeologic Parameters for the 3-D Site-Scale Unsaturated Zone Model of Yucca Mountain, Nevada." *Journal of Contaminant Hydrology*, 38, (1-3), 25-46. New York, New York: Elsevier. TIC: 244160.
- Barnard, R.W.; Wilson, M.L.; Dockery, H.A.; Gauthier, J.H.; Kaplan, P.G.; Eaton, R.R.; Bingham, F.W.; and Robey, T.H. 1992. *TSPA 1991: An Initial Total-System Performance Assessment for Yucca Mountain*. SAND91-2795. Albuquerque, New Mexico: Sandia National Laboratories. ACC: NNA.19920630.0033.
- Barnett, D.B.; Bergeron, M.P.; Cole, C.R.; Freshley, M.D.; and Wurstner, S.K. 1997. *Tritium Monitoring in Groundwater and Evaluation of Model Predictions for the Hanford Site 200 Area*

- Effluent Treatment Facility*. PNNL-11665. Richland, Washington: Pacific Northwest National Laboratory. TIC: 246769.
- Barr, D.L.; Moyer, T.C.; Singleton, W.L.; Albin, A.L.; Lung, R.C.; Lee, A.C.; Beason, S.C.; and Eatman, G.L.W. 1996. *Geology of the North Ramp — Stations 4+00 to 28+00, Exploratory Studies Facility, Yucca Mountain Project, Yucca Mountain, Nevada*. Denver, Colorado: U.S. Geological Survey. ACC: MOL.19970106.0496.
- Bates, J.K.; Bradley, J.P.; Teetsov, A.; Bradley, C.R.; and Buchholtz ten Brink, M. 1992. "Colloid Formation During Waste Form Reaction: Implications for Nuclear Waste Disposal." *Science*, 256, 649-651. Washington, D.C.: American Association for the Advancement of Science. TIC: 239138.
- Bear, J. 1988. *Dynamics of Fluids in Porous Media*. New York, New York: Dover Publications. TIC: 217568.
- Bear, J.; Tsang, C.F.; and de Marsily, G., eds. 1993. *Flow and Contaminant Transport in Fractured Rock*. San Diego, California: Academic Press. TIC: 235461.
- Belyaev, B.N.; Gavrilov, V.N.; Domkin, V.D.; Ivanova, V.P.; Tishkov, V.P.; Tishkova, N.A.; and Tsvetkov, O.S. 1997. "Isotope Composition of Plutonium in Soil and Possibilities of Contamination Source Identification." *Atomnaya Energiya*, 83, (4), 298-304. New York, New York: Consultants Bureau. TIC: 246731.
- Bidaux, P. and Tsang, C.-F. 1991. "Fluid Flow Patterns Around a Well Bore or an Underground Drift with Complex Skin Effects." *Water Resources Research*, 27, (11), 2993-3008. Washington, D.C.: American Geophysical Union. TIC: 247407.
- Birkholzer, J. and Tsang, C.F. 1997. "Solute Channeling in Unsaturated Heterogeneous Porous Media." *Water Resources Research*, 33, (10), 2221-2238. Washington, D.C.: American Geophysical Union. TIC: 235675.
- Birkholzer, J.; Li, G.; Tsang, C.-F.; and Tsang, Y. 1999. "Modeling Studies and Analysis of Seepage into Drifts at Yucca Mountain." *Journal of Contaminant Hydrology*, 38, (1-3), 349-384. New York, New York: Elsevier. TIC: 244160.
- Bish, D.L. and Aronson, J.L. 1993. "Paleogeothermal and Paleohydrologic Conditions in Silicic Tuff from Yucca Mountain, Nevada." *Clays and Clay Minerals*, 41, (2), 148-161. Long Island City, New York: Pergamon Press. TIC: 224613.
- Bish, D.L. and Chipera, S.J. 1989. *Revised Mineralogic Summary of Yucca Mountain, Nevada*. LA-11497-MS. Los Alamos, New Mexico: Los Alamos National Laboratory. ACC: NNA.19891019.0029.
- Bodvarsson, G.S.; Benson, S.M.; Sigurdsson, O.; Stefansson, V.; and Eliasson, E.T. 1984. "The Krafla Geothermal Field, Iceland, 1. Analysis of Well Test Data." *Water Resources Research*, 20, (11), 1515-1530. Washington, D.C.: American Geophysical Union. TIC: 247406.

- Bodvarsson, G.S.; Boyle, W.; Patterson, R.; and Williams, D. 1999. "Overview of Scientific Investigations at Yucca Mountain—The Potential Repository for High-Level Nuclear Waste." *Journal of Contaminant Hydrology*, 38, (1-3), 3-24. New York, New York: Elsevier. TIC: 244160.
- Bodvarsson, G.S.; Pruess, K.; Stefansson, V.; Bjornsson, S.; and Ojiambo, S.B. 1987. "East Olkaria Geothermal Field, Kenya, 1. History Match With Production and Pressure Decline Data." *Journal of Geophysical Research*, 92, (B1), 521-539. Washington, D.C.: American Geophysical Union. TIC: 236629.
- Bradshaw, L.W. 1999. "Nye County Comments on the Department of Energy (DOE) Viability Assessment (VA)." Letter from L.W. Bradshaw (Nye County Department of Natural Resources & Federal Facilities) to L.H. Barrett (DOE/OCRWM), April 13, 1999, 99-020-LB, with enclosure. ACC: MOL.19990609.0149; HQO.19990812.0019.
- Brodsky, N.S.; Riggins, M.; Connolly, J.; and Ricci, P. 1997. *Thermal Expansion, Thermal Conductivity, and Heat Capacity Measurements for Boreholes UE25 NRG-4, UE25 NRG-5, USW NRG-6, and USW NRG-7/7A*. SAND95-1955. Albuquerque, New Mexico: Sandia National Laboratories. ACC: MOL.19980311.0316.
- Brookins, D.G. 1986. "Natural Analogues for Radwaste Disposal: Elemental Migration in Igneous Contact Zones." *Chemical Geology*, 55, 337-344. Amsterdam, The Netherlands: Elsevier. TIC: 246170.
- Brooks, R.H. and Corey, A.T. 1966. "Properties of Porous Media Affecting Fluid Flow." *Journal of the American Society of Civil Engineers, Irrigation and Drainage Division*, 92, (IR2), 61-89. New York, New York: American Society of Civil Engineers. TIC: 216867.
- Broxton, D.E.; Bish, D.L.; and Warren, R.G. 1987. "Distribution and Chemistry of Diagenetic Minerals at Yucca Mountain, Nye County, Nevada." *Clays and Clay Minerals*, 35, (2), 89-110. Long Island City, New York: Pergamon Press. TIC: 203900.
- Bruton, C.J.; Glassley, W.E.; and Bourcier, W.L. 1993. "Testing Geochemical Modeling Codes Using New Zealand Hydrothermal Systems." *Proceedings of the Topical Meeting on Site Characterization and Model Validation, Focus '93, September 26-29, 1993, Las Vegas, Nevada*. Pages 240-245. La Grange Park, Illinois: American Nuclear Society. TIC: 102245.
- Buddemeier, R.W. and Hunt, J.R. 1988. "Transport of Colloidal Contaminants in Groundwater: Radionuclide Migration at the Nevada Test Site." *Applied Geochemistry*, 3, 535-548. Oxford, England: Pergamon Press. TIC: 224116.
- Budnitz, B.; Ewing, R.C.; Moeller, D.W.; Payer, J.; Whipple, C.; and Witherspoon, P.A. 1999. *Peer Review of the Total System Performance Assessment-Viability Assessment Final Report*. Las Vegas, Nevada: Total System Performance Assessment Peer Review Panel. ACC: MOL.19990317.0328.
- Buesch, D.C. and Spengler, R.W. 1998. "Character of the Middle Nonlithophysal Zone of the Topopah Spring Tuff at Yucca Mountain." *High-Level Radioactive Waste Management*,

Proceedings of the Eighth International Conference, Las Vegas, Nevada, May 11-14, 1998. Pages 16-23. La Grange Park, Illinois: American Nuclear Society. TIC: 237082.

Buesch, D.C.; Spengler, R.W.; Moyer, T.C.; and Geslin, J.K. 1996. *Proposed Stratigraphic Nomenclature and Macroscopic Identification of Lithostratigraphic Units of the Paintbrush Group Exposed at Yucca Mountain, Nevada.* Open-File Report 94-469. Denver, Colorado: U.S. Geological Survey. ACC: MOL.19970205.0061.

Buesch, D.C.; Spengler, R.W.; Nelson, P.H.; Vaniman, D.T.; Chipera, S.J.; and Bish, D.L. 1995. "Geometry of the Vitric-Zeolitic Transition in Tuffs and the Relation to Fault Zones at Yucca Mountain, Nevada." *International Union of Geodesy and Geophysics, XXI General Assembly, July 2-14, 1995*, A426. Boulder, Colorado: Geological Society of America. TIC: 237709.

Bullivant, D.P. and O'Sullivan, M.J. 1998. "Inverse Modelling of the Wairakei Geothermal Field." *Proceedings of the TOUGH Workshop '98, Lawrence Berkeley National Laboratory, Berkeley, California, May 4-6, 1998.* Preuss, K., ed. LBNL-41995. Pages 53-58. Berkeley, California: Lawrence Berkeley National Laboratory. TIC: 247159.

Buscheck, T.A. and Nitao, J.J. 1992. "Impact of Thermal Loading on Repository Performance at Yucca Mountain." *High Level Radioactive Waste Management, Proceedings of the Third International Conference, Las Vegas, Nevada, April 12-16, 1992.* 1, 1003-1017. La Grange Park, Illinois: American Nuclear Society. TIC: 204231.

Buscheck, T.A. and Nitao, J.J. 1993. "Repository-Heat-Driven Hydrothermal Flow at Yucca Mountain, Part I: Modeling and Analysis." *Nuclear Technology*, 104, (3), 418-448. La Grange Park, Illinois: American Nuclear Society. TIC: 224039.

Carrera, J. and Neuman, S.P. 1986. "Estimation of Aquifer Parameters Under Transient and Steady State Conditions: 1. Maximum Likelihood Method Incorporating Prior Information." *Water Resources Research*, 22, (2), 199-210. Washington, D.C.: American Geophysical Union. TIC: 245915.

Castor, S.B.; Henry, C.D.; and Shevenell, L.A. 1996. *Volcanic Rock-Hosted Uranium Deposits in Northwestern Nevada and Southeastern Oregon - Possible Sites for Studies of Natural Analogues for the Potential High-Level Nuclear Waste Repository at Yucca Mountain, Nevada.* Reno, Nevada: Nevada Bureau of Mines and Geology. ACC: MOL.19960927.0026.

Chandler, N.; Davidson, C.C.; Gee, G.; LaPointe, P.; and Newman, P. 1999. *A Consensus Peer Review of Predictions of Seepage into Drifts of a Proposed Repository at Yucca Mountain.* Las Vegas, Nevada: Drift Seepage Peer Review Panel. Submit to RPC URN-0078

Clemo, T. and Smith, L. 1997. "A Hierarchical Model for Solute Transport in Fractured Media." *Water Resources Research*, 33, (8), 1763-1783. Washington, D.C.: American Geophysical Union. TIC: 239864.

Crowe, B.; Self, S.; Vaniman, D.; Amos, R.; and Perry, F. 1983. "Aspects of Potential Magmatic Disruption of a High-Level Radioactive Waste Repository in Southern Nevada."

Journal of Geology, 91, (3), 259-276. Chicago, Illinois: University of Chicago Press. TIC: 216959.

CRWMS M&O (Civilian Radioactive Waste Management System Management and Operating Contractor) 1995. *Total System Performance Assessment - 1995: An Evaluation of the Potential Yucca Mountain Repository*. B000000000-01717-2200-00136 REV 01. Las Vegas, Nevada: CRWMS M&O. ACC: MOL.19960724.0188.

CRWMS M&O 1997a. *ISM2.0: A 3D Geologic Framework and Integrated Site Model of Yucca Mountain*. B000000000-01717-5700-00004 REV 00. Las Vegas, Nevada: CRWMS M&O. ACC: MOL.19970625.0119.

CRWMS M&O 1997b. *Unsaturated Zone Flow Model Expert Elicitation Project*. Las Vegas, Nevada: CRWMS M&O. ACC: MOL.19971009.0582.

CRWMS M&O 1997c. *Unsaturated Zone Radionuclide Transport Abstraction/Testing Workshop Results*. B000000000-01717-2200-00185 REV 00. Las Vegas, Nevada: CRWMS M&O. ACC: MOL.19980528.0035.

CRWMS M&O 1998a. "Climatology and Meteorology." Book 2 - Section 4 of *Yucca Mountain Site Description*. B000000000-01717-5700-00019 REV 00. Las Vegas, Nevada: CRWMS M&O. ACC: MOL.19980729.0050.

CRWMS M&O 1998b. "Geochemistry." Book 3 - Section 6 of *Yucca Mountain Site Description*. B000000000-01717-5700-00019 REV 00. Las Vegas, Nevada: CRWMS M&O. ACC: MOL.19980729.0052.

CRWMS M&O 1998c. "Geography and Demography." Book 1 - Section 1 of *Yucca Mountain Site Description*. B000000000-01717-5700-00019 REV 00. Las Vegas, Nevada: CRWMS M&O. ACC: MOL.19980729.0047.

CRWMS M&O 1998d. "Geology." Book 1 - Section 3 of *Yucca Mountain Site Description*. B000000000-01717-5700-00019 REV 00. Las Vegas, Nevada: CRWMS M&O. ACC: MOL.19980729.0049.

CRWMS M&O 1998e. "Hydrologic System." Book 2 - Section 5 of *Yucca Mountain Site Description*. B000000000-01717-5700-00019 REV 00. Las Vegas, Nevada: CRWMS M&O. ACC: MOL.19980729.0051.

CRWMS M&O 1998f. "Nearby Industrial, Transportation, and Military Facilities." Book 1 - Section 2 of *Yucca Mountain Site Description*. B000000000-01717-5700-00019 REV 00. Las Vegas, Nevada: CRWMS M&O. ACC: MOL.19980729.0048.

CRWMS M&O 1998g. "Unsaturated Zone Hydrology Model." Chapter 2 of *Total System Performance Assessment-Viability Assessment (TSPA-VA) Analyses Technical Basis Document*. B000000000-01717-4301-00002 REV 01. Las Vegas, Nevada: CRWMS M&O. ACC: MOL.19981008.0002.

CRWMS M&O 1998h. *Ex-Container System Description Document*. BCA000000-01717-1705-00019 REV 00. Two volumes. Las Vegas, Nevada: CRWMS M&O. ACC: MOL.19981211.0159.

CRWMS M&O 1998i. "Near-Field Geochemical Environment." Chapter 4 of *Total System Performance Assessment-Viability Assessment (TSPA-VA) Analyses Technical Basis Document*. B00000000-01717-4301-00004 REV 01. Las Vegas, Nevada: CRWMS M&O. ACC: MOL.19981008.0004.

CRWMS M&O 1999a. *M&O Site Investigations -- (Q). Activity Evaluation*, September 28, 1999. Las Vegas, Nevada: CRWMS M&O. ACC: MOL.19990928.0224.

CRWMS M&O 1999b. *M&O Site Investigations. Activity Evaluation*, January 23, 1999. Las Vegas, Nevada: CRWMS M&O. ACC: MOL.19990317.0330.

CRWMS M&O 1999c. *Work Package Planning Summary, UZ Flow and Transport Process Model Report FY00*. Work Package 1401213UM1, Rev. 00. WPP-NBS-HS-000002. Las Vegas, Nevada: CRWMS M&O. ACC: MOL.19991020.0177.

CRWMS M&O 1999d. *Machine Readable Media Forms; Compact Disk YMP FEP Database Rev. 00C*. Las Vegas, Nevada: CRWMS M&O. ACC: MOL.19991214.0518.

CRWMS M&O 1999e. *Request for Repository Subsurface Design Information to Support TSPA-SR*. Input Transmittal PA-SSR-99218.Ta. Las Vegas, Nevada: CRWMS M&O. ACC: MOL.19990901.0312.

CRWMS M&O 1999f. *Subsurface Design for Enhanced Design Alternative (EDA) II. Design Input Transmittal SEI-SSR-99172.T*. Las Vegas, Nevada: CRWMS M&O. ACC: MOL.19990409.0100.

CRWMS M&O 2000a. *Unsaturated Zone Flow and Transport Model PMR. Development Plan TDP-NBS-HS-000091 REV 01*. Las Vegas, Nevada: CRWMS M&O. ACC: MOL.20000510.0174.

CRWMS M&O 2000b. *Repository Safety Strategy: Plan to Prepare the Postclosure Safety Case to Support Yucca Mountain Site Recommendation and Licensing Considerations*. TDR-WIS-RL-000001 REV 03. Las Vegas, Nevada: CRWMS M&O. ACC: MOL.20000119.0189.

CRWMS M&O 2000c. *Performance Confirmation Plan*. TDR-PCS-SE-000001 REV 01. Las Vegas, Nevada: CRWMS M&O. ACC: MOL.20000302.0312.

CRWMS M&O 2000 (E0040). *In Drift Microbial Communities*. ANL-EBS-MD-000038 REV 00. Las Vegas, Nevada: CRWMS M&O. ACC: MOL.20000331.0661.

CRWMS M&O 2000 (E0120). *Multiscale Thermohydrologic Model*. ANL-EBS-MD-000049 REV 00. Las Vegas, Nevada: CRWMS M&O. Submit to RPC URN-0019

CRWMS M&O 2000 (EBS PMR). *Engineered Barrier System Degradation, Flow, and Transport Process Model Report*. TDR-EBS-MD-000006 REV 00. Las Vegas, Nevada: CRWMS M&O. ACC: MOL.20000324.0558.

CRWMS M&O 2000 (I0035). *Geologic Framework Model (GFM3.1)*. MDL-NBS-GS-000002 REV 00 ICN 01. Las Vegas, Nevada: CRWMS M&O. ACC: MOL.20000121.0115.

CRWMS M&O 2000 (I0040). *Rock Properties Model (RPM3.1)*. MDL-NBS-GS-000004 REV 00 ICN 01. Las Vegas, Nevada: CRWMS M&O. ACC: MOL.20000121.0117.

CRWMS M&O 2000 (I0045). *Mineralogical Model (MM3.0) Analysis Model Report*. MDL-NBS-GS-000003 REV 00 ICN 01. Las Vegas, Nevada: CRWMS M&O. ACC: MOL.20000120.0477.

CRWMS M&O 2000. (ISM PMR) *Integrated Site Model Process Model Report*. TDR-NBS-GS-000002 REV 00 ICN 01. Las Vegas, Nevada: CRWMS M&O. ACC: MOL.20000121.0116.

CRWMS M&O 2000 (N0120/U0110). *Drift-Scale Coupled Processes (DST and THC Seepage) Models*. MDL-NBS-HS-000001 REV 00. Las Vegas, Nevada: CRWMS M&O. ACC: MOL.19990721.0523.

CRWMS M&O 2000 (N0125). *Abstraction of Drift-Scale Coupled Processes*. ANL-NBS-HS-000029 REV 00. Las Vegas, Nevada: CRWMS M&O. ACC: MOL.20000525.0371.

CRWMS M&O 2000 (U0000). *Development of Numerical Grids for UZ Flow and Transport Modeling*. ANL-NBS-HS-000015 REV 00. Las Vegas, Nevada: CRWMS M&O. ACC: MOL.19990721.0517.

CRWMS M&O 2000 (U0015). *In-Situ Field Testing of Processes*. ANL-NBS-HS-000005 REV 00. Las Vegas, Nevada: CRWMS M&O. ACC: MOL.20000504.0304.

CRWMS M&O 2000 (U0030). *Conceptual and Numerical Models for Unsaturated Zone Flow and Transport*. MDL-NBS-HS-000005 REV 00. Las Vegas, Nevada: CRWMS M&O. Submit to RPC URN-0036

CRWMS M&O 2000 (U0035). *Calibrated Properties Model*. MDL-NBS-HS-000003 REV 00. Las Vegas, Nevada: CRWMS M&O. ACC: MOL.19990721.0520.

CRWMS M&O 2000 (U0050). *UZ Flow Models and Submodels*. MDL-NBS-HS-000006 REV 00. Las Vegas, Nevada: CRWMS M&O. ACC: MOL.19990721.0527.

CRWMS M&O 2000 (U0060). *Radionuclide Transport Models under Ambient Conditions*. MDL-NBS-HS-000008 REV 00. Las Vegas, Nevada: CRWMS M&O. Submit to RPC URN-0064

CRWMS M&O 2000 (U0065). *Particle Tracking Model and Abstraction of Transport Processes*. ANL-NBS-HS-000026 REV 00. Las Vegas, Nevada: CRWMS M&O. ACC: MOL.20000502.0237

CRWMS M&O 2000 (U0070). *Unsaturated Zone Colloid Transport Model*. ANL-NBS-HS-000028 REV 00. Las Vegas, Nevada: CRWMS M&O. Submit to RPC URN-0031

CRWMS M&O 2000 (U0075). *Seepage Model for PA Including Drift Collapse*. MDL-NBS-HS-000002 REV 00. Las Vegas, Nevada: CRWMS M&O. Submit to RPC URN-0023

CRWMS M&O 2000 (U0080). *Seepage Calibration Model and Seepage Testing Data*. MDL-NBS-HS-000004 REV 00. Las Vegas, Nevada: CRWMS M&O. ACC: MOL.19990721.0521.

CRWMS M&O 2000 (U0085). *Analysis of Geochemical Data for the Unsaturated Zone*. ANL-NBS-HS-000017 REV 00. Las Vegas, Nevada: CRWMS M&O. Submit to RPC URN-0048

CRWMS M&O 2000 (U0090). *Analysis of Hydrologic Properties*. ANL-NBS-HS-000002 REV 00. Las Vegas, Nevada: CRWMS M&O. Submit to RPC URN-0055

CRWMS M&O 2000 (U0095). *Analysis of Infiltration Uncertainty*. ANL-NBS-HS-000027 REV 00. Las Vegas, Nevada: CRWMS M&O. ACC: MOL.20000525.0377.

CRWMS M&O 2000 (U0100). *Unsaturated Zone and Saturated Zone Transport Properties*. ANL-NBS-HS-000019 REV 00. Las Vegas, Nevada: CRWMS M&O. Submit to RPC URN-0038.

CRWMS M&O 2000 (U0105). *Mountain-Scale Coupled Processes (TH) Models*. MDL-NBS-HS-000007 REV 00. Las Vegas, Nevada: CRWMS M&O. ACC: MOL.19990721.0528.

CRWMS M&O 2000 (U0120). *Abstraction of Drift Seepage*. ANL-NBS-MD-000005 REV 00. Las Vegas, Nevada: CRWMS M&O. ACC: MOL.20000322.0671.

CRWMS M&O 2000 (U0125). *Abstraction of Flow Fields for RIP (ID:U0125)*. ANL-NBS-HS-000023 REV 00. Las Vegas, Nevada: CRWMS M&O. ACC: MOL.20000127.0089.

CRWMS M&O 2000 (U0135). *Natural Analogs for the Unsaturated Zone*. ANL-NBS-HS-000007 REV 00. Las Vegas, Nevada: CRWMS M&O. ACC: MOL.19990721.0524.

CRWMS M&O 2000 (U0155). *Analysis Comparing Advective-Dispersive Transport Solution to Particle Tracking*. ANL-NBS-HS-000001 REV 00. Las Vegas, Nevada: CRWMS M&O. ACC: MOL.19990721.0518.

CRWMS M&O 2000 (U0160). *Analysis of Base-Case Particle Tracking Results of the Base-Case Flow Fields*. ANL-NBS-HS-000024 REV 00. Las Vegas, Nevada: CRWMS M&O. ACC: MOL.20000207.0690.

CRWMS M&O 2000 (U0170). *Features, Events, and Processes in UZ Flow and Transport*. ANL-NBS-MD-000001 REV 00. Las Vegas, Nevada: CRWMS M&O. ACC: MOL.20000502.0240.

CRWMS M&O 2000 (WFD PMR). *Waste Form Degradation Process Model Report*. TDR-WIS-MD-000001 REV 00. Las Vegas, Nevada: CRWMS M&O. ACC: MOL.20000403.0495.

Cushey, M. and Liu, H.H. 1999. Summary of the UZ Model Workshop, Draft C, held on March 15-16, 1999, Berkeley, California: Lawrence Berkeley National Laboratory. ACC: MOL.20000510.0180.

Czarnecki, J.B.; Nelson, P.H.; O'Brien, G.M.; Sass, J.H.; Thapa, B.; Matsumoto, Y.; and Murakami, O. 1995. "Testing in Borehole USW G-2 at Yucca Mountain: The Saga Continues." *Eos*, 76, (46), 191-192. Washington, D.C.: American Geophysical Union. TIC: 240933.

Czarnecki, J.B.; O'Brien, G.M.; Nelson, P.H.; Sass, J.H.; Bullard, J.W.; and Flint, A.L. 1994. "Is There Perched Water Under Yucca Mountain in Borehole USW G-2?" *1994 Fall Meeting, Supplement to Eos, November 1, 1994*, 75, (44), 249-250. Washington, D.C.: American Geophysical Union. TIC: 226992.

Davis, O.K. 1990. "Caves as Sources of Biotic Remains in Arid Western North America." *Palaeogeography, Palaeoclimatology, Palaeoecology*, 76, (3-4), 331-348. Amsterdam, The Netherlands: Elsevier Science. TIC: 247413.

Day, W.C.; Potter, C.J.; Sweetkind, D.S.; Dickerson, R.P.; and San Juan, C.A. 1998. *Bedrock Geologic Map of the Central Block Area, Yucca Mountain, Nye County, Nevada*. Map I-2601. Washington, D.C.: U.S. Geological Survey. TIC: 237019.

de Marsily, G. 1986. *Quantitative Hydrogeology: Groundwater Hydrology for Engineers*. San Diego, California: Academic Press. TIC: 208450.

Desbarats, A.J. 1990. "Macrodispersion in Sand-Shale Sequences." *Water Resources Research*, 26, (1), 153-163. Washington, D.C.: American Geophysical Union. TIC: 236576.

DOE (U.S. Department of Energy) 1988. *Site Characterization Plan Yucca Mountain Site, Nevada Research and Development Area, Nevada*. DOE/RW-0199. Nine volumes. Washington, D.C.: U.S. Department of Energy, Office of Civilian Radioactive Waste Management. ACC: HQO.19881201.0002.

DOE 1998. *Total System Performance Assessment*. Volume 3 of *Viability Assessment of a Repository at Yucca Mountain*. DOE/RW-0508. Washington, D.C.: U.S. Department of Energy, Office of Civilian Radioactive Waste Management. ACC: MOL.19981007.0030.

DOE 1999. *Draft Environmental Impact Statement for a Geologic Repository for the Disposal of Spent Nuclear Fuel and High-Level Radioactive Waste at Yucca Mountain, Nye County, Nevada*. DOE/EIS-0250D. Summary, Volumes I and II. Washington, D.C.: U.S. Department of Energy, Office of Civilian Radioactive Waste Management. ACC: MOL.19990816.0240.

- Domenico, P.A. and Schwartz, F.W. 1990. *Physical and Chemical Hydrogeology*. New York, New York: John Wiley & Sons. TIC: 234782.
- Doughty, C. 1999. "Investigation of Conceptual and Numerical Approaches for Evaluating Moisture, Gas, Chemical, and Heat Transport in Fractured Unsaturated Rock." *Journal of Contaminant Hydrology*, 38, (1-3), 69-106. New York, New York: Elsevier Science Publishers. TIC: 244160.
- Drozhko, E.G.; Glagolenko, Y.U.; Mokrov, Y.G.; Postovalova, G.A.; Samsonova, L.M.; Glagolev, A.V.; Ter-Saakian, S.A.; Glinsky, M.L.; Vasil'kova, N.A.; Skokov, A.V.; Wollenberg, H.A.; Tsang, C-F.; Frangos, W.; Solbau, R.D.; Stevenson, K.A.; Lowder, W.M.; and Foley, M.G. 1997. "Joint Russian-American Hydrogeological-Geochemical Studies of the Karachai-Mishelyak System." *Environmental Geology*, 29, (3/4), 216-227. Berlin, Germany: Springer-Verlag. TIC: 246744.
- Ehlers, E.G. 1972. *The Interpretation of Geological Phase Diagrams*. San Francisco, California: W.H. Freeman and Company. TIC: 247331.
- Ehrlich, R.; Etris, E.L.; Brumfield, D.; Yuan, L.P.; and Crabtree, S.J. 1991. "Petrography and Reservoir Physics III: Physical Models for Permeability and Formation Factor." *AAPG Bulletin*, 75, (10), 1579-1592. Tulsa, Oklahoma: American Association of Petroleum Geologists. TIC: 246294.
- Ervin, E.M.; Luckey, R.R.; and Burkhardt, D.J. 1994. *Revised Potentiometric-Surface Map, Yucca Mountain and Vicinity, Nevada*. Water-Resources Investigations Report 93-4000. Denver, Colorado: U.S. Geological Survey. ACC: NNA.19930212.0018.
- Fabryka-Martin, J.T.; Wightman, S.J.; Murphy, W.J.; Wickham, M.P.; Caffee, M.W.; Nimz, G.J.; Southon, J.R.; and Sharma, P. 1993. "Distribution of Chlorine-36 in the Unsaturated Zone at Yucca Mountain: An Indicator of Fast Transport Paths." *Proceedings of the Topical Meeting on Site Characterization and Model Validation, Focus '93, September 26-29, 1993, Las Vegas, Nevada*. Pages 58-68. La Grange Park, Illinois: American Nuclear Society. TIC: 102245.
- Farrell, J. and Reinhard, M. 1994. "Desorption of Halogenated Organics from Model Solids, Sediments, and Soil Under Unsaturated Conditions. 2. Kinetics." *Environmental Science and Technology*, 28, (1), 63-72. Washington, D.C.: American Chemical Society. TIC: 246770.
- Faybishenko, B.; Salve, R.; Zawislanski, P.; Doughty, C.; Lee, K.H.; Cook, P.; Freifeld, B.; Jacobsen, J.; Sisson, B.; Hubbell, J.; and Dooley, K. 1998. *Ponded Infiltration Test at the Box Canyon Site, Data Report and Preliminary Analysis*. LBNL-40183. Berkeley, California: Lawrence Berkeley National Laboratory. ACC: MOL.19981002.0035.
- Fetter, C.W. 1993. *Contaminant Hydrogeology*. New York, New York: Macmillan Publishing. TIC: 240691.
- Finch, R.J. and Ewing, R.C. 1991. "Alteration of Natural UO₂ Under Oxidizing Conditions from Shinkolobwe, Katanga, Zaire: A Natural Analogue for the Corrosion of Spent Fuel."

Radiochimica Acta, 52/53, 395-401. München, Germany: R. Oldenbourg Verlag. TIC: 237035.

Finsterle, S. 1999. *ITOUGH2 User's Guide*. LBNL-40040. Berkeley, California: Lawrence Berkeley National Laboratory. TIC: 243018.

Flint, L.E. 1998. *Characterization of Hydrogeologic Units Using Matrix Properties, Yucca Mountain, Nevada*. Water-Resources Investigations Report 97-4243. Denver, Colorado: U.S. Geological Survey. ACC: MOL.19980429.0512.

Flint, L.E. and Flint, A.L. 1995. *Shallow Infiltration Processes at Yucca Mountain, Nevada—Neutron Logging Data 1984-93*. Water-Resources Investigations Report 95-4035. Denver, Colorado: U.S. Geological Survey. ACC: MOL.19960924.0577.

Flury, M.; Flühler, H.; Jury, W.A.; and Leuenberger, J. 1994. "Susceptibility of Soils to Preferential Flow of Water: A Field Study." *Water Resources Research*, 30, (7), 1945-1954. Washington, D.C.: American Geophysical Union. TIC: 247441.

Forester, R.M.; Bradbury, J.P.; Carter, C.; Elvidge, A.B.; Hemphill, M.L.; Lundstrom, S.C.; Mahan, S.A.; Marshall, B.D.; Neymark, L.A.; Paces, J.B.; Sharpe, S.E.; Whelan, J.F.; and Wigand, P.E. 1996. *Synthesis of Quaternary Response of the Yucca Mountain Unsaturated and Saturated Zone Hydrology to Climate Change*. Milestone 3GCA102M. Las Vegas, Nevada: U.S. Geological Survey. ACC: MOL.19970211.0026.

Forester, R.M.; Bradbury, J.P.; Carter, C.; Elvidge-Tuma, A.B.; Hemphill, M.L.; Lundstrom, S.C.; Mahan, S.A.; Marshall, B.D.; Neymark, L.A.; Paces, J.B.; Sharpe, S.E.; Whelan, J.F.; and Wigand, P.E. 1999. *The Climatic and Hydrologic History of Southern Nevada During the Late Quaternary*. Open-File Report 98-635. Denver, Colorado: U.S. Geological Survey. TIC: 245717.

Francis, N.D. 1997. "The Base-Case Thermal Properties for TSPA-VA Modeling." Memorandum from N.D. Francis (SNL) to Distribution, April 16, 1997. ACC: MOL.19980518.0229.

Freeze, R.A. and Cherry, J.A. 1979. *Groundwater*. Englewood Cliffs, New Jersey: Prentice-Hall. TIC: 217571.

Frind, E.O.; Gillham, R.W.; and Pickens, J.F. 1977. "Application of Unsaturated Flow Properties in the Design of Geologic Environments for Radioactive Waste Storage Facilities." *Finite Elements in Water Resources*, 3133-3163. London, United Kingdom: Pentech Press. TIC: 239854.

Gauthier, J.H.; Wilson, M.L.; and Lauffer, F.C. 1992. "Estimating the Consequences of Significant Fracture Flow at Yucca Mountain." *High-Level Radioactive Waste Management, Proceedings of the Third Annual International Conference, Las Vegas, Nevada, April 12-16, 1992*. Pages 891-898. La Grange Park, Illinois: American Nuclear Society. TIC: 204231.

Gauthier-Lafaye F.; Weber F.; and Ohmoto, H. 1989. "Natural Fission Reactors of Oklo." *Economic Geology*, 84, (8), 2286-2295. El Paso, Texas: Economic Geology Publishing Company. TIC: 246605.

Gelhar, L.W.; Welty, C.; and Rehfeldt, K.R. 1992. "A Critical Review of Data on Field-Scale Dispersion in Aquifers." *Water Resources Research*, 28, (7), 1955-1974. Washington, D.C.: American Geophysical Union. TIC: 235780.

Ginn, T.R. and Murphy, E.M. 1997. "A Transient Flux Model for Convective Infiltration: Forward and Inverse Solutions for Chloride Mass Balance Studies." *Water Resources Research*, 33, (9), 2065-2079. Washington, D.C.: American Geophysical Union. TIC: 247422.

Glass, R.J.; Nicholl, M.J.; and Tidwell, V.C. 1996. *Challenging and Improving Conceptual Models for Isothermal Flow in Unsaturated, Fractured Rock through Exploration of Small-Scale Processes*. SAND95-1824. Albuquerque, New Mexico: Sandia National Laboratories. ACC: MOL.19970520.0082.

Glass, R.J.; Parlange, J.Y.; and Steenhuis, R.S. 1991. "Immiscible Displacement in Porous Media: Stability Analysis of Three-Dimensional, Axisymmetric Disturbances with Application to Gravity-Driven Wetting Front Instability." *Water Resources Research*, 27, (8), 1947-1956. Washington, D.C.: American Geophysical Union. TIC: 239458.

Glassley, W.E. and Christensen, B.W. 1992. "Water-Rock Interaction in New Zealand Hydrothermal Systems: Comparison of Some Simulated and Observed Geochemical Processes." *High Level Radioactive Waste Management, Proceedings of the Third International Conference, Las Vegas, Nevada, April 12-16, 1992*. 1, 352-356. La Grange Park, Illinois: American Nuclear Society. TIC: 204231.

Grathwohl, P. 1998. *Diffusion in Natural Porous Media: Contaminant Transport, Sorption/Desorption and Dissolution Kinetics*. Boston, Massachusetts: Kluwer Academic Publishers. On Order Library Tracking Number-247983.

Haukwa, C.B.; Wu, Y.S.; and Bodvarsson, G.S. 1999. "Thermal Loading Studies Using the Yucca Mountain Unsaturated Zone Model." *Journal Of Contaminant Hydrology*, 38, (1-3), 217-255. New York, New York: Elsevier Science Publishers. TIC: 244160.

Hevesi, J.A.; Ambos, D.S.; and Flint, A.L. 1994. "A Preliminary Characterization of the Spatial Variability of Precipitation at Yucca Mountain, Nevada." *High-Level Radioactive Waste Management, Proceedings of the Fifth Annual International Conference, Las Vegas, Nevada, May 22-26, 1994*. 4, 2520-2529. La Grange Park, Illinois: American Nuclear Society. TIC: 210984.

Ho, C.K. 1997a. "Evaporation of Pendant Water Droplets in Fractures." *Water Resources Research*, 33, (12), 2665-2671. Washington, D.C.: American Geophysical Union. TIC: 246969.

Ho, C.K. 1997b. "Models of Fracture-Matrix Interactions During Multiphase Heat and Mass Flow in Unsaturated Fractured Porous Media." *ASME International Mechanical Engineering*

Congress and Exposition, Dallas, Texas, November 16-21, 1997. FED-Vol. 244, 401-412. New York, New York: American Society of Mechanical Engineers. TIC: 241082.

Hoffman, D.C. and Daniels, W.R. 1981. "Assessment of the Potential for Radionuclide Migration from a Nuclear Explosion Cavity." *Groundwater Contamination Symposium*. LA-UR-81-3181. Los Alamos, New Mexico: Los Alamos Scientific Laboratory. TIC: 204725.

Houseworth, J. and Ho, C. 1999. *Unsaturated Zone Flow and Transport Workshop Summary*. Milestone SL948M4. Las Vegas, Nevada: CRWMS M&O. ACC: MOL.19990329.0388.

Isobe, H.; Murakami, T.; and Ewing, R.C. 1992. "Alteration of Uranium Minerals in the Koongarra Deposit, Australia: Unweathered Zone." *Journal of Nuclear Materials*, 190, 174-187. Amsterdam, The Netherlands: Elsevier Science Publishers. TIC: 246371.

Jackson, C.P.; Hoch, A.R.; and Todman, S. 2000. "Self-Consistency of a Heterogeneous Continuum Porous Medium Representation of a Fractured Medium." *Water Resources Research*, 36, (1), 189-202. Washington, D.C.: American Geophysical Union. TIC: 247466.

James, S.C. and Chrysikopoulos, C.V. 1999. "Transport of Polydisperse Colloid Suspensions in a Single Fracture." *Water Resources Research*, 35, (3), 707-718. Washington, D.C.: American Geophysical Union. TIC: 245938.

Jercinovic, M.J. and Ewing, R.C. 1987. *Basaltic Glasses from Iceland and the Deep Sea: Natural Analogues to Borosilicate Nuclear Waste-Form Glass*. JSS Project Technical Report 88-01. Stockholm, Sweden: Swedish Nuclear Fuel and Waste Management Company. TIC: 205668.

Jercinovic, M.J.; Ewing, R.C.; and Byers, C.D. 1986. "Alteration Products of Basalt Glass from Frenchman Springs Flow, Wanapum Basalts, Hanford, Washington." *Advances in Ceramics, Third Annual Symposium on Ceramics in Nuclear Waste Management, April 28-30, 1986, Chicago, Illinois*. Clark, D.E.; White, W.B.; and Machiels, A.J., eds. 20, 671-679. Westerville, Ohio: The American Ceramic Society. TIC: 210019.

Kaplan, M.F. and Mendel, J.E. 1982. "Ancient Glass and the Safe Disposal of Nuclear Waste." *Archaeology*, 35, (4), 22-29. New York, New York: Archeological Institute of America. TIC: 247471.

Karasaki, K.; Segan, S.; Pruess, K.; and Vomvoris, S. 1994. "A Study of Two Phase Flow in Fracture Networks." *High-Level Radioactive Waste Management, Proceedings of the Fifth Annual International Conference, Las Vegas, Nevada, May 22-26, 1994*. 4, 2633-2638. La Grange Park, Illinois: American Nuclear Society. TIC: 210984.

Kersting, A.B.; Efur, D.W.; Finnegan, D.L.; Rokop, D.J.; Smith, D.K.; and Thompson, J.L. 1999. "Migration of Plutonium in Ground Water at the Nevada Test Site." *Nature*, 397, 56-59. London, England: Macmillan Publishers. TIC: 243597.

Khoury, H.N.; Salameh, E.; Clark, I.D.; Fritz, P.; Milodowski, A.E.; Cave, M.R.; Bajjali, W.; and Alexander, W.R. 1992. "A Natural Analogue of High pH Cement Pore Waters from the

- Maqarin Area of Northern Jordan. I: Introduction to the Site." *Journal of Geochemical Exploration*, 46, (1), 117-132. New York, New York: Elsevier Science. TIC: 247469.
- Klavetter, E.A. and Peters, R.R. 1986. *Estimation of Hydrologic Properties of an Unsaturated, Fractured Rock Mass*. SAND-84-2642. Albuquerque, New Mexico: Sandia National Laboratories. TIC: 202727.
- Kneafsey, T.J. and Pruess, K. 1998. "Laboratory Experiments on Heat-Driven Two-Phase Flows in Natural and Artificial Rock Fractures." *Water Resources Research*, 34, (12), 3349-3367. Washington, D.C.: American Geophysical Union. TIC: 247468.
- Koltermann, C.E. and Gorelick, S.M. 1996. "Heterogeneity in Sedimentary Deposits: A Review of Structure-Imitating, Process-Imitating, and Descriptive Approaches." *Water Resources Research*, 32, (9), 2617-2658. Washington, D.C.: American Geophysical Union. TIC: 239856.
- Kotra, J.P.; Lee, M.P.; Eisenberg, N.A.; and DeWispelare, A.R. 1996. *Branch Technical Position on the Use of Expert Elicitation in the High-Level Radioactive Waste Program*. NUREG-1563. Washington, D.C.: U.S. Nuclear Regulatory Commission. TIC: 226832.
- Kwicklis, E.M. and Healey, R.W. 1993. "Numerical Investigation of Steady Liquid Water Flow in a Variably Saturated Fracture Network." *Water Resources Research*, 29, (12), 4091-4102. Washington, D.C.: American Geophysical Union. TIC: 226993.
- LaBolle, E.M.; Fogg, G.E.; and Tompson, A.F.B. 1996. "Random-Walk Simulation of Transport in Heterogeneous Porous Media: Local Mass-Conservation Problem and Implementation Methods." *Water Resources Research*, 32, (3), 583-593. Washington, D.C.: American Geophysical Union. TIC: 245563.
- Lasaga, A.C. 1998. *Kinetic Theory in the Earth Sciences*. Princeton, New Jersey: Princeton University Press. TIC: 246279.
- LeCain, G.D. 1997. *Air-Injection Testing in Vertical Boreholes in Welded and Nonwelded Tuff, Yucca Mountain, Nevada*. Water-Resources Investigations Report 96-4262. Denver, Colorado: U.S. Geological Survey. ACC: MOL.19980310.0148.
- LeCain, G.D. 1998. *Results from Air-Injection and Tracer Testing in the Upper Tiva Canyon, Bow Ridge Fault, and Upper Paintbrush Contact Alcoves of the Exploratory Studies Facility, August 1994 through July 1996, Yucca Mountain, Nevada*. Water-Resources Investigations Report 98-4058. Denver, Colorado: U.S. Geological Survey. ACC: MOL.19980625.0344.
- Leverett, M.C. 1941. "Capillary Behavior in Porous Solids." *AIME Transactions, Tulsa Meeting, October 1940*. 142, 152-169. New York, New York: American Institute of Mining, Metallurgical, and Petroleum Engineers. TIC: 240680.
- Levy, S.S.; Fabryka-Martin, J.T.; Dixon, P.R.; Liu, B.; Turin, H.J.; and Wolfsberg, A.V. 1997. "Chlorine-36 Investigations of Groundwater Infiltration in the Exploratory Studies Facility at Yucca Mountain, Nevada." *Scientific Basis for Nuclear Waste Management XX, Symposium*

held December 2-6, 1996, Boston, Massachusetts. Gray, W.J. and Triay, I.R., eds. 465, 901-908. Pittsburgh, Pennsylvania: Materials Research Society. TIC: 238884.

Lichtner, P.C.; Keating, G.; and Carey, B. 1999. *A Natural Analogue for Thermal-Hydrological-Chemical Coupled Processes at the Proposed Nuclear Waste Repository at Yucca Mountain, Nevada*. LA-13610-MS. Los Alamos, New Mexico: Los Alamos National Laboratory. TIC: 246032.

Lin, W.; Wilder, D.; Blair, S.; Daily, W.; Gdowski, G.; Glassley, W.; Lee, K.; Meike, A.; Ramirez, A.; Roberts, J.; Ruddle, D.; Wagoner, J.; Watwood, D.; Williams, T.; and Carlson, R. 1998. "The Large Block Test of the Exploratory Studies Facility Thermal Tests." *High-Level Radioactive Waste Management, Proceedings of the Eighth International Conference, Las Vegas, Nevada, May 11-14, 1998*. Pages 49-51. La Grange Park, Illinois: American Nuclear Society. TIC: 237082.

Lippmann, M.J. and Bodvarsson, G.S. 1985. "The Heber Geothermal Field, California: Natural State and Exploitation Modeling Studies." *Journal of Geophysical Research*, 90, (B1), 745-758. Washington, D.C.: American Geophysical Union. TIC: 247477.

Liu, H.H. and Dane, J.H. 1996. "An Interpolation-Corrected Modified Method of Characteristics to Solve Advection-Dispersion Equations." *Advances in Water Resources*, 19, (6), 359-368. Amsterdam, The Netherlands: Elsevier Science. TIC: 247478.

Liu, H.H.; Doughty, C.; and Bodvarsson, G.S. 1998. "An Active Fracture Model for Unsaturated Flow and Transport in Fractured Rocks." *Water Resources Research*, 34, (10), 2633-2646. Washington, D.C.: American Geophysical Union. TIC: 243012.

Loeven, C. 1993. *A Summary and Discussion of Hydrologic Data from the Calico Hills Nonwelded Hydrogeologic Unit at Yucca Mountain, Nevada*. LA-12376-MS. Los Alamos, New Mexico: Los Alamos National Laboratory. ACC: NNA.19921116.0001.

Luckey, R.R.; Tucci, P.; Faunt, C.C.; Ervin, E.M.; Steinkampf, W.C.; D'Agnese, F.A.; and Patterson, G.L. 1996. *Status of Understanding of the Saturated-Zone Ground-Water Flow System at Yucca Mountain, Nevada, as of 1995*. Water-Resources Investigations Report 96-4077. Denver, Colorado: U.S. Geological Survey. ACC: MOL.19970513.0209.

Luckner, L.; van Genuchten, M.T.; and Nielsen, D.R. 1989. "A Consistent Set of Parametric Models for the Two-Phase Flow of Immiscible Fluids in the Subsurface." *Water Resources Research*, 25, (10), 2187-2193. Washington, D.C.: American Geophysical Union. TIC: 224845.

Matyskiela, W. 1997. "Silica Redistribution and Hydrologic Changes in Heated Fractured Tuff." *Geology*, 25, (12), 1115-1118. Boulder, Colorado: Geological Society of America. TIC: 236809.

McCarthy, J.F. and Zachara, J.M. 1989. "Subsurface Transport of Contaminants." *Environmental Science & Technology*, 23, (5), 496-502. Easton, Pennsylvania: American Chemical Society. TIC: 224876.

- McKelvey, V. 1976. Major Assets and Liabilities of the Nevada Test Site as a High-Level Radioactive Waste Repository. Letter from Dr. V. McKelvey (USGS) to R.W. Roberts (U.S. Energy Research and Development Administration), July 9, 1976, with enclosure, "Table 1. Assets and Liabilities of Nevada Test Site as Potential High-Level Radioactive Waste Repository." ACC: MOL.19990119.0314.
- McKinley, I.G.; Bath, A.H.; Berner, U.; Cave, M.; and Neal, C. 1988. "Results of the Oman Analogue Study." *Radiochimica Acta*, 44/45, (2), 311-316. Munich, Germany: R. Oldenbourg Verlag. TIC: 247492.
- Mercer, J.W. and Faust, C.R. 1979. "Geothermal Reservoir Simulation: 3. Application of Liquid- and Vapor-Dominated Hydrothermal Modeling Techniques to Wairakei, New Zealand." *Water Resources Research*, 15, (3), 653-671. Washington, D.C.: American Geophysical Union. TIC: 247493.
- Montazer, P. 1987. "Monitoring Hydrologic Conditions in the Vadose Zone in Fractured Rocks, Yucca Mountain, Nevada." Flow and Transport through Unsaturated Fractured Rock. Evans, D.D. and Nicholson, T.J., eds. Geophysical Monograph No. 42, 31-42. Washington, D.C.: American Geophysical Union. TIC: 225379.
- Montazer, P. and Wilson, W.E. 1984. *Conceptual Hydrologic Model of Flow in the Unsaturated Zone, Yucca Mountain, Nevada*. Water-Resources Investigations Report 84-4345. Lakewood, Colorado: U.S. Geological Survey. ACC: NNA.19890327.0051.
- Moridis, G.J. 1999. "Semianalytical Solutions for Parameter Estimation in Diffusion Cell Experiments." *Water Resources Research*, 35, (6), 1729-1740. Washington, D.C.: American Geophysical Union. TIC: 246266.
- Moyer, T.C.; Geslin, J.K.; and Flint, L.E. 1996. *Stratigraphic Relations and Hydrologic Properties of the Paintbrush Tuff Nonwelded (PTn) Hydrologic Unit, Yucca Mountain, Nevada*. Open-File Report 95-397. Denver, Colorado: U.S. Geological Survey. ACC: MOL.19970204.0216.
- Murakami, T.; Ohnuki, T.; Isobe, H.; and Sato, T. 1997. "Mobility of Uranium During Weathering." *American Mineralogist*, 82, 888-899. Washington, D.C.: Mineralogical Society of America. TIC: 246053.
- Murphy, W.M.; Percy, E.C.; Green, R.T.; Prikryl, J.D.; Mohanty, S.; Leslie, B.W.; and Nedungadi, A. 1998. "A Test of Long-Term, Predictive, Geochemical Transport Modeling at the Akrotiri Archaeological Site." *Journal of Contaminant Hydrology*, 29, 245-279. Amsterdam, The Netherlands: Elsevier Science B.V. TIC: 247211.
- Nataraja, M.S. and Brandshaug, T. 1992. Staff Technical Position on Geologic Repository Operations Area Underground Facility Design - Thermal Loads. NUREG-1466. Washington, D.C.: U.S. Nuclear Regulatory Commission. ACC: NNA.19921030.0049.
- National Research Council 1996. *Rock Fractures and Fluid Flow, Contemporary Understanding and Applications*. Washington, D.C.: National Academy Press. TIC: 235913.

- Nativ, R.; Adar, E.; Dahan, O.; and Geyh, M. 1995. "Water Recharge and Solute Transport through the Vadose Zone of Fractured Chalk Under Desert Conditions." *Water Resources Research*, 31, (2), 253-261. Washington, D.C.: American Geophysical Union. TIC: 233563.
- Neretnieks, I. 1993. "Solute Transport in Fractured Rock - Applications to Radionuclide Waste Repositories." Chapter 2 of *Flow and Contaminant Transport in Fractured Rock*. Bear, J.; Tsang, C.F.; and de Marsily, G., eds. 39-127. San Diego, California: Academic Press. TIC: 235461.
- Neuman, S.P. 1990. "Universal Scaling of Hydraulic Conductivities and Dispersivities in Geologic Media." *Water Resources Research*, 26, (8), 1749-1758. Washington, D.C.: American Geophysical Union. TIC: 237977.
- Nicholl, M.J.; Glass, R.J.; and Wheatcraft, S.W. 1994. "Gravity-Driven Infiltration Instability in Initially Dry Nonhorizontal Fractures." *Water Resources Research*, 30, (9), 2533-2546. Washington, D.C.: American Geophysical Union. TIC: 243493.
- Nitao, J. and Buscheck, T. 1991. "Infiltration of a Liquid Front in an Unsaturated, Fractured Porous Medium." *Water Resources Research*, 27, (8), 2099-2112. Washington, D.C.: American Geophysical Union. TIC: 224848.
- Nitao, J.J. 1998. "Thermohydrochemical Alteration of Flow Pathways Above and Below the Repository." Chapter 5.6 of *Near-Field/Altered-Zone Models Report*. Hardin, E.L. UCRL-ID-129179 DR. Livermore, California: Lawrence Livermore National Laboratory. ACC: MOL.19980504.0577.
- NRC (U.S. Nuclear Regulatory Commission) 1997. *Issue Resolution Status Report on Methods to Evaluate Climate Change and Associated Effects at Yucca Mountain (Key Technical Issue: Unsaturated and Saturated Flow Under Isothermal Conditions)*. Washington, D.C.: U.S. Nuclear Regulatory Commission. ACC: MOL.19980219.0880.
- NRC 1999a. *Issue Resolution Status Report Key Technical Issue: Radionuclide Transport*. Rev. 1. Washington, D.C.: U.S. Nuclear Regulatory Commission. ACC: MOL.19991214.0621.
- NRC 1999b. *Issue Resolution Status Report Key Technical Issue: Evolution of the Near-Field Environment*. Rev. 2. Washington, D.C.: U.S. Nuclear Regulatory Commission. ACC: MOL.19990810.0640.
- NRC 1999c. *Issue Resolution Status Report Key Technical Issue: Structural Deformation and Seismicity*. Rev. 2. Washington, D.C.: U.S. Nuclear Regulatory Commission. ACC: MOL.19991214.0623.
- NRC 1999d. *Issue Resolution Status Report Key Technical Issue: Thermal Effects on Flow*. Rev. 2. Washington, D.C.: U.S. Nuclear Regulatory Commission. ACC: MOL.19991021.0156.

- NRC 1999e. *Issue Resolution Status Report Key Technical Issue: Unsaturated and Saturated Flow Under Isothermal Conditions*. Rev. 2. Washington, D.C.: U.S. Nuclear Regulatory Commission. ACC: MOL.19990810.0641.
- NRC 2000. *Issue Resolution Status Report Key Technical Issue: Total System Performance Assessment and Integration*. Rev. 2. Washington, D.C.: U.S. Nuclear Regulatory Commission. TIC: 247614.
- NWTRB (Nuclear Waste Technical Review Board) 1999. *Report to the U.S. Congress and The Secretary of Energy, January to December 1998*. Arlington, Virginia: U.S. Nuclear Waste Technical Review Board. ACC: HQO.19990706.0007.
- NWTRB 2000. *Report to the U.S. Congress and the Secretary of Energy, January to December 1999*. Arlington, Virginia: U.S. Nuclear Waste Technical Review Board. TIC: 247806.
- Oldenburg, C.M. and Pruess, K. 1993. "On Numerical Modeling of Capillary Barriers." *Water Resources Research*, 29, (4), 1045-1056. Washington, D.C.: American Geophysical Union. TIC: 238834.
- Paces, J.B.; Forester, R.M.; Whelan, J.F.; Mahan, S.A.; Bradbury, J.P.; Quade, J.; Neymark, L.A.; and Kwak, L.M. 1996. *Synthesis of Ground-Water Discharge Deposits Near Yucca Mountain*. Milestone 3GQH671M. Las Vegas, Nevada: U.S. Geological Survey. ACC: MOL.19970205.0007.
- Paces, J.B.; Ludwig, K.R.; Peterman, Z.E.; Neymark, L.A.; and Kenneally, J.M. 1998a. "Anomalous Groundwater 234U/238U Beneath Yucca Mountain: Evidence of Local Recharge?" *High-Level Radioactive Waste Management, Proceedings of the Eighth International Conference, Las Vegas, Nevada, May 11-14, 1998*. Pages 185-188. La Grange Park, Illinois: American Nuclear Society. TIC: 237082.
- Paces, J.B.; Newmark, L.A.; Marshall, B.D.; Whelan, J.F.; and Peterman, Z.E. 1998b. "Inferences for Yucca Mountain Unsaturated-Zone Hydrology from Secondary Minerals." *High-Level Radioactive Waste Management, Proceedings of the Eighth International Conference, Las Vegas, Nevada, May 11-14, 1998*. Pages 36-39. La Grange Park, Illinois: American Nuclear Society. TIC: 237082.
- Paleologos, E.K.; Neuman, S.P.; and Tartakovsky, D. 1996. "Effective Hydraulic Conductivity of Bounded, Strongly Heterogeneous Porous Media." *Water Resources Research*, 32, (5), 1333-1341. Washington, D.C.: American Geophysical Union. TIC: 245760.
- Pearcy, E.C.; Prikryl, J.D.; and Leslie, B.W. 1995. "Uranium Transport Through Fractured Silicic Tuff and Relative Retention in Areas with Distinct Fracture Characteristics." *Applied Geochemistry*, 10, 685-704. Oxford, United Kingdom: Elsevier Science. TIC: 246848.
- Pearcy, E.C.; Prikryl, J.D.; Murphy, W.M.; and Leslie, B.W. 1994. "Alteration of Uraninite from the Nopal I Deposit, Pena Blanca District, Chihuahua, Mexico, Compared to Degradation of Spent Nuclear Fuel in the Proposed U.S. High-Level Nuclear Waste Repository at Yucca

Mountain, Nevada." *Applied Geochemistry*, 9, 713-732. New York, New York: Elsevier. TIC: 236934.

Peters, R.R. and Klavetter, E.A. 1988. "A Continuum Model for Water Movement in an Unsaturated Fractured Rock Mass." *Water Resources Research*, 24, (3), 416-430. Washington, D.C.: American Geophysical Union. TIC: 223603.

Philip, J.R.; Knight, J.H.; and Waechter, R.T. 1989. "Unsaturated Seepage and Subterranean Holes: Conspectus, and Exclusion Problem for Circular Cylindrical Cavities." *Water Resources Research*, 25, (1), 16-28. Washington, D.C.: American Geophysical Union. TIC: 239117.

Phillips, F.M. 1994. "Environmental Tracers for Water Movement in Desert Soils of the American Southwest." *Soil Science Society of America Journal*, 58, 15-24. Madison, Wisconsin: Soil Science Society of America. TIC: 240651.

Pickett, D.A. and Murphy, W.M. 1997. "Isotopic Constraints on Radionuclide Transport at Pena Blanca." *Seventh EC Natural Analogue Working Group Meeting: Proceedings of an International Workshop held in Stein am Rhein, Switzerland from 28 to 30 October 1996.* von Maravic, H. and Smellie, J., eds. EUR 17851EN, 113-122. Luxembourg, Luxembourg: European Communities. TIC: 247461.

Pickett, D.A. and Murphy, W.M. 1999. "Unsaturated Zone Waters from the Nopal I Natural Analog, Chihuahua, Mexico - Implications for Radionuclide Mobility at Yucca Mountain." *Scientific Basis for Nuclear Waste Management XXII, Materials Research Society Symposium held November 30-December 4, 1998, Boston, Massachusetts, U.S.A.* Wronkiewicz, D.J. and Lee, J.H., eds. 556, 809-816. Warrendale, Pennsylvania: Materials Research Society. TIC: 246426.

Plummer, M.A.; Phillips, F.M.; Fabryka-Martin, J.; Turin, H.J.; Wigand, P.E.; and Sharma, P. 1997. "Chlorine-36 in Fossil Rat Urine: An Archive of Cosmogenic Nuclide Deposition During the Past 40,000 Years." *Science*, 277, 538-541. Washington, D.C.: American Association for the Advancement of Science. TIC: 237425.

Potter, C.J.; Dickerson, R.P.; and Day, W.C. 1999. *Nature and Continuity of the Sundance Fault*. Open-File Report 98-266. Denver, Colorado: U.S. Geological Survey. TIC: 246609.

Pruess, K. 1987. *TOUGH User's Guide*. NUREG/CR-4645. Washington, D.C.: U.S. Nuclear Regulatory Commission. TIC: 217275.

Pruess, K. 1991. *TOUGH2-A General-Purpose Numerical Simulator for Multiphase Fluid and Heat Flow*. LBL-29400. Berkeley, California: Lawrence Berkeley Laboratory. ACC: NNA.19940202.0088.

Pruess, K. 1997. "On Vaporizing Water Flow in Hot Sub-Vertical Rock Fractures." *Transport in Porous Media*, 28, 335-372. Amsterdam, The Netherlands: Kluwer Academic Publishers. TIC: 238922.

- Pruess, K. 1999. "A Mechanistic Model for Water Seepage through Thick Unsaturated Zones in Fractured Rocks of Low Matrix." *Water Resources Research*, 35, (4), 1039-1051. Washington, D.C.: American Geophysical Union. TIC: 244913.
- Pruess, K. and Narasimhan, T.N. 1985. "A Practical Method for Modeling Fluid and Heat Flow in Fractured Porous Media." *Society of Petroleum Engineers Journal*, 25, (1), 14-26. Richardson, Texas: Society of Petroleum Engineers. TIC: 221917.
- Pruess, K.; Faybishenko, B.; and Bodvarsson, G.S. 1999. "Alternative Concepts and Approaches for Modeling Flow and Transport in Thick Unsaturated Zones of Fractured Rocks." *Journal of Contaminant Hydrology*, 38, (1-3), 281-322. New York, New York: Elsevier. TIC: 244160.
- Pruess, K.; Tsang, Y.W.; and Wang, J.S.Y. 1984. *Numerical Studies of Fluid and Heat Flow Near High-Level Nuclear Waste Packages Emplaced in Partially Saturated Fractured Tuff*. LBL-18552. Berkeley, California: Lawrence Berkeley Laboratory. TIC: 211033.
- Pruess, K.; Wang, J.S.Y.; and Tsang, Y.W. 1990a. "On Thermohydrologic Conditions Near High-Level Nuclear Wastes Emplaced in Partially Saturated Fractured Tuff: 1. Simulation Studies with Explicit Consideration of Fracture Effects." *Water Resources Research*, 26, (6), 1235-1248. Washington, D.C.: American Geophysical Union. TIC: 221923.
- Pruess, K.; Wang, J.S.Y.; and Tsang, Y.W. 1990b. "On Thermohydrologic Conditions Near High-Level Nuclear Wastes Emplaced in Partially Saturated Fractured Tuff: 2. Effective Continuum Approximation." *Water Resources Research*, 26, (6), 1249-1261. Washington, D.C.: American Geophysical Union. TIC: 224854.
- Ramirez, A.L.; Carlson, R.C.; and Buscheck, T.A. 1991. *In Situ Changes in the Moisture Content of Heated, Welded Tuff Based on Thermal Neutron Measurements*. UCRL-ID-104715. Livermore, California: Lawrence Livermore National Laboratory. ACC: NNA.19910701.0097.
- Rasmussen, T.C. 1991. "Steady Fluid Flow and Travel Times in Partially Saturated Fractures Using a Discrete Air-Water Interface." *Water Resources Research*, 27, (1), 67-76. Washington, D.C.: American Geophysical Union. TIC: 247498.
- Rautman, C.A. and McKenna, S.A. 1997. *Three-Dimensional Hydrological and Thermal Property Models of Yucca Mountain, Nevada*. SAND97-1730. Albuquerque, New Mexico: Sandia National Laboratories. ACC: MOL.19980311.0317.
- Reed, M.H. 1982. "Calculation of Multicomponent Chemical Equilibria and Reaction Processes in Systems Involving Minerals, Gases, and an Aqueous Phase." *Geochimica et Cosmochimica Acta*, 46, 513-528. New York, New York: Pergamon Press. TIC: 224159.
- Richards, L.A. 1931. "Capillary Conduction of Liquids Through Porous Media." *Physics*, 1, 318-333. Washington, D.C.: American Physical Society. TIC: 225383.
- Ritcey, A.C. and Wu, Y.S. 1999. "Evaluation of the Effect of Future Climate Change on the Distribution and Movement of Moisture in the Unsaturated Zone at Yucca Mountain, NV."

Journal of Contaminant Hydrology, 38, (1-3), 257-279. New York, New York: Elsevier. TIC: 244160.

Robinson, B.A.; Wolfsberg, A.V.; Viswanathan, H.S.; Bussod, G.Y.; Gable, C.W.; and Meijer, A. 1997. *The Site-Scale Unsaturated Zone Transport Model of Yucca Mountain*. Milestone Report SP25BM3. Los Alamos, New Mexico: Los Alamos National Laboratory. ACC: MOL.19980203.0570.

Robinson, B.A.; Wolfsberg, A.V.; Viswanathan, H.S.; Gable, C.W.; Zyvoloski, G.A.; and Turin, H.J. 1996. *Site Scale Unsaturated Zone Flow and Transport Model, Modeling of Flow, Radionuclide Migration, and Environmental Isotope Distributions at Yucca Mountain*. Milestone 3672. Draft. Los Alamos, New Mexico: Los Alamos National Laboratory. ACC: MOL.19971111.0625.

Robinson, B.A.; Wolfsberg, A.V.; Zyvoloski, G.A.; and Gable, C.W. 1995. *An Unsaturated Zone Flow and Transport Model of Yucca Mountain*. Milestone 3468. Draft. Los Alamos, New Mexico: Los Alamos National Laboratory. ACC: MOL.19960415.0218.

Robison, J.H. 1984. *Ground-Water Level Data and Preliminary Potentiometric-Surface Maps, Yucca Mountain and Vicinity, Nye County Nevada*. Water-Resources Investigations Report 84-4197. Lakewood, Colorado: U.S. Geological Survey. ACC: NNA.19930629.0013.

Roseboom, E.H., Jr. 1983. *Disposal of High-Level Nuclear Waste above the Water Table in Arid Regions*. Geological Survey Circular 903. Denver, Colorado: U.S. Geological Survey. TIC: 216597.

Ross, B. 1990. "The Diversion Capacity of Capillary Barriers." *Water Resources Research*, 26, (10), 2625-2629. Washington, D.C.: American Geophysical Union. TIC: 225235.

Rousseau, J.P.; Kwicklis, E.M.; and Gillies, D.C. 1999. *Hydrogeology of the Unsaturated Zone, North Ramp Area of the Exploratory Studies Facility, Yucca Mountain, Nevada*. Water-Resources Investigations Report 98-4050. Denver, Colorado: U.S. Geological Survey. ACC: MOL.19990419.0335.

Rousseau, J.P.; Loskot, C.L.; Thamir, F.; and Lu, N. 1997. *Results of Borehole Monitoring in the Unsaturated Zone Within the Main Drift Area of the Exploratory Studies Facility, Yucca Mountain, Nevada*. Milestone SPH22M3. Denver, Colorado: U.S. Geological Survey. ACC: MOL.19970626.0351.

Rulon, J.; Bodvarsson, G.S.; and Montazer, P. 1986. *Preliminary Numerical Simulations of Groundwater Flow in the Unsaturated Zone, Yucca Mountain, Nevada*. LBL-20553. Berkeley, California: Lawrence Berkeley Laboratory. ACC: NNA.19870908.0027.

Rumynin, V.G.; Mironenko, V.A.; Sindalovsky, L.N.; Boronina, A.V.; Konosavsky, P.K.; and Pozdniakov, S.P. 1998. *Evaluation of Conceptual, Mathematical and Physical-and-Chemical Models for Describing Subsurface Radionuclide Transport at the Lake Karachai Waste Disposal Site*. LBNL-41974. Berkeley, California: Lawrence Berkeley National Laboratory. TIC: 246562.

Russell, C.E.; Hess, J.W.; and Tyler, S.W. 1987. "Hydrogeologic Investigations of Flow in Fractured Tuffs, Rainier Mesa, Nevada Test Site." *Flow and Transport Through Unsaturated Fractured Rock*. AGU Geophysical Monograph 42. Washington, D.C.: American Geophysical Union. TIC: 247649.

Rybal'chenko, A.I.; Pimenov, M.K.; Kostin, P.P.; Balukova, V.D.; Nosukhin, A.V.; Mikerin, E.I.; Egorov, N.N.; Kaimin, E.P.; Kosareva, I.M.; and Kurochkin, V.M. 1998. *Deep Injection Disposal of Liquid Radioactive Waste in Russia*. Foley, M.G. and Ballou, L.M.G., eds. Columbus, Ohio: Battelle Press. TIC: 247062.

Sammel, E.A.; Ingebritsen, S.E.; and Mariner, R.H. 1988. "The Hydrothermal System at Newberry Volcano, Oregon." *Journal of Geophysical Research*, 93, (B9), 10147-10162. Washington, D.C.: American Geophysical Union. TIC: 247523.

Sass, J.H.; Lachenbruch, A.H.; Dudley, W.W., Jr.; Priest, S.S.; and Munroe, R.J. 1988. *Temperature, Thermal Conductivity, and Heat Flow Near Yucca Mountain, Nevada: Some Tectonic and Hydrologic Implications*. Open-File Report 87-649. Denver, Colorado: U.S. Geological Survey. ACC: MOL.19971027.0303.

Sawyer, D.A.; Fleck, R.J.; Lanphere, M.A.; Warren, R.G.; Broxton, D.E.; and Hudson, M.R. 1994. "Episodic Caldera Volcanism in the Miocene Southwestern Nevada Volcanic Field: Revised Stratigraphic Framework, $^{40}\text{Ar}/^{39}\text{Ar}$ Geochronology, and Implications for Magmatism and Extension." *Geological Society of America Bulletin*, 106, (10), 1304-1318. Boulder, Colorado: Geological Society of America. TIC: 222523.

Scott, R.B. and Bonk, J. 1984. *Preliminary Geologic Map of Yucca Mountain, Nye County, Nevada, with Geologic Sections*. Open-File Report 84-494. Denver, Colorado: U.S. Geological Survey. TIC: 203162.

Selker, J.S.; Steenhuis, R.T.; and Parlange, J.-Y. 1992. "Wetting Front Instability in Homogeneous Sandy Soils Under Continuous Infiltration." *Soil Science Society of America Journal*, 56, (5), 1346-1350. Madison, Wisconsin: Soil Science Society of America. TIC: 247522.

Sharp J.M.; Kreisel, J.I.; and Milliken K.L. 1996. "Fracture Skin Properties and Effects on Solute Transport: Geotechnical and Environmental Implications." *Rock Mechanics, Tools and Techniques, Proceedings of the 2nd North American Rock Mechanics Symposium, NARMS '96, A Regional Conference of ISRM, Montreal, Quebec, Canada, 19-21 June 1996*. 1329-1335. Rotterdam, The Netherlands: A.A. Balkema. TIC: 239941.

Sinnock, S.; Lin, Y.T.; and Brannen, J.P. 1987. "Preliminary Bounds on the Expected Postclosure Performance of the Yucca Mountain Repository Site, Southern Nevada." *Journal of Geophysical Research*, 92, (B8), 7820-7842. Washington, D.C.: American Geophysical Union. TIC: 222650.

Slider, H.C. 1976. *Practical Petroleum Reservoir Engineering Methods, An Energy Conservation Science*. Tulsa, Oklahoma: Petroleum Publishing Company. TIC: 247798.

- Sonnenthal, E.L. and Bodvarsson, G.S. 1999. "Constraints on the Hydrology of the Unsaturated Zone at Yucca Mountain, NV from Three-Dimensional Models of Chloride and Strontium Geochemistry." *Journal of Contaminant Hydrology*, 38, (1-3), 107-156. New York, New York: Elsevier. TIC: 244160.
- Spaulding, W.G. 1985. *Vegetation and Climates of the Last 45,000 Years in the Vicinity of the Nevada Test Site, South-Central Nevada*. Professional Paper 1329. Washington, D.C.: U.S. Geological Survey. TIC: 203210.
- Spengler, R.W.; Braun, C.A.; Martin, L.G.; and Weisenberg, C.W. 1994. *The Sundance Fault: A Newly Recognized Shear Zone at Yucca Mountain, Nevada*. Open-File Report 94-49. Denver, Colorado: U.S. Geological Survey. ACC: NNA.19940128.0119.
- Steeffel, C.I. and Lasaga, A.C. 1994. "A Coupled Model for Transport of Multiple Chemical Species and Kinetic Precipitation/Dissolution Reactions with Application to Reactive Flow in Single Phase Hydrothermal Systems." *American Journal of Science*, 294, (5), 529-592. New Haven, Connecticut: Kline Geology Laboratory, Yale University. TIC: 235372.
- Steeffel, C.I. and Lichtner, P.C. 1998. "Multicomponent Reactive Transport in Discrete Fractures: I. Controls on Reaction Front Geometry." *Journal of Hydrology*, 209, 186-199. Amsterdam, The Netherlands: Elsevier Science B.V. TIC: 247524.
- Stockman, H.; Krumhansl, J.; Ho, C.; and McConnell, V. 1994. *The Valles Natural Analogue Project*. NUREG/CR-6221. Washington, D.C.: U.S. Nuclear Regulatory Commission. TIC: 246123.
- Stroupe, E.P. 2000. "Approach to Implementing the Site Recommendation Design Baseline." Interoffice correspondence from E.P. Stroupe (CRWMS M&O) to D.R. Wilkins, January 26, 2000, LV.RSO.EPS.1/00-004, with attachment. ACC: MOL.20000214.0480.
- Stuckless, J.S.; Peterman, Z.E.; and Muhs, D.R. 1991. "U and Sr Isotopes in Ground Water and Calcite, Yucca Mountain, Nevada: Evidence Against Upwelling Water." *Science*, 254, 551-554. Washington, D.C.: American Association for the Advancement of Science. TIC: 224423.
- Szabo, B.J.; Kolesar, P.T.; Riggs, A.C.; Winograd, I.J.; and Ludwig, K.R. 1994. "Paleoclimatic Inferences from a 120,000-Yr Calcite Record of Water Table Fluctuation in Browns Room of Devils Hole, Nevada." *Quaternary Research*, 41, 59-69. New York, New York: Academic Press. TIC: 234642.
- Thoma, S.G.; Gallegos, D.P.; and Smith, D.M. 1992. "Impact of Fracture Coatings on Fracture/Matrix Flow Interactions in Unsaturated, Porous Media." *Water Resources Research*, 28, (5), 1357-1367. Washington, D.C.: American Geophysical Union. TIC: 237509.
- Thordarson, W. 1965. *Perched Ground Water in Zeolitized-Bedded Tuff, Rainier Mesa and Vicinity, Nevada Test Site, Nevada*. TEI-862. Washington, D.C.: U.S. Geological Survey. ACC: NN1.19881021.0066.

- Tompson, A.F.B. and Gelhar, L.W. 1990. "Numerical Simulation of Solute Transport in Three-Dimensional, Randomly Heterogeneous Porous Media." *Water Resources Research*, 26, (10), 2541-2562. Washington, D.C.: American Geophysical Union. TIC: 224902.
- Tsang, Y.W. and Birkholzer, J.T. 1999. "Predictions and Observations of the Thermal-Hydrological Conditions in the Single Heater Test." *Journal of Contaminant Hydrology*, 38, (1-3), 385-425. New York, New York: Elsevier. TIC: 244160.
- Tucci, P. and Burkhardt, D.J. 1995. *Potentiometric-Surface Map, 1993, Yucca Mountain and Vicinity, Nevada*. Water-Resources Investigations Report 95-4149. Denver, Colorado: U.S. Geological Survey. ACC: MOL.19960924.0517.
- Tyler, S.W.; Chapman, J.B.; Conrad, S.H.; Hammermeister, D.P.; Blout, D.O.; Miller, J.J.; Sully, M.J.; and Ginanni, J.M. 1996. "Soil-Water Flux in the Southern Great Basin, United States: Temporal and Spatial Variations Over the Last 120,000 Years." *Water Resources Research*, 32, (6), 1481-1499. Washington, D.C.: American Geophysical Union. TIC: 235938.
- USGS (U.S. Geological Survey) 2000 (U0005). *Future Climate Analysis*. ANL-NBS-GS-000008 REV 00. Denver, Colorado: U.S. Geological Survey. Submit to RPC URN-0004
- USGS 2000 (U0010). *Simulation of Net Infiltration for Modern and Potential Future Climate*. ANL-NBS-HS-000032 REV 00. Denver, Colorado: U.S. Geological Survey. Submit to RPC URN-0006.
- van Genuchten, M.T. 1980. "A Closed-Form Equation for Predicting the Hydraulic Conductivity of Unsaturated Soils." *Soil Science Society American Journal*, 44, (5), 892-898. Madison, Wisconsin: Soil Science Society of America. TIC: 217327.
- Villar, E.; Bonet, A.; Diaz-Caneja, B.; Fernandez, P.L.; Gutierrez, I.; Quindos, L.S.; Solana, J.R.; and Soto, J. 1985. "Natural Evolution of Percolation Water in Altamira Cave." *Cave Science*, 12, (1), 21-24. Bridgewater, United Kingdom: British Cave Research Association. TIC: 247713.
- Viswanathan, H.S.; Robinson, B.A.; Valocchi, A.J.; and Triay, I.R. 1998. "A Reactive Transport Model of Neptunium Migration from the Potential Repository at Yucca Mountain." *Journal of Hydrology*, 209, 251-280. Amsterdam, The Netherlands: Elsevier. TIC: 243441.
- Wallace, A.B. and Roper, M.W. 1981. *Geology and Uranium Deposits Along the Northeastern Margin, McDermitt Caldera Complex, Oregon*. Uranium in Volcanic and Volcaniclastic Rocks. AAPG Studies in Geology No. 13, 73-80. Tulsa, Oklahoma: American Association of Petroleum Geologists. TIC: 245898.
- Wang, J.S.Y. and Elsworth, D. 1999. "Permeability Changes Induced by Excavation in Fractured Tuff." *Rock Mechanics for Industry, Proceedings of the 37th U.S. Rock Mechanics Symposium, Vail, Colorado, June 6-9, 1999*. Amadei, B., ed. 2, 751-757. Rotterdam, The Netherlands: A.A. Balkema. TIC: 245246.

Wang, J.S.Y. and Narasimhan, T.N. 1985. "Hydrologic Mechanisms Governing Fluid Flow in a Partially Saturated, Fractured, Porous Medium." *Water Resources Research*, 21, (12), 1861-1874. Washington, D.C.: American Geophysical Union. TIC: 225290.

Wang, J.S.Y. and Narasimhan, T.N. 1988. *Hydrologic Modeling of Vertical and Lateral Movement of Partially Saturated Fluid Flow Near a Fault Zone at Yucca Mountain*. SAND87-7070. Albuquerque, New Mexico: Sandia National Laboratories. TIC: 202856.

Wang, J.S.Y. and Narasimhan, T.N. 1993. "Unsaturated Flow in Fractured Porous Media." Chapter 7 of *Flow and Contaminant Transport in Fractured Rocks*. Bear, J., Tsang, C.F., and de Marsily, G., eds. San Diego, California: Academic Press. TIC: 235461.

Wang, J.S.Y.; Cook, N.G.W.; Wollenberg, H.A.; Carnahan, C.L.; Javandel, I.; and Tsang, C.F. 1993. "Geohydrologic Data and Models of Rainier Mesa and Their Implications to Yucca Mountain." *High Level Radioactive Waste Management, Proceedings of the Fourth Annual International Conference, Las Vegas, Nevada, April 26-30, 1993*. 1, 675-681. La Grange Park, Illinois: American Nuclear Society. TIC: 208542.

Wang, J.S.Y.; Trautz, R.C.; Cook, P.J.; Finsterle, S.; James, A.L.; and Birkholzer, J. 1999. "Field Tests and Model Analyses of Seepage into Drift." *Journal of Contaminant Hydrology*, 38, (1-3), 323-347. New York, New York: Elsevier. TIC: 244160.

Warren, J.E. and Root, P.J. 1963. "The Behavior of Naturally Fractured Reservoirs." *Society of Petroleum Engineers Journal*, 3, (3), 245-255. Dallas, Texas: Society of Petroleum Engineers. TIC: 233671.

Watson, P.; Sinclair, P.; and Waggoner, R. 1976. "Quantitative Evaluation of a Method for Estimating Recharge to the Desert Basins of Nevada." *Journal of Hydrology*, 31, (3/4), 335-357. Amsterdam, Netherlands: Elsevier Scientific. TIC: 234481.

Weeks, E.P. 1987. "Effect of Topography on Gas Flow in Unsaturated Fractured Rock: Concepts and Observations." *Flow and Transport Through Unsaturated Fractured Rock*. Evans, D.D. and Nicholson, T.J., eds. Geophysical Monograph 42, 165-170. Washington, D.C.: American Geophysical Union. TIC: 223605.

Weeks, E.P. and Wilson, W.E. 1984. *Preliminary Evaluation of Hydrologic Properties of Cores of Unsaturated Tuff, Test Well USW H-1, Yucca Mountain, Nevada*. Water-Resources Investigations Report 84-4193. Denver, Colorado: U.S. Geological Survey. ACC: NNA.19870407.0037.

Wemheuer, R.F. 1999. "First Issue of FY00 NEPO QAP-2-0 Activity Evaluations." Interoffice correspondence from R.F. Wemheuer (CRWMS M&O) to R.A. Morgan, October 1, 1999, LV.NEPO.RTPS.TAG.10/99-155, with enclosures. ACC: MOL.19991028.0162.

Wilkins, D.R. and Heath, C.A. 1999. "Direction to Transition to Enhanced Design Alternative II." Letter from Dr. D.R. Wilkins (CRWMS M&O) and Dr. C.A. Heath (CRWMS M&O) to Distribution, June 15, 1999, LV.NS.JLY.06/99-026, with enclosures, "Strategy for Baselineing

EDA II Requirements" and "Guidelines for Implementation of EDA II." ACC: MOL.19990622.0126; MOL.19990622.0127; MOL.19990622.0128.

Wilson, M.L.; Gauthier, J.H.; Barnard, R.W.; Barr, G.E.; Dockery, H.A.; Dunn, E.; Eaton, R.R.; Guerin, D.C.; Lu, N.; Martinez, M.J.; Nilson, R.; Rautman, C.A.; Robey, T.H.; Ross, B.; Ryder, E.E.; Schenker, A.R.; Shannon, S.A.; Skinner, L.H.; Halsey, W.G.; Gansemer, J.D.; Lewis, L.C.; Lamont, A.D.; Triay, I.R.; Meijer, A.; and Morris, D.E. 1994. *Total-System Performance Assessment for Yucca Mountain – SNL Second Iteration (TSPA-1993)*. SAND93-2675. Executive Summary and two volumes. Albuquerque, New Mexico: Sandia National Laboratories. ACC: NNA.19940112.0123.

Winograd, I.J. 1981. "Radioactive Waste Disposal in Thick Unsaturated Zones." *Science*, 212, (4502), 1457-1464. Washington, D.C.: American Association for the Advancement of Science. TIC: 217258.

Winograd, I.J. 1986. *Archaeology and Public Perception of a Transscientific Problem – Disposal of Toxic Wastes in the Unsaturated Zone*. Circular 990. Denver, Colorado: U.S. Geological Survey. TIC: 237946.

Winograd, I.J. and Thordarson, W. 1975. *Hydrogeologic and Hydrochemical Framework, South-Central Great Basin, Nevada-California, with Special Reference to the Nevada Test Site*. Professional Paper 712-C. Washington, D.C.: U.S. Geological Survey. TIC: 206787.

Winograd, I.J.; Coplen, T.B.; Landwehr, J.M.; Riggs, A.C.; Ludwig, K.R.; Szabo, B.J.; Kolesar, P.T.; and Revesz, K.M. 1992. "Continuous 500,000-Year Climate Record from Vein Calcite in Devils Hole, Nevada." *Science*, 258, 255-260. Washington, D.C.: American Association for the Advancement of Science. TIC: 237563.

Wittwer, C.; Chen, G.; Bodvarsson, G.S.; Chornack, M.; Flint, A.; Flint, L.; Kwicklis, E.; and Spengler, R. 1995. *Preliminary Development of the LBL/USGS Three-Dimensional Site-Scale Model of Yucca Mountain, Nevada*. LBL-37356. Berkeley, California: Lawrence Berkeley Laboratory. ACC: MOL.19960924.0538.

Wittwer, C.S.; Bodvarsson, G.S.; Chornack, M.P.; Flint, A.L.; Flint, L.E.; Lewis, B.D.; Spengler, R.W.; and Rautman, C.A. 1992. "Design of a Three-Dimensional Site-Scale Model for the Unsaturated Zone at Yucca Mountain, Nevada." *High Level Radioactive Waste Management, Proceedings of the Third International Conference, Las Vegas, Nevada, April 12-16, 1992*. 1, 263-271. La Grange Park, Illinois: American Nuclear Society. TIC: 204231.

WoldeGabriel, G.; Keating, G.N.; and Valentine, G.A. 1999. "Effects of Shallow Basaltic Intrusion into Pyroclastic Deposits, Grants Ridge, New Mexico, USA." *Journal of Volcanology and Geothermal Research*, 92, 389-411. Amsterdam, The Netherlands: Elsevier Science. TIC: 246037.

Wollenberg, H.A. and Flexser, S. 1986. "Contact Zones and Hydrothermal Systems as Analogues to Repository Conditions." *Chemical Geology*, 55, 345-359. Amsterdam, The Netherlands: Elsevier Science B.V. TIC: 246171.

Wu, Y.S.; Chen, G.; and Bodvarsson, G. 1995. *Preliminary Analysis of Effects of Thermal Loading on Gas and Heat Flow Within the Framework of the LBNL/USGS Site-Scale Model*. LBL- 37729. Berkeley, California: Lawrence Berkeley National Laboratory. TIC: 222270.

Wu, Y-S.; Haukwa, C.; and Bodvarsson, G.S. 1999a. "A Site-Scale Model for Fluid and Heat Flow in the Unsaturated Zone of Yucca Mountain, Nevada." *Journal of Contaminant Hydrology*, 38, (1-3), 185-215. New York, New York: Elsevier. TIC: 244160.

Wu, Y.S.; Ritcey, A.C.; and Bodvarsson, G.S. 1999b. "A Modeling Study of Perched Water Phenomena in the Unsaturated Zone at Yucca Mountain." *Journal of Contaminant Hydrology*, 38, (1-3), 157-184. New York, New York: Elsevier. TIC: 244160.

Xu, T. and Pruess, K. 1998. *Coupled Modeling of Non-Isothermal Multi-Phase Flow, Solute Transport and Reactive Chemistry in Porous and Fractured Media: 1. Model Development and Validation*. LBNL-42050. Berkeley, California: Lawrence Berkeley National Laboratory. TIC: 243735.

Xu, T.; Pruess, K.; and Brimhall, G. 1998. *An Improved Equilibrium-Kinetics Speciation Algorithm for Redox Reactions in Variably Saturated Subsurface Flow Systems*. LBNL-41789. Berkeley, California: Lawrence Berkeley National Laboratory. TIC: 240019.

Yang, I.C.; Rattray, G.W.; and Yu, P. 1996. *Interpretation of Chemical and Isotopic Data from Boreholes in the Unsaturated Zone at Yucca Mountain, Nevada*. Water-Resources Investigations Report 96-4058. Denver, Colorado: U.S. Geological Survey. ACC: MOL.19980528.0216.

Yang, I.C.; Yu, P.; Rattray, G.W.; Ferarese, J.S.; and Ryan, J.N. 1998. *Hydrochemical Investigations in Characterizing the Unsaturated Zone at Yucca Mountain, Nevada*. Water-Resources Investigations Report 98-4132. Denver, Colorado: U.S. Geological Survey. ACC: MOL.19981012.0790.

Yao, T-M and Hendrickx, J.M.H. 1996. "Stability of Wetting Fronts in Dry Homogeneous Soils Under Low Infiltration Rates." *Soil Science Society of America Journal*, 60, (1), 20-28. Madison, Wisconsin: Soil Science Society of America. TIC: 246692.

YMP (Yucca Mountain Project) 1999. *Unsaturated Zone Flow and Transport Model Independent Evaluation Panel Preliminary Report*. Las Vegas, Nevada: Yucca Mountain Site Characterization Office. ACC: MOL.20000111.0135.

Zhou, W. and Apted, M.J. 1995. "Flow and Transport Simulation in Yucca Mountain Using Dual-Porosity Model." *High Level Radioactive Waste Management, Proceedings of the Sixth Annual International Conference, Las Vegas, Nevada, April 30-May 5, 1995*. Pages 160-162. La Grange Park, Illinois: American Nuclear Society. TIC: 215781.

Zimmerman, R.M.; Blanford, M.L.; Holland, J.F.; Schuch, R.L.; and Barrett, W.H. 1986. *Nevada Nuclear Waste Storage Investigations Project, Final Report: G-Tunnel Small-Diameter Heater Experiments*. SAND84-2621. Albuquerque, New Mexico: Sandia National Laboratories. ACC: HQS.19880517.2365.

Zimmerman, R.W. and Bodvarsson, G.S. 1996. "Effective Transmissivity of Two-Dimensional Fracture Networks." *International Journal of Rock Mechanics and Mining Sciences & Geomechanics Abstracts*, 33, (4), 433-438. Oxford, United Kingdom: Pergamon Press. TIC: 245649.

6.2 CODES, STANDARDS, REGULATIONS, AND PROCEDURES

64 FR (Federal Register) 8640. Disposal of High-Level Radioactive Waste in a Proposed Geologic Repository at Yucca Mountain. Proposed rule 10 CFR 63. Readily available.

AP-2.14Q, Rev. 0, ICN 1. *Review of Technical Products*. Washington, D.C.: U.S. Department of Energy, Office of Civilian Radioactive Waste Management. ACC: MOL.20000405.0477.

AP-2.16Q, Rev. 0, ICN 0. *Activity Evaluation*. Washington, D.C.: U.S. Department of Energy, Office of Civilian Radioactive Waste Management. ACC: MOL.20000207.0716.

AP-3.10Q, Rev. 2, ICN 1. *Analyses and Models*. Washington, D.C.: U.S. Department of Energy, Office of Civilian Radioactive Waste Management. ACC: MOL.20000512.0066.

AP-3.10Q, Rev. 2, ICN 2. *Analyses and Models*. Washington, D.C.: U.S. Department of Energy, Office of Civilian Radioactive Waste Management. ACC: MOL.20000619.0576.

AP-3.11Q, Rev. 1, ICN 1. *Technical Reports*. Washington, D.C.: U.S. Department of Energy, Office of Civilian Radioactive Waste Management. ACC: MOL.20000726.0216.

AP-3.15Q, Rev. 1, ICN 1. *Managing Technical Product Inputs*. Washington, D.C.: U.S. Department of Energy, Office of Civilian Radioactive Waste Management. ACC: MOL.20000218.0069.

AP-7.5Q, Rev. 0, ICN 1. *Submittal, Review, and Acceptance of Deliverables*. Washington, D.C.: U.S. Department of Energy, Office of Civilian Radioactive Waste Management. TIC: MOL.20000518.0343.

AP-SI.1Q, Rev. 2, ICN 4. *Software Management*. Washington, D.C.: U.S. Department of Energy, Office of Civilian Radioactive Waste Management. ACC: MOL.20000223.0508.

DOE 2000. *Quality Assurance Requirements and Description*. DOE/RW-0333P, Rev. 10. Washington, D.C.: U.S. Department of Energy, Office of Civilian Radioactive Waste Management. ACC: MOL.20000427.0422.

QAP-2-0, Rev. 5. *Conduct of Activities*. Las Vegas, Nevada: CRWMS M&O. ACC: MOL.19980826.0209.

YMP-LBNL-QIP-6.1, Rev. 5, Mod. 0. *Document Review*. Berkeley, California: Lawrence Berkeley National Laboratory. ACC: MOL.19991210.0091.

6.3 SOURCE DATA, LISTED BY DATA TRACKING NUMBER

GS990708312242.008. Physical and Hydraulic Properties of Core Samples from Busted Butte Boreholes. Submittal date: 07/01/1999.

GS990908314224.009. Detailed Line Survey Data for Horizontal and Vertical Traverses, ECRB. Submittal date: 09/16/1999.

LB002181233124.001. Air Permeability and Pneumatic Pressure Data Collected Between October 27, 1999 through November 7, 1999 from Niche 5 (ECRB Niche 1620) of the ESF. Submittal date: 02/18/2000.

LB990501233129.004. 3-D UZ Model Calibration Grids for AMR U0000, "Development of Numerical Grids of UZ Flow and Transport Modeling". Submittal date: 09/24/1999.

LB990701233129.001. 3-D UZ Model Grids for Calculation of Flow Fields for PA for AMR U0000, "Development of Numerical Grids For UZ Flow and Transport Modeling". Submittal date: 09/24/1999.

MO9901MWDISMMM.000. ISM3.0 Mineralogic Models. Submittal date: 01/22/1999. Submit to RPC URN-0074.

MO9901MWDISMRP.000. ISM3.0 Rock Properties Models. Submittal date: 01/22/1999. Submit to RPC URN-0075.

MO9910MWDISMMM.003. ISM3.1 Mineralogic Models. Submittal date: 10/01/1999. Submit to RPC URN-0076.

MO9910MWDISMRP.002. Rock Properties Model (RPM3.1). Submittal date: 10/06/1999. Submit to RPC URN-0080.

6.3.1 Data Tracking Numbers Listed for Tables and Figures in Attachment II

GS000399991221.002. Rainfall/Runoff/Run-on 1999 Simulations. Submittal date: 03/10/2000.

GS000399991221.003. Preliminary Alcove 1 Infiltration Experiment Data. Submittal date: 03/10/2000.

GS000399991221.004. Preliminary Developed Matrix Properties. Submittal date: 03/10/2000.

GS960308312232.001. Deep Unsaturated Zone Surface-Based Borehole Instrumentation Program Data from Boreholes USW NRG-7A, USW NRG-6, UE-25 UZ#4, UE-25 UZ#5, USW UZ-7A, and USW SD-12 for the Time Period 10/01/95 through 3/31/96. Submittal date: 04/04/1996.

GS960908315215.014. Uranium and Thorium Isotope Data for ESF Secondary Minerals Collected Between March 1996 and July 1996. Submittal date: 09/25/1996.

GS980908312242.036. Water Potentials Measured With Heat Dissipation Probes in ECRB Holes from 4/23/98 to 7/31/98. Submittal date: 09/22/1998.

GS980908315215.015. Uranium and Thorium Isotope Data Including Calculated $^{230}\text{Th}/\text{U}$ Ages and Initial $^{234}\text{U}/^{238}\text{U}$ Activity Ratios for in Situ Microdigestions of Outermost Opal-Rich Mineral Coatings from the Exploratory Studies Facility Analyzed Between 12/01/97 and 09/15/98. Submittal date: 09/23/1998.

GS991299992271.001. Preliminary Unsaturated Zone Borehole Hydrochemistry Data. Submittal date: 12/23/1999.

LA0003AM831341.001. Preliminary Revision of Probability Distributions for Sorption Coefficients (K_{DS}). Submittal date: 03/29/2000. Submit to RPC URN-0267

LA0003JC831362.001. Preliminary Matrix Diffusion Coefficients for Yucca Mountain Tuffs. Submittal date: 4/10/2000. Submit to RPC URN-0305

LA0004WS831372.002. Sorption of Np, Pu, and Am on Rock Samples From Busted Butte, NV. Submittal date: 04/19/2000. Submit to RPC URN-0304

LA9909JF831222.005. Chlorine-36 Analyses of ESF and Busted Butte Porewaters in FY99. Submittal date: 09/29/1999.

LA9909JF831222.010. Chloride, Bromide, Sulfate, and Chlorine-36 Analyses of ESF Porewaters. Submittal date: 09/29/1999.

LAJF831222AQ98.004. Chloride, Bromide, Sulfate, and Chlorine-36 Analyses of Salts Leached from ESF Rock Samples. Submittal date: 09/10/1998.

LAJF831222AQ98.011. Chloride, Bromide, Sulfate and Chlorine-36 Analyses of Springs, Groundwater, Porewater, Perched Water and Surface Runoff. Submittal date: 09/10/1998.

LB980001233124.003. Liquid Release Tests Performed to Determine if a Capillary Barrier Exists in Niches 3566 and 3650. Submittal date: 04/23/1998.

LB00032412213U.001. Busted Butte Ground Penetrating Radar Data Collected June 1998 through February 2000 at the Unsaturated Zone Transport Test (UZTT): GPR Velocity Data. Submittal date: 03/24/2000. Submit to RPC URN-0303

LB980901123142.006. Laboratory Test Results of Hydrological Properties from Post-Test Dry-Drilled Cores in the Single Heater Test Area for the Final TDIF Submittal for the Single Heater Test. Submittal date: 08/31/1998.

LB980930123112.001. Surface to ESF Seismic Tomography. Submittal date: 09/30/1998.

LB990051233129.001. Extent of Vitric Region Used to Assign Material Properties in FY 99 UZ Model Layers; Figure 5 From AMR U0000, "Development of Numerical Grids for UZ Flow and Transport Modeling." Submittal date: 09/24/99.

LB990501233129.004. 3-D UZ Model Calibration Grids for AMR U0000, "Development of Numerical Grids of UZ Flow and Transport Modeling." Submittal date: 09/24/1999.

LB990701233129.001. 3-D UZ Model Grids for Calculation of Flow Fields for PA for AMR U0000, "Development of Numerical Grids for UZ Flow and Transport Modeling." Submittal date: 09/24/1999.

LB990801233129.001. TSPA Grid Flow Simulations for AMR U0050, "UZ Flow Models and Submodels" (Flow Field #1). Submittal date: 11/29/1999.

LB990801233129.003. TSPA Grid Flow Simulations for AMR U0050, "UZ Flow Models and Submodels" (Flow Field #3). Submittal date: 11/29/1999.

LB990801233129.004. TSPA Grid Flow Simulations for AMR U0050, "UZ Flow Models and Submodels" (Flow Field #4). Submittal date: 11/29/1999.

LB990801233129.005. TSPA Grid Flow Simulations for AMR U0050, "UZ Flow Models and Submodels" (Flow Field #5). Submittal date: 11/29/1999.

LB990801233129.007. TSPA Grid Flow Simulations for AMR U0050, "UZ Flow Models and Submodels" (Flow Field #7). Submittal date: 11/29/1999.

LB990801233129.009. TSPA Grid Flow Simulations for AMR U0050, "UZ Flow Models and Submodels" (Flow Field #9). Submittal date: 11/29/1999.

LB990801233129.011. TSPA Grid Flow Simulations for AMR U0050, "UZ Flow Models and Submodels" (Flow Field #11). Submittal date: 11/29/1999.

LB990801233129.013. TSPA Grid Flow Simulations for AMR U0050, "UZ Flow Models and Submodels" (Flow Field #13). Submittal date: 11/29/1999.

LB990801233129.015. TSPA Grid Flow Simulations for AMR U0050, "UZ Flow Models and Submodels" (Flow Field #15). Submittal date: 11/29/1999.

LB990801233129.017. TSPA Grid Flow Simulations for AMR U0050, "UZ Flow Models and Submodels" (Flow Field #17). Submittal date: 11/29/1999.

LB990801233129.025. TSPA Grid Flow Simulations for AMR U0050, "UZ Flow Models and Submodels" Flow Field #25: Present Day Mean Infiltration for Flow-Through Perched-Water Conceptual Model. Submittal date: 3/11/2000.

LB990831012027.001. Input to Seepage Calibration Model AMR U0080. Submittal date: 08/31/1999.

LB9908T1233129.001. Transport Simulations for the Low, Mean, and Upper Infiltration Scenarios of the Present-Day, Monsoon, and Glacial Transition Climates for AMR U0050, "UZ Models and Submodels." Submittal date: 3/11/2000.

LB990901233124.002. Alcove 6 Flow Data for AMR U0015, "In Situ Field Testing of Processes." Submittal date: 11/01/1999.

LB990901233124.005. Alcove 4 Flow Data for AMR U0015, "In Situ Field Testing of Processes." Submittal date: 11/01/1999.

LB990901233129.001. Input and Output Data for Verification of Dual-Continua Particle Tracker (DCPT) for AMR U0155, "Analysis Comparing Advect-Dispersion Transport Solution to Particle Tracking." Submittal date: 10/26/1999.

LB991091233129.001. One-Dimensional, Mountain-Scale Calibration for AMR U0035, "Calibrated Properties Model." Submittal date: 10/22/1999.

LB991091233129.003. Two-Dimensional Fault Calibration for AMR U0035, "Calibrated Properties Model." Submittal date: 10/22/1999.

LB991101233129.001. Model Input/Output Files Supporting Seepage Model for PA in AMR U0075, "Seepage Model for PA Including Drift Collapse." Submittal date: 11/30/1999.

LB991121233129.007. Calibrated Parameters for the Present-Day, Mean Infiltration Scenario, Used for Simulations with Perched Water Conceptual Model #3 for the Mean Infiltration Scenarios of the Present-Day, Monsoon and Glacial Transition Climates. Submittal date: 3/1/2000.

LB991131233129.001. Modeling Calcite Deposition and Percolation. AMR U0050, "UZ Flow Models and Submodels". Submittal date: 03/11/2000.

LB991131233129.002. Modeling Seepage and Tracer Tests at Alcove 1. AMR U0050, "UZ Flow Models and Submodels". Submittal date: 03/11/2000.

LB991131233129.003. Analytical and Simulation Results of Chloride and Chlorine-36 Analysis. AMR U0050, "UZ Flow Models and Submodels". Submittal date: 3/11/2000.

LB991200DSTTHC.001. Pore Water Composition and CO2 Partial Pressure Input into Thermal-Hydrological-Chemical (THC) Simulations: Table 3 of AMR N0120/U0110, "Drift-Scale Coupled Processes (Drift-Scale and THC Seepage) Models". Submittal date: 03/11/2000.

LB991200DSTTHC.002. Model Input and Output Files, Excel Spreadsheets and Resultant Figures Which are Presented in AMR N0120/U0110, "Drift-Scale Coupled Processes (Drift-Scale Test and THC Seepage) Models." Submittal date: 3/11/2000.

LB991201233129.001. The Mountain-Scale Thermal-Hydrologic Model Simulations for AMR U0105, "Mountain-Scale Coupled Processes (TH) Models." Submittal date: 3/11/2000.

LB991220140160.012. Model Prediction of 3-D Transport, Present-Day Infiltration, #1 Perched Water Model, Using EOS9nT Input and Output files. AMR U0060, "Radionuclide Transport Models under Ambient Conditions". Submittal date: 3/11/2000.

LB991220140160.017. Model Prediction of 3-D Colloid Transport, Present-Day Infiltration, #1 Perched Water Model, using EOS9nT Input and Output files. AMR U0060, "Radionuclide Transport Models under Ambient Conditions". Submittal date: 3/11/2000.

LB997141233129.001. Calibrated Basecase Infiltration 1-D Parameter Set for the UZ Flow and Transport Model, FY99. Submittal date: 07/21/1999.

MO9804MWDGFM03.001. An Update to GFM 3.0; Corrected Horizon Grids for Four Fault Blocks. Submittal date: 04/14/1998.

MO9901MWDGFM31.000. Geologic Framework Model. Submittal date: 01/06/1999.

MO9901MWDISMMM.000. ISM 3.0 Mineralogic Models. Submittal date: 01/22/1999.
Submit to RPC URN-0074.

MO9910MWDISMMM.003. ISM3.1 Mineralogic Models. Submittal date: 10/01/1999. Submit to RPC URN-0076.

MO9901MWDISMRP.000. ISM3.0 Rock Properties Models. Submittal date: 01/22/1999.
Submit to RPC URN-0075.

MO9910MWDISMRP.002. Rock Properties Model (RPM3.1). Submittal date: 10/06/1999.
Submit to RPC URN-0080.

MO9912SPAPAI29.002. PA Initial Abstraction of THC Model Chemical Boundary Conditions. Submittal date: 01/11/2000. Submit to RPC URN-0282.

SN0001T0581699.004. Supplemental Files to Support Base-Case Particle-Tracking Analysis for TSPA-SR (Total System Performance Assessment-Site Recommendation) (In Analysis/Model Report U0160, ANL-NBS-HS-000024). Submittal date: 01/06/2000.

SN0003T0503100.001. Weighting Factors for Low, Middle and High Climate Infiltration Rate Maps. Submittal date: 03/20/2000.

SN9908T0581699.001. Files to Support 1-D Comparison Between FEHM Particle Tracking and T2R3D Advective-Dispersive Transport Simulations Along SD-9. Submittal date: 08/16/1999.

SN9912T0511599.002. Revised Seepage Abstraction Results for TSPA-SR (Total System Performance Assessment-Site Recommendation). Submittal date: 12/15/1999.

SN9912T0581699.003. Files to Support Base-Case Particle-Tracking Analyses (AMR U0160) for TSPA-SR. Submittal date: 12/13/1999.

INTENTIONALLY LEFT BLANK

7. ATTACHMENTS

Attachment I – UZ Data and Associated Data Tracking Numbers (DTNs)

Attachment II – List of DTNs for Figures and Tables

Attachment III – Figures

INTENTIONALLY LEFT BLANK